



**Cristina Montagner**

Mestre em Ciências Químicas para a  
Conservação e Restauro

## **The brushstroke and materials of Amadeo de Souza-Cardoso combined in an authentication tool**

Dissertação para obtenção do Grau de Doutor em  
Conservação e Restauro,  
especialidade de Ciências da Conservação

Orientador: Prof. Doutora Maria João Seixas de Melo, FCT-UNL

Co-orientadores:

Prof. Doutor Rui Manuel Feliciano de Jesus, ISEL-IPL  
Prof. Doutora Márcia Vilarigues, FCT-UNL

Júri:

Presidente: Professor Doutor Fernando Manuel Anjos  
Henriques

Arguentes: Prof. Doutor João Pedro Martins de Almeida Lopes  
Doutora Jilleen Nadolny

Vgais: Prof. Doutora Maria Raquel Henriques da Silva  
Prof. Doutora Leslie Anne Carlyle

**The brushstroke and materials of Amadeo de Souza-Cardoso combined in an authentication tool**

Copyright © Cristina Montagner, Faculdade de Ciências e Tecnologia, Universidade Nova de Lisboa.

A Faculdade de Ciências e Tecnologia e a Universidade Nova de Lisboa têm o direito, perpétuo e sem limites geográficos, de arquivar e publicar esta dissertação através de exemplares impressos reproduzidos em papel ou de forma digital, ou por qualquer outro meio conhecido ou que venha a ser inventado, e de a divulgar através de repositórios científicos e de admitir a sua cópia e distribuição com objetivos educacionais ou de investigação, não comerciais, desde que seja dado crédito ao autor e editor.

## ACKNOWLEDGEMENTS

This thesis was written in three different countries, Italy, Portugal and The Netherlands. These countries represent my origin, my recent past and my future. In the same way, I would like to thank all the people who have shared with me these last four years and with whom I will create my future.

First, I want to thank my supervisor Professor Maria João Melo for introducing me with enthusiasm into the world of Amadeo and also for helping me to recognize my limits. I am also very grateful to my co-supervisors: Professor Márcia Vilarigues, for her support and the ideas that we have shared in these four years. Professor Rui Jesus for the dedication and patience with which he introduced me to computer science, but also for his constructive criticism towards my work.

Thanks to Professor Fernando Pina for receiving me at the Department of Conservation and Restoration and in the Photochemistry group and for his kind chats about Italy.

I am very grateful to all team members of Centro de Arte Moderna da Fundação Gulbenkian for the fruitful collaboration, in particular to director Isabel Carlos and curator Ana Vasconcelos e Melo. Thanks to Helena de Freitas for her contribution in the selection of the artworks studied and for her suggestions during my research.

I would like to thank Professor Nuno Correia of Center for Informatics and Technologies (CITI) of UNL for receiving me in the Department of Informatics and for his contribution to this project. I am very grateful to Professors Sérgio Nascimento, João Linhares and their colleagues at the Department of Physics of the University of Minho, for their work and the time spent together in the missions in Lisbon and Minho.

To Professor Rita Macedo for her contributions in the research and for the positive attitude and interest in my work. Many thanks to Ana Maria, thanks for making me feel home. I am very grateful to Professor Leslie Carlyle for her support during the research and for the inexhaustible enthusiasm and passion that she transmitted me during all our chats.

I am grateful to all the people that I met in these four years. I can imagine the effort you have made to understand my own Portuguese dialect, and you know that I appreciate this effort. Thanks to Ana Margarida, Marta, Ângela, Elia, Solange, Augusta, Andreia, Ana Isabel, Catarina, Emanuele and Joana. Thanks also to Sara and Isabel: I learned so much with you but also found two good friends. Thank you Joana: it was a pleasure working with you, I'm proud of you. I shared this journey, the laboratory, and the *aquário* with some important friends. They have supported me when I have needed it. With them I have never spent a single day without a smile. They are the people on whom I could always count on, and they will be also part of my future: Rita, Tatiana, Diogo and Vanessa, thank you.

Thanks to Ughetta and Renato for their friendship and for the "Italian" moments that we shared in Lisbon. I have to thank my supporters from abroad, thanks to Eleonora for encouraging me to finish this experience that we started together several years ago. I also thank Chiara, who has patiently waited for me to get a real job. Thanks for your support in the last 28 years.

Everything I've lived in the last four years in Portugal has been shared with Jorge. He was my main support, he has always encouraged me to do my best and with him I am making our future.

A special thanks to my family: thank you for your support and for teaching me to work to achieve my dreams. This thesis is dedicated to you.

\*\*\* This is a revised version of my thesis. I have benefited much from the suggestions and comments from my examiners: Prof. João Pedro Martins de Almeida Lopes, Dr. Jilleen Nadolny, Prof. Maria Raquel Henriques da Silva and Prof. Leslie Anne Carlyle.





## RESUMO

Hoje em dia, os estudos de autenticação de pinturas requerem a utilização de uma abordagem multidisciplinar, baseada não apenas na contribuição feita pela análise de características visuais, mas também na caracterização dos materiais e técnicas. Para além disso, é importante que a atribuição da autoria de uma pintura seja confirmada através de estudos técnicos realizados num determinado número de obras de arte originais que percorra toda a carreira do artista.

Esta dissertação está relacionada com o trabalho do pintor modernista Amadeo de Souza-Cardoso, encontrando-se dividida em três partes. Na primeira parte, propomos uma ferramenta baseada no processamento de imagem, que relaciona informação acerca da pincelada de Amadeo com informação sobre os materiais utilizados na sua obra. O sistema resultante proporciona uma avaliação qualitativa e quantitativa acerca da autoria da pintura; o elemento quantitativo é particularmente relevante, uma vez que pode ser crucial para a resolução de controvérsias relacionadas com a autoria de obras de arte, como por exemplo disputas judiciais. A análise de pinceladas foi efectuada através da combinação de dois algoritmos utilizados para detectar características, nomeadamente Gabor Filter e Scale Invariant Feature Transform. Devido a esta combinação (e ao uso do modelo Bag-of-Features), o método proposto revela uma precisão superior a 90% ao distinguir entre imagens de pinturas de Amadeo e imagens de obras de arte de outros artistas contemporâneos. De modo a incluir a análise molecular, implementámos um sistema semi-automático que utiliza imagiologia hiperespectral e análise elementar. Este sistema apresenta como resultado final uma imagem que representa o mapeamento dos pigmentos presentes, juntamente com as áreas realizadas com materiais não coerentes com a paleta de Amadeo, caso estas existam. Este resultado visual constitui uma forma simples e eficaz de confirmar os resultados do sistema. A ferramenta proposta baseada na combinação de pinceladas e informação molecular foi testada em doze pinturas, tendo-se obtido resultados prometedores.

A segunda parte da tese apresenta um estudo sistemático de quatro pinturas seleccionadas, feitas por Amadeo em 1917. Apesar de não terem título, três destas pinturas são comumente conhecidas como *BRUT*, *Entrada* e *Coty*; estas pinturas são consideradas as obras melhor sucedidas e mais genuínas deste artista. Porém, os materiais e as técnicas destas obras de arte nunca foram estudados. As pinturas foram estudadas através de uma abordagem multi-analítica, que envolveu a utilização das técnicas micro-espectroscopia de fluorescência de raio-X dispersiva de energias, micro-espectroscopias de infravermelho e Raman, micro-espectrofluorimetria e microscopia electrónica de varrimento. A caracterização dos materiais e técnicas utilizados por Amadeo nas suas últimas pinturas, assim como a investigação de alguns dos problemas de conservação que afectam estas obras, é essencial para enriquecer o conhecimento obtido acerca do artista. Para além disso, o estudo dos materiais das quatro pinturas revela semelhanças entre as pinturas *BRUT* e *Entrada*. Esta observação é também comprovada pela análise dos elementos presentes numa fotografia de uma colagem (pertencente à Biblioteca de Arte da Fundação Calouste Gulbenkian), a única prova existente de uma suposta maquete destas pinturas.

A parte final da tese descreve a aplicação da ferramenta de processamento de imagem desenvolvida na primeira parte do trabalho a um conjunto de casos de estudo; esta experiência demonstra o potencial da ferramenta para apoiar a análise de pinturas e estudos de autenticação. A análise de pinceladas foi utilizada como análise adicional durante o processo de avaliação de quatro pinturas atribuídas a Amadeo, e o sistema baseado na análise das imagens hiperespectrais foi aplicado na pintura datada de 1917. Os casos de estudo servem portanto como uma ponte entre as duas primeiras partes da dissertação.

**Palavras-chaves-** Autenticação; Amadeo de Souza-Cardoso; análise de pinceladas; processamento de imagem; mapeamento de imagens hiperespectrais; análise de pinturas.

## ABSTRACT

Nowadays, authentication studies for paintings require a multidisciplinary approach, based on the contribution of visual features analysis but also on characterizations of materials and techniques. Moreover, it is important that the assessment of the authorship of a painting is supported by technical studies of a selected number of original artworks that cover the entire career of an artist.

This dissertation is concerned about the work of modernist painter Amadeo de Souza-Cardoso. It is divided in three parts. In the first part, we propose a tool based on image processing that combines information obtained by brushstroke and materials analysis. The resulting tool provides qualitative and quantitative evaluation of the authorship of the paintings; the quantitative element is particularly relevant, as it could be crucial in solving authorship controversies, such as judicial disputes. The brushstroke analysis was performed by combining two algorithms for feature detection, namely Gabor filter and Scale Invariant Feature Transform. Thanks to this combination (and to the use of the Bag-of-Features model), the proposed method shows an accuracy higher than 90% in distinguishing between images of Amadeo's paintings and images of artworks by other contemporary artists. For the molecular analysis, we implemented a semi-automatic system that uses hyperspectral imaging and elemental analysis. The system provides as output an image that depicts the mapping of the pigments present, together with the areas made using materials not coherent with Amadeo's palette, if any. This visual output is a simple and effective way of assessing the results of the system. The tool proposed based on the combination of brushstroke and molecular information was tested in twelve paintings obtaining promising results.

The second part of the thesis presents a systematic study of four selected paintings made by Amadeo in 1917. Although untitled, three of these paintings are commonly known as *BRUT*, *Entrada* and *Coty*; they are considered as his most successful and genuine works. The materials and techniques of these artworks have never been studied before. The paintings were studied with a multi-analytical approach using micro-Energy Dispersive X-ray Fluorescence spectroscopy, micro-Infrared and Raman Spectroscopy, micro-Spectrofluorimetry and Scanning Electron Microscopy. The characterization of Amadeo's materials and techniques used on his last paintings, as well as the investigation of some of the conservation problems that affect these paintings, is essential to enrich the knowledge on this artist. Moreover, the study of the materials in the four paintings reveals commonalities between the paintings *BRUT* and *Entrada*. This observation is supported also by the analysis of the elements present in a photograph of a collage (conserved at the Art Library of the Calouste Gulbenkian Foundation), the only remaining evidence of a supposed *maquete* of these paintings.

The final part of the thesis describes the application of the image processing tools developed in the first part of the thesis on a set of case studies; this experience demonstrates the potential of the tool to support painting analysis and authentication studies. The brushstroke analysis was used as additional analysis on the evaluation process of four paintings attributed to Amadeo, and the system based on

hyperspectral analysis was applied on the painting dated 1917. The case studies therefore serve as a bridge between the first two parts of the dissertation.

**Keywords-** Authentication; Amadeo de Souza-Cardoso; brushstroke analysis; image processing; hyperspectral imaging; painting analysis.

## PUBLICATIONS

C. Montagner, D. Sanches, J. Pedroso, M. J. Melo and M. Vilarigues. « Ochres and earths: matrix and chromophores characterization of 19<sup>th</sup> and 20<sup>th</sup> century artist materials » *Spectrochimica Acta Part A*, 103 (2013) 409–416.

V. Otero, D. Sanches, C. Montagner, M. Vilarigues, L. Carlyle, J. A. Lopes and M. J. Melo « Characterisation of metal carboxylates by Raman and infrared spectroscopy in works of art » *Journal of Raman Spectroscopy* (published online: 10 JUL 2014 DOI: 10.1002/jrs.4520).

C. Montagner, R. Jesus, N. Correia, M. J. Melo, M. Vilarigues, R. Macedo and H. de Freitas. « Unveiling the hand of a 19<sup>th</sup> Century artist with binary image classification and Bag-of-Features » *International Conference On Systems, Signals and Image Processing (IWSSIP)*, April, 2012.

C. Montagner, P. Almeida, R. Jesus, N. Correia, M. J. Melo, M. Vilarigues, R. Macedo, H. de Freitas and S. Nascimento « Behind the surface - Hyperspectral image spectroscopy for artist authentication » *12<sup>th</sup> International AIC Congress*, UK, 2013.

C. Montagner, S. M.C. Nascimento, J. M.M. Linhares, M. J. Melo, M. Vilarigues and R. Macedo « Assessing the power of colour in Amadeo's paintings » *12<sup>th</sup> International AIC Congress*, UK, 2013.

P. Almeida, C. Montagner, R. Jesus, N. Correia, M. Vilarigues, M.J. Melo and S. Nascimento « Analysis of paintings using multi-sensor data » *21<sup>th</sup> European Signal Processing Conference (Eusipco)*, Marrocco, 2013.

## SYMBOLS AND NOTATIONS

Ap.	Appendix
$\delta$	Bending vibration
$p(B/Am)$	Brushstroke probability
CAM	Centro de Arte Moderna da Fundação Calouste Gulbenkian (Center for Modern art of Calouste Gulbenkian's Foundation)
DCR-FCT	Department Conservation and Restoration- Faculdade de Ciências e Tecnologia
DoG	Difference-of-Gaussian
EMD	Euclidean Minimum distance
ESRF	European Synchrotron Radiation Facility
HPLC-DAD	High Performance Liquid Chromatography – Diode Array Detector
HART	Historically Accurate Reconstruction Techniques
$I_a(Am)$	Indicator for authenticity considering brushstroke and material analysis.
$I_a(M/Am)$	Indicator for authenticity considering material analysis
Inv.	Inventory number: it refers to the inventory number used at CAM and reported on the Catalogue Raisonné of the painting of Amadeo, unless otherwise stated.
$\mu$ -EDXRF	Micro-Energy Dispersive X-Ray Fluorescence spectroscopy
$\mu$ - FTIR	Micro-Fourier Transform Infrared spectroscopy
$\mu$ -Raman	Micro-Raman spectroscopy
$\mu$ -SPEX	Micro-spectrofluorimetry
$\mu$ -XANES	Micro-X-ray Absorption Near-Edge spectroscopy
RLSC	Regularized Least Squared Classifier
SAM	Spectral Angle Mapper
SIFT	Scale Invariant Feature Transform
SEM-EDS	Scanning Electron Microscopy and Energy Dispersive X-ray Spectrometry
$v_{as}$	Stretching vibration (asymmetric)
$v_s$	Stretching vibration (symmetric)
SVM	Support Vector Machine
SR	Synchrotron Radiation
TF-IDF	Term Frequency– Inverse Document Frequency
W&N	Winsor & Newton



# CONTENTS

<b>CONTEXT OF THE WORK</b>	<b>1</b>
<b>PART I: DIGITAL IMAGE PROCESSING FOR OIL PAINTING ANALYSIS</b>	
<b>INTRODUCTION TO PART I</b>	<b>7</b>
<b>CHAPTER 1: AUTHENTICATION AND COMPUTER VISION</b>	<b>11</b>
<b>1.1 Authenticity issues</b>	<b>11</b>
1.1.1 The authentication process	12
<b>1.2 Computer vision in the conservation field</b>	<b>14</b>
1.2.1 Digital image processing	14
1.2.2 Challenges in art conservation	16
1.2.3 Imaging processing for brushstroke analysis	17
1.2.4 Hyperspectral imaging for pigment identification	19
<b>1.3 Our contributions</b>	<b>21</b>
<b>CHAPTER 2: METHODOLOGY AND RESULTS</b>	<b>23</b>
<b>2.1 Features combination for painting authentication</b>	<b>23</b>
<b>2.2 Brushstroke Analysis</b>	<b>24</b>
2.2.1 Image pre-processing and features extraction	25
2.2.2 Bag-of-Features	29
2.2.3 Classifier	30
2.2.4 Parameters setting and evaluation of the strategy proposed	31
<b>2.3 Molecular Analysis</b>	<b>34</b>
2.3.1 Painting system	36
2.3.2 Paint data and pre-processing step	39
2.3.3 Pigment analysis	40
2.3.4 Image mapping	43
2.3.5 Setting up the parameters	44
2.3.6 Evaluation of the strategy proposed	46
<b>2.4 Features combination: results</b>	<b>50</b>
<b>2.5 Final remarks</b>	<b>54</b>

## **PART II: MATERIALS AND TECHNIQUES OF AMADEO'S PAINTINGS DATED 1917**

<b>INTRODUCTION TO PART II</b>	<b>57</b>
<b>CHAPTER 1: AMADEO DE SOUZA-CARDOSO</b>	<b>59</b>
<b>1.1 Amadeo: an artist in his time</b>	<b>59</b>
1.1.1 Paris (1906-1914)	60
1.1.2 Back to Portugal (1914-18)	62
1.1.3 Looking at Amadeo's paintings	65
<b>1.2 Dealing with ageing: conservation issues</b>	<b>72</b>
1.2.1 Drying and ageing of the oil binder	73
1.2.2 Metal soaps in paint formulations and the Ripolin case study	75
1.2.3 Pigment alteration	77
<b>CHAPTER 2 ANALYSIS OF THE PAINTINGS</b>	<b>83</b>
<b>2.1 The paintings of 1917</b>	<b>83</b>
2.1.1 Unconventional materials	87
2.1.2 Preparation layer	90
2.1.3 Amadeo's colour language	91
2.1.4 Chrome yellow samples	100
<b>2.2 Conservation issues</b>	<b>105</b>
2.2.1 Metal carboxylates	107
2.2.2 Fading	115
2.2.3 Cracking and darkening of the green area	119
<b>2.3 Final remarks</b>	<b>121</b>

## **PART III: CASE STUDIES**

<b>1.1 Brushstroke analysis to support authentication processes</b>	<b>125</b>
1.1.1 The methodology	125
1.1.2 Results and discussion	127
1.1.3 Final remarks	135
<b>1.2 Hyperspectral imaging analysis</b>	<b>136</b>
1.2.1 The system proposed	136



1.2.2 Results and discussion	136
1.2.3 Final remarks	141
<b>CONCLUSION AND FUTURE WORKS</b>	<b>143</b>
<b>REFERENCES</b>	<b>149</b>
<b>APPENDICES PART I</b>	
Appendix I: k-means method	165
Appendix II: Term Frequency–Inverse Document Frequency (TF-IDF)	166
Appendix III: Hyperspectral imaging	167
Appendix IV: Analysis of the painting <i>Mucha</i> using hyperspectral imaging and $\mu$ -EDXRF	168
Appendix V: Paint tubes samples database	174
<b>APPENDICES PART II</b>	
Appendix I: Paintings cited in the main text	179
Appendix II: Experimental Section, Instrumentation	181
Appendix III: Colorimetric analysis of Amadeo’s paintings.	184
Appendix IV: Area of analysis	189
IV.1. <i>BRUT</i>	189
IV.2. <i>Entrada</i>	191
IV.3. <i>Coty</i>	193
IV.4. <i>Untitled</i>	195
Appendix V: Representative spectra of <i>BRUT</i> , <i>entrada</i> , <i>Coty</i> and <i>Untitled</i> .	197
V.1 $\mu$ -EDXRF	201
V.2 $\mu$ -FTIR	218
V.3 $\mu$ -Raman	227
V.4 $\mu$ -SPEX	235
V.5 Reflectance spectroscopy (hyperspectral imaging)	238
Appendix VI: SEM-EDS analysis on cross-sections and micro-samples	243
VI.1 Sampling areas	243
VI.2 Cross-sections	245
VI.3 Micro-samples	254

Appendix VII: Chrome yellow samples analysis	258
VII.1 SEM-EDS analysis of Entrada, BRUT and Untitled samples	258
VII.2 $\mu$ -FTIR	260
VII.3 Synchrotron analysis	264
Appendix VIII: Oil paint tubes	269
Appendix IX: Ripolin chart	272
<b>APPENDICES PART III</b>	
Appendix I: Images painting <i>Collage</i>	275
Appendix II: Area of analysis case studies paintings.	276
II.1 Painting A: <i>Collage</i>	276
II.2 Painting B: <i>geometric composition</i>	277
II.3 Painting C: <i>the embroiderers</i>	278
II.4 Painting D: <i>the café</i>	279
Appendix III: Analysis and representative spectra of the case studies paintings	280
III.1 Results	280
III.2 $\mu$ -EDXRF	283
III.3 $\mu$ -FTIR	290
III.4 $\mu$ -Raman	295
III.5 FORS	304
Appendix IV: Image documentation	305
Appendix V: Paintings cited in the main text	308

## LIST OF FIGURES

### PART I

- Figure 1.** An example of spontaneity, in this case the rapidity of the movements may be related to the absence of inhibition (Image taken from [www.ascuoladiguggenheim.it](http://www.ascuoladiguggenheim.it)) **13**
- Figure 2.** Fusion data system overview **23**
- Figure 3.** System architecture for the brushstroke analysis. **24**
- Figure 4.** Bank of 24 Gabor's filters used in this work with 6 orientations and 4 scales. **25**
- Figure 5.** Gabor filter processing, **A** RGB image of the painting *Ar livre nù*, Amadeo de Souza-Cardoso (1914); **B** scale 4 and 45° filter; **C** representation of the convolution of the image with the filter (scale 4, 45°); **D** resulted image filtered with 24 filters. **26**
- Figure 6.** Image processing of RGB image *Ar livre nù*, Amadeo de Souza-Cardoso, (1914), using SIFT (left) and Gabor filter (right). **27**
- Figure 7.** Representation of Gabor (3); **A** Identification of the keypoints localization and orientation; **B** Selection of a area around the keypoint; **C** Rotation of the area in accordance with the orientation detected by SIFT; **D** Selection of an area of 64x64 pixels around the keypoint. **28**
- Figure 8.** Representation of the construction of the vocabulary used for Bag-of-Features, positive and negative patches are collected from the images of the training set belongs to the corresponding classes. Image adapted from [Maaten and Postma 2009]. **29**
- Figure 9.** The performance of the classifier while changing the number of positive images in the training set, %Hits means the number of painting images correctly classified: the images of the *positive* class (Amadeo) correctly classified are represented by the black lines; the *negative* class (Not Amadeo) by the dot lines. **A** The texture features are extracted using Gabor filter; **B** the features are extracted by SIFT using the Bag-of-Features model. **32**
- Figure 10.** Representation of the hyperspectral imaging data-cube, the hyperspectral analysis includes the visible range between 400 to 720 nm. For each painting 33 images with a spectral resolution of 10 nm were acquired. In this way, a data-cube of 1344 x 1024 x 33 is created, where the first two dimensions are the spatial resolution of the images (expressed in pixels) and the third dimension is the reflectance value of each pixel in the 33 images. From the data-cube it is possible to extract a reflectance spectra for each one of the pixels of the image. **34**
- Figure 11.** System overview of the combination of hyperspectral imaging and elemental analysis. **37**
- Figure 12.** System overview of the step 1 where are mapped the areas that could not painted by Amadeo (violet) and those where the analysis was not performed (pink). The other pigments are considered unclassified and will be analysed in Step 2. **41**
- Figure 13.** System overview of Step 2, where by comparing the reflectance spectra from the painting with those in the reflectance database we compute the first pigment attribution. This attribution can be confirmed if the elements detected on the paint area are coherent with those corresponding to the proposed pigment. If the attribution is not confirmed then the pixel is considered unclassified and goes to Step 3. **41**
- Figure 14.** Representation of the measure of the distance between two vectors using Euclidian Minimum Distance (left) and Spectral Angle Mapper (right). **42**
- Figure 15.** System overview of Step 3. The reflectance spectrum of the unknown pixels is compared with a set of spectra of mixtures. **43**
- Figure 16.** **A** Selection of a pixel (291; 304) in the segmented image; **B** mapping of the areas where it was detected vermilion and chrome yellow. **44**
- Figure 17.** Tests performed to define the best values for the interval of colour tolerance ( $C$ ) in the pre-processing step. The two points (orange and blue), indicated in the coloured image of the painting *Mucha* (1915-16) were used as samples in the tests. In white are mapped the pixels that satisfied the Equation 10 considering the different values of  $C$  indicated close to the image. The  $\Delta E^*$  indicates the **46**

difference between the sample pixel and those mapped in white. The percentage indicates the portion of the area mapped in white.

**Figure 18.** *Mucha* painting (1915-16) and DCR (2013) **C** and **E** RGB images of the paintings; k-means cluster analysis of *Mucha* using **A** 15 clusters; **B** 70 clusters; segmented image obtained with our system **D** *Mucha* **F** DCR, the *No Analyzed* is coloured in pink and the *No Amadeo* in purple. 48

**Figure 19.** Comparison between the measured reflectance spectra on *Mucha* hyperspectral image (solid lines) and estimated proposed by our system (dot-dashed lines). The sample points are indicated in Figure 17C; **A** spectrum of Cobalt blue pigment sample B1; **B** spectrum of mixture of viridian and chrome yellow sample G1; **C** spectrum of mixture of chrome yellow and vermilion sample point O1; **D** spectrum of vermilion sample point R1. 49

**Figure 20.** Relation between the percentage of the *Analysed area* and the *Indicator of authenticity* for molecular analysis. 51

**Figure 21.** Paintings analysed by fusion data. The paintings of Amadeo de Souza-Cardoso belong to the Centro de Arte Moderna, Fundação Calouste Gulbenkian [Freitas *et al.* 2008]. The painting DCR was made by the DCR-FCT. 52

## PART II

**Figure 1.** Alexandre Ferraz de Andrade, Luice e Amadeo (seated), Brussels 1910. Image from [Alfaro 2007, pg 118]. 61

**Figure 2.** La Légend de St Julien L'Hospitalier, illustrated manuscript version of Gustave Flaubert's book, 1912. Collection of Centro de Arte Moderna, Fundação Calouste Gulbenkian (Inv.DP1822) [Freitas 2008 *et al.* pg. 208] 62

**Figure 3.** Paintings of Amadeo de Souza-Cardoso dated 1917. Collection of Centro de Arte Moderna, Fundação Calouste Gulbenkian. **A** *Untitled (Entrada)*, 93 x 76 cm. Collection of CAM (Inv. 77P9); **B** *Untitled (Coty)*, 93 x 76 cm. Collection of CAM (Inv. 68P11); **C** *Untitled (Máquina registadora - Cash Register)* (P198), 93 x 76 cm. Collection of CAM (Inv. 68P10); **D** *Untitled*, 93.5 x 93.5 cm. Collection of CAM (Inv. 77P8); **E** *Untitled*, 100 x 70.3 cm. Collection of CAM (Inv. 86P19); **F** *Untitled (BRUT 300 TSF)*, 85.8 x 66.2 cm. Collection of CAM (Inv. 77P20) and **G** *Untitled (Zinc)*, Private collection. [Freitas *et al.* 2008, pgs. 355, 356, 358, 360, 362, 364, 367, 355]. 64

**Figure 4.** Oil paint tubes from the box of Amadeo, from left to right: carminic red (Bourgeois); viridian (Lefranc), chrome yellow (Lefranc) and vermilion (Winsor & Newton) [Melo *et al.* 2008] 66

**Figure 5.** The pigment palette of Amadeo between 1912 and 1916, with details from his paintings. Image adapted from Melo *et al.* 2008. 67

**Figure 6A.** Paintings of Amadeo de Souza-Cardoso on cardboard. **A** *Untitled* (1914), 18 x 33 cm. Collection CAM (Inv. 77P5); **B** *Untitled* (1914) 10.7 x 41.2 cm. Collection CAM (Inv.91P219); **C** *Ar livre nú* (1914) 18.8 x 13 cm. Collection CAM (Inv.91P217); **D** *Untitled* (1914) 18.7 x 12.5 cm. Collection CAM (Inv.91P220); **E** *Untitled* (1914) 17.4 x 13.3 cm. Collection CAM (Inv.87P158); **F** *Untitled (Cabeça)* (1914) 18.6 x 16.2 cm. Collection CAM (Inv.91P218); **G** *Untitled* (1914) 20.1 x 12.9 cm. Private Collection; **H** *Untitled* (1914) 18.7 x 12.8 cm. Private Collection; **I** *Untitled* (1913) 14.6 x 17.9 cm. Collection CAM (Inv. 91P225); **L** *Untitled* (1914) 26.8 x 32.9 cm. Collection CAM (Inv. 91P224); **M** *Untitled* (1913) 34.4 x 28.2 cm Collection CAM (Inv. 92P209) [Freitas 2008, pgs. 228, 229, 236, 237, 239, 264, 268, 269, 286, 285, 287]. 68

**Figure 6B.** Paintings of Amadeo de Souza-Cardoso on canvas. Collection of Centro de Arte Moderna, Fundação Calouste Gulbenkian **A** *Untitled (O Jockey)* (1913) 61 x 50 cm. (Inv. 77P5) [Freitas 2008, pg. 209]; **B** *(Paysagem figura negra)* (1914-15) 50 x 50 cm (Inv. 86P23) [Freitas 2008, pg. 297]; **C** *Gemälde G /Quadro G* (1912) 51 x 29.5 cm (Inv. 77P2) [Freitas 2008, pg. 182]; **D** *Untitled*, 100 x 70.3 cm. (Inv. 86P19) [Freitas 2008, pg. 362]; **E** *Mucha* (1915-16) 27.3 x 21.4 cm. (Inv. 86P21) [Freitas 2008, pg. 322]; **F** *(Janellas do pescador)* (1915-16) 27.4 x 34.8 cm. (Inv. 77P16) [Freitas 2008, pg. 318]; **G** *Untitled* (undated) 99.6 x 64.6 cm. (Inv. 91P222) [Freitas 2008, pg. 373] 69

**Figure 7.** Paintings of Amadeo de Souza-Cardoso Collection CAM. *Untitled* (1913) (Inv. 92P209) **A** visible light photograph; **B** X-ray image [Melo *et al.* 2009]; **C** *Untitled* (1914) (Inv. 88P159); **D** Infrared photograph [Melo *et al.* 2008]. 70

- Figure 8.** Amadeo de Souza-Cardoso **A** *Mucha*, Oil painting (1915-16), 27.3 x 21.4 cm. Collection CAM (Inv. 86P21); **B** and **C** *Untitled*, watercolour 25 x 16 cm. and 28 x 18 cm. Private collection; **C** Oil painting *A casita clara – paisagem (The clear little house-landscape)* (1915-16) 30.5 x 40.5 cm. Collection CAM (Inv. 77P15); **D** (*Maisonatte*), watercolour (1915-16), 14.7 x 23.8 cm. Collection CAM (Inv. 87DP340) [Freitas 2008, pgs. 322, 323, 316]. **71**
- Figure 9.** Macro images of different texture patterns in the paintings of Amadeo de Souza-Cardoso. Collection of Centro de Arte Moderna, Fundação Calouste Gulbenkian **A** *Untitled*, (1912-13) (Inv. 77P3); **B** *A chalupa* (1914-15), (Inv. 77P22); **C** *Untitled (Entrada)* (1917) (Inv. 77P9); **D** *Untitled* (1914) (Inv. 92P210); **E** *Mucha* (1915-16) (Inv. 86P21); **F** *Untitled* (1913-14) (Inv. 87P158) [Freitas 2008, pgs. 179, 237, 241, 285, 322, 364]. **72**
- Figure 10.** Hydrolysis of a triglyceride composed of two unsaturated acids, (a) linolenic and (b) linoleic, and one saturated acid, (c) stearic. **74**
- Figure 11.** Schematic model of the different stages of the drying of the oil **A** fresh oil; **B** representation of the polyanionic network (after curing); **C** after hydrolysis of the ester bond due to the ageing processes (after maturation). Image adapted from [Boon *et al.* 1996]. **74**
- Figure 12.** Example of darkening of chrome yellow pigments in Vincent van Gogh painting. Bank of the Seine (F 293s 77v/1962) (mid 1887), oil on canvas (32 x 46 cm); Van Gogh Museum, Amsterdam (Vincent van Gogh Foundation). Painting analysed by Monico *et al.* in [Monico *et al.* 2011b]. **77**
- Figure 13.** Detection of Cr (VI) and Cr (III) species using K-edge XANES spectra. In black the spectrum of Cr(III) oxide (Cr<sub>2</sub>O<sub>3</sub>) and in orange the reference Crocoite mineral (Department of Conservation and Restoration of the Universidade NOVA de Lisboa). **78**
- Figure 14.** Molecular structures of fluorescein, eosin and erythrosine, image adapted from [Geldof *et al.* 2013]. **80**
- Figure 15.** iPad application of the digital reconstruction of van Gogh painting *The bedroom* (1888). The user can observe the differences between the present state of the painting and its colour reconstruction [Vet 2014]. **81**
- Figure 16.** Paintings of Amadeo de Souza-Cardoso dated 1917. Collection of Centro de Arte Moderna, Fundação Calouste Gulbenkian. *Untitled (BRUT 300 TSF)* Inv. 77P20; *Untitled (Entrada)* Inv. 77P9; *Untitled (Coty)* Inv. 69P11; *Untitled* Inv. 77P8. **84**
- Figure 17.** **A** Image of the Collage (Art Library of the Calouste Gulbenkian Foundation ASC09/16); **B** Headline of the Madrid's edition of the newspaper "La correspondencia de España"; **C** Flyer included in the album "12 Reproductions" (1916) (Art Library of the Calouste Gulbenkian Foundation ASC 221). Image of the flyer from [Alfaro 2007, pg 235]. **85**
- Figure 18.** Image details of the word ZINC on (top) the maquette and on (down) *Untitled (ZINC)*, c. 1917, 59 x 49 cm. Private Collection [Freitas 2008, pg. 355]. **85**
- Figure 19.** Image details (from left to right) of the rag doll in: the *maquette*; *Canção popular a Russa e o Figaro*, 1916, 80 x 60 cm. Collection of Centro de Arte Moderna, Fundação Calouste Gulbenkian (Inv. 77P18) [Freitas *et al.* 2008, pg. 333] and *Trou de la serrure PARTO DA VIOLA Bon ménage Fraise avant garde*, 1916, 70 x 58 cm. Collection of Centro de Arte Moderna, Fundação Calouste Gulbenkian (Inv. 68P17) [Freitas *et al.* 2008, pg. 336]. Appendix Part II Ap.I. shows the images of the paintings **86**
- Figure 20.** Comparison between *maquette* (upper part) and *Entrada* painting (lower part) **A** Images details of the word ENTRADA **B** word BRUT 300 KK and **C** advertising of the lamp Wotan. **87**
- Figure 21.** Mapping of ● silica, sand, calcium carbonate; ● glass and mirrors; ● day-by-day materials, hair clips, matches and box of matches; ● starch. **88**
- Figure 22.** Image details of found objects on *Coty* paintings, from left to right: mirrors; paint glass and one mirror; pearl necklace; hair clips. **89**
- Figure 23.** **A** Image detail of the representation of the matches in *Entrada (7x)* **B** Image detail of the wax matches and **C** of the box label applied on *Untitled* painting **D** wood matchbox like this in the painting *Untitled* conserved by the Portuguese Association of Phillumenism. **90**

<b>Figure 24.</b> SEM image in BSE mode of the preparation layers <b>A</b> <i>Coty</i> ( $\mu 6$ ); <b>B</b> <i>Entrada</i> ( $\mu 33$ ); <b>C</b> <i>BRUT</i> ( $\mu 12$ ); <b>D</b> <i>Untitled</i> ( $\mu 6$ ), (Appendix Part II Ap.IV.1 shows the sampling areas).	<b>91</b>
<b>Figure 25.</b> Red layer in <i>BRUT</i> <b>A</b> Detail image from the back of the painting; <b>B</b> Photomicrographs of the paint surface (10x); <b>C</b> Cross-section of the sample $\mu 12$ where it is possible to observe the red layer (the sampling area indicated in Fig. IV.2 Appendix Part II Ap.IV.1).	<b>91</b>
<b>Figure 26.</b> Colours distribution on the CIE(a*b*) colour space. The CIEL*a*b* values were calculated by the spectral reflectance of the hyperspectral images of the 4 paintings.	<b>92</b>
<b>Figure 27.</b> Violet sample ( $\mu 13$ ) from <i>Coty</i> painting; <b>A</b> Infrared spectrum ( $\star$ ) cobalt violet pigment; <b>B</b> Raman spectrum.	<b>94</b>
<b>Figure 28.</b> Green sample ( $\mu 19$ ) from <i>Untitled</i> painting; <b>A</b> Infrared spectrum ( $\bullet$ ) viridian pigment; <b>B</b> Raman spectra from the sample (black) and from the reference strontium yellow (grey).	<b>95</b>
<b>Figure 29.</b> Blue sample (B12) from <i>Untitled</i> painting; <b>A</b> reflectance spectrum; <b>B</b> EDXRF spectrum.	<b>95</b>
<b>Figure 30.</b> Yellow sample ( $\mu 3$ ) from <i>Coty</i> painting; <b>A</b> Infrared spectrum ( $\bullet$ ) cobalt yellow pigment; <b>B</b> Raman spectrum.	<b>97</b>
<b>Figure 31.</b> Yellow sample ( $\mu 3$ ) from <i>Coty</i> painting SEM image in BSE mode.	<b>97</b>
<b>Figure 32.</b> <b>A</b> Infrared spectra of the red sample $\mu 6$ from <i>Coty</i> <b>B</b> section of A between 1800 and 650 $\text{cm}^{-1}$ : sample $\mu 6$ (black line), cochineal carmine lake reproduction (grey line), carminic acid (red line) and ( $\bullet$ ) barium sulphate.	<b>98</b>
<b>Figure 33.</b> Sample $\mu\text{Red}1$ from <i>BRUT</i> : <b>A</b> Cross-section; <b>B</b> and <b>C</b> SEM image in BSE mode details of the white particles present in the top layer, in the area Z1 was $\text{PbSO}_4$ and in area Z2 $\text{BaSO}_4$ .	<b>98</b>
<b>Figure 34.</b> (Left) Raman spectrum of <i>Coty</i> $\mu 2$ ; in black the bands attributed to PR49 $\beta$ -naphthol pigment, in orange those attributed to minium and in blue the characteristic band of the barium sulphate. (Right) Molecular structure of Lithol red (PR49) [Scherren <i>et al.</i> 2009].	<b>99</b>
<b>Figure 35.</b> Percentage of the use of lead and zinc white in the paintings analysed.	<b>99</b>
<b>Figure 36.</b> White sample ( $\mu 14$ ) from <i>Entrada</i> painting; <b>A</b> Infrared spectra of the sample (black) and reference $\text{SrSO}_4$ (Alfa Aesar); <b>B</b> Raman spectra of the sample (black) and reference $\text{SrSO}_4$ ( $\bullet$ ) lead carbonate.	<b>100</b>
<b>Figure 37.</b> CIE(a*b*) colour values for the chrome yellow samples: pure lead chromate (in blue) and mixed-crystals of lead chromate and lead sulphate (in grey). E = <i>Entrada</i> ; B= <i>BRUT</i> and U= <i>Untitled</i> .	<b>101</b>
<b>Figure 38.</b> SEM image in BSE mode of the pure chrome yellow sample <b>A</b> <i>Entrada</i> $\mu 32$ ; <b>B</b> sample of paint tube of Chrome deep ( $\mu 17\_3128$ ) of W&N.	<b>102</b>
<b>Figure 39.</b> Infrared spectra of the sample $\mu 8$ <i>Entrada</i> . In the inset, comparison with a chrome deep pigment reconstruction, M3 (based on W&N process) (in grey) $\bullet$ $\text{PbCrO}_4$ ; $\blacklozenge$ $\text{CaCO}_3$ ; $\blacklozenge$ kaolinite.	<b>103</b>
<b>Figure 40.</b> Infrared spectra of the sample $\mu 17$ <i>Entrada</i> . In the inset, comparison with a Lemon chrome yellow pigment reconstruction, L3b (based on W&N process) (in grey); $\bullet$ $\text{Pb}(\text{Cr},\text{S})\text{O}_4$ .	<b>103</b>
<b>Figure 41.</b> XRF chromium map intensity with the XANES points of analysis ( $^\circ$ ) <b>A</b> <i>BRUT</i> and <b>C</b> <i>Entrada</i> ; average XANES spectrum <b>B</b> <i>BRUT</i> and <b>D</b> <i>Entrada</i> .	<b>105</b>
<b>Figure 42.</b> Conservation problems detected in <i>BRUT</i> : <b>A</b> localization of the areas; image details <b>B</b> crack (10x); <b>C</b> network of cracks, macro image acquired with transmitted light; <b>D</b> network of cracks (10x); <b>E</b> cracks and lacuna of the paint and preparation layer (25x); <b>F</b> cracking (32x); <b>G</b> delamination of the white and green paint (16x).	<b>106</b>
<b>Figure 43.</b> Photomicrographs of the white and dark green areas in the word <i>BRUT</i> <b>A</b> delamination of the white area in the letter "R", sample $\mu 4$ (10x); <b>B</b> delamination of the green area in the letter "R", sample $\mu 5$ (32x); <b>C</b> sampling area in the letter "T" where no delamination was observed, sample $\mu 25$ (20x); <b>D</b> identification of the sampling area in the word "BRUT".	<b>108</b>

<b>Figure 44.</b> Infrared spectra of samples collected from the word “BRUT” in the painting BRUT; <b>A</b> from yellow area under the letter “R” ( $\mu 4$ ); <b>B</b> white area in the letter “T” ( $\mu 25$ ).	<b>108</b>
<b>Figure 45.</b> (Top) Mapping of the carboxylates areas in painting BRUT and Entrada: the pink area corresponds to the samples of the group 1, characterized by the presence of IR defined bands at 1551, 1534 $\text{cm}^{-1}$ (spectrum Fig. 44A). The green area corresponds to the samples of the group 2, characterized by the presence of IR broad band centred at 1589 $\text{cm}^{-1}$ (spectrum Fig. 44B); (Down) Identification of the samples analysed for each type of carboxylates group.	<b>109</b>
<b>Figure 46.</b> Infrared spectra of $\mu$ -samples collected from the paint tube Lefranc Zinc white applied on glass slide, the samples were collected on the dried surface (external) and from the not-completed dried paint (internal).	<b>110</b>
<b>Figure 47.</b> Infrared spectra of reference zinc carboxylates synthesized in DCR laboratory, details in [Otero <i>et al.</i> 2014].	<b>110</b>
<b>Figure 48.</b> Infrared spectra of the tube samples Lefranc Zinc White, the white of Ripolin and the white BRUT $\mu 4$ .	<b>110</b>
<b>Figure 49. A</b> Optical microscope image of cross-section from Lefranc zinc white paint sample; <b>B</b> SEM image in BSE mode of cross-section from Lefranc zinc white paint sample; <b>C</b> Optical microscope image of cross-section from Blanc Ripolin sample.	<b>112</b>
<b>Figure 50.</b> Raman spectra <b>A</b> ASC8 zinc white inside the area delimited with red dashed line in the cross-section image. In blue the contribution of the resin used to prepare the cross-section; <b>B</b> zinc azelate reference.	<b>112</b>
<b>Figure 51.</b> Raman spectra of Ripolin blanc sample on diamond cell, the region between 1320 and 1350 $\text{cm}^{-1}$ was excluded because it corresponds to the diamond band; in red the band attributed to azelaic acid.	<b>113</b>
<b>Figure 52.</b> SEM image in BSE mode of <b>A</b> zinc white Lefranc (ASC8). The EDS analysis detected the presence of: Zn (Z6) and Si (Z5); <b>B</b> Blanc Ripolin sample. The EDS analysis detected the presence of: Zn (Z2) and Al in (Z3).	<b>113</b>
<b>Figure 53.</b> SEM image in BSE mode of <b>A</b> zinc white by Lefranc (ASC8); <b>B</b> Blanc by Ripolin; <b>C</b> BRUT sample $\mu 4$ ; <b>D</b> BRUT sample $\mu 5$ .	<b>114</b>
<b>Figure 54.</b> Cross-section ( $\mu 19$ ), <b>A</b> visible light; <b>B</b> Ultraviolet light (filter 5); <b>C</b> Ultraviolet light (filter 8).	<b>116</b>
<b>Figure 55.</b> Cross-section of the sample BRUT $\mu 19$ <b>A</b> MO image; <b>B</b> SEM image in BSE mode; <b>C</b> distribution of aluminium (Al line K); <b>D</b> distribution of the cobalt (Co line K); <b>E</b> distribution of the zinc (Zn line K).	<b>117</b>
<b>Figure 56. A</b> Reflectance spectrum acquired with hyperspectral camera; <b>B</b> Infrared spectrum of purple BRUT $\mu$ -19 (+) cerulean blue; (●) zinc carboxylate; (▲) magnesium carbonate.	<b>117</b>
<b>Figure 57.</b> $\mu$ -EDXRF spectrum acquired on the BRUT painting in the purple area.	<b>118</b>
<b>Figure 58. A</b> BRUT ( $\mu 19$ ) Emission spectra ( $\lambda_{\text{ex}} = 490 \text{ nm}$ ; $\text{df} = 500 \text{ nm}$ ) and excitation ( $\lambda_{\text{em}} = 610 \text{ nm}$ ; $\text{df} = 600 \text{ nm}$ ) from the purple (violet line) and bluish (blue line); <b>B</b> Eosin in MeOH:H <sub>2</sub> O (70:30, v/v) with Al <sup>3+</sup> at pH 2.9, applied on filter paper [Claro 2009].	<b>118</b>
<b>Figure 59.</b> Image detail using ranking light of the green area at the bottom right corner in the painting BRUT (Left); <b>A</b> Photomicrographs of the light green area (10x); <b>B</b> Photomicrographs of the dark green area (25x).	<b>119</b>
<b>Figure 60.</b> Infrared spectra of the green sample ( $\mu 33$ ) from BRUT painting (green line); barium sulphate (orange line) and starch (grey line).	<b>120</b>
<b>Figure 61.</b> Cross-section dark green sample $\mu 33$ <b>A</b> OM image; <b>B</b> and <b>C</b> SEM image in BSE mode.	<b>120</b>
<b>Figure 62.</b> The pigment palette of Amadeo for the paintings dated 1917, with details from his paintings.	<b>121</b>

## PART III

- Figure 1.** The pigment palette of Amadeo between 1912 and 1916, with details from his paintings. Image adapted from Melo *et al.* 2009 **126**
- Figure 2.** Images of the four paintings assigned Amadeo de Souza-Cardoso but that were not included in the Catalogue Raisonné of his paintings [Freitas *et al.* 2008]. **127**
- Figure 3.** Image documentation of the *Painting B* (Left) X-ray image (Right) Infrared image, in orange the line used as sketch to create the composition. **129**
- Figure 4.** Photomicrographs of the brushstroke details from: **A** and **B** painting Geometric (10x); **C** and **D** Amadeo de Souza-Cardoso, Quadro G (7x), dated 1912, collection of Centro de Arte Moderna, Fundação Calouste Gulbenkian (Inv. 77P2). **130**
- Figure 5.** Painting C Embroiderers; visible light photograph (left); X-ray image of the, the red rectangle indicates the region that has no correspondence to that of the surface of the painting (right). **131**
- Figure 6.** Detail image of the group of women, here the brushstroke is used to create the figures more that fill it and the colours seem mixed directly on the support. **132**
- Figure 7.** Mapping performed on the x-ray image: (●) *lacune* filled probably during the first conservation treatment; (●) chromatic integrations made over the varnish layer. **133**
- Figure 8.** Image of the painting and in detail the four areas selected for the brushstroke analysis and the relative brushstroke probability, where 1 is the probability to be painted by Amadeo e 0 by another artist; the accuracy of the answer is 91%. **134**
- Figure 9.** **A** Image *Coty* painting; **B** segmented image; **C** mapping of Not-Amadeo area. **137**
- Figure 10.** **A** Image *Entrada* painting; **B** segmented image; **C** mapping of the emerald green pigment. **138**
- Figure 11.** Comparison between the reflectance spectra acquired on the **A** *Entrada* painting in the green area (a) with a mixture of viridian and Prussian blue; **B** from the oil paint tube samples viridian and emerald green, used as reference materials in the data-base. **138**
- Figure 12.** **A** *BRUT* painting (a), (b) black areas, (c) Prussian blue with whiteness surface, (c) area of fading; **B** segmented image. **139**
- Figure 13.** Photomicrographs of the area with problems of colour alteration: (left) the blue area, indicated with the letter (c) in Figure 12A, shows a whiteness due to the delamination of the varnish; (right) violet area, indicated with the letter (d) in Figure 12A, the fading of the eosin lake leaved visible the bluish tone of the cerulean blue pigment present. **139**
- Figure 14.** **A** Image *Untitled* painting; **B** segmented image; mapping of **C** vermilion; **D** chrome yellow. **140**

## APPENDICES PART I

- Figure I.1** **A**  $k$  centroids of  $K$ -clusters are chosen randomly; **B** Each sample is assign to the nearest centroid; **C** For each cluster a new centroid is calculated. Move the centroid to the new position. If centroids are unchanged, the clustering is done. Otherwise, go to step A and new centroids are computed. **165**
- Figure IV.1** *Mucha* painting **A** EDXRF points of analysis; **B** segmented image made by the system. **168**
- Figure IV.2.** Comparison between reflectance spectrum acquired on one pixel (red line) and the mean spectra obtained using an area of 9x9 pixels (black line). **169**
- Figure IV.3** **A** Reflectance spectrum acquired on yellow (Y1); orange (O1) and red (R1) area. Mapping of the pigments identified by the system: **B** chrome yellow; **C** mixture chrome yellow and vermilion and **D** vermilion. **170**
- Figure IV.4** **A** first derivative of the reflectance spectra from the painting Y1, R1, O1; **B** reflectance spectra acquired on the Amadeo's paint tubes Jaune de Chrome foncé – Lefranc (ASC17) and French Vermilion - Winsor & Newton (MG3). **171**



<b>Figure IV.5 A</b> Reflectance spectra from the painting; <b>B</b> Reflectance spectra acquired from the paint tube samples of Amadeo Cobalt Blue - Winsor & Newton (MG4) and Cerulean Blue – Winsor & Newton (ACS7); <b>C</b> mapping of the area B2.	<b>172</b>
<b>Figure IV.6 A</b> Reflectance spectra from the painting; <b>B</b> Reflectance spectrum acquired from the paint tube sample of Amadeo Vert Emerald – Lefranc (ASC20) <b>C</b> mapping of the area G1.	<b>173</b>
<b>Figure V.</b> Reflectance spectra from the samples used to as reference materials in the hyperspectral imaging analysis. *Spectra acquired by hyperspectral camera.	<b>176</b>

## APPENDICES PART II

<b>Figure I.1</b> Amadeo de Souza-Cardoso, <i>Canção popular a Russa e o Figaro</i> (P180), 1916, 60x80 cm, Centro de Arte Moderna, Fundação Calouste Gulbenkian	<b>179</b>
<b>Figure I.2</b> Amadeo de Souza-Cardoso, <i>Trou de la serrure PARTO DA VIOLA Bon ménage Fraise avant garde</i> (P182), 1916, 58x 80 cm, Centro de Arte Moderna, Fundação Calouste Gulbenkian.	<b>179</b>
<b>Figure I.3.</b> Amadeo de Souza-Cardoso, <i>Untitled (ZINC)</i> , (P195), c. 1917, 59 x 49 cm, Centro de Arte Moderna, Fundação Calouste Gulbenkian.	<b>180</b>
<b>Figure III.1.</b> The paintings of Amadeo de Souza-Cardoso from the collection of Center of Modern Art of Calouste Gulbenkian Foundation in Lisbon digitalized by hyperspectral imaging and used in this study. Images by courtesy of CAM [Freitas <i>et al.</i> 2008].	<b>185</b>
<b>Figure III.2</b> Lightness distribution of Amadeo paintings.	<b>186</b>
<b>Figure III.3</b> Average CIE(a*,b*) value and chronologic distribution of the paintings	<b>186</b>
<b>Figure III.4</b> Numbers of discernible colours.	<b>187</b>
<b>Figure III.5 A</b> Amadeo de Souza-Cardoso, <i>Untitled (O jockey)</i> , 1913, 61 x 50 cm. Collection of Centro de Arte Moderna, Fundação Calouste Gulbenkian (Inv. 77P5) [Freitas 2008, pg. 208] and <b>B</b> Colour distribution; <b>C</b> Amadeo de Souza-Cardoso, <i>Untitled</i> , 1917, 93,5 x 93,5 cm. Collection of Centro de Arte Moderna, Fundação Calouste Gulbenkian (Inv. 77P8) [Freitas 2008, pgs. 358] and <b>D</b> Colour distribution <i>Untitled</i> .	<b>188</b>
<b>Figure IV.1</b> Painting <i>Untitled (BRUT 300 TSF)</i> , area where it was performed EDXRF analysis (●).	<b>189</b>
<b>Figure IV.2</b> Painting <i>Untitled (BRUT 300 TSF)</i> samples for FTIR and Raman analysis (●).	<b>190</b>
<b>Figure IV.3</b> Painting <i>Untitled (Entrada)</i> , area where it was performed EDXRF analysis (●).	<b>191</b>
<b>Figure IV.4</b> Painting <i>Untitled (Entrada)</i> , samples for FTIR and Raman analysis (●)	<b>192</b>
<b>Figure IV.5</b> Painting <i>Untitled (Coty)</i> area where it was performed EDXRF analysis (●).	<b>193</b>
<b>Figure IV.6</b> Painting <i>Untitled (Coty)</i> , samples for FTIR and Raman analysis (●).	<b>194</b>
<b>Figure IV.7</b> Painting <i>Untitled</i> , area where it was performed EDXRF analysis (●).	<b>195</b>
<b>Figure IV.8</b> Painting <i>Untitled</i> , samples for FTIR and Raman analysis (●)	<b>196</b>
<b>Figure V.1</b> Representative $\mu$ -EDXRF spectra of preparation layer and white, black, violet, blue, green, yellow, ochre, brown, pink, red areas from <i>BRUT</i> painting.	<b>204</b>
<b>Figure V.2</b> Representative $\mu$ -EDXRF spectra of preparation layer and white, black, violet, blue, green, yellow, orange, brown, pink, red, glass, mirror, golden areas from <i>Entrada</i> painting.	<b>208</b>
<b>Figure V.3</b> Representative $\mu$ -EDXRF spectra of preparation layer and white, black, grey, violet, blue, green, yellow, orange, brown, pink, red, golden, areas and glass, pearl, metal hair clip from <i>Coty</i> painting.	<b>212</b>
<b>Figure V.4</b> Representative $\mu$ -EDXRF spectra of preparation layer and white, black, grey, violet, blue, green, yellow, orange, brown, red, pink, golden areas and matches from <i>Untitled</i> painting.	<b>216</b>

<b>Figure V.5</b> Representative infrared spectra of preparation layer and white, violet, blue, green, yellow, red areas from <i>BRUT</i> painting.	<b>219</b>
<b>Figure V.6</b> Representative infrared spectra of preparation layer and white, violet, blue, green, yellow areas from <i>Entrada</i> painting.	<b>221</b>
<b>Figure V.7</b> Representative infrared spectra of varnish, preparation layer and white, violet, blue, yellow, red areas from <i>Coty</i> painting.	<b>222</b>
<b>Figure V.8</b> Representative infrared spectra of varnish, preparation layer and white, black, violet, dark blue, green, light green, yellow, red areas and transparent sphere from <i>Untitled</i> painting.	<b>224</b>
<b>Figure V.9</b> Representative Raman spectra of red, yellow, green blue areas from <i>BRUT</i> painting.	<b>228</b>
<b>Figure V.10</b> Representative Raman spectra of yellow, brown, green areas from <i>Entrada</i> painting.	<b>229</b>
<b>Figure V.11</b> Representative Raman spectra of violet, blue, green, red, orange, brown areas from <i>Coty</i> painting.	<b>230</b>
<b>Figure V.12</b> Representative Raman spectra of green, yellow, white, areas and transparent sphere from <i>Untitled</i> painting.	<b>231</b>
<b>Figure V.13</b> Representative spectra of Emission and excitation spectra ( $\lambda_{exc} = 490$ nm; dichroic = 500 nm; $\lambda_{em} = 610$ nm; dichroic = 600 nm) acquired on pink, red and violet samples from <i>BRUT</i> painting.	<b>236</b>
<b>Figure V.14</b> Representative spectrum of Emission and excitation spectra ( $\lambda_{exc} = 490$ nm; dichroic = 500 nm; $\lambda_{em} = 610$ nm; dichroic = 600 nm) acquired on pink sample from <i>Entrada</i> painting.	<b>237</b>
<b>Figure V.15</b> Representative spectra of Emission and excitation spectra ( $\lambda_{exc} = 490$ nm; dichroic = 500 nm; $\lambda_{em} = 610$ nm; dichroic = 600 nm) acquired on pink and red samples from <i>Untitled</i> painting.	<b>237</b>
<b>Figure V.16</b> Representative Reflectance (hyperspectral imaging) spectra of violet, blue, green, yellow, red areas from <i>BRUT</i> painting.	<b>239</b>
<b>Figure V.17</b> Representative Reflectance (hyperspectral imaging) spectra of violet, blue, green, yellow, orange, red areas from <i>Entrada</i> painting.	<b>240</b>
<b>Figure V.18</b> Representative Reflectance (hyperspectral imaging) spectra of violet, blue, green, yellow, red areas from <i>Coty</i> painting.	<b>241</b>
<b>Figure V.19</b> Representative Reflectance (hyperspectral imaging) spectra of violet, blue, green, yellow, red, pink, areas from <i>Untitled</i> painting.	<b>242</b>
<b>Figure VI.1</b> <i>BRUT</i> , areas of sampling of cross-section (●) and micro-samples (●)	<b>243</b>
<b>Figure VI.2</b> <i>Entrada</i> , areas of sampling of cross-section (●) and micro-samples (●)	<b>243</b>
<b>Figure VI.3</b> <i>Coty</i> , areas of sampling of cross-section (●) and micro-samples (●)	<b>244</b>
<b>Figure VI.4</b> <i>Untitled</i> , areas of sampling of cross-section (●) and micro-samples (●)	<b>244</b>
<b>Figure VII.1.</b> Infrared spectra sample $\mu 8$ <i>Entrada</i> ; Columbano Tube T17_3128 and 735.5 reconstruction ●PbCrO <sub>4</sub> ; ♦ CaCO <sub>3</sub> ; ♦ kaolinite.	<b>260</b>
<b>Figure VII.2</b> Infrared spectra sample $\mu 32$ <i>Entrada</i> ; Columbano Tube T17_3128 and 735.5 reconstruction. ● PbCrO <sub>4</sub> ; ♦ CaCO <sub>3</sub> ; ♦ kaolinite	<b>260</b>
<b>Figure VII.3.</b> Infrared spectra sample $\mu 19$ <i>Entrada</i> ; Columbano Tube T17_3128 and 735.5 reconstruction. ● PbCrO <sub>4</sub> ; ♦ Gypsum; *CaCO <sub>3</sub> ; ● SrSO <sub>4</sub>	<b>261</b>
<b>Figure VII.4.</b> Infrared spectra sample $\mu 37$ <i>Entrada</i> ; Columbano Tube T17_3128 and magnesium sulfate heptahydrate. ● PbCrO <sub>4</sub> ; ♦ CaCO <sub>3</sub> ; ♦ MgSO <sub>4</sub> 7H <sub>2</sub> O	<b>261</b>
<b>Figure VII.5.</b> Infrared spectra sample $\mu 17$ <i>Entrada</i> ; Columbano tube T24_3128 and CR.C7 0.4 Molar fraction chromate and 0.6 sulphate. ● Pb(Cr,S)O <sub>4</sub> .	<b>262</b>

<b>Figure VII.6.</b> Infrared spectra sample $\mu 3$ BRUT; CR.C.8 with 0.3 Molar fraction chromate and 0.7 sulphate • Pb(Cr,S)O <sub>4</sub> ; ♦ BaSO <sub>4</sub> ; ● MgCO <sub>3</sub> .	<b>262</b>
<b>Figure VII.7.</b> Infrared spectra sample $\mu 4$ BRUT; ● BaSO <sub>4</sub> ; ♦ gypsum; * quartz.	<b>263</b>
<b>Figure VII.8.</b> Infrared spectra sample $\mu 16$ BRUT, CR.C7 0.4 Molar fraction chromate and 0.6 sulphate. ● MgCO <sub>3</sub>	<b>263</b>
<b>Figure VII.9.</b> Visible light microscope with the mapping area marked in red; RGB composite images obtained by $\mu$ -IR: <b>B</b> mixed lead chromate (975-966 cm <sup>-1</sup> ); <b>C</b> Quartz (1170-1157 cm <sup>-1</sup> ); <b>D</b> MgCO <sub>3</sub> (1500-1398 cm <sup>-1</sup> ); <b>E</b> broad band centred at 1580 cm <sup>-1</sup> ; <b>F</b> Carboxylate (1525-1560 cm <sup>-1</sup> ).	<b>265</b>
<b>Figure VII.10.</b> XRF Chromium map intensity; RGB composite images obtained by $\mu$ -XRF at a primary beam energy of 6.12 keV <b>B</b> Ba in green, Cr in red; <b>C</b> Mg in blue; <b>D</b> Si in green.	<b>265</b>
<b>Figure VII.11.</b> Infrared spectra sample am17 BRUT acquired with SR- $\mu$ IR in BaF <sub>2</sub> cell (top) and sample am15 BRUT acquired with $\mu$ -FTIR in diamond cell (down); ● MgCO <sub>3</sub> ; ♦ Quartz.	<b>266</b>
<b>Figure VII.12.</b> XRF chromium map intensity with the XANES points of analysis; <b>B</b> average XANES spectrum.	<b>266</b>
<b>Figure VII.13.</b> RGB composite images obtained by $\mu$ -XRF at a primary beam energy of 6.12 keV with K in green, Ba in red and Cr in blue; <b>B</b> XRF Chromium map intensity in black the area used to create the calculate the intensity profile reported in C; <b>C</b> intensity profile of Cr K line on the XRF maps at beam energy of 6.12 keV (black) and 6.02 keV (red); <b>D</b> XANES points of analysis; <b>E</b> average XANES spectrum.	<b>267</b>
<b>Figure IX.1</b> Front of the Ripolin's colour chart: <i>Glacis Ripolin a Finir Spécial Pour Voitures</i> , dated 1925.	<b>272</b>
<b>Figure IX.2</b> Inside of the Ripolin's colour chart: <i>Glacis Ripolin a Finir Spécial Pour Voitures</i> , dated 1925. In the red squared is identified the swatch Blanc 1401.	<b>272</b>
<b>APPENDICES PART III</b>	
<b>Figure I.1.</b> Painting (A) <i>Collage</i> , assigned Amadeo de Souza-Cardoso.	<b>275</b>
<b>Figure I.2 A</b> Image of Painting (A) <i>Collage</i> with normal light; <b>B</b> mapping of the areas painted with pigments not included in the Amadeo's palette: (●) copper phthalocyanine and dioxazine violet; (●) $\beta$ -naphthol; (●) dioxazine violet and $\beta$ -naphthol; (●) Hansa yellow and red $\beta$ -naphthol; (●) dioxazine violet and copper phthalocyanine; (●) red $\beta$ -naphthol and yellow ochre. The green line indicates the papers glued.	<b>275</b>
<b>Figure II.1</b> Painting (A) <i>Collage</i> , points where it was performed EDXRF analysis (○).	<b>276</b>
<b>Figure II.2</b> Painting (A) <i>Collage</i> , samples for FTIR (●) and Raman analysis (○).	<b>276</b>
<b>Figure II.3</b> Painting (B) <i>Geometric</i> , points where it was performed EDXRF analysis (●).	<b>277</b>
<b>Figure II.4</b> Painting (B) <i>Geometric</i> , samples for FTIR (●) and Raman analysis (●)	<b>277</b>
<b>Figure II.5</b> Painting (C) <i>Embroiderers</i> , points where it was performed EDXRF and FORS analysis (○); Raman <i>in-situ</i> (●); points of sampling for FTIR and Raman (●); samples for cross-sections (●).	<b>278</b>
<b>Figure II.6</b> Painting (C) <i>Embroiderers</i> , points where it was performed EDXRF analysis (○); points of sampling for FTIR and Raman (●); samples for cross-sections (●).	<b>279</b>
<b>Figure III.1</b> Representative $\mu$ -EDXRF spectra of the paper support; blue; green; red; yellow; violet; brown; white; black areas and the signature from Painting (A) <i>Collage</i> .	<b>284</b>
<b>Figure III.2</b> Representative $\mu$ -EDXRF spectra of white; blue; green; red; pink; yellow; brown areas from Painting (B) <i>Geometric</i> .	<b>285</b>
<b>Figure III.3</b> Representative $\mu$ -EDXRF spectra of the support; blue; green; red; yellow; pink; brown; white areas; signature and preparation layer from Painting (C) <i>Embroiderers</i> .	<b>287</b>
<b>Figure III.4</b> Representative $\mu$ -EDXRF spectra of the support; blue; green; red; yellow; violet; brown; white; black areas and preparation layer from Painting (D) <i>Café</i> .	<b>289</b>

<b>Figure III.5</b> Representative $\mu$ -FTIR spectra of the red and yellow areas from Painting (A) <i>Collage</i> and the reference pigments $\beta$ -naphthol PR4 (Clariant) and Hansa yellow PY1 (Clariant).	<b>290</b>
<b>Figure III.6</b> Representative $\mu$ -FTIR spectra of the white and brown areas from Painting (B) <i>Geometric</i> .	<b>291</b>
<b>Figure III.7</b> Representative $\mu$ -FTIR spectra of the grey, red, green and blue areas from Painting (C) <i>Embroiderers</i> .	<b>292</b>
<b>Figure III.8</b> Representative $\mu$ -FTIR spectra of the varnish and the green; white; yellow; blue and violet areas from Painting (D) <i>Café</i> .	<b>293</b>
<b>Figure III.9</b> Representative $\mu$ -Raman spectra of the blue; red; yellow painted areas and blue area on paper B from Painting (A) <i>Collage</i> and the reference pigments Copper phthalocyanine blue PB15 (Aldrich); dioxazine violet PV23 (Clariant); $\beta$ -naphthol PR4 (Clariant), Hansa yellow PY1 (Clariant) and indigo (Thermo Database).	<b>297</b>
<b>Figure III.10</b> Representative $\mu$ -Raman spectra of the yellow; brow and red from Painting (B) <i>Geometric</i> .	<b>298</b>
<b>Figure III.11</b> Representative $\mu$ -Raman spectra of the preparation layer and white area from Painting (C) <i>Embroiderers</i> .	<b>289</b>
<b>Figure III.12</b> Representative $\mu$ -Raman spectra of the white; blue; green and yellow areas from Painting (D) <i>Café</i> .	<b>299</b>
<b>Figure III.13</b> Representative FORS spectra of the support; blue; green; red; pink; yellow; brown areas from Painting (C) <i>Embroiderers</i> .	<b>304</b>
<b>Figure IV.1.</b> Infrared photography Painting (A) <i>Collage</i> , attributed Amadeo de Souza-Cardoso.	<b>305</b>
<b>Figure V.2.</b> Infrared photography Painting (C) <i>Embroiderers</i> , attributed Amadeo de Souza-Cardoso.	<b>306</b>
<b>Figure V.3.</b> Ultraviolet photograph (covered in black and white) Painting (D) <i>Café</i> , attributed Amadeo de Souza-Cardoso.	<b>307</b>
<b>Figure V.4.</b> X-ray image Painting (D) <i>Café</i> , attributed Amadeo de Souza-Cardoso.	<b>307</b>
<b>Figure VI.1</b> Amadeo de Souza-Cardoso, Untitled, 1910, graphite on paper. 36 x 24.7 cm. Collection of Centro de Arte Moderna, Fundação Calouste Gulbenkian (Inv. 92DP1586).	<b>308</b>
<b>Figure VI.2</b> Amadeo de Souza-Cardoso, Untitled, 1910, graphite on paper. 25 x 35 cm. Collection of Centro de Arte Moderna, Fundação Calouste Gulbenkian (Inv. 86DP372).	<b>309</b>

## LIST OF TABLES

### PART I

<b>Table 1.</b> Strategies adopted in the features extraction block.	<b>25</b>
<b>Table 2.</b> Number of keypoints detected with SIFT and with Gabor (3) on SIFT keypoint analysing an area of 64x64 and 128x128 pixels	<b>28</b>
<b>Table 3.</b> Number of <i>positive</i> images in the training and test sets.	<b>32</b>
<b>Table 4.</b> Evaluation of the performance of the classifier using: SIFT; Gabor (1) in a global approach; Gabor (2) in regular points and Gabor (3) in the localization of SIFT keypoints. Hits refers the percentage of Amadeo's paintings correctly classified.	<b>33</b>
<b>Table 5.</b> Evaluation of the role of the number of clutters in the construction of the vocabulary in bag-of-features strategy. The value indicated is the sum of the positive and negative word with the same proportion 50:50.	<b>34</b>
<b>Table 6.</b> Set of oil paint tube used to create the database of reference materials.	<b>38</b>
<b>Table 7.</b> Example of the Excel file used to introduce the chemical elements and the corresponding L*a*b* values.	<b>39</b>
<b>Table 8.</b> Percentage of areas detected by pigment analysis on <i>Mucha</i> and <i>DCR</i> paintings.	<b>47</b>
<b>Table 9.</b> Indicator of authenticity that the paintings were made by Amadeo, considering brushstroke and materials analysis separately, and joined together by the fusion data. The value range is 0-1 where 0 is Not Amadeo and 1 Amadeo.	<b>53</b>

### PART II

<b>Table 1.</b> Percentage area of paintings busy with unusual materials and glass and mirrors.	<b>89</b>
<b>Table 2A.</b> Colour construction in the <i>BRUT</i> and <i>Entrada</i> paintings.	<b>93</b>
<b>Table 2B.</b> Colour construction in the <i>Coty</i> and <i>Untitled</i> paintings.	<b>93</b>
<b>Table 3.</b> Characteristic infrared and Raman bands assigned to cobalt yellow ( $K_3[Co(NO_2)_6]$ ,) pigment [Cornman 1986; Hitchman and Rowbottom 1982; Miller and Wilkins 1952; Vendilo et al. 2011].	<b>96</b>
<b>Table 4.</b> Characterization of micro-samples of chrome yellows.	<b>101</b>

### PART III

<b>Table 1.</b> Palette of pigments detected in the Painting <i>Geometric</i> .	<b>130</b>
<b>Table 2.</b> Percentage of Not-analysed and Not-Amadeo area in <i>BRUT</i> , <i>Entrada</i> , <i>Coty</i> and <i>Untitled</i> paintings.	<b>137</b>
<b>Table 3.</b> Colorimetric analysis on the <i>BRUT</i> blue areas.	<b>140</b>

### APPENDICES PART I

<b>Table IV.1.</b> Elements detected for each area and the attribution performed by the system combining hyperspectral imaging and EDRF.	<b>168</b>
<b>Table IV.2</b> Colorimetric values acquired on the yellow, orange and red areas of the painting <i>Mucha</i> and on the paint tube samples.	<b>171</b>
<b>Table. IV.3</b> Colorimetric values acquired on three blue areas of the painting <i>Mucha</i> and on the paint tube samples.	<b>172</b>

<b>Table IV.4</b> Colorimetric values acquired on two green areas of the painting <i>Mucha</i> and on the paint tube sample.	<b>173</b>
--	------------

## APPENDICES PART II

<b>Table V.1</b> Colour areas analysed on <i>BRUT</i> by $\mu$ -EDXRF; $\mu$ -FTIR; $\mu$ -Raman; $\mu$ -SPEX; Reflectance spectroscopy (hyperspectral imaging) and SEM-EDS.	<b>197</b>
<b>Table V.2</b> Colour areas analysed on <i>Entrada</i> by $\mu$ -EDXRF; $\mu$ -FTIR; $\mu$ -Raman; $\mu$ -SPEX; Reflectance spectroscopy (hyperspectral imaging) and SEM-EDS.	<b>198</b>
<b>Table V.3</b> Colour areas analysed on <i>Coty</i> by $\mu$ -EDXRF; $\mu$ -FTIR; $\mu$ -Raman; $\mu$ -SPEX; Reflectance spectroscopy (hyperspectral imaging) and SEM-EDS.	<b>199</b>
<b>Table V.4</b> Colour areas analysed on <i>Untitled</i> by $\mu$ -EDXRF; $\mu$ -FTIR; $\mu$ -Raman; $\mu$ -SPEX; Reflectance spectroscopy (hyperspectral imaging) and SEM-EDS.	<b>199</b>
<b>Table V.5.</b> Characteristic energies of the X-rays (KeV) used to identify the elements in the EDXRF analysis.	<b>217</b>
<b>Table V.6.</b> Characteristic bands of FTIR spectra of the pigments identified.	<b>225</b>
<b>Table V.7.</b> Raman band assignments cobalt violet pigment.	<b>232</b>
<b>Table VII.1</b> Roi region in $\text{cm}^{-1}$ used for IR mapping.	<b>268</b>
<b>Table VII.2</b> X-ray adsorption edges and X-ray line energies (KeV) used for XRF mapping.	<b>268</b>
<b>Table VIII.1</b> Oil pain tubes analysed in Melo et al. 2009, relative code and label's transcription	<b>269</b>

## APPENDICES PART III

<b>Table III.1</b> Colour areas analysed on Painting (A) <i>Collage</i> by $\mu$ -EDXRF; $\mu$ -Raman and $\mu$ -FTIR.	<b>280</b>
<b>Table III.2</b> Colour areas of the paper analysed on Painting (A) <i>Collage</i> by $\mu$ -EDXRF and $\mu$ -Raman.	<b>280</b>
<b>Table III.3</b> Colour areas analysed on Painting (B) <i>Geometric</i> by $\mu$ -EDXRF; $\mu$ -Raman and $\mu$ -FTIR.	<b>281</b>
<b>Table III.4</b> Colour areas analysed on Painting (C) <i>Embroiderers</i> by $\mu$ -EDXRF; FORS; $\mu$ -Raman and $\mu$ -FTIR.	<b>281</b>
<b>Table III.5</b> Colour areas analysed on Painting (D) <i>Café</i> by $\mu$ -EDXRF; $\mu$ -Raman and $\mu$ -FTIR.	<b>282</b>
<b>Table III.6.</b> Characteristic energies of the X-rays (KeV) used to identify the elements in the EDXRF analysis.	<b>289</b>
<b>Table III.7.</b> Characteristic bands of FTIR spectra of the pigments identified.	<b>294</b>
<b>Table III.8.</b> Characteristic bands of Raman spectra of the pigments identified.	<b>300</b>

## CONTEXT OF THE WORK

This thesis is inserted in the multidisciplinary project “*Crossing Borders: History, Materials, and Techniques of Portuguese Painters from 1850 to 1918 (Romanticism, Naturalism and Modernism)*” which has been supported by the Portuguese Foundation for Science and Technology (FCT). The objective of the project was to analyse three important periods of the history of Portuguese art from the perspective of the materials and the painting techniques. A particular effort was done to relate art history with the analysis of the painting materials. As its name suggests, the project aimed at crossing the borders between areas such as conservation science, art history, and computer science. In fact, the work presented in this thesis was developed at the NOVA University of Lisbon through a collaboration between the Department of Conservation and Restoration and Professor Nuno Correia’s group at the Center for Informatics and Information Technologies (CITI). The *Crossing Borders* project involved also important museums in Lisbon, namely Casa Museu Anastácio Gonçalves, the Center for Modern Art of Calouste Gulbenkian Foundation, and Museu Nacional de Arte Contemporânea - Museu do Chiado. Furthermore, the section of the Portuguese police in charge of art crimes was a project participant. The analysis of selected artworks was followed by investigations on bibliographical and archival sources; the objective of such investigations was to shed light on how art was taught in Portugal and on the materials used by the artists and the providers of such materials. A number of projects were carried out in parallel to the study of the paintings; these activities were aimed at the analysis of conservation problems and at the development of new analytical methodologies.

Amadeo de Souza-Cardoso (1887-1918), the artist studied in this thesis, could be considered as an “unconventional representative” of Portuguese modernism. His education and career took place mainly in Paris, a city whose artistic offering he exploited fully; this is clearly recognizable in the influence that international artists had in his artworks [Freitas *at al.* 2006]. Unfortunately, the critics’ attention on Amadeo arrived rather late, through the studies of art historian José Augusto França [França 1956]. This late discovery, together with the absence of a Catalogue Raisonné (which was published only in 2008), could be considered among the reasons why the art market (in Portugal and elsewhere) is full of forgeries of Amadeo’s artworks. The edition of the Catalogue Raisonné motivated the first systematic study of the materials and techniques used by Amadeo in artworks dated between 1912 and 1917 [Melo *et al.* 2008]. Art historical analyses as well as scientific examination of the paintings provided the basis for and against being including in the catalogue a set of ambiguous paintings.

Attribution and authenticity are challenging issues in art conservation. The lucrative business of forging art is the fourth largest world criminal enterprise [Kaplan 2010]. The section of the Portuguese police in charge of art crimes highlights how the current economic crisis opens new opportunities for illicit activities. As referred by João Oliveira, coordinator of criminal investigation of Judicial Police, Portugal is already situated in the major international routes of painting falsification. In general, addressing authentication issues calls for a multidisciplinary approach.

This recent multidisciplinary approach to authentication is to be contrasted with a more traditional view, mostly related to historical and aesthetic aspects—this view is referred to as a whole as *connoisseurship*: the expert knowledge of style and techniques that art historians develop through the course of a career [Barrett 1995]. Even today the formal analysis of the artworks and connoisseurship play a significant role in the authentication process. The detailed and systematic observation of a set of artworks of a given artist allows the identification of markers that could be used to assess the artworks' authorship [Dantzig Foundation 1973; Morelli 1893].

The artist's *brushstroke* is a natural feature for observation in a painting. This may be well considered as the artist's signature marks, for it captures the personal movements performed during the act of painting. Similar to handwriting, the brushstroke of an artist may change during his/her life; however, the defining characteristics of the personality of the artist remain uniform and visible [Morelli 1893]. Recent progresses in the realm of machine learning have allowed the simulation of the formal analyses of artworks through computer vision techniques. In particular, given an image of the artwork, the application of algorithms of image segmentation and feature extraction allows the detection of texture information which can be used to classify the image. In fact, this process enables computation of the probability that a given artist produced the painting. A notable work in this direction, focused on van Gogh's paintings, was carried out by Professor Rick Johnson Jr of Cornell University and Professor Eric Postma (1961) at Tilburg University [Johnson *et al.* 2008].

Nevertheless, Dantzig himself [Dantzig Foundation 1973] demonstrated that the visual aspect of an artwork cannot be considered independently from its constituent materials. Dantzig's studies on van Gogh's paintings showed that brushstrokes are related to the materials' properties and handling, but also that the choice of the support and of the kind of preparation have an influence on the final appearance of the surface. Recently, these aspects have been studied in the context of the HART project (Historically Accurate Paint Reconstruction Techniques), which was supported by the NWO (Netherlands Organization for Scientific Research) [Carlyle and Witlox 2005].

Based on the above observations, and the work done in collaboration with art historian Helena de Freitas (curator of the most important exhibition of Amadeo and co-author of his Catalogue Raisonné), raised the need for carrying out a study which integrates visual and molecular information in Amadeo's artwork, i.e., information derived from the study of the constituent materials of the artwork. The goal of this study is to use the information on Amadeo's materials and techniques to create a tool based on image processing to support authentication processes. It is important to note that the authentication of an artwork can also base on the use of the detailed knowledge of the artist's materials and techniques, and the developmental evolution throughout the artist's career [Barrett 1995]. To follow the evolution of Amadeo's career we studied his last paintings. These artworks were made in Portugal in 1917 and are considered as a homogenous core, different from all his previous works.



In this context, this dissertation has two main objectives: (i) the development of a tool, based on image processing, supporting the authentication of Amadeo's artworks, and (ii) the analysis of his artworks produced in Portugal in 1917. Given that this work involves separate areas, the thesis is presented in three separate yet interrelated parts.

- PART I focuses on the work developed on image processing. Chapter 1 includes the presentation of some aspect of the authentication process and the recent contribution of computer vision techniques in the conservation field. Chapter 2 presents the tool developed for the study for the paintings of Amadeo: the method combines brushstroke analysis performed by two algorithms of image processing (Gabor filter and Scale Invariant Feature Transform) and the molecular analysis using hyperspectral imaging and elemental analysis ( $\mu$ -EDXRF).
- PART II introduces Amadeo de Souza-Cardoso and his works (Chapter 1). The analysis of the paintings of Amadeo produced in Portugal in 1917 and the main important conservation problems are given in Chapter 2. According to art historians, the paintings studied in this part constitute a homogeneous core [França 1992] and are among his best work [Silva 1995; Freitas 2008b]. The materials and techniques of these paintings (namely, *Untitled (Brut 300 TSF)*, *Untitled (Entrada)*, *Untitled (Coty)* and *Untitled*) are studied for the first time in this thesis. The results obtained thus enrich the study performed previously in 2008 [Melo *et al.* 2008]. The experimental style that Amadeo adopts in these artworks (in particular, the use of new materials) constitutes new challenges for their conservation.
- In PART III the contributions and results of Parts I and II are jointly exploited in the analysis of 2 set of paintings. The aim of this part is to assess the potentialities and the limitations of the proposed systems; the results obtained by the application of the tools developed in Part I are compared with those obtained by the multi-analytical approach described and used in Part II:
  - (1) Four paintings attributed to Amadeo de Souza-Cardoso but not included in his Catalogue Raisonné were studied in order to assess their authenticity. The paintings are called *Collage*, *Geometric*, *Embroiderers* and *Café*. The results obtained by the materials and techniques characterization were compared with the classification obtained by the brushstroke analysis performed using image processing.
  - (2) The system based on the combination of hyperspectral imaging and elemental analysis was applied on the paintings of Amadeo dated 1917, *BRUT*, *Entrada*, *Coty*, and *Untitled* studied in Part II. The aim of this analysis is evaluate the capacity of the system developed in the characterization of the pigments present in the paintings.



**PART I: DIGITAL IMAGE PROCESSING  
FOR OIL PAINTING ANALYSIS**



## INTRODUCTION TO PART I

In 2007, the Calouste Gulbenkian Foundation published the first volume of the Catalogue Raisonné of Amadeo de Souza Cardoso - the photo biography [Freitas *et al.* 2007]. One year after, the second volume was published: the **Catalogue Raisonné of Amadeo's paintings** [Freitas *et al.* 2008]. The second volume includes 201 paintings of Amadeo. The research made by Helena de Freitas and her team to prepare the edition of the Catalogue Raisonné of paintings took 8 years. In these years a large set of material<sup>1</sup> was collected and organized [Alfaro 2008]. A significant part of the investigation studies the relation of Amadeo with his contemporary artistic context; this research resulted in the exhibition *Amadeo de Souza-Cardoso Diálogo de Vanguardas-Avant-Garde Dialogues*, at the Gulbenkian Foundation between November 2006 and January 2007. The exhibition was attended by over 700.000 visitors in four mounts. The exhibition and the associated catalogue [Freitas *et al.* 2006] present a sort of dialogue between a selection of Amadeo's paintings and artworks from other artists that influenced the Portuguese painter. Such artists include Gino Severini, August Macke, Amadeo Modigliani, Liubov Popova, Kazimir Malevitch, Albert Gleizes, Lyonel Feininger, Jean Metzinger, Otto Freundlich, Pablo Picasso, Ivan Puni, and Olga Rozanova. Moreover, the Catalogue documents how Amadeo became familiar with these artists, their friendship or exhibitions in which Amadeo had the opportunity to see their paintings. During the edition of the Catalogue Raisonné of paintings Helena de Freitas and her team asked the DCR-FCT to analyse 5 ambiguous paintings attributed to Amadeo. Before analysing these paintings, a systematic study of the **materials and techniques of Amadeo** was developed; this study covered artistic materials that belonged to Amadeo as well as a selection of 19 paintings representative of the Amadeo's production between 1912 and 1917. Such materials include a palette and a box of paint tubes (from the CAM collection) and 31 oil paint tubes from two paint boxes conserved in the Family house of Amadeo in Manhufe<sup>2</sup>. The paint tubes were from the French Lefranc and Bourgeois and the English Winsor & Newton (W&N) [Melo *et al.* 2009]. The analysis of the oil paint tubes and of the paintings made it possible to reconstruct the palette of pigments used by Amadeo between 1912 and 1916 [Melo *et al.* 2008]. During the analysis of the paintings it appeared clear that the visual investigation of the painting surface carried out by the team of art historians and curators and the analysis of the materials were often in agreement, complementing each other.

Based on the experience of the Catalogue Raisonné it was decided to address the challenging topic of the **Amadeo's painting authentication**. Specifically, it was decided to create a model based on the *modus operandi* used in laboratory for the evaluation of the authenticity of a painting attribute to Amadeo. The aim of the model was to combine two information: (i) brushstroke information (visual

---

<sup>1</sup> The research was based on the analysis of documentary sources: catalogs of exhibitions, album "12 Reproductions" (published by Amadeo in 1916, Porto), Amadeo's agendas, published articles, photographs of the time and personal correspondence of Amadeo [Alfaro 2006].

<sup>2</sup> In the Family house of Amadeo are conserved 6 boxes, 3 of which contain materials that would be used by Amadeo: a box assigned "Amadeo Cardoso" with 60 crayons. A box assigned "Amadeo" with 21 oil paint tubes and a box with the name "Maria da Graça 34" with 18 oil paint tubes. The oil tube paints were studied in [Melo *et al.* 2009].

analysis), were extracted from RGB images; (ii) molecular information (pigments' characterization) were extracted by the analysis of hyperspectral images and by elemental analysis (performed by  $\mu$ -EDXRF). The combination of these two information (fusion analysis) provides a qualitative and quantitative evaluation of the authenticity of the paintings attributed to Amadeo. For different reasons Amadeo de Souza-Cardoso resulted the perfect subject for developing the authentication tool: (i) previous art historian studies highlighted the unique features belonging to Amadeo's works (brushstroke and colour) used in the developed system. (ii) The Catalogue Raisonné offered a base of information on which the system was built on. (iii) Amadeo used a restricted and consistent palette of pigments that was used as reference database for the mapping the pigments in the hyperspectral images.

The use of image processing for **brushstroke analysis** was successfully applied in van Gogh's paintings [Johnson *et al.* 2008; Li *et al.* 2012]. The methodologies used on the analysis of van Gogh's brushstrokes were the starting point in the definition of Amadeo's system. At the same time, complementing the brushstroke analysis with information on the materials (molecular analysis) made the system more robust and helped to overcome problems when distinguishing similar or ambiguous brushstroke. In this thesis was used one of the algorithms applied with positive results on the study of van Gogh's paintings, namely the Gabor filter [Johnson *et al.* 2008]. In Amadeo's system, Gabor was combined with an algorithm for feature detection, called Scale Invariant Features Transform (SIFT). This algorithm was chosen because it is able to detect features present in different images also when they are in different scale and position. The system developed for brushstroke analysis is based on a binary classification. This means that the features extracted from images of Amadeo's paintings (called *positive* class) were compared with the features extracted from image of not Amadeo's paintings (called *negative* class). For the *positive* class 200 images of paintings of Amadeo present in his Catalogue Raisonné were used. As for the *negative* class paintings of artists as close as possible to Amadeo were chosen: these include 109 images from the paintings present in the Catalogue *Diálogo de Vanguardas-Avant-Garde Dialogues* described above [Freitas *et al.* 2006] and from paintings of artists that belonged to Amadeo's circle, such as Sonia and Robert Delaunay, Eduardo Viana, Mario Eloy and José Almada Negreiros from the CAM collection. The images in these two classes are divided in two sets called training and test. The training set is used to create the model, while the test set is used to evaluate the performance of the classifier. To provide a statistically significant evaluation of the classifier's performance, the test set should be as large as possible. The selection of the images for the training and test sets is therefore a crucial step. On the one hand, the *positive* images in the training set should be as representative as possible of the different brushstrokes of the artist. On the other hand, to enhance the performance of the classifier, the images of paintings by not Amadeo should have a brushstroke similar to that present in Amadeo's paintings. The selection of the images in both sets was carried out in collaboration with Helena de Freitas.

The **molecular analysis** was performed by hyperspectral imaging technique combined with and elemental analysis ( $\mu$ -EDXRF). To perform this analysis, a database of 16 reference materials was created. The selection of the materials in the database was based on the analysis of the 19 paintings

and of the paint materials made at the time of the Catalogue Raisonné of Amadeo's paintings [Melo *et al.* 2008] described above. The hyperspectral imaging technique was selected because it provides molecular information but also colour information that together with brushstroke is considered a relevant feature in Amadeo's paintings. By analysing the hyperspectral images, the system produces a mapping of the pigments but also identifies the areas that could have been painted with materials different from those in the database. These areas are quantified and used as information in authentication studies. Moreover, the detection of these areas helps to better focus the use of methods that require sampling. The system shows a limitation in the characterization of the pigments in areas affected by colour changing; such as in the case of the analysis of the paintings by Amadeo *BRUT* dated 1917.

The combination of brushstroke and molecular analysis provides a quantitative **indicator for authenticity** with a value between 0 (considered not Amadeo) and 1 (considered Amadeo). The model developed for brushstroke analysis was created specifically for Amadeo's paintings. Due to this specificity, the performance evaluation of the classifier cannot be calculated using standard existing databases, as done in other works in computer vision. For this reason, this evaluation was done using test sets and case studies. The best results obtained have an accuracy of 93% in the classification of 198 images from Amadeo and not Amadeo paintings. The classifier gave a correct answer for 133 of the 138 images of Amadeo's paintings tested. Moreover, the brushstroke analysis was used as an additional analysis on the evaluation of 4 paintings (called *Collage*, *Geometric*, *Embroiderers* and *Café*) attributed to Amadeo but not included in the Catalogues Raisonné. The brushstroke analysis provided results coherent with those achieved by the analysis of the materials and techniques. In one case (*Café*) it was observed that the presence of a varnish layer can reduce the detection of the brushstroke by the image process and can compromise the performance of the classifier. The brushstroke and the molecular models were also tested in a set of 12 paintings, 11 of which by Amadeo and a deliberate falsification of an Amadeo's painting. The same 12 paintings were used to evaluate the behaviour of the system combining the two information (brushstroke and molecular) by *SUM-Combination* technique. The combination technique chosen is simple: the two analyses are weighted and summed. To the two analysis has been given the same weight because are considered equally relevant to the authentication study. In the case of the molecular and fusion analysis the 12 paintings were correctly classified. In the case of the brushstroke analysis the classifier gave a correct answer for 10 of the 11 images of Amadeo's paintings tested.





## CHAPTER 1: AUTHENTICATION AND COMPUTER VISION

This chapter introduces some concepts that are central to the research developed in this thesis. This introduction does not aim at giving a detailed overview of the history of connoisseurship and falsification; rather, it intends to offer essential information on how the different disciplines involved in this thesis address the problem of painting authenticity. In the first part of the chapter, the formal analysis and the notion of connoisseurship are presented using the approach proposed by Giovanni Morelli (1816-1891) and Maurits M. van Dantzig (1903-1960). Their studies on the use of visual features to prove authenticity are at the heart of recent applications on painting classification developed by computer vision. The second part of the chapter introduces the challenges posed by the conservation community to computer science. The state of the art in the use of digital image processing for brushstroke analysis and the use of hyperspectral imaging for painting analysis complete this section. Finally, the last section presents the contribution given by this work to the authentication process of paintings attributed to Amadeo.

### 1.1 Authenticity issues

*“Yesterday, this painting was worth millions of guilders and experts and art lovers would come from all over the world and pay money to see it. Today, it is worth nothing and nobody would cross the street to see it for free. But the picture has not changed. What has?”* - Hans van Meegeren, 1947- [Todd 2008].

Hans van Meegeren (1889-1947) was one of the well-known forgers of all time. He became famous for producing, among others, a dozen fake Vermeers which were sold to museums and private collectors [Coremans 1948]. His most famous painting is *Christ and the Disciples at Emmaus*, discovered by Professor Abraham Bredius at the Boymans Museum in Rotterdam in 1937. The size and the religious theme made the painting an “unusual Vermeer”; still, Bredius defined it as *quite different from all his other paintings and yet every inch a Vermeer* [Dutton 2009, pg.177]. Within a few days after the end of the Second World War, van Meegeren was arrested, since he sold one of his Vermeer paintings to the German politician and military leader Reichsmarschall Hermann Göring he was accused of treason. In prison van Meegeren confessed to the falsification of the Vermeer paintings. From that moment all his paintings present in museum collections, including the *The Disciples*, were relegated to basement storage. So, what had changed in the *magnificent* painting and in the *splendid luminous effect* so appreciated by Bredius after the van Meegeren’s confession? It is generally assumed that artistic forgery is related to the absence of aesthetic values but the story of the van Meegeren paintings demonstrated that forgery is not only a matter of aesthetic; in other words, *pure aesthetics cannot explain forgery* [Lessing 1983]. The term authenticity is still one of the most elusive and debated qualities to be associated with cultural work [Matero 2007]. Moreover, the concept of authenticity is never absolute, *it varies from place to place, over time, and with context* [Lowenthal 1994]. One of the aspects of attribution in determining authenticity is related to the identification of the origins, authorship, or provenance of the object, which Dutton calls *nominal authenticity*. However, when we evaluate an artwork we deal with an

*object's character as a true expression of an individual's or a society's values and beliefs*<sup>3</sup> [Dutton 2003, pg. 259] for that reason we can consider a work of art a forgery if it does not allow you to answer a series of questions related to its creation by the artist, to the cultural context and to the audience experience; all of this information is usually considered in the frame work of the artist's intentions [Dutton 2003].

In spite of the elusiveness of the term, in contemporary conservation practice authenticity<sup>4</sup> is a requirement to be deemed the Outstanding Universal Value of UNESCO. The conditions of authenticity are discussed in the Nara document (1994). The term authenticity was introduced, for the first time in the international heritage community, by the Venice Charter<sup>5</sup> in 1964: *It is our duty to hand them [historic monuments] on in the full richness of their authenticity* [Hassard 2006, pg.147]. In the Venice Charter, the term authenticity is used without any definition or contextualization; some decades will be necessary to fully understand the complexity of this concept [Hassard 2006, pg.147]. In 1994 the Nara Document defined authenticity as the *essential qualifying factor concerning values*. This document was drafted at the Conference on Authenticity<sup>6</sup> with the aim of extending the Venice Charter in response to the expanding scope of cultural heritage concerns and interests in our contemporary world. The preservation of authenticity is considered in the Nara Document as a way to protect local cultural identities from being increasingly subject to the forces of globalization and homogenization and to the aggressive nationalism. The Nara Document attributed to technical and the political institutional sectors (such as museums and universities) a key role in authenticity research: *"The understanding of authenticity plays a fundamental role in all scientific studies of the cultural heritage, in conservation and restoration planning, as well as within the inscription procedures used for the World Heritage Convention and other cultural heritage inventories"*<sup>7</sup>.

### 1.1.1 The authentication process

Attribution and authenticity analyses were for a long time related to matters of aesthetics, identified as *connoisseurship*. The eighteenth-century French term *connoisseur* initially carried broad connotations *of discrimination which were implicitly the prerogatives of a culture's upper class* [Sutton 2004, pg.30]. In the twenty-first century the term connoisseurship was related to the process that, involving intuitive recognition of an artist's hand, allowed the determination of authorship of an artwork [Sutton 2004]. In

---

<sup>3</sup> "Set of distinctive spiritual, material, intellectual and emotional features of society or a social group, that encompasses, not only art and literature, but lifestyles, ways of living together, value systems, traditions and beliefs", definition of Culture in UNESCO Framework for Cultural Statistics (2009).

<sup>4</sup> "A property must also meet the conditions of integrity and/or authenticity and must have an adequate protection and management system to ensure its safeguarding". Operational Guidelines for the Implementation of the World Heritage Convention, UNESCO, 2011.

<sup>5</sup> International Charter for the Conservation and Restoration of Monuments and Sites: 'The Venice Charter', Venice, 1964.

<sup>6</sup> Nara Conference on Authenticity in relation to the World Heritage Convention in Nara, Eighteenth session, Phuket, Thailand 12-17 December 1994.

<sup>7</sup> Point 10 of Values and authenticity in Information note: Nara Document on Authenticity. Experts meeting, 1-6 November 1994. <http://whc.unesco.org/archive/nara94.htm>, last access 3/3/2015.

the English edition of Morelli [Morelli 1893] he explain the parallelism that exist between speaking and painting “as most men, both speakers and writers, make use of habitual modes of expression, favourite words and saying, which they often employ involuntarily [...] so almost every painter has his own peculiarities, which escape him without his being aware of it” [Morelli 1893, pg.75]. Morelli in his visual glossary, included material aspects: disembodied, hands, ears and other body parts from different Renaissance masters and suggests: *The study of all the individual part, which go to make up “form” in a work of art, is what I would recommend to those who are [...] really desire to find a way through the intricacies of the history of art, and to attain, if possible, to a scientific knowledge of art* [Morelli 1893, pg.75]. As discussed by Hendriks [Hendriks et al. 2009], the consistency of an artist’s hand, as proposed by Morelli, formed the basis of the *Pictology* method developed by Maurits M. van Dantzig (1903-1960) [Dantzig Foundation 1973]. The *Pictology* method has two functions: the identification of markers and the use of these marker to define the quality of the work. Through the qualitative<sup>8</sup> classification proposed by Dantzig, he developed a systematic method to identify a list of the painting characteristics. Dantzig observed that these characteristics were more common in the artworks of the great masters and less common in the work of their followers [Dantzig Foundation 1973]. Dantzig related the spontaneity with the speed of the stroke and with the confidence that the artist has when he/she is going to draw a line (which is important in drawings and underdrawings): *a true work of art maintains a high degree of spontaneity; an inferior work, or a forgery, is full of inhibitions* [Dantzig Foundation 1973, pg.3].



**Figure 1.** An example of spontaneity, in this case the rapidity of the movements may be related to the absence of inhibition (Image taken from [www.ascuoladiguggenheim.it](http://www.ascuoladiguggenheim.it))

The presence of *pentimenti* is another feature usually related with the creative process of an original artwork. In general, the visual analysis of the painting surface developed by Dantzig is closely related to the manipulation of the materials: *The artist has a nearly infinite number of choices- not just his materials, colours, composition but the direction, width, and length of each stroke-all of which he handles in a way specific for him* [Dantzig Foundation 1973, pg.4]. Besides this Dantzig shows how the physical properties

---

<sup>8</sup> Dantzig used the term superior for the authentic and inferior for the forgery art works.

of the materials affect the visual appearance of the surface. The analysis that Dantzig developed for the van Gogh paintings and, in particular the analysis of the brush work, is a clear example of how the materials properties and their handling can lead to surface characteristics. Dantzig identified 93 constant features for van Gogh's paintings, including 25 related to brush work. The selection of the support, a smooth surface instead a *rough one, such as the choice of slow-drying and quick-drying paint* influence the appearance of the painting surface [Dantzig Foundation 1973, pg.14].

From his analysis, Dantzig concluded that van Gogh combined long and very short brush strokes; sometimes the contours of the figures are formed by long brush strokes obtained with one movement. The horizontal brushstroke is applied from left to right and the vertical in a downward direction. The pressure varies and heavy pressure is mainly observed in thick layers of paint. The brush was handled sometimes obliquely and sometimes at a right angle with respect to the canvas [Dantzig 1952, pg.69]. Van Gogh did not mix his paint on the canvas, but applied the colours just as they come out of the tube; sometimes he squeezed the paint direct from the tube on to the canvas, causing little "worms" or rolls of paint, the height and size of which varied according to the thickness of the layer of paint [Dantzig 1952, pg.79].

Dantzig argued with his studies on the paintings of van Gogh that the visual appearance of a painting cannot be considered separately from the materials of the work of art. The warning given by Giovanni Urbani, former director of the Istituto Centrale del Restauro in Rome, is clear: the determination of the authenticity exercised only with the appreciation of aesthetic qualities, delegating to the science to provide simple confirmations, is open to objection and concern [Urbani 2000]. Considering that in art as well as in archaeology the evidence from the past are not constituted by verbal testimony, but mainly from objects, the authentication process must verify both the sensitive experience stimulated by the objects themselves and the characterization of the *material dell'arte* [Brandi 1977] using experimental methods [Urbani 2000].

## 1.2 Computer vision in the conservation field

The application of image processing in the conservation field and in particular, in terms of painting analysis is quite recent, in the following sub-sections the concept of image processing and the most important applications of this discipline in the art-historian domain will be introduced.

### 1.2.1 Digital image processing

The research developed in the first part of the dissertation concerns the application of computer vision methods in the conservation field. The goal of **computer vision** research is to provide computers with humanlike perception capabilities, that means that the computers can understand the sensed data, take appropriate actions and learns from their experiences to enhance future performance [Sebe *et al.* 2005]. Machine learning offers methods for computer vision for automating the model acquisition and updating

the process: the aim of machine learning is that computer algorithms and systems can improve their own performance with time [Sebe *et al.* 2005]. The integration of machine learning techniques in image processing gives a great benefit to the field. **Image processing** develops methods that include the acquisition, the processing and the analysis of digital images. An image may be represented with a two-dimensional function,  $f(x, y)$ , where  $x$  and  $y$  are spatial (plane) coordinates, and the amplitude of  $f$  at any pair of coordinates  $(x, y)$  is the intensity or the grey level of the image at that point. We have a digital image when  $x, y$  and the amplitude values of  $f$  are discrete quantities [Gonzales and Woods 2001].

Gonzalez and Woods in their book [Gonzales and Woods 2001, pgs.1-2] classified the image processing into three levels:

- Low-level processing, characterized by the fact that both inputs and outputs are images. In this level are simple operations, called pre-processing, such as the reduction of the noise, contrast enhancement, and image sharpening.
- Mid-level processing is characterized by the fact that its inputs are images, but its outputs are features extracted from those images, such as image segmentation (partitioning an image into regions or objects). These kind of processes reduce the image to a form suitable for computer classification.
- Higher-level processing involves the objects recognition that in the final stage can lead the program to perform the cognitive functions normally associated with vision.

The studies performed on painting brushstrokes (Section 1.2.3) are based on the concept of **texture**, for that it is important to define the visual texture and the image texture. An image of a real object often exhibits regions with different intensities. An example could be the image of a wooden surface, it contains variations in intensities which form repeated patterns; the presence of this non-uniform intensity defines the **visual texture** [Rosenfeld 1975; Tamura *et al.*1978]. The physical meaning of visual texture include all the characteristics that define the surface properties (such as roughness); often the surface properties have a tactile quality. On the other hand **image texture** is defined as a function of the spatial variation in pixel intensities (grey values) [Tuceryan and Jain 1998]. The Image texture of an image can be extracted and used to perform a texture classification. The aim of this process is to produce a map where each uniform textured region is identified with the texture class it belongs to [Varma and Zisserman 2005]. An image can be also be **segmented** in terms of the texture information present in it. Most of the algorithms for texture segmentation are based on two properties of intensity values: discontinuity and similarity. In the first approach the image is segmented based on abrupt changes in intensity, such as edge detection; in the second one the image is divided into regions that present similarity according to a set of predefined criteria [Gonzales and Woods 2001; Awate *et al.* 2006]. Finally the textures can be **synthetized**, this is an important topic in computer graphics where the goal is to render object surfaces as realistic looking as possible [Tuceryan and Jain 1998].

## 1.2.2 Challenges in art conservation

Large database of artworks are always more common in museum and cultural-institute [Berezhnoy *et al.* 2009]. **Image documentation** of artworks includes, in addition to the digitalization process introduced in the past years, the use of widespread methods based on a specific range of the electromagnetic spectrum, such as X-ray images; infrared photography; fluorescence and ultra-violet and the more recent hyperspectral imaging. All these methods are used to extract information about the painting materials and techniques. In such techniques, the resulting image is generally interpreted by an art scholar [Stork 2008] but in the past few years, thanks to the advances in image segmentation, object recognition and scene analysis, it has been possible to use computer vision to extract information from the image documentation [Stork 2006].

Stork in his work [Stork 2008] gives an overview of the most recent computer vision techniques and how they have been used to support research in art. Colour and texture are the two main features used in painting authentication, the colour and texture features analysed by content-based image-retrieval techniques allow to express the contents of an image with a vector, simplifying the calculation of the similarity between images (e.g., Euclidean distance) [Berezhnoy *et al.* 2009].

As reported by Cornelis [Cornelis *et al.* 2009] the challenges in the conservation field explored by computer vision tools were:

- *Author attribution and authentication*, this issues was mainly addressed through the extraction of texture and colour features that can be used for classification [Lyu *et al.* 2004; Hendriks *et al.* 2009; Li *et al.* 2012; Irfan and Stork 2009; Jafarpour *et al.* 2009; Polatkan *et al.* 2009];
- *Dating*, proposing a date or at least a chronology according to a stylistic evolution identified by the analysis of the brushstroke (see previous point) [Li and Wang 2004; Li *et al.* 2012];
- *Object detection*, development of an automatic search of an object, such as a person or other figurative entities, in a large historical image database [Bergboer *et al.* 2005];
- *Image enhancement*, fusion of information extracted by images acquired using different wavelengths (such as visible, infrared and X-ray) with the aim to enhance features related to damage, painting techniques, or historical documentation [Dik *et al.* 2008; Johnson *et al.* 2013];
- *Inpainting*, consisting of on the digitally reconstructing missing areas within an artwork [Fornasier *et al.* 2009].

In addition to the brushstroke analysis used in classification issues (attribution, authentication and dating) that will be discussed in the following sub-section, there are two recent applications of computer vision methods based on art *connoisseurship*: the first one is related to the detection and analysis of **craquelure**. Similar to the case of the brushstroke, in the paintings construction there are many elements such as support type, ground layer thickness, pigments particle size and type of binder used in the ground layer that may be inferred from craquelure patterns. For that reason variations in craquelure may provide information on the nature of the painting [Bucklow 1997]. Automatic methods to extract craquelure patterns from digital images were developed in a project carried out at the Uffizi Gallery in Florence where the automatic classification of the craquelure in paintings was used to support

damage assessment [Berezhnoy *et al.* 2009] and more recently in Abas's work [Abas 2004], where he used craquelure patterns visible at the surface to classify paintings. The second application concerns the measure of **weave densities** in the painting's canvas. Usually the measurement of weave density (threads/cm) is performed manually from a radiographic image. Johnson *et al.* [Johnson *et al.* 2013] proposed an algorithm to perform automatic measuring from radiographs of the weaving densities of the horizontal and vertical threads that comprise the canvas. The results obtained from the analysis of a set of radiography of van Gogh paintings provide evidence to determine which paintings' support could have been cut from the same piece of canvas.

### 1.2.3 Image processing for brushstroke analysis

As introduced below, the traditional painting surface is characterized by a large number of brushstroke patterns, created by a series of touches arranged in a specific way. Based on connoisseurship, the orientation, shape, and distribution of brushstrokes are identified as unique signatures of the painter. The work of Taylor *et al.* [Taylor *et al.* 1999] was of the first in the use of computerized fractal analysis to detect features from the painting surface and use them to support the authentication process. Taylor *et al.* worked on a specific class of paintings, the dripped paintings of the American abstract expressionist, Jackson Pollock. The analyses developed were based on fractals, a mathematical structure that exhibits regularities at different scales or sizes. Dripped paintings by Pollock were also studied by Al-Ayyoub *et al.* [Al-Ayyoub *et al.* 2011] through the application of traditional image measurements for the analysis of Pollock's works, for instance curvature and fractality features. Al-Ayyoub *et al.* applied supervised classification techniques on a data set of 42 paintings by Pollock and 38 by other artists, the best result (85% accuracy) was achieved using a conjunction of six texture features. Concerning the classified, AdaBoost algorithm showed better results compared with the use of Support Vector Machine (SVM).

The AUTHENTIC project (2003-2007) funded by the Netherlands Organization for Scientific Research (NWO) was developed by Igor Berezhnoy, Eric Postma, and Jaap van den Herik with the aim of creating software tools to support art experts in their assessments of the authenticity of van Gogh's paintings [Berezhnoy *et al.* 2005]. An important contribution to the study ---and in general, in the development of a new application of computer vision tools in art--- was given by Professor Rick Johnson Jr. at Cornell University. In 2005, Johnson invited three researchers who were using statistics for image analysis: Ingrid Daubechies at Princeton University, James Wang at Penn State University, and Eric Postma at Maastricht University to work on images of van Gogh's paintings [Sipics 2009]. The goal of the project was to generate a mathematical and computational characterization of the technique of the Dutch artist, including brushwork, composition, and colour choices. The results of the project were presented in a series of workshops with the title *IP4AI- Image Processing for Artist Identification*, from 2006 to 2010. A database of 101 high-resolution grey-scale film scans of 82 van Gogh paintings (vG), 6 non-van Gogh, and 13 which were currently questioned by experts was given to the three mathematical teams [Johnson *et al.* 2008]. The groups worked on a patch of images with a size of 512x512, 128x128 or 256x256

pixels. To detect texture, geometry, style and fluency of the painting surface, the three groups used different kinds of wavelets transform and different classifiers. The Penn State group worked on 78 images: 59 images from vG and 19 images of paintings belonging to the other two classes. Textured features were extracted by 4D wavelets; the classifier that they selected was the Maximum Likelihood classifier which works with only one class in the training set (the training set was composed by 23 vG paintings). The classification of the images in the test set was performed considering the distance between the tested image and the images of the training set: a low average distance indicates a measure of stylistic proximity to the work of van Gogh. Among the five least similar to vG paintings they correctly identified 3 images, while among the most similar ones they correctly identified 4 images. The Princeton group used complex wavelets with a Multidimensional Scaling classifier on a set of 75 images, 65 of which were vG paintings. They represented all paintings in a 3D space, and calculated the center in the van Gogh cluster (called CvG): 55 of the 65 paintings by van Gogh were represented close to the CvG, as well as 2 of the images from no-van Gogh paintings. Gabor filter and Support Vector Machine classifier were tested by the Maastricht group. They were able to detect dissimilarities in the brushstroke texture of paintings, and to correctly identify four of the six non-van Gogh paintings included in the database at the cost of incorrectly classifying two van Gogh paintings [Johnson *et al.* 2008].

The Gabor filter was used also by Shen [Shen 2009] to perform an automatic classification of a large western painting image collection (including paintings of Caravaggio, Rubens, Vermeer, Tiepolo, Monet, Turner and Goya). Shen tested two strategies for feature extraction: the first one, a global visual feature which include colour analysis, using a colour histogram, texture using the Gabor filter and shape with the Canny edge detector. The second strategy included the analysis of local visual features; each image was partitioned into 16 sub-blocks and the Gabor filter was extracted. The best result in terms of identification accuracy (69.7%) was obtained by joining together the global and local strategies. In this work the classification was based on RBF (Radial Basis Function) a neural network. In the same year, Berezhnoy *et al.* developed an interesting approach to extract brushstroke orientation [Berezhnoy *et al.* 2009]. The model proposed was based on the Prevailing Orientation Extraction Technique (POET). Their strategy consists of two stages: a filtering stage and an orientation-extraction stage. That work analysed 169 digitalized reproductions of paintings by van Gogh, obtained by scanning Ektachromies at a resolution of 2000 dpi with 48 bits colour depth. The results obtained showed that POET has the same capacity to distinguish the brushstroke orientation as the observation of the paintings by human participants.

In 2012 Li *et al.* [Li *et al.* 2012] continued the investigation on van Gogh's brushstrokes and developed a novel extraction method using an integration of edge detection and clustering-based segmentation. The analysis of the repetitive and patterned impression of the brushstroke allowed the definition of features that distinguish between van Gogh's paintings produced in separate periods in his career: Paris and the Arles, and Saint-Rémy. The strategy proposed distinguishes his work from those of his contemporaries. This result is relevant to attribution studies because there are paintings made by artists, also included in his circle, that were not made as deliberate copies or forgeries but have become



mistakenly attributed to van Gogh. While the strategies described achieved good performance for brushstroke detection, the study of authentication remains a challenge: “*the computer doesn’t show clear separation between the real [van Gogh] and the fake paintings, which is logical because the forgers really intend to mimic the van Gogh brushstroke*”<sup>9</sup>. For this reason, authenticity studies must be complemented with analytical characterization of his materials. Given this approach, in this thesis it was decided to explore the combination of brushstroke information extracted by image processing with the materials analysis performed using hyperspectral imaging techniques.

#### 1.2.4 Hyperspectral imaging for pigment identification

Hyperspectral imaging consists of the collection of a set of images using narrow spectral bands in the UV, visible and NIR range (imaging spectroscopy). By assembling the images in a data-cube, it is possible to extract a reflectance spectrum for each pixel of the image. For this reason imaging spectroscopy may be considered as an extension of Fiber Optic Reflectance Spectroscopy (FORS). Thanks to the development of Fiber optic technology in the last 20 years, it has been possible to improve the use of portable instruments in the UV-Vis, NIR and more recently, in the Mid-Infrared regions of the electromagnetic spectrum. FORS has been widely used in examination of artwork, in particular for pigment identification [Bacci *et al.* 2006; Leona *et al.* 2004], dyes [Montagner *et al.* 2011] and paintings [Bacci *et al.* 2003]. At the same time, significant contributions have been made by the group of John Delaney at the National Gallery of Washington combining FORS and multispectral imaging for paintings [Delaney *et al.* 2010] and illuminated manuscripts [Ricciardi *et al.* 2011; Delaney *et al.* 2014].

The characterization of coloured matter by reflectance spectroscopy is usually performed by comparing the unknown spectra with a database of reference materials. The spectra in the database must be collected on mock-up paintings prepared following the techniques and pictorial materials used by the artist as closely as possible [Boselli *et al.* 2011]. In the case of painting materials, the particle size of the pigments, the concentration and types of binders could influence the shape of the reflectance spectrum [Feller 2004]. The absence of a comprehensive database is one of the main limitations of this analysis. A number of groups have their own reference pigment sets; however, few have a comprehensive set that has been systematically prepared and measured, such as the online database of CNR-IFAC<sup>10</sup>, which contains a collection of a reflectance spectra in the 270-820 nm, 350-100 and 980-1700 nm ranges.

Considering the extensive number of spectra that can be obtained with hyperspectral cameras, it was necessary to develop an automatic strategy to analyse it. Chemometric methods for spectral analysis were proposed by Baronti *et al.* [Baronti *et al.* 1997] for the study of 16th-century Italian painting and

---

<sup>9</sup> Mentioned on the on the video “Digital analysis of van Gogh paintings” of Laurens van der Maaten and Eric Postma, based on the work [Maaten *et al.* 2009]. The video winner the Most Innovative video Award at AAAI Conference on Artificial Intelligence in 2008.[<http://www.quizover.com/oer/course/2-digital-analysis-of-van-gogh-paintings-by-laurens-der-videolectures>, last login 26-08-214]

<sup>10</sup> <http://fors.ifac.cnr.it/>

Comelli *et al.* [Comelli *et al.* 2011] for the study of the Italian Renaissance paintings by Masolino da Panicale. Delaney *et al.* [Delaney *et al.* 2010] applied standard remote sensing software (ENVI) to analyse the multispectral image of Picasso's Harlequin Musician. ENVI decomposes the spectra into mutually independent end members. The method described proved to be efficient for identifying groups of materials based on their spectroscopic characteristics. Since the end members do not necessarily have any physical meaning, they cannot therefore be compared to the spectra of reference materials [Liang 2012].

Spectral Angle Mapper (SAM) and Euclidian Minimum Distance (EMD) have been also applied to compare reflectance spectra with the aim of classifying pigments [Keshava 2004; Pelagotti *et al.* 2008; Deborah *et al.* 2014]. Deborah *et al.* [Deborah *et al.* 2014] compared the classification accuracy achieved by SAM and Spectra Correlation Mapper (SCM). SCM was found to be superior to SAM, as it enabled the detection of negative correlations between spectra; nevertheless, the SCM method results were suitable only for homogeneous regions and failed to classify mixed regions.

The analysis of a mixture of pigments is another problem in the interpretation of reflectance data. The investigation based on the Kubelka–Munk theory provided good results [Zhao 2008] but the method proposed requires measurement of pigment mixtures with materials whose absorption and scattering coefficients are known. Spectral unmixing was developed for the analysis of hyperspectral imaging of soil. Using the unmixing algorithm, the unknown spectrum is decomposed into a collection of constituent spectra, called *end members*, and a set of relative abundances. The term end members corresponds to familiar macroscopic objects in the scene, such as water, soil, vegetation, etc. The decomposition of the unknown spectrum can be performed using both linear and nonlinear combination of the end members, however the linear combination cannot be applied when the components are intimately associated, that is, when multiple scatterings are involved [Keshava and Mustard 2002].

An important line of research concerns the combination of multispectral imaging with other spectroscopic techniques. An example is the recent work proposed by Cesaratto *et al.* [Cesaratto *et al.* 2013] for the analysis of a painting on paper by van Gogh. In this work, multispectral imaging is combined with portable Raman spectroscopy; the analysis of multispectral imaging data was performed with the Sequential Maximum-Angle Convex Cone (SMACC) and the spectral angle mapper (SAM). The complementarity of reflectance spectroscopy with the X-ray fluorescence is also well-known [Liang 2012]. This technique allows the determination of the elements present in the painting based on the interaction of the materials with X-ray; local analysis is performed on an area of a few microns ( $\mu$ ) of diameter. Some studies have used the combination of hyperspectral images with Energy Dispersive X-ray Fluorescence (EDXRF) [Liang 2012; Delaney *et al.* 2014]. Still, to date the correlation between reflection imaging spectroscopy and EDXRF is performed by the user without an automatic process.

### 1.3 Our Contributions

This work proposes for the first time a method based on data fusion to support authentication processes of Amadeo's paintings. The information that are combined concern: the brushstroke and materials analysis (molecular information). The basic idea of the system used in this work originated from experience in 2008 [Melo *et al.* 2008] during the edition of Amadeo's Catalogue Raisonné [Freitas *et al.* 2008]. On that occasion, a group of ambiguous paintings were analysed; the visual and technical information were correlated with the analysis of the materials to aid the decision about their authorship. That experience defined the key features in Amadeo's work: brushstroke, colour and materials.

The brushstroke information is extracted from RGB images by Gabor filter. Gabor filter was already used for the analysis of van Gogh brushstroke [Johnson *et al.* 2008; Shen 2009] but in this work Gabor was combined with Scale Invariant Feature Transform (SIFT). By combining these two algorithms we focused the texture analysis (Gabor) on the relevant keypoint detected by SIFT. Moreover the use of this localized version of Gabor allowed the application of the Bag-of-feature method, which resulted appropriate to reduce the problems of having a training set with a small number of images (this problem is frequent in analysing images from painting collections).

The analysis of the pigments is performed using hyperspectral imaging combined with the analysis of the elements by X-ray fluorescence analysis ( $\mu$ EDXRF). The use of hyperspectral imaging in painting documentation is evolving and this technique is increasingly being coupled with other analytical techniques. X-ray fluorescence analysis has always been considered one of the techniques that best complement the image spectroscopy, and even more so today with the development of systems of macro-XRF<sup>11</sup>. Until now, users would have to manually correlate the results obtained by these two techniques. For this reason, the semi-automatic method proposed in this thesis offers an important contribution in this line of research. As introduced above, one of the limitations in the use of reflectance spectroscopy (FORS or hyperspectral imaging) for pigments characterization is the need of a database of reference materials as close as possible to the analysed materials; in this work this limitation has been exceeded using as reference historical paint samples. The reflectance and the elemental data acquired on the painting are compared with a database collected from samples of paint tubes belong to the artist. The system develop is also able to detect areas were not perfect match- between the data collected in the painting and those present in the database- is found. These areas can be related with the use of pigments not consistent with the pigment palette of Amadeo and therefore areas that may be not original. The quantification of these areas is combined with the probability of authenticity calculated by the brushstroke analysis.

---

<sup>11</sup> Macro-XRF allows to perform the scanning X-ray fluorescence analysis [Alfeld *et al.* 2013].



## CHAPTER 2: METHODOLOGY AND RESULTS

This chapter presents the system developed based on the combination of brushstroke and molecular analysis (Section 2.1). The system was developed using Matlab® programming language. The following two sections present the strategies proposed for each one of the analyses: the brushstroke detection, was developed by a combination of Gabor filter and Scale Invariant Feature Transform (Section 2.2); the molecular examination was performed combining hyperspectral imaging with elemental analysis (Section 2.3). The results obtained by features combination analysis of 12 paintings are presented at the end of this Chapter.

### 2.1 Features combination for painting authentication

As introduced in the previous chapter, the texture of the painting is directly related with the materials and the techniques used by the artist. For this reason, the tool proposed to support the authentication process of paintings attributed to Amadeo combines information on texture and materials. Figure 2 shows the overview of the system proposed, where RGB images are used to extract information concerning the brushstroke [Montagner *et al.* 2012] and hyperspectral images are analysed to extract information on the materials (molecular analysis) used in the painting [Almeida *et al.* 2013; Montagner *et al.* 2013].

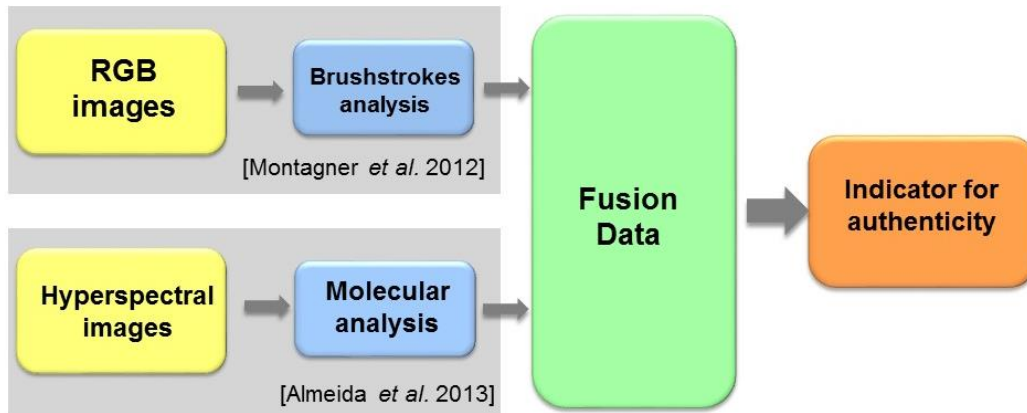


Figure. 2 Fusion data system overview.

The results obtained by the two analyses are combined using *SUM-Combination*:

$$I_a(Am) = \alpha p(B/Am) + (1 - \alpha)I_a(M/Am) \quad (1)$$

That is,  $I_a(Am)$  is a quantitative indicator for authenticity, the value range of the indicator is 0-1 where 0 is Not Amadeo and 1 Amadeo. The indicator is obtained by a weighted sum of the brushstroke probability  $p(B/Am)$  and the quantitative indicator for molecular analysis  $I_a(M/Am)$ . The coefficient  $\alpha$  may be chosen by the user considering the weight attributed for each analysis or estimated using the cross validation method [Browne 2000]. For the Amadeo's system was chosen a coefficient of 0.5 for

each component, this means that the two analysis are considered equally relevant for the authentication study of Amadeo' paintings.

## 2.2 Brushstroke Analysis

The strategy proposed to perform the brushstroke analysis is based on binary classification and depicted in Figure 3, where the block *Paintings* represents the database of images used. The selection of the images was performed in collaboration with Helena de Freitas, art historian expert of Amadeo's works and curator in the Calouste Gulbenkian Foundation. The database is composed of two classes, called *positive* and *negative*. The *positive* class includes 200 images from Amadeo's paintings from his Catalogue Raisonné [Freitas *et al.* 2008]; the *negative* class includes 109 images of paintings of Amadeo's contemporary artists. In the *negative* class are included paintings presented at the exhibition *Amadeo de Souza-Cardoso - Diálogo de Vanguardas* [Freitas *et al.* 2006]. This exhibition featured a large number of international artists that had stylistic correlations with Amadeo, such as Gino Severini, August Macke, Liubov Popova, Kazimir Malevitch, Albert Gleizes, Lyonel Feininger, Jean Metzinger, Otto Freundlich, Pablo Picasso, Sonia and Robert Delaunay, Ivan Puni, Olga Rozanova and Franz Marc. In the *negative* class are also included images from paintings by Eduardo Viana, Mario Eloy and José Almada Negreiros, these artists belonged to the Amadeo's circle.

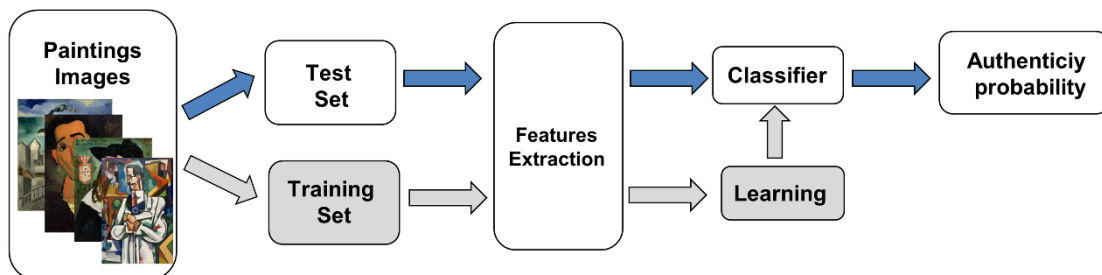


Figure 3. System architecture for the brushstroke analysis.

To train the classifier and to validate its performance, the database is divided in two sub-sets called *training* and the *test* set, respectively (Fig.3). The *training* set is used in the *learning* stage to build the model, whereas the *test* set is used in the classification stage. In this stage the image, for which the model does not know the label, is processed to test the capacity of the model in recognize the class that the image belongs to. The *Feature extraction* block (Fig. 3) represents the step where each image of the datasets is processed to extract texture features. Table 1 presents the four strategies tested in this step: (1) Gabor filter; (2) Scale Invariant Feature Transform (SIFT) and in addition, two localized variations of Gabor filter: (3) Gabor in regular point and (4) Gabor in the localization of the keypoints. Wavelength analysis was used with good results in related work [Johnson *et al.* 2008; Shen 2009] and SIFT was chosen because it has been already used with success in image classification [Nowak *et al.* 2006]. SIFT and the two localized variations of Gabor allowed the employment of the Bag-of-Features

model (presented in Section 2.2.2), that demonstrably improved the performance of the classifier. The classifier used was Regularized Least Squared Classifier (RLSC) (presented in section 2.2.3).

**Table 1.** Strategies adopted in the features extraction block.

	Strategy	Feature extractor	Bag-of-Features
1.	Gabor (1)	Gabor	-
2.	SIFT	SIFT	√
3.	Gabor (2) in regular points	Gabor	√
4.	Gabor (3) in keypoints	SIFT+ Gabor	√

### 2.2.1 Image pre-processing and feature extraction

From the literature it is known that images of equal size are more easily compared [Cornelis *et al.* 2009]. For this reason, before the texture extraction, the size of all the images was reduced so that the smallest dimension was equal to 512 pixels. In order to preserve the texture information the ratio between the number of lines and columns of each image was not changed.

#### *Gabor (1)*

A Gabor filter is defined as the product of a sinusoid times a Gaussian kernel. The Gabor function is named after Dennis Gabor who used it in the 1940s for edge detection [Gabor 1946]; later on, John Daugman [Daugman 1988] proposed this function to describe the spatial response of cells in visual stimuli experiments and in 1996 Manjunath *et al.* [Manjunath *et al.* 1996] proposed the use of Gabor for texture analysis. In this work a bank of 24 filters with 4 scales and 6 directions, as represented in Figure 4 was used.

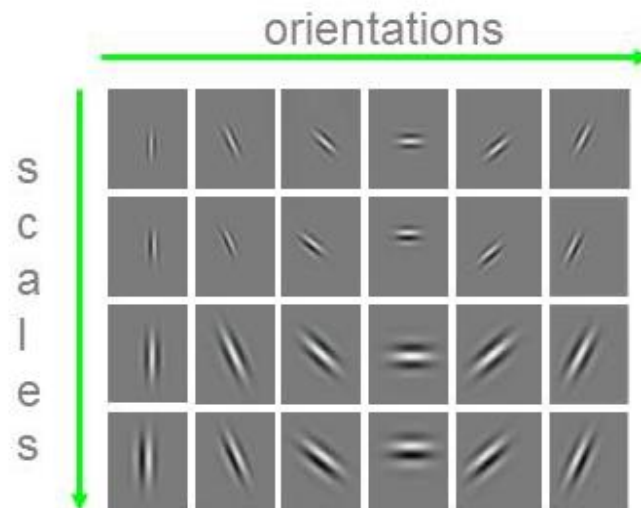


**Figure 4.** Bank of 24 Gabor's filters used in this work with 6 orientations and 4 scales.

Figure 5 shows a representation of the result obtained (C) by the application of the filter at 45° (B) on the image of the painting *Ar livre nù* of Amadeo (A) as well as the final convolution of the images obtained by the application of the 24 filters (D).

Given an image  $I(x, y)$ , its Gabor wavelet transform is defined to be [Jesus 2009]:

$$W_{x,y} = \int I(x_1, y_1) g_{mn} * (x - x_1, y - y_1) dx_1 dy_1 \quad (2)$$

where  $g_{nm}$  indicates the Gabor filter. The image  $I(x_1, y_1)$  will be represented by the mean ( $\mu_{o,s}$ ) and the standard deviation ( $\sigma_{o,s}^2$ ) of the modulus of the filtered image,  $W_{w;x}$ . For each orientation  $o$  and scale  $s$  the vector

$$x_k = [\mu_{1,1}, \sigma_{1,1}^2, \dots, \mu_{N_{orientation}, N_{scale}}, \sigma_{N_{orientation}, N_{scale}}^2]^T \quad (3)$$

is obtained from the filtered image. The texture features extracted with Gabor are represented as 48-dimension vectors.

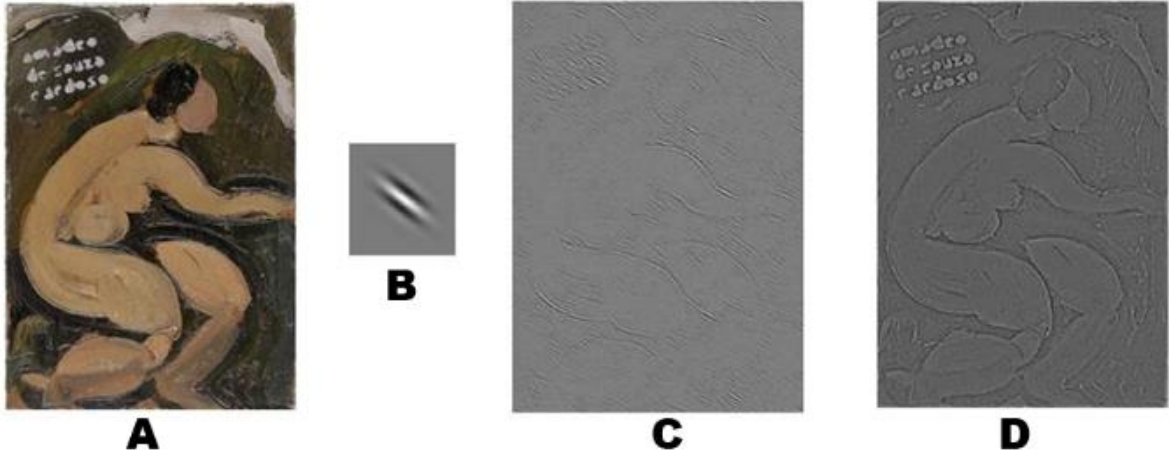


**Figure 5.** Gabor filter processing, **A** RGB image of the painting *Ar livre nù*, Amadeo de Souza-Cardoso (1914); **B** scale 4 and 45° filter; **C** representation of the convolution of the image with the filter (scale 4, 45°); **D** resulted image filtered with 24 filters.

### Scale Invariant Feature Transform (SIFT)

Lowe proposed this method in 1999 [Lowe 1999] as a way of extracting distinctive invariant features from images. These features were used to perform reliable matching between different views of an object or scene. One of the most important properties of this algorithm is that the extracted features are invariant to image scale and rotation. The algorithm provides robust matching across a substantial range of distortion: change in viewpoint, addition of noise and change in illumination of the object. SIFT has been successfully used in several areas [Nowak *et al.* 2006; Lew *et al.* 2006; Jesus *et al.* 2010]. The strategy proposed by Lowe can be summarized in four steps:



(1) *Scale-space extreme detection* consists in a search over all the scales of the image. It is implemented by using a difference-of-Gaussian (DoG) function. The aim of this step is to identify potential interest points that are invariant to scale and orientation.

(2) *Keypoint localization*: at each candidate interest point (keypoint) a detailed model is built to determine the stability of this point at the different scales.

(3) *Orientation assignment*: one or more orientations are assigned to each keypoint location based on local image gradient directions.

(4) *Keypoint descriptor*: the local image gradients are measured at the selected scale in the region around each keypoint. For each image of the database around 2000 keypoints are calculated.

For this work the SIFT descriptor is computed in a region of 16x16 pixels which is divided in 4x4 pixels blocks. An orientation histogram is calculated with 8 directions in each block. This results in a representation vector of 128 dimensions (4x4x8). Figure 6 shows the same RGB image processed with SIFT (left) and Gabor filter (right).



**Figure 6.** Image processing of RGB image *Ar livre nù*, Amadeo de Souza-Cardoso, (1914), using SIFT (left) and Gabor filter (right).

### *Gabor (2) in regular points*

To increase the amount of texture information extracted, each image of the database was divided into squares of 128 pixels with an overlap of 64 pixels. In case that the dimension of the image was not a multiple of 128, the remaining part was equally divided in the left and in the right part. The analysis was performed on each of these parts with the same condition described previously (Gabor (1)).

### *Gabor (3) in the localization of the keypoint*

SIFT was used to detect the keypoints of each image (Figure 7A). Then, an area of  $N \times N$  pixels around each key point was selected (Fig.7B) and rotated according to the orientation assignment by SIFT

(Fig.7C). Finally, the area was processed with the Gabor filter bank (Gabor (1)) (Fig.7D). It is important to take into account that not all the keypoints detected with SIFT can be used in this strategy. Indeed, it is necessary that the distance from the edge of the image and the key point localization should be greater or equal than  $\frac{N}{2}$ . Table 2 shows the number of keypoints detected with SIFT and the number of keypoints which can be used with Gabor (3) considering an area of 64x64 and 128x128 pixel around the keypoint. For this work the larger area was chosen for comparison with the strategy Gabor (2).

**Table 2.** Number of keypoints detected with SIFT and with Gabor (3) on SIFT keypoint analysing an area of 64x64 and 128x128 pixels.

	Number of keypoints		
	SIFT	Gabor (3)	
		64 x 64	128 x 128
<b>Positive Set</b>	384237	246423	184248
<b>Negative Set</b>	174537	122634	93612
<b>Tot</b>	558774	369057	277860

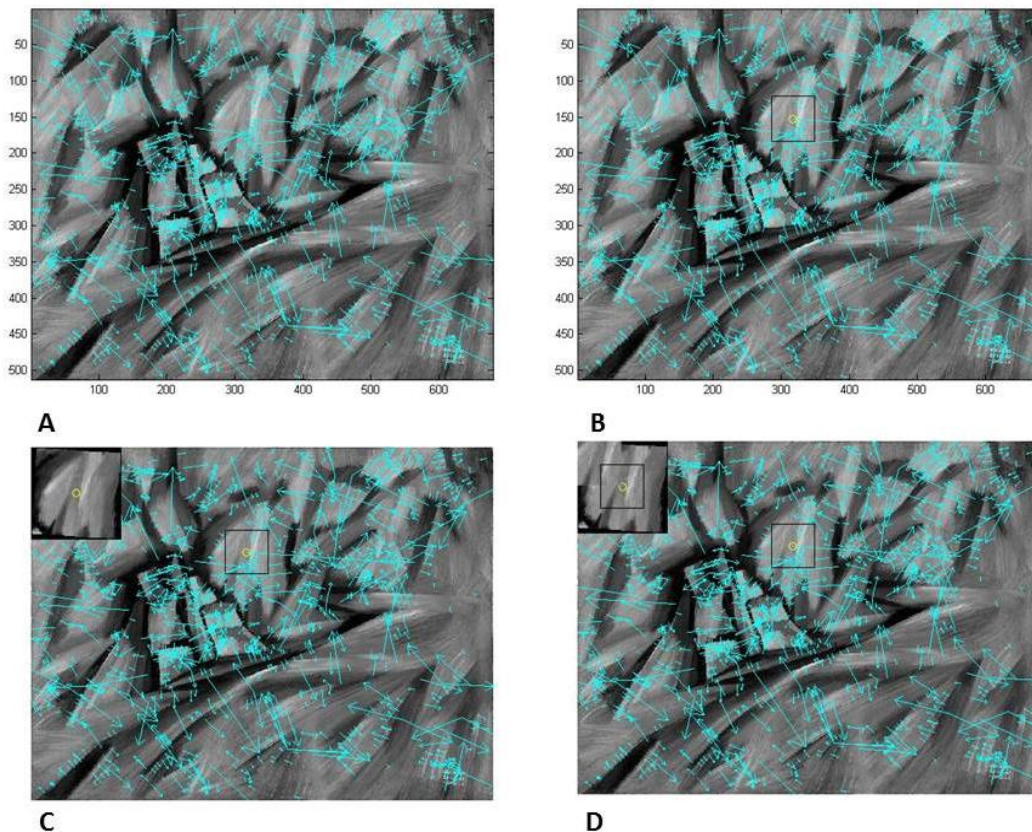


**Figure 7.** Representation of Gabor (3); **A** Identification of the localization and orientation of the keypoints; **B** Selection of an area around the keypoint; **C** Rotation of the area in accordance with the orientation detected by SIFT; **D** Selection of an area of 64x64 pixels around the keypoint.

## 2.2.2 Bag-of-Features

An intermediate step between the extraction of features and the classification stage is the use of Bag-of-Features, called also Bag-of-Words. This model was developed in the field of Natural Language Processing to study the interactions between computers and human (natural) languages and was later applied to image classification. In the Bag-of-Features each image is considered as a loose collection of patches (features) collected from both the classes used (*positive* and *negative*<sup>12</sup>).

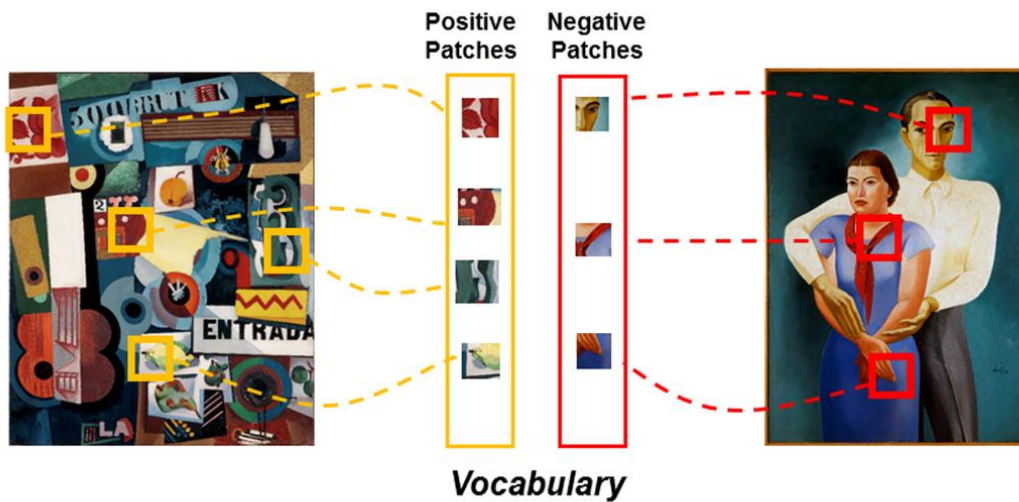


**Figure 8.** Representation of the construction of the *vocabulary* used for Bag-of-Features, *positive* and *negative* patches are collected from the images of the training set belongs to the corresponding classes. Image adapted from [Maaten and Postma 2009].

The Bag-of-features model requires the creation of a *vocabulary* using the features extracted from the images of the training set. The *vocabulary* must contain *positive* and *negative* words (Fig. 8). In this work the *vocabulary* was created using clustering analysis, (K-means method which will be presented in Appendix Part I Ap.I). The number of clusters was selected based on tests presented in the following section. The features extracted from the images of the *test* set are compared with the features presented in the *vocabulary*; in this way, it is possible to count, how many *positive* and *negative* words (features) are present in each unknown image. Bag-of-Features considers the possibility that a *positive* image presents some features that may also be present in a *negative* image and vice versa.

It is possible to formalize the Bag-of-Features model as follows: given a data-set composed of a set of  $N$  images  $D_B = \{I_1, \dots, I_N\}$  and a *vocabulary*  $V_w = \{w_1, \dots, w_M\}$  of *words*, the Bag-of-Features for an

---

<sup>12</sup> In this work the *positive* class includes all the paintings of Amadeo and the *negative* class all the not Amadeo paintings.

image  $I_k$  is represented by a histogram that counts the occurrences, of each  $W_{l,k}$  of each  $w_l$  word in the  $I_k$  picture [Nowak *et al.* 2006]:

$$x_k(l) = \sum_{i=0}^{M-1} W_{i,k} \delta(l-i) \quad (4)$$

where  $\delta(l)$  is the impulse unitary function. To normalize the vector of occurrence, the Term Frequency–Inverse Document Frequency was applied (more information about TF-IDF in Appendix Part I Ap.II) [Robertson 2004]:

$$W_{jk} = \frac{N_{l,k}}{\sum N_{l,k}} \log \left( \frac{N}{n_l} \right) \quad (5)$$

where  $n_l$  denotes the number of images in which the term  $l$  is present and  $N_{l,k}$  is the number of occurrences of the term  $l$  in the  $k$  image. Bag-of-Features is very useful in the case of SIFT keypoints because it reduces the number of features that will go then to the classifier and reduces the imbalance between the two classes. Using SIFT approximately 2000 key points, with 128 dimensions can be calculated; Bag-of-Features allows the reduction of this number and the performance of a sort of normalization, because all the images are described with the same number of features, that is, the number of *words* of the *vocabulary*. Furthermore, this strategy takes into account that an image can have both negative and positive features. The presence of characteristic features from both of the classes is expected in paintings made by artists that belong to the same entourage.

### 2.2.3 Classifier

For the classification stage we used Regularized Least Squared Classifier (RLSC) [Poggio and Smale 2003], a simplified variant of the popular Support Vector Machines (SVM) [Müller *et al.* 2001], which provides comparable results. Given a training set:

$$S_m = \{(x_i, y_i)_{i=1}^m\} \quad (6)$$

where  $y$  is a label with a value -1 for the *negative* class and 1 for the *positive* one,  $y_i \in \{-1, 1\}$  and  $x_i$  are the feature vector. This feature vector comes from the algorithms of feature extraction by Gabor and SIFT. The discriminant function used to define the boundary between the two classes is:

$$f(x) = \sum_{i=1}^m c_i K(x_i, x) \quad (7)$$

$K(x_i, x) = e^{-\frac{\|x-x_i\|^2}{2\sigma^2}}$  is a Gaussian kernel;  $m$  is the number of training points and  $c = [c_1, \dots, c_m]^T$ , is a vector of coefficients obtained by the least squares method. The minimization of (7) leads to  $(m\gamma I + K)c = y$  where,  $I$  is the identity matrix,  $K$  is a square positive definite matrix with the elements,

$K_{i,j} = K(x_i, x_j)$  and  $y$  is a vector with coordinates  $y_j$ . To choose the optimal values for  $\gamma$  and  $\sigma$  cross-validation method was used. The points  $\{x_i\}$  with  $f(x_i) \leq 0$  are classified in the *Negative* class and label as *Not Amadeo* ( $y_i = -1$ ), whereas the points with  $f(x_i) > 0$  are classified in *Positive* class and label as *Amadeo* ( $y_i = 1$ ).

## 2.2.4 Parameters setting and evaluation of the strategy proposed

Due to the specificity of the system developed, based on Amadeo's features, the evaluation of the performance of the classifier cannot be calculated using standard existing databases, as done in other works in computer vision. For this reason, this evaluation was done using test sets and case studies<sup>13</sup>. The number of the images used in the database is limited to the number of the paintings made by Amadeo. Besides that, Amadeo changed brushstroke several times along his career; for this reason, the selection of the images for the training set was a crucial step. The images selected for the training set should represent all the different periods of the artist. We selected this set with the help of Helena de Freitas, an expert on Amadeo's work. To reduce the number of used images to a minimum, and to optimize the performance of the classifier, we developed a series of tests based on the following questions:

- (1) The unbalanced number of *positive* (200) and *negative* (109) images may influence the performance? May the number of *positive* class images used in the training set influence the performance of the classifier?
- (2) The use of Bag-of-Features may improve the performance of the classifier?
- (3) Which one of the four strategies (Gabor filter; SIFT and the two localized versions of Gabor) allows the best discrimination between the images of Amadeo and Non-Amadeo painting?

The first test performed aims to evaluate the role of the number of the *positive* images (Amadeo's paintings) in the training set. Nine training sets were built keeping the number of the *negative* images constant (60) and changing the number of *positive* images (from 62 to 105). The other images were used in test sets to evaluate the performance of the classifier. Figure 8 shows the performance of the classifier expressed as a percentage of correct answers (% Hits) versus the number of the *positive* images in the training set. The green lines indicate the percentage of the images of Amadeo's paintings that were correctly classified, while the red lines the Not Amadeo images correctly classified. In Figure 8A the texture features were detected using Gabor filter and in Figure 8B using SIFT. It is important to remember that by using SIFT it was possible to apply the Bag-of-Features strategy.

---

<sup>13</sup> Four paintings attributed to Amadeo but not included in his Catalogue Raisonné were used as case studies in Part III of this thesis.



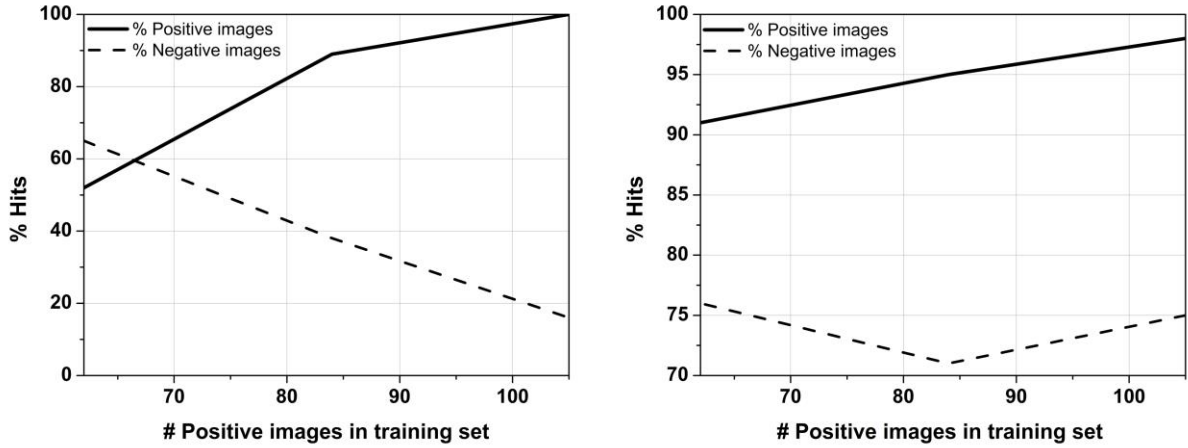


**Figure 9.** The performance of the classifier while changing the number of positive images in the training set, %Hits means the number of painting images correctly classified: the images of the *positive* class (Amadeo) correctly classified are represented by the black lines; the *negative* class (Not Amadeo) by the dot lines. **A** The texture features are extracted using Gabor filter; **B** the features are extracted by SIFT using the Bag-of-Features model.

The test performed using Gabor (Fig. 9A) shows by increasing the number of *positive* images in the training set the classifier increases the number of *positive* images correctly classified; however, at the same time, it reduces the capacity to classify *negative* images. That may be explained as a sort of over fitting due to the large number of images of Amadeo's paintings used, compared to the number of Not Amadeo. The over fitting produces an excess of false positives (that is, images belonging to the *negative* class classified as *positive*). In the case of the tests performed using SIFT (Fig. 9B) the number of *positive* images in the training set does not influence the performance of the classifier directly because the Bag-of-Feature model, based on a vocabulary of words, allows the reduction of the unbalance between the two classes. The performance obtained with the four strategies proposed (Gabor filter; SIFT and the two localized versions of Gabor) were tested through the second test. Also in this set of tests, the number of the *negative* images was kept constant: 60 images for the training set and 49 for the test set, while the number of *positive* images was changed according to Table 3. The performance of the classification is expressed with accuracy, as follows:

$$Ac = \frac{T_p + T_n}{(T_p + T_n + F_p + F_n)} \quad (8)$$

where  $T_p$  is true positive;  $T_n$  is true negative;  $F_p$  is false positive and  $F_n$  is false negative.

**Table 3.** Number of *positive* images in the training and test sets.

Test	Training set	Test set
#1	62	138
#2	84	116
#3	105	95

Table 4 shows the results obtained using the four strategies for feature extraction. In the Table, “Hits” refers to the percentage of Amadeo’s images correctly classified. From the tests it is clear that the use of localized variants of the Gabor filter (Gabor (2) and (3)) improves the performance of the classifier, obtaining an accuracy > 90%. The test performed using Gabor (2) and (3) give results slightly better than those performed with SIFT and Gabor (1), with an accuracy between 91% and 94%.

Comparing the different test sets (# 1, 2, 3) we can see, as expected, that the increment of the *positive* images in the training set in Gabor (1) improves the classification of the images of Amadeo’s painting but at the same time increases the number of false positives. In the case of Gabor (1), to correctly detect the textures in Amadeo’s paintings, the classifier requires a large set of images in the training set. In the three cases where we used the Bag-of-Features strategy (SIFT, Gabor (2) and Gabor (3)) the classifiers seem to be more invariant to the learning stage. These results confirm those obtained in the previous one, as showed in Figure 8.

**Table 4.** Evaluation of the performance of the classifier using: SIFT; Gabor (1) in a global approach; Gabor (2) in regular points and Gabor (3) in the localization of SIFT keypoints. Hits refers to the percentage of Amadeo’s paintings correctly classified.

Test	%	SIFT*	Gabor (1)	Gabor (2)*	Gabor (3)*
#1	Hits	91	65	97	97
	False Positive	24	20	14	10
	Accuracy	83	73	92	93
#2	Hits	95	87	99	97
	False Positive	29	43	12	12
	Accuracy	84	72	94	93
#3	Hits	98	97	100	99
	False Positive	25	61	18	14
	Accuracy	86	68	91	92

\* Use of bag-of-features model, choosing 1000 positive and 1000 negative words.

The third test performed concerns the selection of the best number of features that can be used to create the *vocabulary*. The number of features is determined by the number of clusters used in the K-means method. Table 5 shows the results obtained with this set of tests: we always used the same training and test sets and the number of clusters were changed to select the *positive* and the *negative* words in the Gabor (3) strategies. The results obtained show that the performance of the classifier is partially influenced by the number of features used by the Bag-of-Features; increasing the numbers of features the accuracy increase until it reaches a plateau around 95%. After this value by increasing the number of features does not increase the accuracy of the classifier.

**Table 5.** Evaluation of the role of the number of clutters in the construction of the vocabulary in bag-of-features strategy. The value indicated is the sum of the positive and negative word with the same proportion 50:50.

<b>Words</b>	100	200	400	1000	1200	1400	1600	2000
<b>Accuracy (%)</b>	67	74	82	90	95	93	94	95

Based on the tests performed, it is possible to give some answer to the question formulated at the beginning of this sub-section: the number of the *positive* images in the training set has a role in the accuracy of the classifier; the performance of the classifier can be improved using the Bag-of-Feature strategy by choosing a balanced number of *positive* and *negative words*. In the case of Gabor (1) increasing the number of images of Amadeo's paintings increases also the number of false positive, which do not happen using the SIFT strategy; for that reason it can be seen that Bag-of-Features improves the correct distinction between positive and negative class images reducing the number of false positives. The selection of the number of features to be used in the Bag also has an influence on the classification; a larger number of features does not necessarily mean better results. Finally, the two localized variants of Gabor, that Gabor analysis performed in regular points and in the localization of SIFT keypoints, show better results when compared with Gabor (1) and SIFT.

## 2.3 Molecular Analysis

Besides texture, colour is considered as one of the most relevant features in the works of Amadeo: *the impact of his [Amadeo's] paint stems, largely, from the combination of the maximum energy of the forms with the maximum power of colours* [Gonçalves 2006]. **Hyperspectral imaging** in the visible range allows for an accurate reproduction of the colours of the painting. Moreover, this technique performs a spectroscopic analysis over all the surface of the painting. Based on the spectral features is possible the characterization of the pigments present in the painting. The camera used for this work is a low-noise Peltier-cooled digital camera (Hamamatsu) of the Centre of Physics of the University of Minho in Portugal. The camera works in the visible range between 400 and 720 nm, with a resolution step of 10 nm, which means that for each painting are acquired 33 images. Assembling these images are obtained a data-cube (Fig. 10). The third dimension of the cube is the intensity assumed by the 33 pixels with the same coordinates in the 33 images. This intensity is used to calculate a reflectance spectra (one for each pixel). The RGB colours used to visualize the final image are calculated from the reflectance spectra that guarantee a colour reproduction more accurate comparing with the normal digital camera.



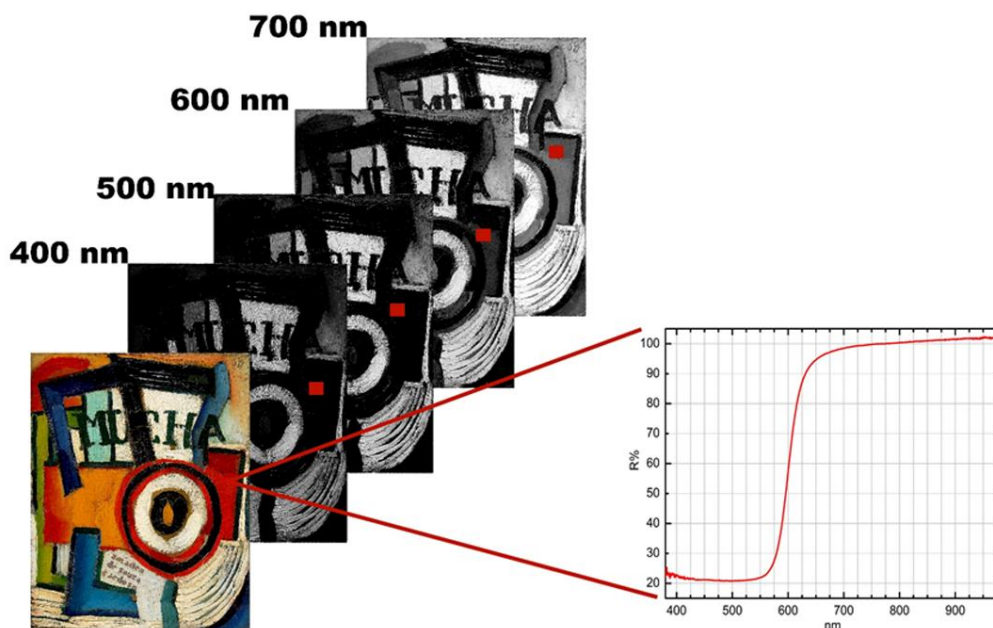


**Figure 10.** Representation of the hyperspectral imaging data-cube, the hyperspectral analysis includes the visible range between 400 to 720 nm. For each painting 33 images with a spectral resolution of 10 nm were acquired. In this way, a data-cube of 1344 x 1024 x 33 is created, where the first two dimensions are the spatial resolution of the images (expressed in pixels) and the third dimension is the reflectance value of each pixel in the 33 images. From the data-cube it is possible to extract a reflectance spectra for each one of the pixels of the image.

In the developed system the hyperspectral imaging data are combined with the information concerning the chemical elements present in the paint. This information is extracted by **X-ray fluorescence technique** ( $\mu$ -EDXRF). The elemental analysis was chosen as a complementary technique to hyperspectral imaging.  $\mu$ -EDXRF is an *in-situ* technique that allows a rapid analysis on different areas of the painting. This technique is quite effective to detect or to exclude the presence of elements that may be related to the use of pigments not coherent with those used by Amadeo. The use of elemental analysis overcomes some limitations in the use of hyperspectral imaging to perform pigment characterization; such as the difficult in the discrimination between vermilion and cadmium orange or between blue cobalt based pigments. Another limitation in the use of hyperspectral imaging (and in general in reflectance spectroscopy techniques) is that the interpretation of the spectra is usually performed by comparing the unknown spectra with a **database of reference materials**. To solve this problem it was used a database of reference materials most representative as possible of the materials used by Amadeo. The database is composed by 16 samples from historic oil paint tubes. The selection of the reference materials was based on the previous study on the materials and techniques of Amadeo [Melo *et al.* 2008; Melo *et al.* 2009]. Comparing the information extracted from the painting with that collected in the database of reference materials it is possible to detect the pigments present in the painting but also the areas made using pigments not included in the database. In the features combination step (Section 2.4) the quantification of the areas where the system detected the presence of pigments don't included in the database of reference materials is used to calculate the *indicator of*

authenticity  $I_a(M/Am)$  based on the materials information. This indicator is added (in Equation 1) to the probability of authenticity calculated from the brushstroke analysis.

One of the outputs produced by the system is a mapping of the pigments detected in the painting. The **mapping image** is in false colours: in areas with the same colour the system detected the same pigment or mixture of pigments. The user can select a pixel from the mapping image and see which pigment(s) the system detected in it or the user can visualize the distribution of a specific pigment(s) selected from a list.

The results obtained by the developed system were compared with those obtained by K-means cluster method<sup>14</sup> (an unsupervised strategy) that is used to perform the analysis of the hyperspectral image (Section 2.3.6).

### 2.3.1 Painting system

Figure 11 shows the overview of the system proposed, the input data used by the system are: the hyperspectral images and the chemical elements (acquired by  $\mu$ -EDXRF) of the paintings and of 16 samples used as database of reference materials. The database represents the materials used by Amadeo (more information below). The core of the system is composed of 3 steps. In step 1 the algorithm detected: (i) the areas painted with materials that are not present in the database of reference materials (these areas are called the *Not Amadeo* areas); (ii) the areas where the elemental analysis is missing<sup>15</sup> (these areas are called the *Not analysed* area); (iii) the black and white areas. In steps 2 and 3 to each pixel of the hyperspectral image is attributed a pigment or a mixture of pigments. That part is performed by comparing the reflectance data and the elemental information acquired on painting with those present in the database of reference materials. To compare the unknown reflectance spectra with the database we used a combination of two popular metrics [Keshava 2004; Pelagotti *et al.* 2008] Spectral Angle Mapper (SAM) and Euclidian Minimum Distance (EMD).

The output of the system is mapping image where the areas painted with the same pigments are represented with the same colour. Besides that, is reported in a table jointly with the image the percentage of the area occupied by each pigment or mixture as well as the areas that may not be original (*Not Amadeo*) or where part of the data are missing (*Not analysed*). The percentages of these areas are used in Equation (1) to calculate the quantitative indicator for molecular analysis  $I_a(M/Am)$ .

---

<sup>14</sup> More information on K-means cluster method in Appendix Part I. Ap.I

<sup>15</sup> The selection of the points for the elemental analysis is preceded by the observation of the painting by naked eye and by microscope. Some areas may not be included because they are considered consistent with other areas already selected.

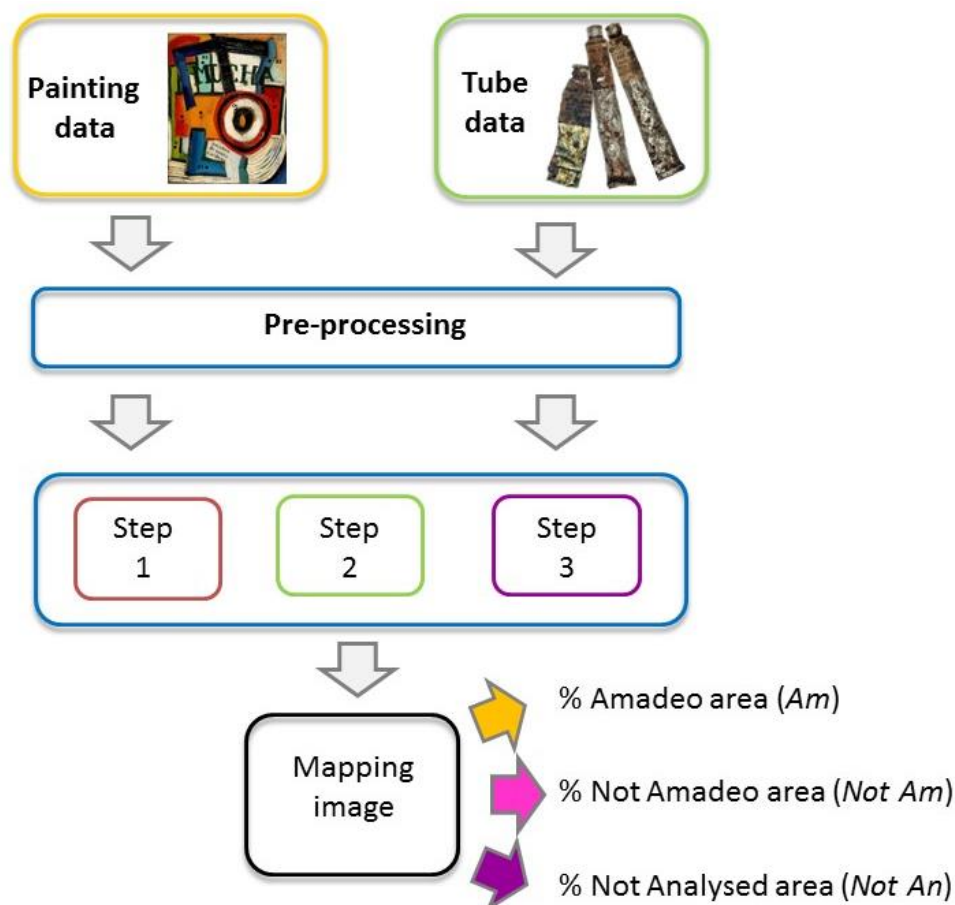


**Figure 11.** System overview of the combination of hyperspectral imaging and elemental analysis.

### *Paint tubes samples database*

As referred before to characterize the pigments present in the paintings is used a database of reference materials from paint tubes. The paint tube samples were digitalized by hyperspectral camera and analyzed by  $\mu$ -EDXRF. Table 6 shows the 16 oil paint tubes<sup>16</sup> chosen to create the database. The database represents the paint materials used by Amadeo between 1912 and 1916. The selection of the pigments used as reference materials was based on the analysis of 19 selected paintings produced by Amadeo between 1912 and 1917; as well as 31 oil paint tubes from two paint boxes belong to Amadeo and preserved in Manhufe at the Family house of the artist. The paintings and the paint tubes were analysed at the time of the edition of the Catalogue Raisonné of Amadeo (more information in Part II, Chapter 1, Section 1.1.3) [Melo *et al.* 2008; Melo *et al.* 2009]. The reflectance spectra from the selected paint tube samples (acquired by hyperspectral camera) were compared with those collected on the Amadeo's paintings to guarantee that the spectral features extracted were comparable. The reflectance spectroscopy analysis in the visible range is not able to detect the presence of fillers or additives in the

<sup>16</sup> The paint tubes were previously analyzed also by FORS;  $\mu$ -FTIR,  $\mu$ -Raman and HPLC in [Melo *et al.* 2009; Silva *et al.* 2011 Montagner *et al.* 2013b].

paint. The spectra features used to characterize the samples are related to transitions that occur between energy levels that interest the metal atoms (for inorganic) or molecular orbitals (for organic) of the pigments. For these reasons, even if there are differences in term of paint formulation, between the paints of the database and those used in the paintings, these differences do not affect the identification of the pigments used by the artist. From the 16 oil paint tubes used as reference materials (Table 6): 13 were selected from those conserved in the Amadeo's house and 3 are from a paint box that has been used by the Portuguese painter Columbano Bordalo-Pinheiro (Lisbon 1857-1929). The Columbano's tubes belong to the collection of the Museu Nacional de Arte Contemporânea do Chiado in Lisbon and were analysed in the context of the Crossing Borders project at DCR-FCT; part of the analyses are published in Silva *et al.* [Silva *et al.* 2011] and Montagner *et al.* [Montagner *et al.* 2013b]. The reflectance spectra acquired on the 16 reference materials are presented in Appendix Part I Ap.V.

**Table 6.** Set of oil paint tube used to create the database of reference materials.

<b>Pigment</b>	<b>Paint tube*</b>
Cobalt violet	ASC13 – Lefranc §
Vermillion	MG6 - Winsor & Newton §
Carmine lake	ASC14 – Lefranc §
Terra rossa	MG18 - Rembrandt Oil Colors §
Raw Siena	MG7- Winsor & Newton §
Ochre yellow	MG11 - Winsor & Newton §
Chrome yellow	ASC17- Lefranc §
Cadmium orange	MG2 - Winsor & Newton §
Cobalt blue	MG4 - Winsor & Newton §
Cerulean blue	ASC7 - Winsor & Newton §
Prussian blue	ASC19 - Winsor & Newton §
Ultramarine	21_3130 - Winsor & Newton ♦
Viridian	ASC20 – Lefranc §
Emerald green	20_3128 - Morin et Janet ♦
Lead white	10_3130 - Paul Denis ♦
Ivory Black	MG17- Winsor & Newton §

\* Paint tube samples from the Family house of Amadeo studied in [Melo *et al.* 2008]. With ASC the samples take from the oil pant tubes from the box with the 'Amadeo'. With MG the samples take from the oil pant tubes from the box with the 'Maria da Graça' [Melo *et al.* 2009].

§ Samples studied in [Melo *et al.* 2008].

♦ Paint tubes belonged to the Portuguse artist Columbano Bordalo Pinheiro (1857-1929), the paint tubes are from the collection of the Museu Nacional de Arte Contemporânea do Chiado (Lisbon). The paint tubes were analysed at DCR-FCT, part of the characterization was published in [Silva *et al.* 2011].

### 2.3.2 Painting data and pre-processing step

Each painting was digitalized using **hyperspectral camera** in the range 400–720 nm, with a resolution step of 10 nm. The data for each painting can be represented in a matrix  $M \times N \times W$ , where  $M$  and  $N$  are the spatial resolution of the images and  $W$  represents the 33 values of reflectance over the spectral range (Fig.10). The samples used as reference materials (each sample was applied on a glass slide) were digitalized using the same set-up described above. For samples we calculated the average spectrum considering an area of 5x5 pixels. To improve the comparison between the reflectance spectra acquired from the painting and those present in the database it was used the first derivative. The **first derivative** allows us to point out the inflection point of the reflectance bands; that is usually an important feature in the interpretation of this type of spectra. Because spectra are acquired stepwise, usually they must be smoothed for the calculation of their derivatives. Various algorithms are available for this purpose; we selected the method of Savitzky and Golay [Savitzky and Golay 1964]. This method uses a least-squares methodology to fit a polynomial curve into a set of contiguous data points (usually from 13 to 31, in our case 9 points were used) and calculates the ordinate at the central value of the abscissa (wavelength).

Relating to the **elemental analysis**, each samples used as reference materials was analysed in three points. The number of points of analysis for a painting change depending on the number of colours and the dimension. In the paintings studied in this work were collected between 30-100 points for each painting. One of the main problems in combining hyperspectral and elemental analysis was that  $\mu$ -EDXRF is a local analysis; for this reason, it was necessary to define a strategy that allowed the extension of the results obtained by the analysis of a limited number of points over the entire painting surface. We thus created a matrix where the user introduces the elements detected by the  $\mu$ -EDXRF jointly with the **colour parameters** (CIEL\*a\*b\*). The colour parameters are calculated from the reflectance spectra (extracted by the hyperspectral image) in the same area of analysis<sup>17</sup>. The user introduces in an Excel file only the elements responsible for providing the colour of the pigment; this means that elements that could be related to the preparation layer or to the presence of fillers. Table 7 shows an example of the table produced by the user to introduce the data.

**Table 7.** Example of the Excel file used to introduce the chemical elements and the corresponding L\*a\*b\* values.

Point	Elements	L*	a*	b*
Am 1c	Cr	74,6	-3,22	53,7
Az 1a	Fe,S	25,7	6,89	-27,1
C1 a	Cr,Fe	54,5	13,6	49,2
...	...	...	...	...

<sup>17</sup> The colour parameter are calculated by the reflectance spectra assuming the CIE D65 illuminant and a 10° standard observer (CIE 1964) [Feller 2004]. More information in Appendix Part I Ap.III.

The elemental information is then organized in the following structure:

$$XRF_{el} = \{el_1, el_2, \dots, el_P\} \quad (9)$$

where  $P$  is the number of points where the analysis was performed and  $elp = \{sq_1, sq_2, sq_k\}$  is the list of the chemical elements detected on the painting. To extend the local chemical analysis introduced by the user to all the painting surface, we assume that pixels of the hyperspectral image with the same (CIELAB) values are made with the same material: the list of the elements detected for each point of analysis was considered valid for all the pixels of the image with close colorimetric data, following:

$$\exists_x \in XRF_{lab} : Lab_i \geq (x - c) \wedge Lab_i \leq (x + c) \quad (10)$$

where  $c$  is a constant that defines the interval of the colour margin. The selection of the value of  $c$  is a crucial step in the strategy proposed below. For this reason its value was selected based on experimental tests (Section 2.3.4). In addition, in the fragment image obtained at the end of the analysis all the areas in which the elemental analysis has not been done or where there is a mismatch between the colour of the pixels and the colorimetric values introduced by the user in the matrix, will be highlighted (*Not analysed* area in Section 2.3.3). In that way, the user can check and analyse what type of error was made. In the meantime these faulty areas will not be considered in the analysis of the pigment.

### 2.3.3 Pigment analysis

#### *Step 1: Area identification*

Figure 12 shows the diagram of the first step, in which the algorithm detects three areas: (1) called *Not analysed* area, corresponds to the pixels in which the X-ray fluorescence analysis was not performed (in pink in Fig.12). That selection avoids performing the classification based on incomplete analytical data. The area (2) called *Not Amadeo*, includes the area painted with pigments that are not included in the Amadeo database, that is, probably not the original areas (in violet in Fig.12). The area (3) includes the white and black pixels (in black and white in Fig.12).

To detect the white and black areas all the reflectance spectra of the hyperspectral image are compared with two reference spectra of white and black sample from the paint tubes: lead white and carbon black respectively. The comparison is performed using SAM, Spectral Angle Mapper (more details in Step 2). SAM computes the angle between the unknown spectra and the reference and then all the unknown pixels whose angle is lower than a threshold defined by the user are classified in agreement with the reference spectra (black or white); the others are considered unclassified, that is, coloured pixels. The threshold was defined experimentally by a parameter sweep; that is, the value of the threshold was adjusted by sweeping the parameter values through a user defined range. The tests are presented in

Section 2.3.5. All the pixels that do not belong to *Not Amadeo*, *Not analysed* and *black and white* areas will not be further classified. The other pixels (shown in grey in Fig. 11) will be analysed in Step 2.

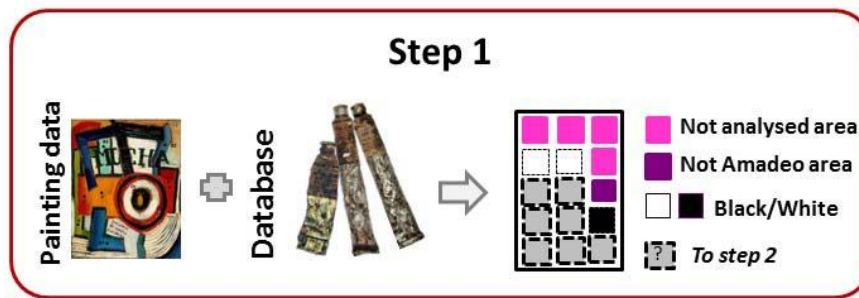


**Figure 12.** System overview of Step 1 where the areas are mapped that could not have been painted by Amadeo (violet) and those where the analysis was not performed (pink). The other pigments are considered unclassified and will be analysed in Step 2.

### Step 2: Pigment Identification

In this step (Fig. 13) and in the following, each pixel of the hyperspectral image will be classified according to its similarity with the spectra of a pigment that constitute the reference database or with a mixture of those. The similarity between the derivative of the unknown spectra and those present in the reference database is calculated using a combination of Spectral Angle Mapper (SAM) and Euclidian Minimum Distance (EMD) (Fig. 14).

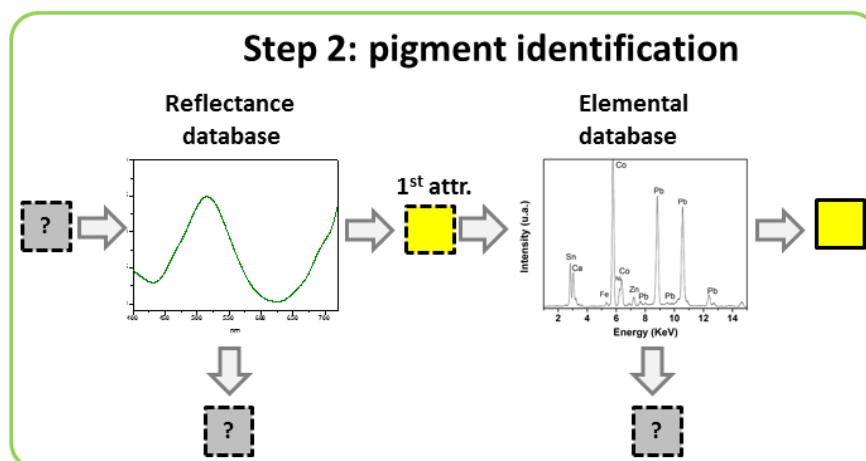


**Figure 13.** System overview of Step 2, where by comparing the reflectance spectra form the painting with those in the reference reflectance database we compute the first pigment attribution. This attribution can be confirmed if the elements detected in the paint area are consistent with those corresponding to the proposed pigment. If the attribution is not confirmed then the pixel is considered unclassified and goes to Step 3.

SAM and EMD are two of the most popular metrics used to compare reflectance spectra [Pelagotti *et al.* 2008]. In both cases, the spectrum is considered as a vector: EMD measures the distance between the two vectors (blue line in Fig. 14), while SAM considers the dimension of the angle between them. In

both cases, it is possible to impose a threshold to define the limit of similarity. It is important to take into account that SAM is insensitive to illumination changes because it uses only the vector direction and not the vector length [Pelagotti *et al.* 2008]. On the other hand, the sensitivity of EMD to illumination changes may provide an excessive number of clusters, thus making their interpretation quite difficult.

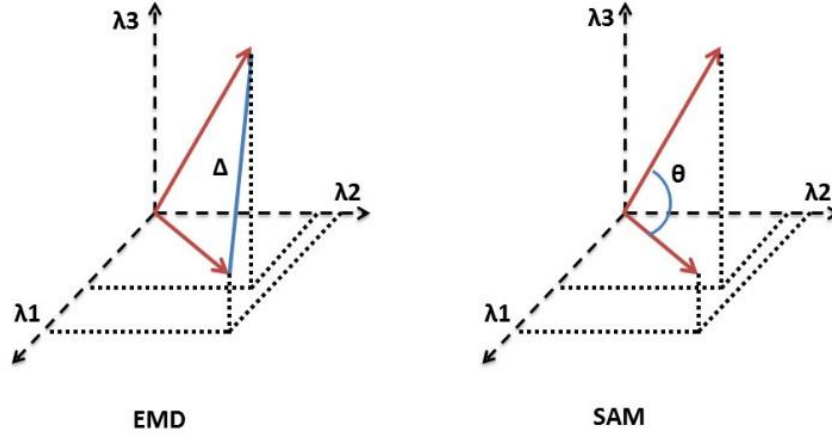


**Figure 14.** Representation of the measure of the distance between two vectors using Euclidian Minimum Distance (left) and Spectral Angle Mapper (right).

The combination of SAM and EMD is based on the method of matching proposed by Lowe [Lowe 2004]. The first step consists of calculating the angle  $\alpha$  between the spectrum of the pixel  $p$  of the HS image and the reflectance spectra for each reference material  $r$  present in the database:

$$\alpha_{p,r} = \cos^{-1} \left[ \frac{\sum_{i=1}^n R_{p,i} R_{r,i}}{\sqrt{\sum_{i=1}^n R_{p,i}^2 \sum_{i=1}^n R_{r,i}^2}} \right] \quad (11)$$

Where  $n$  is the number of values in the reflectance spectra (in our case 33);  $R_{r,i}$  is the value of the derivative of the reference spectrum  $r$  in the wavelength  $i$ . Then, we sort all the materials by ascending order; finally the pixel  $p$  is labelled according to material  $r_1$  if the angle  $\alpha_{p,r_1}$  is inferior to a percentage  $P_x$  of the second lower angle  $\alpha_{p,r_2}$ :

$$\alpha_{p,r_1} < P_x \alpha_{p,r_2} \quad (12)$$

The pixel is labelled according to the material whose spectrum is lower or equal to the threshold; otherwise, the pixel will be labelled as unclassified. For the pixels not classified by SAM, the similarity will be re-calculated using the Euclidean Minimum Distance, as described above:

$$EMD_{p,r} = \sqrt{\sum_{i=1}^n (R_{p,i} - R_{r,i})^2} \quad (13)$$



The first attribution based on the reflectance spectra will be confirmed by relying on elemental analysis performed on the painting. The algorithm compares the elements that characterize the pigment proposed (first attribution) with the elements detected by X-ray fluorescence in the corresponding area on the painting. If the hypothesis proposed is consistent, that is, if the element(s) detected on the painting are the same as the pigment proposed, then the pixel will be classified according to the given assignment; otherwise, if this condition is not satisfied, the pixel is defined unclassified and passes to Step 3.

### Step 3: Mixture Identification

In this step (Fig. 15), the algorithm classifies the pixels that belong to a mixture of pigments. Based on the elemental analysis performed on the painting, the algorithm makes a selection of pigments and calculates all the possible mixtures considering the following proportions: 100%:0%; 90%:10%; 80%:20%; 70%:30%; 60%:40%; and 50%:50%. For each mixture, hypothetical reflectance spectra of the mixture are computed as a linear sum of the spectra of the pigments. The mixture and their hypothetical reflectance spectra constitute a new database, which will be used to classify the pixels hitherto unclassified. The similarity between the spectra and the database of mixtures is calculated using SAM.

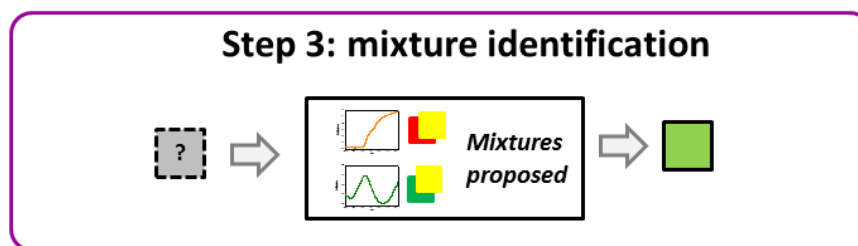


**Figure 15.** System overview of Step 3. The reflectance spectrum of the unknown pixels is compared with a set of spectra of mixtures.

#### 2.3.4 Image mapping

Based on the analysis performed on the three previously described steps, the system is able to associate one label to each pixel in the hyperspectral image. The possible labels are: black; white; *Not analysed* and *Not Amadeo*; one of the pigments presented in the database or one of the mixture made by the pigments presented in the database. The output of our system consists of an RGB image in which all the pixels within the same label are represented with the same colour. Therefore, the colours of the segmented image do not aim to reproduce the colours of the painting; the goal of the RGB image is to map the distribution of the different materials. The RGB colours used in the false colour image are selected as follows: the pixels labelled as black and white are represented by the corresponding RGB values (0 0 0 and 255 255 255); the *Not analysed* and *Not Amadeo* pixels can be represented with colours selected by the user. Colours are chosen that are easily recognizable and different from those present

in the painting. All those pixels labelled according to a pigment present in the database are represented by the RGB values calculated from the reflectance spectrum of the corresponding pigment. The same method is used in the case of mixtures of pigments.

In addition to the image, the system produces:

- A table that reports the pigments or mixtures and the percentage of the area they occupy considering the area of the painting analysed.
- The percentage value of the *Not Amadeo* and *Not analysed* areas.
- The user has the possibility of visualizing the mapping of the areas where the system detected the presence of specific pigments or specific mixtures of two or three pigments.
- The user can select a pixel and check which pigment(s) was detected in it.



**Figure 16.** **A** Selection of a pixel (291; 304) in the segmented image; **B** mapping of the areas where vermilion and chrome yellow were detected.

Through the coloured image the user can made a preliminary check of the answer proposed by the system. The user also has the possibility of selecting a specific pixel and of checking which pigments were detected in it (Fig.16A) or, can chose a pigment or a mixture (with a maximum 3 pigments) and visualize the distribution of these pigments in the painting (Fig.16B).

### 2.3.5 Setting up the parameters

In the system developed there are two parameters that may significantly influence the classification of the pixels of the hyperspectral image. The values for these parameters were chosen through tests presented below:

- (1) the value  $c$  in the pre-processing data, Equation (10);
- (2) the threshold ( $P_x$ ) for the SAM analysis used in Step 1, Equation (12).

(1) The parameter  $c$  (Equation 10) is used in the pre-processing step to extend the elemental analysis (EDXRF) to over all the surface of the painting, assuming the same elements for the pixels with close  $L^*a^*b^*$  values. The value  $c$  defines the interval of colour tolerance. Considering Equation 10, it is possible to write the colorimetric values of two candidate pixels as:

$$L_2^* = L_1^* + c ; a_2^* = a_1^* + c ; b_2^* = b_1^* + c$$

the difference ( $\Delta E$ ) between two colours in the  $L^*a^*b^*$  space is calculated as [Feller 2004]:

$$\Delta E = \sqrt{(L_2^* - L_1^*)^2 + (a_2^* - a_1^*)^2 + (b_2^* - b_1^*)^2} \quad (14)$$

To define the parameter  $c$  it was selected a set of pixels from the *Mucha* hyperspectral image; their  $L_1^*a_1^*b_1^*$  values were introduced in Equation (10); then 20 values of  $L_2^*a_2^*b_2^*$  it were calculated changing the parameter  $c$  in the range from 1 to 20. Figure 17 shows two examples of the tests performed, using two pixels from orange and blue areas; Figure 17 shows the mapping of the pixels that satisfied the Equation (10) changing the value  $c$  from 13 to 18. The percentage of the area mapped in each image and the corresponding  $\Delta E$  (calculated from Equation 14) is also presented. The value chosen for  $c$  was 14: that value allowed the selection of only the pixels with a colour very close to the test sample. The value was selected by comparing the mapping obtained using different coloured samples.

(2) In Step 1 the white and black areas are selected by comparing all the reflectance spectra of the hyperspectral image with two reference spectra of white and black from the paint tubes: lead white and carbon black, respectively. The comparison between the spectra is performed using SAM (Section 2.3.3). The threshold ( $P_x$ ) in Equation (12), used to define the similarity between the angles is crucial to avoid coloured pixels being classified as white or black and excluded from Steps 2 and 3. The threshold ( $P_x$ ) was adjusted by a sweeping parameter method: from 14 paintings of Amadeo we selected 122 areas of 3x3 or 5x5 pixels from known white, black and coloured areas. 61 of these areas were used as a training set; the value of the threshold was changed from 0.01 to 5 with a step of 0.01. The values that allowed the correct classification of larger number of white, black and coloured pixels were used in a set of 122 areas (test set) selected from the same paintings. The test was performed on 1722 pixels: 400 white; 425 black and the remaining coloured. The best threshold was 4: it allows a correct classification of 100% of the black and white areas and 87% of the coloured areas.

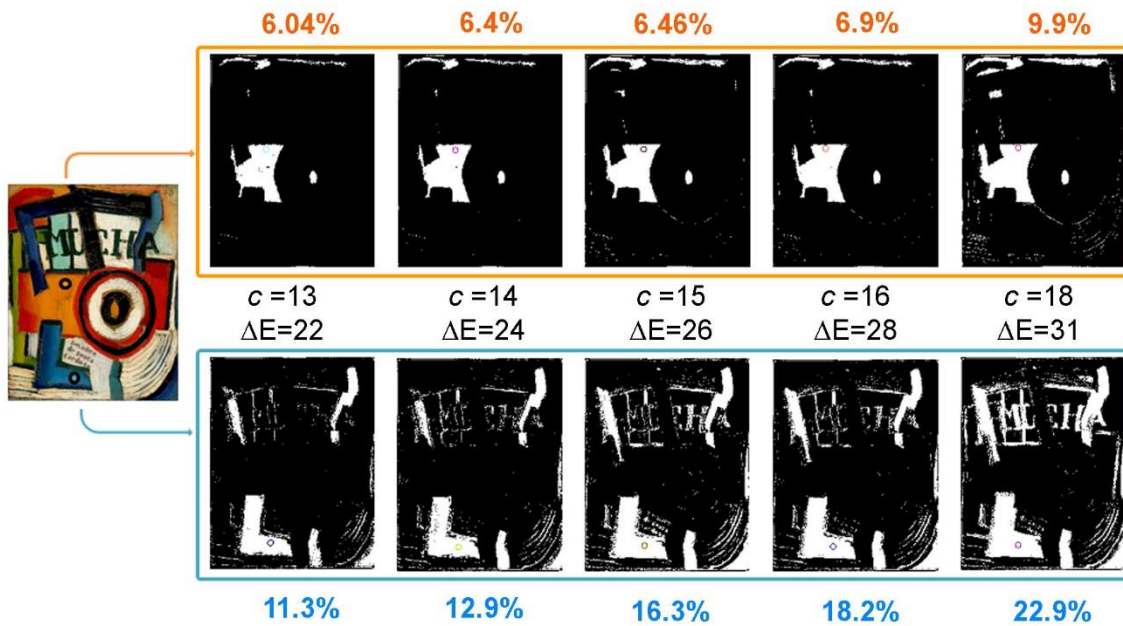


**Figure 17.** Tests performed to define the best values for the interval of colour tolerance ( $c$ ) in the pre-processing step. The two points (orange and blue), indicated in the coloured image of the painting *Mucha* (1915-16) were used as samples in the tests. In white are mapped the pixels that satisfied the Equation 10 considering the different values of  $C$  indicated close to the image. The  $\Delta E$  indicates the difference between the sample pixel and those mapped in white. The percentage indicates the portion of the area mapped in white.

### 2.3.6 Evaluation of the strategy proposed

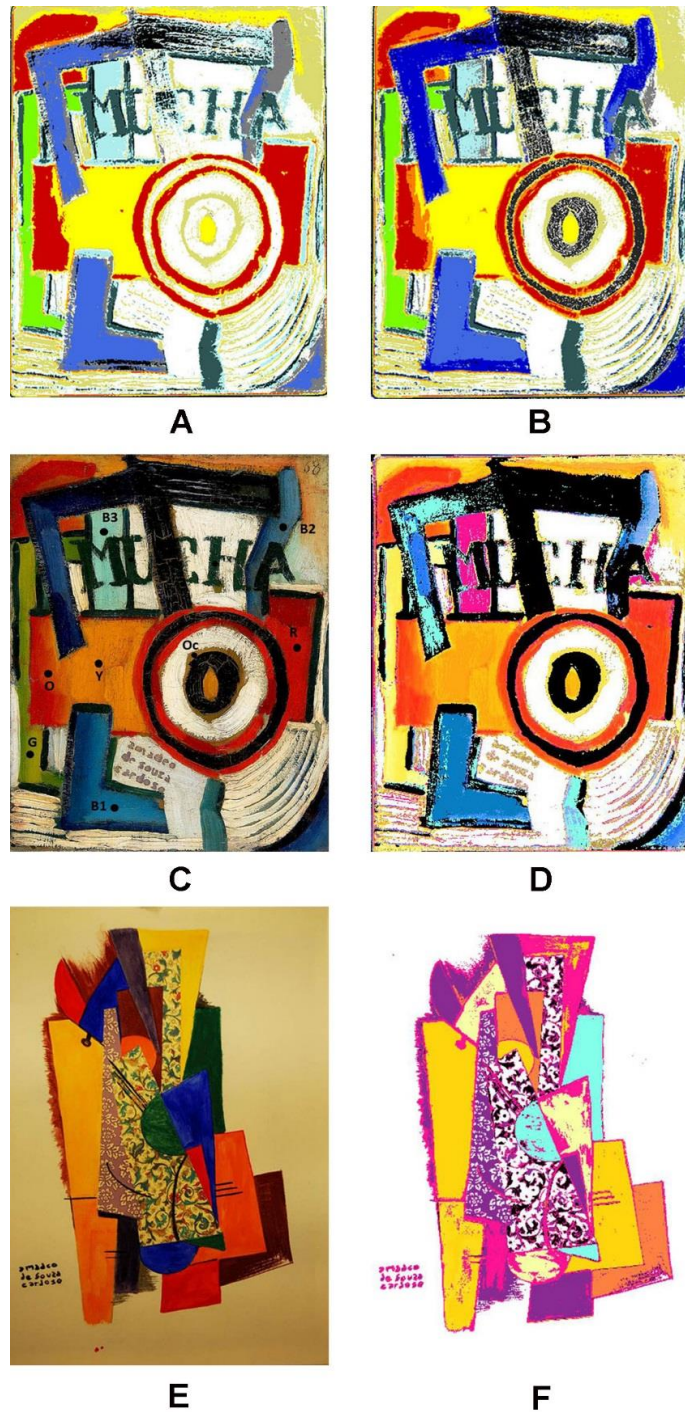
To evaluate the output made by the proposed system we used the analysis of Amadeo's painting *Mucha* (1915-16), the mapping obtained by our system was compared with those obtained using k-means cluster strategy (more information about k-means method in Appendix Part I Ap.I. The analysis of the reflectance spectra and the elemental data acquired in *Mucha* painting is presented in Appendix Part I Ap.IV). Along with this, will be presented the analysis of the false painting called *DCR* (2013). This second painting was prepared in our laboratory using both materials present in the Amadeo's palette and pigments introduced in to the market after the death of the artist.

Figure 18C shows the original RGB image of the *Mucha* paintings that was analysed using k-means clustering method (Figs 18A and B) and using our segmented method proposed in this chapter (Fig. 18D). With k-means clustering, SAM was used to calculate the spectra angle between each centroid of the clusters and the pixels of the images. All the angles calculated were sorted by ascending order. If the first and the second angles follow the condition in Equation (12) then, the pixel is included in the cluster corresponding to the first angle. The algorithm produces an image mapping in which all pixels that belong to the same cluster are visualized with the same RGB values. The RGB values are calculated from the reflectance spectra of the centroid of the cluster. Observing Figures 18A and B it is clear that the classification based on k-means is strongly influenced by the number of clusters chosen, 15 and 70 clusters, respectively. The image obtained using 70 clusters shows a region segmentation closer to the

original image when compared to that obtained using 15 clusters. This method performs a mapping of the pixels with similar reflectance spectra but it does not provide information about the pigments present in the painting. Comparing the segmented image calculated with our method (Fig. 18D) we can see that it is closer to the original by comparing with those obtained by the cluster analysis. It is important to remember that the RGB values used in our segmented image are computed starting from the reflectance spectra proposed by the classifier; in that way, the visual output is a simple and efficient way to evaluate the results obtained by the system and it is accessible for people with different background. We chose pink to colour the *Not Analysed* area and purple to colour the *Not Amadeo* area. Figures 18E and F are another example of the segmented image obtained by the analysis of a painting prepared in our laboratory, *DCR* (2013). In this case, by analysis of the materials a large area was detected corresponding to *Not Amadeo* (coloured in purple in Fig.18F). The percentage of the areas are presented in Table 8.

**Table 8.** Percentage of the coloured areas detected by pigment analysis on *Mucha* and *DCR* paintings.

<b>Area (%)</b>	<b><i>Mucha</i></b>	<b><i>DCR*</i></b>
Not Analysed	4.2	3.5
Not Amadeo	0.0	41.5
Amadeo	95.8	55



**Figure 18.** *Mucha* painting (1915-16) and DCR (2013) **C** and **E** RGB images of the paintings; k-means cluster analysis of *Mucha* using **A** 15 clusters; **B** 70 clusters; segmented image obtained with our system **D** *Mucha* **F** DCR, the *Not Analysed* is coloured in pink and the *Not Amadeo* in purple.

To evaluate the quality of the reflectance spectra proposed by the classifier for the analysis of *Mucha* we selected a few spectra and compared them with those acquired from the painting. More information on the results of the analysis of this painting are presented in Appendix Part I Ap.IV.



Figure 18C shows the point where it were collected the spectra presented in Figure 19. According to our analysis the yellow, orange and red shades (indicated in Fig.18C with the letters Y, O and R) were painted using different amount of chrome yellow ( $\text{PbCrO}_4$ ) mixed with vermilion ( $\text{HgS}$ ) (Fig. 19C and D). Figure 19C gives an example of reflectance spectrum measured in the area Y (solid line) and the spectrum proposed by our method (dashed line). Chrome yellow is also used in mixture with viridian ( $\text{Cr}_2\text{O}_3 \cdot \text{H}_2\text{O}$ ) to obtain the green tone of the area G (Figure 18C). The spectrum collected in the green area of the painting and that proposed by the system are show in Fig. 19B.

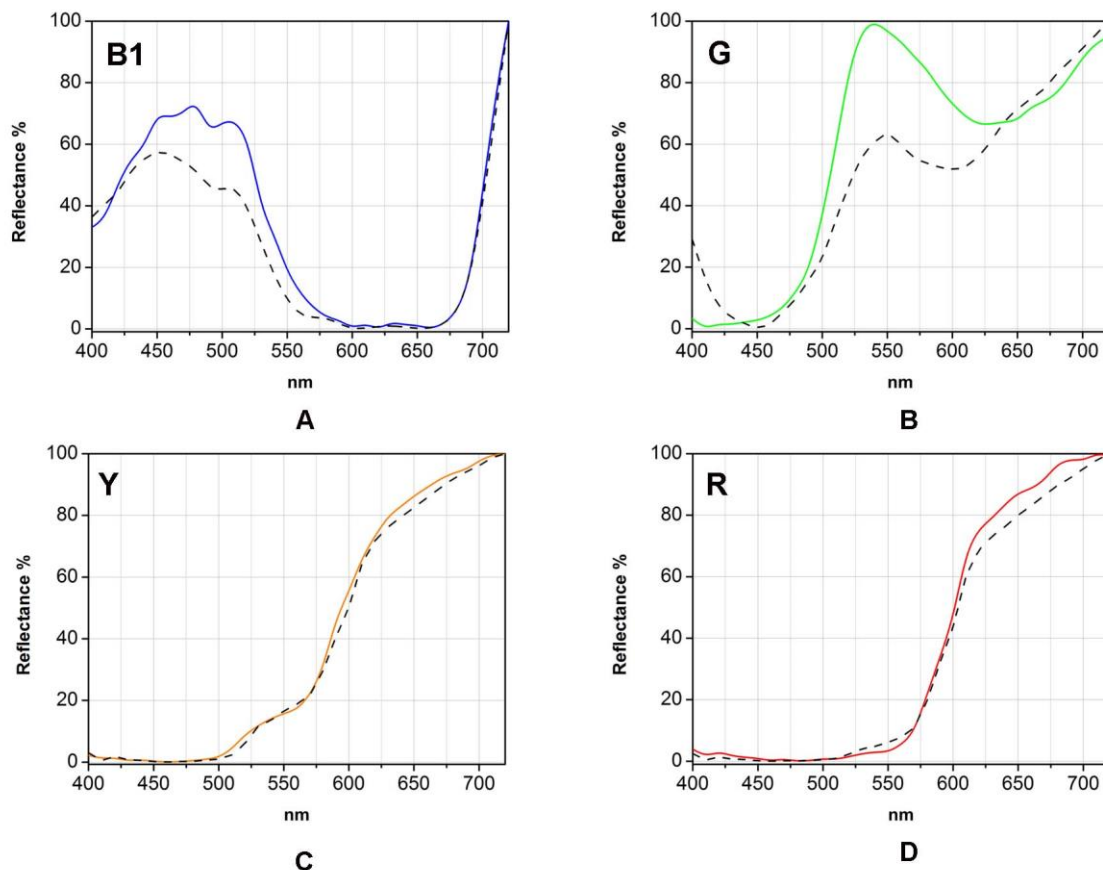


**Figure 19.** Comparison between the measured reflectance spectra on *Mucha* hyperspectral image (solid lines) and proposed by our system (dashed lines). The point of analysis are indicated in Figure 18C; **A** Cobalt blue pigment detected in area B1; **B** Mixture of viridian and chrome yellow detected in area G1; **C** Mixture of chrome yellow and vermilion detected in area Y; **D** Mixture of vermilion and chrome yellow detected in area R.

As described before the system developed combine the elemental and the molecular information acquired using EDXRF and reflectance spectroscopy (hyperspectral imaging), the combination of these two techniques overcomes the limitations of the two techniques when they are used alone. An example of limitation concern the discrimination of chrome yellow from viridian using EDXRF in our system. That limitation is related with the element that are introduced in the system; both of the pigments are characterized by the presence of Chromium (Cr). This sort of limitation in the use of the EDXRF data is overcomes by the analysis of the reflectance spectra: the spectral features of the two pigment are sufficient to obtain a correct identification.

The example of the analysis of the Blue area, B in Figure 18C, shows the opposite case: in this area the reflectance spectroscopy (Fig. 19A) indicated the presence of a cobalt based pigment, but it is not able to discriminate between cerulean blue ( $\text{CoO} \cdot n\text{SnO}_2$ ) and cobalt blue (CoO). The reflectance spectra of these two pigments are characterized by the presence of a broad reflectance band between 430-550 nm [Boselli 2010]. On the other hand the elemental analysis allows the discrimination of the two pigments thanks to the presence or to the absence of the tin element (Sn). In this case the elemental information guarantees a correct identification of the materials present in the blue area.

## 2.4 Features combination: results

The fusion data is computed using *SUM-Combination* technique (as shows in Equation 1):

$$I_a(Am) = \alpha p(B/Am) + (1 - \alpha)I_a(M/Am)$$

That is,  $I_a(Am)$  is a quantitative indicator for authenticity, the value range of the indicator is 0-1 where 0 is No Amadeo and 1 Amadeo. The indicator is obtained by a weighted sum of the brushstroke probability  $p(B/Am)$  and the quantitative indicator for molecular analysis  $I_a(M/Am)$ .

The probability based on the brushstroke analysis is calculated as follows:

$$p(B/Am) = \frac{1}{1 + e^{-Af(x)B}} \quad (14)$$

The function  $f(x)$  represents the discriminant function of the classifier: Regularized Least Squared Classifier (RLSC) expressed in Equation 7.

The *indicator of authenticity* based on molecular analysis is calculated considering the area where the system detected pigments coherent with the Amadeo's palette ( $Am$ ), considered proportionally with the full analysed area ( $1 - NotAn$ ):

$$I_a(M/Am) = Am * (1 - NotAn) \quad (15)$$

Where *NotAn* (*Not analysed*) is the percentage of the area where the elemental analysis was not performed. That means all the pixels of the hyperspectral image which do not satisfy Equation 10;  $Am$  (*Amadeo*) is the percentage of the area where the results obtained are consistent with those present in the database. In Equation 16 the percentage of area not analysed ( $NotAn$ ) has subtracted in the calculation of *indicator of authenticity* as no information can be extracted from it. Figure 20 shows the relation between the percentage of the analysed area, and the indicator of authenticity (expressed in %)



of the painting to be classified as authentic. Different curves were calculated considering different percentage of *Not Amadeo* area detected.

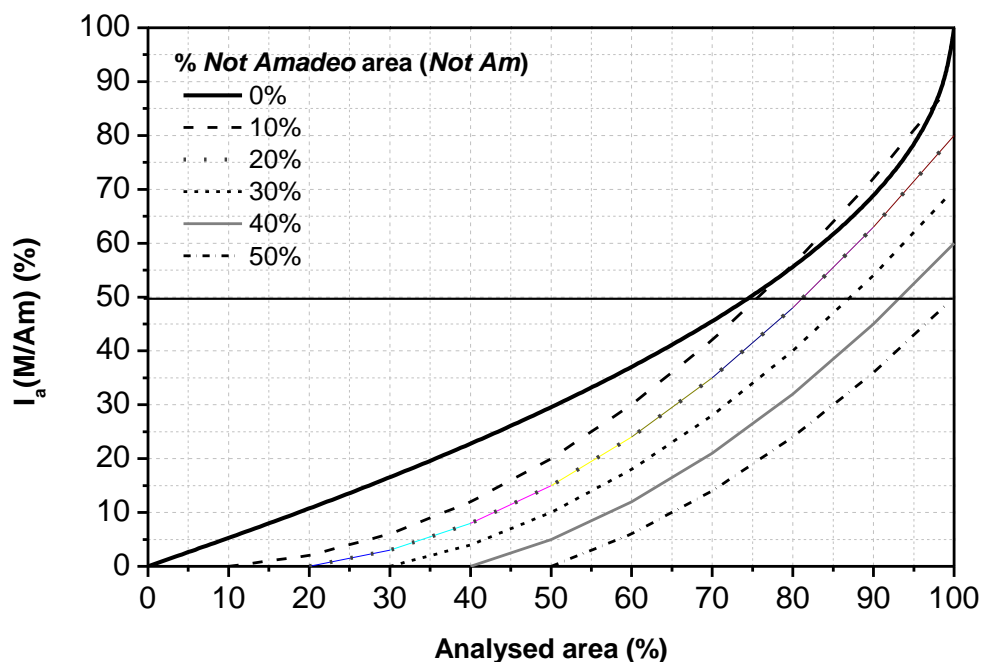


**Figure 20.** Relation between the percentage of the *Analysed area* and the *indicator of authenticity* for molecular analysis.

As shown in Figure 20, the relation between *Analysed area* and *Indicator of authenticity* is not linear. Considering the simplest case, where all the pigments found in the painting are consistent with Amadeo's palette (*Not Amadeo* area = 0%), to obtain an *Indicator of authenticity* higher than 50% it is necessary to analyse at least 75% of the area of the painting. The other curves represent cases in which the *Not Amadeo* percentage is higher than 0% (using steps of 10% from 10 to 50%). These curves show the influence of the *Not Amadeo* area in the analysis and which is the level of accuracy in the analysis necessary to achieve at least 50% of authenticity.

For a set of 12 paintings, shown in Figure 21, we calculated their *indicator of authenticity* of being painted by Amadeo considering the brushstroke analysis, the material information and through the fusion of the data from both. The first 11 paintings belong to Amadeo, while the last was made by the DCR-FCT as a deliberate falsification of a painting by Amadeo.

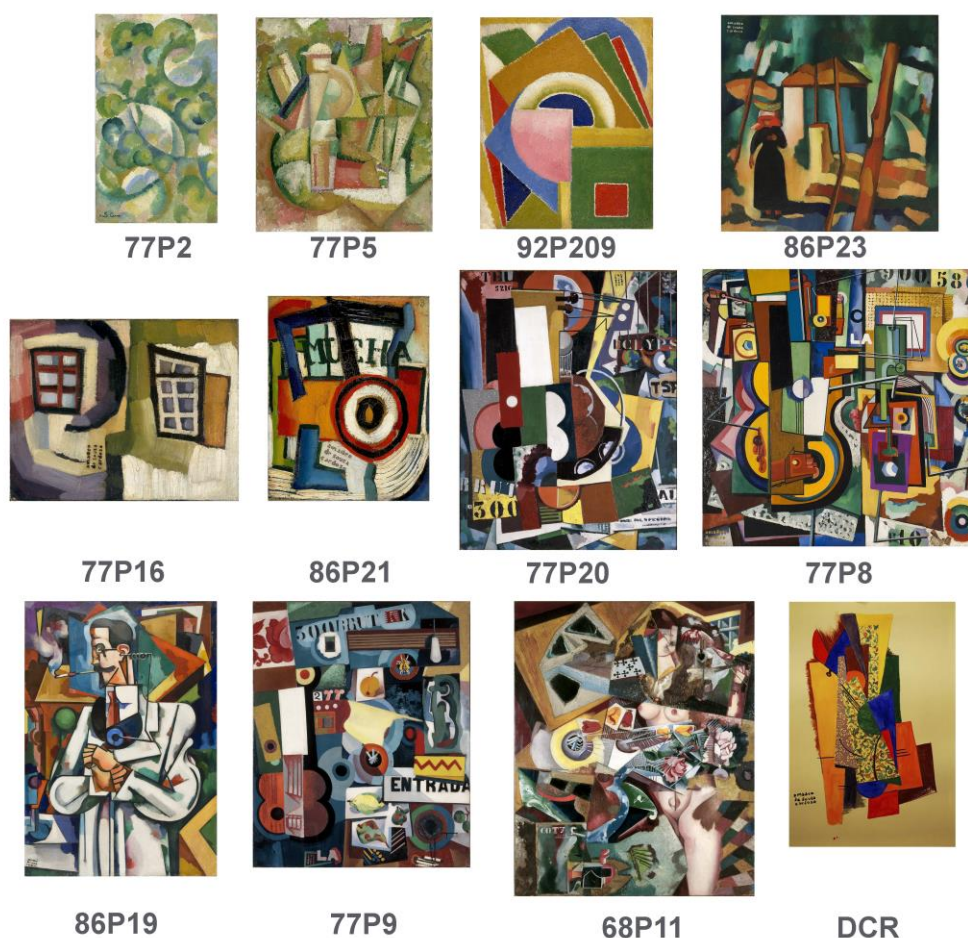


**Figure 21.** Paintings analysed by fusion data. The paintings of Amadeo de Souza-Cardoso belonging to the Centro de Arte Moderna, Fundação Calouste Gulbenkian [Freitas *et al.* 2008]. The painting DCR was made at DCR-FCT.

Table 9 shows the quantitative indicator for authenticity that each painting was made by Amadeo considering the brushstroke, the molecular analysis and with both (fusion data). The fusion data was calculated giving the same weight to for each analysis (Equation 1  $\alpha = 0.5$ ). The accuracy of the answer of the brushstroke analysis, calculated as in Equation (8) is 88% (94% true positive; 89% true negative and 20% false positive answers). Using the same formula to calculate the accuracy of the molecular analysis (Table 9) we obtain 100% of accuracy, considering the limited number of paintings analysed with this strategy, it seems more appropriate to report the percentage of the area correctly identified in the 11 original paintings of Amadeo---this value is 94%.

**Table 9.** Indicator of authenticity that the paintings were made by Amadeo, considering brushstroke and materials analysis separately, and joined together by the fusion data. The value range is 0-1 where 0 is *Not Amadeo* and 1 *Amadeo*.

#	Paintings	Brushstroke	Materials	Fusion data
1	77P2* <i>Quadro G</i>	0.8	0.99	<b>0.89</b>
2	77P5 <i>O jockey</i>	0.95	1	<b>0.97</b>
3	92P209 <i>Untitled</i>	0.98	0.97	<b>0.97</b>
4	86P23 <i>Paisagem, figura negra</i>	0.98	0.84	<b>0.91</b>
5	77P16 <i>Janellas do pescador</i>	0.99	1	<b>0.99</b>
6	<b>86P21 <i>Mucha</i></b>	<b>0.7</b>	0.91	<b>0.8</b>
7	<b>77P20 <i>Untitled (BRUT 300 TFS)</i></b>	<b>0.71</b>	1	<b>0.83</b>
8	<b>77P8 <i>Untitled</i></b>	<b>0.82</b>	0.99	<b>0.91</b>
9	<b>86P19 <i>Untitled (Medico)</i></b>	<b>0.73</b>	0.74	<b>0.73</b>
10	<b>77P9 <i>Untitled (Entrada)</i></b>	<b>0.35</b>	1	<b>0.67</b>
11	<b>68P11 <i>Untitled (Coty)</i></b>	<b>0.89</b>	0.91	<b>0.9</b>
12	<i>DCR painting</i>	0.42	0.49	<b>0.45</b>

\*the numbers refer to the inventory code at CAM [Freitas *et al.* 2008]

Considering the results of the materials and the fusion data analysis all the paintings were correctly classified, including the negative case study (12). Observing the results of the brushstroke analysis we can see that the paintings 6-9 and 11 show close values. This sort of cluster may be explain by the presence in composition of these paintings of similar elements. Moreover, the values of these paintings are also lower comparing with the paintings 1-5, in particular for the case of the painting 10 *Entrada*. This result may be related with the missing in the database of element such as the letters (see for example the word “ENTRADA” in the painting 10 and the word “MUCHA” in 6). Additionally it is possible that the letters are not well identified by SIFT because this algorithm is not considered apt for text analysis. To note that paintings between 7 and 11 are dated 1917 and are considered by art historians as a homogeneous nucleus, different from previous works. The analysis of their materials and techniques show a use of similar palate of pigments, moreover the paintings 7, 8, 10 and 11 are characterized for the presence of founded materials such as mirrors, glasses, and sand (See Part II Section 2.1.1). The painting 6 (*Mucha*) dated 1915, is not usually associated to the group of painting dated 1917, identified above, anyway the brushstroke analysis associates this painting with the number 7 and 9. To confirm the relation of *Mucha* with the other paintings it was performed a test in which 3 of the paintings dated 1917 (7, 10 and 11) were included in the training set. By introducing these paintings the brushstroke probability of *Mucha* increases to 0.91. This result confirm the influence of the selection of the images in the training set on the performance of the classifier and suggests a similarity between the brushstroke of *Mucha* and those of the paintings dated 1917.

## 2.5 Final remarks

The brushstroke strategy proposed which used a combination of Gabor filter and SIFT was able to discriminate between images of paintings of Amadeo (*positive* class) and paintings of other contemporaneous artists (*negative* class) with an accuracy higher than 90%; the classifier gave a correct answer for 133 of the 138 images of Amadeo's paintings tested (please see Table 4 Section 2.2.3). The use of Bag-of-Features model reduced the problems of the unbalance between the numbers of images included in each one of the class.

The system proposed to extract the molecular information using hyperspectral and elemental analysis provides reasonable results in terms of image mapping and in the detection of areas that could be no painted by Amadeo works as expected (please see Figure 18D). The image produced as output of the system is an easy way to confirm the results obtained. The performance of the system is influenced by: the number of points of  $\mu$ -EDXRF analysis and by the threshold ( $c$ ) used in the pre-processing to extend the elemental analysis over all the painting surface. In our work the same threshold was used for all of the paintings, this value was chosen empirically. In the future it would be useful to implement a method that defines a specific threshold for each painting. An alternative solution would be to run the elemental analysis using macro-XRF, which extend the examination over the whole surface of the painting.

The test performed on the 12 paintings using the data-fusion strategy demonstrated the usefulness of the integration of material analysis to solve a problem of a false negative obtained by the classifier using only the brushstroke analysis.

**PART II: MATERIALS AND TECHNIQUES OF  
AMADEO'S PAINTINGS DATED 1917**



## INTRODUCTION TO PART II

At the time of the edition of the Catalogue Raisonné of Amadeo de Souza-Cardoso [Freitas *et al.* 2008] 19 selected paintings were systematically studied<sup>1</sup> with the aim of defining the materials and techniques used by the artist. 18 of these paintings are dated between 1912 and 1916<sup>2</sup> (the other is dated 1917); all the paintings belong to the CAM's collection [Melo *et al.* 2008]. The selection of these paintings was made by the teams of the DCR-FCT and CAM led by Helena de Freitas. The selection privileged: paintings representing different periods of Amadeo's artistic production in the timeframe described above; paintings that had not been restored, and similar (in terms of dating and/or style) to the 5 doubtful paintings analyzed in the same mission [Melo *et al.* 2009]. The analysis of these paintings and the analysis of artist materials that belonged to Amadeo (31 samples from oil paint tubes conserved in the artist's Family house as well as the painter's palette from the CAM's collection) were the basis to define the palette of pigments representative of Amadeo's production between 1912 and 1916<sup>3</sup> [Melo *et al.* 2008; Melo *et al.* 2009]. It was decided to restrict the data of the pigment's palette to 1916, even if the painting *Untitled* (Inv. CAM 86P19, dated 1917) was analyzed. This decision is related to the fact that art historians consider the period between the end of 1916 and the end of 1917 as a homogeneous nucleus inside the career of Amadeo [França 1992; Silva 1995; Freitas 2008]. These nucleus of paintings were made in Portugal where Amadeo has been forced to remain due to the World War I. In Manhufe Amadeo found a sort of productive isolation that allowed him to create his most successful paintings [Silva 1995]. Due to the isolation that Amadeo experienced while in Portugal, to his difficulties in obtaining artists' materials in his homeland,<sup>4</sup> and also to the evident experimentation of materials<sup>5</sup> that he made in the last paintings, it was decided to dedicate a separate study for the paintings dated 1917.

Part II of this thesis presents the study on the materials and techniques of 4 **selected paintings of Amadeo dated 1917**; these paintings are untitled but 3 of them are known with the names *BRUT*, *Entrada* and *Coty*<sup>6</sup>. These paintings are characterized by the presence of founded objects such as glasses, mirror, sand and matches. The analysis of the pigments used in these paintings confirmed the palette defined for the period 1912-1916 [Melo *et al.* 2008] and included also some new elements such

---

<sup>1</sup> The analyses included investigation by images (X-ray; UV and IR images); observation of the paintings under microscope; in-situ elemental analysis by  $\mu$ -EDXRF; spectroscopic analysis of micro-samples by  $\mu$ -FTIR and  $\mu$ -Raman spectroscopy and HPLC analysis for the identification of organic dyes [Melo *et al.* 2009].

<sup>2</sup> Form the 18 paintings: 3 are dated between 1912 and 1913; 11 are dated between 1913 and 1914; 3 are dated between 1915 and 1916; 1 is undated.

<sup>3</sup>In the palette are included: cobalt blue ( $\text{CoO}\cdot\text{Al}_2\text{O}_3$ ); ultramarine blue ( $\text{Na}_8[\text{Al}_6\text{Si}_6\text{O}_{24}]\text{S}_n$ ); cerulean blue ( $\text{CoO}\cdot n\text{SnO}_2$ ); viridian ( $\text{Cr}_2\text{O}_3\cdot 2\text{H}_2\text{O}$ ); vermilion ( $\text{HgS}$ ); carmine lake (cochineal lake); chromium yellow ( $\text{PbCrO}_4$ ); cadmium yellow ( $\text{CdS}$ ); lead white ( $2\text{PbCO}_3\cdot\text{Pb}(\text{OH})_2$ ) and barium sulfate ( $\text{BaSO}_4$ ) [Melo *et al.* 2008].

<sup>4</sup> Amadeo in the letters to Robert Delaunay (dated January 9 and March 18 of 1916) referred about his difficult trip to Porto to buy artist materials, the letters are transcript by Ferreira in [Ferreira 1972, pgs. 97-98].

<sup>5</sup> An example of experimentation in term of materials is the inclusion it the paintings composition of founds materials.

<sup>6</sup> To simplify the text, in this thesis the 4 paintings are identified with the attributed name *BRUT* for the painting *Untitled*, (*BRUT 300 TSF*) Inv. 77P20; *Entrada* for the painting *Untitled*, (*Entrada*) Inv. 77P9; *Coty* for the painting *Untitled*, (*Coty*) Inv. 68P11 and *Untitled* for the painting *Untitled*, Inv. 77P8 [Freitas *et al.* 2008].

as the use of golden and silver tones (in *Entrada*, *Coty* and *Untitled*); these tones were detected only in *La Légend de St Julien L'Hospitalier* (the manuscript illustrated by Amadeo in 1912) but they were never found in his oil paintings. Moreover, it was found red organic dyes that belong to the  $\beta$ -naphthol class (in *Coty*) and cobalt yellow used alone and in mixture with chrome yellow (in *Coty* and *Untitled*). In *BRUT* and *Entrada* the hue violet was obtained by the mixture of blue pigment and a red lake. With respect to the palette defined for the period 1912-1916, these differences are localized in restricted areas of the paintings or in some cases to a specific painting. A relevant difference that was found in the pigments' palette of Amadeo before and after 1916 was the use of zinc white, alone and in mixture with the other pigments. In the paintings before 1916 the white used by Amadeo was lead white. Zinc white had already been found but in a small area in the painting the painting dated 1917 *Untitled* (Inv. 86P19) studied in 2008 [Melo *et al.* 2009]. In *BRUT* and *Entrada* zinc carboxylates were found associated with the use of this pigments.

In addition to the pigments characterization, it was performed a comparative study of the colorimetry properties of 24 selected paintings by Amadeo dated between 1911 and 1917. The paintings were digitized by hyperspectral imaging with the aim of comparing their colour properties. The number of discriminable colours and the colour distribution in the CIE(a\*b\*) colour space of the paintings dated 1917 show very close values, different from his previous paintings. This analysis, together with the pigments characterization, are now qualitative data that can support the art historians' thesis that this paintings should be considered as a nucleus; in the 4 paintings analysed Amadeo was developing a new research on the use of colour<sup>7</sup>. Moreover the analyses described above show a relation between the paintings *BRUT* and *Entrada* that seems also visible in the elements of the composition represented in the photograph (conserved at archive of the Art Library of the Calouste Gulbenkian Foundation Inv. ASC09/16). This is the photograph of a collage work made by Amadeo and that probably was a *maquette* for these paintings.

---

<sup>7</sup> Personal communication by Helena de Freitas.



## CHAPTER 1: AMADEO DE SOUZA-CARDOSO

In the Second Part of the thesis, the focus is on Amadeo's last artworks dated 1917. This chapter introduces the artist Amadeo de Souza-Cardoso (1887-1918), his works and the paintings dated 1917 that are analysed in detail in the next chapter. Chapter 1 presents: a short biographical account of Amadeo considering two periods (i) his experience in Paris from 1906 to 1914 and (ii) the period that Amadeo spent in Portugal between 1914 and 1918. The chapter also presents a description of the main characteristics of his painting techniques and the materials that he used; these information are based on the analysis of 19 paintings and a set of artist materials performed by DCR-FCT in 2008 [Melo *et al.* 2008; Melo *et al.* 2009]. In the second part of the chapter are introduced the paintings produced by Amadeo at the end of the Portuguese period (1917). Secondly, this chapter introduces the main problems of conservation that have been encountered in Amadeo's paintings dated 1917 (Section 1.2.)

### 1.1 Amadeo: an artist in his time

Amadeo was born in 1887 in Manhufe, near Amarante in Northern Portugal and died at the age of 30 years, in Espinho in 1918, a victim of the Spanish flu [Freitas 2008b]. The critical reception of Amadeo was uneven, in which the attention on this artist appeared and disappeared in accordance with the irregular rhythm of exhibitions [Freitas 2008c]. This could be also related with the absence in Portugal of a proper museum of contemporary art. Only in 1942 two paintings by Amadeo entered in The Museu Nacional de Arte Contemporânea do Chiado (National Museum of Contemporary Art - Museu do Chiado) collection [Freitas 2008c]

Amadeo was selected to be one of the artists to represent modern art by the Secretariado da Propaganda Nacional (SPN - the Portuguese regime's propaganda office of the *Estado Novo*<sup>8</sup>). The role of the SPN was to disseminate nationalist ideas and organize culture and the arts. In 1935, the SPN created the Amadeo de Souza-Cardoso Prize; in 1958 and 1959, a series of exhibitions were organized in Paris, Lisbon and Porto. The first monograph dedicated to the artist was written by José Augusto França in 1956 [França 1956]. In his work, França made for the first time made an analysis of Amadeo's artworks.

A number of documents related to Amadeo, including a collection of photographs, was donated by his widow, Lucie Cardoso, and his friend Paulo Ferreira at the end of the 1980s to the Calouste Gulbenkian Foundation (FCG). The Center of Modern Art (CAM)<sup>9</sup> -- conserves 200 of Amadeo's artworks including 63<sup>10</sup> paintings; 136 drawings and watercolours and 1 illustrated manuscript. The FCG developed an important role in the promotion and preservation of Amadeo's work. In 1987, the centenary of the birth

---

<sup>8</sup> *Estado Novo* (New State) was the dictatorial regime that ruled Portugal during 1933 and 1974.

<sup>9</sup> CAM was created in the 1983.

<sup>10</sup> There are 201 paintings included in the Catalogue Raisonné of Amadeo de Souza-Cardoso.

of Amadeo, the CAM presented his major retrospective. More recently, in 2006, CAM organized an exhibition entitled *Amadeo de Souza-Cardoso. Avant-Garde Dialogues*. The aim of the exhibition, curated by Helena de Freitas, was to establish a reunion between the works of Amadeo and the works of international contemporary artists, inside and outside of his circle of friends, which had an influence on his career.

The research developed for the exhibition *Amadeo de Souza-Cardoso. Avant-Garde Dialogues*, presented in the catalogue of the exhibition [Freitas *et al.* 2006], enabled significant progress in the recognition of Amadeo relations with the international culture of his time. The Portuguese origins of Amadeo and his European experience have been well described by different generations of artists and critics. The first one was the Portuguese painter José de Almada Negreiros; in 1916, during the exhibition of Amadeo in Lisbon, Negreiros defined Amadeo as *Portugal's first discovery in 20<sup>th</sup> Century Europe* [França 1992]. José Augusto França and José Escada underlined the desirable international relevance of this artist, França described him as *reluctant Portuguese*, while Escada excluded the nationalism aspect by defining him as a *European painter* [Freitas 2008b].

The Gulbenkian Foundation promoted the edition of the Catalogue Raisonné of Amadeo, which was published in two volumes: the first one is a photo-biography of the artist [Freitas *et al.* 2007] and the second is the catalogue of his painted artworks [Freitas *et al.* 2008]. A Catalogue Raisonné of his drawings has not been published as yet.

### 1.1.1 Paris (1906-1914)

In 1906, Amadeo left Portugal for Paris to study architecture. Very quickly, however, he became more interested in the *emerging artistic energies irradiation from the city* [Freitas 2008b] and left his studies. At the time Paris offered the best of contemporary art; Amadeo had the opportunity to visit the most important exhibition, such as Cézanne's retrospective at the *Salon d'Automne* (1907).

The caricature was, probably, the way by which Amadeo approached the art world; he started this practice in Portugal in 1905 and continued it until about 1910. Out of his original country, Amadeo made close friendships with several Portuguese artists, including Thomaz Costa, Francis Smith, Acacio Lino, Alberto Nunes Cardoso, and Eduardo Viana [Alfaro 2007] (Fig.1). Very soon, he widened his circle of friends. His friendship with Italian artist Amedeo Modigliani was well-known. Modigliani had also arrived in Paris in 1906; in 1911, the two artists organized an exhibition at Cardoso's studio in Paris. Picasso, Guillaume Apollinaire, Max Jacob and Ortiz de Zárate were invited to the event [Freitas 2008b]. The contact with Russian culture was very influential for Amadeo's artistic production. It is known that Amadeo saw the first performance of Serge Diaghilev's *Ballets Russes* and that the Russian artists Zadkine, Archipenko and Sonia Delaunay entered also in his circle of friends. According to Ferreira [Ferreira and Pernes 1972], in 1911 Amadeo appeared at the home of Robert and Sonia Delaunay in

Paris to present his works. From that moment, the Delaunay and Amadeo started a friendship and collaborations that continued even after his return to Portugal in 1914 due to the First World War (see the following sub-section).



**Figure 1.** Alexandre Ferraz de Andrade, Lucie e Amadeo (seated), Brussels 1910. Image from Alfaro 2007, pg 118.

The years 1911 and 1912 were the most productive years for Amadeo both for exhibition and for the artwork he produced. Amadeo presented at the most significant salons of the time: the *Salon des Indépendants*, in the editions of 1911 and 1912, and the *Salon d'Automne* in 1912; in the same year, he produced an exhibition in the *Der Sturm* Gallery in Berlin. Also in 1912, he was invited to the first exhibition of Modern Art in the United States; the year after, thanks to the help of the American painter and art critic Walter Pach, Amadeo sent eight paintings to the *Armory Show* in New York. The relationship with Pach was very important for Amadeo, in particular during the last years of his life. *The XX Dessins* album of drawings and *La Légende de St Julien L'Hospitalier* (Fig. 2) are two unusual artworks that Amadeo produced in 1912. *La Légende*, produced during Amadeo's holiday in Brittany [Freitas 2008b], is the illustrated manuscript version of Gustave Flaubert's book; in this work his reference to medieval art is quite evident.



**Figure 2.** *La Légende de St Julien L'Hospitalier*, illustrated manuscript version of Gustave Flaubert's book, 1912. Collection of Centro de Arte Moderna, Fundação Calouste Gulbenkian (Inv.DP1822) [Freitas et al. 2008 pg. 208].

### 1.1.2 Back to Portugal (1914-18)

In July of 1914, Amadeo and Lucie left Paris travel to Rocamadour in the south-west of France, and from there to London and subsequently to Barcelona. At the *Salon of the Allied Artist's Association* (London) Amadeo presented the paintings *Le Jardinier*, *Musiciens de Nuit*, *Les Oeillets* which received enthusiastic reviews [Alfaro 2008]. In Barcelona, Amadeo and Lucie joined their friend Leon Solá [Alfaro 2006] who introduced Amadeo to the architect Antoni Gaudí. Then their travel continued to Porto (north of Portugal); while there the war between France and German was declared of the (August 3); this forced Amadeo and Lucie to stay in Portugal more time than they desired [Alfaro 2006]. In 1915 Sonia and Robert Delaunay arrived at Vila do Conde, in the north of Portugal [Freitas 2008b]. During the time spent in Portugal, the couple developed an artistic project on the light and on the local culture features as pottery, traditional dolls in textile [Alfaro 2006]. They created the *Corporation Nouvelle* which also involved Portuguese artists Almada Negreiros, Eduardo Viana, José Pacheco and also Amadeo, as well as poets the Guillaume Apollinaire and Blaise Cendrars. The relation between Sonia and Robert Delaunay with Portuguese artists is well documented in the works of Paulo Ferreira [Ferreira and Pernes 1972] and in the book of correspondence between this group of artists<sup>11</sup> [Ferreira 1972]. One of the projects of the *Corporation Nouvelle* was the edition of an album produced with *pochoir* (stencil). According to the correspondence between Amadeo and the Delaunays, Amadeo declared his disinterest in the *pochoir* technique, considering himself absolutely mediocre in the use of gouache, pigmented wax also. Despite his initial rejection, Amadeo worked on the album's project and started to use the *pochoir* to sign his oil paintings [Alfaro 2006]. The projects of the *Corporation Nouvelle* as well as the ambitious project for the second exhibition in New York were not successful: *America is our great market [...] if*

<sup>11</sup> Correspondence of Almada-Negreiros, José Pacheco, Amadeo de Souza-Cardoso, Eduardo Vianna, Robert and Sonia Delaunay.

*the war had not started I could have achieved [...] one of my dreams: to exhibit one of my paintings on board of a large transatlantic-including the return trip. How beautiful that would be!*<sup>12</sup>

Amadeo showed his works in Portugal for the first time in 1916, in Porto (November) and in Lisbon (December). Before the exhibition in Porto Amadeo published an album entitled *12 Reproductions* to promote his works; the album included a flyer where he announces the cities of the future exhibitions: Munich, Paris, Berlin, London, Colonia, Hamburg, New York and Chicago. The exhibition in Porto was entitled *Exposição de Pintura (Abstraccionismo) Amadeo de Souza Cardoso* [Alfaro 2007, pg.238], Amadeo described to Walter Pach the exhibition with these words: *over thirty thousand people visited the exhibition, it was the first exhibition of modern painting in Portugal. People were overwhelmed by this new expression of art, by the new techniques and process*<sup>13</sup>. This exhibition surprised the visitors and local media and promoted controversial reactions. Amadeo was also physically assaulted [Alfaro 2007, pg. 243]. The second exhibition was in Lisbon at the Liga Naval's Palace; the Portuguese newspaper *A Nação* defined the exhibition in Lisbon as *an excellent exhibition of abstractionist painting [...] The exhibition was indeed an event in our tiny art world, not only due to the quality of the people from our social elite that visited it, but also because of the number of painting that were bought*<sup>14</sup>.

Despite these results in Portugal, Amadeo waited anxiously to return to Paris, in a letter that he sent to Sonia Delaunay he imagines the streets of Paris through postcards sent by Eduardo Viana: *I do from time to time my trip to Paris, the Galleries Lafayette and get some provisions, while our brave soldiers fighting gloriously*<sup>15</sup>. At the end of 1916, everything seemed ready and Amadeo wrote to Walter Pach: *send the cards to Portugal, where I will be until the 1st January. [...] But after that I will be in Paris, I am planning to leave at the latest on January 3 - the latest! Or even before Christmas* [Freitas 2008b]. Unfortunately he could not embark into this trip, as he died in October 1918 victim of the Spanish flu pandemic.

---

<sup>12</sup> "A América é o nosso grande Mercado [...] se a guerra não houvesse estalado teria eu conseguido, [...] realizar um dos meus sonhos: fazer uma exposição de um mês dos meus quadros a bordo de um grande transatlântico - na viagem de ida e de regresso. Como isso seria bello!" Amadeo's interview to the newspaper *O Dia*, 4 December 1916 [Freitas 2008b].

<sup>13</sup> "Mais de 30 mil pessoas visitaram a exposição, que causou um grande ruído, foi a primeira grande exposição de pintura moderna em Portugal. As pessoas ficaram abismadas pela nova expressão da arte, pelas técnicas e processo novos." Letter of Amadeo to Walter Pach, November 1916 [Alfaro 2007, pg 243]

<sup>14</sup> *A Nação*, December 19, 1916 [Alfaro 2006, pg. 487].

<sup>15</sup> "Je travaille et reçois des cartes postales de Vianna, et ça me fait rappeler l'élémi et le petit pharmacien. Je fais de temps en temps mon voyage d'agrément à Paris ; aux Galleries Lafayette je fais quelques provisions - pendant que nos braves soldats se battent glorieusement..." Letter to Sonia Delaunay 19 May 1916 [Ferreira 1972, pgs 134-135].



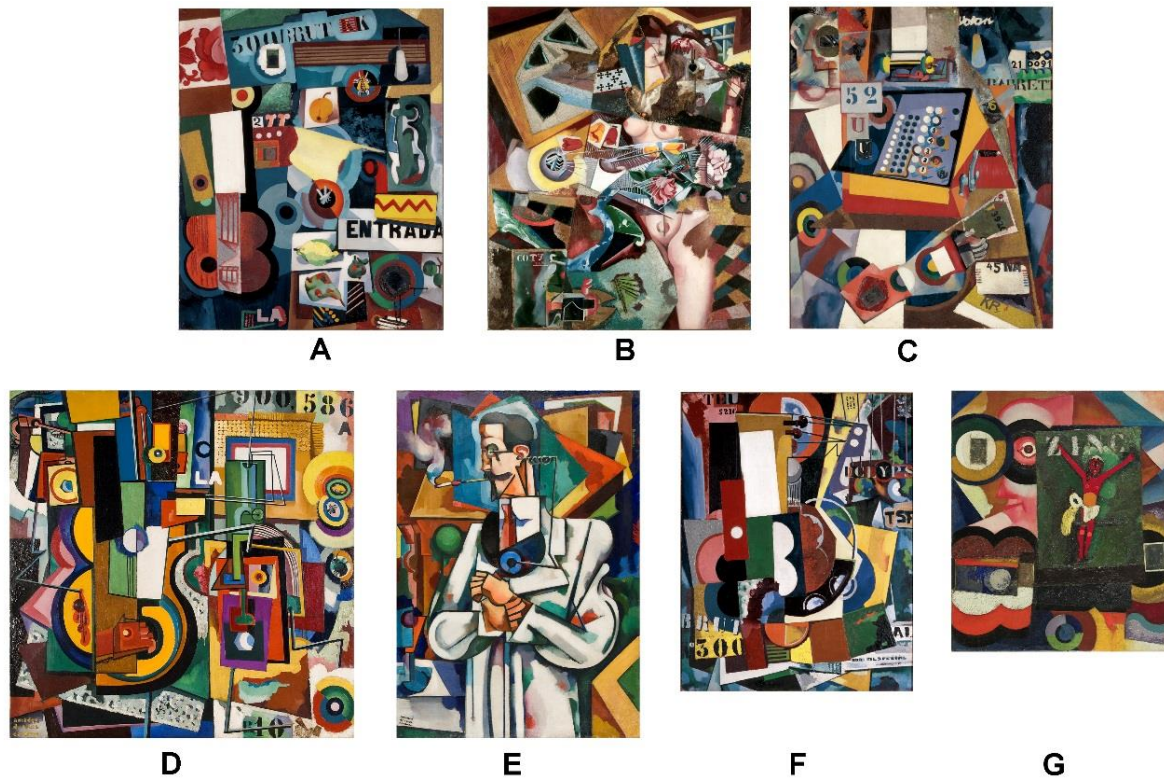


**Figure 3.** Paintings of Amadeo de Souza-Cardoso dated 1917. Collection of Centro de Arte Moderna, Fundação Calouste Gulbenkian. **A** *Untitled (Entrada)*, 93 x 76 cm. Collection of CAM (Inv. 77P9); **B** *Untitled (Coty)*, 93 x 76 cm. Collection of CAM (Inv. 68P11); **C** *Untitled (Máquina registadora - Cash Register)* (P198), 93 x 76 cm. Collection of CAM (Inv. 68P10); **D** *Untitled*, 93.5 x 93.5 cm. Collection of CAM (Inv. 77P8); **E** *Untitled*, 100 x 70.3 cm. Collection of CAM (Inv. 86P19); **F** *Untitled (BRUT 300 TSF)*, 85.8 x 66.2 cm. Collection of CAM (Inv. 77P20) and **G** *Untitled (Zinc)*, Private collection. [Freitas *et al.* 2008, pgs. 355, 356, 358, 360, 362, 364, 367, 355].

Art historians have recognized the paintings realized in 1917 as the most successful of his career: *in Manhufe Amadeo come back to the productive isolation, he perform his most qualified paintings* [Silva 1995]. In Portugal Amadeo developed an increasingly profound and complex pictorial research [Freitas 2008b]. According to França, between 1916 and 1917, Amadeo painted at least 6 or 7 untitled paintings<sup>16</sup>, three of these with the same dimensions (93x76 cm) that form a homogenous nucleus (Fig.3 A, B and C) [França 1992]. In these three paintings we find figure elements already present in previous works, such as violins and lithographic letters and numbers. França has suggested that Amadeo realized these group of artworks after the paintings reproduced on the album *12 Reproductions* of 1916 and before the publication of the Futurist Portugal manifest (late 1917) [França 1992]. The images of paintings indicated by França as the last works of Amadeo are reported in Figure 3; paintings A, B and C are the three works with the same dimension. The materials and the techniques of the paintings A, B, D and E have been studied in this thesis. The painting in Figure 3E was already studied at the Conservation and Restoration Department in 2008 [Melo *et al.* 2008].

<sup>16</sup> For more information about the art of Amadeo between 1915 and 1917 [França 1986].

### 1.1.3 Looking at Amadeo's paintings

The materials and the techniques of Amadeo<sup>17</sup> all within in the context of modern art of the twentieth century. Amadeo himself defined his art as far from the academism and in general not classifiable: *I do not follow any school. The schools died. [...] I'm an impressionist, cubist, futurist, or abstractionist? A bit of everything*<sup>18</sup>. The palette used by Amadeo (Fig.4) is characterized by the presence of traditional pigments, such as lead white<sup>19</sup>, vermilion red and Cochineal lake and the brown tones of the ochres (iron and manganese oxide), with new colours introduced in the XIX century artist's palette. *I'm currently studying the wonderful technique from the ancient monk painters, which I adapted to modern chemistry, because the ancients did not know for example the colours cedenio [Selenium?<sup>20</sup>], which are wonderful, and the emerald green, [...]. Their techniques adapted to modern chemistry can be used today!*"<sup>21</sup> In these words we can appreciate the passion for experimentation and for the relation between antiquity and modernity expressed by the artist. Amadeo introduced in his palette pigments discovered by inorganic chemistry at the time, and that had quickly entered as material for artists. As we will see, he essentially used inorganic pigments of chromium, cadmium, cobalt, copper and arsenic.

During the edition of the Catalogue Raisonné the team of the DCR that worked in collaboration with Helena de Freitas analysed a group of materials that belong to Amadeo. In the Amadeo's house in Manhufe were found three boxes containing artist materials that should be used by Amadeo. The box n° 1 show the inscription "Amadeo Cardoso" and contained 60 crayons<sup>22</sup>; the box n°2 with the inscription "Amadeo" and contained 21 oil paint tubes, the box n°3 with the inscription "Maria da Graça 34" contained 18 oil paint tubes. The paint tubes were from French Lefranc and Bourgeois and the English Winsor & Newton (W&N) [Melo *et al.* 2009]. Thanks to the analysis of the labels and the shape of the tubes, W&N identified these paint tubes as earlier than 1914<sup>23</sup> [Melo *et al.* 2008; Melo *et al.* 2008]. Figure 4 shows four of the 39 paint tubes.

---

<sup>17</sup> Data based on the study of 18 painting between 1913 and 1916 and 1 painting dated 1917; a palette and 31 paint tubes belonging to him [Melo *et al.* 2008; Melo *et al.* 2009].

<sup>18</sup> Amadeo's interview to the journal *O Dia* (1916) [Alfaro 2006].

<sup>19</sup> Lead white is used alone or mixed with barium sulphate. The use of the zinc white is localized in a small detail of the painting *Untitled* (86P19) in 1917.

<sup>20</sup> It is possible that the term cedenio is a typing error. The term Selénio (Selenium in English) was already present in a Portuguese dictionary in 1898 [Almeida 1898, p.1834] "Selénio, chim. Corpo simples, metálico, avermelhado, muito friável." ("Selenium, chem. Simple body metallic red, very friable.")

<sup>21</sup> "Eu estou até atualmente estudando a técnica maravilhosa dos antigos frades pintores, que, adaptada à química moderna, porque os antigos não conheciam por exemplo as cores de cedénio, que são maravilhosas, e o verde esmeralde, que nem sequer se encontra nos verdes profusos do Grego, que, adaptada à química moderna, repito, se pode usar hoje" Amadeo's interview to the journal *O Jornal de Coimbra* (1916) [Ferreira and Ribeiro 1987].

<sup>22</sup> The crayons were not analysed.

<sup>23</sup> Information provided by Jessica Montgomery, of Winsor & Newton [Melo *et al.* 2008].



**Figure 4.** Four of the oil paint tubes analysed by DCR in 2008. From left to right: red carmine (Bourgeois); viridian (Lefranc), chrome yellow (Lefranc) and vermilion (Winsor & Newton) [Melo *et al.* 2008]

From the 39 oil paint tubes, it was possible to collect samples from 31 tubes; the samples were analysed by  $\mu$ -EDXRF,  $\mu$ -FTIR,  $\mu$ -Raman and HPLC was used for the organic dyes. In Appendix Part II Ap. VIII the transcription of the 31 labels from the oil paint tubes analysed from the box n°2 and n°3, for more details please see Melo *et al.* 2008. The results of the analysis of the tube samples were compared with the analysis of 19 selected paintings representative of the Amadeo's production between 1912 and 1917 (Fig. 6A and 6B). This comparison shows that these tubes are representative of the materials used by the artist. Considering that at the time of the Catalogue Raisonné it was studied only one painting dated 1917 (CAM Inv. 86P19), the palette of pigments presented in Figure 5 should be considered valid for the period 1912-1916. Moreover, the information acquired on the paintings and the paint tubes was compared with those found on five doubt paintings attributed to Amadeo [Melo *et al.* 2009]. Three of these paintings resulted forged [Melo *et al.* 2009], while two are presented as Case Studies at the end of the Catalogue Raisonné, because technical analysis and the art historian investigation were not able to prove the authorship of these paintings [Freitas *et al.* 2008].

Cobalt blue, is the most common blue in Amadeo's paintings; it is used pure and in mixture with ultramarine. Amadeo made a limited use of the purple tones that were usually obtained with Cobalt violet pigment. Viridian can be considered as the green of Amadeo; it is used pure or mixed with chrome yellow to obtain the light tones, or with Prussian blue for the dark green tones; emerald green is less common. The chemical element chromium was discovered in 1797 by Vauquelin and thanks to its synthesis of lead chromate (1809) the artists enjoyed not only a brilliant yellow but also variance of orange and reddish hues [Schaefer *et al.* 2008]. Amadeo used chrome yellow to achieve a specific hue; this pigment is present in many mixtures, with viridian, with vermilion and with the ochre. The presence of cadmium in the yellow and orange tones is limited. Finally, the use of a pure black pigment, such



carbon black, is less frequent in the paintings of Amadeo. To obtain the black tones Amadeo used mixtures of viridian, vermilion, ultramarine and Prussian blue.



**Figure 5.** The pigment palette of Amadeo between 1912 and 1916, with details from his paintings. Image adapted from Melo *et al.* 2008.

For his oil paintings Amadeo chose two types of support: cardboard and canvas. Figures 6A and B show the paintings analysed [Melo *et al.* 2008] divided according to their support. Unlike the canvas paintings, which always present a preparation layer<sup>24</sup> (usually thin, made of gypsum, lead white and barium sulphate), the artworks on cardboard may or may not present this layer; when it exists, the layer is a commercial preparation of lead white. In the cardboard works without preparation layer the colour of the support itself is used as a colour in the composition.

The infrared image technique allows us to see that Amadeo sketched a few lines to organize the space of his paintings (Fig. 7D). The absence of *pentimenti* is also remarkable as well as the absence of overlapping between the figures of the composition; this becomes evident by using an X-ray image technique (Fig. 7B). All these features may be achieved only with a precise planning of the painting before its execution [Melo *et al.* 2008].

<sup>24</sup> The role of the preparation layer is to create a proper surface to be paint. The untreated canvas is absorbent and has a texture, the excessive absorption of the canvas may promote the extraction of the binder from the paint, as consequence of that the painting surface appears very mat with and in some case it may induce poor paint adhesion [Kirby 2011]. To reduce the absorbency of the canvas usually it is also apply a layer, called sizing, in general prepared with a solution of glue, between the canvas and the preparation layer.

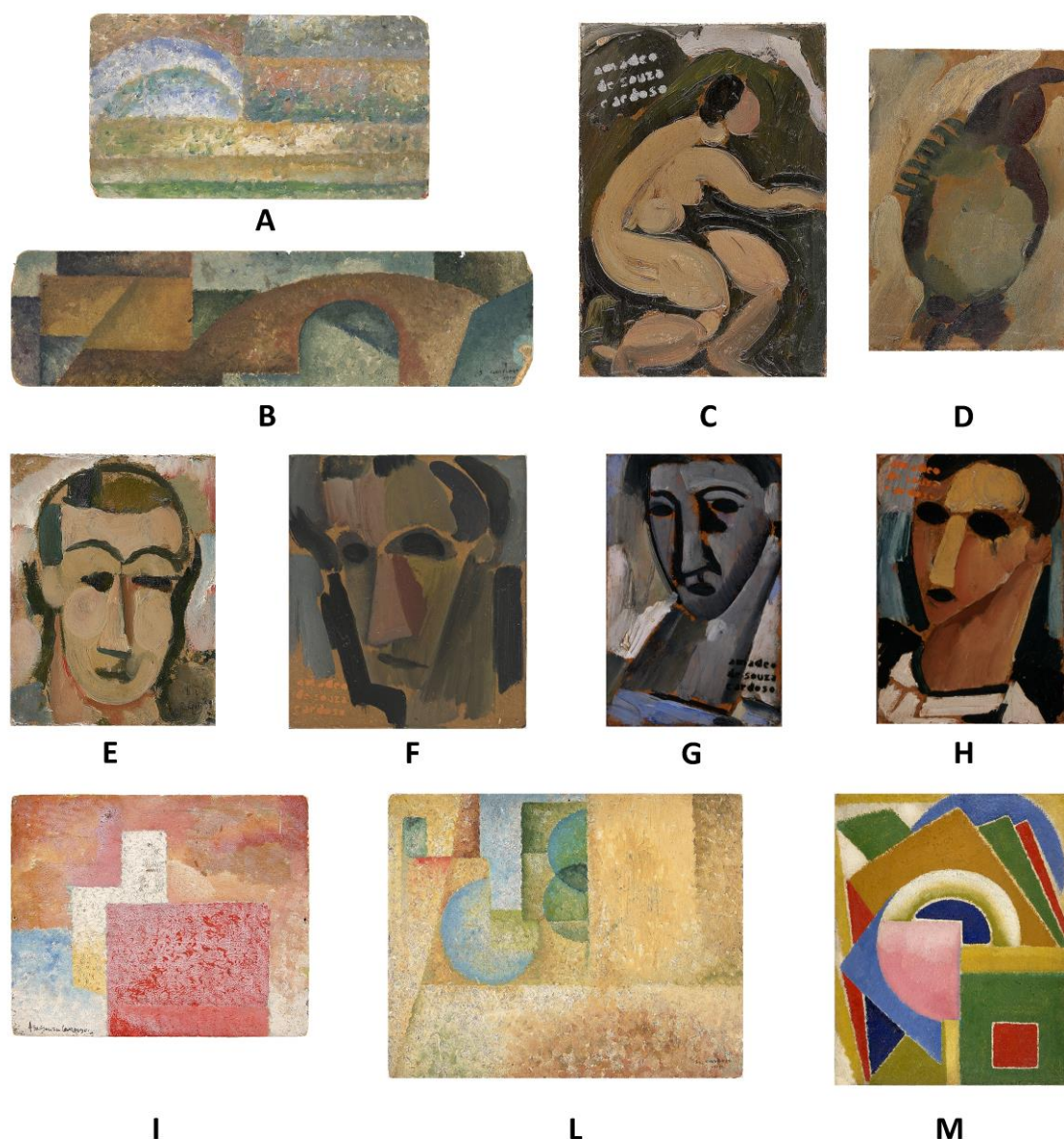


**Figure 6A.** Paintings of Amadeo de Souza-Cardoso on cardboard. **A** *Untitled* (1914), 18 x 33 cm. Collection CAM (Inv. 77P5); **B** *Untitled* (1914) 10.7 x 41.2 cm. Collection CAM (Inv.91P219); **C** *Ar livre nú* (1914) 18.8 x 13 cm. Collection CAM (Inv.91P217); **D** *Untitled* (1914) 18.7 x 12.5 cm. Collection CAM (Inv.91P220); **E** *Untitled* (1914) 17.4 x 13.3 cm. Collection CAM (Inv.87P158); **F** *Untitled (Cabeça)* (1914) 18.6 x 16.2 cm. Collection CAM (Inv.91P218); **G** *Untitled* (1914) 20.1 x 12.9 cm. Private Collection; **H** *Untitled* (1914) 18.7 x 12.8 cm. Private Collection; **I** *Untitled* (1913) 14.6 x 17.9 cm. Collection CAM (Inv. 91P225); **L** *Untitled* (1914) 26.8 x 32.9 cm. Collection CAM (Inv. 91P224); **M** *Untitled* (1913) 34.4 x 28.2 cm Collection CAM (Inv. 92P209) [Freitas *et al.* 2008, pgs. 228, 229, 236, 237, 239, 264, 268, 269, 286, 285, 287].

However, there exist only a few examples of drawings that can be considered as sketches of Amadeo's paintings. Figure 8 shows two examples of this: one example concerns the *Mucha* painting (1915-16), probably the most emblematic of Amadeo's artworks; the second one concerns *A casita clara-paysagem (The clear little house-landscape)* (1915). The use of patches of colours, called *tache*<sup>25</sup>, is a

<sup>25</sup> This term, introduced by Zola in his study of Manet's paintings, was used to describe the Impressionist's use of coloured patch or stroke in contrast the Academic techniques. In Impressionist paintings the forms are not



characteristic of Amadeo's technique. Overall the texture is a relevant element in his compositions and is complemented by the use of the colour.



**A**



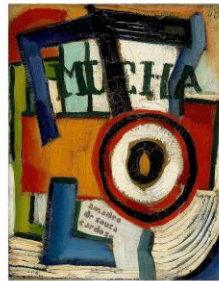
**B**



**C**



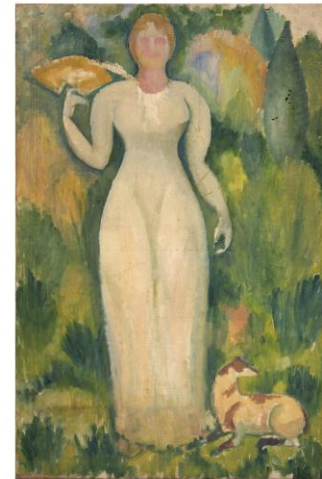
**D**



**E**



**F**



**G**

**Figure 6B.** Paintings of Amadeo de Souza-Cardoso on canvas. Collection of Centro de Arte Moderna, Fundação Calouste Gulbenkian **A** Untitled (O Jockey) (1913) 61 x 50 cm. (Inv. 77P5); **B** (*Paysagem figura negra*) (1914-15) 50 x 50 cm (Inv. 86P23); **C** *Gemälde G /Quadro G* (1912) 51 x 29.5 cm (Inv. 77P2); **D** Untitled, 100 x 70.3 cm. (Inv. 86P19); **E** *Mucha* (1915-16) 27.3 x 21.4 cm. (Inv. 86P21); **F** (*Janellas do pescador*) (1915-16) 27.4 x 34.8 cm. (Inv. 77P16); **G** Untitled (undated) 99.6 x 64.6 cm. (Inv. 91P222) [Freitas *et al.* 2008, pg. 209, 297, 182, 362, 322, 318, 373]

represented by the shape of the objects themselves but using differentiated patches of colour, which gives the effect of light surrounding the object [Bomford *et al.* 1990].



**A**



**B**



**C**



**D**

**Figure 7.** Paintings of Amadeo de Souza-Cardoso Collection CAM. *Untitled* (1913) (Inv. 92P209) **A** visible light photograph; **B** X-ray image [Melo *et al.* 2009]; **C** *Untitled* (1914) (Inv. 88P159); **D** Infrared photograph [Melo *et al.* 2008].



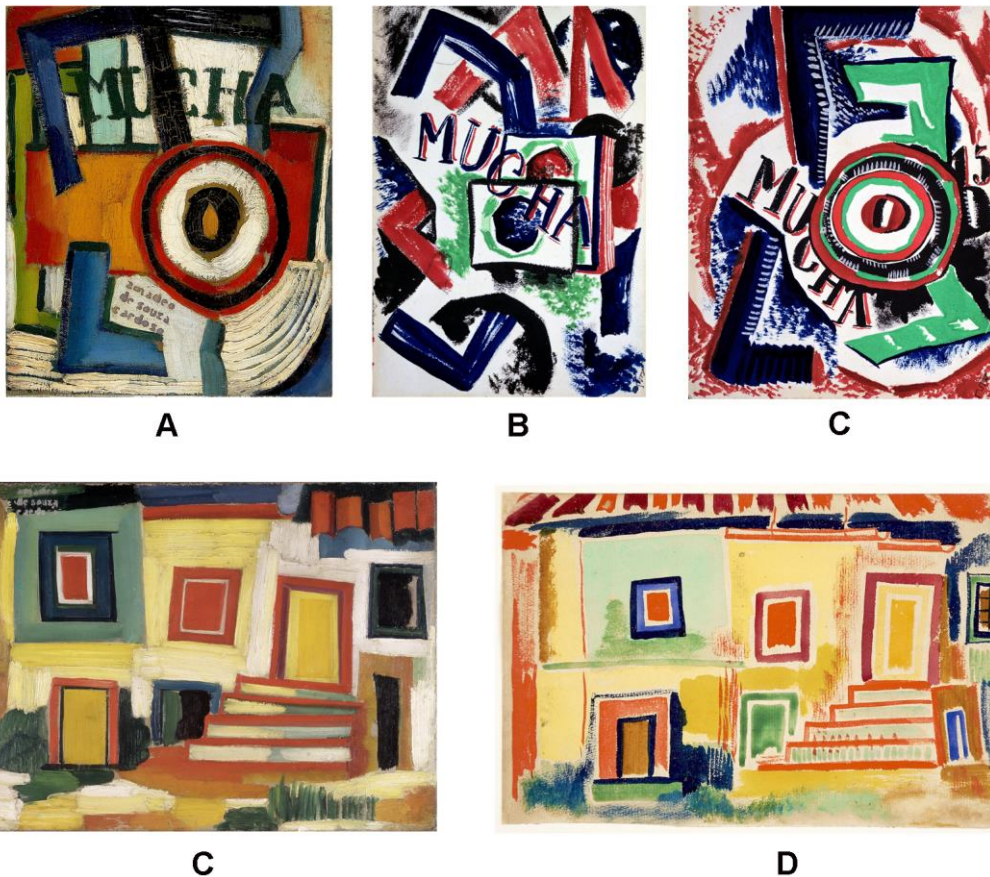


**Figure 8.** Amadeo de Souza-Cardoso **A** *Mucha*, Oil painting (1915-16), 27.3 x 21.4 cm. Collection CAM (Inv. 86P21); **B** and **C** *Untitled*, watercolour 25 x 16 cm. and 28 x 18 cm. Private collection; **C** Oil painting *A casita clara – paisagem (The clear little house-landscape)* (1915-16) 30.5 x 40.5 cm. Collection CAM (Inv. 77P15); **D** (*Maisonatte*), watercolour (1915-16), 14.7 x 23.8 cm. Collection CAM (Inv. 87DP340) [Freitas et al. 2008, pgs. 322, 323, 316].

By observing his paintings, it is possible to identify different types of textures; some examples are reported in Figure 7. In general, the word *rapidity* describes his execution well. The texture is created by the used of short and, presumably quick movements, keeping the brush in a vertical position. In some works the paints are not mixed on the palette but directly on the canvas; by juxtaposition of different tones; in that way the surface is characterized by the heterogeneity in terms of colour and also in texture (Fig. 9D). In other works, the paints are previously mixed on the palette and then applied onto the canvas; however, the mixture is never homogeneous and in the microscope it is possible to distinguish the different pigments used, this technique maintains the brilliance of the colour also when the pigments are mixture. In a few cases, the brushstroke is elongated and it is used to define the figure more than to fill it (Fig. 9C); in these cases the colour is obtained by dragging more than one tone in the same brushstroke (Fig. 9B). Sometimes, the marks left by the brush are visible (Fig. 9E and F).



**Figure 9.** Macro images of different texture patterns in the paintings of Amadeo de Souza-Cardoso. Collection of Centro de Arte Moderna, Fundação Calouste Gulbenkian **A** *Untitled*, (1912-13) (Inv. 77P3); **B** *A chalupa* (1914-15), (Inv. 77P22); **C** *Untitled (Entrada)* (1917) (Inv. 77P9); **D** *Untitled* (1914) (Inv. 92P210); **E** *Mucha* (1915-16) (Inv. 86P21); **F** *Untitled* (1913-14) (Inv. 87P158) [Freitas *et al.* 2008, pgs. 179, 237, 241, 285, 322, 364].

## 1.2 Dealing with ageing: conservation issues

Oil painting is a dynamic system resulting for the drying and natural ageing processes that begin at the moment the paint is applied. Even if we consider aging as a natural process, we know that there exist a large number of factors that may promote it. One of these factors is human intervention, for instance restoration processes, which may affect the chemical reactions that take place in the paint [van Loon *et al.* 2012]. As revealed in the research of Marion Mecklenburg and his team, large groups of surrounding elements, usually identified with environmental conditions, are also strictly related to the promotion of the ageing process; examples include light, temperature, moisture and pollution [Tumosa *et al.* 1994]. Moreover, the voluntary or involuntary<sup>26</sup> selection of the materials by the artist plays an important role: differences in the quality of the materials, that can be related to manufacture, washing, purification processes and particle size can affect the stability of the painting [van Loon *et al.* 2012]. In the nineteenth

---

<sup>26</sup> Here the term involuntary refers to two aspects related with paint manufacture: (i) the incorrect labelling of paint tubes, that pigments could be substituted in the paint formulation and still sold under their original names [Carlyle 1993]; (ii) the adulteration of the industry artist's materials (wax, pigment, oil) by additions of cheaper ingredients and by artificial enhancement of the paint properties with the introduction of lower-quality materials. Cheaper and brighter pigments could be added during paint manufacture *to make them attractive to the buyer* [Muckley 1882 cited in Carlyle 1993]. This practice was reported in many painting manuals of 18<sup>th</sup> and 19<sup>th</sup> century [Carlyle 1993].

century, British instruction books on oil painting advised artists to anticipate changes in their materials, such as the yellowing of the binder. To offset this they were advised to use the more coloured in linseed oil, with dark pigment and the lighter poppy and nut oils for the light colours. Very often, the manuals also offered advice and methods to avoid material changes [Carlyle 1990].

The oil painting is a product of a natural aging process also associated with the drying of the oil binder. The research developed in the last 20 years, by the group led by Professor Boon at the FOM Institute AMOLF (Foundation for Fundamental Research on Matter) has clarified many aspects of the drying process of the oil and its interaction with pigments. In the oil paint, pigments, additives and binders may interact to form new compounds such as metal salts or soaps (metal carboxylates). The drying oils, the metal soaps formation and their impact on the state of preservation of the paint, are introduced in the following sub-section. However, the presence of metal soaps cannot be attributed only to a degradation process. In fact, they were introduced at the end of the 19<sup>th</sup> century, in the enamel paint industry to modify the oil paint properties. Sub-section 1.2.2 presents a brief history of metal soaps in paint formulations, and in particular the Ripolin case study. Finally, two cases of pigment alteration (of chrome yellow and eosin based lake) will be presented.

### 1.2.1 Drying and ageing of the oil binder

A drying oil is a natural product composed mainly of triglycerides, i.e., esters of glycerol linked to three long-chain carboxylic acids (Fig. 10). The fatty acid portion of the drying oils generally used in oil paints is mostly composed of C18 polyunsaturated acids: oleic acid (C18 : 1), linoleic (C18 : 2) and linolenic (C18 : 3); and a small percentage of saturated fatty acids with 12–18 carbon atoms, e.g., palmitic (C16 : 0) and stearic (C18 : 0) [Lazzari and Chiantore 1999; van den Berg 2002].

During the drying process it is possible to identify three main stages, represented in Fig. 9: curing, maturation and degradation stage [Boon *et al.* 1996]. The reactivity of the double bonds of the unsaturated fatty acids promotes the initiation of the process, which is mainly based on photooxidation and autoxidation reactions (Fig. 11) [Meilunas *et al.* 1990; Boon *et al.* 1996; van den Berg and Boon 1999; van der Mallégo *et al.* 1999; Weerd *et al.* 2005; Cotte *et al.* 2006]. The curing stage is rapid and involves the formation of hydroperoxide, followed by the breakdown of hydroperoxide giving rise to highly reactive radicals, and subsequent cross-linking. The breakdown of the hydroperoxide is accelerated by the presence of transition metals from pigments and driers. This process results in a complex three-dimensional polyanionic network (Fig. 11B) [van den Berg and Boon 1999]. The network is based on the glycerol ester with a cross-linked fraction of carboxylate anions and it is stabilised by metal cations from the pigments or the driers (e.g., lead oxide or acetate) (Fig. 11C) [Osawa 1988; van den Berg 2002; van der Weerd *et al.* 2005; Tumosa and Mecklenburg 2005]. Painters and paint manufacturers used to promote the drying by pre-heating the oil, in order to (pre)polymerize it or by using alkaline washing steps [van den Berg and Boon 1999]. During the maturation stage, in addition to the cross-linking,



degradation reactions that transform the triglyceride radicals into low weight molecular products also occur: a variety of carboxylic acid, aldehydes, ketones, alcohols and hydrocarbons. Most of these smaller molecules will leave the paint film by evaporation, although short chain of fatty acids may be trapped within the paint film for a long time [van den Berg and Boon 1999]. This volatile fraction, called the mobility phase, determines the flexibility of the film. Unlike the polyanionic network, the volatile fractions can move and diffuse through the paint layers. However, the paint system has been recently characterised as capable of a self-repair mechanism [Boon 2006; Boon *et al.* 2007]. Mono and dicarboxylic acids that are not incorporated in the network may migrate to react with metal cations, leading to the formation of an increased proportion of metal carboxylates (metal soaps). In some cases, metal soaps form aggregates within the paint film (predominantly in the preparation layers). Their formation is still not fully understood, but it appears that aggregation depends on the paint composition (pigments, extenders and driers), the availability of free fatty acids, the build-up of the layers, the environmental conditions (temperature, relative humidity, etc.) and the conservation history of the painting [Robinet and Corbeil 2003; Plater *et al.* 2003; van der Weerd *et al.* 2005; Boon 2006].

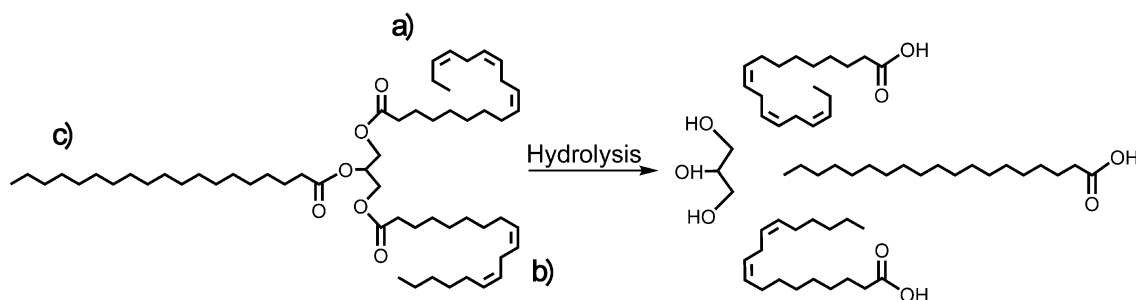


**Figure 10.** Hydrolysis of a triglyceride composed of two unsaturated acids, (a) linolenic and (b) linoleic, and one saturated acid, (c) stearic.

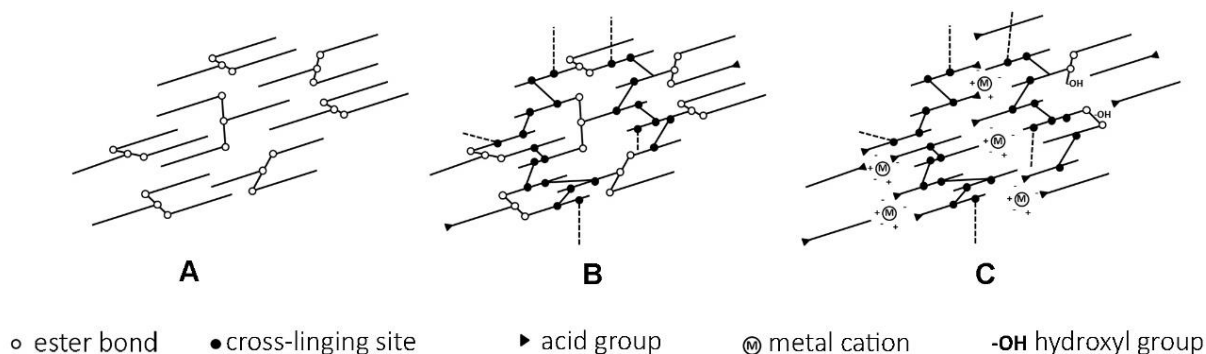


**Figure 11.** Schematic model of the different stages of the drying of the oil **A** fresh oil; **B** representation of the polyanionic network (after curing); **C** after hydrolysis of the ester bond due to the ageing processes (after maturation). Image adapted from [Boon *et al.* 1996].

The formation of a metal soap may promote the dissolution of an original pigment [Weerd 2002] with a consequent increment in volume [Boon *et al.* 2002]. The mass formed may protrude through the paint layers to the surface of the painting (protrusions). Protrusions are visually evident as whitish masses



that give to the painting surface a granular texture [Keune 2005; Weerd 2002]. As well, the presence of metal soaps may also increase the transparency or darkening of paint [Keune 2005; Noble *et al.* 2005; Shimadzu *et al.* 2008].

### 1.2.2 Metal soaps in paint formulations and the Ripolin case study

Mayer describes three classes of materials added to colours by manufacturers in order to keep the pigment in suspension; to avoid the separation of oil and pigment and in order to *impart the desirable short (buttery)* [Mayer 1982, pg.147]. The classes of materials described by Mayer are: (1) *waxes or waxes-like materials, which produce a colloidal or gelatinous condition in the oil/pigment system;* (2) *water or aqueous solutions, which produce emulsifying effect and* (3) *certain inert pigments, such as alumina hydrated, which produce very short pastes. The addition of beeswax, or aluminium<sup>27</sup> and zinc stearates or palmitates, will result in good buttery pastes, and when used in very small amount there is probably little danger on the structural strength of the film.*

Mayer advised that *the use if used in sufficient quantity, metallic soap will tend to cause the oil film become spongy and to get brittle with age [...] two per cent by volume in the total amount of oil color is usually considered permissible* [Mayer 1982, pg.148].

Lead compounds<sup>28</sup>, were recommended in the artists' literature not only as driers: lead-treated oils, in the presence of certain resins, will gelatinize. These buttery transparent gels were used to enhance the paint's brushability and to achieve greater transparency [Carlyle 1999]. Gardner in the test protocols of 1911 [Gardner 1911] describes the tendency of lead and zinc to form metal linoleates. In the edition of 1930 [Gardner 1930] he describes the use of aluminium stearate to coat the surface of pigment particles and helped prevent settling as well as reducing the amount of oil needed to wet. Aluminium stearate was ground with the pigment before the bulk of the oil was added [Tumosa 2001] and it is still used as coating for titanium dioxide in order to control dispersion in the oil [Terry *et al.* 2005].

The zinc soaps used in the paint industry [Stanley 1946] were linoleate; naphthenate; oleate, resinate and stearate, the last defined as the most usual soap. Zinc soaps are considered quite effective when are incorporated in the oil before grinding the pigments<sup>29</sup>. Zinc stearate has long been one of the most widely used compounds to produce matte or flat finishes in varnish and lacquers [Stanley 1946].

---

<sup>27</sup> The use of aluminium stearate in the paint formulation was patent in 1920 [Tumosa 2001]. The use of "linoleate or oleate of alumina" in vermilion tubes was mentioned by Church<sup>27</sup> in 1901 [Church 1901, pg.67].

<sup>28</sup> Lead acetate was the only metallic drier, offered in artists' colormen catalogues until the last decades of the 19<sup>th</sup> century and the most mentioned in the artists' instruction books and handbooks. Litharge, white lead, and red lead were mentioned as additions to slow-drying pigments to enhance their drying properties [Carlyle 1999]

<sup>29</sup> To a careless manufacture, the metal soaps present a simple solution of all colour-grinding problems and because they have great bulk and are comparatively inexpensive, they are well suited for use as deliberate adulterants or cheapeners [Mayer 1982, pg.148].

Ripolin<sup>30</sup> was the first company to use zinc-oxide<sup>31</sup> enamel paints on a large scale [Casadio and Rose 2013a]. The presence of high concentration of ZnO is considered an indicator of enamel paint; anyway zinc white emerges as an artist's pigment in the second quarter of the 19<sup>th</sup> century and its use increased simultaneously with the rise of the use of the house paint [Arslanoglu *et al.* 2013].

Compared to artist's oil paint, commercial prepared enamel paint offered the artist different visual and handling properties, including a unique range of surface gloss and colours, great fluidity, and relatively short drying times [Gautier *et al.* 2009]. High gloss exterior paints could be achieved by including zinc stearate, among other methods [Standeven 2011]. The research led<sup>32</sup> by The Art Institute of Chicago (AIC) characterized the Ripolin enamel products and its use as an artist's materials in the works of Picasso [Muir *et al.* 2013; Casadio *et al.* 2013c; Arslanoglu *et al.* 2013] Picabia [King *et al.* 2013], Sidney Nolan [Dredge *et al.* 2013], and Kandinsky [McMillan *et al.* 2013]. Based on the work of Gautier *et al.* [Gautier *et al.* 2009] the presence of metal soaps is defined as one of the features that indicates the presence of enamel paint. They has suggested that zinc carboxylates are products of interaction between zinc white and oil, as well as the presence of driers based on cobalt and lead [Gautier *et al.* 2009]. However, it is meaningful that Standeven reports the addition of zinc stearate in gloss exterior paint formulations [Standeven 2011]. However, the distinction between oil paint tubes and enamel paints is not straightforward [McMillan *et al.* 2013]. Arslanoglu *et al.* [Arslanoglu *et al.* 2013] report that the characterization of the binder by mass spectrometry could be affected by the addition of metal soaps in the manufacture process, because it changes the ratios of the fatty acid used to characterize the oil.

Based on the literature, there exist other features that can be used to differentiate Ripolin from artist's tube paint: (1) the dominance of zinc-based whites instead of the basic lead carbonate [Gautier *et al.* 2009]; (2) French Ripolin contains only trace amount of fillers [McMillan *et al.* 2013]; (3) small particle size (150-300 nm length/diameter range) [McMillan *et al.* 2013]; (4) absence of many common pigments<sup>33</sup> used in artists' tube paints [McMillan *et al.* 2013; Gautier *et al.* 2009]; (5) the use of mixtures of primary colours (yellow, blue and red) to achieve secondary (orange, violet, green) and tertiary colours (yellow-orange; red-orange; red-violet; blue-violet; blue-green; yellow-green) [Gautier *et al.* 2009].

---

<sup>30</sup> Ripolin was developed in the Netherlands in the early 1890s by Carl Julius Ferdinand Riep. In 1897 Riep's Briegleb paint company formed a partnership with the French artist's paint manufacture, Lefranc. The merged company was called Ripolin with the first factory opening in France in that year [Standeven 2013].

<sup>31</sup> Zinc white replaced the lead white in the preparation of the house paints. Lead white is toxic and has a tendency to darken when exposed to polluted atmospheres rich in sulphur [Casadio and Rose 2013a].

<sup>32</sup> Recent interest on enamel paint was reflected in the popularity of conference such as "Issues in Contemporary Oil paint" (Amersfoort, The Netherlands March 2013) and "From Can to Canvas: Early uses of house paints by Picasso and his contemporaries in the first half of the 20<sup>th</sup> century" (Marseille and Antibes, France, May 2011) [Casadio *et al.* 2013b].

<sup>33</sup> Cadmium pigments, cobalt-based blue pigments, emerald green, and cobalt violets.

### 1.2.3 Pigment alteration

#### *The darkening of Chrome yellow*

Luis Nicolas Vauquelin identified the chromium element in 1797, and his first synthesis of the lead chromate is dated 1809 [Kühn and Curran 1986]. Process modifications such as the pH condition in the synthesis of the lead chromate result in different crystal structures and different hues: the hues change from the orange-red tone, of the basic lead chromate ( $\text{Pb}_2\text{CrO}_5$ ) obtained in alkaline condition to a deep lemon yellow (mixed-crystals of lead chromate and lead sulphate<sup>34</sup>,  $\text{Pb}(\text{Cr},\text{S})\text{O}_4$ ) if the synthesis is carried out in acidic conditions.. The yellow-orange pure lead chromate ( $\text{PbCrO}_4$ ) is obtained using a neutral pH [Harley 2001; Erkens *et al.* 2001].

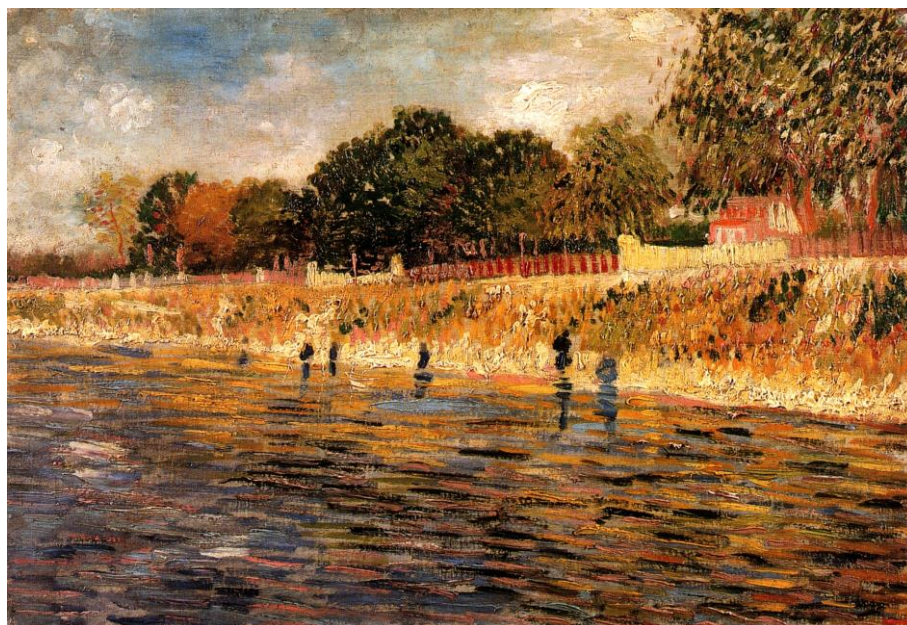


**Figure 12.** Example of darkening of chrome yellow pigments in Vincent van Gogh painting. *Bank of the Seine* (F 293s 77v/1962) (mid 1887), oil on canvas (32 x 46 cm); Van Gogh Museum, Amsterdam (Vincent van Gogh Foundation). Painting analysed by Monico *et al.* [Monico *et al.* 2011b].

The lower stability of the lead chromate pigments were discussed by 19<sup>th</sup> century chemists and artist's colourmen. Vibert in *The science of painting* [Vibert 1892], classified chrome yellow as bad pigment: *Lead, in combination with other bodies, furnishes many yellow colours more or less bad. Such as [...] Chrome yellows (chromate of lead) [...]. All these colours get black or decompose the metallic combinations with which they are associated* [Vibert 1892, pg.166]. Nowadays, the darkening of the

---

<sup>34</sup> A mixed-crystal is a solid solution, i.e., a crystalline structure in which one or more atoms are substituted by others that can assume the same geometry, without changing the structure. The term mixed-phase pigment is also commonly used [Buxbaum 1998; Erkens *et al.* 2001].

chromate pigments affects important oil artworks such as some van Gogh (Fig.12) [Monico *et al.* 2011a] and Georges Seurat [Zanella *et al.* 2011] paintings.

The inconsistency<sup>35</sup> of this phenomenon may be related to numerous variables (such as ambient conditions and/or related to restoration procedures) that are part of the history of painting. Moreover, the diversity of chrome yellow formulations and the complexity of the ageing process in an oil matrix play a relevant role [Otero *et al.* 2012]. Recently, important contributions have been made to further our understanding of the degradation processes involved in the darkening of chromate based pigments. Analysis of degraded paint samples from painting by George Seurat and van Gogh, using  $\mu$ -X-ray Absorption Near Edge Structure ( $\mu$ -XANES), demonstrated that the alteration of chromate pigments: zinc yellow (zinc potassium chromate  $K_2O \cdot 4ZnCrO_4 \cdot 3H_2O$ ) [Zanella *et al.* 2011] and chrome yellow [Monico *et al.* 2011a; Monico *et al.* 2013], is associated with the reduction of the original Cr (VI) of the chromate based pigments to Cr (III) (Fig.13).

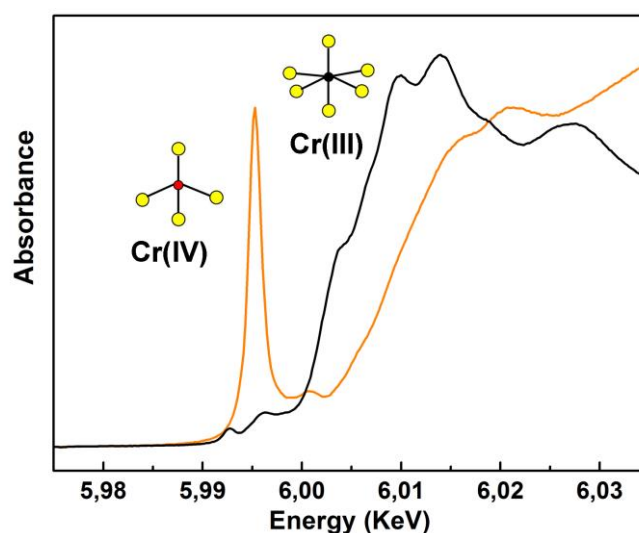


**Figure 13.** Detection of Cr (VI) and Cr (III) species using K-edge XANES spectra<sup>36</sup>. In black the spectrum of Cr(III) oxide ( $Cr_2O_3$ ) and in orange the reference Crocoite mineral, Cr(VI) (Department of Conservation and Restoration of the Universidade NOVA de Lisboa).

Zanella *et al.* [Zanella *et al.* 2011] studied the degradation of zinc yellow (zinc potassium chromate) using artificial aging of paint samples containing modern Zn yellow in oil. This work proposes two different degradation processes depending on the relative humidity conditions. They observed a changing of the colour of the paint sample from yellow to ochre after aging in the presence of  $SO_2$  and under low relative humidity (50%). On the other hand a dark green tone was observed in the samples aged under high relative humidity (90%) and in the presence of  $SO_2$ . By artificial aging of historical 19<sup>th</sup>

<sup>35</sup> Degradation phenomenon was not observed in all the paintings of van Gogh, even where this problem appeared it doesn't affect all areas uniformly where chrome yellow pigment is used. Fortunately, in the works of Amadeo that we have studied, chrome yellows appear to be unchanged [Melo *et al.* 2008; Otero *et al.* 2012].

<sup>36</sup> The pre-edge peak around 5.993 KeV for the Cr K-edge is caused by a bound state 1s to 3d transition. It is allowed in the non-centrosymmetric tetrahedral coordination, such as Cr(VI) compounds. In the case of Cr(III) compounds that commonly exist in a centrosymmetric octahedral geometry the same pre-edge have a low intensity [Pantelouris *et al.* 2004].

century oil paint tube samples, Monico *et al.* [Monico *et al.* 2011a] observed a relation between the structure of the pigment and its tendency to darkening. Solid solutions of lead chromate and lead sulphate shows more tendency to degradation compared with pure lead chromate. Moreover, a high amount of lead sulphate in the solid solution promotes the instability of the pigment. Samples from van Gogh paintings<sup>37</sup> that show brown degradation of chrome yellow layer were analysed by synchrotron techniques, in these samples the reduction of Cr appears to be associated with the presence of (one or more) sulphate compounds. Moreover the alteration was especially evident in areas rich in Ba, S, and/or Al/Si [Monico *et al.* 2011b].

Based on the fitting of a combination of XANES spectra of several chromium reference compounds with the spectra of degraded paint samples, Casadio *et al.* [Casadio *et al.* 2011] and Monico *et al.* [Monico *et al.* 2013] suggested that the degradation products may be chromium oxide ( $\text{Cr}_2\text{O}_3$ ) and viridian ( $\text{Cr}_2\text{O}_3 \cdot 2\text{H}_2\text{O}$ ), chromium(III) acetate ( $\text{Cr}(\text{C}_2\text{H}_3\text{O}_2)_3$ ) or potassium sulphate dodecahydrate [ $\text{KCr}(\text{SO}_4)_2 \cdot 12\text{H}_2\text{O}$ ]. Artificial ageing using UVA/Vis light of a paint sample from a 19<sup>th</sup> century oil-paint tube was also investigated in nanoscale by Tan *et al.* [Tan *et al.* 2013]. The model proposed is based on a core-shell structure, where the lead chromate degrades by the dissolution of  $\text{CrO}_4^{2-}$  ions, which react with the organic binder of the paint at the interface with micro-droplets of aqueous solution. This results in the reduction of Cr(VI) to Cr(III),  $\text{Cr}_2\text{O}_3$  precipitates at the surface of pigment particles. This model is based on different behaviours for the pure chrome yellow sample and the solid solution of chromate and lead sulphate: after that the samples were taken out of the paint tubes, the particles gradually evolved to  $\text{PbCrO}_4\text{-Cr}_2\text{O}_3$  core-shell and  $\text{PbCrO}_4\text{-PbSO}_4$  core-shell, respectively. Artificial aging leads them to the formation of  $\text{Cr}_2\text{O}_3$  and  $\text{PbCrO}_4\text{-PbSO}_4\text{-Cr}_2\text{O}_3$ .

In order to develop a model able to explain this phenomenon, it is essential to have an accurate characterization of the chrome yellow in the paintings as well as aging tests on samples prepared by Historically Accurate Reconstructions Technique (HART). This methodology is currently being used at the Department of Conservation and Restoration of the Universidade NOVA de Lisboa<sup>38</sup>; in April 2014 a mission to the European Synchrotron Radiation Facility (ESRF) in Grenoble took place. During this mission unaged and aged paint reconstructions and painting samples, including two samples from the paintings studied in this thesis (*BRUT* and *Entrada*) were analysed by  $\mu$ -XANES and  $\mu$ -FTIR. The results obtained by the analysis of artificially aged HART samples confirmed the reduction of Cr(VI) to Cr(III) in the degraded samples. The preliminary analysis of the HART samples reveals that pigments based on mixed-crystals (Primrose and Lemon) show a higher relative stability than those composed of pure lead chromate in mixture with calcium carbonate and gypsum (Middle Chrome Yellow). These results may

---

<sup>37</sup> Identified in the samples from the van Gogh paintings was monoclinic  $\text{PbCrO}_4$ , monoclinic  $\text{PbCr}_{1-x}\text{S}_x\text{O}_4$ , and mixtures of monoclinic and orthorhombic  $\text{PbCr}_{1-x}\text{S}_x\text{O}_4$  species [Monico *et al.* 2013].

<sup>38</sup> Research developing under the PhD thesis project of Vanessa Otero «Bright colours: historically accurate reconstructions of Amadeo's palette » at DCR-UNL.

be explained by the pigment absorption in the formulation, which we consider to be lower for the mixed crystals, and by the light effect on fillers such as calcium carbonate [Otero *et al.* 2014c].

### *The fading of Eosin based lake*

Lake pigments based on eosin were synthesized in the 19<sup>th</sup> century and with the name Geranium Lake very early became popular among the impressionist painters. A large number of studies show that this class of pigments is responsible for the fading of many of van Gogh's paintings [Peres *et al.* 1991; Rioux 1999; Burnstock *et al.* 2005; Claro *et al.* 2010; Geldof and Steyn 2013].

In 1860 the German chemist Adolf Baeyer synthesized the first compound of the hydroxy-phthalein group, the fluorescein (Fig. 14). The sodium salt of the fluorescein was introduced very soon in the market by the Badische Anilin & Soda Fabrik (BASF) and other German companies. In 1873 the research director of BASF, Heinrich Caro, discovered that by bromination of fluorescein was possible to obtain a red dye, that he called Eosin (Fig. 14). Eosin was introduced in the market the year after. The iodination of fluorescein, named erythrosin (Fig.14) was synthesized in 1875 by the chemist Emilio Nölting. The Eosin-based lake pigments are obtained by precipitating the soluble dyes with aluminium and lead salts, the colour range of the pigment is from orange scarlet to bluish-red [Geldof and Steyn 2013]. The instability of this pigment was known already in the 19<sup>th</sup> century, Jehan-Georges Vibert (1892) advised against the use of synthetic reds that had recently become available for artists. Adolf Lehne (1893) described that the pigment "appeared pale only 5 days after and completely faded after 18 days". Van Gogh in 1888 wrote to his brother about the fading that was occurring in his paintings and explained that he intended to overcome the problem by the application of excessively pronounced colours [Rioux 1999; Geldof and Steyn 2013].

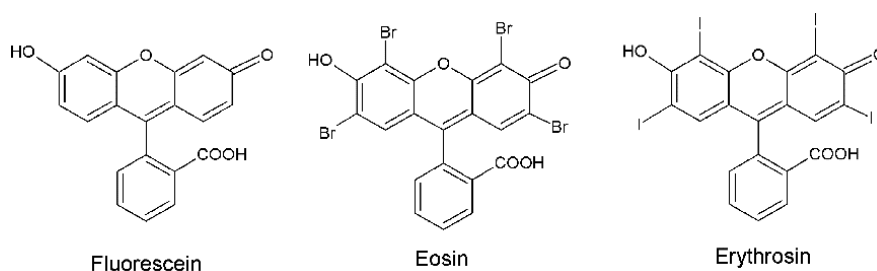


**Figure 14.** Molecular structures of fluorescein, eosin and erythrosine, image adapted from [Geldof and Steyn 2013].

Aside from the light exposure other factors are recognized to accelerate this phenomenon, such as high conditions of humidity, or the gaseous pollutants [Salmon and Cass 1993]. The method of extraction, in the case of the natural lake, the substrate used for the precipitation can also influence in the lightfastness of the lake. Burnstock *et al.* [Burnstock *et al.* 2005] tested the stability<sup>39</sup> of lakes made from cochineal,

<sup>39</sup> The lakes were light aged at 25 °C and 60% relative humidity, using 36 W Philips colour 96 fluorescent lamps (10,000 lux) for 2850 hours [Burnstock *et al.* 2005].



brazilwood (on aluminium- and tin-containing substrates), eosin, madder, and Kopp's purpurine. The paint was prepared with water-washed linseed oil. Each paint was also mixed with lead white paint, zinc white paint, Megilp or chalk. The study suggests that cochineal and madder lake paints are more stable comparing with brazilwood/madder combinations, and that brazilwood and eosin lakes are the most fugitive. Comparable results was obtained by Saunders and Kirby [Saunders and Kirby 1994]. Lakes with a tin-containing substrate are usually less stable than those on an aluminium-containing substrate. Fading is also influenced by the thickness of the layer and by the concentration of the dyestuff. The presence of lead white in the mixture accelerates the fading. Lead white and zinc white were also found in the two van Gogh's paintings with the most evident problem of fading.

Recently digital colour reconstruction was applied for van Gogh paintings, such as the case of *The bedroom* (1888). Van Gogh described this painting to his brother Theo "[...] the walls are of a pale violet. The floor — is of red tiles [...] the doors lilac. And that's all — nothing in this bedroom, with its shutters closed<sup>40</sup>. Actually, this colour turned into pale blue tone due to fading of the lake pigment leaving the cobalt blue alone visible [Geldof and Steyn 2013].

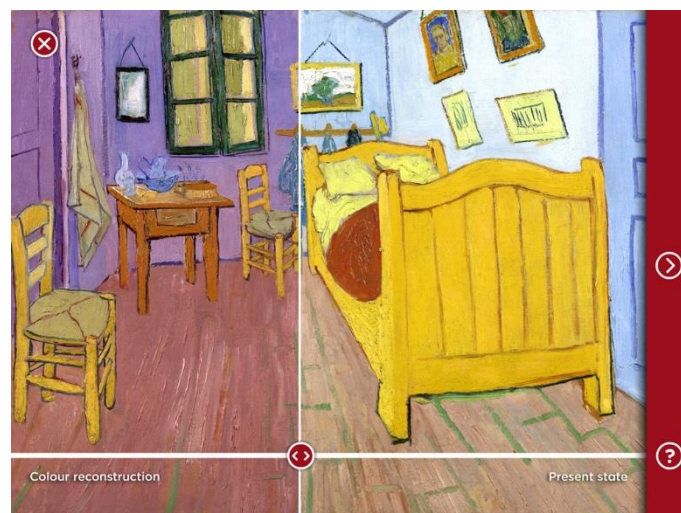


**Figure 15.** iPad application of the digital reconstruction of van Gogh painting *The bedroom* (1888). The user can observe the differences between the present state of the painting and its colour reconstruction [Vet and van Kregten 2014].

A digital reconstruction of the original colours of van Gogh's paintings was carried out by Dr. Roy Berns. The reconstruction of the colour was based on reflectance spectroscopy analysis in the visible region performed on the painting where colour changes were not observed and when possible, on protected regions. When these areas were not available for measurement, reference samples were prepared using materials to the original. By the application of a linear algebra model, the original colour was recalculated and shown as a RGB image [Berns 2005]. This research was part of the eight years project on the study of the materials and techniques of van Gogh that culminated with the exhibition *Van Gogh*

---

<sup>40</sup> Letter from Vincent van Gogh to his brother Theo, Arles, 16 October 1888. From Vincent van Gogh *The Letters* archive available on line <http://vangoghletters.org/vg/> (last accessed October 2014)

*at Work*. For this exhibition, installed tactile supports were installed (as iPads) that offered to the visitor the possibility to see “underneath the visible paint layer”. An example of this application is the colour reconstruction of *The bedroom painting* showed in Figure 15.



## CHAPTER 2: ANALYSIS OF THE PAINTINGS

This chapter presents the main results on the study of the materials and techniques of four of the last paintings produced by Amadeo in 1917, including a description of what we consider to be the *maquette* of his last works. The selection of the four paintings, between those dated 1917, was performed with the help of the art historian Helena de Freitas. These paintings were chosen because they have the whole colour palette that Amadeo uses in his oil works, but at the same time show the peculiar elements of his last period such as the use of unconventional and found materials such as sand, mirrors and glass. Particular attention will be given to the analysis of Amadeo's colour *language* comparing it with that used in his previous works (Section 2.1.3). This chapter also presents the main important conservation issues related to these paintings (Section 2.2). Part of the analysis and the sampling of the paintings took place in situ at the Center of Modern Art of the Gulbenkian Foundation in Lisbon in April 2013. The analysis of these paintings enriches the study of Amadeo's techniques developed by DCR-FCT in 2008 [Melo *et al.* 2009; Melo *et al.* 2009]. The details on the analytical techniques used are presented in Appendix Part II, Ap. II. The areas of analysis, the main representative spectra and the results obtained by the analysis of micro-samples are presented in Appendices of the Part II from Ap. IV to VII.

### 2.1 The paintings of 1917

The four paintings dated 1917 studied in this thesis are presented in Figure 16. Although these paintings are untitled, three of them are usually known as *BRUT 300 TSF*, *Entrada*, and *Coty*<sup>1</sup>. These paintings were exhibited for the first time in Paris after the death of Amadeo (*BRUT*, *Entrada* and *Coty* in 1925; *Untitled* in 1958). These works are considered as a homogenous nucleus and probably the most relevant and innovative art works by Amadeo (Section 1.1.2).

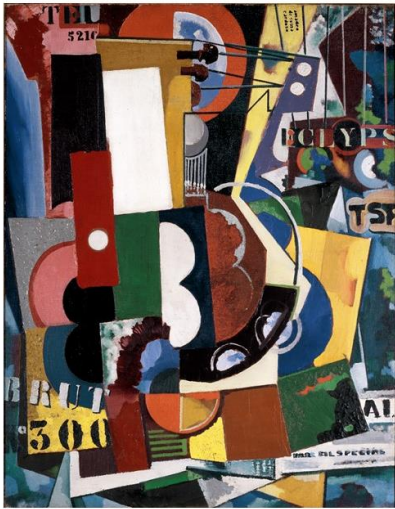
The archive of Amadeo at the Art Library of the Calouste Gulbenkian Foundation includes a photograph that represents a *collage* work, Figure 17A. This *collage* shows many similarities with some of the Amadeo's oil paintings and in particular with *BRUT* and *Entrada*; for this reason we suggest the hypothesis that it is a *maquette* made before these paintings were executed. This photograph, probably taken by Amadeo himself, is the only evidence of this work that has ever been found. The *collage* was likely made by gluing pieces of paper and objects onto a support. The collage shows half of the headline of the Madrid edition of the newspaper "*La correspondencia de España*" (Fig. 17B), which was published in Spain between October 19, 1912 and December 31, 1918<sup>2</sup>. In the collage also visible are two portions of the flyer that Amadeo included in the album "*12 Reproductions*" (Fig. 17C) which was published at the time of his Porto exhibition in November 1916 (Section 1.1.2). This flyer might suggest a date after

---

<sup>1</sup> To simplify the text, the 4 paintings are called *BRUT* for the painting *Untitled*, (*BRUT 300 TSF*) Inv. 77P20; *Entrada* for the painting *Untitled*, (*Entrada*) Inv. 77P9; *Coty* for the painting *Untitled*, (*Coty*) Inv. 68P11 and *Untitled* for the painting *Untitled*, Inv. 77P8 [Freitas *et al.* 2008].

<sup>2</sup> Personal communication with the Spanish newspaper archive.

which this work was performed. Comparing the dimension of the headline of the newspaper with that present in the collage it is possible to deduce that *maquette* could measure 100x70 cm.



*Untitled (BRUT 300 TSF)*



*Untitled (Entrada)*



*Untitled (Coty)*



*Untitled*

**Figure 16.** Paintings of Amadeo de Souza-Cardoso dated 1917. Collection of Centro de Arte Moderna, Fundação Calouste Gulbenkian. *Untitled (BRUT 300 TSF)* Inv. 77P20 (85.8 x 66.2 cm); *Untitled (Entrada)* Inv. 77P9 (93 x 76 cm); *Untitled (Coty)* Inv. 69P11 (93 x 76 cm); *Untitled* Inv. 77P8 (93.5 x 93.5 cm).

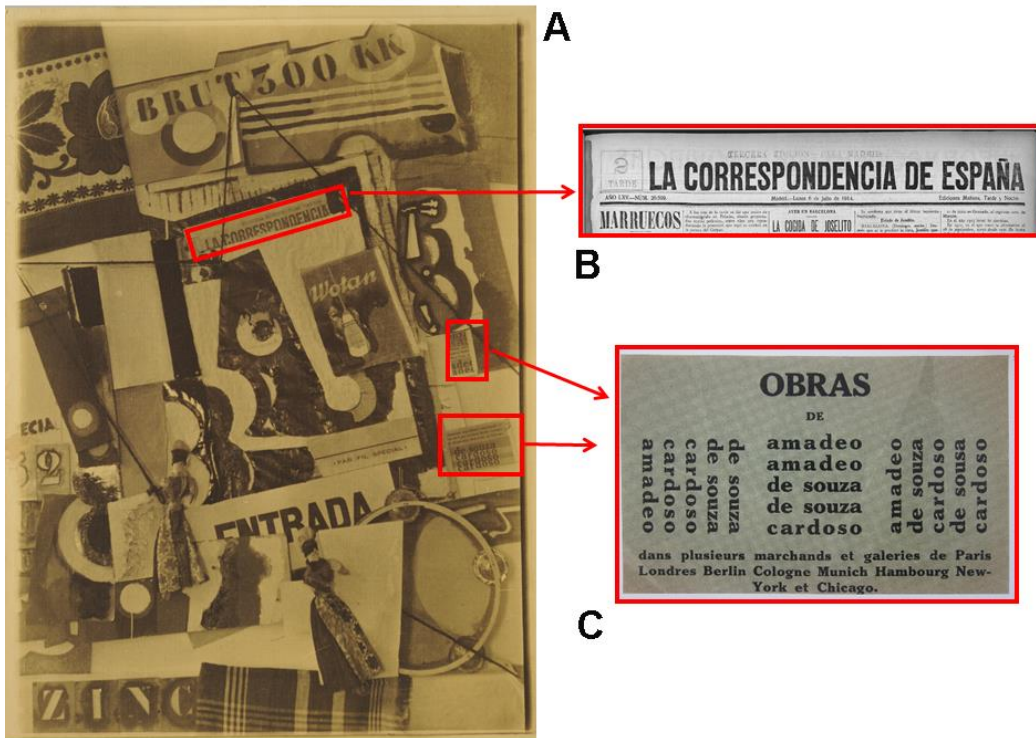


**Figure 17.** **A** Image of the Collage (Art Library of the Calouste Gulbenkian Foundation ASC09/16); **B** Headline of the Madrid edition of the newspaper “La correspondencia de España”; **C** Flyer included in the album “12 Reproductions” (1916) (Art Library of the Calouste Gulbenkian Foundation ASC 221). Image of the flyer from Alfaro 2007, pg. 235.



**Figure 18.** Image details of the word ZINC on the *maquette* (top) and on *Untitled (ZINC)*, c. 1917, 59 x 49 cm. Private Collection (down) [Freitas et al. 2008, pg. 355].

In the collage are visible four *pochoirs* of the letters Z, I, N and C. Figure 18 shows the comparison between these four letter and the word ZINC, in the painting *Untitled ZINC* (1917) (Appendix Part II



Ap.I). The dimension of the letters of the *pochairs*<sup>3</sup> and those in the painting are comparable. This suggest that the *pochairs* in the collage were used for the painting ZINC. Based on this hypothesis it is possible that the painting ZINC (or at least the word in the painting) was completed before the collage and therefore before the paintings *BRUT* and *Entrada*.

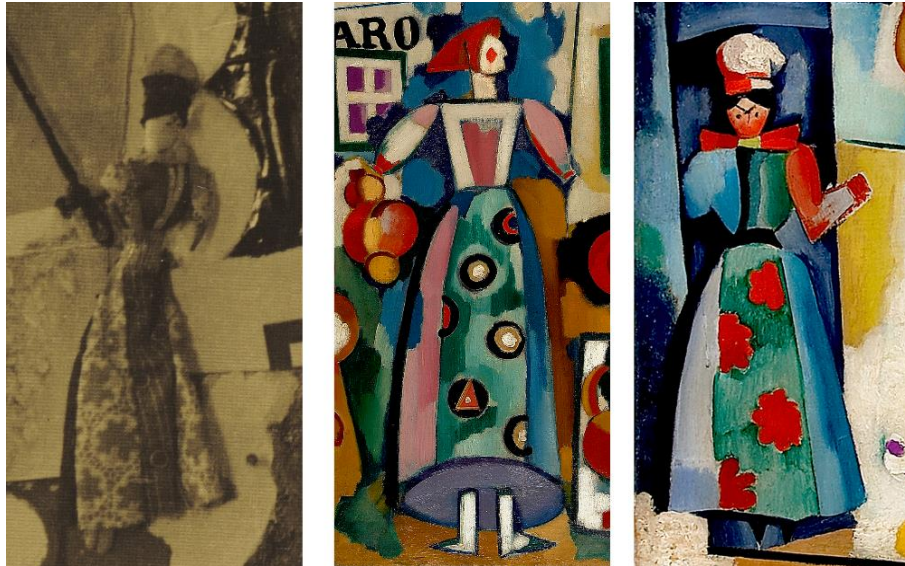


**Figure 19.** Image details (from left to right) of the rag doll in: the *maquette*; *Canção popular a Russa e o Figaro*, 1916, 80 x 60 cm. Collection of Centro de Arte Moderna, Fundação Calouste Gulbenkian (Inv. 77P18) [Freitas *et al.* 2008, pg. 333] and *Trou de la serrure PARTO DA VIOLA Bon ménage Fraise avant garde*, 1916, 70 x 58 cm. Collection of Centro de Arte Moderna, Fundação Calouste Gulbenkian (Inv. 68P17) [Freitas *et al.* 2008, pg. 336]. Appendix Part II Ap.I. shows the images of the paintings.

The *maquette* presents also other elements reproduced in the oil paintings of Amadeo: Figure 19 shows the comparison between the rag doll<sup>4</sup> applied in the *maquette* and its representation in two of Amadeo's paintings. The relation between the collage and the paintings *BRUT* and *Entrada* is exemplified by the presence in the *maquette* of the words that give the titles of these two artworks (Fig. 20A, B). The meaning of the word ENTRADA was explored by Rui Mario Gonçalves [Gonçalves 2006, pg. 27] who related it to the sign for a bullring. Rui Afonso Santos suggested that it could be the indication of a theatre entrance [Lapa 1999]. More recently, Cunha Leal [Cunha 2010] identified in the painting *Entrada* a few elements related to Portugal and the United States entering in the First World War (1914-1918).

The representation of the guitar is another element common to the *collage* and Amadeo's paintings. The piece present in the up left corner of the *collage* (probably of wallpaper) is accurately reproduced in the same position in the painting *Entrada*. The construction of the black lines visible in the *maquette* is interesting: they are obtained with wire fixed with nails and they seem to reproduce the mechanism represented in *Untitled*. In *maquette* we also find what seems to be a tambourine which is represented

<sup>3</sup> The dimensions (h. 4.3 cm) of the letters Z, I, N and C were calculated considering the 100 x 70 cm proposed as dimension of the collage.

<sup>4</sup> The rag doll is a handcraft product of the north of Portugal. The collection of Modern Art Centre of the Calouste Gulbenkian Foundation conserves an example of a doll that belonged to Amadeo.

stylized in the painting *BRUT*. Another stylized element, reproduced in *Entrada*, is the lamp Wotan whose advertisement is glued in the *maquette* (Fig.20C).

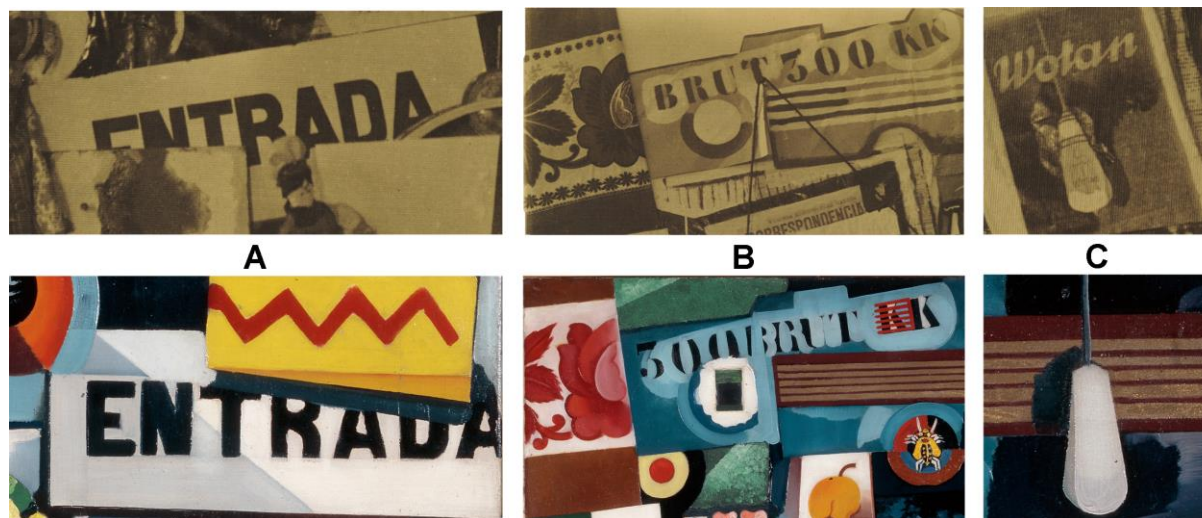


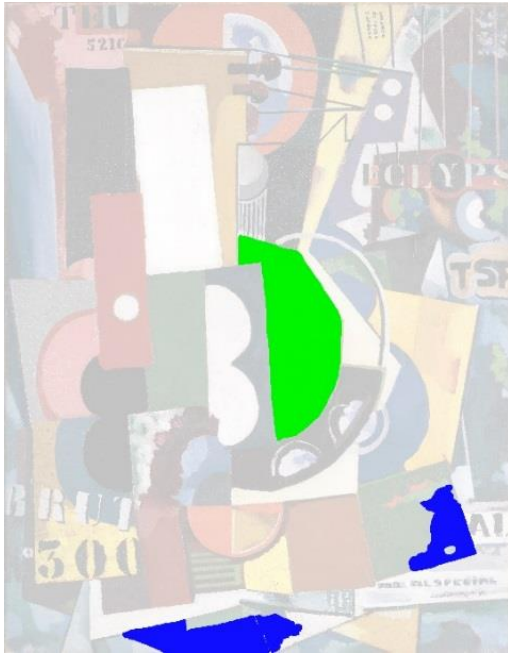
**Figure 20.** Comparison between *maquette* (upper part) and *Entrada* painting (lower part) **A** Images details of the word ENTRADA **B** word BRUT 300 KK and **C** advertising of the lamp Wotan.

As mentioned in Section 1.1.3, the absence of *pentimenti* and overlaps between the figures of the composition, together with the *alla prima* technique used by Amadeo, suggests that the artist precisely planned the painting before its execution. In the case of the last paintings, the existence of the photograph of the *collage* strongly suggest that the collage may have been a *maquette* for his last works.

### 2.1.1 Unconventional materials

One of the main differences between the paintings analysed for this thesis and those analysed in previous works [Melo *et al.* 2008] is the use of unconventional and found materials. Figure 21 shows the mapping of these materials, while Table 1 shows the percentage of the area occupied for each class of object. Unconventional materials such as spheres of silica or calcium carbonate and sand were added to the paint to create a new texture, while the found objects seem to be used with a narrative meaning. *Coty* is the painting in which Amadeo developed this technique the most: in this painting the artist applied a pearl necklace and hair clips (Fig. 22) but also potash-silicate mirrors and painted glasses ( $\mu$ -EDXRF analysis in Appendix Part II Ap.V.1). An example is the glass painted with the silhouette of a bottle of the perfume<sup>5</sup> that gives the name to the painting (*Coty*) glued in the lower left corner of the painting. This glass is applied to the canvas using oil mixture of calcium carbonate and gypsum; on the surface of the white dirty mass was found traces of a golden layer; EDS-SEM analysis detected the presence zinc and copper ( $\mu$ 11) (please see Appendix Part II Ap.VI.3) that suggest the surface originally have been gilded with foils. Unfortunately, at present this golden effect is no longer evident visually.

<sup>5</sup> The advertisement of the perfume *Coty* appears in the futuristic poem *Apotheosis* written by Sá-Carneiro in *Orpheus 2* in 1915.



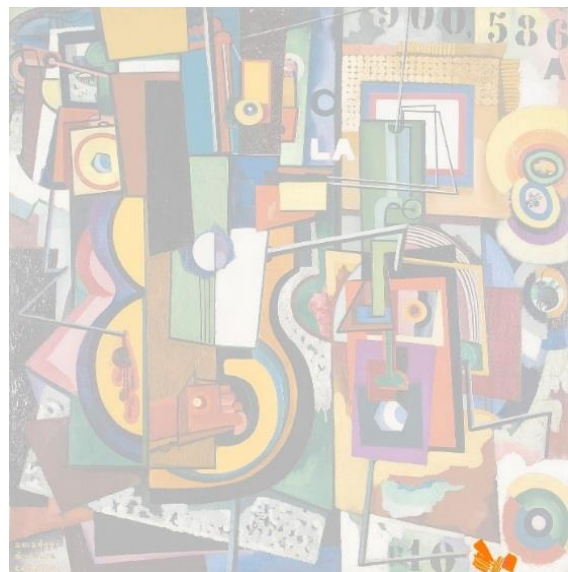
*Entrada*



*BRUT*



*Coty*



*Untitled*

**Figure 21.** Mapping of ● silica, sand, calcium carbonate; ● glass and mirrors; ● found materials, hair clips, matches and a box of matches; ● starch.



**Table 1.** Percentage area of paintings with unusual materials and with glass and mirrors.

	Unusual materials (% area)	Glass and mirrors (% area)
<i>BRUT</i>	5,3	--
<i>Entrada</i>	12,6	1,15
<i>Coty</i>	29,2	8

The use of four mirrors on the top of *Coty* is interesting: they are glued at the same height of the stylized face of the female figure. Rui Mario Gonçalves [Gonçalves 2006] assigns two functions to the use of mirrors in that painting: the first one is related to the "impossibility of visually reproducing a mirrored surface" and the second related to the "creation of a virtual space, beyond or below the plane of the screen [...] also a willingness to subvert the position of voyeur: the observer who ends up watching himself <sup>6</sup>".



**Figure 22.** Image details of found objects in *Coty*, from left to right: mirrors; painted glass and one mirror; necklace; hair clips.

In the lower right corner of the paintings *Entrada* and *Untitled* some matches are represented: in the first case the matches are painted (Figs. 23A and B) while in the second case 13 wax matches are glued onto the surface together with a piece of the wooden matchbox. The matchbox is covered with spheres of calcium carbonate and a thin golden layer. Thanks to the help of the Portuguese Association of Phillumensism it was possible to discover the origin of the matchbox. It was produced between 1895 and 1911 by the *Companhia Portuguesa de Phosphoros*<sup>7</sup> (Portuguese's matches company). Figure 23 compares the label present in the painting (C) and an example of the same box conserved by the Association (D).

<sup>6</sup> [...] A presença de espelhos é frequente na fase final [...] noa tem apenas a função de resolver dois problemas pictóricos: um, a impossibilidade pictórica de reproduzir visualmente uma superfície espelhada; outra a criação de um espaço virtual, para além ou para aquém do plano da tela. A presença de fragmentos de espelhos corresponde também a uma vontade de subverter a posição de voyeur: o observador acaba por se observar a se próprio [Gonçalves 2006].

<sup>7</sup> The matchbox present in the *Untitled* was produced by the Company of Portuguese Phosphoros between 1895 and 1911. In 1895, Francisco Borges created a consortium that included six match companies of Porto and Lisbon [Sottomayor 2011, pgs.59-60]. The matchbox found in the painting was produced in the factory of Lordelo (north of Portugal). The monopoly remained until 1925, when the deregulation of the matches manufacture was instituted.

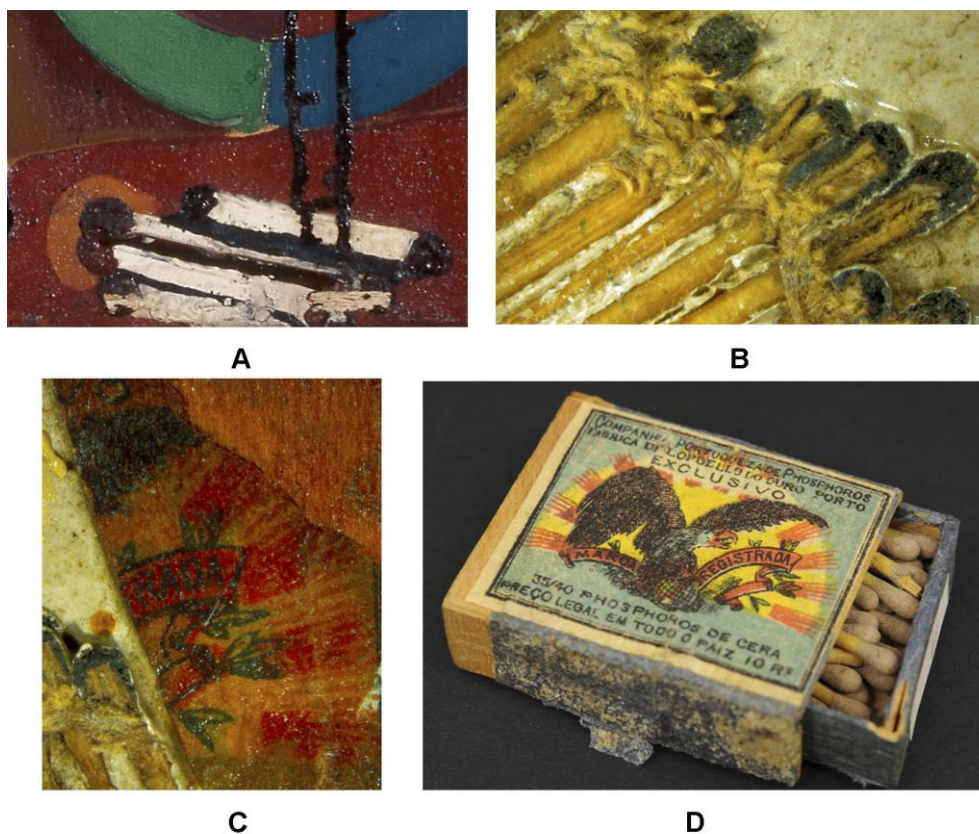


**Figure 23.** **A** Detail of the painted representation of the matches in *Entrada* (7x) **B** Detail of the wax matches and **C** of the box label applied on *Untitled* **D** Wooden matchbox very similar to that in *Untitled* which is in the collection of the Portuguese Association of Phillumenism.

### 2.1.2 Preparation layer

FTIR, Raman and SEM-EDS analyses show that the preparation layers of the four paintings are a mixture of lead white (*Dutch process*) and calcium carbonate, with oil as binder. Figure 24 shows a SEM image in BSE mode of the 4 cross-sections from the paintings: in the samples taken the thickness of the preparation layers is around 140  $\mu\text{m}$  for *BRUT*; 100  $\mu\text{m}$  for *Entrada* and between 42 e 30  $\mu\text{m}$  for *Coty* and *Untitled*.

In *BRUT* a red layer has been applied over the preparation layer; this is the only case of coloured layer in Amadeo's artworks studies. Figure 25A shows the back of the painting where the red layer is visible; the presence of white spot where the red layer was not applied suggests that it was applied when the canvas was fixed with round nails, probably before the application on the current frame (the actual frame is not original). As mentioned before, Amadeo did not made overlaps between the elements of the composition; for this reason the red layer is visible also in the front of the painting (Figure 25B). The thin red layer (around 6  $\mu\text{m}$ ) appears in the cross-section in Figure 25C and is composed of a mixture of vermilion, ochre and barium sulphate (Raman analysis of  $\mu\text{1}$  presented in Appendix Part II Ap.V.3. Cross-section ( $\mu\text{12}$ ) analysis presented in Appendix Part II Ap.VI.2).



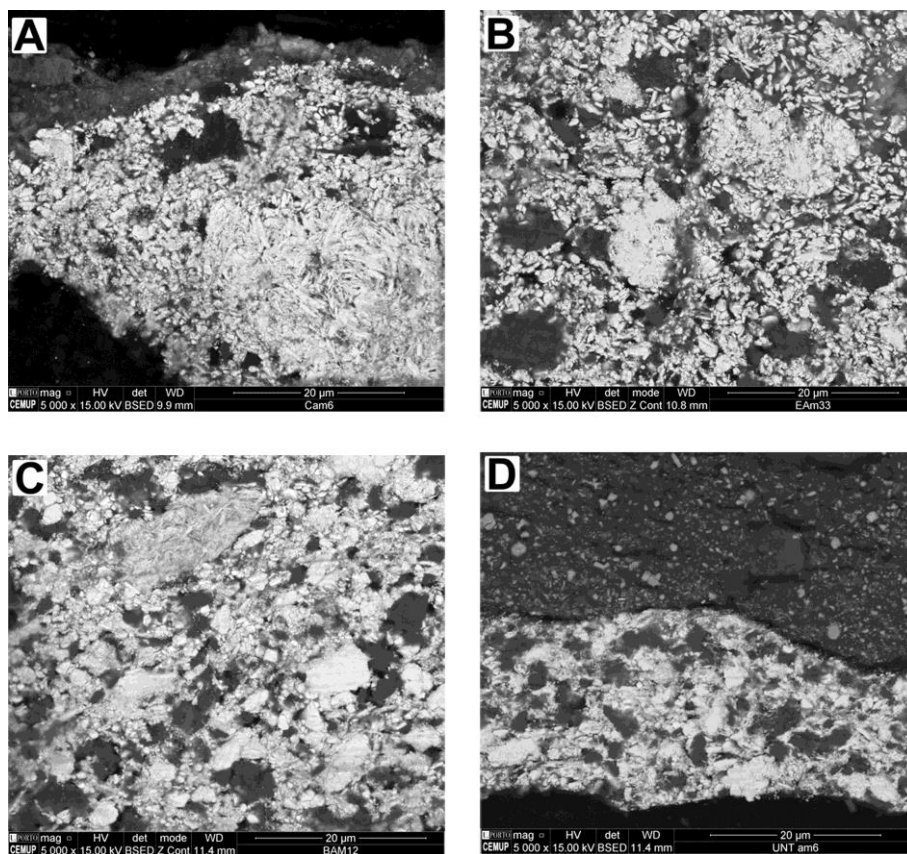


**Figure 24.** SEM image in BSE mode of the preparation layers **A** *Coty* ( $\mu 6$ ); **B** *Entrada* ( $\mu 33$ ); **C** *BRUT* ( $\mu 12$ ); **D** *Untitled* ( $\mu 6$ ), (Appendix Part II Ap.IV.1 shows the sampling areas).

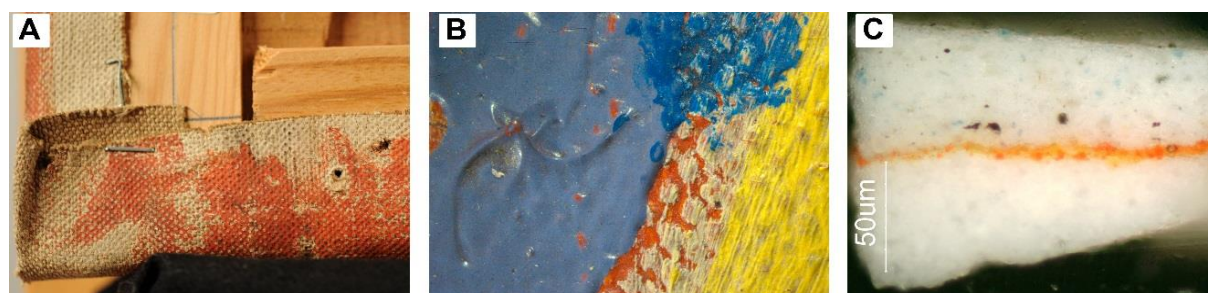


**Figure 25.** Red layer in *BRUT* **A** Detail image from the back of the painting; **B** Photomicrographs of the paint surface (10x); **C** Cross-section of the sample  $\mu 12$  where it is possible to observe the red layer (the sampling area indicated in Fig. IV.2 Appendix Part II Ap.IV.1).

### 2.1.3 Amadeo's colour language

Twenty four paintings by Amadeo were digitalized by hyperspectral imaging with high spectral and spatial resolution. The paintings were chosen considering different periods of the Amadeo's career, between 1911 and 1917. The reflectance spectrum of each pixel of the hyperspectral image was estimated and its colour was computed assuming the D65 standard illumination. The colorimetric data obtained was represented in the CIEL\*a\*b\* uniform colour space. The analysis of the 24 paintings is presented in Appendix Part II Ap.III, here is presented the analysis of the four analysed paintings dated

1917. The colorimetric analysis shows that the four paintings have a similar number of discernible colours<sup>8</sup> and a similar distribution. The paintings dated 1917 are characterized by a higher number of discernible colours (80.000) compared with previous works, where a mean average of 53.000 colours was calculated (Appendix Part II Ap.III). Figure 26 shows the colour range of each painting represented in the CIE(a\*b\*) plot, where the blue area is the sum of the colorimetric coordinates of each pixel of the hyperspectral image. In general the colour range goes between  $-30 > a^* < 40$  and  $-40 > b^* < 60$  with lightness ( $L^*$ ) values uniformly distributed around 50 ( $\pm 15$ ). In these paintings, in contrast to those dated before 1917, Amadeo used a palette of saturated hues; the tones used almost reach the limit of the CIE(a\*b\*) colour space. As well, the shape of *island-like* colour distribution suggests the use of patches of colours. The distribution of the colours shows a high similarity between the paintings *BRUT* and *Entrada*. This similarity, suggested also by the analysis of images in the *maquette* (Section 2.1.1) was also detected by the paint materials used (presented below).

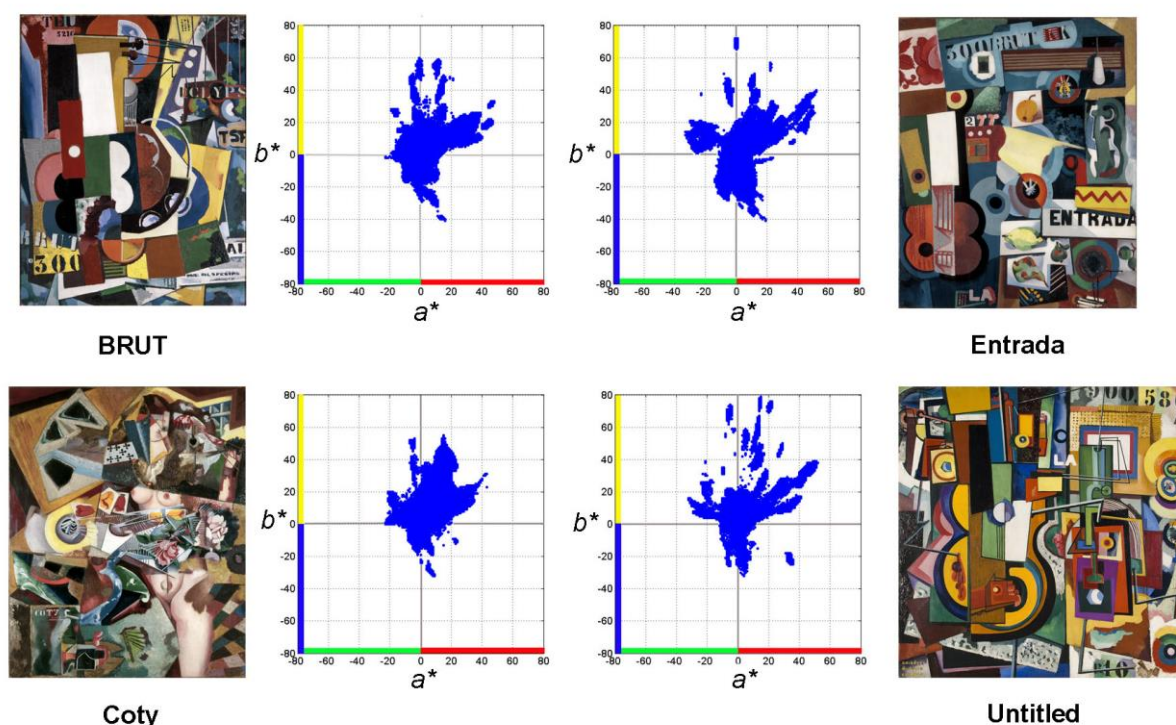




























**Figure 26.** Colour distribution on the CIE(a\*b\*) colour space. The CIE L\*a\*b\* values were calculated from the spectral reflectance of the hyperspectral images of the 4 paintings.

























The analysis of the four paintings shows the use of an oil binder. In the case of *BRUT* and *Entrada* the presence of zinc carboxylates suggested the addition of metal soaps to the paint; this point will be discussed in Section 2.2.1. Tables 2A and 2B present the pigments identified in the four paintings dated 1917. The representative spectra for each pigment acquired using multi-analytical techniques are presented in Appendix Part II.V.1-5.

<sup>8</sup> The number of discernible colours were estimated assuming the CIE 1931 standard observer by segmenting the CIE L\*a\*b\* colour volume into unitary volumes; the just noticeable difference (JND) was assumed to be  $\Delta E=1$  in CIE L\*a\*b\*.

**Table 2A.** Colour construction in the *BRUT* and *Entrada* paintings.

	Violet	Blue	Green	Yellow	Red
<b>BRUT</b>	 cobalt blue +eosin	 cerulean blue	 emerald	 chrome yellow	 vermilion
		 Prussian + ultramarine	 viridian + cerulean	 cadmium yellow	 lake
			 Prussian+ chrome y.	 chrome y. + cadmium y.	 lake + minium
				 chrome y. + ochre	
<b>Entrada</b>	 ultramarine +lake	 cobalt blue	 emerald	 chrome yellow	 vermilion
		 Prussian +cobalt	 viridian + Prussian	 cadmium yellow	 lake
		 Prussian + ultramarine	 Prussian+chrome y.	 strontium yellow	
				 chrome y. + cadmium y.	

**Table 2B.** Colour construction in the *Coty* and *Untitled* paintings.

	Violet	Blue	Green	Yellow	Red
<b>Coty</b>	 cobalt violet	 Prussian	 viridian	 chrome yellow	 vermilion
		 Prussian + cobalt	 viridian+ultramarine	 chrome + cadmium	 lake
			 viridian+cadmium y.	 chrome y. + ochre	 β-naphthol + minium
			 emerald + chrome y.	 cobalt yellow	
<b>Untitled</b>	 cobalt violet	 cerulean	 Viridian	 chrome yellow	 vermilion
			 emerald	 cadmium yellow	 vermilion + minium
			 viridian + strontium y.	 chrome y. + cobalt y.	

In general we can see that the palette used by Amadeo in the 1917 paintings is very close to that used in the previous paintings (Section 1.1.3). However during the analysis of the paintings some differences were detected that will be discussed in this section. The application of golden and silver tones present in *Coty*, *Entrada* and *Untitled* is unique in his oil paintings; it is obtained with an alloy of zinc and copper and zinc and aluminium, respectively ( $\mu$ -EDXRF analysis presented in Appendix Part II Ap.V.1; *Coty*



micro-samples analysis in Appendix Part II Ap.VI.1-3). These metallic tones were found only in *La Légend de St Julien L'Hospitalier*, the illustrated manuscript dated 1912 (Part II, Section 1.1.1). In this work they were obtained with foils of gold and silver, respectively<sup>9</sup>.

The analysis of the **violet** samples<sup>10</sup> collected from the four paintings show that Amadeo obtained this colour using cobalt violet pigment in *Coty* (samples  $\mu$ 13,15) and *Untitled* (sample  $\mu$ 9) and using a mixture of blue and red in *BRUT* and *Entrada*. Cobalt violet ( $\text{Co}_3(\text{AsO}_4)_2$ ) was also present in the *palette* before 1917; in contrast, the mixture of blue and red pigment was not detected in previous artworks. FTIR spectra of cobalt violet is characterized by the strong absorption band at  $878\text{ cm}^{-1}$  attributed to anti-symmetric As-O stretching [Casadio *et al.* 2012]. Cobalt violet was also confirmed by Raman spectroscopy based on its characteristic bands at  $842$  and  $872\text{ cm}^{-1}$  attributed to the anti-symmetric and symmetric As-O stretching, respectively [Casadio *et al.* 2012; Martens *et al.* 2003] (Figure 27A and B). In *BRUT* the purple tone is obtained with a mixture of cobalt blue ( $\text{CoO}\cdot\text{Al}_2\text{O}_3$ ) and eosin (sample  $\mu$ 19) and in *Entrada* with a mixture of Prussian blue ( $\text{Fe}_4[\text{Fe}(\text{CN})_6]_3$ ) and Madder lake (sample  $\mu$ 20). The instability of eosin is well known [Claro *et al.* 2010; Geldof and Steyn 2013]; this instability is visible in *BRUT* where the fading of the eosin-based lake revealed the bluish of the cobalt blue pigment; this point will be presented in more detail in Section 2.2.2.

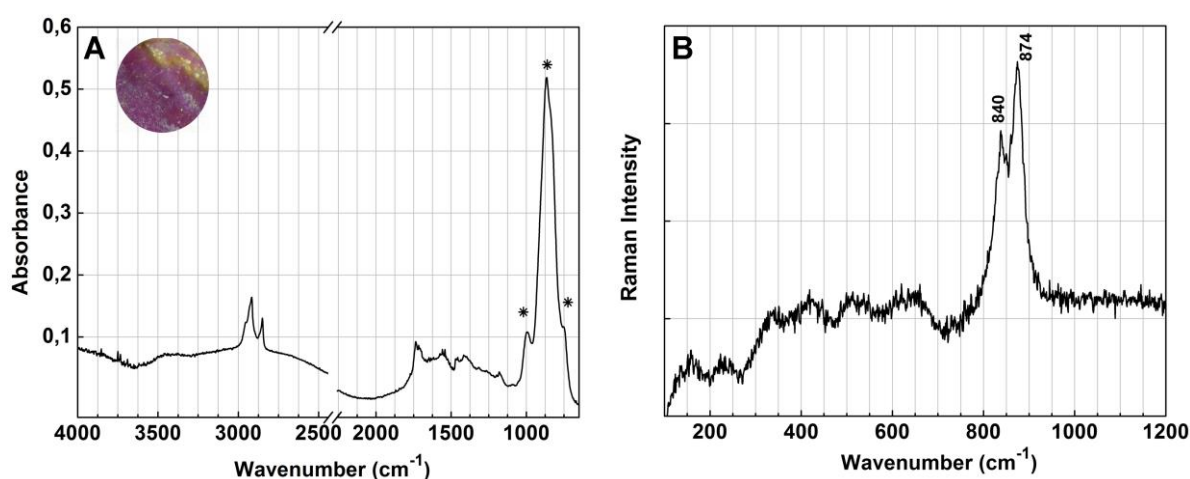


**Figure 27.** Violet sample (sample  $\mu$ 13) from *Coty* painting; **A** Infrared spectrum (\*) cobalt violet pigment; **B** Raman spectrum.

Viridian ( $\text{Cr}_2\text{O}_3\cdot 2\text{H}_2\text{O}$ ) was the main **green** pigment in Amadeo's *palette* before 1917; in *Coty* and *Untitled*, it continues to be the most frequently used green pigment; alone (in *Coty*, sample  $\mu$ 14 and in *Untitled* sample  $\mu$ 14) and in mixture with ultramarine (*Coty* sample  $\mu$ 14); with the cadmium yellow (*Coty* area of EDXRF analysis Gr6 and Gr8) and strontium yellow  $\text{SrCrO}_4$  (*Untitled* sample  $\mu$ 19). Figure 28A

<sup>9</sup> Result obtained in the PhD thesis ongoing project of Ana Margarida Cruz da Silva «Crossing Borders. History, materials and techniques of Amadeo de Souza-Cardoso and Eduardo Viana» at DCR-UNL.

<sup>10</sup> The samples (identified with the letter  $\mu$ ) collected from the paintings *BRUT*, *Entrada*, *Coty* and *Untitled* are indicated in the Figs. IV.2; IV.4; IV.6; IV.8, respectively in the Appendix Part II Ap.IV.1-4.

shows the FTIR spectra of *Untitled* sample  $\mu 19$  with the characteristic bands of viridian at 3630–2630, 1288, 1064, 794 and 650  $\text{cm}^{-1}$  [Zumbuehl *et al.* 2009]. Figure 28B shows the Raman analysis performed on the same samples compared with the spectra of a reference  $\text{SrCrO}_4$  synthesized in laboratory. The bands detected in the sample are the anti-symmetric  $\text{CrO}_4^{2-}$  stretching at 892 and 864  $\text{cm}^{-1}$  and the bending at 399, 372 and 347  $\text{cm}^{-1}$  [Frost 2004]. In the case of *BRUT* and *Entrada* viridian was substituted by emerald green ( $\text{Cu}(\text{C}_2\text{H}_3\text{O}_2)_2 \cdot 3\text{Cu}(\text{AsO}_2)_2$ ) (*BRUT* samples  $\mu 6$ ,  $\mu 7$  and  $\mu 33$ ; *Entrada* sample  $\mu 5$ ). In these two paintings the dark green tones were obtained also with a mixture of Prussian blue and chrome yellow (*BRUT* samples  $\mu 3$  and  $\mu 5$ ; *Entrada* EDXRF analysis on area Gr3) or Prussian blue and viridian (*Entrada* sample  $\mu 31$ ). In the emerald green samples from *BRUT* the presence of starch was detected (discussed in Section 2.2.3).

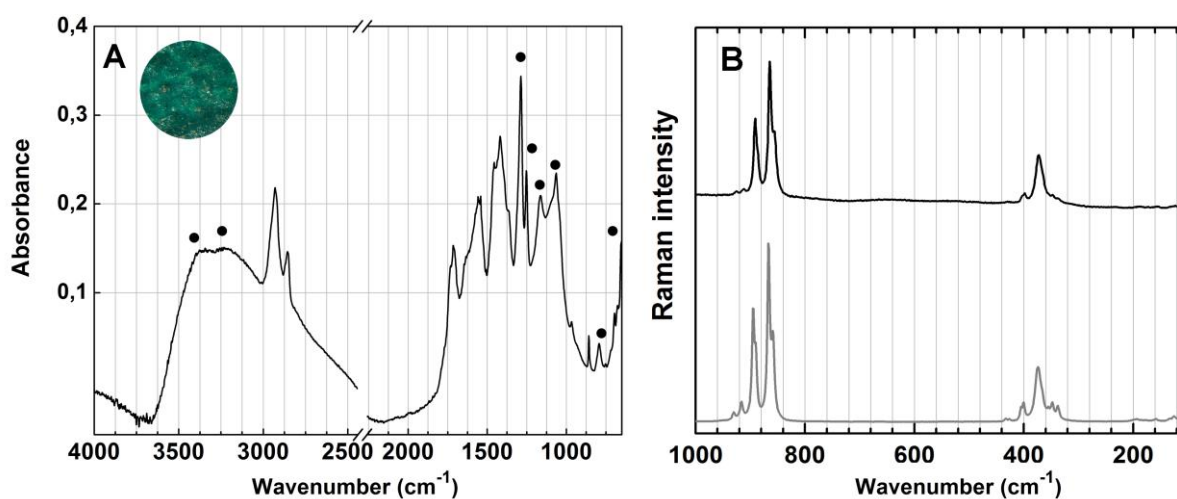


**Figure 28.** Green sample ( $\mu 19$ ) from *Untitled*; **A** Infrared spectrum (●) viridian pigment; **B** Raman spectra from the sample (black) and from the reference strontium yellow (grey).

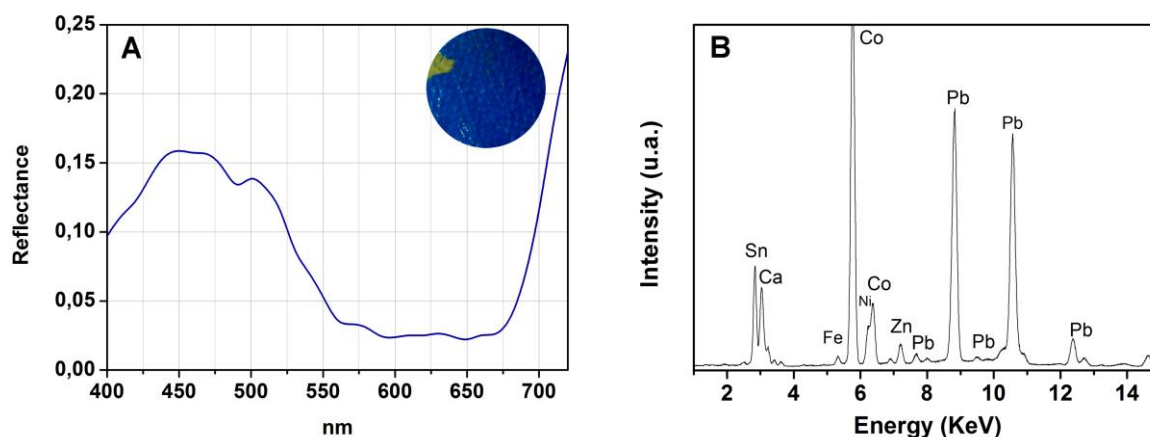


**Figure 29.** Blue sample (BI2) from *Untitled*; **A** reflectance spectrum; **B** EDXRF spectrum.

The **blue** tones are mainly obtained by cobalt pigments used pure (*BRUT* sample  $\mu 18$ ; *Entrada* EDXRF analysed BI4, BI9 and BI10) or in mixture with Prussian blue ( $\text{Fe}_4[\text{Fe}(\text{CN})_6]_3$ ) (*Entrada* EDXRF analysis on the areas BI11-15). In *Entrada* it is also used the mixture of Prussian and ultramarine ( $\text{Na}_8[\text{Al}_6\text{Si}_6\text{O}_{24}]\text{S}_n$ ) (*Entrada* samples  $\mu 2$  and  $\mu 3$ ).

In *Coty* and *Untitled* the mixture of blue pigments is less common; Prussian blue (*Coty* sample  $\mu 12$ ; EDXRF analyses BI10-11 and BI15) and cerulean blue ( $\text{CoO} \cdot n\text{SnO}_2$ ) (*Untitled* EDXRF analyses BI1-6) are mainly used pure. Figure 29A and B shows the characterization of the cerulean pigment using reflectance spectra in the visible region and  $\mu$ -EDXRF. The discrimination between cobalt ( $\text{CoAl}_2\text{O}_4$ ) and cerulean blue using reflectance spectroscopy is not straightforward: both pigments are characterized by three absorption bands between 550 and 670 nm related to the crystal field transition between in the orbital  $d-d$  of Co(II) ion [Boselli 2010]. In the case of cobalt blue the three bands are usually less visible, and in the case of the cerulean the bands are shifted to higher wavelengths of about 20 nm [Bacci *et al.* 2009].

In the paintings analysed in this chapter the **yellow** tones occupy a large percentage of the surface: 24% in *Untitled*, 11% in *Entrada* and *BRUT*, and only 9% in *Coty*. Chrome yellow continues to be the main yellow pigment in Amadeo's palette followed by cadmium yellow. The proportion between the use of chrome and cadmium yellow pigments is 2:1 in *BRUT* and *Entrada*; 3:1 in *Coty* and 4:1 in *Untitled*. Due to the tendency of chrome yellow to degrade, all samples were fully characterised and two of these were analysed by  $\mu$ -XANES and  $\mu$ -FTIR at European Synchrotron Radiation Facility (ESRF) in Grenoble, France. The results are presented in Section 2.1.5. In addition to the chrome and the cadmium yellow, strontium and cobalt yellow were occasionally detected. Cobalt yellow is used alone in the base of the neck of the female figure in *Coty* (sample  $\mu 3$ ) and in mixture with chrome yellow in *Untitled* (sample  $\mu 33$ ). In previously analysed paintings this pigment was found in *Untitled* (*O Jockey*) (Inv. 77P5, Fig. 5B). Cobalt yellow, called Aureolin, is a potassium cobalt nitrite  $\text{K}_3[\text{Co}(\text{NO}_2)_6]$ , but the related compound also exists, dipotassium monosodium hexanitrocobalt(III)  $\text{K}_3[\text{NaCo}(\text{NO}_2)_6]$  [Gates 1995]. This pigment was introduced as an artists' material in 1851 [Cornman 1986]. Figure 30 shows the characterization of *Coty* sample  $\mu 3$  using (A) FTIR and (B) Raman. Table 3 lists the band wavenumbers and the relative assignments for FTIR and Raman analysis of cobalt yellow.

**Table 3.** Characteristic infrared and Raman bands assigned to cobalt yellow ( $\text{K}_3[\text{Co}(\text{NO}_2)_6]$ ,) pigment [Cornman 1986; Hitchman and Rowbottom 1982; Miller and Wilkins 1952; Vendilo *et al.* 2011].

FTIR		Raman	
cm <sup>-1</sup>	Assignment	cm <sup>-1</sup>	Assignment
2704 (w)	--	1326 (s)	$\nu_{\text{as}}$ (N-O)
2649 (w)	--	836 (m)	$\delta$ (N-O)
1390 (vs)	$\nu_{\text{as}}$ ( $\text{NO}_2$ )	821 (s)	$\delta$ (N-O)
1334 (vs)	$\nu_{\text{s}}$ ( $\text{NO}_2$ )	302 (vs)	$\nu$ (Co-N)
827 (m)	$\delta$ (ONO)	178 (w)	--

w=weak; m=medium; s=strong; vs= very strong.

The BSE mode images of *Coty* sample  $\mu 3$  show rhomb's particles, in the particles surface it is possible to observe small holes (Fig. 31). SEM-EDS analysis detected the presence of cobalt associated with the presence of potassium and sodium, which suggest the presence of the potassium-sodium

compound. However, the amount of sodium in the sample is very low because no band shifts in the stretching and bending bands are visible.

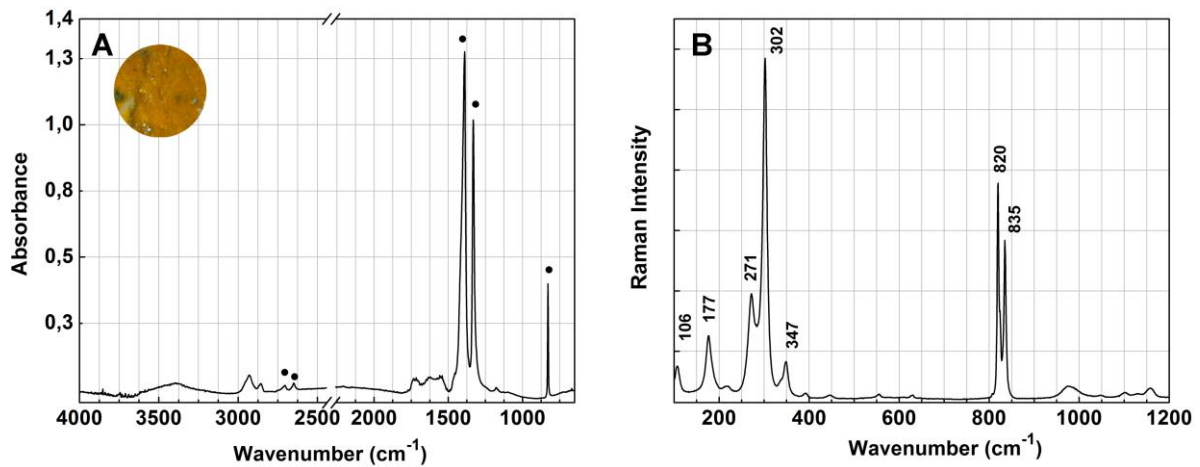


Figure 30. Yellow sample ( $\mu\text{3}$ ) from *Coty*; **A** Infrared spectrum (●) cobalt yellow pigment; **B** Raman spectrum.

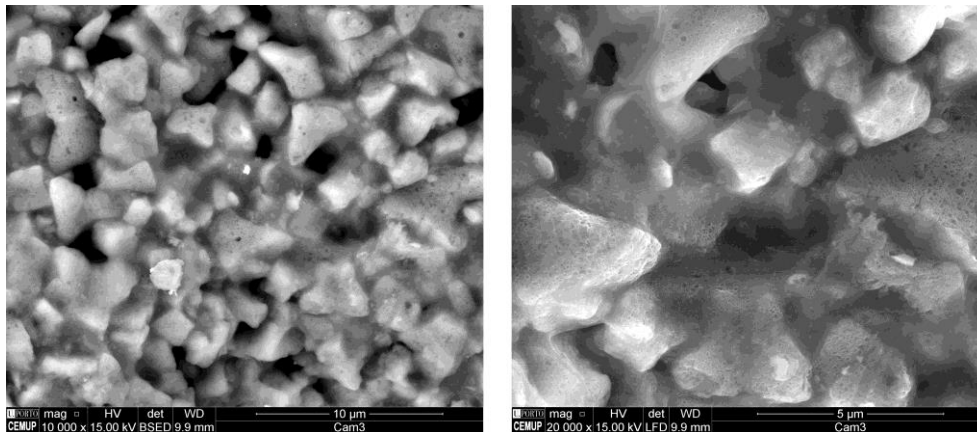
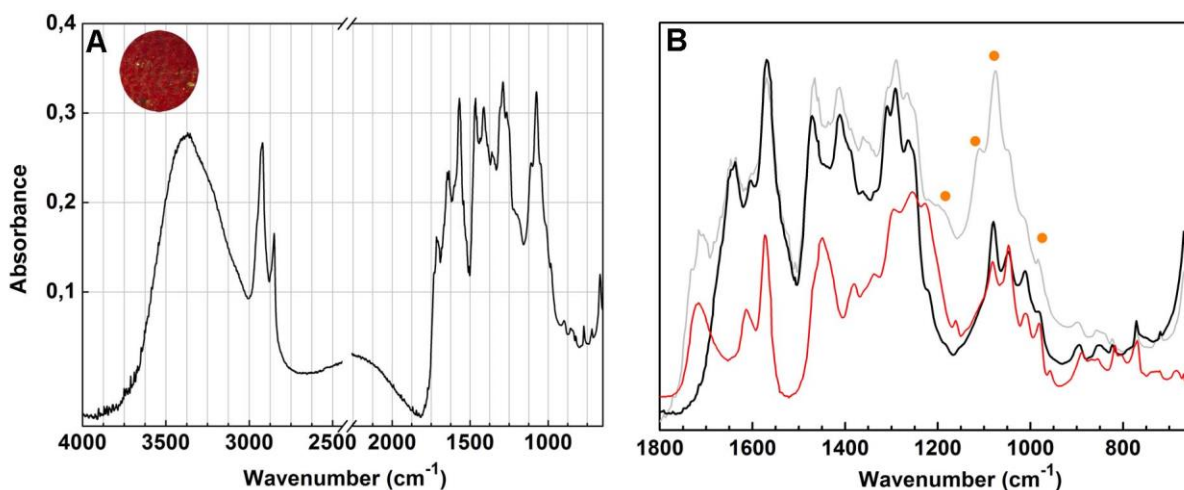


Figure 31. Yellow sample ( $\mu\text{3}$ ) from *Coty* SEM image in BSE mode.

In the paintings previously analysed Amadeo used mainly vermilion ( $\text{HgS}$ ) for a **red** hue and less frequently, cochineal lake. In these last paintings vermilion continues to be used but at the same time the use of lakes of alizarin and purpurin appears. In *BRUT*, 7% of the surface is painted with red lakes. FTIR analysis shows a good match of the *BRUT* samples  $\mu\text{Red1}$ ,  $\mu\text{11}$ ,  $\mu\text{26}$ ,  $\mu\text{28}$  and  $\mu\text{30}$  and the paint tube of Brown Madder<sup>11</sup> of Winsor & Newton (identified with the code MG1). From the same painting the sample  $\mu\text{14}$  shows a good match with the oil paint sample of Laque Andrinople<sup>12</sup> by Lefranc (identified with the code MG10). Figure 32 shows the comparison between the FTIR analysis of the red sample  $\mu\text{6}$  from *Coty* (black line); the spectrum of cochineal carmine lake reproduction based on a recipe from the W&N archive (grey line) and the spectrum of carminic acid (red line).

<sup>11</sup> HPLC analysis of the paint tube sample detected the presence of alizarin and purpurin [Melo *et al.* 2009].

<sup>12</sup> HPLC analysis of the paint tube sample detected the presence of alizarin [Melo *et al.* 2009].



**Figure 32.** A Infrared spectra of the red sample  $\mu 6$  from *Coty* B section of A between 1800 and 650  $\text{cm}^{-1}$ : sample  $\mu 6$  (black line), cochineal carmine lake reproduction (grey line), carminic acid (red line) and (●) barium sulphate.

Figure 33 shows the morphology of the red paint (sample  $\mu\text{Red}1$ ) in *BRUT*: in the red top layer elongated white particles are visible in a matrix of aluminium associated with the presence of red lake. The white particles show a core of barite ( $\text{BaSO}_4$ ) covered by lead sulphate ( $\text{PbSO}_4$ ); the particles measure 7.5  $\mu\text{m}$  in length and 2  $\mu\text{m}$  thick. The core measures a thickness of 0.3  $\mu\text{m}$ . This type of particle has never been found in other analysed Amadeo's paintings.

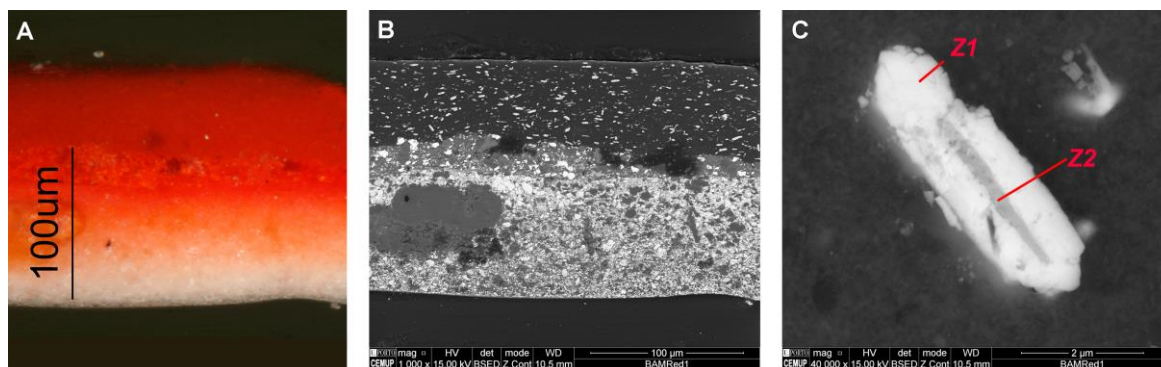


**Figure 33.** Sample  $\mu\text{Red}1$  from *BRUT*: **A** Cross-section; **B** and **C** SEM image in BSE mode details of the white particles present in the top layer, in the area Z1 was  $\text{PbSO}_4$  and in area Z2  $\text{BaSO}_4$ .

In *Coty* Raman analysis detected the use of the red organic dye  $\beta$ -naphthol in mixture with minium (sample  $\mu 2$ ). The Raman spectra collect on the painting sample was compared with those present in the Raman spectra reference collection [Scherren *et al.* 2009], the best match was found with the spectrum of the  $\beta$ -naphthol pigment PR49 C.I. 15630 (Fig. 32 left) (molecular structure in Fig. 34 right) belongs to the class of Lithol red<sup>13</sup>.

<sup>13</sup> Lithol red was discovered and patented by P. Julius in 1899. It was widely available in the early 1920s. Sodium (PR 49), barium (PR 49:1), calcium (PR49:2), and strontium (PR 49:3) salts of diazotised (2-naphthylamine-1-sulfonic) acid coupled with 2-naphthol [Craver 2000; Eastaugh *et al.* 2004; Stenger *et al.* 2010; Standeven 2012] belong to the Lithol group.



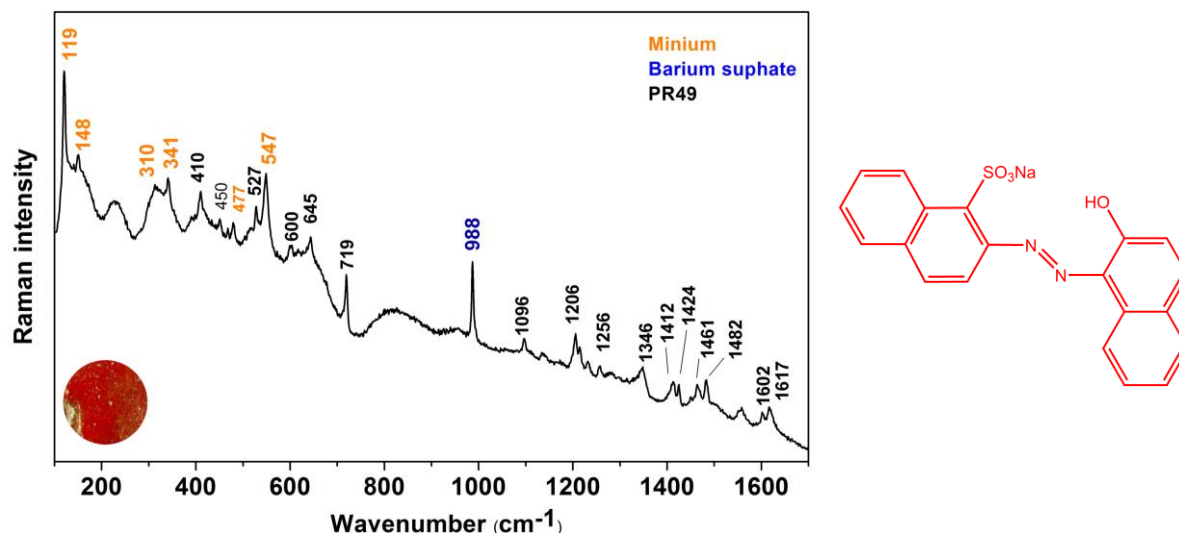


**Figure 34.** (Left) Raman spectrum of *Coty*  $\mu 2$ ; in black the bands attributed to PR49  $\beta$ -naphthol pigment, in orange those attributed to minium and in blue the characteristic band of the barium sulphate. (Right) Molecular structure of Lithol red (PR49) [Scherren *et al.* 2009].

In the paintings analysed dated before 1917, the **white** areas were obtained with a mixture of lead white ( $2\text{PbCO}_3 \cdot \text{Pb(OH)}_2$ ) and barium sulphate ( $\text{BaSO}_4$ ). In these last 4 paintings Amadeo continued to use the lead but in *BRUT* and *Entrada* it was also found a large use of zinc white ( $\text{ZnO}$ ). In the previous works zinc white was just found in small areas of another painting dated 1917, the *Untitled* (Inv. 86P19) (Fig.5B). Figure 35 shows the proportion in the use of the two white pigments in the paintings.

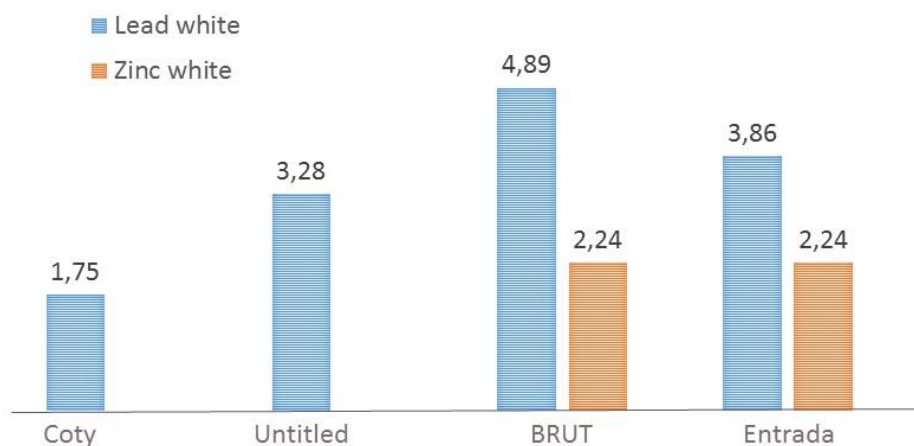


**Figure 35.** Percentage of the use of lead and zinc white in the paintings analysed.

FTIR and Raman analysis of the samples collected from the white areas show that lead white was always used in mixture and in similar proportion with other white sulphate compounds. In the paintings *Entrada* (samples  $\mu 14$  and  $\mu 23$ ) lead white was used in mixture with strontium sulphate (Fig.36); In *BRUT* (samples  $\mu 25$ ,  $\mu 29$  and  $\mu 27$ ) and *Untitled* (samples  $\mu 4$ ,  $\mu 20$  and  $\mu 43$ ) lead white was used in mixture with gypsum. The proportion between lead white and the strontium sulphate in *Entrada* is similar to that found in the painting *Untitled* (CAM Inv. 86P19) analysed in 2008 [Melo *et al.* 2008].

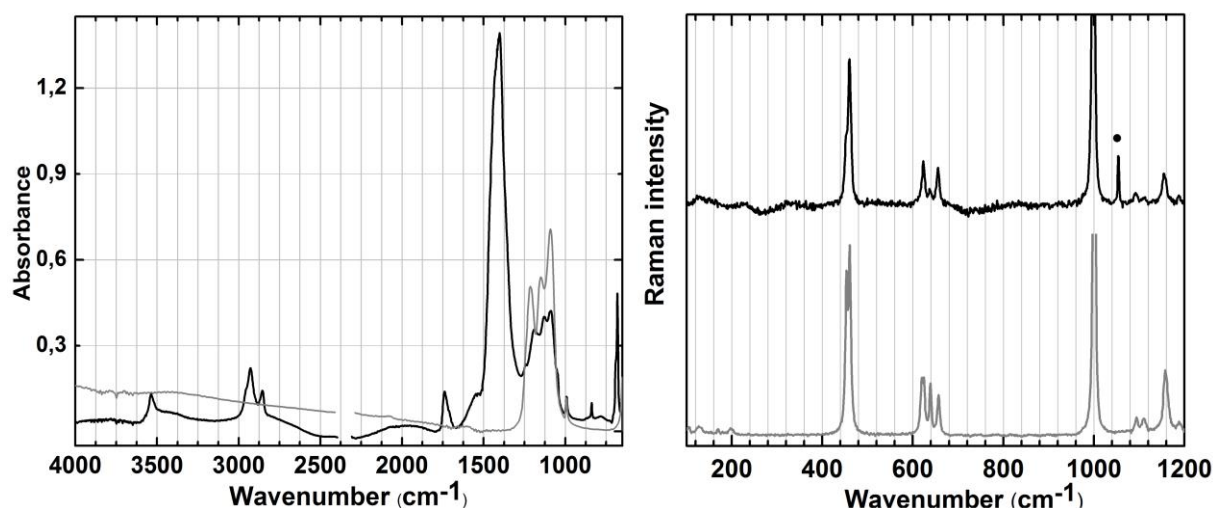


**Figure 36.** White sample ( $\mu 14$ ) from *Entrada* painting; **A** Infrared spectra of the sample (black line),  $\text{SrSO}_4$  (grey line); **B** Raman spectra of the sample (black line),  $\text{SrSO}_4$  (grey line) and lead carbonate (●).

The first attempt to introduce zinc with was introduced as artists' material was in 1780 [Kühn and Curran 1986]. W&N started to sell it in watercolour in 1834 and the French producer Leclaire produced oil zinc white in industrial scale in 1845 [Kühn and Curran 1986]. This pigment was also the white of the enamel paint brand Ripolin (Section 1.2.2). It is well known the predisposition of zinc to form metal carboxylates due to the interaction of the metal ions with the free fatty acids of the oil (Section 1.2.2). In *BRUT*, in the areas where the use of zinc white was found, FTIR analysis detected a large amount of metal soaps. For that reason a full characterization was performed of the zinc white samples to evaluate the state of preservation of the paint and to see if there is the possibility that Amadeo used enamel paints in his last artworks; the results of the analysis is presented in Section 2.2.1.

#### 2.1.4 Chrome yellow samples

The colour range of chrome yellow pigments varies from light yellow (mixed crystals of lead chromate and lead sulphate,  $\text{Pb}(\text{Cr},\text{S})\text{O}_4$ ) to yellow (lead chromate,  $\text{PbCrO}_4$ ) and orange-red (basic lead chromate,  $\text{Pb}_2\text{CrO}_5$ ). In the paintings presented in this chapter Amadeo used different yellow tones, obtained using pure lead chromate and mixed crystals of lead chromate and lead sulphate. This was also found in the paintings previously studied [Otero *et al.* 2012]. These pigments were also mixed with cadmium yellow, ochre and in one case with cobalt yellow to achieve specific hues.

Figure 37 shows the different CIE( $a^*b^*$ ) values of some of the chrome yellow samples from the paintings *BRUT*, *Entrada* and *Untitled*; as expected the pure lead chromate ( $\text{PbCrO}_4$ ) (blue squares) has a more reddish tone (higher  $a^*$  values) compared with the mixed crystals of lead chromate and lead sulphate ( $\text{Pb}(\text{Cr},\text{S})\text{O}_4$ ) formulation (grey squares). The mixed crystals of lead chromate and lead found in Amadeo's paintings are characterized by a similar proportion between the two components.

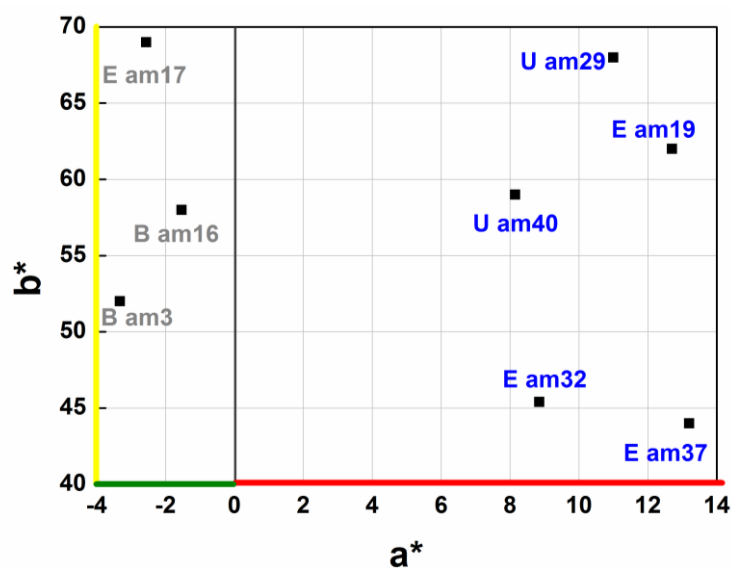


**Figure 37.** CIE(a\*b\*) colour values for the chrome yellow samples: pure lead chromate (in blue) and mixed-crystals of lead chromate and lead sulphate (in grey). E = *Entrada*; B= *BRUT* and U= *Untitled* paintings.

Table 4 shows the characterization of the samples analysed in the paintings of Amadeo, dated 1917. Recently, a comprehensive study of the W&N 19<sup>th</sup> century manufacture of their yellow lead chromate based pigments was carried out [Otero *et al.* 2014b]. It was possible to conclude that W&N used a limited number of manufacturing processes to produce their **chrome yellow** and **chrome deep** colours. Lemon and Pale production records were used to produce chrome yellow and Middle and Deep to produce their chrome deep. In blue are indicated the related W&N processes with the pigment composition identified in Amadeo's works [Otero *et al.* 2014b].

**Table 4.** Characterization of micro-samples of chrome yellows.

	Pigments Composition		Samples
Pure	<b>PbCrO<sub>4</sub> + CaCO<sub>3</sub></b> (Chrome Deep) Process M3a*	No fillers	Untitled μ29, 40
		Gypsum	SrSO <sub>4</sub> Entrada μ19
		Kaolin	Entrada μ8, 32
		MgSO <sub>4</sub> 7H <sub>2</sub> O	CdS Entrada μ37
Mixed crystals	<b>Pb(Cr,S)O<sub>4</sub></b> (Chrome Yellow)	No fillers Lemon Process L3b*	Entrada μ17
		Barite	-- Untitled μ1
		Process L3a*	MgCO <sub>3</sub> BRUT μ 3
		MgCO <sub>3</sub> , Quartz	BRUT μ16

\* The codes of the processes are L = Lemon/Pale and M = Middle. When process variations exist, the main pathway presents the letter a and the process variation the letter b.

In the paint samples with the pure lead chromate (*Entrada* samples μ8, μ19; μ32 and μ37 and *Untitled* sample μ29 and μ40) it was detected the presence of calcium carbonate used as filler, the proportion of the calcium carbonate and lead chromate are constant in all the painting samples. SEM-EDS analysis on these yellow samples show the presence coccolith shells of the CaCO<sub>3</sub>, which indicates that the material was formed by organogenic sedimentation (Fig.38) [Gysau 2006, pg.21].

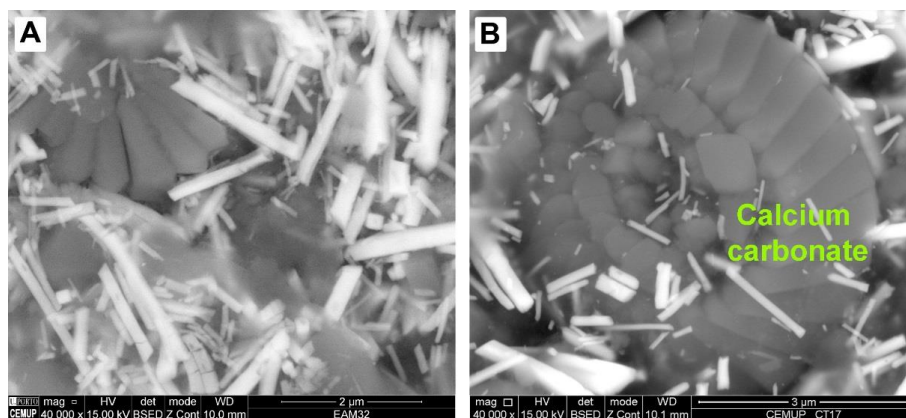


**Figure 38.** SEM image in BSE mode of the pure chrome yellow sample **A** *Entrada*  $\mu$ 32; **B** sample of paint tube of Chrome deep ( $\mu$ 17\_3128) of W&N.

Comparing the pigment reconstruction based on the W&N archive [Otero *et al.* 2014b] a correlation was found between the pure lead chromate samples with calcium carbonate and the middle process M3a<sup>14</sup>. As stated, this process is associated with the W&N chrome deep colour. This composition corresponds to what found in a W&N oil paint tube labelled Chrome Deep ( $\mu$ 17-3128) that belonged to the painter Columbano Bordalo Pinheiro<sup>15</sup> (1857–1929) [Silva *et al.* 2011]. Figure 39 shows the FTIR spectra of the *Entrada* sample  $\mu$ 8 and a M3 pigment reconstruction, where the characteristic bands of the  $\text{CaCO}_3$  are visible at  $1422\text{ cm}^{-1}$  and  $875\text{ cm}^{-1}$ . This second band shows an overlapping with the band of the asymmetric stretching of the  $\text{CrO}_4^{2-}$  group and the shoulders at  $831$  and  $820\text{ cm}^{-1}$ .

Also for the sample characterized by the presence of a solid solution of lead chromate and lead sulphate ( $\text{Pb}(\text{Cr,S})\text{O}_4$ ) were compared with the reconstruction based on the W&N archive. A good match was found between the sample from *Entrada*  $\mu$ 17 and the Lemon chrome yellow, W&N process L3b<sup>16</sup> (in this process no fillers were added). The samples from *Untitled*  $\mu$ 1 and *BRUT*  $\mu$ 3,  $\mu$ 16 can be correlated with the W&N process L3a<sup>43</sup> (characterized by the presence of barium sulphate). As noted, these methods are associated with the W&N chrome yellow colour and this type of composition also corresponds to what found in a W&N oil paint tube labelled Chrome Yellow ( $\mu$ 26-3130) that also belonged to Columbano [Silva *et al.* 2011]. Figure 40 shows the comparison of the FTIR spectrum from the sample *Entrada*  $\mu$ 17 with a pigment reconstruction based on the W&N archive (L3b).

<sup>14</sup> In this process the chromate source is obtained from  $\text{K}_2\text{Cr}_2\text{O}_7$  and  $\text{Na}_2\text{CO}_3$ ; the lead source is  $\text{Pb}(\text{NO}_3)_2$  and  $\text{CaCO}_3$  is used as extender. However, in this particular formulation, M3,  $\text{Na}_2\text{CO}_3$  was not added [Otero *et al.* 2012].

<sup>15</sup> Two boxes with 63 oil paint tubes belonged to the Portuguese painter Columbano Bordalo-Pinheiro (Lisbon 1857-1929) and conserved at the Museu Nacional de Arte Contemporânea do Chiado in Lisbon were analysed in the context of the Crossing Borders project at DCR-FCT; part of the analyses are published in Silva *et al.* [Silva *et al.* 2011] and Montagner *et al.* [Montagner *et al.* 2013b]. The tubes belong to several companies: 32 from Winsor & Newton; 14 from Morin et Janet; 10 from P. Denis (C. Bourgès – Maison Merlin); 5 from Lefranc. Two tubes are not labelled.

<sup>16</sup> In L3a process the chromate source is obtained from  $\text{K}_2\text{Cr}_2\text{O}_7$  and  $\text{Na}_2\text{CO}_3$ ; the lead source is  $\text{Pb}(\text{NO}_3)_2$ ; the sulphate source is sodium sulphate ( $\text{Na}_2\text{SO}_4$ ) with sulphuric acid ( $\text{H}_2\text{SO}_4$ ) and  $\text{BaSO}_4$  is used as extender. In L3b no extender is added [Otero *et al.* 2012].

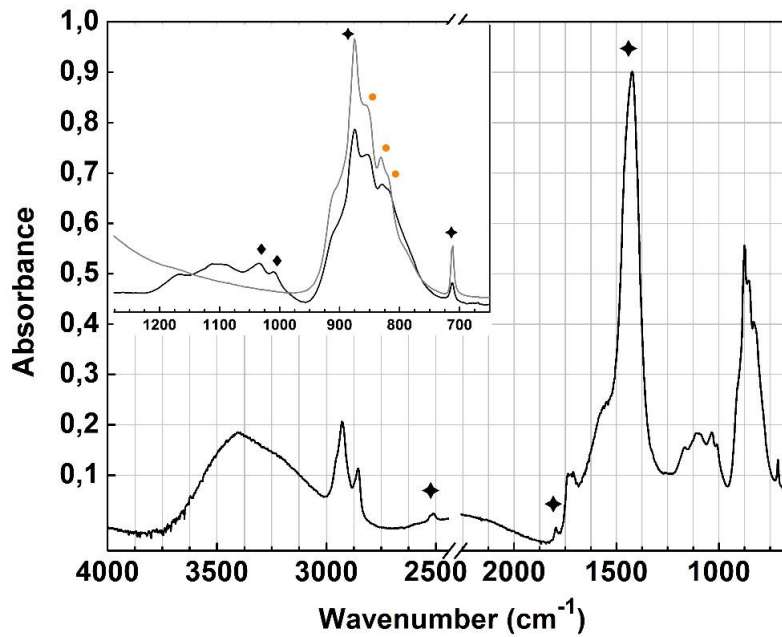


**Figure 39.** Infrared spectra of the sample  $\mu 8$  *Entrada*. In the inset, comparison with the chrome deep pigment reconstruction, M3 (based on W&N process) (in grey) ●  $\text{PbCrO}_4$ ; ◆  $\text{CaCO}_3$ ; ◆ kaolinite.

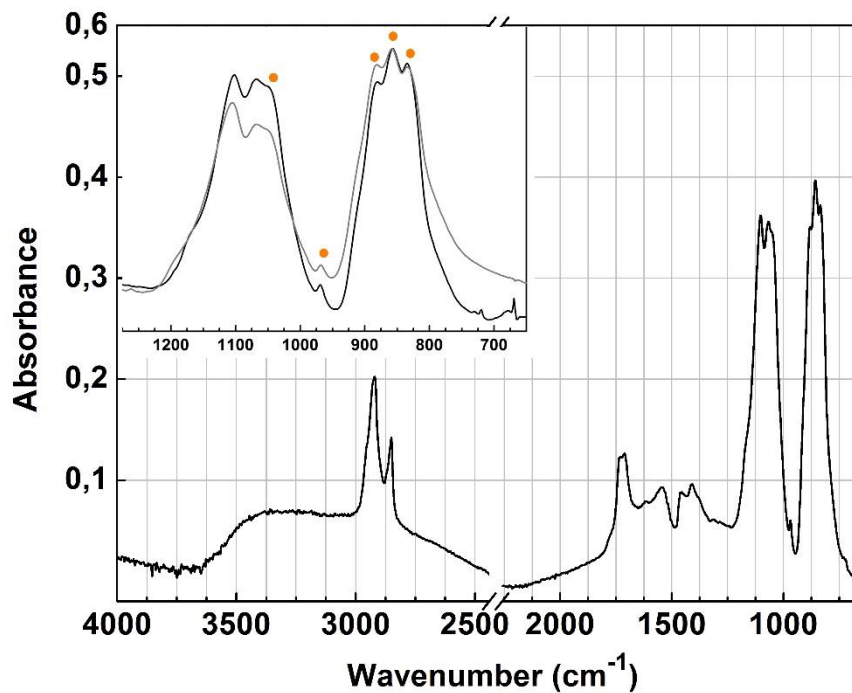


**Figure 40.** Infrared spectra of the sample  $\mu 17$  *Entrada*. In the inset, comparison with a Lemon chrome yellow pigment reconstruction, L3b (based on W&N process) (in grey); ●  $\text{Pb}(\text{Cr,S})\text{O}_4$ .

Other additives, such as gypsum, kaolin, the barium and the strontium sulphate and magnesium sulphate heptahydrate (Table 4). The presence of magnesium carbonate is associated to the W&N 19<sup>th</sup> century oil paint manufacture [Otero *et al.* 2014b]. No correlations were found between the additives indicated below and the recipes of chrome yellow pigment in the W&N archive; this should be suggest the used by Amadeo of a different manufacturer. SEM-EDS and FTIR analysis of the other chrome

yellow samples collected from the analysed paintings are presented in Appendixes of Part II Ap.VII.1 and Ap.VII.2, respectively.

The tendency to darkening of the chrome yellow is well-known (Section 1.2.3); for this reason a set of 4 samples from 19<sup>th</sup> century oil paint tubes and 5 historically accurate reconstructions (HART)<sup>17</sup> samples (powders, unaged and artificially aged oil paints) and 14 micro-samples from Amadeo's paintings, including two samples from *BRUT* and *Entrada*, were analysed by synchrotron radiation (SR)-based techniques, X-ray Absorption Near Edge Structure ( $\mu$ XANES), X-ray fluorescence microspectrometry ( $\mu$ XRF) and Fourier transform infrared microspectroscopy mapping ( $\mu$ FTIR), at the ESRF during a mission of April 2014. Unaged and aged<sup>18</sup> paint reconstructions were analysed with the aim of understanding which pigment and/or paint formulation shows more tendency to change colour and what are the degradation products. The painting samples were analysed to see if there are any signs of degradation process in Amadeo's artwork.

Both *Entrada* and *BRUT* samples are composed of mixed crystals of lead chromate and lead sulphate; in the first one no filler was detected. While in the *BRUT* sample magnesium carbonate was found, along with barite, quartz and zinc azelate (the characterization of the metal soap will be developed in Section 2.2.1).

The absorption of the carboxylate is homogenous in all the samples, no aggregates are visible. As introduced in section 1.2.3 the degradation of the chrome yellow is related to the reduction of the original species Cr(VI) to Cr(III). To evaluate the presence or not of Cr(III) species compared the profile of the Cr K line obtained from the XRF maps performed at different beam energies (Fig. VII.13 Appendix Part II Ap.VII.3). In both samples, no alteration was found and consequently, we can assume that no degradation has occurred. To confirm this result in each sample a set of analysis was performed using  $\mu$ -XANES, Figure 41A and C show the points where the analysis was performed; in all points the  $\mu$ -XANES spectra obtained are very similar with that of lead chromate (crocoite) reference spectra, supporting the conclusion that no degradation is occurring. Figure 41B and D show the average XANES spectra. More information of the SR analysis in Appendix Part II Ap.VII.3

---

<sup>17</sup> Result obtained in the ongoing PhD thesis project of Vanessa Otero «Bright colours: historically accurate reconstructions of Amadeo's palette» at DCR-UNL.

<sup>18</sup> The samples were irradiated for 1500 hours using a Xenon-light apparatus ( $\lambda_{irr}>310$  nm).

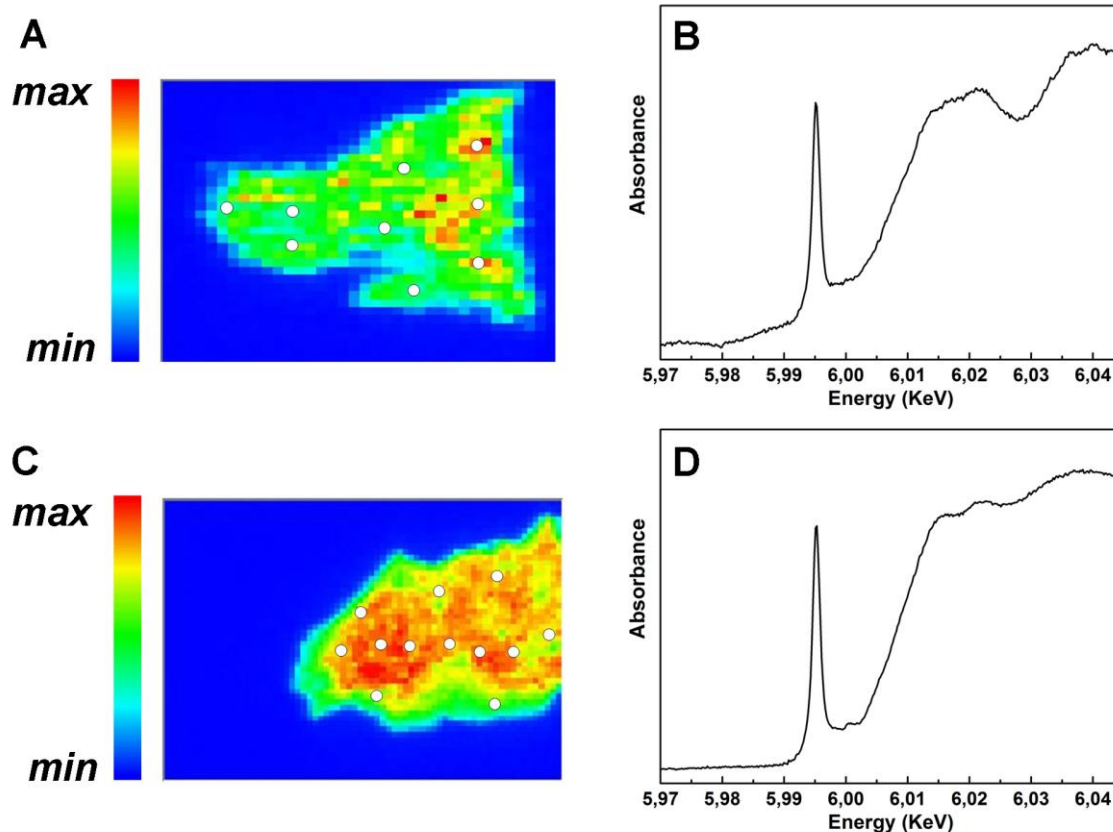


**Figure 41.** XRF chromium map intensity with the XANES points of analysis (°) **A** *BRUT* and **C** *Entrada*; average XANES spectrum **B** *BRUT* and **D** *Entrada*.

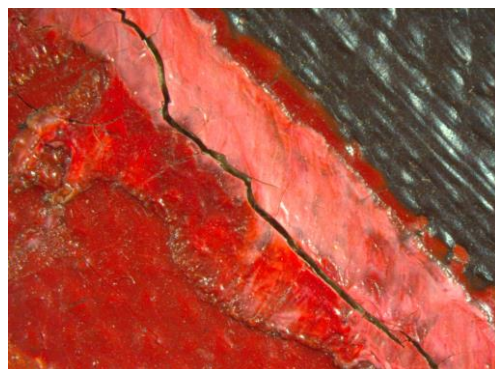
## 2.2 Conservation issues

From the studied paintings, *BRUT* was the one where more problems of conservation were detected. Figure 42 shows the problems detected and their location. Cracks were detected in the red area close to the up left corner (Fig. 42B). The detail images in Figure 42C in the brown and red areas were acquired using transmitted light, these image shows that the paint layer is very thin, and characterized by the presence of network of micro-cracks network. The light (Fig. 42D) and the dark green areas in the lower-right angle also show the presence of a network of cracks but in this case the paint layer is very thick. In this area was detected the presence of starch mixed with emerald green (discussed in 2.2.3). In the same dark green area a lacuna is present that leaves the canvas visible (Fig. 42E). The white and the green paint (Fig. 42C) of the letter R shows problems of adhesion, part of the letter was already loss. FTIR analysis in this area detected the presence of zinc carboxylate (discussed in 2.2.1). In *BRUT* also two areas were detected with colour alteration: part of the dark blue area around the guitar silhouette (Fig.42H) shows whitish tone due to the delamination of the varnish (ketone resin). In the area of the head of the guitar (Fig. 42I) it was detected a fading of the purple dyes (eosin-based lake), that caused the colour change from purple to blue given by the presence of cobalt blue pigment (discussed in 2.2.2).

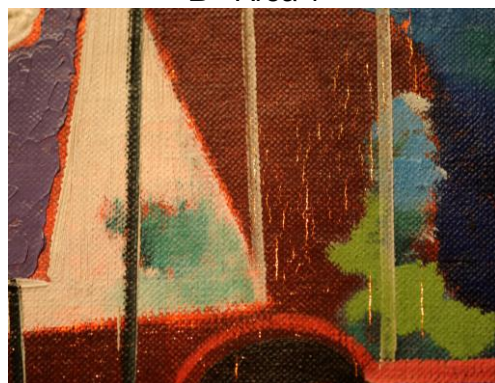




A



B - Area 1



C - Area 2



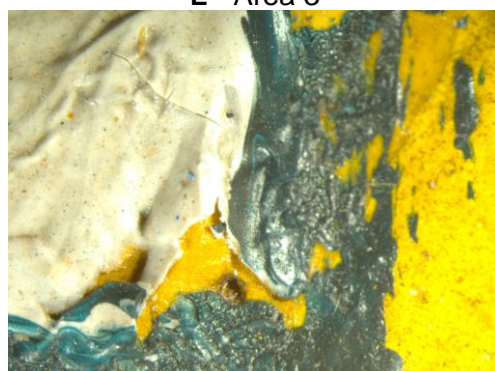
D - Area 2



E - Area 3



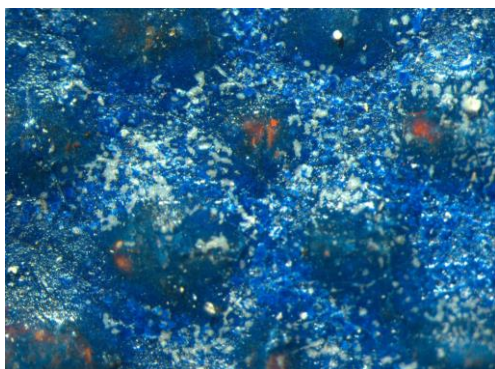
F - Area 4



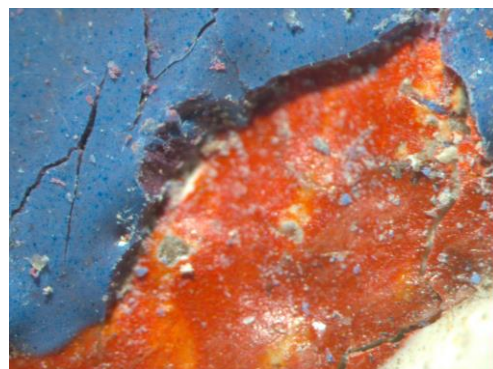
G - Area 5

**Figure 42.** Conservation problems detected in *BRUT*: **A** localization of the areas. Image details **B** crack (10x); **C** network of cracks (macro image acquired with transmitted light); **D** network of cracks (10x); **E** cracks and lacuna of the paint and preparation layer (25x); **F** cracking (32x); **G** delamination of the white and green paint (16x).





H - Area 6



I - Area 7

**Figure 42 (continued).** H White patches on the surface (50x); I fading (40x).

### 2.2.1 Metal carboxylates

The word “BRUT” in the *BRUT* painting (Fig. 43D) shows problems of adhesion that in some cases involve the loss of paint. To note that the problems of adhesion are visible in the letter “R” (Fig.43A and B) but not in the letter “T” (Fig. 43C). FTIR analysis in the samples collected in the letters “R” and “T” (Fig. 43D) detected a large amount of zinc carboxylates. Based on the spectral features the FTIR spectra were divided in two groups. Figure 44 shows a representative spectrum of each group:

- (1) In the FTIR spectrum in Figure 44A, are visible the characteristic absorption bands of the zinc soaps: stretching C-H at 2919, 2850  $\text{cm}^{-1}$ , stretching  $\text{COO}^-$  ( $\nu_{\text{as}}$  1551, 1534  $\text{cm}^{-1}$  and  $\nu_{\text{s}}$  1402  $\text{cm}^{-1}$ ); bending  $\text{CH}_2$  at 1461  $\text{cm}^{-1}$  and rocking  $\text{CH}_2$  at 745  $\text{cm}^{-1}$ , bending  $\text{COO}^-$  at 669  $\text{cm}^{-1}$ . Based on these spectral features it was suggest the presence of a zinc carboxylate with a well-defined molecular structure. The well structure identified by the spectroscopic analysis may be related to the presence of a compound add to the paint and not formed in it, such as an additive in the paint. This type of carboxylate was found in the samples  $\mu_4$  and  $\mu_5$  from the letter “R” (Fig.43A and B)
- (2) FTIR spectrum in Figure 44B shows the presence of lead white, gypsum and a broad band centred at 1582  $\text{cm}^{-1}$  related to a not-defined structure of carboxylate compounds, may related to an ongoing process, such as a degradation process between the zinc and the oil. This type of carboxylate was found in the sample  $\mu_{25}$  from the letter “T”

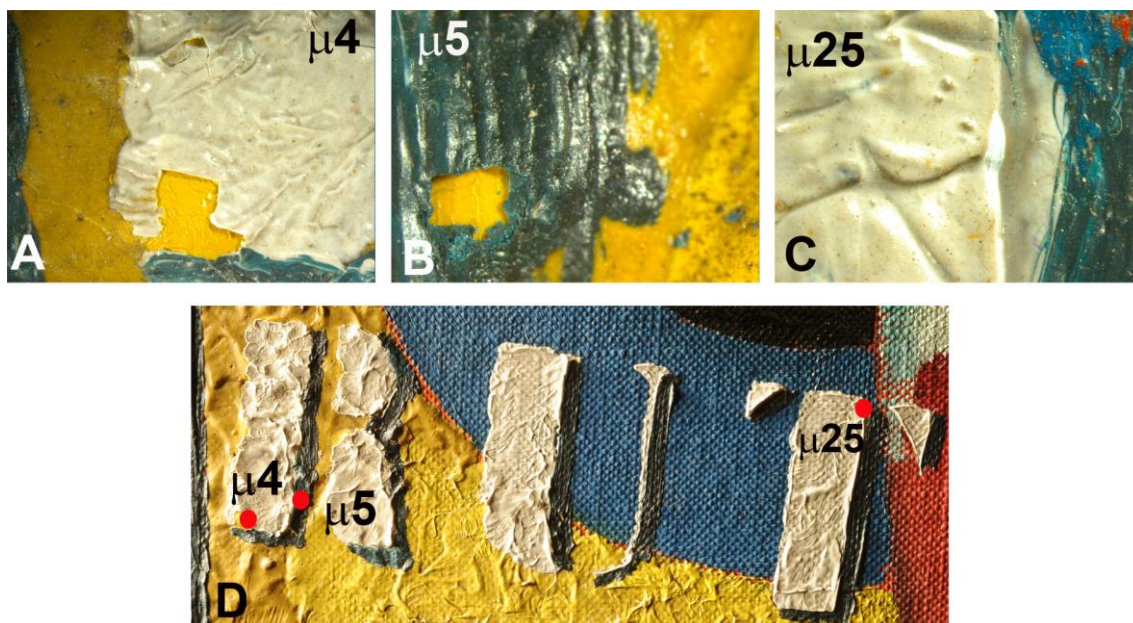


**Figure 43.** Photomicrographs of the white and dark green areas in the word “BRUT” **A** delamination of the white area in the letter “R”, sample  $\mu 4$  (10x); **B** delamination of the green area in the letter “R”, sample  $\mu 5$  (32x); **C** sampling area in the letter “T” where no delamination was observed, sample  $\mu 25$  (20x); **D** identification of the sampling area in the word “BRUT”.

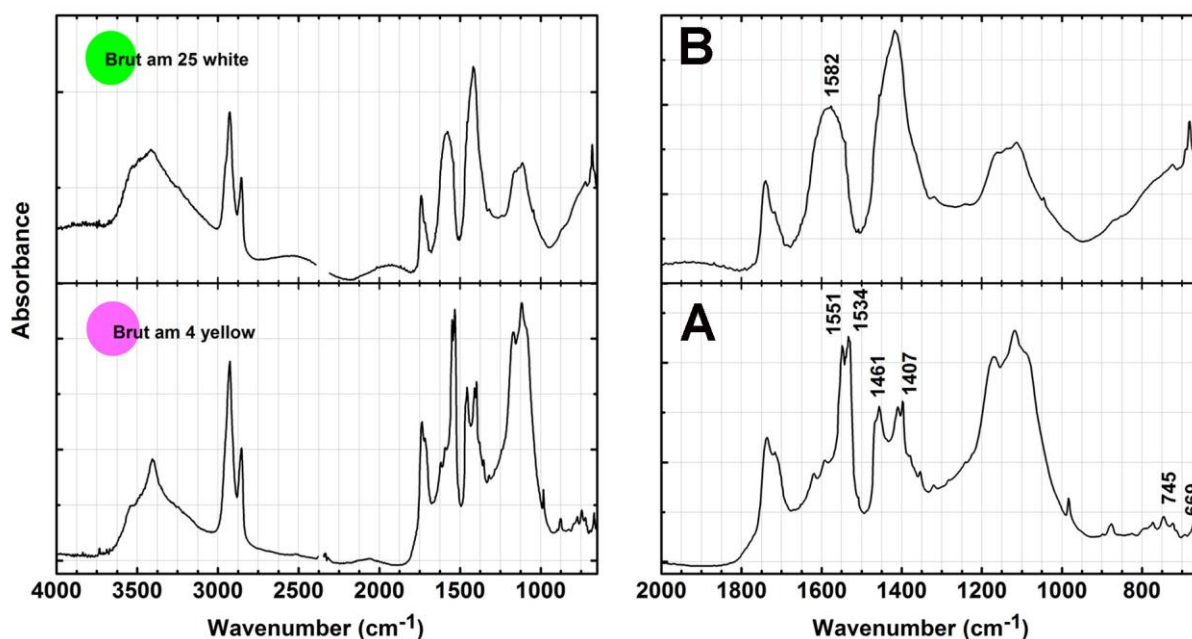


**Figure 44.** Infrared spectra of samples collected from the word “BRUT” in the painting *BRUT*; **A** from yellow area under the letter “R” ( $\mu 4$ ) (group 1); **B** white area in the letter “T” ( $\mu 25$ ) (group 2).

The two types of carboxylates described for the letter “R” and “T” were found also in other *BRUT* samples. FTIR analysis was performed on of 71 samples collected on the *BRUT* and *Entrada*. Figure 45 shows the mapping of the areas where the two types of carboxylates were found. In pink the areas where it were detected carboxylates form the group (1) characterised by the presence of a defined

structure (Fig. 44A). These areas were quantified in 15.5% of the surface of the painting *BRUT*. In green the areas where it were detected carboxylates form the group (2) characterised by the broad band at 1589  $\text{cm}^{-1}$  (Fig. 44A). These areas were quantified in 18.3% of the surface of the painting *BRUT*.

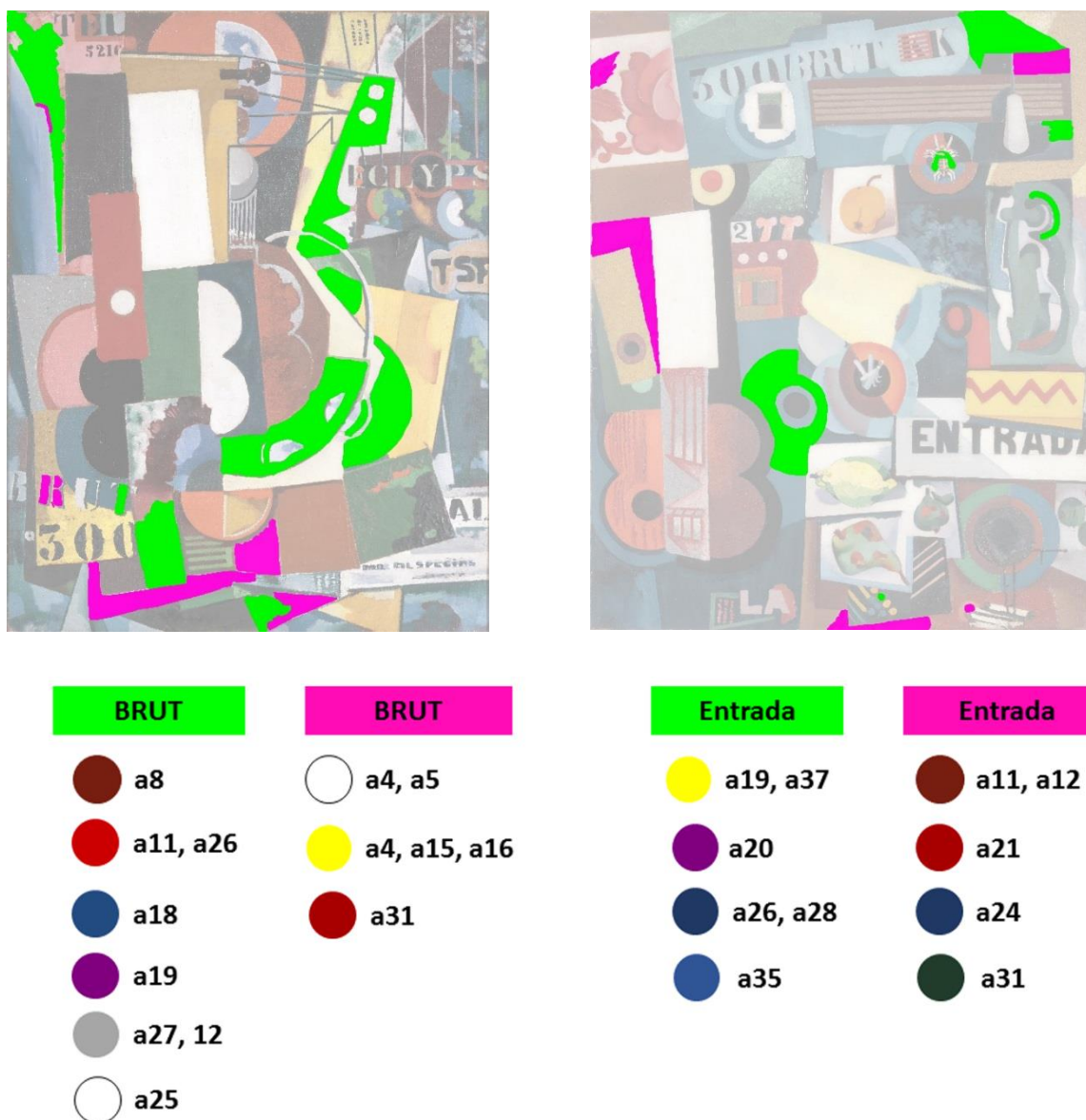


**Figure 45.** (Top) Mapping of the carboxylates areas in painting *BRUT* and *Entrada*: the pink area corresponds to the samples of the group 1, characterized by the presence of IR defined bands at 1551, 1534  $\text{cm}^{-1}$  (spectrum Fig. 44A). The green area corresponds to the samples of the group 2, characterized by the presence of IR broad band centred ad 1589  $\text{cm}^{-1}$  (spectrum Fig. 44B); (Down) Identification of the samples analysed for each type of carboxylates group.

To better characterize the samples collected from the paintings *BRUT* and *Entrada* their FTIR spectral features were compared with spectra collected on (i) reference zinc soap synthesized at DCR; (ii) samples collected from oil paint tube ASC8 “Blanc de Zinc” by Lefranc Paris that was found in the box in preserved in the Amadeo’s house in Manhufe (please see Part II, Section 1.1.3) and (iii) a sample

from a swatch of “Blanc 1401” by Ripolin colour chart dated 1925<sup>19</sup> belong to DCR (Image of the Ripolin chart in Appendix Part II Ap.IX).

A paint from the Lefranc zinc white tube (ASC8) was applied in 2008 on a microscope glass slide, the slide was leaved opened in a box protected by the light. In 2014 FTIR analysis was performed sampling different areas of the paint: a dried area (external surface) and in a not complete dried area (on the internal of the paint). Figure 46 shows the FTIR spectra from these two areas, the figure is divided in the 3 part to help the identification of the characteristic regions: (i) 2919, 2850  $\text{cm}^{-1}$   $\nu(\text{C-H})$ ; (ii) 1547, 1527  $\nu_{\text{as}}(\text{COO}^-)$  and 1398  $\text{cm}^{-1}$   $\nu_{\text{s}}(\text{COO}^-)$ ; (iii) 745, 721  $\text{cm}^{-1}$   $\delta(\text{CH}_3)$  and 681  $\text{cm}^{-1}$   $\delta(\text{COO}^-)$ . It is interesting to note that the samples from the zinc tube show the same types of IR features identified in the *BRUT* and *Entrada* samples (Fig.44). The sample from the surface shows a broad band at 1580  $\text{cm}^{-1}$ , while the sample from the internal area show peaks at 1549 and 1534  $\text{cm}^{-1}$ . These peaks may suggest the presence of **zinc azelate and/or oleate**. Figure 47 shows FTIR spectra of the zinc carboxylate synthesized at DCR [Otero *et al.* 2014a] and used as a reference in this work. Zinc azelate and oleate are characterized by the presence of the doublet absorption at 1556/1535  $\text{cm}^{-1}$  and at 1547/1527  $\text{cm}^{-1}$ . Zinc oleate (and palmitate) are characterized also by the two bands 743, 722  $\text{cm}^{-1}$   $\delta(\text{CH}_3)$ . The oleates present an additional characteristic band around 3005  $\text{cm}^{-1}$  due to the C=C-H stretching vibrations. This absorption is not visible in the spectrum of the samples from the Lefranc tube.

Observing the FTIR spectra form the *BRUT* samples with a well-defined structure. It was possible to identify: zinc **stearate or palmitare** in the sample  $\mu 5$  and zinc **zinc azelate and/or oleate** in the samples  $\mu 4$ , 15-16 and 31.

The swatch Blanc by Ripolin was sampled in 3 areas from the surface to the internal of the swatch. All the spectra acquired show the same features. Figure 48 shows an example of FTIR spectrum collected from the swatch Blanc. FTIR spectrum shows a broad band centred at 1580  $\text{cm}^{-1}$  similar to the dried sample of the Lefranc paint and in the samples of the group (2) in the painting *BRUT*. Casadio *et al.* 2013 and Hanspach-Bernal and Bezur show the same IR spectral features in samples collected from Ripolin’s swatch on different colour charts from the collection of the Art Institute of Chicago [Casadio *et al.* 2013c; Hanspach-Bernal and Bezur 2013]. The authors identified the presence of metal carboxylates but they didn’t characterize the type of acid involved. Moreover, Dredge *et al.* analysed samples from Ripolin’s cans dated 1927 by the Infrared Beam-line at the Australian Synchrotron. They identified two types of zinc carboxylate: (i) characterized by doublet peaks at 1551 and 1533  $\text{cm}^{-1}$  and a shoulder at 1597  $\text{cm}^{-1}$  attribute to zinc oleate; (ii) characterized by a broad non-specific carboxylate peak in the area 1650-1500  $\text{cm}^{-1}$  [Dredge *et al.* 2013]. The authors doesn’t provide a characterization for the second type of carboxylate.

---

<sup>19</sup> Ripolin’s colour chart: *Glacis Ripolin a Finir Spécial Pour Voitures*, dated 1925.



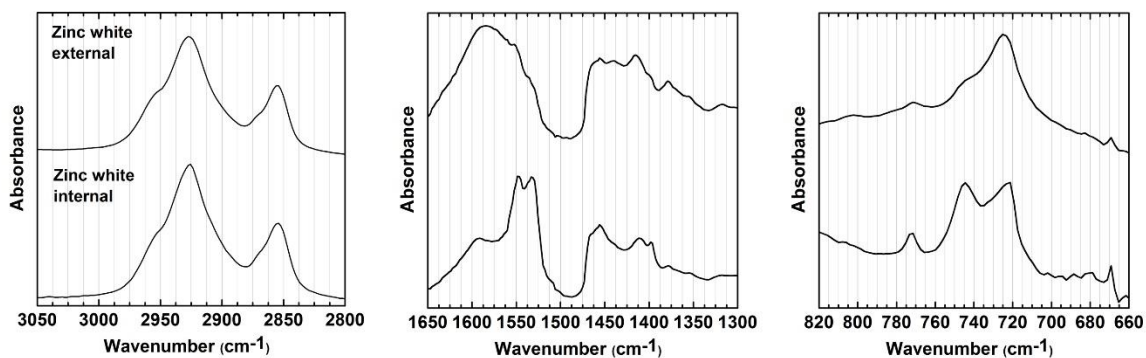


**Figure 46.** Infrared spectra of  $\mu$ -samples collected from the paint tube by Lefranc Zinc white applied on glass slide, the samples were collected on the dried surface (external) and from the not-completed dried paint (internal).

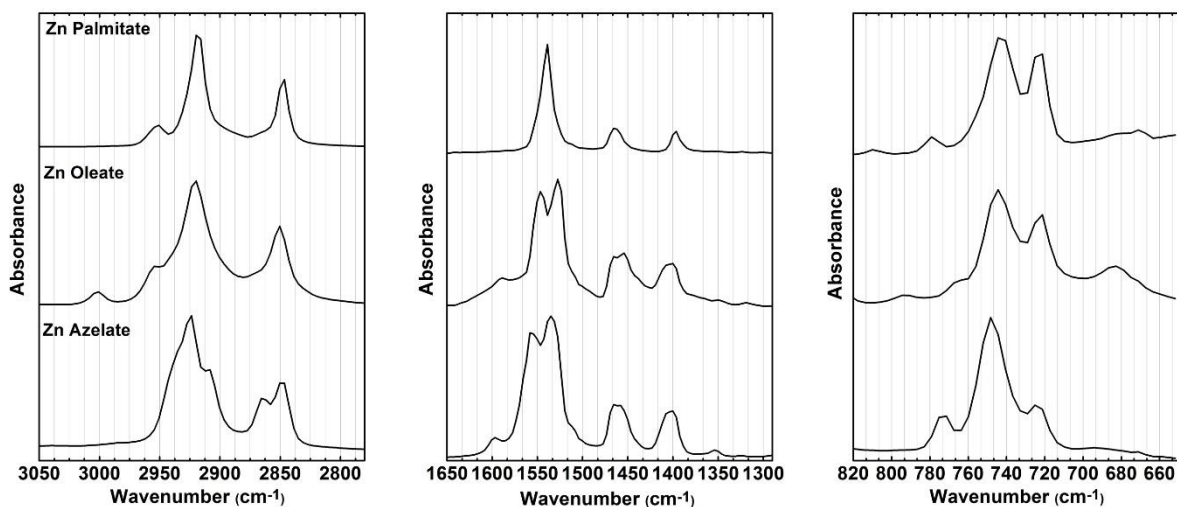


**Figure 47.** Infrared spectra of reference zinc carboxylates synthesized in DCR laboratory, details in [Otero *et al.* 2014a].

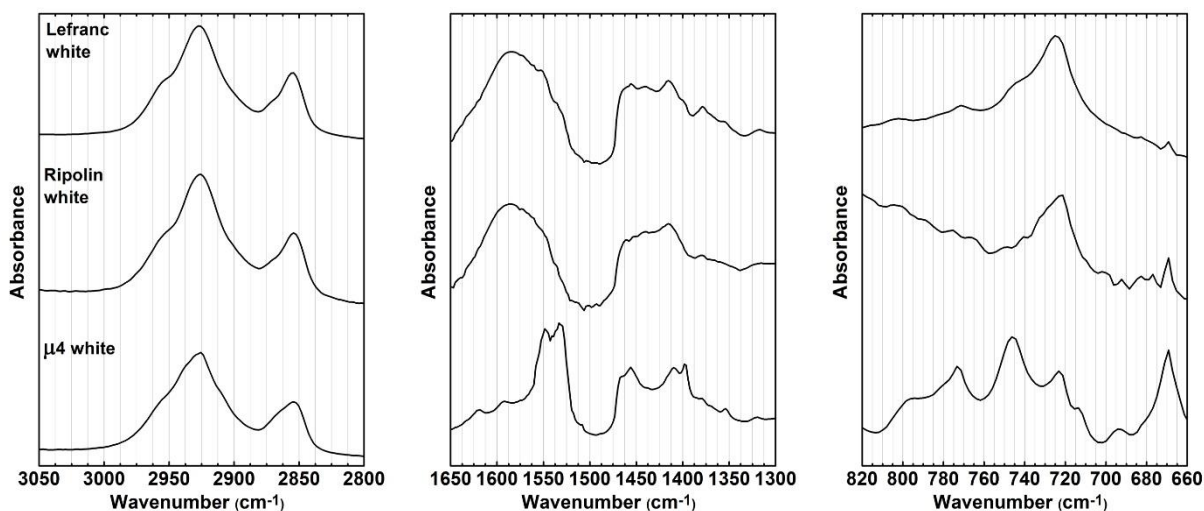


**Figure 48.** Infrared spectra of the tube samples Lefranc Zinc white tube; the Blanc by Ripolin and the white sample from BRUT  $\mu$ 4.

To cross-sections were prepared from the Lefranc zinc white oil paint tube (Fig. 49A) sample the Blanc Ripolin sample (Fig. 49C). In the cross-section of the oil samples the presence of an aggregate is visible, delimited by the red dashed line in Fig. 49A). The cross-section from the Ripolin sample does not show any aggregate (Fig. 49C).

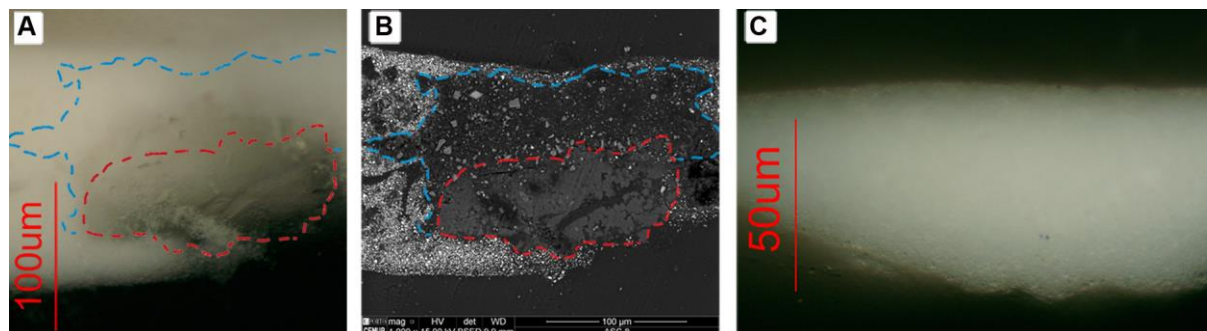


**Figure 49.** **A** Optical microscope image of cross-section from Lefranc zinc white paint sample; **B** SEM image in BSE mode of cross-section from Lefranc zinc white paint sample; **C** Optical microscope image of cross-section from Blanc Ripolin sample.

Raman analysis performed inside the aggregate in zinc white oil sample in the area delimited by the red dashed line in Figure 49A. The Raman spectrum collected in the sample (Fig.50A) was compared with those collected on the carboxylic acids and the zinc carboxylates synthesized at the DCR [Otero *et al.* 2014a], the best match was found with the **zinc azelate** (Fig.50B). In the surrounding area (delimited by the blue in Figure 49A) no Raman signal was obtained due to the high fluorescence.

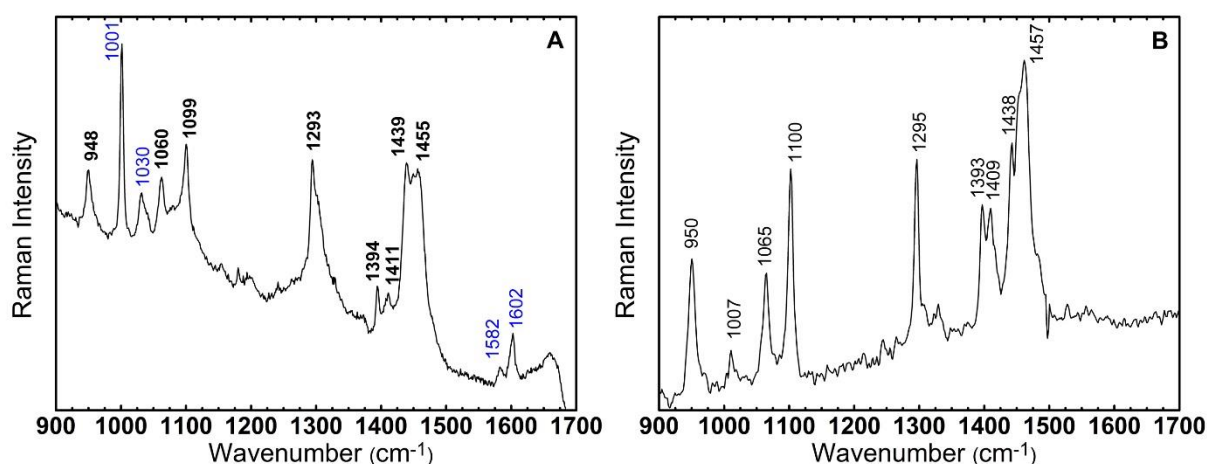


**Figure 50.** Raman spectra **A** ASC8 zinc white inside the area delimited with red dashed line in the cross-section image. In blue the contribution of the resin used to prepare the cross-section; **B** zinc azelate reference.

The Blanc Ripolin sample was analysed by Raman (Fig.51) and also compared with the reference spectra from carboxylic acids and the zinc carboxylates [Otero *et al.* 2014a] in this case the best match found was with the azelaic acid. The Raman spectrum of azelaic acid is characterized by the presence

of band and  $664\text{ cm}^{-1}$   $\delta(\text{COO}^-)$ ; at  $905\text{ cm}^{-1}$   $\nu(\text{C-C})$ ;  $1060$  and  $1097\text{ cm}^{-1}$  of the  $\delta(\text{C-C-C})$  and at  $1412$  and  $1440\text{ cm}^{-1}$   $\delta(\text{CH}_2)$  [Otero *et al.* 2014a].

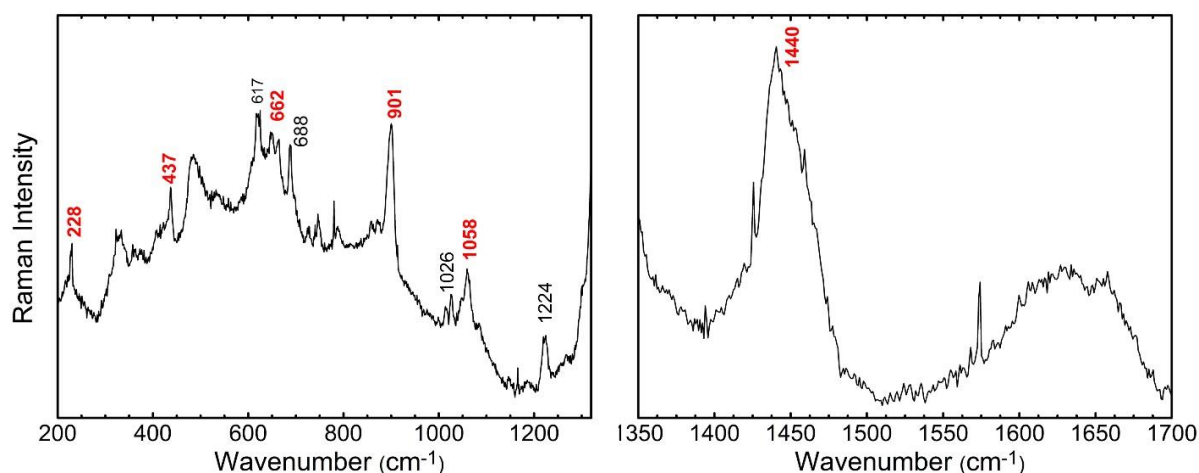


**Figure 51.** Raman spectra of Ripolin blanc sample on diamond cell, the region between  $1320$  and  $1350\text{ cm}^{-1}$  was excluded because it corresponds to the diamond band; in red the band attributed to azelaic acid.

The cross-section from the zinc white oil paint; the Blanc Ripolin and the samples  $\mu 4$  and  $\mu 5$  from *BRUT* were analysed by SEM-EDS. The sample from Lefranc (Fig. 52A) and Ripolin (Fig. 52B) show morphological differences, such as the shape and the dimension of the particles<sup>20</sup>: the particles of the oil pant tube sample show non-homogenous dimension with a medium size of  $0.152\text{ }\mu\text{m}$  ( $\pm 0.341$ ) while the particles on Ripolin's sample have  $0.071\text{ }\mu\text{m}$  ( $\pm 0.212$ ). Casadio and Rose [Casadio and Rose 2013a] relates the reduction of the dimension (high concentration of particles in the  $0.15\text{--}0.3\text{ }\mu\text{m}$  length/diameter range) of the ZnO particles in Ripolin paint to the grinding process used by the industry.

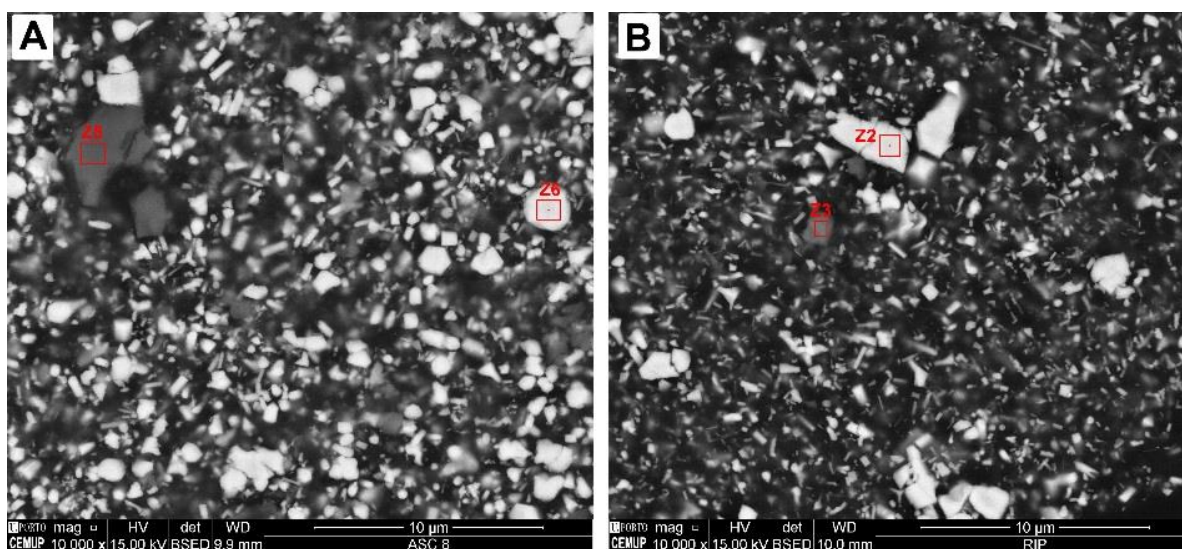


**Figure 52.** SEM image in BSE mode of **A** zinc white Lefranc (ASC8). The EDS analysis detected the presence of: Zn (Z6) and Si (Z5); **B** Blanc Ripolin sample. The EDS analysis detected the presence of: Zn (Z2) and Al in (Z3).

<sup>20</sup> The size of the particles was measured using the open source program for image processing ImageJ (<http://imagej.net>). For the analysis the SEM images in BSE mode were used.



The EDS analysis detected the presence of silicon (that suggest the presence of silica) in the Lefranc paint sample; while in the sample from Ripolin it was detected aluminium (that suggest the presence of aluminium oxide).

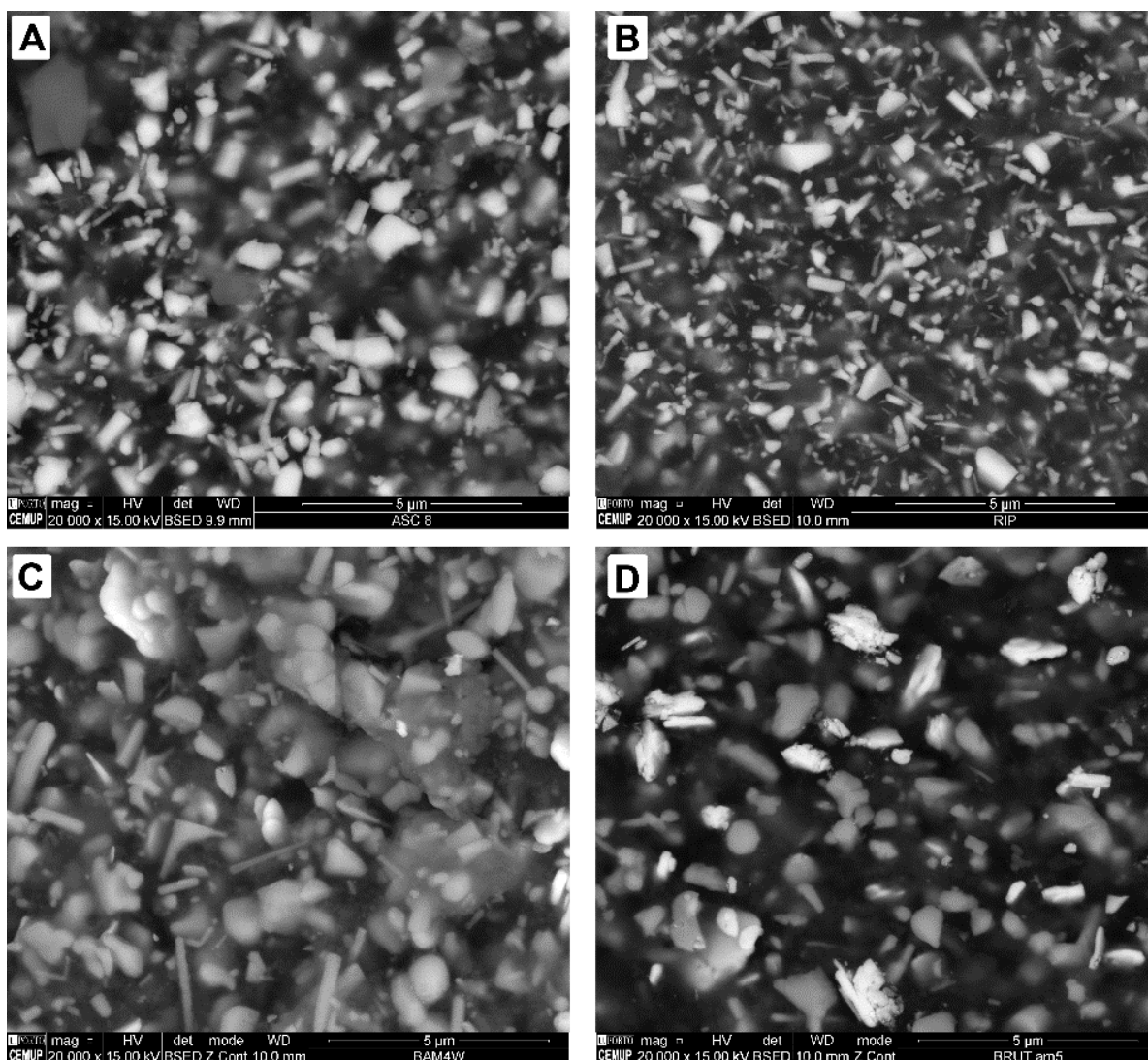


**Figure 53.** SEM image in BSE mode of **A** zinc white by Lefranc (ASC8); **B** Blanc by Ripolin; **C** BRUT sample  $\mu$ 4; **D** BRUT sample  $\mu$ 5.

The data acquired from Lefranc and Ripolin were compared with those from the paint samples. The morphology and the size of the pigment particles of zinc white in samples from *BRUT* is closer to that of the oil paint tube sample. In the SEM image from the painting samples (Fig. 53 C and D) rounded and acicular particles are visible. The size of the particles identified as ZnO in the painting's samples show a ranges from 0.6 to 1.5  $\mu$ m.

In conclusion, the spectral features of the FTIR spectra from 71 samples collected from the paintings *BRUT* and *Entrada* suggest the presence of the two types of carboxylates: the first is characterized by a well-defined structure may be related with the presence of an additive. In the areas where problems

of paint adhesion are visible (Fig.43 A and B) it were detected zinc stearate or palmitate (in sample  $\mu 5$ ) and zinc azelate and/or oleate (in sample  $\mu 4$ ). Zinc azelate and/or oleate were also detected on the samples  $\mu 15-16$  and  $\mu 31$ . The second type of carboxylate is characterized by a broad IR band centred on  $1580\text{ cm}^{-1}$ . It was not possible a complete characterization of the carboxylates. The not-defined structure of the carboxylate suggest the presence of a compound formed in the paint and not added to it. It could be the case of the product of an ongoing degradation process between the metal of the pigment and the oil. Based on the analysed samples 18.3% of the area of the painting present this type of carboxylate. To note that this type was detected also in the *BRUT* sample  $\mu 25$ . This sample was collected from the letter "T" where no signal of delamination are visible (Fig.43 C).

The same two types of carboxylates described for the *BRUT* samples were found in the Lefranc paint tube of zinc white used by Amadeo. Raman analysis performed in an aggregate in an oil zinc white sample detected the presence of zinc azelate.

The FTIR analysis of the samples collected from the Blanc swatch from of Ripolin's colour chart (dated 1925) detected only the presence of the broad band around  $1580\text{ cm}^{-1}$  as in the case of the Lefranc sample and the second group of *BRUT* samples. This band was detected also in [Casadio *et al.* 2013c; Dredge *et al.* 2013; Hanspach-Bernal and Bezur 2013] by the analysis of Ripolin samples from different production. The band at  $1580\text{ cm}^{-1}$  cannot be considered as an unequivocal signature of the presence of enamel paint. In the Ripolin cross-section no aggregates were detected and the Raman analysis suggest the presence of azelaic acid.

On the other hand, the particle size of the Ripolin sample (calculated from SEM image) is smaller compared with the Lefranc zinc white sample. The samples from the painting *BRUT* ( $\mu 4$  and  $\mu 5$ ) are in the same range of size of those calculated in the oil paint tube sample.

### 2.2.2 Fading

In *BRUT* the head of a guitar presents a purple-bluish tone; by micro sampling the area it was clear that the colour at the surface was different from the colour in the internal part of the layer, which characterized by a strong pink tone. In the cross-section of the sample ( $\mu 19$ ) collected in that area, the purple-bluish tone has a thickness of  $15\text{ }\mu\text{m}$  (Fig. 54A). The pink area in the visible light image shows an orange fluorescence under ultraviolet illumination (Fig.54B). This fluorescence is not visible at the surface of the paint layer that had been in contact with the light. The orange fluorescence is one of the features in the identification of the eosin based lakes [Geldof and Steyn 2013]. In Figure 54C it visible the fluorescence of the zinc particles, homogeneously distributed throughout the layer. The distribution of the zinc is also confirmed by the mapping performed by SEM-EDS (Fig. 55E).

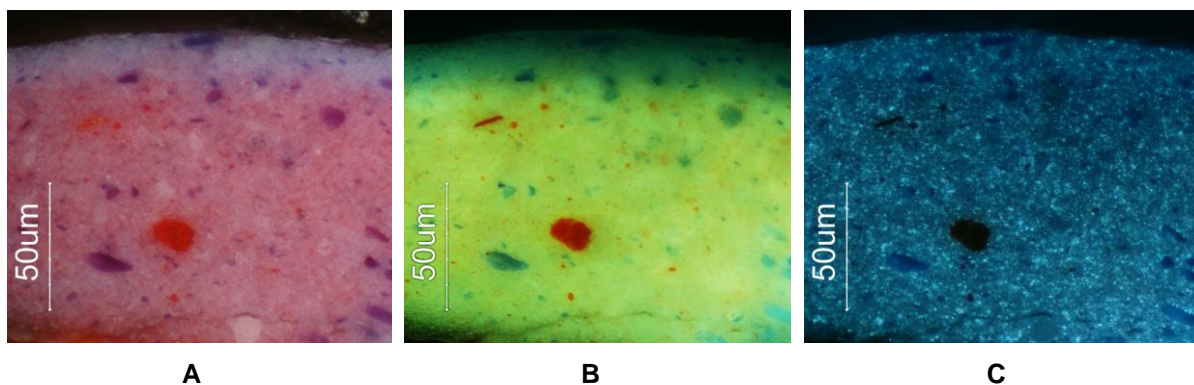


**Figure 54.** Cross-section ( $\mu 19$ ), **A** visible light; **B** Ultraviolet light (filter 5); **C** Ultraviolet light (filter 8).

SEM-EDS performed on the same cross-section (Fig.55B) shows the homogenous distribution of the zinc in the layer; besides that, BSE image does not show a separation between the pink and blue layers as it is visible in the image with visible light. Aluminium<sup>21</sup> is clearly associated to the presence of dark purple, blue and red crystals (Fig. 55C). In the dark purple and blue crystal the presence of cobalt was also detected (Fig. 55D). The results obtained suggest the presence of a mixture of cobalt based pigment with a lake.

FTIR detected a large amount of zinc carboxylate, characterized by the presence of a broad band corresponding of the COO<sup>-</sup> stretching, at 1580 cm<sup>-1</sup> (Fig. 56B). The presence of zinc carboxylates are discussed in Section 2.2.1. FTIR and reflectance spectroscopy confirmed the presence of a cobalt blue based pigment by the absorption band at 680 cm<sup>-1</sup> corresponding to the stretching Co-O. In the reflectance spectrum (Fig. 56A) is visible the absorption bands between 550-560 nm of the *d-d* transition of the Co(II) (Section 2.1.3). The detection of aluminium by SEM-EDS in the correspondence to the blue crystals confirms the presence of Cobalt blue.

As introduced in Section 1.2.3, eosin was discovered by Hofmann and marketed by BASF in 1874. Eosin derives from the bromination of fluorescein and erythrosin from its iodination; the presence of bromine or iodine supports the discrimination between bromination and fluorescein. In the van Gogh paintings bromine was still detected after discolouration of the lake [Geldof and Steyn 2013]. X-ray fluorescence performed on BRUT in the correspondence with the purple area detected the presence of Zn, Co, Pb Hg and Fe. The presence of Hg is related to the red layer of vermilion, iron oxide pigments applied over the ground, In the EDXRF spectrum (Fig. 57) the presence of the K $\beta$  line of the Hg (11.82 keV) overlaps with the K $\alpha$  of the Br (11.87 keV) and for that reason the attribution of the presence of Br may be suggested only based on the K $\beta$  peak at 13.3 keV. It was not possible to confirm or exclude the presence of Br by SEM-EDS due to the overlapping between the L $\beta$  line of the Br (1.52 keV) and the K $\alpha$  of the Al.

<sup>21</sup> Aluminium can be related to the presence of a lake pigment. Metal salt, such as alum is used to precipitate the lake pigment from the chromophore in solution.

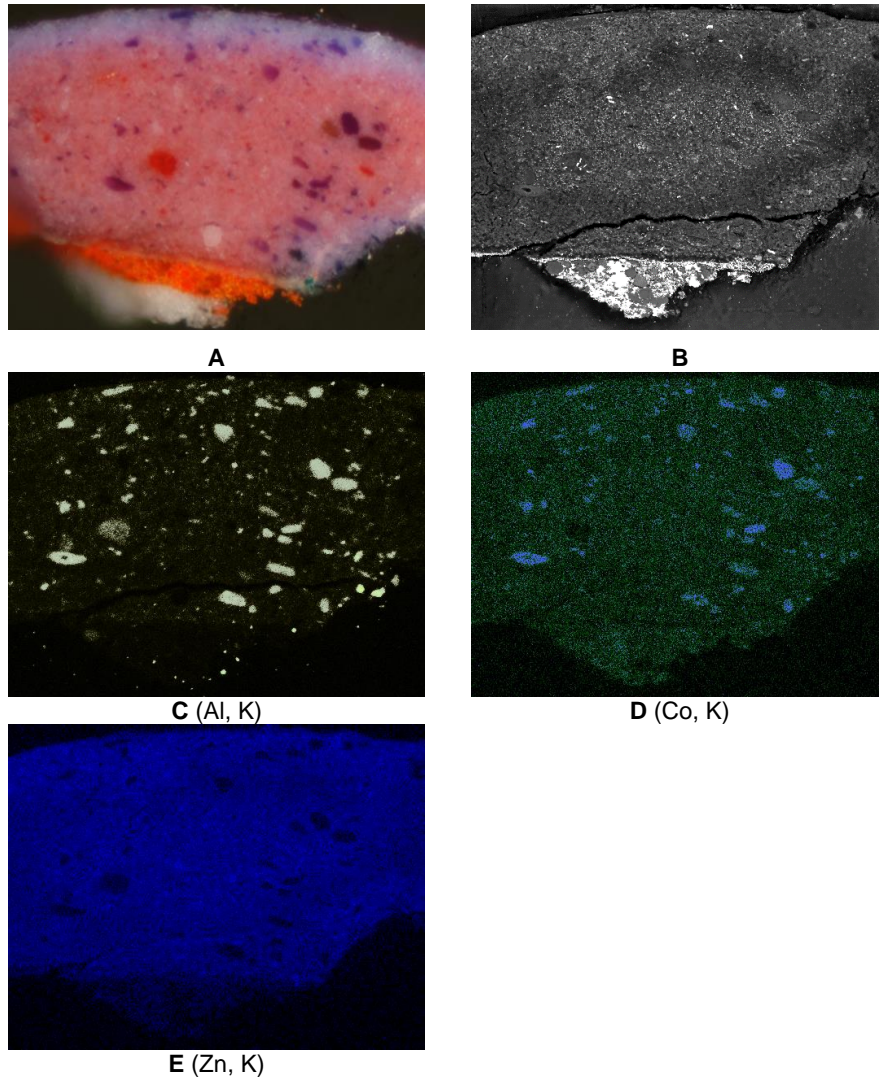


**Figure 55.** Cross-section of the sample BRUT  $\mu$ 19 **A** MO image; **B** SEM image in BSE mode; **C** distribution of aluminium (Al line K); **D** distribution of the cobalt (Co line K); **E** distribution of the zinc (Zn line K).

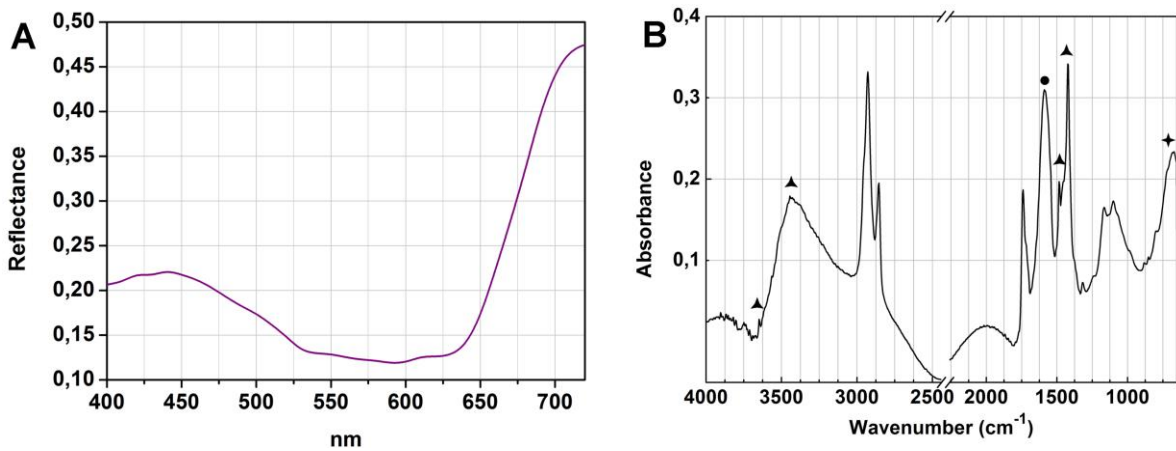


**Figure 56.** **A** Reflectance spectrum acquired with hyperspectral camera; **B** Infrared spectrum of purple BRUT  $\mu$ -19 (+) cerulean blue; (●) zinc carboxylate; (▲) magnesium carbonate.

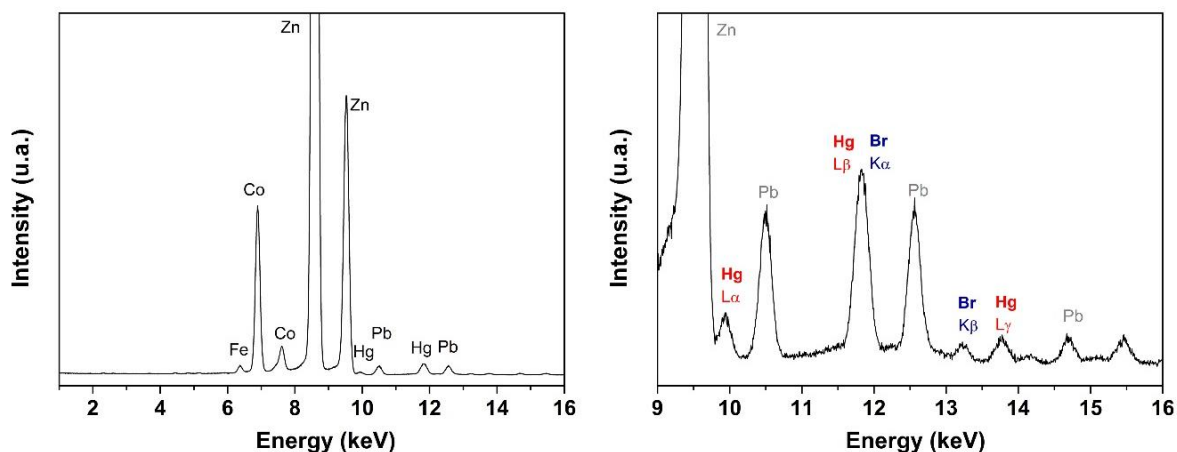


**Figure 57.**  $\mu$ -EDXRF spectrum acquired on the *BRUT* painting in the purple area.

Microspectrofluorimetry offers high sensitivity, selectivity, and good spatial resolution that make this technique invaluable in the identification of dyes and lake pigments in art work [Melo *et al.* 2009]. Figure 58A shows the emission and excitation spectrum acquired on the cross-section *BRUT* ( $\mu$ 19); in Figure 58B the spectrum acquired on a reference sample of eosin complexed with  $\text{Al}^{3+}$  applied on paper filter [Claro 2009]. The sample from the painting shows an excitation maxima at 528 nm and the emission maxima at 544 nm (collected in the violet area) and 556 nm (in the bluish area). As reported in Claro [Claro 2009] the metal ion used as complexing agent in the preparation of the lake influence the intensity and the position of the excitation and the emission band we can suggest a presence of an eosin based lake complexed with aluminium.

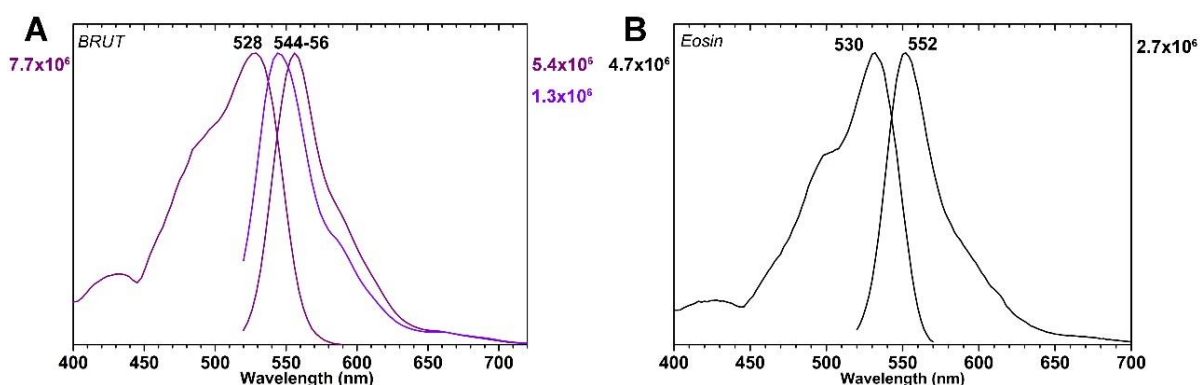


**Figure 58. A** *BRUT* ( $\mu$ 19) Emission spectra ( $\lambda_{\text{ex}} = 490 \text{ nm}$ ;  $\text{df} = 500 \text{ nm}$ ) and excitation ( $\lambda_{\text{em}} = 610 \text{ nm}$ ;  $\text{df} = 600 \text{ nm}$ ) from the purple (violet line) and bluish (blue line); **B** Eosin in  $\text{MeOH}:\text{H}_2\text{O}$  (70:30, v/v) with  $\text{Al}^{3+}$  at pH 2.9, applied on filter paper [Claro 2009].



### 2.2.3 Cracking and darkening of the green area

Figure 59 shows detail images of a green area in the bottom right corner of *BRUT*. In this area the surface presents an extended *craquelé*, with a local loss in the paint layer. The dark colour visible in the green area seems restricted to the surface: the photomicrographs acquired in correspondence to the *lacuna* (Fig.59B) shows that the green colour in the bulk of the paint layer is lighter than the colour at the paint surface. EDXRF analysis performed in the light and dark green areas detect copper and arsenic (Areas of analysis G9a-c; Bk9a-b in Fig. IV.1 Appendix Part II Ap. IV; EDXRF spectra in Fig. V.1 Appendix Part II Ap.V.1).

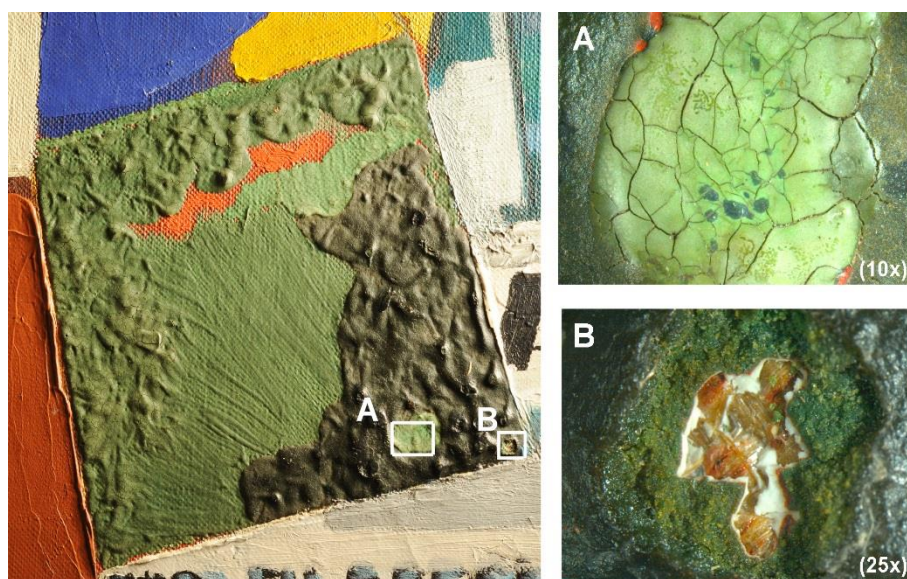


**Figure 59.** Image detail using raking light of the green area at the bottom right corner in the painting *BRUT* (Left); **A** Photomicrographs of the light green area (10x); **B** Photomicrographs of the dark green area (25x).

FTIR analysis detected the presence of emerald green (mixed with barium sulphate) in the light green. In the dark area FTIR analysis (samples  $\mu 6$ ,  $\mu 33$  and  $\mu 34$ ) it was detected the presence of starch<sup>22</sup> and barium sulphate. Figure 60 shows IR spectrum of a green sample where it is visible the absorption bands of the starch at 1152, 1180 and 1030  $\text{cm}^{-1}$  of the absorption of the C-O bond stretching [Stuart and Ando 1997]. In the same spectrum it is also visible the contribution of the barium sulphate with the increase of the absorption at 1180  $\text{cm}^{-1}$ , the presence of a shoulder at 1080 and the weak band at 985  $\text{cm}^{-1}$ , all related to the stretching of the  $\text{SO}_4^{2-}$  group. From the FTIR analysis no signal of oil as binder. No further analyses were done to identify the origin of the starch.

---

<sup>22</sup> As reported by Carlyle in [Carlyle 2001, pg. 110] Field (in the edition 1841, pg. 350) listed starch as material used to gelatinise oil paint “Indeed starch, as prepared by the laundress, has been lately recommended with high encomiums for this purpose”. The use of starch mixed with oil paints was reported by various art magazines from 1839 and 1841 [Carlyle 2001, pg. 110]. The only one other reference is related to the use of medium containing starch for dead colouring on an absorbent white ground [Carlyle 2001, pg.110].

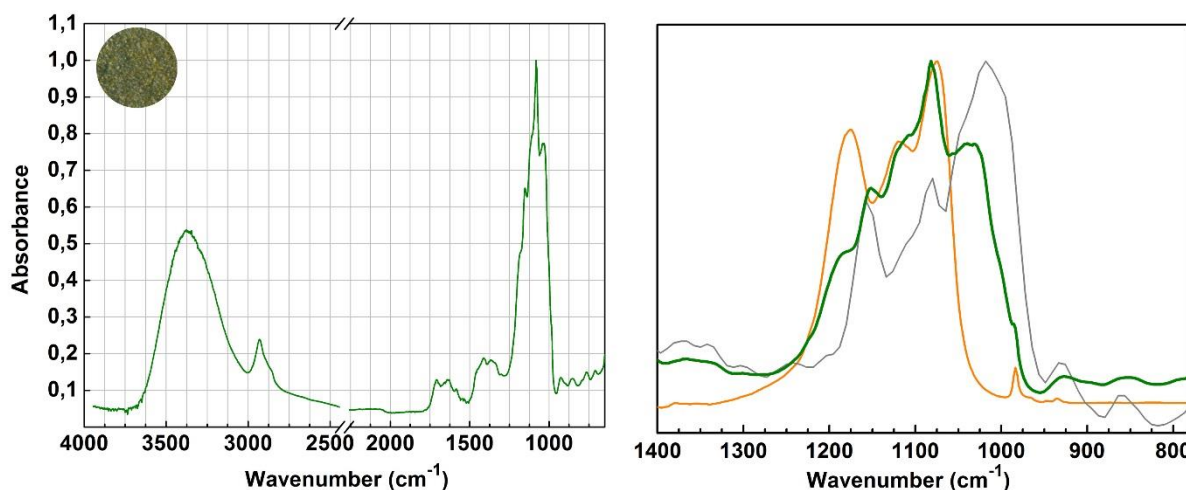


**Figure 60.** Infrared spectra of the green sample ( $\mu 33$ ) from *BRUT* painting (green line); barium sulphate (orange line) and starch (grey line).

Raman (Fig. V.9 Appendix Part II Ap.V.3) and SEM-EDS (Appendix Part II Ap.VI.2.1 am 33) performed on a cross-section confirmed the presence of emerald green mixed with barium sulphate also in the dark area. SEM image in BSE mode (Fig.61) of the green layer of the cross-section ( $\mu 33$ ) shows dark circular areas, similar to *bubbles*. These areas present different sizes, from 10  $\mu\text{m}$  to ca. 40  $\mu\text{m}$ . In these areas SEM-EDS analysis detected a high content of carbon and low amounts of lead, arsenic and calcium. The area around the *bubbles* is fractured. The shape of the fractures, visible in the edge of the *bubbles*, suggests that the presence of an organic material that has filled the cavities. This organic material would then reduce its volume (shrink), causing fractures on the adjacent area. To exclude the possibility that the cavity was filled by the resin used to prepare the cross-section a micro-sample  $\mu 6$  that shows the same phenomenon was analysed.

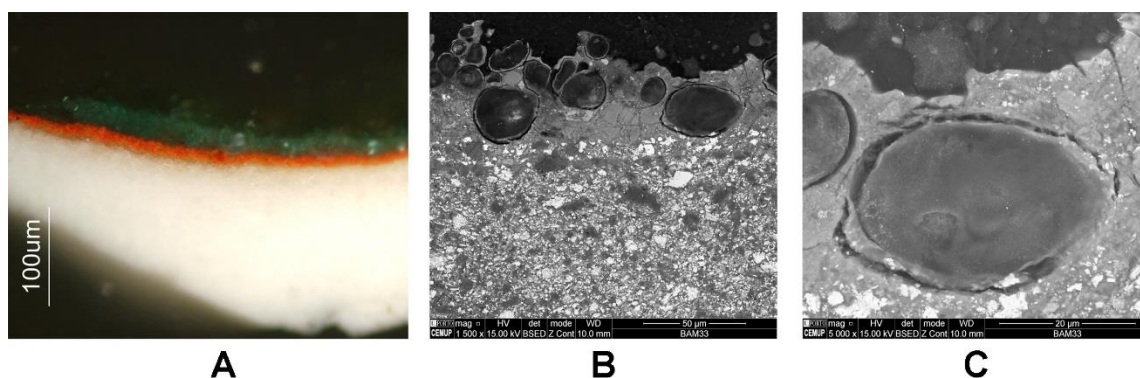


**Figure 61.** Cross-section dark green sample  $\mu 33$  **A** OM image; **B** and **C** SEM image in BSE mode.

Considering the results presented it is possible that starch has been applied on the surface of the green of emerald green and barium sulphate. FTIR analysis on the dark green surface doesn't detect the presence of oil, that suggest that the starch was not mixed with oil paint. The surface, where starch was detected, shows a dark green hue, while the internal part of the layer show a lighter green. The difference of the colour between the surface and the interior part should be explain by the presence of starch: the



starch filled the space between the pigment particles, reducing the scattering of the light promoting the darkening of the surface.

## 2.3 Final remarks

The analyses of the four paintings dated 1917 enrich the knowledge on the materials and techniques of Amadeo de Souza-Cardoso created at the time of the edition of his Catalogue Raisonné [Melo *et al.* 2008; Melo *et al.* 2009]. In these paintings Amadeo experimented with the use of found materials. In *Coty* and in *Untitled* Amadeo seems to be more faithful to his classic palette but at the same time it is curious that *Coty* is the painting where he experimented more the use of founded materials in almost 30% of the paint area.



**Figure 62.** The pigment palette of Amadeo for the paintings dated 1917, with details from his paintings.

The characterization of the pigments allow the identification of the palette for the paintings dated 1917 (Fig.62). Moreover, the analysis of the colour distribution (based on the colour data acquired using hyperspectral imaging) shows that in the last paintings Amadeo developed a coherent colour *language* different from that used in the previous works. In the last works Amadeo used saturated tones applied as patches without colour gradient. It is very interesting to see that the artist achieved this effect basically using the same palette of the previous works. To note the localized use of golden and silver tones in particular in *Coty* and *Entrada*. The difference that were detected from the palette of pigments before (Fig. 5) and after 1917 (Fig. 62) are the use of mixture of blue pigments and red lake to achieve the purple hue. Before 1917 the main important green pigment used by Amadeo was viridian; in the case of *BRUT* and *Entrada* it was detected viridian but the main areas were painted by emerald green. Cobalt yellow was already detected mixed with chrome yellow in a sample from the painting *Untitled (O Jockey)* Inv. 77P5 dated 1913. In these last paintings cobalt yellow was found alone and in mixture with chrome yellow in *Coty* and *Untitled*. The main relevant difference between the two palette of pigments is the use of zinc white in particular in *BRUT* and *Entrada*.

The analysis of a photograph of a supposed *maquette* shows a correlation between the collage represented in the photograph and the oil paintings, in particular with *BRUT* and *Entrada*. These two

paintings show a very similar colour distribution and construction, such as the use of the same proportion of chrome yellow and cadmium yellow, and the use of zinc white. The *maquette* should be realized before the paintings *BRUT* and *Entrada* and after the edition of the album “12 Reproductions” (November 1916). Taking into consideration the interpretation of some elements present in the *maquette* and the *pochoirs* of the letters Z, I, N, and C it is suggested that the artwork *Untitled (ZINC)* was completed before the *maquette* and therefore before the paintings *BRUT* and *Entrada*.

In the analysis of the paintings particular attention was given to the chrome yellow samples. Thanks to the parallel investigation developed within the project Crossing Borders on the W&N 19<sup>th</sup> archive it was possible to correlate the results obtained from the painting analysis with the industrial synthesis of the chrome yellow. Two samples of chrome yellow from *BRUT* and *Entrada* were analysed by Synchrotron radiation techniques; in these samples no signs of degradation process were detected. The data obtained from the samples characterization will be very important to continue the study on the process of alteration of this pigment.

In general these paintings are well conserved, however *BRUT* shows more problems comparing with the others. It was detected the presence of craquelé and micro-craquelé that in some cases compromise the stability of the paint layer. Related with the use of zinc white FTIR analysis detected a large amount of zinc carboxylates. Based on infrared analysis, and in particular observing the carboxylic region between 1530 and 1580  $\text{cm}^{-1}$  two types of metal soaps were identified: (i) is characterized by the presence of a broad band centred at 1580  $\text{cm}^{-1}$ . This not defined structure of the carboxylate suggest the presence of a compound formed in the paint and not added to it, such as the case of an alteration product between the zinc and the oil. (ii) The second type is characterized by the presence of a doublet absorption at 1551-1534  $\text{cm}^{-1}$ , the well-defined structure of the zinc carboxylate suggest that it is a compound added to the paint more than a product of degradation. This second type of zinc carboxylate was detected in the samples from the area with conservation problems: paint delamination in white and green area of the letter “R” of the word “BRUT” (samples  $\mu 4$  and  $\mu 5$ ). In the sample  $\mu 5$  FTIR detected the presence of zinc stearate or palmitate and in the sample  $\mu 4$  of zinc azelate and/or oleate. In *BRUT* it was also detected a fading problem related to the presence of an eosin-based lake used in mixture with cobalt blue that caused the change of the colour in the figure of the head of guitar. For the first time in Amadeo's paintings it was detected the presence of starch in the green areas of the painting *BRUT*; the presence of the starch may be related with the dark tone of the area.

**PART III:  
CASE STUDIES**



In this part of the thesis the image processing tools described in Part I are applied to two sets of painting case studies (described below). The goal of this chapter is to compare the results obtained using the image tools with the results obtained by the analysis of the painting materials, performed using multi-analytical approach.

The first set of paintings (Section 1.1) are called here as *Collage*; *Geometric*; *Embroiderers* and *Café*. These paintings are attributed to Amadeo de Souza-Cardoso but not included in the Catalogue Raisonné and they were studied at the DCR-UNL in order to assess their authenticity. These paintings were used to evaluate the brushstroke analysis based on image processing (please see Part I, Section 2.2) as tool to support authentication processes. The answer provide by the materials examination was compared with the answer provide by the tool developed to perform brushstroke analysis. To evaluate the authenticity of the paintings their materials and techniques were compared with those used by Amadeo in the paintings studied until now (including the 19 paintings analysed in [Melo *et al.* 2008] and the four paintings: *BRUT*, *Entrada*, *Coty* and *Untitled* studied in this these and presented in Part II Chapter 2).

The second group of paintings (Section 1.2) are the paintings of Amadeo dated 1917 *BRUT*, *Entrada*, *Coty* and *Untitled*. The study of the materials of these paintings is presented in Part II of this thesis. The system that perform the analysis of the materials based on hyperspectral images and elemental data (please see Part I, Section 2.3) was applied in these four paintings. The results obtained by the system are then compared with the results obtained by the analysis of paintings, this comparison is useful to appreciate the success and limitations of the system proposed.

## **1.1 Brushstroke analysis to support authentication processes**

### **1.1.1 The methodology**

The study performed on 19<sup>1</sup> selected paintings of Amadeo's at the time of the edition of his Catalogue Raisonné [Melo *et al.* 2008] allows to reconstruct the palette of colours used by the artist between 1912 and 1916 (Fig.1). For more details please see Part I, Section 1.1.3.

The characterization of the materials includes also the evaluation of the mixtures used. During the evaluation of a painting it is also studied the technique used by the artist; this includes the stratigraphy of the painting, the presence of underdrawings, the way in which the colour is constructed, and the brushstroke. The analysis of the painting technique and its structure is performed by combining the information extracted by image documentation (infrared, ultraviolet, normal and raking light and X-ray images), by the observation of the painting under microscope, and by the analysis of the cross-sections. This part of the Chapter summarizes the main results obtained by the analysis of the 4

---

<sup>1</sup> During the edition of the Catalogue Raisonné were analyzed 19 paintings of Amadeo, 18 of these dated between 1912 and 1916 and 1 dated 1917 [Melo *et al.* 2009].

paintings with a focus on the elements that are in agreement or not with the features of Amadeo's technique defined in the previous work [Melo *et al.* 2008; Melo *et al.* 2009]. More details on the analyses are presented in the Appendices of Part III, the areas of analysis of each case study are presented in Ap.II and the results in Ap.III.1: The representative spectra of:  $\mu$ -EDXRF in Ap.III.2;  $\mu$ -FTIR in Ap.III.3;  $\mu$ -Raman in Ap.III.4 and FORS in Ap.III.5.



**Figure 1.** The pigment palette of Amadeo between 1912 and 1916, with details from his paintings. Image adapted from Melo *et al.* 2009.

As noted below, the results obtained by the analysis of the materials and the techniques used in the four paintings is compared with the analysis of the brushstroke performed using image processing. The shape, orientation and distribution of brushstrokes are considered as distinctive markers left by the artist on the surface of a painting; the recent application of image processing allows to develop an algorithm to detect these features (for more information in Part I, Section 1.2.3). In the case of Amadeo a method that combines two algorithms used in texture analysis was developed: Scale Invariant Feature Transform (SIFT) and Gabor filter. To summarize from Part I, the first one is used to detect points of interest (called key-points) in the image. Usually the key-points are related to the presence of texture patterns. The second algorithm is applied in a selected region of 64x64 pixels around each key-point. Gabor filter allows extract texture information, representing it as a vector of 24 values; the vectors of each image (ca. 1200) are used to perform a binary classification. The classifier (Regularized Least Squared Classified-RLSC) is previously trained to recognise images of Amadeo's paintings (called positive class) and images of paintings from other contemporaneous artists (called negative class). The aim of the classification is to attribute to each unknown painting a value between 0 and 1, where 0 indicates the similarity of the painting with the negative class and 1 with the positive class. For more details please see Part I Section 2.2.



### 1.1.2 Results and discussion

Figure 2 shows the images of three of the paintings that were used as case studies. The painting (A) *Collage* is subject of a legal dispute. For this reason the images of the painting are not presented in the main text but can be found in the Appendix PIII.I. Paintings (A) is a collage on paper, while (B) *Geometric* and (C) *Embroiderers* are oil paintings on cardboard. The painting (D) *Café* is an oil painting on paper that was lining on a canvas. The following is a summary of the main results regarding the analysis of four paintings.



*B. Geometric*



*C. Embroiderers*



*D. Café*

**Figure 2.** Images of the four paintings assigned Amadeo de Souza-Cardoso but that were not included in the Catalogue Raisonné of his paintings [Freitas *et al.* 2008].

## *Painting (A) Collage*

The artwork (A) presents collage of three papers; based on our knowledge this is the only paper collage attributed to Amadeo, with the exception of the drawing *L' Athlète* (1913) conserved at CAM (Inv. DP3339) which is a collage and ink on paper and cardboard. The pigment characterization was performed using as much as possible in-situ techniques. Raman analysis shows that a large part of the artwork is made with pigments not included in Amadeo's palette; these areas are mapped in Figure I.2 in Appendix Part III Ap.I. The blue tone is a mixture of ultramarine blue, copper phthalocyanine and dioxazine violet. Dioxazine violet is used also in the dark brown tone and in the violet one. The red area is made with  $\beta$ -naphthol: this red organic pigment is also used in mixture with the orange tone and with yellow ochre in the brown-orange tone. The ochre tone is made by iron based pigments and carbon black.

Three of the four organic pigments found in the painting were introduced as materials for artists after the dead of Amadeo:

- Copper phthalocyanine: discovered in 1927 [Herbst and Hunger 1997] and patented in 1929 [Lomax 2005];
- Dioxazine violet: discovered in the 1920s [Keijzer 1990] and patented in 1935 [Lomax and Learner 2006].
- Hansa yellow: used on textile since 1909 and introduces as artist materials since 1925 [Ropret 2008; Lomax and Learner 2006].

Considering that an important area of the collage was painted with pigments introduced after the dead of the artist, this indicates that the painting could not be authored by Amadeo

Due to the presence of a varnish<sup>2</sup> layer applied over the papers glued on the artwork it was not possible to obtain a Raman signal. Only indigo was identified in the blue tone in the paper (b) indicated in Figure I.2 in Appendix Part III Ap.I. EDXRF on the green area of the paper (a) detected arsenic and copper; these results suggest the presence of a copper-based pigment such as emerald green or Scheel's green. The latter was used in wall paper in the XVII and XIX centuries [Fiedler and Bayard 1997].

The brushstroke analysis of this painting gives a value of 0.21 - where 1 is the probability to be painted by Amadeo and 0 by another artist; the accuracy of the answer is 91%. This result support the conclusions made based on the analysis of the materials.

---

<sup>2</sup> The varnish was not analysed.

### *Painting (B) Geometric*

The X-ray image acquired for this painting (Fig.3) does not show overlapping between the figures of the composition. Besides this, the infrared photography shows few lines used to define the space (Fig.3), these lines are not used as preliminary drawing but just to sketch the outline of the composition. Both these features were also detected in the Amadeo's paintings analysed in previous work [Melo *et al.* 2008]. The cardboard used as support is also not unusual in his artworks of small dimension (Part II, Section 1.1.3).

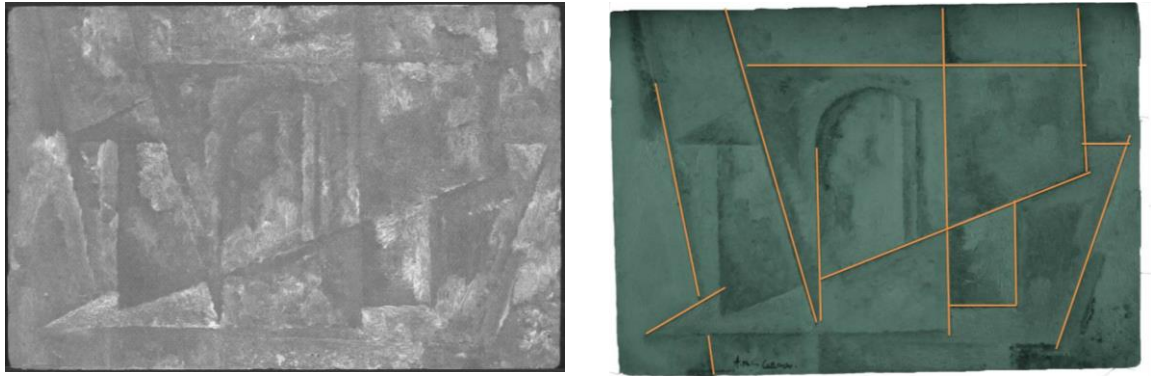


**Figure 3.** Image documentation of the *Painting B* (Left) X-ray image (Right) Infrared photography, in orange the line used as sketch to create the composition.

Figure 4 compares two photomicrographs from the *painting B* and two from the painting *Quadro G* (1912) (this painting belongs to the CAM collection, Inv. 77P2): the shape, the texture and the density of the brushstrokes of the painting *Geometric* are very similar to those observed in the CAM's painting of Amadeo dated 1912-14. As indicated by the X-ray image there are no overlaps between the different geometric figures, observing the painting surface at the microscope, in few point it is possible to see the white preparation layer, this feature is quite also not unusual in the Amadeo's technique.



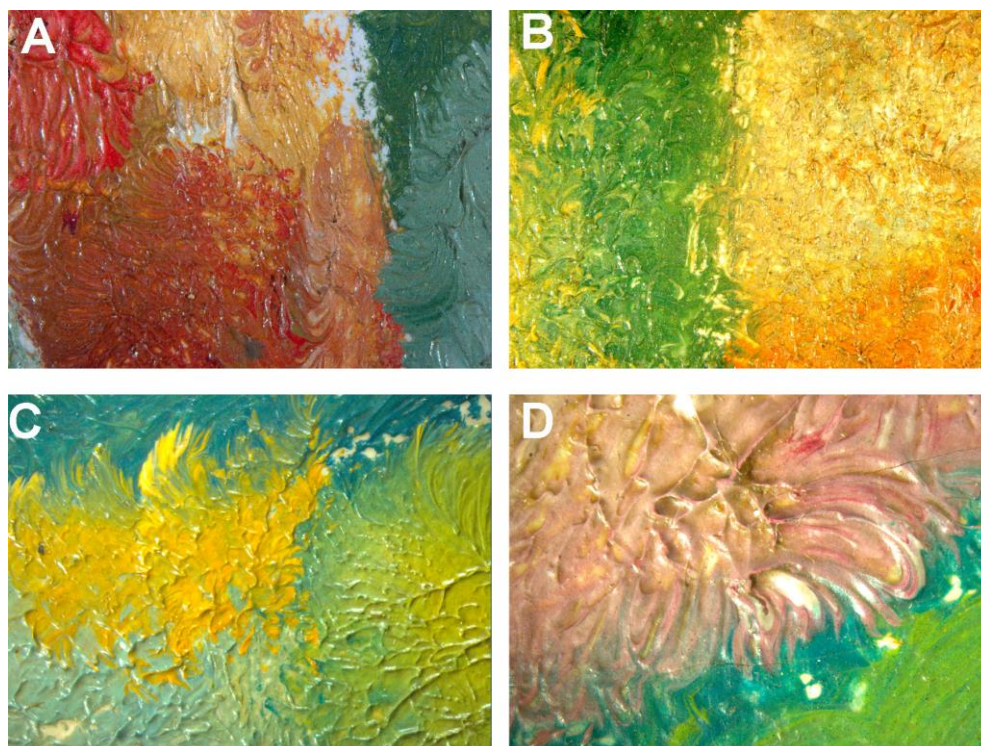


**Figure 4.** Photomicrographs of the brushstroke details from: **A** and **B** painting *Geometric* (10x); **C** and **D** Amadeo de Souza-Cardoso, *Quadro G* (7x), dated 1912, collection of Centro de Arte Moderna, Fundação Calouste Gulbenkian (Inv. 77P2).

The palette of pigments used in painting is *Geometric* restricted (Table 1): FTIR and Raman analysis detected the presence of viridian, cobalt blue, vermilion and ochre. Chrome yellow (solid solution of chromate and sulphate) was detected only by Raman and in mixture with ochre. All these pigments are consistent with Amadeo's palette based on previous study [Melo *et al.* 2008].

**Table 1.** Palette of pigments detected in the Painting *Geometric*.

Cobalt blue	Viridian	Vermilion	Chrome yellow	Ochre yellow	Lead white
CoO.Al <sub>2</sub> O <sub>3</sub>	Cr <sub>2</sub> O <sub>3</sub> .2H <sub>2</sub> O	HgS	Pb(Cr,S)O <sub>4</sub>	Fe <sub>2</sub> O <sub>3</sub> .H <sub>2</sub> O	2PbCO <sub>3</sub> .Pb(OH) <sub>2</sub>
●	●	●	●	●	○

Brushstroke analysis based on image processing gives a value of 0.9, where 1 is the probability to be painted by Amadeo and 0 by another artist; with an accuracy of 91%. In contrast to what was observed in the case of the collage (Painting (A) *Collage*), both technical and brushstroke analysis did not identified any elements that suggest that this painting could have not been painted by Amadeo.

### *Painting (C) Embroiderers*

The painting support used is a cardboard with a preparation layer of lead white and barium sulphate. No underdrawings or even lines to orient the composition were observed with IR photography (Appendix Part III Ap.IV).

X-ray image (Fig.5, left) shows only a difference between the compositions visible with normal light (Fig. 5, right) in correspondence with the windows in top of the painting. Nevertheless, it seems more a *pentimento* of the artist than an underpainting.



**Figure 5.** Painting C *Embroiderers*; visible light photograph (left); X-ray image of the, the red rectangle indicates the region that has no correspondence to that of the surface of the painting (right).

Also in this painting the palette of colour is restricted: the blue tone is obtained with a mixture of cobalt blue and iron oxide pigments (goethite and hematite); viridian and chrome yellow were also identified. All these pigments belong to the Amadeo's palette, less common is the use of  $\beta$ -naphthol red pigment. This organic pigment was detected by  $\mu$ -Raman in the red area. FORS analysis suggest the presence of an organic pigment also in the pink tone, anyway it was not confirmed by other examination. The  $\beta$ -naphthol red pigment was only found in the painting *Coty* (1917) in mixture with minium ( $Pb_3O_4$ ) (Part II, Section 2.1.4) and in the illustrated manuscript version of Gustave Flaubert's book *La Légend de St Julien L'Hospitalier* (1912) (Part II, Section 1.1.1). The first  $\beta$ -naphthol pigment (PR1) was introduced in the artistic market in 1895; most of the other pigments of this family were introduced in the early 1900s [Lomaxa and Learner 2006]. For this reason, it cannot be considered as an evidence that the painting is forged. However, it is important to stress that this would be the first painting of Amadeo in which the vermilion has been completely replaced by an organic red.



The texture of the painting is quite evident: the paint layer is thick and the brushstroke is used to create the figure more than to fill it, this characteristic is clearly visible in the standing female figure (Fig. 6).



**Figure 6.** Detail image of the group of women, here the brushstroke is used to create the figures more that fill it.

In addition, these observations are supported by the analysis of the brushstroke using image processing: the probability of the brushstroke to be of Amadeo is 0.92 (where 0 is not Amadeo and 1 Amadeo), with an accuracy of 91%.

To conclude, the analysis performed did not detect elements indicating that this painting could not have been painted by Amadeo, except to the extensive use of organic pigments belongs to the class of  $\beta$ -naphthol instead of his usual vermilion. Pigments from the  $\beta$ -naphthol class has been found only in Flaubert's book *La Légend de St Julien L'Hospitalier* (1912) and in *Coty* (1917).

### *Painting (D) Café*

The scene represented in this work appears related to drawing and the caricatures<sup>3</sup> that Amadeo made at the beginning of his career more than to oil paintings. The painting was realize on paper and then lining on the actual canvas; moreover a thick layer of varnish cover the painting surface. Combining the information acquired by the X-ray and the UV photograph<sup>4</sup> we can see that the painting underwent at least two important conservation treatments (these are mapped in Figure 7 in green and in red). The X-ray image show areas with low radiopacity, these areas do not show any relation with

---

<sup>3</sup> Appendix Part II Ap. V shows an example of drawing and a caricature by Amadeo present in the Collection of Centro de Arte Moderna, Fundação Calouste Gulbenkian.

<sup>4</sup> The X-ray image and the UV photograph are presented in Appendix Part III Ap.IV

the figures represented in the composition and were probably filled in the past (mapped with red in Fig. 7). The UV photograph shows areas with a fluorescence less intense comparing with that of the varnish. These areas seems related with a chromatic integrations was made over the varnish layer (mapped with green in Fig. 7).

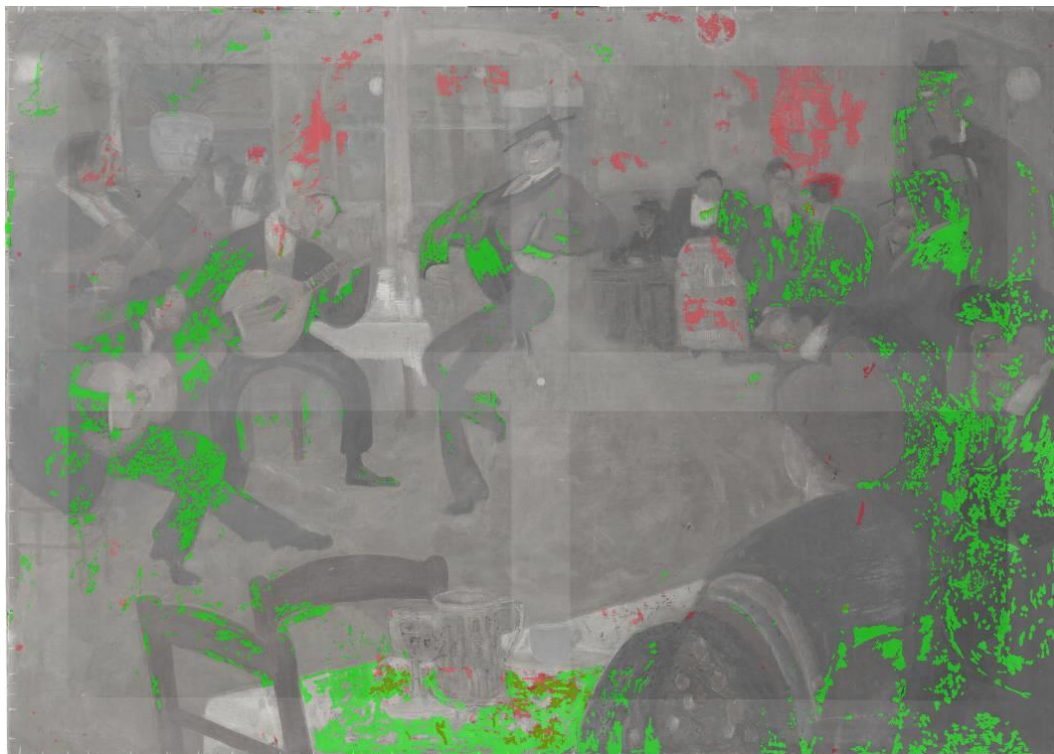


**Figure 7.** Mapping of the conservation treatments, based on the X-ray image the UV photograph (●) in these areas the X-ray image shows the presence of a material less radiopaque comparing with the rest of the painting. (●) In the UV photograph are visible areas where the chromatic integrations was made over the varnish layer.

Concerning the material analysis, Raman and FTIR analysis detected viridian, vermilion and chrome yellow, all found frequently in Amadeo's paintings. The violet tone is a mixture of ultramarine blue, vermilion and a red lake (not identified) with lead white and barium sulphate. The creation of a purple hue by the mixture of a blue inorganic pigment and a red organic dyes was found only in the painting *Entrada* of 1917; in the earlier works, as well as in *Coty* and *Untitled* (both of 1917), Amadeo used cobalt violet (Part II, Section 2.1.4). The white area analysed are a mixture of lead white and barium sulphate, this mixture was found also in the painting on cardboard<sup>5</sup> analysed in 2008 [Melo *et al.* 2009]. Concerning the blue hue, EDXRF analysis detected the presence of cobalt but it was no possible to confirm the presence of cobalt blue pigments by other spectroscopic techniques; Raman detected the presence of ultramarine (Appendix Part III Ap.III.1 and III.3).

---

<sup>5</sup> Paintings form the CAM collection: Inv. 77P5; Inv. 91P219; Inv. 91P224; Inv. 91P225; Inv. 88P159; Inv. 91P220; Inv. CP0143 and Inv. CP0137 [Melo *et al.* 2009].



The overall image processing analysis gives a value of 0.35 (where 0 is not Amadeo and 1 Amadeo, with an accuracy of 91%), this result inserts the painting in the negative class (Not Amadeo). However we note that the presence of the layer of varnish compromise the observation of the brushstroke of the painting, which can be appreciated only at the microscopic level. For that reason four areas, where no conservation treatments were detected and in which the brushstroke was evident, were photographed and used as additional information in the brushstroke analysis (Fig. 8). The brushstroke analysis was also performed on the images acquired in these areas. Figure 8 shows the four areas analysed and the results obtained by the brushstroke analysis: in these areas the analyses give values higher than 0.85. This result can be explain in two ways: (i) the analysis of the overall image was influenced by the presence of the varnish; (ii) in this painting there are the contributions of two artists (at least) one of these used a brushstroke with features similar to that used by Amadeo. It is important to take into account that the application of image processing on images collected on areas of the painting was made for the first time on the painting *Café*. This method was not tested on other Amadeo's paintings because it was beyond the scope of this thesis, for that reason this result must be considered as a suggestion and in the future will be important to evaluate this strategy.

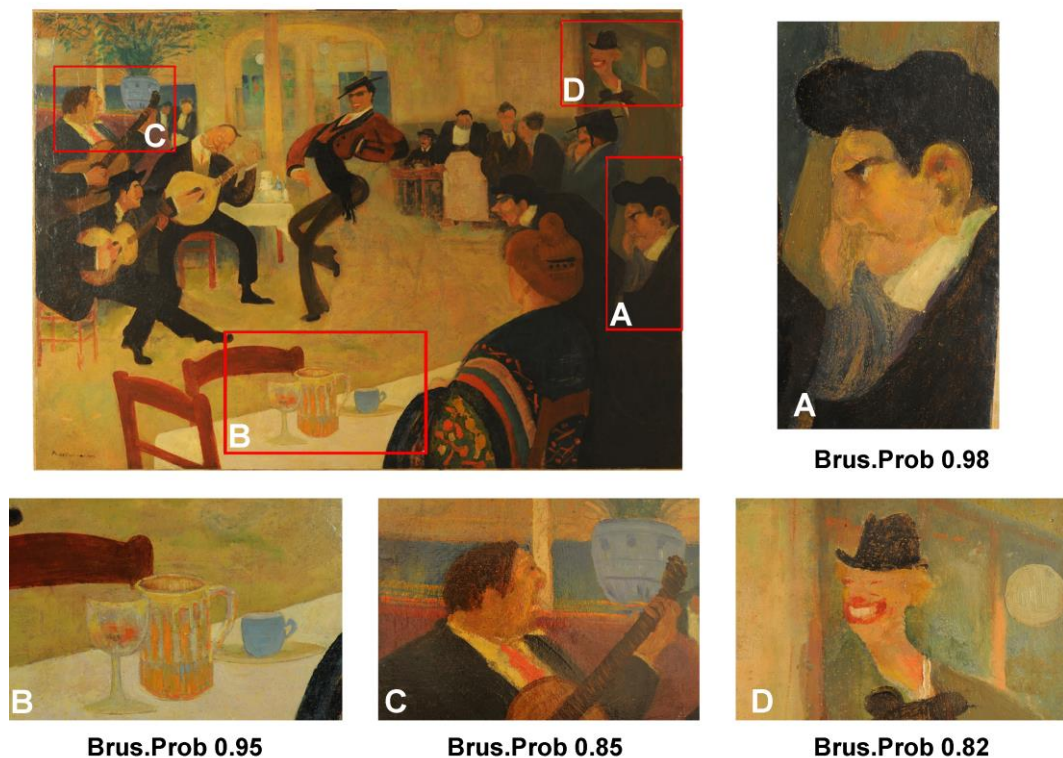


**Figure 8.** Image of the painting and in detail the four areas selected for brushstroke analysis and the relative brushstroke probability (Brus. Prob.), where 1 is the probability to be painted by Amadeo e 0 by another artist; the accuracy of the answer is 91%.

The contrast between the results obtained by the analysis of the painting with those obtained in the selected areas could be related to the presence of the varnish and/or the conservation treatment that

compromised the analysis of the texture. Another hypothesis is that the painting was partially made by Amadeo and completed later on by another artist.

### 1.1.3 Final Remarks

The case studies presented show that the analysis of the brushstroke using image processing, are in agreement with observations of the painting surface (with the naked eye and by the microscope) and with the conclusion made by the analysis of the pigments. In the first two paintings (*Collage* and *Geometric*) the technical investigation and the image processing analysis give the same unambiguous result. In the case of the painting *Embroiderers* representing the embroiderers, the brushstroke analysis clearly includes the artwork in the *positive* class (Amadeo) and material analysis did not detect pigments introduced after the 1918. The pigments used in the painting *Embroiderers* are the same found in previous analysed paintings of Amadeo [Melo *et al.* 2009] to note the use of the red pigment belongs to  $\beta$ -naphthol class has been found only in Flaubert's book *La Légende de St Julien L'Hospitalier* (1912) and in *Coty* (1917). The study of the painting *Café* shows the limitation of this technique in the case of painting with varnish layer that reduce the visibility of the brushstroke. By the analysis of this painting it was possible to identify the presence of pigments frequently used by Amadeo: viridian, vermilion and chrome yellow. The purple hue is obtained by a mixture of ultramarine blue, vermilion and a red lake (not identified). The use of a mixture of blue pigment and red lake was found only in the paintings *BRUT* and *Entrada* dated 1917, while in the earlier works, as well as in *Coty* and *Untitled* (both of 1917), it was found cobalt violet pigment. The analysis of the brushstroke of the painting *Café* classified this painting as *Not Amadeo*, while the brushstroke analysis performed on four selected areas of the painting given positive results (high similarity with the brushstroke of Amadeo). This experience identifies an important limitation in the use of the classifier based on image processing: the presence of varnish can compromise the identification of the brushstroke and consequently the classification of the painting. The analysis of images acquired on selected areas of the painting, was used for the first time here, in the future this method should be tested on more known paintings to evaluate its efficiency. Moreover this method should be tested to identify the contribution of more than one artist in the same painting.

## 1.2 Hyperspectral imaging analysis

In this following section the system based on the combination hyperspectral imaging and elemental analysis is used to analyse of the four paintings dated 1917 (*BRUT*, *Entrada*; *Coty* and *Untitled*). This analysis is useful to evaluate the potentialities and limitations of the system developed.

### 1.2.1 The system proposed

In Part I Chapter 2 of this thesis it is presented the system based on the combination hyperspectral imaging and elemental analysis. To resume, it provides the characterization of the pigments present in the painting and identifies areas painted that may not painted by Amadeo. The system was developed based on the information acquired by the analysis of 19 selected paintings of Amadeo: 18 dated between 1912 and 1916; 1 dated 1917 and a set of 16 oil paint tubes (tube database) used as reference materials (more information of the paint tube in Part I Section 1.1.3 and Part II Section 2.3.1) [Melo *et al.* 2008; Melo *et al.* 2009]. The identification of the pigment is performed by comparing the data (reflectance spectra and elemental data) acquired on the painting and those present in the tube database. The elemental analysis is performed by  $\mu$ -Energy Dispersive X-ray Fluorescence ( $\mu$ -EDXRF), an in-situ technique used for the identification of chemical elements with atomic number higher than sodium. The comparison of reflectance spectra is achieved using a combination of Spectral Angle Mapper (SAM) and Euclidian Minimum Distance (EMD). Besides that, the system indicates the areas made with materials that are not consistent with those present in the tube database (this area is labelled as *Not Amadeo area*) and the areas where it was not possible to perform the analysis due to the missing of the elemental information (labelled *Not Analysed area*).

The output image created by the system is an easy way to check the attributions proposed by the system. The RGB values used to create the output image are computed from the reflectance spectrum according with the classification of the area; while the colours for the other two areas (*Not Amadeo* and *Not Analysed*) are pink and grey, respectively.

### 1.2.2 Results and discussion

Table 2 shows the percentage of the *Not Analysed* and *Not Amadeo* areas in the four paintings analysed. As expected the percentage of *Not Amadeo* area is always 0 with the exception of the *Coty*, where the percentage is 7.5%. This percentage corresponds to the area with cobalt yellow pigment. Cobalt yellow pigment is present alone and in mixture with chrome yellow (Fig.9); this pigment was not

included in the Amadeo's paint database<sup>6</sup> because it was found in a relevant amount for the first time in the painting *Coty*.

**Table 2.** Percentage of *Not analysed* and *Not Amadeo* area in *BRUT*, *Entrada*, *Coty* and *Untitled* paintings.

	Not Analysed area (%)	Not Amadeo area (%)
<i>BRUT</i>	2.7	0
<i>Entrada</i>	0	0
<i>Coty</i>	0	7.5
<i>Untitled</i>	0.5	0



**Figure 9.** **A** Image *Coty* painting; **B** segmented image; **C** mapping of Not-Amadeo area based on the reference pigments from the previous study [Melo *et al.* 2008].

It is worth noticing that the mirrors present in the paintings (*Coty* and *Entrada*) appeared black in the hyperspectral images and the resulting segmented images. This is due to the way in which the data are acquired<sup>7</sup>.

The mapping image obtained by the analysis of the hyperspectral image of the painting *Entrada* shows good results (Fig.10). Anyway, in the mapping of the emerald green pigment (Fig. 10C) the system includes the area indicated with the letter (a), where  $\mu$ -Raman and  $\mu$ -FTIR detected the presence of viridian and Prussian blue.

<sup>6</sup> The tube database of reference materials includes: cobalt violet; vermilion; carmine lake; terra rossa; raw Siena; ochre yellow; chrome yellow; cadmium orange; cobalt blue; cerulean blue; Prussian blue; ultramarine blue; viridian; emerald green; lead white; ivory black.

<sup>7</sup> For each painting 33 images are acquired in the range 400-720 nm, as well other two images are acquired and used to correct (i) the noise signal of the detector and (ii) the eventually non-homogeneous distribution of the light intensity from the centre to the periphery of the acquired image. The first image is taken with the lens camera corked; while the "light-reference" image is taken using a uniform diffuse surface. On the mirrored surface the intensity of the reflected radiation is very close to that reflected by the "light-reference" surface for that reason, after the correction, the reflectance spectra in the mirror area is close to 0 (black).

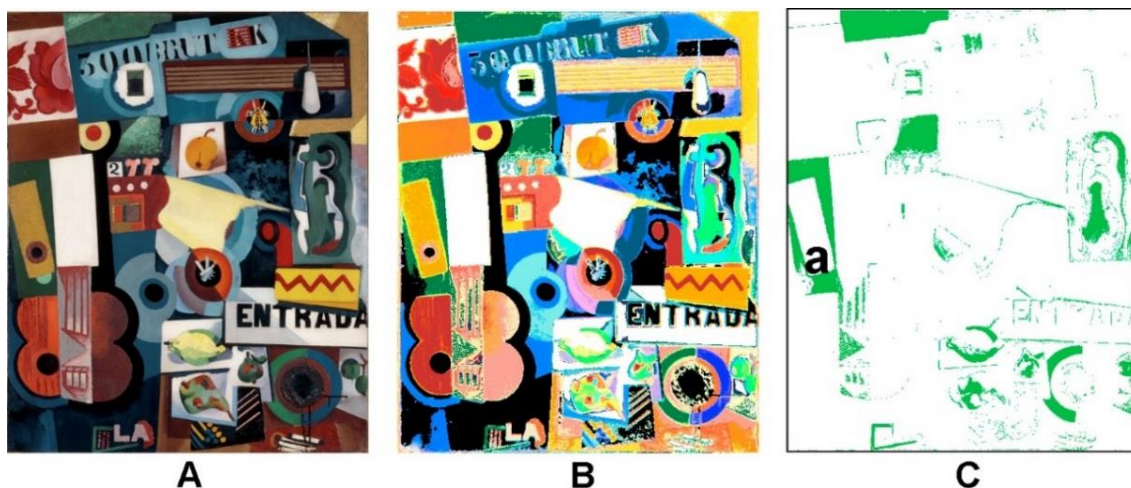


**Figure 10.** A Image of *Entrada*; B segmented image; C mapping of the emerald green pigment.

In Figure 11 the reflectance spectra of this mixture is compared with those from the emerald green and viridian oil paint tubes include in the database of reference materials. In the spectra acquired from the painting the reflectance absorption band in the region 600-720 nm shows low values comparing to the spectrum of viridian, probably due to the presence of the Prussian blue. Which would account for the misclassification.

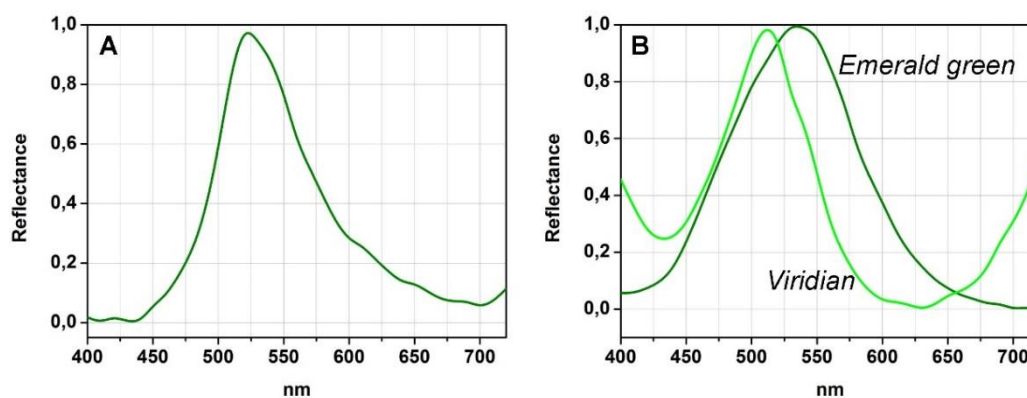


**Figure 11.** Comparison between the reflectance spectra acquired on **A** *Entrada* in the green area (a) with a mixture of viridian and Prussian blue; **B** from the oil paint tube samples viridian and emerald green, used as reference materials in the data-base.

The mapping of *BRUT* shows a differentiation between the black areas indicated in Figure 12A with the letters (a) and (b). The reflectance values of the area (a) are higher than the area (b) with  $\Delta E = 20$ . Raman analysis in area (b) detected the presence of hematite, vermilion and carbon black; the EDXRF analysis in the two areas shows a higher amount of iron in the area (a) comparing in the area (b). The different proportion of iron based-pigments and vermilion in the mixture used in the two areas could explain the difference in the reflectance values and the resulting difference in the mapping.



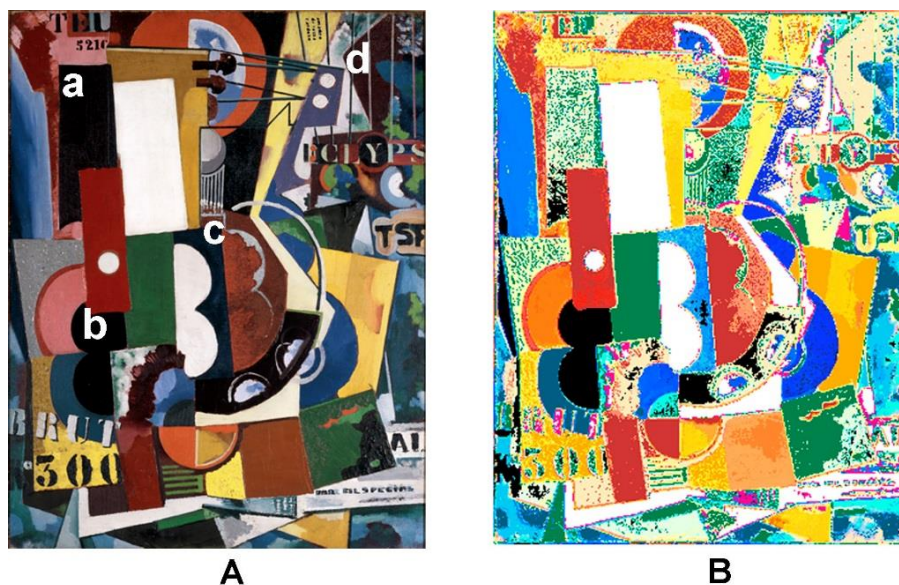


**Figure 12.** A *BRUT* (a), (b) black areas, (c) Prussian blue with whiteness surface, (d) area of fading; B segmented image.

In the painting *BRUT* we found two areas where it appears that the original colours have changed:

- (i) The blue area, indicated by (c) in Figure 12A, is made by Prussian blue but the delamination of the varnish induced white patches on the surface. A photomicrograph of the area is in Figure 13.
- (ii) The area of the head of the guitar, indicated with (d) in Figure 12A and presented in Part II, Section 2.2.2, shows a bluish tone though to be due to the fading of the eosin-based lake used in mixture with cobalt blue (Fig. 13).

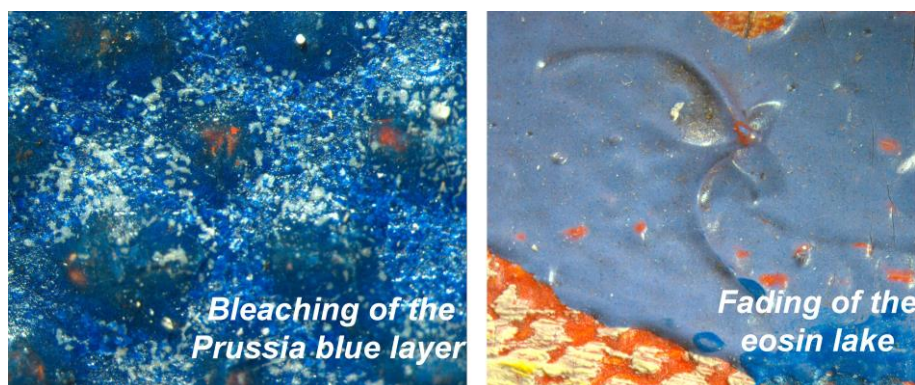


**Figure 13.** Photomicrographs of the area with problems due to colour alteration: (left) the blue area, indicated with the letter (c) in Figure 12A, shows a whiteness due to the delamination of the varnish; (right) violet area, indicated with the letter (d) in Figure 12A, the fading of the eosin lake left a bluish tone from cerulean blue visible.

Hyperspectral analysis associated with the blue area (i) shows the presence of cobalt blue pigment. This error could be explained due to the current colour of the surface. Table 3 shows the colorimetric values of three points in the paintings: Prussian blue area altered and not altered and a cobalt blue area. The colorimetric values of the altered area are closer to cobalt blue ( $\Delta E=11$ ) than the unchanged Prussian blue ( $\Delta E=37$ ).



**Table 3.** Colorimetric analysis on the *BRUT* blue areas.

Colour area	$L^*$	$a^*$	$b^*$	$\Delta E$
Prussian blue not altered	28	5.99	-34.5	37
Prussian blue altered	31.8	0.2	-12.3	
Cobalt blue	33	-7.05	-15.3	11

In the case of the violet area (ii) the hyperspectral analysis is associated with the presence of cerulean blue, since the eosin-based lake does not contribute at the surface colour.

The mapping image (Fig. 14B) produced by the analysis of the *Untitled* hyperspectral image shows good results. In Figure 14C the example of the mapping of vermilion, in the red areas this pigment was used alone or in mixture with ochre and chrome yellow. This last pigment is mapped in Figure 14D.

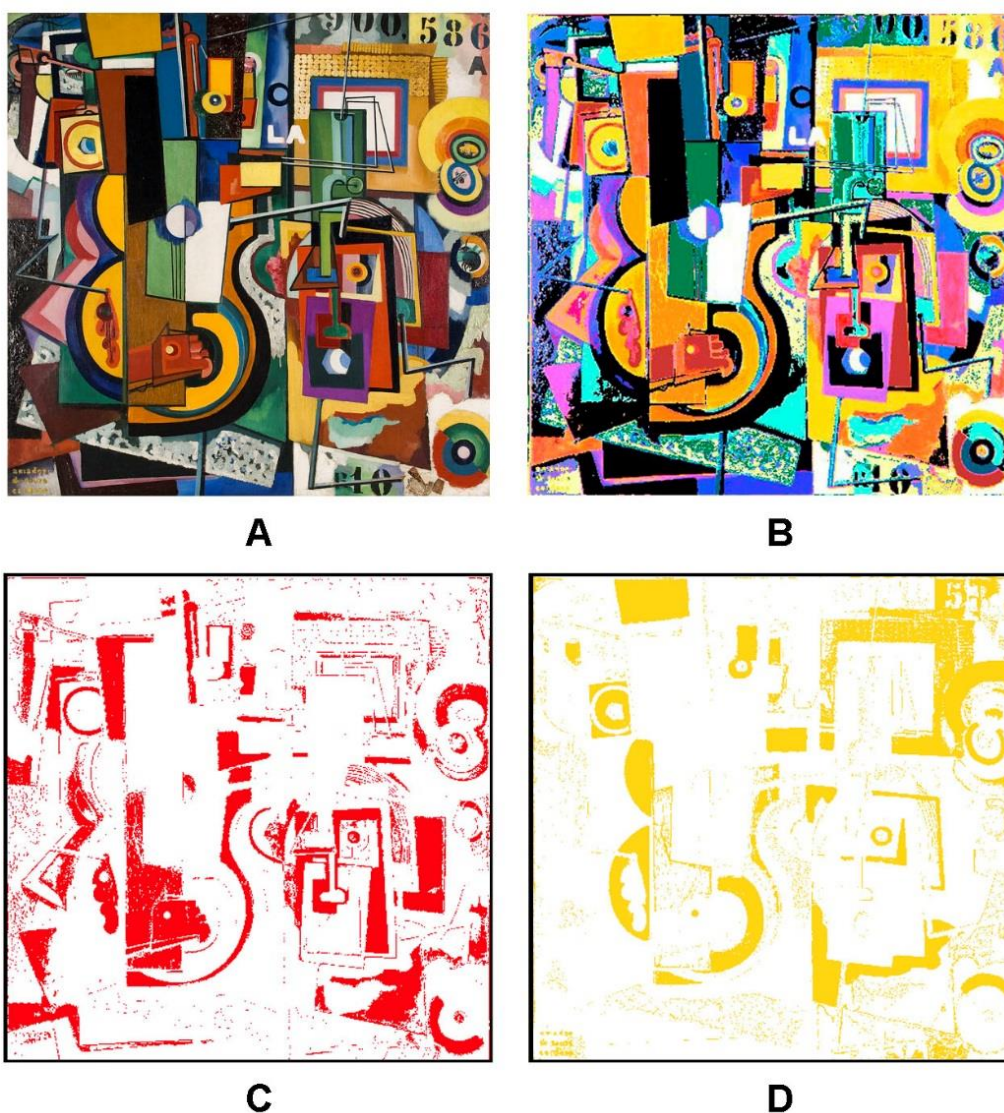


**Figure 14.** A Images of *Untitled*; B segmented image; mapping of C vermilion; D chrome yellow.

According with the paintings previously analysed, Amadeo rarely used pure black pigment in the black areas; usually this tone was achieved using a mixture of carbon black, blue pigments (such as cobalt or Prussian blue), vermilion and iron-based pigments; the identification of these mixtures by reflectance spectroscopy is challenging, and in the proposed system it is mainly performed using colorimetric values and elemental analysis. It is notable that in *Untitled* a problem appeared similar to that observed in the black areas in *BRUT*: the rectangle close to the left edge of the painting is mapped as a blue hue (Fig.14B) because the system identified a mixture of cerulean, cobalt violet and vermilion; EDXRF analysis in this area (Bk10b) detected Hg; Fe, Zn, Pb and Ca (Appendix Part II Ap.V.1). In the hyperspectral image in the black area, and in black part we observed a stray-light<sup>8</sup> of the surface.

### 1.2.3 Final remarks

The analysis of the paintings dated 1917 by the system based on hyperspectral imaging and elemental data show the potentialities but also some limitations of the system. The case study *Coty* shows the role of the database of reference materials used to characterize the pigments in the painting; *Coty* was analysed using a database built using the information collected by the analysis of the 19 paintings dated (1912-1917) and the set of paint tube samples (Part I Section 2.3.1) where the cobalt yellow was not included. By the analysis of the hyperspectral and elemental data acquired on *Coty* the system identified the area painted with cobalt yellow (alone and in mixture with chrome yellow) as a *Not Amadeo* area. In the future will be important to extend the database of reference materials including the pigments found in the paintings dated 1917 and analysed in this thesis. In this case the system results useful as preliminary screening tool that can help the user to identify areas of interest were it is necessary to perform further analysis requiring micro-sampling.

The analysis of the *BRUT* painting shows that the presence of conservation problems related with colour alteration can affect the performance of the system. This problem affects mainly the pre-processing step (presented in Part I, Section 2.3.2), where the colorimetric values (CIEL\*a\*b\*) are used to extend the localized information obtained by  $\mu$ -EDXRF to all the painting surface. The system associates to areas with the same colour the same chemical elements selected from a list of points analysed by  $\mu$ -EDXRF. It was note that in presence of fading or colour alteration this association can be uncorrected; this error may have repercussions in the next steps and then in the characterization of the pigments. This problem could be reduced using a macro-XRF [Alfeld *et al.* 2013] that allows to perform the elemental analysis directly over all the painting surface. Using macro-XRF each pixel of the hyperspectral image should directly associated to the elemental analysis performed in the same area, this will avoid the pre-processing step and reduce the error related to the association between colour and elements.

---

<sup>8</sup> Stray-light, gives reflections and light scatter usually resulting from the presence of imperfections, dust, or other particles or similar [Hunt 1991].

To improve the system it could be useful to extend it with a function that allows the possibility of enabling manual intervention from an expert user. The aim of the manual intervention could be “to force” the results of the mapping in the most challenging areas, such as those with pigments which are too dark and/or too light.

## **CONCLUSIONS AND FUTURE WORK**

The unique features belonging to an artist are a fundamental factor in assessing painting attribution. It is possible to define these features as those features that remain invariant in his/her work even when the artist changes subject or period. These features can be identified only after a systematic study of a selected set of paintings, so as to cover the longest period possible in his/her career.

Based on previous work made at the DCR-FCT in cooperation with Helena de Freitas [Melo *et al.* 2008], it appeared clear that authentication issues in the case of Amadeo de Souza-Cardoso could only be addressed by combining the information extracted from his brushstrokes and from the analysis of his painting materials. The system developed in this thesis is promising for addressing this requirement: it shows potential to provide a quantitative answer concerning painting authorship. The system is based on the **fusion** of the (i) texture analysis performed using two algorithms (namely, Gabor and Scale Invariant Feature Transform) in combination with the Bag-of-Features model, and (ii) molecular analysis performed using hyperspectral imaging and micro-Energy Dispersive X-ray Fluorescence spectroscopy ( $\mu$ -EDXRF). The image output (produced by the analysis of the hyperspectral images) maps those areas made with the same pigments (or mixture of pigments). The resulting images can also indicate the areas where (i) the system detected the presence of pigments not consistent with Amadeo's palette (called *Not Amadeo*) and (ii) where analyses were not carried out (called *Not analysed*). The *Not Amadeo* area is useful to identify the portions of the painting where further or complementary analysis are required; the *Not analysed* option alerts the user about the presence of areas where the  $\mu$ -EDXRF was not performed yet. The RGB values used to create the output mapping image are not meant to reproduce the original colours of the painting; they are calculated starting from the reflectance spectrum of the pigment (or the mixture of pigments) detected by the system in each pixel. In this way, the user may perform a "visual check" on the quality of the system response. For a more accurate analysis, the user can choose a specific pixel and check which pigments were detected in it; the user may also request the mapping of a single pigment or a mixture. The system based on the combination of brushstroke and molecular information was tested with promising results on 12 paintings. In the future, it would be useful to use the system on additional case studies; in particular, paintings of artists in Amadeo's circle who may have shared techniques and materials with him.

The analysis of the **brushstroke** using image processing achieved an accuracy higher than 90% in distinguishing between images of Amadeo's paintings and images of artworks by other contemporary artists. The classifier give a correct answer for 133 of the 138 images of Amadeo's paintings tested. This technique was also used to evaluate the authorship of four paintings attributed to Amadeo (called here as *Collage*, *Geometric*, *Embroiderers* and *Café*); the obtained results were consistent with those acquired by the analysis of the materials and techniques. The application of the texture analysis on the four case studies shows also that the performance of this technique could be influenced by the presence of varnish or previous conservation treatments, as these reduce the visibility of the painting texture (case study painting *Café*). An interesting future work consists in exploring the application of this analysis on detailed images taken from the paintings (as tested for the analysis of *Café*); this

approach could be useful in settings with limited brushstroke visibility and when there is the hypothesis that more than one artist could have worked on the painting.

In the case of **molecular analysis** using hyperspectral imaging and  $\mu$ -EDXRF spectroscopy, the mapping of the pigments could be compromised by the presence of change that affect the colour of the surfaces (e.g., fading or bleaching). Alterations in the colour of the painting surface interfered mainly with the pre-processing step; in this step the colorimetric values ( $L^*a^*b^*$ ) calculated by the reflectance spectra are used to extend the localized information obtained by  $\mu$ -EDXRF to the whole painting surface. If it is known a priori which areas are affected by colour alteration, she could minimize the problem by introducing data ( $L^*a^*b^*$  and detected elements) acquired on the altered areas. In that way the pre-processing step could make the correct association between colour and elements. Another solution should be the use of a macroXRF to perform the elemental analysis directly over the whole painting [Alfeld *et al.* 2013]; in that case a pre-processing step would no longer be necessary. Moreover, a trained user must confirm the results proposed by the system; for this reason, in the future it could be very useful to create a user interface to make the system accessible also to users with no background in informatics.

The **analysis of the paintings** dated 1917, usually known as *BRUT*, *Entrada*, and *Coty and the Untitled*, complements the knowledge on Amadeo developed in previous work [Melo *et al.* 2008]. These paintings are characterized by the presence of **unconventional** and found materials; in fact, in *Coty* this type of materials are used in almost 30% of the painting surface. Thanks to the application of colorimetric analysis based on hyperspectral images of 24 paintings of Amadeo, it was possible to compare the colour distribution of these paintings with the previous works of Amadeo. In his paintings dated 1917 Amadeo used a consistent **colour language** characterized by the presence of saturated tones mainly applied by patches of colours without colour gradient<sup>9</sup>. The colour distribution shows an equilibrium between the greens and the reds ( $-30 < a^* < 60$ ) and a slight predominance of yellow tones when compared to blue tones ( $-40 < b^* < 65$ ). This results, together with the characterization of the pigments used in this group of paintings dated 1917 are a qualitative data that can support the art historian's studies. The research performed by Helena de Freitas and her team on these paintings and their documentary sources indicate these paintings as nucleus where Amadeo was developing a new research on the use of colour<sup>10</sup>. The results obtained by the analysis of the materials and techniques, suggest a relation between the works *BRUT* and *Entrada*: these two paintings show characteristics that separate them from the other two. *BRUT* and *Entrada* show a very close colour distribution and the same pigment palette (e.g., the use of chrome and cadmium yellow in the same proportion and the extensive use of zinc white). Moreover, the analysis of objects, and the elements present in a collage (undated) made by Amadeo (the only document of this object is a photograph conserved at the Art Library of the Calouste Gulbenkian Foundation) supports this hypothesis. The photographed object

---

<sup>9</sup> In this context colour gradient means that the colours vary continuously producing smooth colour transitions.

<sup>10</sup> Personal communication by Helena de Freitas.



should be a *maquette* that Amadeo made before the realization of *BRUT* and *Entrada*. The presence in the collage of the headline of the newspaper “La Correspondencia de España” allowed to calculate the original dimension of the object: 100x70 cm. In the collage are also visible 4 *pochoirs* with the letters Z, I, N and C. The dimensions of the letters (calculated considering the dimensions of the collage proposed above) suggest that the painting *Untitled (ZINC)*<sup>11</sup>, 1917) or at least the word “ZINC” could have been completed before the *maquette*; while *BRUT* and *Entrada* should be realized after the *maquette*.

FTIR analysis performed on *BRUT* and *Entrada* detected the presence of **metal carboxylates** related with the use of zinc white. Differently from the painting, dated 1912-1916, analysed in the previous work [Melo *et al.* 2008; Melo *et al.* 2009] where Amadeo used only lead white, in the paintings (*BRUT*, *Entrada*; *Coty* and *Untitled*) Amadeo used zinc white alone and in mixture with other pigments. To note that in the paint tube box conserved by the family and analysed in 2008 [Melo *et al.* 2008] only a tube of zinc white was found. Considering the infrared features of 71 samples collected on the *BRUT* and *Entrada* two types of metal soaps were identified: (i) the first type is characterized by the presence of a doublet absorption 1551/1534 cm<sup>-1</sup>, the well-defined structure of the zinc carboxylate suggest that it is a compound add to the paint more than a product of degradation; (ii) the second type is characterized by the presence of a broad band centred at 1580 cm<sup>-1</sup>. The not-defined structure of the carboxylate suggest the presence of a compound formed in the paint, such as the case of an alteration product between the zinc and the oil. The first type of zinc carboxylate was detected in the areas with more conservation problems, such as the letter “R” of the word “BRUT”, where in the sample  $\mu$ 5 it was detected zinc stearate or palmitate and in the sample  $\mu$ 4 zinc azelate and/or oleate.

The conservation of **chrome yellow** in Amadeo’s paintings is a major concern. This pigment is very important in his palette and also in these last paintings it is still the principal yellow pigment: it covers 19% *Untitled*’s paint surface. For this reason, a change in the colour of this pigment, similar to what happened in the painting of van Gogh [Monico *et al.* 2011b], would compromise the appearance of the painting, losing the original colour balance. The samples of chrome yellow were fully characterized and compared with the paint reconstruction based on the W&N archive [Otero *et al.* 2012]. Two chrome yellow painting samples from *BRUT* and *Entrada* were analysed by Synchrotron radiation techniques; the analysis of the painting samples does not show any signal of degradation. In the context of colour alteration phenomenon in *BRUT*, we detected fading and a colour changing at the paint surface. The fading of the paint is associated with the use of an eosin-based lake; the fading of this pigment causes the changing of the paint layer from pink to bluish-purple. The blue tone is related to the presence of cobalt blue present in mixture with the lake. In a dark green area of the painting it was detected the presence of starch. Starch was detected in the surface of the layer made by emerald green, under the surface it is still visible the original colour of the green pigment. Observing the SEM

---

<sup>11</sup> Amadeo de Souza-Cardoso, *Untitled (ZINC)*, 1917, 59 x 49 cm. Private collection [Freitas *et al.* 2008, pg. 355].

images seems that the starch has filled the space between the particles of the pigment with the consequent reduction of the light scattering that due the darkening of the surface.

The drawings, water colours and caricatures of Amadeo are important elements in his career; however, a Catalogue Raisonné has not yet been produced. In the future, it could be important to develop an approach similar to that developed for the oil paintings, applied to the study of the drawings and watercolours. Moreover, the application of the tool developed by combining hyperspectral imaging and  $\mu$ -EDXRF would made an important contribution on the characterization of the pigments used.



## REFERENCES

- Abas, F.S. 2004. "Analysis of craquelure patterns for content-based retrieval". Ph.D. Dissertation, University of Southampton, UK.
- Al-Ayyoub, M.; Irfan, M. and Stork, D.G. 2011. "Computer Vision and Image Analysis of Art II". Proceedings *SPIE* Vol. 7869.
- Alfaro, C. 2006. "Amadeo de Souza-Cardoso: 1887-1918" in Catalogue *Diálogo de Vanguardas-Avant-Garde Dialogues*. Assírio & Alvim and Fundação Calouste Gulbenkian, Lisbon.
- Alfaro, C. 2007. "Fotobiografia" in *Catalogo Raisonné V1. Amadeo de Souza Cardoso fotobiografia*. Assírio & Alvim and Fundação Calouste Gulbenkian, Lisbon.
- Alfaro, C. 2008. "Critérios e metodologia" in *Catálogo Raisonné V.2 – Amadeo de Souza-Cardoso, pintura*. Assírio & Alvim and Fundação Calouste Gulbenkian, Lisbon.
- Alfeld, M.; Pedrosa Vaz, P.; van Eikema Hommes, M.; Van der Snickt, G.; Tauber, G.; Blaas, J.; Haschke, M.; Erler, K.; Dik, J. and Janssens, K. 2013. "A mobile instrument for in situ scanning macro-XRF investigation of historical paintings", *Journal of Analytical Atomic Spectrometry*, 28:760-767.
- Almeida, F. and Henrique, B. 1898. *Diccionario Ilustrado da Lingua Portuguesa Histórico, Geográfico, Científico, Mythológico, Biográfico, Bibliográfico, etc.*, Lisboa: Francisco Pastor.
- Almeida, P.; Montagner, C.; Jesus, R.; Correia, N.; Vilarigues, M.; Melo, M.J. and Nascimento, S. 2013. "Analysis of paintings using multi-sensor data". 21<sup>th</sup> European Signal Processing Conference (Eusipco), Marrocco.
- Arslanoglu, J.; Centeno, S.A.; Digney-Peer, S. and Duvernois, I. 2013. "Picasso in the Metropolitan Museum of Art": An investigation of materials and techniques, *Journal of the American Institute for Conservation*, 52:140-155.
- Awate, S. P.; Tasdizen, T. and Whitaker, R.T. 2006 "Unsupervised Texture Segmentation with Nonparametric Neighborhood Statistics", *Proc. European Conference on Computer Vision*, 2:494-507
- Bacci, M.; Casini, A.; Cucci, C.; Picollo, M.; Radicati, B. and Vervat, M. 2003. "Non-invasive spectroscopic measurements on the Il ritratto della figliastra by Giovanni Fattori: identification of pigments and colourimetric analysis". *Journal of Cultural Heritage*, 4:329-336.
- Bacci, M.; Magrini, D.; Picollo, M.; Radicati, B.; Trumpy, G.; Tsukada, M. and Kunzelman, D. 2006. "Modern white pigments: their identification by means of non-invasive ultraviolet, visible and infrared fiber optic reflectance spectroscopy". *Congress Modern Paints Uncovered*, London.
- Bacci, M.; Magrini, D.; Picollo, M. and Vervat, M. 2009. "A study of the blue colors used by Telemaco Signorini (1835–1901)". *Journal of Cultural Heritage*, 10: 275–280.
- Baronti, S.; Casini, A.; Lotti, F. and Porcinai S. 1997. "Principal component analysis of visible and near-infrared multispectral images of work of art". *Chemom. Intell. Lab. Syst.* 39(1): 103-114.
- Berezhnoy, I.E.; Postma, E.O. and Herik van den, H.J. 2005. "Computerized visual analysis of paintings" in *XVI international conference of the Association for History and Computing*, Amsterdam, 14-17 September.
- Berezhnoy, I.E.; Postma, E.O. and Herik, H.J. van den 2009. "Automatic extraction of brushstroke orientation from paintings. POET: prevailing orientation extraction technique". *Machine Vision and Applications*, 20: 1–9.

- Berg, van den, J. D. and Boon, J. J. 1999. "Chemical changes in curing and ageing oil paints", proceedings *ICOM-CC Triennial 12th Conference*, Lyon.
- Berg, van den, J.D. 2002. *Analytical chemical studies on traditional linseed oil paints*, PhD Dissertation, University of Amsterdam.
- Bergboer, N.; Postma, E.O. and Herik, H.J. van den 2005. "Visual object detection for the cultural heritage", proceedings of the *XVI international conference of the Association for History and Computing*, Amsterdam.
- Berns, R.S. 2005 Rejuvenating the appearance of cultural heritage using color and imaging science techniques, proceedings *10<sup>th</sup> Congress of the International Colour Association, AIC Colour 05*, Granada, Andalucia, Spain, 369-375.
- Bersani, D.; Lottici, P.P. and Montenero, A. 1999. "Micro-Raman investigation of iron oxide films and powders produced by Sol-Gel syntheses". *Journal of Raman Spectroscopy* 30:355–360.
- Bomford, D.; Kirby, J.; Leighton, J. and Roy, A. 1990. *Art in the making, Impressionism*, National Gallery Publications Limited.
- Boon, J.J.; Peulvé, S.; Brink, O. F. van den; Duursma, M. C. and Rainford, D. 1996. "Molecular aspects of mobile and stationary phases in ageing tempera and oil paint films in Early Italian Paintings", proceedings *Techniques and Analysis Symposium*, Maastricht.
- Boon, J.J.; Weerd, J. van der; Keune, K.; Noble, P. and Wadum, J. 2002. "Mechanical and chemical changes in Old Master paintings: dissolution, metal soap formation and remineralization processes in lead pigmented ground/intermediate paint layers of 17th century paintings", proceedings *ICOM-CC Triennial 13<sup>th</sup> Conference*, Rio de Janeiro.
- Boon, J.J. and Ferreira, E.S.B. 2006. *Reporting Highlights of the De Mayerne Programme*, Netherlands Organisation for Scientific Research (NWO), The Hague, The Netherlands.
- Boon, J.J.; Hoogland, F. G. and Keune, K. 2007. "Chemical processes in aged oil paints affecting metal soap migration and aggregation", in *AIC paintings specialty group Postprints*, Washington.
- Boselli, L. 2010. *Non-invasive spectroscopic study of 19th century artists' materials*. PhD Dissertation in Scienze e Tecnologie per l'archeologia e i beni culturali, Università degli Studi di Ferrara, 2010
- Boselli, L.; Picollo, M. and Radicati, B. 2011. "UV, Vis, NIR Fibre Optic Reflectance Spectroscopy (FORS)" in *Practical handbook on diagnosis of paintings on movable support*, Editors D. Pinna, R. Mazzeo, B. Brunetti, European Project ARTECH.
- Bouchard, M.; Rivenc, R.; Menke, C. and Learner, T. 2009. "micro-FTIR and micro-Raman study of paints used by Sam Francis, *e-PRESERVATIONScience* 6:27-37.
- Bouchard, M. and Gambardella, A. 2010. "Raman microscopy study of synthetic cobalt blue spinels used in the field of art", *Journal Raman Spectroscopy* 41(11): 1477–1485.
- Brandi, C. 1977. *Teoria del restauro*, Edizioni di Storia e Letteratura, Roma, Einaudi, Torino.
- Browne, M.W. 2000. "Cross-Validation Methods", *Journal of Mathematical Psychology*, 44(1):108–132.
- Bucklow, S. 1997. "The Description of Craquelure Patterns," *Studies in Conservation*, 42(3):129-40.

- Burnstock, A.; Lanfear, I.; van der Berg, K.J.; Carlyle, L.; Clarke, M. and Hendricks, E. 2005. "Comparison of the fading and surface deterioration of red lake pigments in six paintings by Vincent van Gogh with artificially aged paint reconstructions", in: A.B. Paterakis, M. Cassar, D. Thickett, C. Villers, J.Wouters (Eds.), *Preprints of the 14<sup>th</sup> Triennial Meeting of the ICOM Committee for Conservation*, 1:459–466.
- Buxbaum, G. 1998. *Industrial Inorganic Pigments*, 1998, pg. 58 and 116–119.
- Carlyle, L. 1990. "The artists' anticipation of change as discussed in British nineteenth century instruction books for oil painting", preprints *Appearance, Opinion, Change: Evaluating the Look of Paintings*, United Kingdom Institute of Conservation, London, 62-67.
- Carlyle, L. 1993. "Authenticity and Adulteration: What Materials Were Nineteenth-Century Artists Really Using?" *The Conservator*, United Kingdom Institute for Conservation, Number 17:56-60.
- Carlyle, L. 1999. "Paint driers discussed in 19th-century British oil painting manuals", *JAIC*, 38(1):69-82.
- Carlyle, L. 2001. *The Artist's Assistant. Oil Painting Instruction Manuals and Handbooks in Britain 1800–1900. With Reference to Selected Eighteenth-century Sources*. London: Archetype Publications.
- Carlyle, L. and Witlox, M. 2005. *HART Project Report. Report of the De Mayerne Programme project: Historically Accurate Reconstructions of Oil Paint and Painting Composites*. De Mayerne Programme, Netherlands Organisation for Scientific Research (NWO).
- Casadio, F.; Xie, S.; Rukes, S. C.; Myers, B.; Gray, K. A.; Warta, R. and Fiedler, I. 2011. "Electron energy loss spectroscopy elucidates the elusive darkening of zinc potassium chromate in Georges Seurat's *A Sunday on La Grande Jatte—1884*", *Anal. Bioanal. Chem.*, 399:2909–2920.
- Casadio, F.; Bezúr, A.; Fiedler, I.; Muir, K.; Trad, T. and Maccagnola, S. 2012. "Pablo Picasso to Jasper Johns: a Raman study of cobalt-based synthetic inorganic pigments", *Journal Raman Spectrosc.*, 43: 1761–1771.
- Casadio, F. and Rose, V. 2013a. "High-resolution fluorescence mapping of impurities in historical zinc oxide pigments: hard X-ray nanoprobe applications to the paints of Pablo Picasso", *Applied Physics A*, 111:1-8.
- Casadio, F.; Muir, K. and Bezur, A. 2013b. "Introduction part two of special issue: From Can to Canvas", *Journal of the American Institute for Conservation*, 52(4):211-212.
- Casadio, C.; Miliani, C.; Rosi, F.; Romani, A.; Anselmi, C.; Brunetti, B.; Sgamellotti, A.; Andral, J.-L. and Gautier, G. 2013c. "Scientific investigation of an important corpus of Picasso paintings in Antibes: New insights into technique, condition, and chronological sequence", *Journal of the American Institute for Conservation*, 52(3):182-204.
- Cesaratto A.; Nevin, A.; Valentini, G.; Brambilla, L.; Castiglioni, C.; Toniolo, L.; Fratelli, M. and Comelli, D. 2013. "A novel classification method for multispectral imaging combined with portable Raman spectroscopy for the analysis of a painting by Vincent Van Gogh", *Appl Spectrosc.*, 67(11):1234-41.
- Church, A.H. 1901. *The Chemistry of Paints and Painting*, 3rd Edition, Seeley and Co. Ltd, London.
- Claro, C. 2009. *An interdisciplinary approach to the study of the colour in Portuguese manuscripts illuminations*. PhD Dissertation. Lisboa: Universidade NOVA de Lisboa.
- Claro, A.; Melo, M.J.; Seixas de Melo, J.S.; van den Berg, K.J.; Burnstock, A.; Montague, M. and Newman, R. 2010. "Identification of red colorants in van Gogh paintings and ancient Andean textiles by microspectrofluorimetry", *Journal of Cultural Heritage*, 11:27–34.



- Comelli, D.; Nevin, A.; Valentini, G.; Osticioli, I.; Castellucci, E.M.; Toniolo, L.; Gulotta, D.; and Cubeddu, R. 2011. "Insights into Masolino's Wall Paintings in Castiglione Olona: Advanced Reflectance and Fluorescence Imaging Analysis", *Journal Cultural Heritage*, 12(1):11-18.
- Coremans, P. 1948. *Van Meegeren's faked Vermeers and De Hooghs, a scientifica examination*, Cassel & Co. LTD Amsterdam.
- Cornelis, B.; Dooms, A.; Daubechies I. and Schelkens, P. 2009. "Report on Digital Image Processing for Art Historians", proceedings *International conference on Sampling Theory and Applications*, Marseille, France.
- Cornman, M. 1986. 'Cobalt Yellow (Aureolin),' in *Artists' Pigments. A Handbook of their History and Characteristics*, vol 1, National Gallery of Art.
- Cotte, M.; Checroun, E.; Susini, J.; Dumas, P.; Tchoreloff, P.; Besnard, M. and Walter, Ph. 2006. "Kinetics of oil saponification by lead salts in ancient preparations of pharmaceutical lead plasters and painting lead mediums Original Research Article", *Talanta*, 70(5):1136-1142
- Craver, C. 2000. *Applied polymer science 21<sup>th</sup> century*, Edited by Clara D. Craver, Charles E. Carraher, Jr. Elsevier.
- Cunha Leal, J. 2010. "Uma entrada para Entrada. Amadeo, a historiografia e os territórios da pintura", *Intervalo*, 4:133-153.
- Dantzig van, M.M. 1952. *Vincent? A new method of identifying the artist and his work and of unmasking the forger and his products*, publisher: Keesing, Amsterdam.
- Dantzig van, M.M. Foundation 1973. *Pictology*, Edit by van Dantzig Foundation, The Netherlands.
- Daugman, J. G. 1988. "Complete Discrete 2-D Gabor Transforms by Neural Networks for Image Analysis and Compression", *IEEE Transactions on Acoustics, Speech, and Signal processing*, 36(7):1169-1179
- Deborah, H.; George, S. and Hardeberg, J.Y. 2014. "Pigment mapping of the Scream (1893) based on hyperspectral imaging", proceedings of *International Conference on Image and Signal Processing*, Cherbourg, France, 247-256.
- Delaney, J. K.; Zeibel, J.G.; Thoury, M.; Littleton, R.; Palmer, M.; Morales, K. M.; Rene, E. and Hoenigswald, A. 2010. "Visible and infrared imaging spectroscopy of Picasso's Harlequin musician: mapping and identification of artist materials in situ," *Applied Spectroscopy*, 64(6):584-594.
- Delaney, J. K.; Ricciardi, P.; Deming Glinsman, L.; Facini, M.; Thoury, M.; Palmer, M. and de la Rie, R. E. 2014. "Use of imaging spectroscopy, fiber optic reflectance spectroscopy, and X-ray fluorescence to map and identify pigments in illuminated manuscripts", *Studies in Conservation*, 59(2): 91-101.
- Derrick, M.R.; Stulik, D. and Landry, J.M. 1999. *Infrared Spectroscopy in Conservation Science, – Scientific Tools for Conservation*. Los Angeles: The Getty Conservation Institute.
- Dik, J.; Janssens, K.; van der Snickt, G.; van der Loeff, L.; Rickers, K. and Cotte, M. 2008. "Visualization of a lost painting by Vincent van Gogh using synchrotron radiation based X-ray fluorescence elemental mapping", *Analytical Chemistry*, 80:6436-6442.
- Dredge, P.; Schilling, M. R.; Gautier, G.; Mazurek, J.; Learner, T. and Wuhrer, R. 2013. "Lifting the Lids off Ripolin: a collection of paint from Sidney Nolan's studio", *Journal of the American Institute for Conservation*, 52(4):213-226.
- Dutton, D. 2003. "Authenticity in Art" in *The Oxford Handbook of Aesthetics*, edited by Jerrold Levinson, New York: Oxford University Press. 258-274

- Dutton, D. 2009. *The art instinct*, Oxford University Press, Oxford.
- Eastaugh, N.; Walsh, V.; Chaplin, T. and Siddall, R. 2004. *Pigment Compendium: A Dictionary and Optical Microscopy of Historical Pigments*, Elsevier, Amsterdam.
- Erkens, L.J.H.; Hamers, H.; Hermans, R. J. M.; Claeys, E. and Bijmens, M. 2001. "Lead chromates: areview of the state of the art in 2000". *Surface Coatings International Part B: Coatings Transactions*, 84(3):169-176.
- Feller, R.J. 2004. *Color science in the examination of museum objects: non-destructive procedures*, Los Angeles: The Getty Conservation Institute.
- Ferreira, P. 1972. *Correspondance de quatre artistes Portugais : Almada-Negreiros, José Pacheco, Souza-Cardoso, Eduardo Vianna Avec Robert et Sonia Delaunay*, Fundação Calouste Gulbenkian, Lisbon.
- Ferreira, P. and Pernes, P. 1972. *Sónia e Robert Delaunay em Portugal: e os seus amigos Eduardo Vianna, Amadeo De Souza-Cardoso, José Pacheco, Almada Negreiros*, Fundação Calouste Gulbenkian, Lisbon.
- Ferreira, P. and Ribeiro, J. S. 1987. *Centenário de Nascimento de Amadeo de Souza-Cardoso*. Lisboa: Fundação Calouste Gulbenkian, Lisbon.
- Fiedler, I. and Bayard, M. 1997. "Emerald Green and Scheele's Green" in *Artists' pigments. a handbook of their history and characteristics*, 3. Fitzhugh, Elisabeth (Ed.) 1<sup>a</sup> ed. Washington: National Gallery of Art.
- Fornasier, M.; Ramlau, R. and Teschke, G. 2009. "The application of joint sparsity and total variation minimization algorithms to a real-life art restoration problem", *Advances in Computational Mathematics*, 31:157-184.
- França, J.A. 1956. *Amadeo de Souza-Cardoso*, Lisbona:Sul, Lisbon.
- França, J.A. 1986. "A Febre da vida Moderna" in *Amadeo & Almada*, Venda Nova:Bertand, Lisbon, 87-145
- França, J.A. 1992. "As últimas pinturas de Amadeo de Souza-Cardoso" in *Amadeo de Souza-Cardoso 1887-1918*, Porto Ed. Fundação de Serralves, 23-26.
- Freitas, H.; Alfaro, C. and Rosa, M. 2006. *Diálogo de Vanguardas-Avant-Garde Dialogues*. Assírio & Alvim and Fundação Calouste Gulbenkian, Lisbon.
- Freitas, H.; Alfaro, C. and Miranda, A.T. 2007. *Catálogo Raisonné V1. Amadeo de Souza-Cardoso fotobiografia*. Assírio & Alvim and Fundação Calouste Gulbenkian, Lisbon.
- Freitas, H. and Alfaro, C. 2008. *Catálogo Raisonné V.2 – Amadeo de Souza-Cardoso, pintura*. Assírio & Alvim and Fundação Calouste Gulbenkian, Lisbon.
- Freitas, H. 2008b. "Amadeo de Souza-Cardoso 1887-1918" in *Catálogo Raisonné V.2 – Amadeo de Souza-Cardoso, pintura*. Assírio & Alvim and Fundação Calouste Gulbenkian, Lisbon.
- Freitas, H. 2008c. "Elements on the critical reception of Amadeo de Souza-Cardoso." in *Catálogo Raisonné V.2 – Amadeo de Souza-Cardoso, pintura*. Assírio & Alvim and Fundação Calouste Gulbenkian, Lisbon.
- Frausto-Reyes, C.; Ortiz-Morales, M.; Bujdud-Pérez, J.M.; Magaña-Cota, G.E. and Mejía-Falcón, R. 2009. "Raman spectroscopy for the identification of pigments and color measurement in Dugès watercolours", *Spectrochimica Acta Part A*, 74(5):1275–1279.

- Frost, R. L. 2004. "Raman microscopy of selected chromate minerals", *Journal of Raman Spectroscopy*, 35(2):153-158.
- Frost, R.L.; Bahfenne, S. and Keeffe, E.C. 2010. "Raman spectroscopic study of the mineral gerstleyite  $\text{Na}_2(\text{Sb,As})_3\text{S}_{13}\cdot 2\text{H}_2\text{O}$  and comparison with some heavy-metal sulphides", *Journal of Raman Spectroscopy*, 41(12):1779-1783.
- Gabor, D. 1946. "Theory of communication", *Electrical Engineers - Part III: Radio and Communication Engineering*, 93(26):429 – 441
- Gardner, H. A. 1911. *Paint Technology and Tests*, McGraw-Hill Book Co., New York.
- Gardner, H. A. 1930. "Physical and Chemical Examination of Paints, Varnishes, Lacquers, and Colors", 5<sup>th</sup> Edition, pp. 884-896.
- Gates, G. 1995. "A Note on the Artists' Pigment Aureolin", *Studies in Conservation*, 40(3): 201-206.
- Gautier, G.; Bezur, A., Muir, K., Casadio, F. and Fiedler, I. 2009. "Chemical fingerprinting of ready-mixed house paints of relevance to artistic production in the first half of the twentieth century. Part I: Inorganic and organic pigments", *Applied Spectroscopy*, 63(6):597-603.
- Geldof, M.; Keijzer de, M.; Bommel van, M.; Pilz, K.; Salvant J.; Keulen van, H. and Megens, L. 2013. "Van Gogh's Geranium lake", in *van Gogh Studio practice*, Mercatorfonds, Brussels.
- Geldof, M. and Steyn, L. 2013b. "Van Gogh's Cobalt blue", in *van Gogh Studio practice*, Mercatorfonds, Brussels.
- Genestar, C. and Pons, C. 2005. "Earth pigments in painting: characterization and differentiation by means of FTIR spectroscopy and SEM-EDS microanalysis", *Analytical Bioanalytical Chemistry*, 382(2):269–274.
- Gonçalves, R.M. 2006. *Amadeo de Souza-Cardoso: A ânsia de originalidade*, Caminho Ed., Lisbon. 25-28
- Gonçalves, M.T. 2013. *Fakes in Art*. PhD Dissertation, Estudos in Literatura e Cultura Teoria da Literatura, Faculdade de Letras, Universidade de Lisboa.
- Gonzalez, R.C. and Woods, R.E. 2001. *Digital Image Processing*, 2<sup>nd</sup> Edition. Prentice Hall Upper Saddle River, New Jersey 07458.
- Gysau, D. 2006. *Fillers for Paints: Fundamentals and Applications*, Hannover: Vincentz Network.
- Hanspach-Bernal, E. and Bezur, A. 2013. "Mixed media: an example of Pablo Picasso's combination of non-artist's paints with tube colors from the Menil collection", *Journal of the American Institute for Conservation*;52(3):173-183.
- Harley, R.D. 2001, *Artists' Pigments c. 1600-1835*, London: Archetype Publications, 10-102.
- Hassard, F. 2006. *Heritage, Hermeneutics and Hegemony A Study of Ideological Division in the field of Conservation-Restoration*, PhD Dissertation Faculty of Creativity and Culture Buckinghamshire Chilterns University College Brunel University.
- Hendriks, E. and Hughes, S. 2009. "Van Gogh's brushstrokes: marks of authenticity?", in *Art, conservation and authenticities: material, concept, context International conference*, Archetype, London, 143-154.
- Herbst, W. and Hunger, K. 1997. *Industrial Organic Pigments. Production, properties, application*, Second, completely revised, WILEY-VCH Verlag GmbH & Co. KGaA.

- Hitchman, M.A. and Rowbottom, G.L., 1982. "Transition metal nitrite complexes", *Coordination Chemistry Reviews*, 42(1):55-132.
- Humel, D.O. 2002. *Atlas of plastics additives - Analysis by spectrometric methods*. Verlag Berlin Heidelberg New York: Springer.
- Hunt, R. W. G. 1991. *Measuring Colour*, Ellis Horwood.
- Irfan, M. and Stork, D.G. 2009. "Multiple visual features for the computer authentication of Jackson Pollock's drip paintings: Beyond box-counting and fractals", in Niel; David Fofi, Editor(s) *SPIE Electronic Imaging: Machine vision application II*, 7251.
- Jafarpour, S.; Polatkan, G.; Brevdo, E.; Hughes, S.; Brasoveanu, A. and Daubechies, I. 2009. "Stylistic analysis of paintings using wavelets and Machine Learning", *Proceedings 16<sup>th</sup> IEEE international conference on Image processing*, Cairo, Egypt.
- Jesus, R. 2009. *Recuperação de Informação Multimédia em Memórias Pessoais*, PhD Dissertation, Universidade Nova de Lisboa, Faculdade de Ciências e Tecnologia.
- Jesus, R.; Abrantes, A. and Correia, N. 2010. "Methods for automatic and assisted image annotation", *Multimedia Tools and Applications*, 1-20.
- Johnson, C. R.; Hendriks, E.; Bereznoy, I.J.; Brevdo, E.; Hughes, S.M.; Daubechies, I; Li, J.; Postma, E.O. and Wang, J. Z. 2008. "Image Processing for Artist Identification Computerized analysis of Vincent van Gogh's painting brushstrokes", *IEEE Signal Processing Magazine*, 37:37-48.
- Johnson, D.H.; Johnson Jr, C.R and Erdmann, R.G. 2013. "Weave analysis of paintings on canvas from radiographs", *Signal Processing*, 93:527–540.
- Kaplan, B. 2010. "Forgeries: as seen on TV! Art crimes are on the rise, and Canada", *National Post*, 8 April.
- Keijzer, de, M.1990. "Microchemical analysis on synthetic organic artists pigments discovered in the Twentieth Century" in *ICOM preprints*, Dresden, 221-225.
- Keshava N. and Mustard, J.F. 2002. "Spectral unmixing". *IEEE Signal Processing Magazine*, 19(1):44-57.
- Keshava, N. 2004. "Distance metrics and band selection in hyperspectral processing with applications to material identification and spectral libraries," *IEEE Transactions On Geoscience And Remote Sensing*, 42(7):1552-1565.
- Keune, K. 2005. *Binding medium, pigments and metal soaps characterised and localised in paint cross-sections*, PhD Dissertation MOLART (Project); Universiteit van Amsterdam.
- King, A.; Townsend, J. H.; Ormsby, B. and Gautier, G. 2013. "The use of Ripolin by Picabia in "The Fig Leaf (1922)", *Journal of the American Institute for Conservation*, 52(4):246-257.
- Kirby, J. 2011. *A closer look techniques of painting*, National Gallery Company Limited.
- Kühn, H. and Curran, M. 1986. *Artists' Pigments: a handbook of their history and characteristics*, vol. 1:170-172; 187–200; 208–211.
- Lapa, P. 1999. "A modernist through the memory of a distant present" in *At the edge: a Portuguese futurist*. Lisboa: GRI, Corcondan Gallery. 101-109.
- Lazzari, M. and Chiantore, O. 1999. "Drying and oxidative degradation of linseed oil", *Polymer Degradation and Stability*, 65:303-313.

- Leona, M.; Casadio, F.; Bacci, M. and Picollo, M. 2004. "Identification of the pre-Columbian pigment Maya blue on works of art by non-invasive UV-Vis and Raman spectroscopic techniques", *Journal of the American Institute for Conservation*, 43(1):39-54.
- Lessing, A. 1983. "What is wrong with forgery?", in *The forger's art*, Edit by Denis Dutton, University of California Press, London. 58-76
- Lew, M. S.; Sebe, N.; Djeraba, C. and Jain. R. 2006. "Content-based multimedia information retrieval: State of the art and challenges". *ACM Transactions on Multimedia Computing, Communications and Applications*, 2(1):1-19.
- Li J. and Wang, J. Z. 2004. "Studying digital imagery of ancient paintings by mixtures of stochastic models", *IEEE Transactions on Image Processing* 13(3):340-353.
- Li, J.; Yao, L.; Hendriks. L. and Wang, J.Z. 2012 "Rhythmic brushstrokes distinguish van Gogh from his contemporaries: findings via automated brushstroke extraction", *Pattern Analysis and Machine Intelligence, IEEE Transactions*, 34(6).
- Liang, H. 2012. "Advances in multispectral and hyperspectral imaging for archaeology and art conservation", *Applied Physics A*, 106:309-323.
- Likas, A.; Vlassis, N. and Verbeek, J. J. 2003. "The global k-means clustering algorithm", *Pattern Recognition* 36:451-461.
- Lomax, S.Q. 2005. "Phthalocyanine and quinacridone pigments: their history, properties and use", *Reviews in Conservation*, 6:19-29.
- Lomax, S.Q. and Learner, T. 2006. "A review of the classes, structures and methods of analysis of synthetic organic pigments", *Journal of the American Institute for Conservation (JAIC)*, 45:107-125.
- Lowe, D.G. 1999. "Object recognition from local scale-invariant features," *International Conference on Computer Vision*, Corfu, Greece, 1150-1157.
- Lowe, D.G. 2004. "Distinctive image features from scale-invariant keypoints", *International Journal of Computer Vision*, 91-110.
- Lowenthal, D. 1994. "Changing criteria of authenticity" in *Nara conference on authenticity*, proceedings published by UNESCO World Heritage Centre, Japan. 121-135
- Loon, van, A.; Noble, P. and Burnstock, A. 2012. "Ageing and deterioration of traditional oil and tempera paints" in *Conservation of Easel Paintings*, edit by Joyce Hill Stoner, Rebecca Rushfield. Routledge, Oxford. 214-241
- Lyu, S.; Rockmore, D. and Farid, H. 2004. "A digital technique for art authentication", *Proceedings of National Academy of Sciences (PNAS)*, 101(49):17006-17010.
- Maaten, van der, L. and Postma, E. 2009. "Identifying the real van Gogh with Brushstroke Textons", Technical Report TiCC TR.
- Mallégol, J.; Gardette, J. and Lemaire, J. 1999. *Journal of the American Oil Chemists' Society*, 76:967-976
- Manjunath, B.S. and Ma, W.Y. 1996. "Texture Features for Browsing and Retrieval of Image Data". *IEEE Transactions on Pattern Analysis And Machine Intelligence*, 18(8): 837-842.
- Martens, W.; Frost, R. L. and Kloprogge, J. T. 2003. "Raman spectroscopy of synthetic erythrite, partially dehydrated erythrite and hydrothermally synthesized dehydrated erythrite", *Journal of Raman Spectroscopy*, 34(1):90-95.

- Matero, F.G. 2007. "Loss, Compensation, and authenticity: the contribution of Cesare Brandi to architectural conservation in America", in *Future Anterior: Journal of Historic Preservation History Theory*, 4(1):45-63.
- Mayer, R. 1982. *The Artist's handbook of materials and techniques*. 4<sup>th</sup> Edition, Revised and Up, Faber & Faber.
- McMillan, G.; Casadio, F.; Fiedler, I. and Sorano-Stedman, V. 2013. "An investigation into Kandinsky's use of Ripolin in his paintings after 1930", *Journal of the American Institute for Conservation*, 52(4): 258-277.
- Meilunas, R. J.; Bentsen, J. G. and Steinberg, A. 1990. "Analysis of ages FTIR spectroscopy", *Studies in Conservation*, 35:33-51.
- Melo, M.J.; Vilarigues, M.; Babo, S.; Alfaro, C.; Freitas, H. and Sandu, I. 2008. "Uma mão cheia de cores, o Século XX e o nascimento da arte Moderna" in *Amadeo de Souza-Cardoso, Catalogue Raisonné, Pintura, V.2*, 81–104.
- Melo, M.J.; Vilarigues, M.; Babo, S.; Alfaro, C.; Freitas, H. and Sandu, I.; 2009. "Estudo dos materiais e técnicas de Amadeo de Souza-Cardoso", technical report Departamento de Conservação e Restauro da Faculdade de Ciências e Tecnologia Universidade Nova de Lisboa.
- Miller, F. A. and Wilkins, C. H. 1952. "Infrared Spectra and Characteristic Frequencies of Inorganic Ions", *Analytical Chemistry*, 24(8):1253-1294.
- Monico, L.; Snickt, G.; Janssens, K.; Noft, W.; Miliani, C.; Verbeeck, J.; Tian, H.; Tan, H.; Dik, J.; Radepont, M. and Cotte, M. 2011a. "Degradation process of lead chromate in paintings by Vincent van Gogh studied by means of synchrotron X-ray spectromicroscopy and related methods. 1. Artificially aged model samples", *Analytical Chemistry*, 83:1214–1223.
- Monico, L.; Snickt, G.; Janssens, K.; W. Noft, W.; Miliani, C.; Verbeeck, J.; Tian, H.; Tan, H.; Dik, J.; Radepont, M. and Cotte, M. 2011b. "Degradation process of lead chromate in paintings by Vincent van Gogh studied by means of synchrotron X-ray spectromicroscopy and related methods 2. Original paint layer samples", *Analytical Chemistry*, 83, 1224–1231.
- Monico, L.; Janssens, K.; Miliani, C.; Snickt, G.; Brunetti, B. G.; Cestelli Guidi, M.; Radepont, M. and Cotte, M. 2013. "Degradation process of lead chromate in paintings by Vincent van Gogh studied by means of synchrotron X-ray spectromicroscopy and related methods 4. Artificial aging of model samples of co-precipitates of lead chromate and lead sulfate", *Analytical Chemistry*, 85:860-867.
- Montagner, C.; Bacci, M.; Bracci, S.; Freeman, R. and Picollo, M. 2011. "Library of UV–Vis–NIR reflectance spectra of modern organic dyes from historic pattern-card coloured papers", *Spectrochimica Acta Part A*, 79:1669-1680
- Montagner, C.; Jesus, R.; Correia, N.; Melo, M.J.; Vilarigues, M.; Macedo, R. and de Freitas, H. 2012. "Unveiling the hand of a 19<sup>th</sup> century artist with binary image classification and bag-of-features," *International Conference On Systems, Signals and Image Processing (IWSSIP)*, Vienna, Austria.
- Montagner, C.; Almeida, P.; Jesus, R.; Correia, N.; Melo, M.J.; Vilarigues, M.; Macedo, R.; Freitas, H. and Nascimento, S. 2013. "Behind the surface - Hyperspectral image spectroscopy for artist authentication", proceedings *12<sup>th</sup> International AIC Congress*, UK.
- Montagner, C., Sanches, D., Pedroso, J. Melo, M.J. and Vilarigues, M. 2013b. "Ochres and earths: matrix and chromophores characterization of 19<sup>th</sup> and 20<sup>th</sup> century artist materials", *Spectrochimica Acta Part A*, 103:409–416.
- Morelli, G. 1893. *Italian painters: critical studies of their works*. With an introduction by A. H. Layard. Translated from the German by Constance Jocelyn Ffoulkes. 2<sup>nd</sup> impression. John Murray, 1900. London.



- Muckley, W.L. 1882. *A Handbook for painters and art students*, London.
- Muir, K.; Langley, A.; Bezur, A.; Casadio, F.; Delaney, J. and Gautier, G. 2013. "Scientifically investigating Picasso's suspected use of Ripolin house paints in still life, 1922 and the Red Armchair, 1931", *Journal of the American Institute for Conservation*, 52(3):156-172.
- Müller, K. R.; Mika, S.; Rätsch, G.; Tsuda, K. and Schölkopf, B. 2001. "An Introduction to Kernel-based Learning Algorithms", *IEEE Neural Networks*, 12(2):181-201.
- Noble, P.; van Loon, A. and Boon, J. J. 2005. "Chemical changes in old master paintings II: darkening due to increased transparency as a result of metal soap formation processes", proceedings *ICOM-CC Triennial 14th Conference*, The Hague, Holland, (Ed. I. Verger). James & James, London. 496-503
- Nowak, E.; Jurie, F. and Triggs, B. 2006. "Sampling strategies for bag-of features image classification". Proceedings *European Conference on Computer Vision*, Graz, Austria, Springer, 3954:490-503.
- Osawa Z. 1988. "Role of metals and metal-deactivators in polymer degradation", *Polymer Degradation and Stability*, 20(3-4):203-36.
- Plater, M.J.; De Silva, B.; Gelbrich, T.; Hursthouse, M.B.; Higgitt, C. L. and Saunders, D.R. 2003. "The characterisation of lead fatty acid soaps in 'protrusions' in aged traditional oil paint", *Polyhedron*, 22(24): 3171-3179.
- Otero, V.; Carlyle, L.; Vilarigues, M. and Melo, M.J. 2012. "Chrome yellow in nineteenth century art: historic reconstructions of an artists' pigment", *RSC Advances*, 2:1798-1805
- Otero, V.; Sanches, D.; Montagner, C.; Vilarigues, M.; Carlyle, L.; Lopes J.A. and Melo, M.J. 2014a. "Characterisation of metal carboxylates by Raman and infrared spectroscopy in works of art", *Journal of Raman Spectroscopy*, published online: 10 JUL 2014 DOI: 10.1002/jrs.4520.
- Otero, V.; Carlyle, L.; Vilarigues, M.; Cotte, M. and Melo, M.J. 2014b. "19<sup>th</sup> century chrome yellow and chrome deep from Winsor & Newton", to be submitted.
- Otero, V.; Montagner, C.; Carlyle, L.; Vilarigues, M.; Cotte, M. and Melo, M.J. 2014c. *Synchrotron Radiation and Historically Accurate Reconstruction for the preservation of chrome yellow in 19th c. works of art*, User Report ESRF.
- Pantelouris, A.; Modrow, H.; Pantelouris, M.; Hormes, J. and Reinen, D. 2004. "The influence of coordination geometry and valency on the K-edge absorption near edge spectra of selected chromium compounds", *Chemical Physics*, 300(1-3):13-22.
- Pelagotti, A.; Del Mastio, A.; de Rosa, A. and Piva, A. 2008. "Multispectral imaging of paintings, a way to material identification," *IEEE Signal Processing Magazine*, 36:27-36.
- Peres, C.; Hoyle, M. and van Tilborgh, L. 1991. *A Closer Look: Technical and Art-Historical Studies on Works by Van Gogh and Gauguin*, Zwolle: Waanders Publishers.
- Poggio, T. and Smale, S. 2003. "The mathematics of learning: Dealing with data", *Notice of American Mathematical Society*, 50(5):537-544.
- Polatkan, G.; Jafarpour, S.; Brasoveanu, A.; Hughes, S. and Daubechies, I. 2009. "Detection of forgery in painting using supervised learning", proceedings *IEEE International Conference on Image Processing*, Cairo.
- Prasad, P.S.R.; Chaitanya, K.V.; Prasad, K.S. and Rao, D.N. 2005. "Direct formation of the  $\gamma$ -CaSO<sub>4</sub> phase in dehydration process of gypsum: in situ FTIR study", *American Mineralogist*, 90:672-678.
- Quilès, F. and Burneau, A. 1998. "Infrared and Raman spectra of alkaline-earth and copper II/acetates in aqueous solutions", *Vibrational Spectroscopy*, 16:105-117.

Ricciardi, P. and Delaney, J. K. 2011. "New trends in the study of medieval illuminated manuscripts: combining visible and infrared imaging spectroscopy with site specific, in-situ techniques for material identification and mapping", *Revista de Historia da Arte*, 254-263 (available online: <http://revistadehistoriadaarte.wordpress.com>).

Rioux, J.P. 1999. "The discolouration of pinks and purples in Van Gogh's paintings from Auvers", in *Cézanne to Van Gogh: the collection of Doctor Gachet*, New York, 104-14.

Robertson, S. 2004, "Understanding Inverse Document Frequency: On theoretical arguments for IDF", *Journal of Documentation*, 60(5):503–520.

Robinet L. and Corbeil, M.C. 2003. "The characterization of metal soaps", *Studies in Conservation*, 48:23-40.

Roncaglia, D. I.; Botto, I. L. and Baran, E. J. 1985 "Vibrational spectrum of  $Pb_2CrO_5$ ", *Journal of Materials Science Letters*, 4(11):1427-1428.

Ropret, P.; Centeno, S.A. and Bukovec, P. 2008. "Raman identification of yellow synthetic organic pigments in modern and contemporary paintings: Reference spectra and case studies", *Spectrochimica Acta Part A*, 69:486-497.

Rosenfeld, A. 1975. *Visual texture analysis: An overview*, Computer Science Center, Univ. Maryland, College Park, Technical Report TR-406.

Salmon, L.G. and Cass, G.R. 1993 "The fading of artist's colorants by exposure to atmospheric nitric acid", *Studies in Conservation*, 38:73-91.

Salton, G. and McGill, M. 1986. *Introduction to modern information retrieval*, McGraw-Hill, Inc., New York, NY, USA.

Saunders, D. and Kirby J. 1994. "Light-induced colour changes in red and yellow lake pigments", *National Gallery Technical Bulletin*, 15.

Savitzky, A. and Golay, M. J. E. 1964. "Smoothing and differentiation of data by simplified least squares procedures," *Analytical Chemistry*, 36:1627-1639.

Schaefer, I.; von Saint-George, C. and Lewerentz, K. 2008. *Painting light the hidden techniques of the Impressionists*, Skira editore, Milano, Italy.

Scherren, F.; Brzeninka, K.; Lutzenberger, K.; Stege, H. and Panne, U. 2009. "Synthetic organic pigments of the 20<sup>th</sup> and 21<sup>th</sup> century relevant to artist's paints: Raman spectra reference collection", *Spectrochimica Acta A*, 73:505-524.

Schulte, F.; Brzezinka, K-W.; Lutzenberger, K.; Stege, H. and Panne, U. 2008. "Raman spectroscopy of synthetic organic pigments used in 20<sup>th</sup> century works of art", *Journal of Raman Spectroscopy*, 39:1455-1463.

Sebe, N.; Cohen, I.; Garg, A.; and Huang, T.S. 2005. *Machine Learning in Computer Vision* Springer Verlag.

Shebanova, O.N. and Lazor, P. 2003. "Raman spectroscopic study of magnetite ( $FeFe_2O_4$ ): a new assignment for the vibrational spectrum", *Journal of Solid State Chemistry*, 174:424-430.

Shen, J. 2009. "Stochastic modeling western paintings for effective classification", *Pattern Recognition* 42:293-301.

Shimadzu, Y.; Keune, K.; Boon, J. J.; Townsend, J. H. and van den Berg, K. J. 2008. "The effects of lead and zinc white saponification on surface appearance of paint", proceedings *ICOM-CC Triennial 15th Conference*, New Delhi.

- Silva, A.M.; Sanches, D.; Montagner, C.; Vilarigues, M.; Melo, M.J. and Picollo, M. 2011. "The palette of Columbano Bordalo Pinheiro (1857-1929): characterization of oil paint colours from his tubes", proceedings *Science for Contemporary Art, AiAr conference*, Florence (Italy).
- Silva, R. H. 1995. "Os anos do Orpheus e de Portugal futurista", in *História da Arte Portuguesa*, ed. Paulo Pereira, Círculo de Leitores, Lisbon 372-377
- Sipics, M. 2009. "The van Gogh project: art meets mathematics" in *Ongoing international study*, in *SIAM News*, 42(4).
- Sottomayor, F.A. 2011. *Indústria dos Fósforos: das Origens ao Monopólio (1862-1926). O caso do Porto*, Dissertação de Mestrado em História Contemporânea, Departamento de História e de Estudos Políticos e Internacionais. Porto.
- Standeven, H.A. L. 2011. *House paints 1900-1960*, ed. T. Ball, Research in Conservation. The Getty Conservation Institute, Publications, Los Angeles.
- Standeven, H.A. L. 2012. "The history and manufacture of Lithol red, a pigment used by Mark Rothko in his Seagram and Harvard murals of the 1950s and 1960s", *Tate's Online Research Journal*, ISSN 1753-9854.
- Standeven, H.A.L. 2013. "Oil-based house paints from 1900 to 1960: an examination of their history and development, with particular reference to Ripolin enamels", *Journal of the American Institute for Conservation*, 52(3):127-139.
- Stenger, J.; Kwan, E.E.; Eremin, K.; Speakman, S.; Kirby, D.; Stewart, H.; Huang, S.G.; Kennedy, A.R.; Newman, R. and Khandekar, N. 2010. "Lithol red salts: characterization and deterioration", *e-PRESERVATION Science*, 7:147-157.
- Stanley B.E. 1946. *The alkaline-earth and heavy metal soaps*, American Chemical Society Monograph series, Reinhold publishing corporation.
- Stork, D.G. 2006. "Computer Vision, Image Analysis, and Master Art: Part 1," *IEEE MultiMedia*, 13(3):16-20.
- Stork, D.G. 2008. "Computer image analysis of paintings and drawings: An introduction to the literature," Proceedings *Image processing for artist identification workshop*, van Gogh Museum, Amsterdam, The Netherlands.
- Stuart, B.; George, B. and McIntyre, P. 1996. *Modern Infrared Spectroscopy*, John Wiley & Sons, England.
- Stuart, B. and Ando, D.J. 1997. *Biological Application of Infrared Spectroscopy*. New York: John Wiley and Sons.
- Sutton, P.C. 2004. "Rembrandt and brief history of connoisseurship" in *The expert versus the object - judging fakes and false attributions in the visual arts*, Edit by Ronald D. Spencer, Oxford University Press. 29-38.
- Tamura, H.; Mori, S. and Yamawaki, Y. 1978. "Textural Features Corresponding to Visual Perception", *IEEE Transactions on Systems, Man, and Cybernetics*, SMC-8, 460-473.
- Tan, H.; Tian, H.; Verbeeck, J.; Monico, L.; Janssens, K. and van Tendeloo, G. 2013. "Nanoscale investigation of the degradation mechanism of a historical chrome yellow paint by quantitative electron energy loss spectroscopy mapping of chromium species, *Angewandte Chemie International Edition*, 52:1-5.
- Taylor, R. P.; Micolich, A. P. and Jonas, D. 1999. Fractal analysis of Pollock drip paintings. *Nature*, 399, 422.

- Terry, A.E.; Overall, N.J. and Tooley, I.R. 2005. "Characterization of TiO<sub>2</sub> nanoparticles surface modified with aluminium stearate", *Langmuir*, 21:3172-3178.
- Todd, R. 2008. *The thing itself: on the search for authenticity*, Riverhead books, New York.
- Tuceryan, M. and Jain, A. K. 1998. *Texture Analysis, The handbook of pattern recognition and computer vision* (2<sup>nd</sup> Edition), World Scientific Publishing Co.
- Tumosa, C.S., Erhardt, W.D.; Marion F.M and McCormick-Goodhart, M.H. 1994. "The effects of relative humidity and temperature on exhibited objects", *Special ICOM Study Series*, 9.
- Tumosa, C.S. 2001. "A brief history of aluminium stearate as a component of paint", WAAC Newsletter 23(3) [on line <http://cool.conservation-us.org/waac/wn/wn23/wn23-3/wn23-304.html> (March 2014)].
- Tumosa, C.S. and Mecklenburg, M. F. 2005. "The influence of lead ions on the drying of oils", *Reviews in Conservation*, 6:39-47.
- Urbani, G. 2000. "Il restauro tra scienza e estetica" in *Intorno al restauro*, Edit by Bruno Zanardi, Skira editor Milan. 65-68
- Varma, M. and Zisserman, A. 2005. "A statistical approach to texture classification from single images", *International Journal of Computer Vision: Special Issue on Texture Analysis and Synthesis*, 62:61-81.
- Vandenabeele, P.; Moens, L.; Edwards, H.G.M. and Dams, R. 2000. "Raman spectroscopic database of azo pigments and application to modern art studies", *Journal of Raman Spectroscopy*, 31:509-517.
- Vendilo, A.G.; Kovaleva, N.E.; Chistov, V.I. and Retivov, V.M. 2011. "Potassium cobaltinitrite", *Russian Journal of Inorganic Chemistry*, 56(4):501-505.
- Vet, de, M. and van Kregten, J. 2014. "Touch van Gogh and Be Touched – How New Media Are Transforming the Way We Present Complex Research", *Conference of Museums and the Web*, Baltimore, MD, USA.
- Vibert, J. G. 1892. *The science of painting*, translation from 8<sup>th</sup> revised edition by Percy Young.
- Weerd, van der, J. 2002. *Microspectroscopic analysis of traditional oil paint*, PhD Dissertation Faculty of Science, University of Amsterdam.
- Weerd, van der, J.; van Loon, A. and Boon, J. J. 2005. "FTIR Studies of the effects of pigments on the aging of oil", *Studies in Conservation*, 50(1):3-22.
- Yang, J.J.; Martens, W.N. and Frost, R.L. 2010. "Transition of chromium oxyhydroxide nanomaterials to chromium oxide: a hot stage Raman spectroscopic study", *Journal of Raman Spectroscopy*, 42(5):1142-1146.
- Zanella, L.; Casadio, F.; Xie, S.; Gray, K. A.; Warta, R.; Ma, Q. and Gaillard, J. 2011. "The darkening of zinc yellow: XANES speciation of chromium in artist's paints after light and chemical exposures", *Journal of Analytical Atomic Spectrometry*, 26:1090-1097.
- Zhao, Y. 2008. *Image segmentation and pigment mapping of Cultural Heritage based on spectral imaging*, PhD. Dissertation, Rochester, New York, United States.
- Zumbuehl, S.; Scherrer, N.C.; Burger, A. and Eggenberger, U. 2009. "Early viridian pigment composition characterization of a (hydrated) chromium oxide borate pigment", *Studies in Conservation*, 54(3):149-159.



## **APPENDICES PART I**





## Appendix I: K-means method

The goal of a cluster method is to divide a set of objects into a number ( $k$ ) of clusters. Suppose a data set  $X = \{x_1; \dots; x_N\}$  and  $x_n \in R^d$ , the M-clustering problem aims at partitioning this data set into  $M$  disjoint subsets (clusters)  $C_1, \dots, C_M$ , such that a clustering criterion is optimized.

The most widely used clustering criterion is the sum of the squared Euclidean distances between each data point  $x_i$  and the centroid  $m_k$  (cluster center) of the subset  $C_k$  which contains  $x_i$ .

$$E(m_1, \dots, m_M) = \sum_{i=1}^N \sum_{k=1}^M l(x_i \in C_k \|x_i - m_k\|)^2$$

Where  $l(x) = 1$  if  $x$  is true and 0 otherwise [Likas *et al.* 2003].

The clustering algorithm works as represented in the figure below:

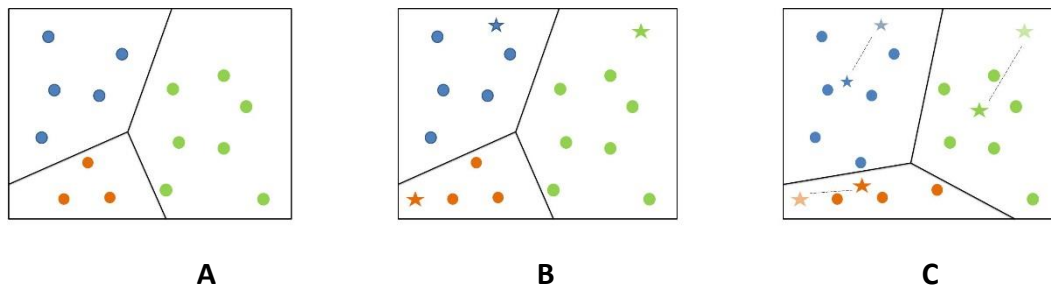


**Figure I.1** **A**  $k$  centroids of  $K$ -clusters are chosen randomly; **B** Each sample is assign to the nearest centroid; **C** For each cluster a new centroid is calculated. Move the centroid to the new position. If centroids are unchanged, the clustering is done. Otherwise, go to step A and new centroids are computed.

## Appendix II: Term Frequency–Inverse Document Frequency (TF-IDF)

Consider a collection of objects in which each object is characterized by one or more properties, each property could be weighted to reflect its importance in the representation of the given object [Salton and McGill 1986]. Salton proposed the concept of term frequency (TF) using a text as examples. The TF weighting system is based on the notion that constructs (words, phrases, word groups) that frequency occur in the text of documents have some bearing on the content of the texts. Hence the weight of term  $k$  in document  $i$ ,  $WEIGHT_{ik}$  might be set equal to the frequency of occurrence of word construct  $k$  in the document  $i$ :  $WEIGHT_{ik} = FREQ_{ik}$

The term weighting function known as Inverse Document Frequency (IDF) was proposed in 1972, and has since been extremely widely used, usually as part of a TF-IDF function. Karen Spärck Jones introduced the concept of IDF: it is based on counting the number of documents in the collection being searched which contain (or are indexed by) the term in question. The intuition was that a query term which occurs in many documents is not a good discriminator, and should be given less weight than one which occurs in few documents [Salton and McGill 1986].

With the Bag-of-Features each image  $I$  is represented by a vector of occurrence of words:

$$d_i = [W_{1,i}, W_{2,i}, \dots, W_{N_t,i}]^T$$

to normalize this vector, the Term Frequency–Inverse Document Frequency is applied,

$$W_{l,k} = \frac{N_{i,k}}{\sum N_{l,k}} \log \left( \frac{N}{n_l} \right)$$

with  $n_l$  denotes the numbers of images where the term  $l$  is present and  $N_{l,k}$  is the number of occurrences of the term  $l$  in the  $k$  image.

### Appendix III: Chromatic values

Reflectance spectra can be related to colour using established international conventions developed by Commission International d'Eclairage (CIE)<sup>1</sup>. The tristimulus values (X,Y,Z) in the  $400 \leq \lambda \leq 700$  nm spectral range for the 10° standard observer (CIE 1964) are computed as follows [Feller 2004]:

$$X_{10} = K \sum S(\lambda)x_{10}(\lambda)R(\lambda); \quad Y_{10} = K \sum S(\lambda)y_{10}(\lambda)R(\lambda); \quad Z_{10} = K \sum S(\lambda)z_{10}(\lambda)R(\lambda)$$

where:  $K = \frac{100}{\sum S(\lambda)y_{10}R(\lambda)}$ ;

$\lambda$  indicates the wavelength at a 10 nm pitch;

$S(\lambda)$  is the relative spectral power distribution of the illuminant;

$x(\lambda)$ ,  $x_{10}(\lambda)$ ,  $y(\lambda)$ ,  $y_{10}(\lambda)$ ,  $z(\lambda)$  and  $z_{10}(\lambda)$  are colour-matching functions;

$R(\lambda)$  is the spectral reflectance of the specimen.

Several colour spaces have been defined based on the tristimulus values  $X$ ,  $Y$ ,  $Z$ . For this work we chose the  $L^*a^*b^*$  colour space. This space can be visualized as a spherical space in which the axis is the lightness ( $L^*$ ), ranging from 0% to 100% and the radius are the chromaticity variables  $a^*$  and  $b^*$ . Variable  $a^*$  is the green (negative) to red (positive) axis and variable  $b^*$  is the blue (negative) to yellow (positive) axis. The variables are defined as follows [Feller 2004]:

$$L^* = 116(Y/Y_n)^{1/3} - 16; \quad a^* = [500(X/X_n)^{1/3} - (Y/Y_n)^{1/3}]; \quad b^* = [200(Y/Y_n)^{1/3} - (Z/Z_n)^{1/3}]$$

where  $X_n$ ,  $Y_n$ ,  $Z_n$  are the CIE tristimulus values of the illuminant.

---

<sup>1</sup> Information concerning the activities of *The International Commission on Illumination* and the and the technical report can be found in [www.cie.co.at/](http://www.cie.co.at/)

## Appendix IV: Analysis of the painting *Mucha* give date using hyperspectral imaging and $\mu$ -EDXRF

This appendix shows the analysis of the results produced by the system of molecular analysis (Part I Chapter 2) obtained combining hyperspectral image and elemental analysis on the painting *Mucha*.

### Results and discussion

Figure IV.4.A show the points where the elemental analysis was performed, the elements detected are resumed in Table IV.1. Figure IV.1B show the segmented image obtained by the system.

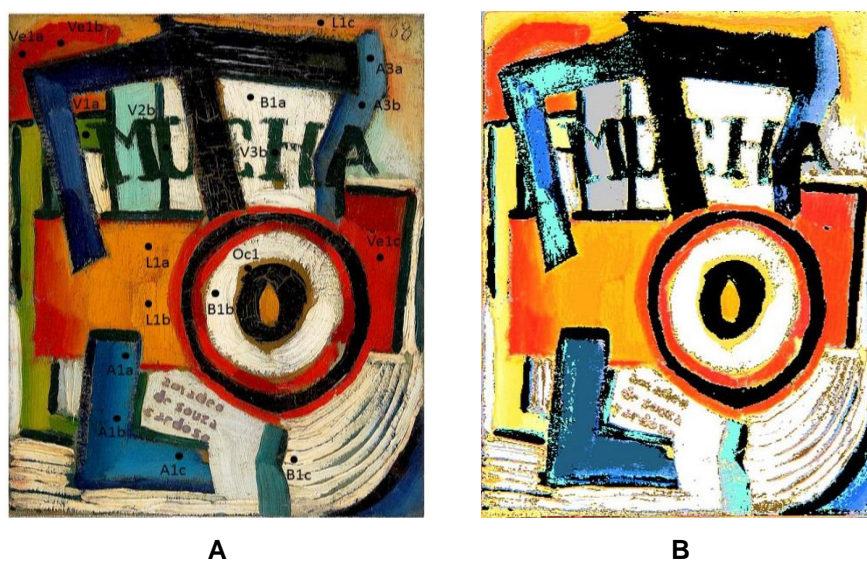


**Figure IV.1** *Mucha* painting **A** EDXRF points of analysis; **B** segmented image made by the system.

**Table IV.1.** Elements detected for each area and the attribution performed by the system combining hyperspectral imaging and EDXRF.

Colour	EDXRF	Attribution made by the system
Yellow	Pb, Ba, (Zn) Ca, Cr, Hg, (Fe)	Chrome Yellow + Vermilion
Orange	Pb, Ba, (Zn), Ca, Cr, Hg, (Fe)	Vermilion + Chrome Yellow
Red	Pb, Ba, Zn, Hg, (Cr, Fe)	Vermilion + Chrome Yellow
Light brown	Pb, Ba, Zn, Cr, Fe, Hg	Yellow Ochre + Chrome Yellow + Vermilion
Green	Pb, Ba, Zn, Cr (Fe)	Cr Yellow +Viridian + Yellow ochre
Blue	Pb, Zn, Ba, (Cr, Fe)	Cerulean blue
	Pb, Zn, Ba, Co, Ni, Sn, (Fe)	Cerulean
	--	n.a.
White	Pb, Ba	--
Black	Pb, Ba, Zn, Hg, Ca, Cr, Fe, Co	--

The results obtained by the system are compared with the analysis of the reflectance spectra. Besides that Spectra Angle Mapped (SAM) was used to visualize the distribution of the pigments in the hyperspectral imaging.

Base on the dimension of the detector used to acquire the hyperspectral image and the distance between the camera and the painting it was calculated that each pixel of the image represent 0,2 mm of the painting surface. All the spectra presented in this appendix are the mean of a 9x9 pixels. The use of a mean value, instead of the single pixel, allows the reduction of the noise of the reflectance spectrum (Fig. IV.2).

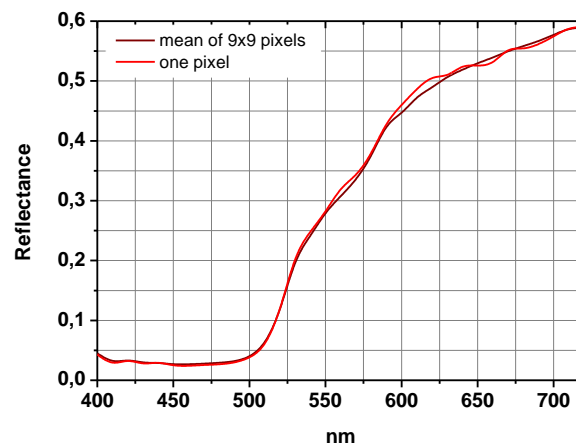
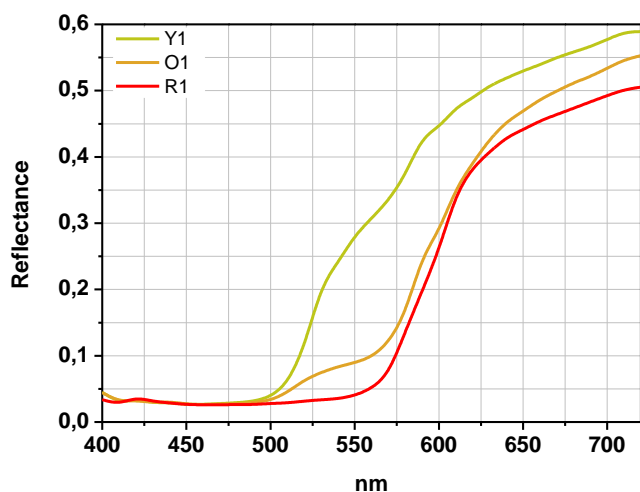


**Figure IV.2.** Comparison between reflectance spectrum acquired on one pixel (red line) and the mean spectra obtained using an area of 9x9 pixels (black line).

### *Yellow, orange and red areas*

The spectrum of the point Y1 (Fig. IV.3A) show a maximum of absorption in the between 400 and 500 nm. The first derivative of point Y1 (Fig. IV.4A) showed a well-defined maximum peak at around 524 nm and another less intense at 580 nm. It is visible a good correlation between the spectrum Y1 and the spectrum form the chrome yellow paint tube sample ASC17 (Fig. IV.4B). The strong absorption band, around 460 nm, of the chrome yellow ( $\text{PbCrO}_4$ ) is due to electronic transition metal-ion. In the region 580 -720 nm the spectrum of the ASC17 show a linear increase of the reflectance, in different way the spectrum of Y1 shows a shoulder at 580 ca. nm. The two inflection points of the spectrum are clearly in the first derivative (Fig. IV.4A), the presence of inflection point suggest the presence of contribution of a red tone.

Concerning the point R1 the spectrum shows high reflectance values between 400 to 550 nm (Fig. IV.3A). The first derivative (Fig. IV.4A) shows a maximum at 600 nm and a shoulder at 580 nm similar to that observed in Y1. The reflectance spectrum of the vermilion ( $\text{HgS}$ ) (Fig. IV.4B) shows a typical shape, called "S", with an inflection point at 600 nm. The absorption band of this due to the electronic transition band to band [Boselli 2010].



**A**

**B**



**C**

**D**

**Figure IV.3** **A** Reflectance spectrum acquired on yellow (Y1); orange (O1) and red (R1) area. Mapping of the pigments identified by the system: **B** chrome yellow; **C** mixture chrome yellow and vermilion and **D** vermilion.

Concerning the orange (Fig. IV.3A) the spectrum shape suggests the presence of yellow (Y1) and red (R1). The curve of the first derivative (Fig. IV.4A) of O1 show two peaks at 515 nm, 584 the maximum and a shoulder at 609 nm. In this case the peak around 580 nm is the maximum. The XRF analysis presented in Table IV.1 confirms the presence of vermilion and chromium in the orange tones. Table IV.2 shows the L\*a\*b\* values acquired in the 3 areas of the painting and in the paint tube samples.



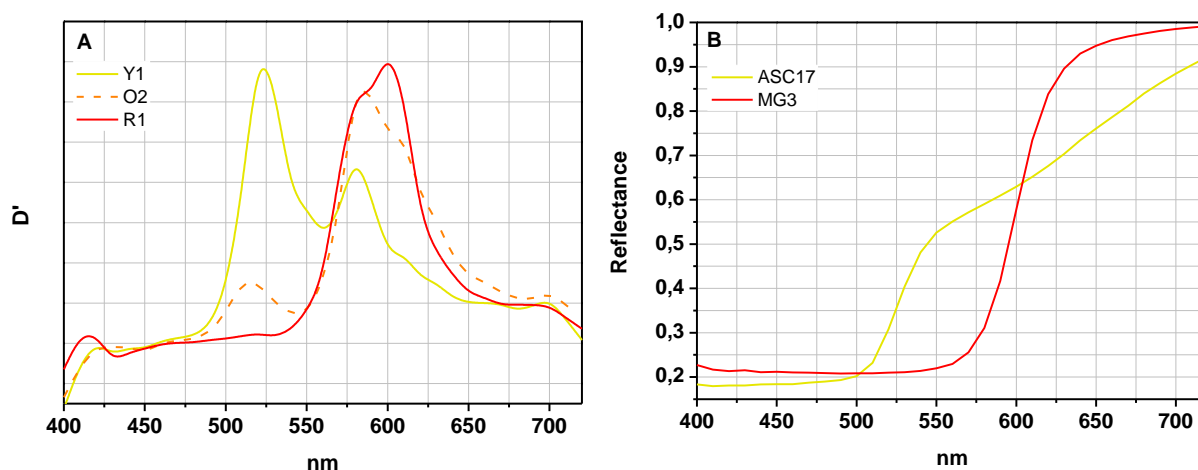


**Figure IV.4** **A** first derivative of the reflectance spectra from the painting Y1, R1, O1; **B** reflectance spectra acquired on the Amadeo's paint tubes Jaune de Chrome foncé – Lefranc (ASC17) and French Vermilion - Winsor & Newton (MG3).

**Table IV.2** Colorimetric values acquired on the yellow, orange and red areas of the painting *Mucha* and on the paint tube samples.

	Y1	O1	R1	ASC17	MG3
<b>L*</b>	59,03 ± 1,9	48,76 ± 0,58	39,6 ± 0,61	77,42 ± 4,73	71,38 ± 7,15
<b>a*</b>	21,16 ± 1,5	32,3 ± 2,1	44,63 ± 1,069	12,52 ± 4,32	49,64 ± 13,54
<b>b*</b>	64,4 ± 4,53	50,53 ± 0,4	35,03 ± 0,85	32,59 ± 12,14	30,28 ± 13,19

### Blue areas

The reflectance spectrum of B2 (Fig. IV.5A) show as maximum of reflectance a broad band centred around 477 nm with a shoulder at 510 nm. Associated to this reflectance band is visible an absorption band between 550-670 nm due to the overlaps of three bands at around 567, 606 and 667 nm. This spectrum is comparable with the spectrum of MG4 and ASC7 Cobalt ( $\text{CoAl}_2\text{O}_4$ ) and Cerulean blue ( $\text{CoO} \cdot n\text{SbnO}_2$ ) respectively (Fig. IV.5B). In the case of Cobalt blue (MG4) the three absorption bands between 550 and 670 nm are less visible comparing with the cerulean blue due to the dark tone of the sample. The absorption bands in the visible region of the cobalt based pigments is related to the crystal field transition between the orbital  $d-d$  of Co(II) ion [Boselli 2010]. The reflectance spectrum of cerulean blue shows spectral features similar to Cobalt blue, but its absorption bands are shifted at higher wavelengths of about 20 nm [Bacci *et al.* 2009]. The sample B1 (Fig. IV.5A) shows a reflectance band at 474 nm, associated with an absorption band centred at 620 nm. The spectrum shows a good correlation with the ultramarine spectra. Ultramarine blue ( $\text{Na}_8[\text{Al}_6\text{SiO}_6\text{O}_{24}]\text{S}_n$ ) spectrum is characterized by a strong absorption band centred at about 600 nm, which is caused by the charge transfer of the ion  $\text{S}_3$  and a maximum of reflectance at 475 nm [Boselli *et al.* 2011; Bacci *et al.* 2009]. Table IV.3 shows the  $L^*a^*b^*$  values acquired in the 3 areas of the paintings and in the paint tube samples.

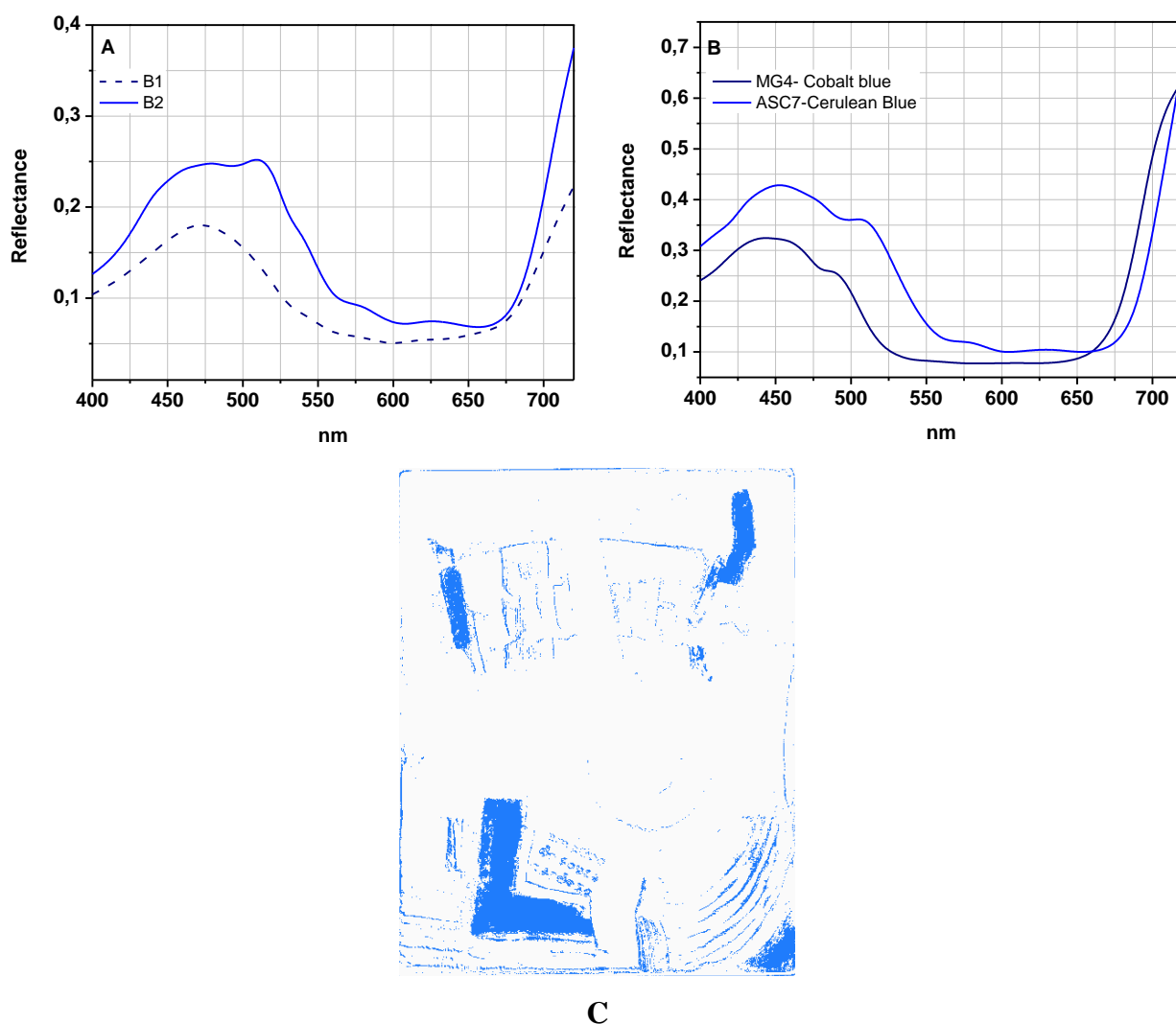


**Figure IV.5** **A** Reflectance spectra from the painting; **B** Reflectance spectra acquired from the paint tube samples of Amadeo Cobalt Blue - Winsor & Newton (MG4) and Cerulean Blue – Winsor & Newton (ACS7); **C** mapping of the area B2.

**Table. IV.3** Colorimetric values acquired on three blue areas of the painting *Mucha* and on the paint tube samples.

	B1	B2	B3	MG4 Cobalt blue	ASC7 Cerulean
<b>L*</b>	38,46 ± 0,65	45,16 ± 1,1	68,63 ± 1,61	53,68 ± 18,23	49,23 ± 4,85
<b>a*</b>	-7,13 ± 0,54	-15,46 ± 2,06	-18,9 ± 1,73	2,95 ± 3,7	-14,29 ± 0,04
<b>b*</b>	-15,86 ± 2,17	-16,06 ± 1,02	6,73 ± 1,61	-27,96 ± 11,73	-30,18 ± 1,1

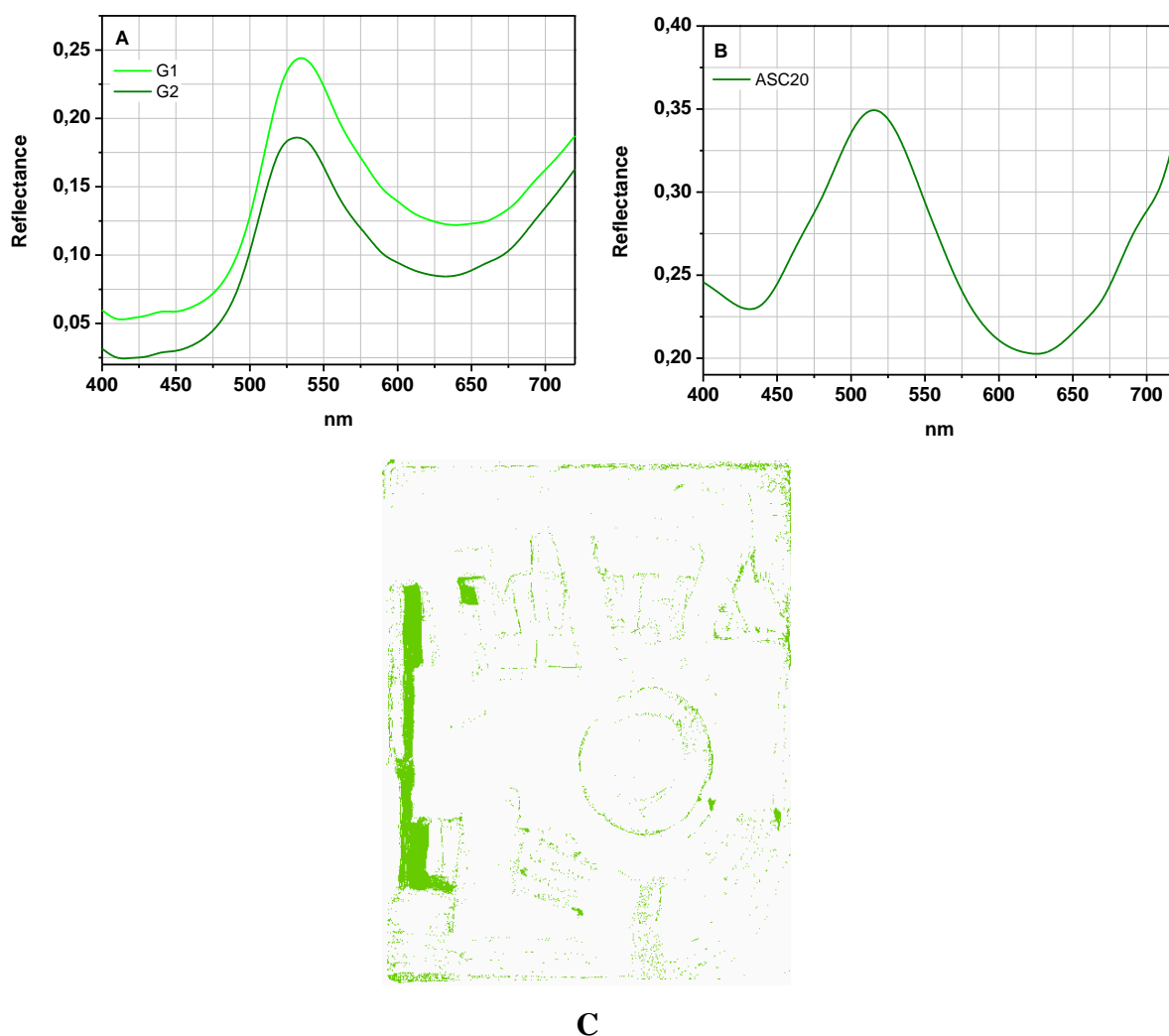
### Green areas

Figure IV.6 shows the comparison between the reflectance spectra in the points G1 and G2 from the painting and that acquired on the paint tubes sample ASC20. That tube is labelled as Vert Emerald but FTIR and Raman analysis confirmed the presence of viridian ( $\text{Cr}_2\text{O}_3 \cdot 2\text{H}_2\text{O}$ ). The maximum of reflectance of tube sample is 524 nm, with an absorption band centered on 630 nm. In the cases of *Mucha* points the maximum reflectance is shifted of about 20 nm comparing with the paint tube. Moreover the

absorption band in the region around 630 nm is less intense comparing with the viridian sample. The green tones in the painting are significantly more yellow (high  $b^*$ ) comparing with the tube sample (Table IV.4). The system developed proposed the presence of a mixture of viridian and chrome yellow, the hypothesis was confirmed by the analysis a cross-section collect in this area [Melo *et al.* 2009].

**Table IV.4** Colorimetric values acquired on two green areas of the painting *Mucha* and on the paint tube sample.

	G1	G2	ASC20
$L^*$	$49,3 \pm 1,5$	$43,26 \pm 0,2$	$49,37 \pm 14,69$
$a^*$	$-23,16 \pm 3,45$	$-26,33 \pm 2,13$	$-10,98 \pm 7,18$
$b^*$	$43,2 \pm 5,08$	$34,5 \pm 1,49$	$2,66 \pm 1,52$

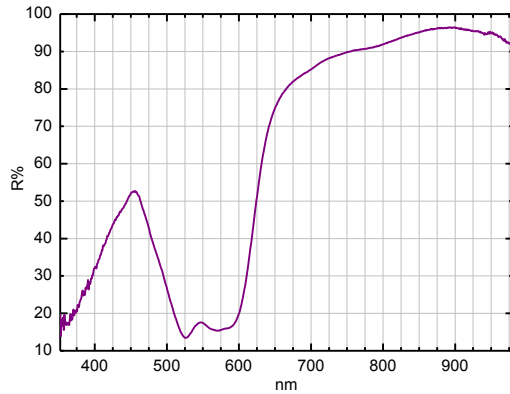


**Figure IV.6** A Reflectance spectra from the painting; B Reflectance spectrum acquired from the paint tube sample of Amadeo Vert Emerald – Lefranc (ASC20) C mapping of the area G1.

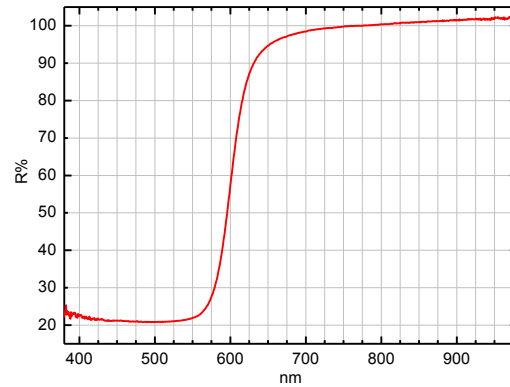
## Appendix V: Paint tubes samples database

This appendix present the reflectance spectra (collected by FORS) paint tube samples used to create the database of reference materials. The system use only the reflectance values between 400 and 720 nm.

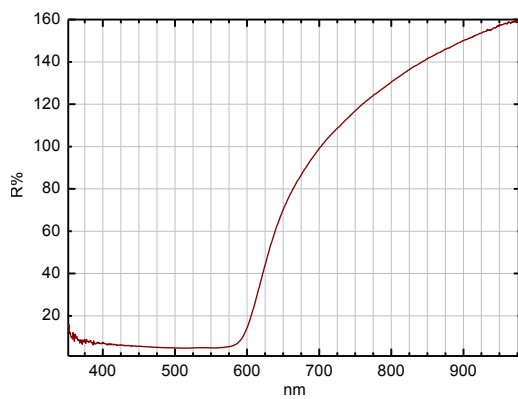
### Reflectance spectra



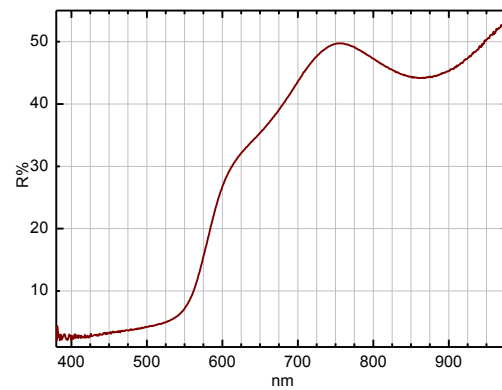
Cobalt violet, ASC13 - Lefranc



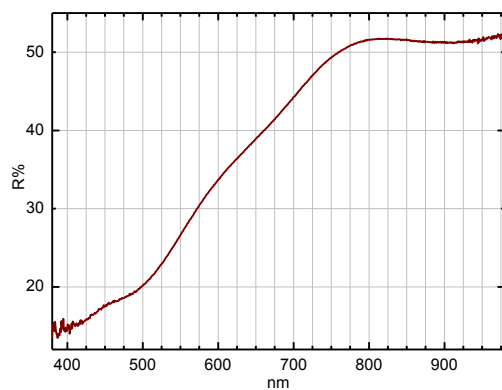
Vermillion, MG6 - Winsor & Newton



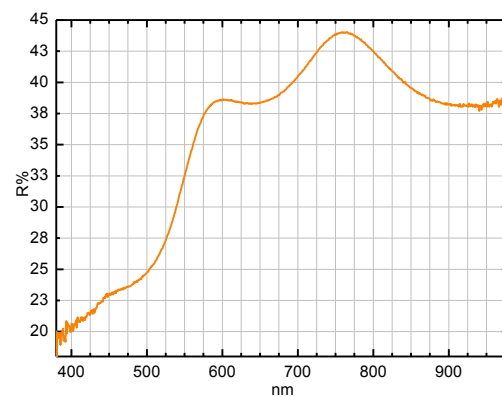
Carmine lake, ASC14 - Lefranc



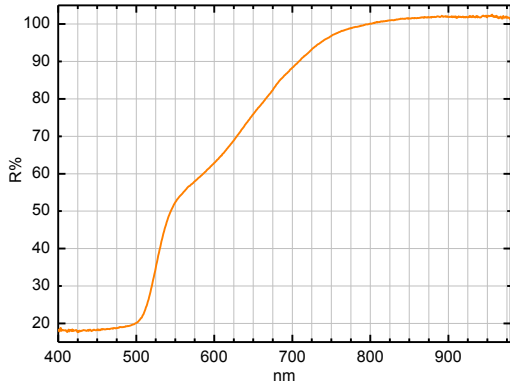
Terra rossa, MG18 - Rembrandt Oil Colors



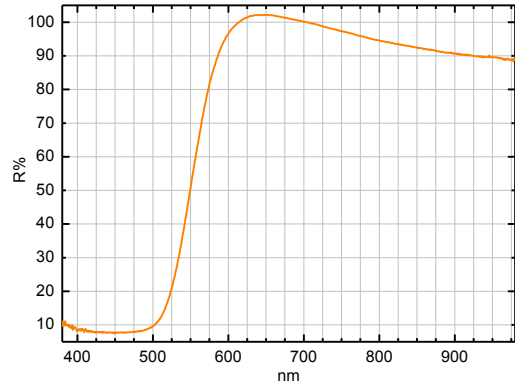
Raw Siena, MG7 - Winsor & Newton



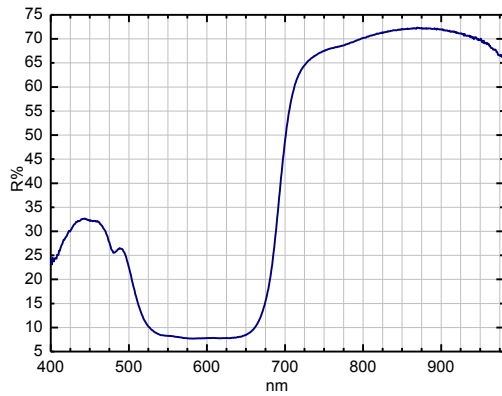
Ochre yellow, MG11 - Winsor & Newton



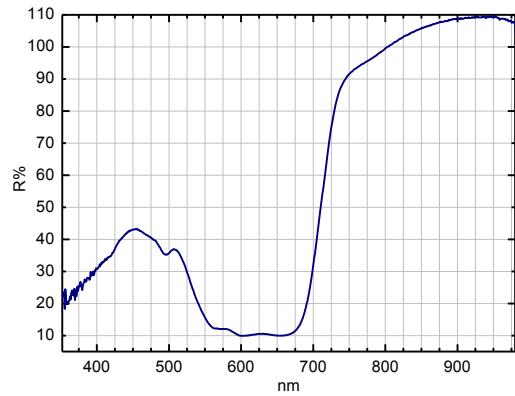
Chrome yellow, ASC17- Lefranc



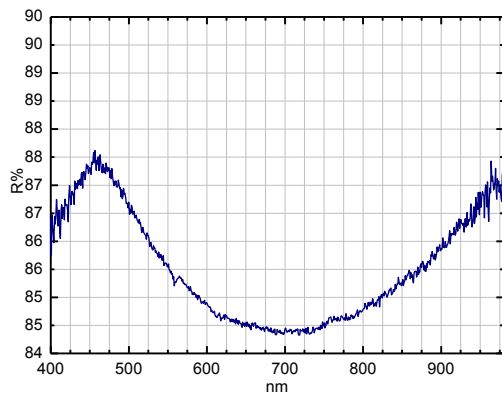
Cadmium orange, MG2 - Winsor & Newton



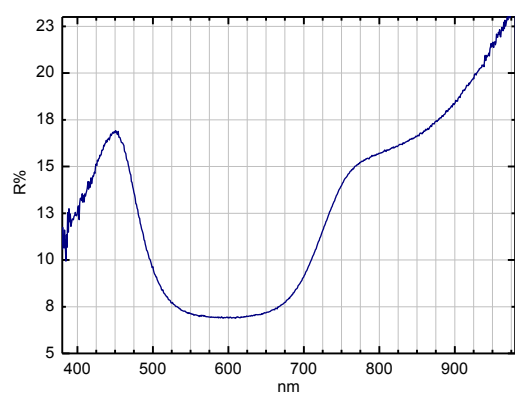
Cobalt blue, MG4 - Winsor & Newton



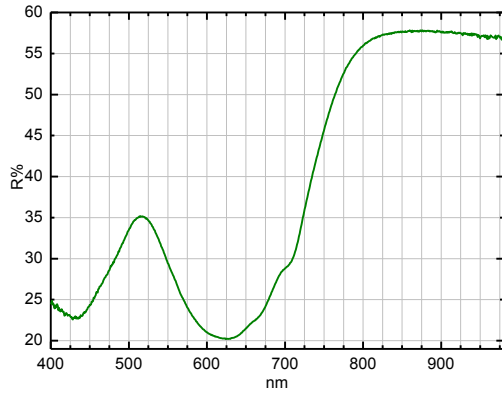
Cerulean blue, ASC7 - Winsor & Newton



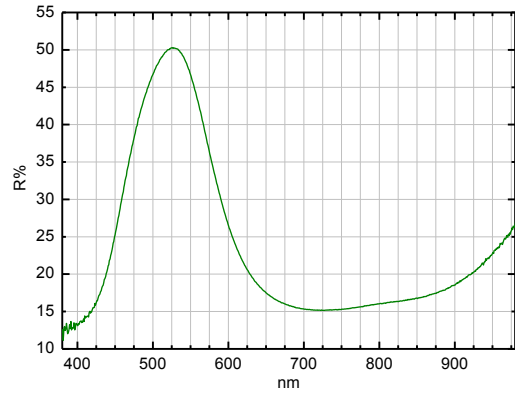
Prussian blue, ASC19 - Winsor & Newton



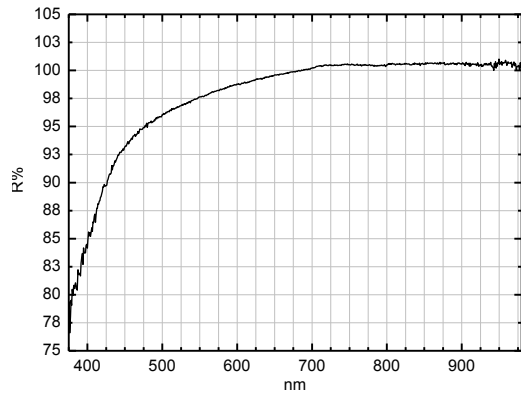
Ultramarine Blue, 21\_3130 - Winsor & Newton



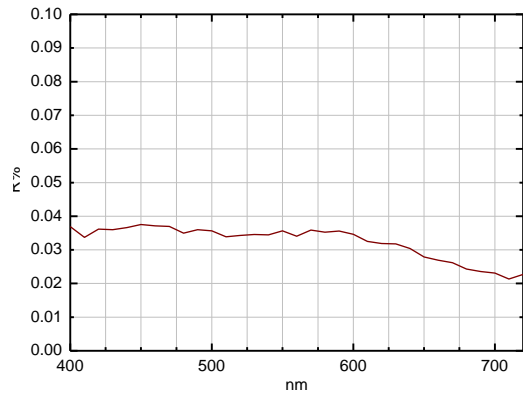
Viridian, ASC20 - Lefranc



Emerald green, 20\_3128 - Morin et Janet



Lead white, 10\_3130 - Paul Denis



Ivory Black, MG17- Winsor & Newton\*

**Figure V.** Reflectance spectra from the samples used to as reference materials in the hyperspectral imaging analysis. \*Spectra acquired by hyperspectral camera.

## **APPENDICES PART II**





## Appendix I: Paintings cited in the main text

This section presents the paintings cited in the main text but that are not shown in it.



**Figure I.1** Amadeo de Souza-Cardoso, *Canção popular a Russa e o Figaro*, 1916, 80 x 60 cm. Collection of Centro de Arte Moderna, Fundação Calouste Gulbenkian (Inv. 77P18) [Freitas et al. 2008, pg. 333].



**Figure I.2** Amadeo de Souza-Cardoso, *Trou de la serrure PARTO DA VIOLA Bon ménage Fraise avant garde*, 1916, 70 x 58 cm. Collection of Centro de Arte Moderna, Fundação Calouste Gulbenkian (Inv. 68P17) [Freitas et al. 2008, pg. 336].

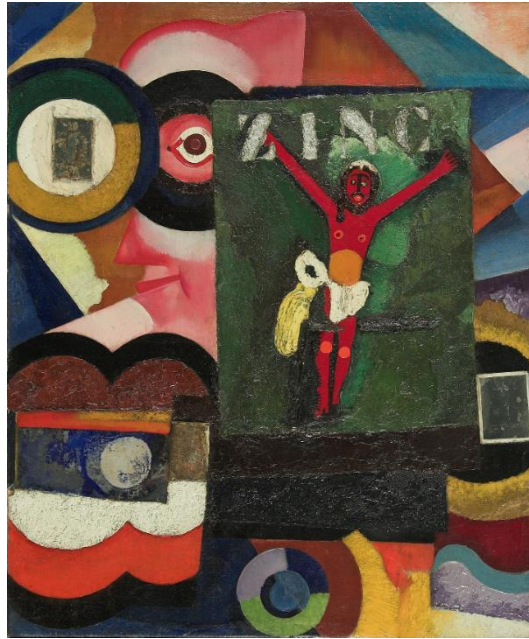


**Figure I.3.** Amadeo de Souza-Cardoso, *Untitled (ZINC)*, 1917, 59 x 49 cm. Private collection [Freitas *et al.* 2008, pg. 355].

## Appendix II: Experimental Section, Instrumentation

### *Digital X-ray image*

The digital radiography system used is *ArtXR*ay from NTB GmbH. X-ray Generator Y.MBS/160-F01 with directional beam type. Focal Spot size of 1,9 mm. The system works with a voltage of 40-160 kV and X-ray account of 0.2-5 mA. The digital camera has radiation sensibility range from 10 kV to 160 kV. A minimum of pixelsize of 0.083 mm and a resolution of 12 pixel / mm.

The condition of acquisition were 62kV; 2.2mA with an integration time of 100ms.

### *Infrared photography*

Infrared photograph acquired using *Sony DSC-F828* camera, infrared filter, *Hoya Filter*, Infrared (R72).

### *Stereo microscope*

Model *Leica MZ16* (7.1x to 115x), equipped with digital camera *Leica IC D* and a fiber optics system of illumination (*Leica KI 1500 LCD*).

### *Optical Microscope (OM)*

*Axioplan 2ie* Zeiss microscope equipped with transmitted and incident halogen light illuminator (tungsten light source, HAL 100); UV light (mercury light source, HBO 100 illuminator); and a digital Nikon camera *DXM1200F*, with *Nikon ACT-1* application program software, for microphotographs. Samples can be analysed with 10x ocular lenses and 5x/10x/20x/50x objective Epiplan lenses (giving total optical magnification of 50x, 100x, 200x, and 500x). For the incident and transmitted light the samples were analysed under crossed polars –polariser and analyser filters; for UV light the Zeiss filter set 05 [BP 395-440, FT 460, LP 470], with this filter the excitation is at 395-440 nm and the emission is from 470 nm onwards. The set 8 [G365; FT395; LP420] were also used, with this filter the excitation is at 365 nm and emission from 420 nm onwards. The scales for all objectives were calibrated within the *Nikon ACT-1* software. For all the images on this thesis, acquired with ultraviolet illumination, was used the filter set 8, otherwise the filter is reported in the caption of the figure.

### *μ-EDXRF*

X-Ray fluorescence spectra were obtained using an *ArtTAX* spectrometer from *Intax GmbH*. Operating with a molybdenum (Mo) X-ray tube, focusing polycapillary lens and silicon drift electro-thermally cooled detector and a *xFlash* (Si drift) detector, with 170 eV resolution. The accurate positioning system and polycapillary optics enable a small area of primary radiation ( $\varnothing \sim 70 \mu\text{m}$ ) at the sample. Elemental compositions were obtained from the average of three independent spots, analysed with a tube voltage of 40KV and a current intensity of 300 $\mu\text{A}$  and live time 200s.

### *$\mu$ -Raman*

Raman microscopy was carried out using a Labram 300 Jobin Yvon spectrometer, equipped with a HeNe laser 17mW operating at 632.8nm and a solid state laser operating at 532 nm. Spectra were recorded as an extended scan. The laser beam was focused with 50x and 100x Olympus objective lens. The laser power at the surface of the samples was varied with the aid of a set of neutral density filters (optical densities 0.3, 0.6 and 1).

### *$\mu$ -FTIR*

Infrared analyses were carried out with a Nicolet Nexus spectrophotometer coupled to a Continuum microscope (15x objective) with a MCT-A detector cooled by liquid nitrogen. Spectra were obtained in transmission mode, between 4000 and 650  $\text{cm}^{-1}$ , resolution of 8  $\text{cm}^{-1}$  and 256 scans. Samples were previously compressed using a Thermo diamond anvil compression cell. Spectra are shown here as acquired, without corrections or any further manipulations, except for the occasional removal of the CO<sub>2</sub> absorption at ~2300–2400  $\text{cm}^{-1}$ .

### *$\mu$ -SPEX*

Measurements were obtained with a microSPEX instrument using a setup where the Spex Fluorog apparatus 3-2.2 is connected to an Olympus BX51 M confocal microscope. Standard dichroic filters of 600 nm and 500 nm were used to collect the excitation and emission spectra, respectively. Excitation spectra (M) were performed collecting the signal at 610 nm and emission spectra (X) were acquired exciting at 490 nm. All spectra were acquired in a 30  $\mu\text{m}$  area, using a pinhole 8 with a 50x lens, and the following slits set: emission slits = 3 / 3 / 3 mm and excitation slits = 5 / 3 / 0.8 mm. In each micro-sample, at least six analyses were performed.

### *Fiber optical reflectance spectroscopy*

Reflectance spectra were acquired using an Ocean Optics equipment composed by a single-beam dispersive fibre optic spectrometer (model MAYA 200 PRO) equipped with 2048- linear silicon CCD array detector (Sony ILX511B). The MAYA 200 PRO has a spectral response from 200 nm to 1050 nm. The illumination is an Ocean Optics HL-200-HP with 20 Watt halogen light source in a single optical path covering the 360-2400 nm range. Spectra were obtained with integration time of 8 ms and 15 scans to average. The measuring head, in a 45°/45° (illumination/acquisition angles) configuration, gives a diameter of analysis of about 2 mm. As reference a Spectralon® standard was used.

### *Hyperspectral imaging*

The paintings and the paint samples were imaged from 400 to 720 nm in 10 nm intervals using a fast-tunable liquid-crystal filter (Varispec, model VS-VIS2-10-HC-35-SQ, Cambridge Research & Instrumentation, Inc., Massachusetts) and a low-noise Peltier-cooled digital camera (Hamamatsu, mod. C4742-95-12ER, Hamamatsu Photonics K. K., Japan), capable of a spatial resolution of 1344 x 1024

pixels and 12 bit output. The spectral reflectance of each pixel of each scene was estimated from a grey reference, presented at the scene at the time of acquisition after corrections for dark noise, spatial non-uniformities and stray light.

### *SEM-EDS*

SEM images were obtained using a FEI Quanta 400 FEG ESEM, which uses a Schottky emitter field emission gun, operating at low vacuum conditions and at 15 kV, equipped with an EDAX Genesis X4M detector. Images were acquired using secondary (SE) and backscattered (BSE) electron detectors.

### *Synchrotron Radiation $\mu$ -XRF and $\mu$ -XANES*

High resolution SR  $\mu$ -XRF maps (at 6.12 and 6.02 keV) were collected on the  $\mu$ -samples to identify the elemental composition of the samples. SR  $\mu$ -XANES analyses at the Cr K-edge were performed on selected areas of each paint sample.  $\mu$ -XANES spectra were acquired by scanning the primary energy around the Cr K-edge (5.96-6.09 keV). The energy calibration was performed using a metallic Cr foil.

### *Synchrotron Radiation $\mu$ -IR*

Infrared analyses were carry out with Nicolet Nexus spectrophotometer coupled to a Continuum microscope (15x objective) with a MCT-A detector cooled by liquid nitrogen. Spectra were obtained in transmission mode, between 4000–700  $\text{cm}^{-1}$ , resolution of 8  $\text{cm}^{-1}$  and 100 or 150 scans. The mapping was performed using step size of 10 nm with an aperture of the beam of 10 nm also. Only for the map of the sample BRUT am17 in BaF2 the aperture was reduced to 8 nm and step size to 6 nm.

## **Appendix III: Colorimetric analysis of Amadeo's paintings.**

This Appendix shows the colorimetric analysis performed on 24 paintings digitalized by hyperspectral imaging with high spectral and spatial resolution.

*This work was presented at 12th International AIC Congress, UK, 2013. C. Montagner, S. M.C. Nascimento, J. M.M. Linhares, M. J. Melo, M. Vilarigues and R. Macedo, "Assessing the power of colour in Amadeo's paintings".*

### **III.1 Materials and Method**

#### **Paintings**

Twenty four paintings belonging to Amadeo (Fig. III.1) were digitalized by hyperspectral imaging at the Center of Modern Art (CAM) of Calouste Gulbenkian Foundation in Lisbon. The paintings were chosen considering different period of the Amadeo's career, between 1911 and 1917. The code used to identified the paintings (P#) refer to the numeration used in the Catalogue Raisonné [Freitas *et al.* 2008] in which the paintings are presented in chronological order.

#### **Hyperspectral imaging technique**

The paintings and the paint samples were imaged from 400 to 720 nm in 10 nm intervals using a fast-tunable liquid-crystal filter (Varispec, model VS-VIS2-10-HC-35-SQ, Cambridge Research & Instrumentation, Inc., Massachusetts) and a low-noise Peltier-cooled digital camera (Hamamatsu, mod. C4742-95-12ER, Hamamatsu Photonics K. K., Japan), capable of a spatial resolution of 1344 × 1024 pixels and 12 bit output. The spectral reflectance of each pixel of each scene was estimated from a grey reference, presented at the scene at the time of acquisition after corrections for dark noise, spatial non-uniformities and stray light. The spectral radiance of each pixel of the paintings was estimated from the correspondent reflectance assuming the CIE D65 illuminant. The colorimetric properties of the paintings were analyzed in the CIELAB colour space. Also, the colorimetric analyses performed on the paintings were correlated with that performed on a set of 22 oil paint tube samples which belonged to Amadeo and which were digitalized using the same technique.





**Figure III.1.** The paintings of Amadeo de Souza-Cardoso from the collection of Center of Modern Art of Calouste Gulbenkian Foundation in Lisbon digitalized by hyperspectral imaging and used in this study. Images by courtesy of CAM [Freitas *et al.* 2008].

### III.2 Results and discussion

#### *Lightness*

Figure III.2 represents the lightness values for all paintings analysed. Results show that Amadeo's paintings have a lightness value uniformly distributed around the mean value  $L^* 50$  with a variation of about  $L^* \pm 15$ .

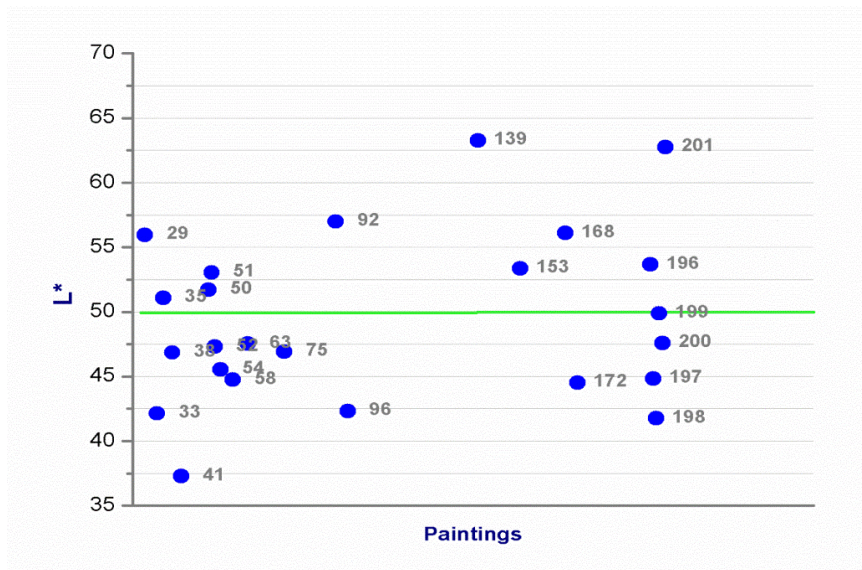


Figure III.2 Lightness distribution of Amadeo paintings.

*Correlation between artistic period and average colour*

Figure III.3 shows the average values of the Amadeo paintings in the CIE(a\*,b\*) representation. The 24 analysed paintings are set in the 2 upper quadrants of the colour space. The of the paintings have a a\* values between -5 and 5; this means that they cover an area equilibrated divided between red and green components. By correlating their colorimetric properties and the chronology of the artworks, it is possible to see that the group of paintings dated 1911-12 (indicated in red by the numbers 29-41) is characterised by lower a\* values, so more close to the green comparing with the others. Otherwise the paintings of the last period, 1917 (in orange) are characterized by higher a\* values, so more close to the red. The paintings dated 1913-14 (in blue) are set at high yellow component (b\* between 20 and 27). In general, a shift is evident from the green-yellow tone of the first period to a reddish tonality in the last period.

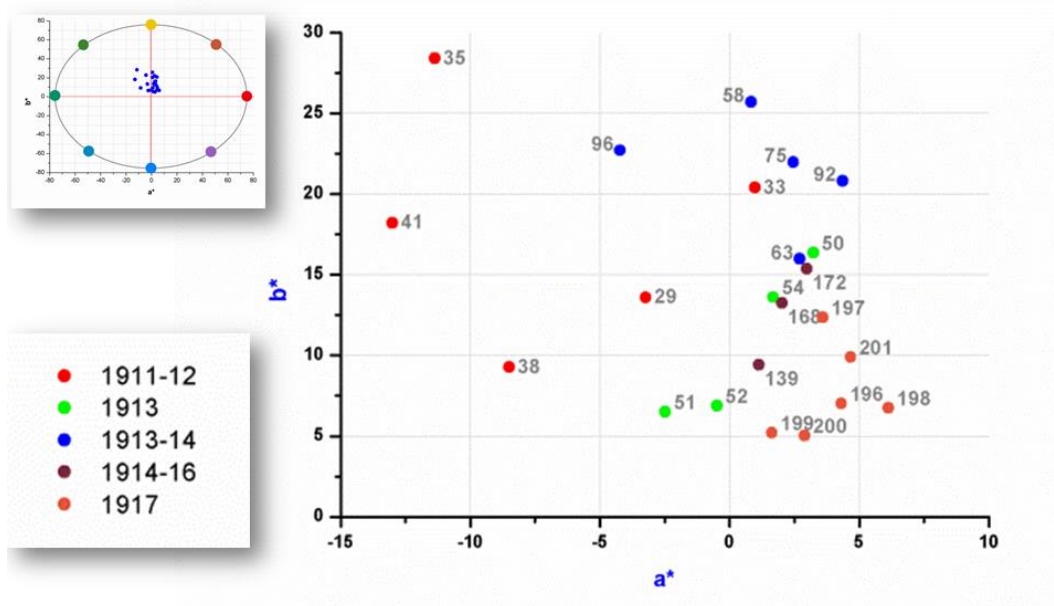


Figure III.3 Average CIE(a\*,b\*) value and chronologic distribution of the paintings.

### Numbers of discernible colours

Figure III.4 shows the number of discernible colours calculated for each analysed painting. Paintings are arranged by chronological order from P29 to P201. The number of discernible colours are estimated assuming the CIE 1931 standard observer by segmenting the CIELAB colour volume into unitary volumes; the just noticeable difference (JND) was assumed to be  $\Delta E=1$  in CIELAB.

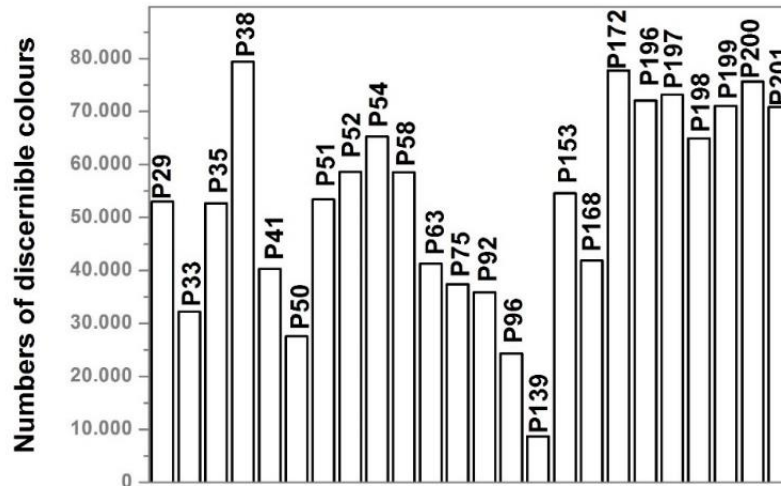


Figure III.4 Numbers of discernible colours. The code P# indicates the paintings in Figure III.1

It was found that Amadeo's paintings have about 8.700 to 80.000 discernible colours, with a mean value of 53.000. Observing the number of discernible colours it is possible to identify two subgroups: i) the paintings from P29 to P168 (dated between 1911 and 1916) displaying a random distribution of the number of discernible colours, and ii) the painting from P172 to P201 may be considered as a cluster with a mean value of 72.200. In the second subgroup are included artworks produced by Amadeo in 1917 (P196-P201), which are considered by art historians as a homogenous groups. These paintings show a similar number of discernible colours higher than the others paintings (with the exception of P38). In this second group it is also included the painting P172 *Mucha* dated 1915-16, produced during the artist's last creative period and therefore it may be related with his last works.

### Colour distribution

Using colour distribution analysis it is possible to visualize each pixel of the hyperspectral image using its colorimetric values. Considering the 24 paintings analysed we can identify two types of distributions; Figure III.5 reports one example for each type: (i) all the pixels occupy an elliptical area extended along the  $a^*$  axis, with values between -20 and 60 (Fig. III.5B). The pixels present contiguous values; this suggests the use that the colours were applied by a gradient that vary continuously, producing smooth colour transitions. (ii) The area occupied by the second type, represented by the painting P197 (Fig. III.5C) does not show a regular form, but an island like shape, where most of the shades are used pure without a colour gradient. The area of the colour gamut in this second type is larger compared to that of the first one, it is particular noticeable in the yellow tones. This distribution suggests the use of more saturated colours when compared with those observed in the first type. The second type of distribution was observed only for the paintings of the period 1916-1917.

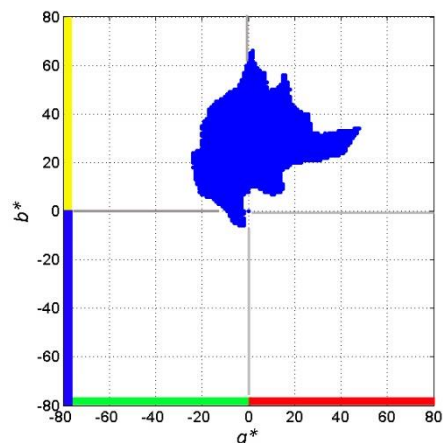


### III.3 Conclusions

The colorimetric analysis performed on 24 paintings of Amadeo disclosed that the colour analysis on the paintings of the last period (from P196 to 201) differ from the others concerning the numbers of discernible colours and their distribution. The distribution of colours calculated for each painting in the CIE( $a^*$   $b^*$ ) colour space revealed two characteristic shapes: one elliptic shape distributed along the CIE  $b^*$  axes; and a second one characterized by an island like shape, characterized by the presence of higher saturation colours. This second type of distribution is associated with the paintings of the Amadeo's last period (1917) where a larger number of discernible colours was also observed.



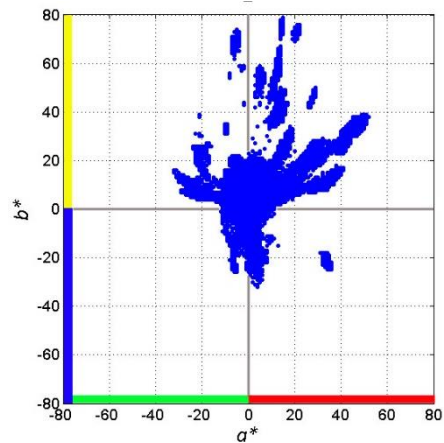
**A**



**B**



**C**



**D**

**Figure III.5** **A** Amadeo de Souza-Cardoso, *Untitled (O jockey)*, 1913, 61 x 50 cm (P58). Collection of Centro de Arte Moderna, Fundação Calouste Gulbenkian (Inv. 77P5) [Freitas *et al.* 2008, pg. 208] and **B** Colour distribution; **C** Amadeo de Souza-Cardoso, *Untitled*, 1917, 93,5 x 93,5 cm (P197). Collection of Centro de Arte Moderna, Fundação Calouste Gulbenkian (Inv. 77P8) [Freitas *et al.* 2008, pgs. 358] and **D** Colour distribution *Untitled*.

## Appendix IV: Area of analysis

### IV.1. BRUT

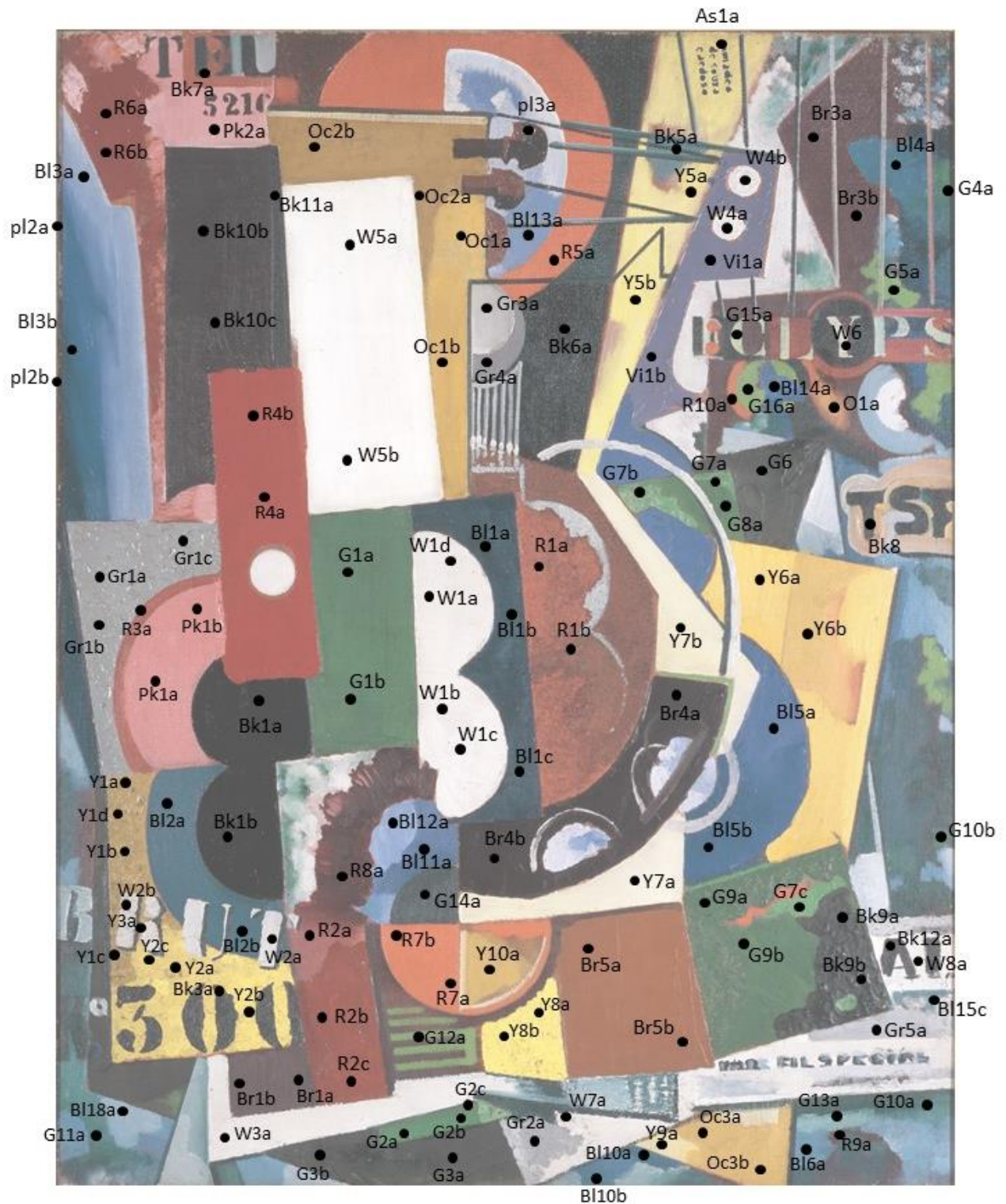


Figure IV.1 Painting *Untitled (BRUT 300 TSF)*, areas where EDXRF analysis was performed (●).





Figure IV.2 Painting *Untitled (BRUT 300 TSF)* samples for FTIR and Raman analysis (●).

IV.2 Entrada



Figure IV.3 Painting *Untitled (Entrada)*, areas where EDXRF analysis was performed (●).



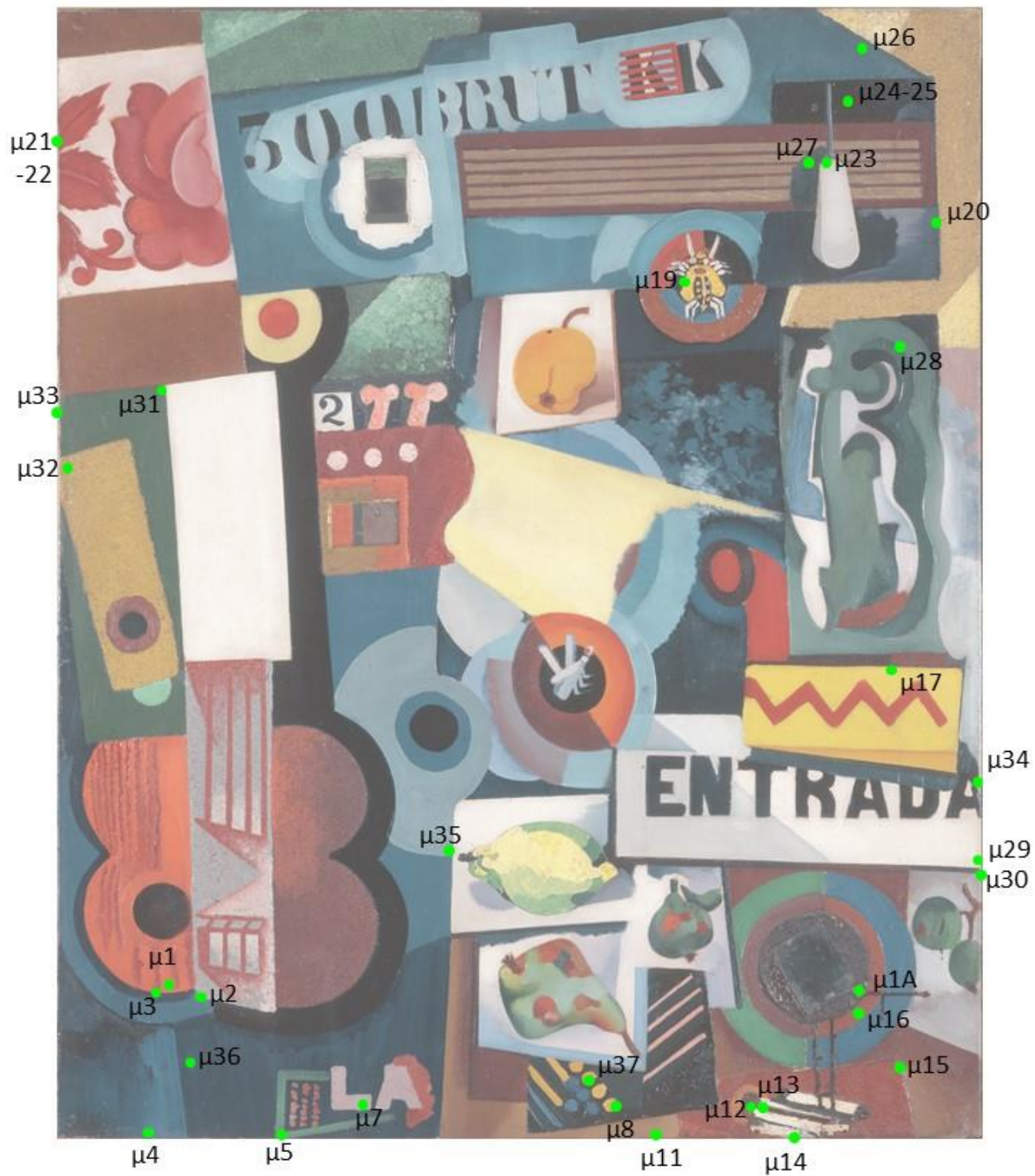


Figure IV.4 Painting *Untitled (Entrada)*, samples for FTIR and Raman analysis (●)







Figure IV.6 Painting *Untitled (Coty)*, samples for FTIR and Raman analysis (●).







Figure IV.8 Painting *Untitled*, samples for FTIR and Raman analysis (●)

## Appendix V: Representative spectra of *BRUT*, *entrada*, *Coty* and *Untitled*.

In this appendix are presented the representative spectra of  $\mu$ -EDXRF,  $\mu$ -FTIR,  $\mu$ -Raman,  $\mu$ -SPEX, reflectance spectra acquired by hyperspectral imaging acquired in the painting *BRUT*, *Entrada*, *Coty* and *Untitled* studied in the Part II, Chapter 2. SEM-EDS analysis will be presented in the Appendix VI and the characterization of chrome yellow samples in Appendix VII. To help the reader in the following tables (Tables V.1-4) are presented the samples analysed, divided for colour and analytical techniques used.

**Table V.1** Colour areas analysed on *BRUT* by  $\mu$ -EDXRF;  $\mu$ -FTIR;  $\mu$ -Raman;  $\mu$ -SPEX; Reflectance spectroscopy (hyperspectral imaging) and SEM-EDS.

Ref.	Colour	$\mu$ -EDXRF *	$\mu$ -FTIR	$\mu$ -Raman	$\mu$ -SPEX	Reflectance spectroscopy *	SEM-EDS
$\mu$ 1	red <i>imprimitura</i>	✓	✓	✓	-	-	-
	preparation	✓	✓	✓	-	-	-
$\mu$ 2	varnish	-	✓	-	-	-	-
$\mu$ 3	dark green	✓	✓	✓	-	✓	-
	yellow	✓	✓	✓	-	✓	✓
$\mu$ 4	white	✓	✓	✓	-	✓	✓
	yellow	✓	✓	✓	-	✓	✓
$\mu$ 5	dark green	✓	✓	✓	-	✓	✓
	white	✓	✓	✓	-	-	✓
$\mu$ 6	dark green	✓	✓	✓	-	✓	✓
$\mu$ 7	light green	✓	✓	✓	-	✓	-
$\mu$ 8	brown	✓	✓	✓	-	✓	-
$\mu$ 9	red	✓	✓	✓	-	✓	-
$\mu$ 10	blue	✓	-	✓	-	✓	-
	varnish	-	✓	-	-	-	-
$\mu$ 11	red	✓	✓	✓	✓	✓	-
$\mu$ 12	grey	✓	✓	✓	-	✓	✓
	red <i>imprimitura</i>	-	-	✓	-	-	✓
	preparation	-	-	✓	-	-	✓
$\mu$ 13	black	✓	✓	✓	-	✓	-
$\mu$ 14	red	✓	✓	n.s	✓	✓	-
$\mu$ 15	yellow	✓	✓	✓	-	-	-
$\mu$ 16	yellow	✓	✓	✓	-	✓	✓
	orange	-	✓	-	-	-	✓
$\mu$ 17	yellow	✓	✓	✓	-	✓	-
$\mu$ 18	blue	-	✓	✓	-	✓	-
$\mu$ 19	violet	✓	✓	✓	✓	✓	✓
$\mu$ 20	yellow	✓	✓	✓	-	✓	-
$\mu$ 21	yellow	✓	✓	✓	-	✓	-
$\mu$ 22	yellow	✓	✓	✓	-	✓	-
$\mu$ 23	yellow	✓	✓	✓	-	✓	-
$\mu$ 24	yellow	✓	✓	✓	-	✓	-
$\mu$ 25	white	✓	✓	✓	-	✓	-
$\mu$ 26	red	✓	✓	n.s	✓	✓	-
	blue	-	-	✓	-	-	-
$\mu$ 27	white	✓	✓	-	-	✓	-
	grey	✓	-	✓	-	✓	-

**Table V.1 (continued)**

μ28	red	✓	✓	✓	✓	✓	-
μ29	white	✓	✓	✓	-	✓	-
μ30	red	✓	✓	✓	✓	✓	-
μ31	red	✓	✓	n.s	-	✓	-
μ32	brown	-	✓	✓	-	✓	-
μ33	dark green	✓	-	-	-	✓	✓
μ34	dark green	✓	✓	✓	-	✓	✓
μRed1	red	✓	✓	✓	✓	✓	✓

\*Acquired on the painting surface; n.s. No signal

**Table V.2** Colour areas analysed on *Entrada* by μ-EDXRF; μ-FTIR; μ-Raman; μ-SPEX; Reflectance spectroscopy (hyperspectral imaging) and SEM-EDS.

Ref.	Colour	μ-EDXRF *	μ-FTIR	μ-Raman	μ-SPEX	Reflectance spectroscopy *	SEM-EDS
μ1	brown	✓	✓	✓	-	✓	✓
μ2	orange	✓	✓	✓	-	✓	-
μ3	dark blue	✓	✓	✓	-	-	-
μ4	blue	✓	✓	✓	-	✓	-
μ5	light green	✓	✓	✓	-	-	-
μ7	pink	✓	✓	✓	-	✓	-
μ8	yellow	✓	✓	✓	-	-	-
μ11	brown	✓	✓	✓	-	✓	-
μ12	brown	✓	✓	✓	-	-	-
μ14	white	-	✓	✓	-	✓	-
	green	-	✓	✓	-	-	-
μ15	red	✓	✓	✓	-	✓	-
	black	-	✓	✓	-	-	-
μ16	brown	✓	✓	✓	-	✓	-
μ17	yellow	✓	✓	✓	-	✓	✓
μ19	yellow	✓	✓	✓	-	✓	✓
μ20	violet	✓	✓	✓	n.s	✓	-
μ21	red	✓	✓	✓	n.s	✓	-
μ22	red	✓	✓	✓	n.s	✓	-
μ23	white	✓	✓	✓	-	✓	-
μ24	violet	✓	✓	✓	-	✓	-
μ25	violet	✓	✓	✓	-	✓	-
μ26	blue	✓	✓	-	-	✓	-
	yellow	-	✓	✓	-	✓	-
μ27	green	✓	✓	✓	-	✓	-
μ28	blue	✓	✓	✓	-	✓	-
μ29	white	✓	✓	✓	-	✓	-
μ30	preparation	✓	✓	✓	-	-	-
	brown	✓	✓	✓	-	-	-
μ31	white	✓	✓	✓	-	-	-
	green	✓	✓	✓	-	-	-
μ32	yellow	✓	✓	✓	-	✓	✓
μ33	preparation	✓	✓	✓	-	✓	✓
μ34	dark blue	✓	✓	✓	-	✓	-
μ35	light blue	✓	✓	-	-	✓	-
μ36	dark blue	✓	✓	✓	-	✓	-
μ37	yellow	✓	✓	✓	-	-	✓

\*Acquired on the painting surface; n.s. No signal



**Table V.3** Colour areas analysed on *Coty* by  $\mu$ -EDXRF;  $\mu$ -FTIR;  $\mu$ -Raman;  $\mu$ -SPEX; Reflectance spectroscopy (hyperspectral imaging) and SEM-EDS.

Ref.	Colour	$\mu$ -XEDRF *	$\mu$ -FTIR	$\mu$ -Raman	$\mu$ -SPEX	Reflectance spectroscopy *	SEM-EDS
$\mu$ 1	brown	-	✓	✓	-	✓	-
	preparation	✓	-	-	-	✓	✓
	varnish	-	✓	-	-	-	-
$\mu$ 2	red	✓	✓	✓	-	✓	-
$\mu$ 3	yellow	✓	✓	✓	-	✓	✓
$\mu$ 4	yellow	✓	✓	✓	-	✓	-
$\mu$ 5	yellow	✓	✓	✓	-	✓	-
	brown	✓	-	✓	-	-	-
$\mu$ 6	red	✓	✓	n.s.	n.s.	✓	✓
	preparation	-	-	✓	-	-	✓
$\mu$ 7	red	✓	✓	✓	-	✓	-
$\mu$ 8	brown	✓	✓	✓	-	✓	-
	transparent sphere	-	-	✓	-	-	✓
$\mu$ 9	glue	-	✓	-	-	-	-
$\mu$ 10	white	✓	✓	-	-	-	-
$\mu$ 11	golden	-	-	n.s.	-	-	✓
$\mu$ 12	dark blue	✓	✓	✓	-	✓	-
$\mu$ 13	violet	✓	✓	✓	-	✓	-
$\mu$ 14	green	✓	✓	✓	-	✓	-
$\mu$ 15	violet	✓	✓	✓	-	✓	-

\*Acquired on the painting surface; n.s. No signal

**Table V.4** Colour areas analysed on *Untitled* by  $\mu$ -EDXRF;  $\mu$ -FTIR;  $\mu$ -Raman;  $\mu$ -SPEX; Reflectance spectroscopy (hyperspectral imaging) and SEM-EDS.

Ref.	Colour	$\mu$ -EDXRF *	$\mu$ -FTIR	$\mu$ -Raman	$\mu$ -SPEX	Reflectance spectroscopy *	SEM-EDS
$\mu$ 1	yellow	✓	✓	✓	-	✓	✓
	blue	-	✓	✓	-	-	✓
	preparation	-	-	✓	-	-	✓
$\mu$ 2	preparation	✓	✓	✓	-	-	-
$\mu$ 3	black	✓	✓	✓	-	-	-
$\mu$ 4	white	✓	✓	✓	-	✓	-
$\mu$ 5	green	✓	-	✓	-	✓	-
$\mu$ 6	light green	✓	-	✓	-	✓	✓
$\mu$ 7	white	✓	✓	✓	-	✓	-
$\mu$ 8	red	✓	✓	✓	-	-	-
$\mu$ 9	violet	✓	✓	✓	-	✓	-
$\mu$ 10	yellow	✓	✓	✓	-	✓	-
$\mu$ 11	matches	✓	-	✓	-	-	✓
$\mu$ 12-13	varnish	-	✓	-	-	-	-
$\mu$ 14	white	✓	✓	✓	-	-	-
$\mu$ 15	golden	✓	-	-	-	-	-
$\mu$ 16	Transparent sphere	-	✓	✓	-	-	-
$\mu$ 17	paper	-	✓	-	-	-	-
$\mu$ 18	fiber of the matches	-	✓	-	-	-	-
$\mu$ 19	green	✓	✓	✓	-	✓	-
	yellow	✓	✓	✓	-	-	-

\*Acquired on the painting surface. n.s. No signal

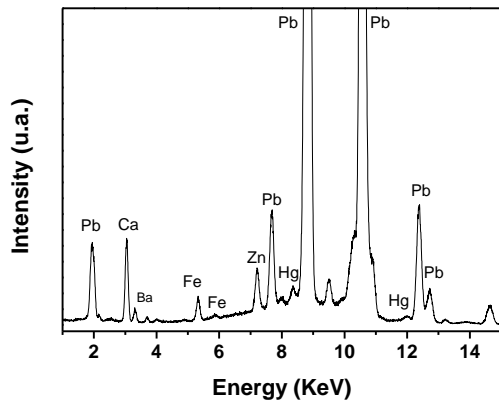
**Table V.4 (continued)**

Ref.	Colour	μ-EDXRF *	μ-FTIR	μ-Raman	μ-SPEX	Reflectance spectroscopy *	SEM-EDS
μ20	white	✓	✓	✓	-	✓	-
	red	-	-	✓	-	-	-
μ21	pink	✓	✓	✓	✓	-	-
μ22-23	varnish	-	✓	-	-	-	-
μ24-25	pink	✓	✓	✓	-	✓	✓
	preparation	-	✓	✓	-	-	-
μ26	black	✓	✓	✓	-	-	-
μ27	yellow	✓	✓	✓	-	✓	-
μ28	red	✓	✓	n.s	✓	-	-
μ29	yellow	✓	✓	✓	-	✓	-
μ30	yellow	✓	✓	✓	-	-	-
μ31	light green	✓	✓	n.s	-	✓	-
μ32	dark blue	✓	✓	✓	-	-	-
μ33	yellow	✓	✓	✓	-	✓	-
μ34	yellow	✓	✓	✓	-	✓	-
μ35	violet	✓	✓	✓	-	✓	-
μ36	blue	✓	✓	n.s	-	✓	-
μ37	yellow	✓	✓	✓	-	✓	-
μ38	orange	✓	✓	✓	-	-	-
μ39	yellow	✓	✓	✓	-	✓	-
μ40	yellow	-	✓	✓	-	✓	-
μ41	light green	✓	✓	✓	-	-	-
μ42	orange	✓	✓	✓	-	-	-
μ43	white	✓	✓	✓	-	✓	-
μ44	black	✓	✓	✓	-	-	-

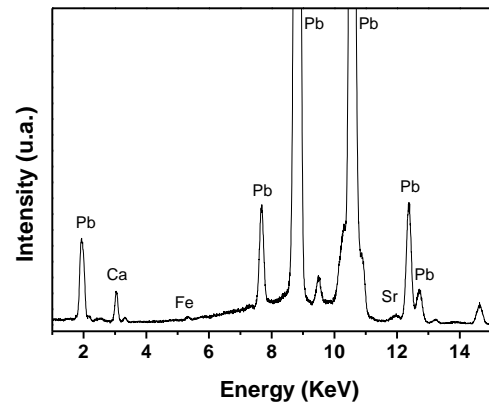
\*Acquired on the painting surface. n.s. No signal

## V.1 $\mu$ -EDXRF

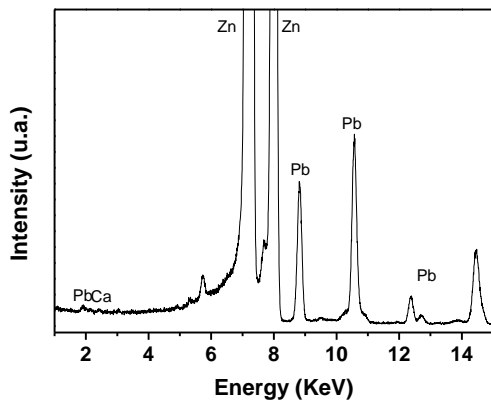
### Representative $\mu$ -EDXRF spectra from *BRUT* painting



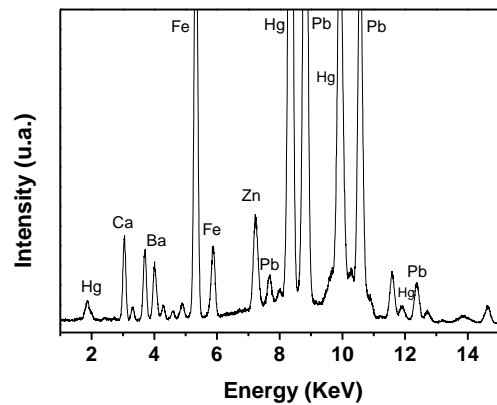
*Preparation layer (Pl1a)*



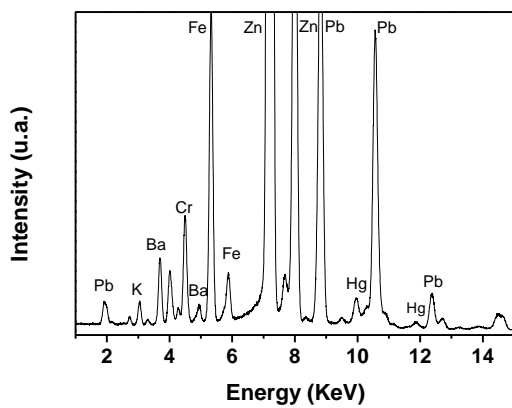
*White (Wh1a)*



*White (Wh1b)*

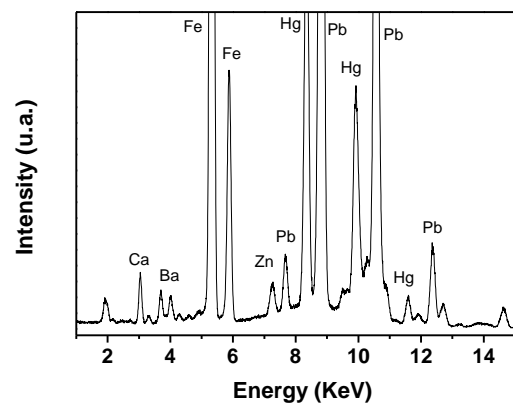


*Black (Bk1a)*

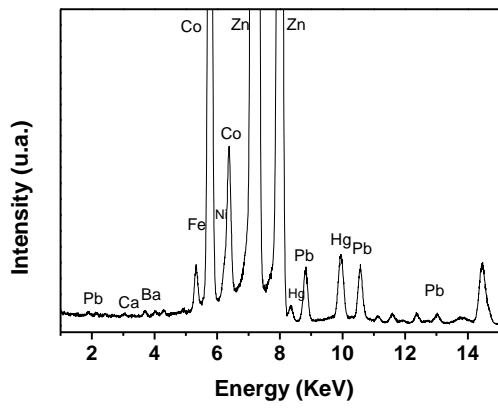


*Black (Bk7a)*

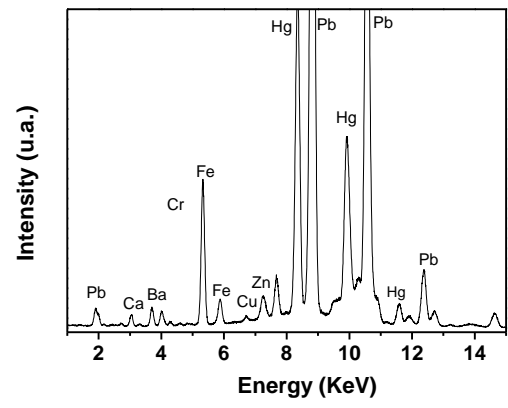
Ba



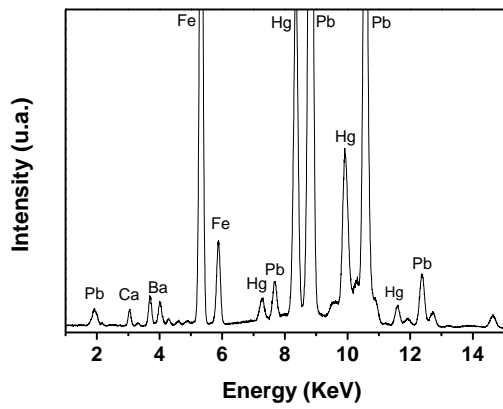
*Black (Bk10b)*



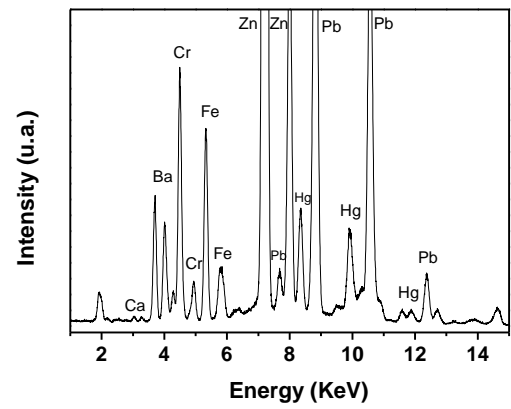
Violet (Vi1a)



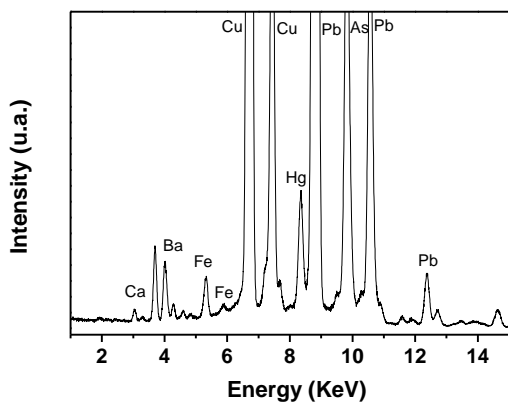
Blue (Bl1a)



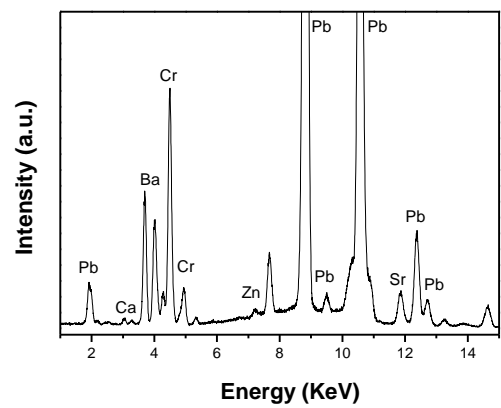
Blue (Bl2a)



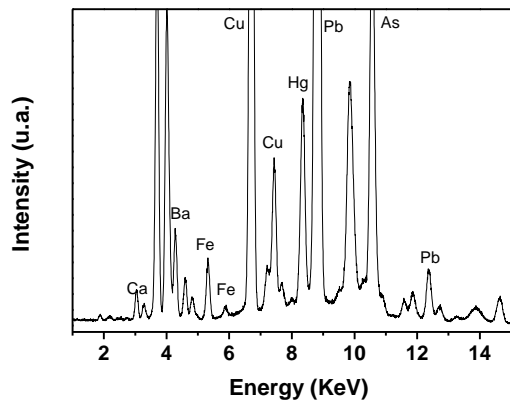
Green (G5a)



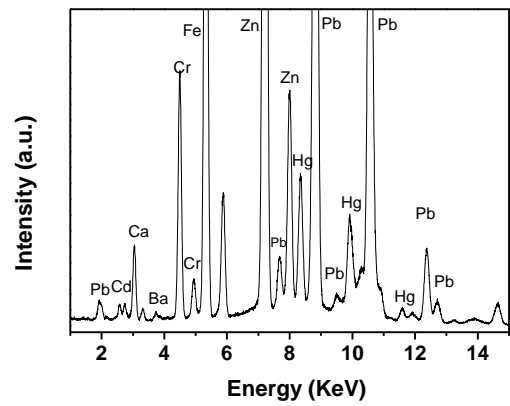
Green (G9a)



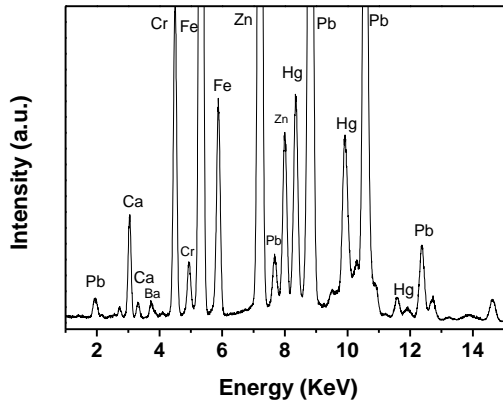
Yellow (Y2a)



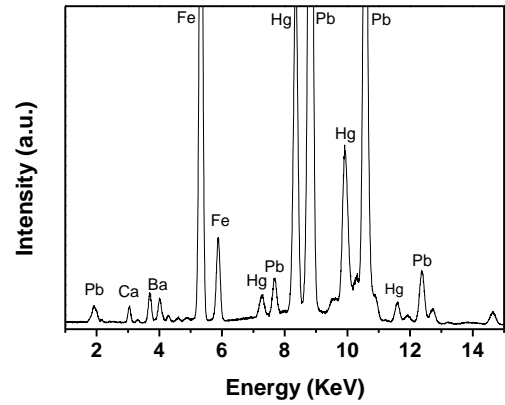
Dark green (Bk9a)



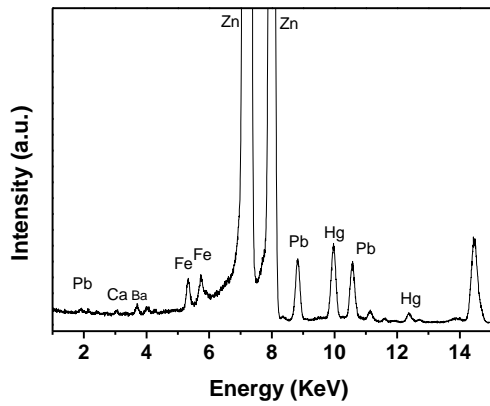
Yellow (Y6b)



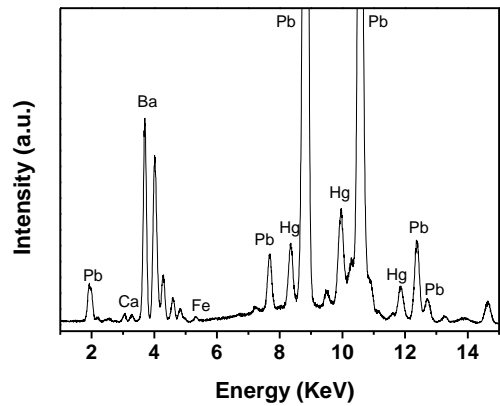
Ochre (Oc3a)



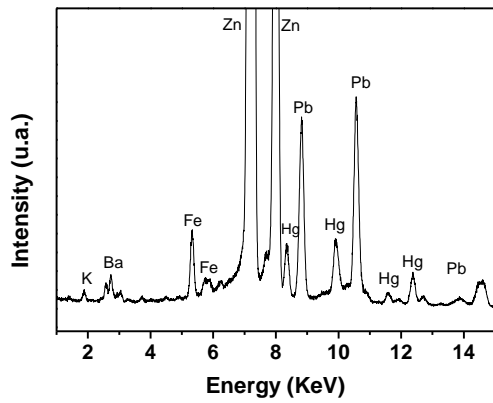
Brown (Br2a)



Pink (Pk1b)



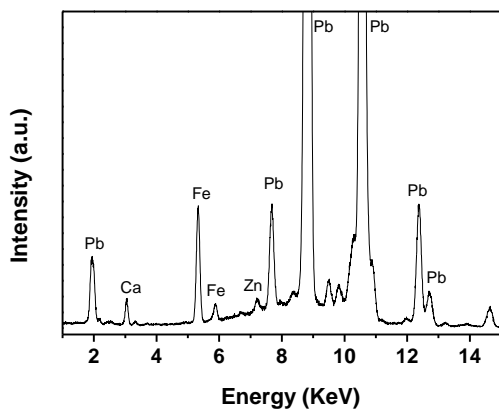
Red (R4a)



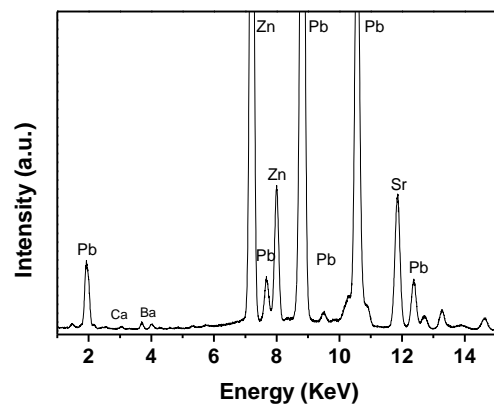
Signature (As1a)

**Figure V.1** Representative  $\mu$ -EDXRF spectra of preparation layer and white, black, violet, blue, green, yellow, ochre, brown, pink, red areas from *BRUT* painting.

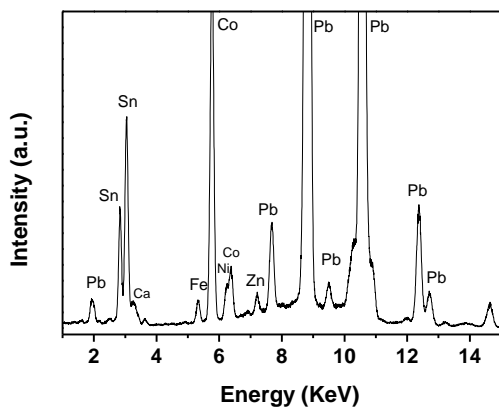
**Representative  $\mu$ -EDXRF from *Entrada* painting.**



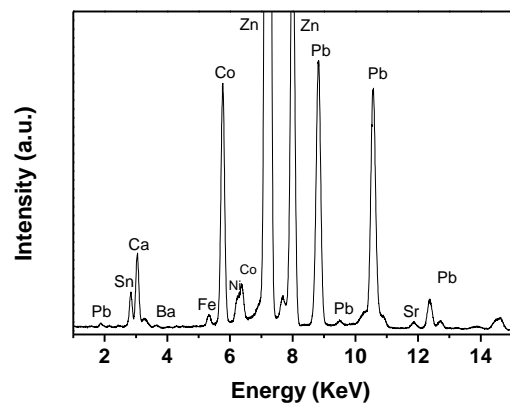
Preparation (PI1a)



White (Wh1b)

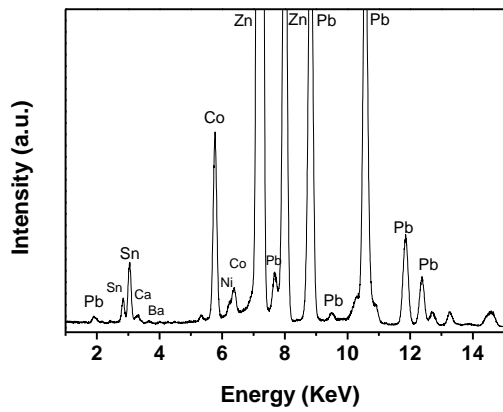


Black(Bk1a)

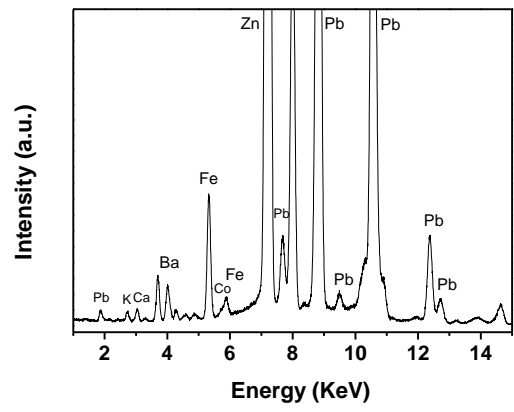


Violet (Vi1b)

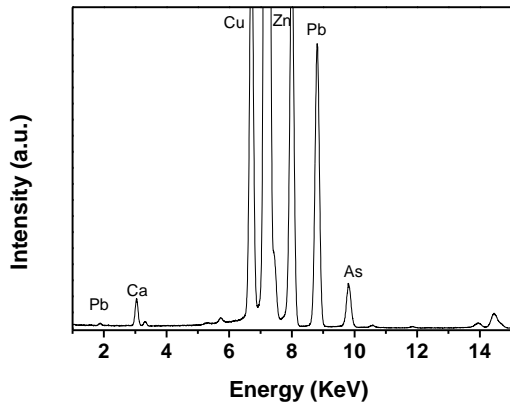




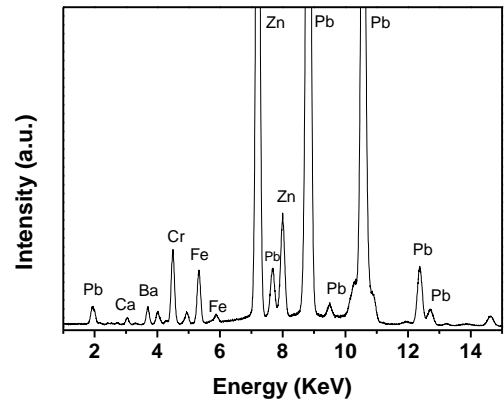
Blue (B11a)



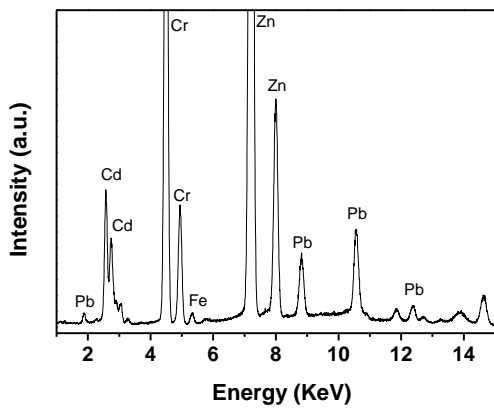
Blue (B11b)



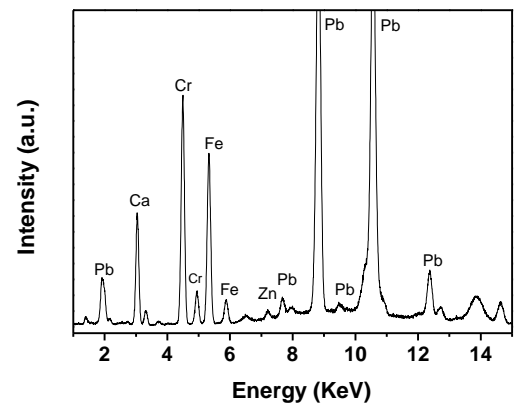
Green (Gr1a)



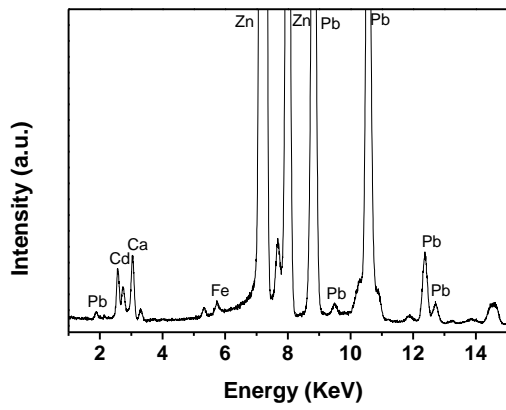
Green (Gr3b)



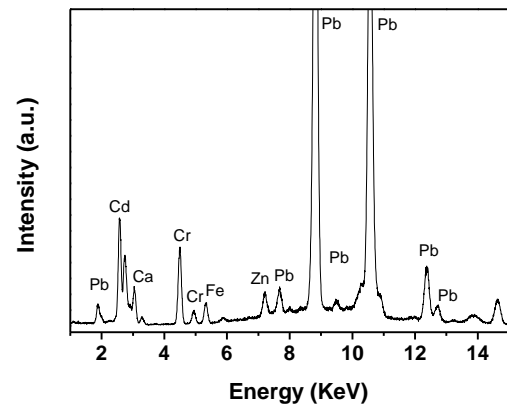
Green (Gr6b)



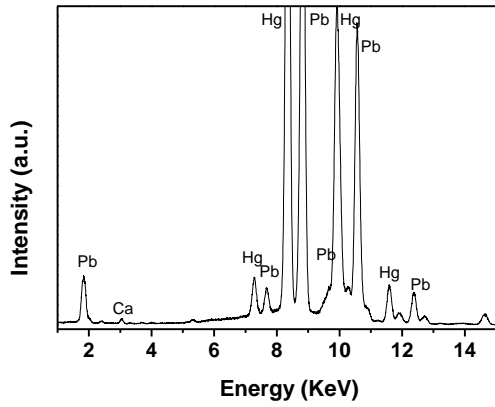
Yellow (Y2a)



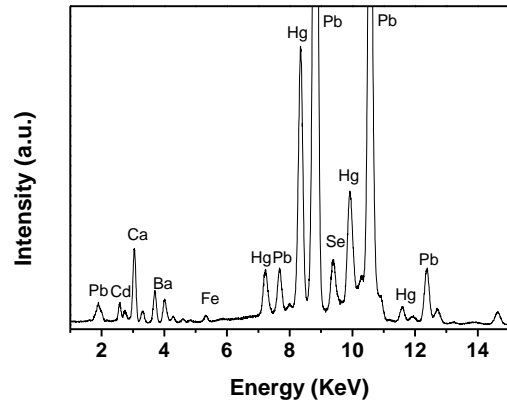
Yellow (Y8a)



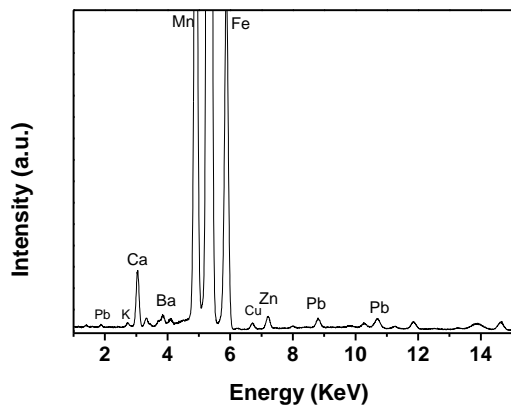
Yellow (Y13b)



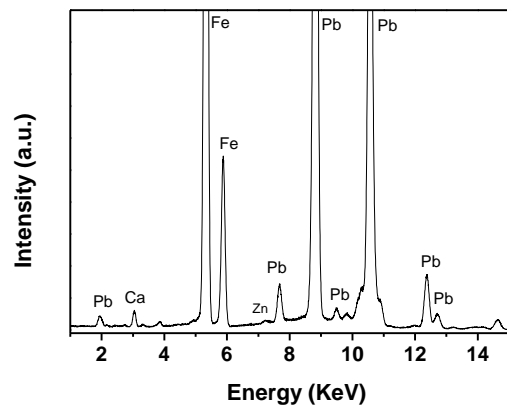
Orange (O2a)



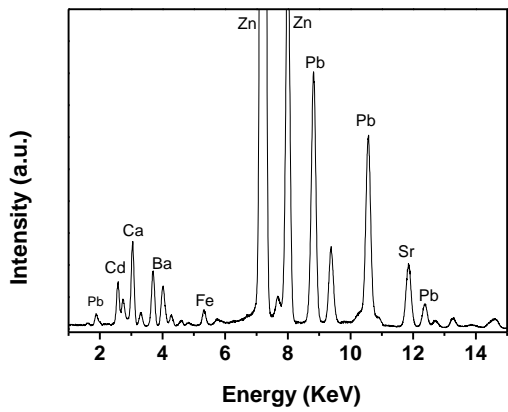
Orange (O2d)



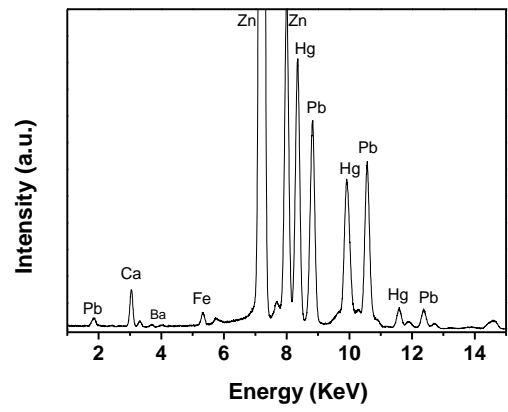
Brown (Br1a)



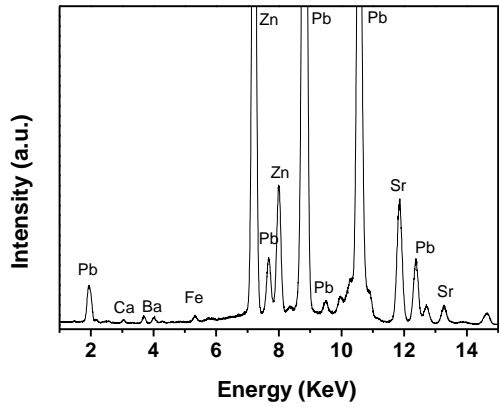
Brown (Br3a)



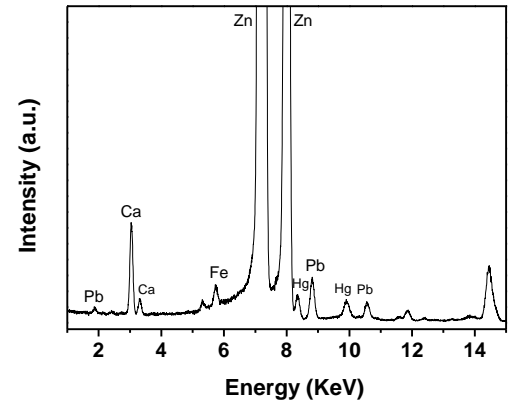
Red (R2a)



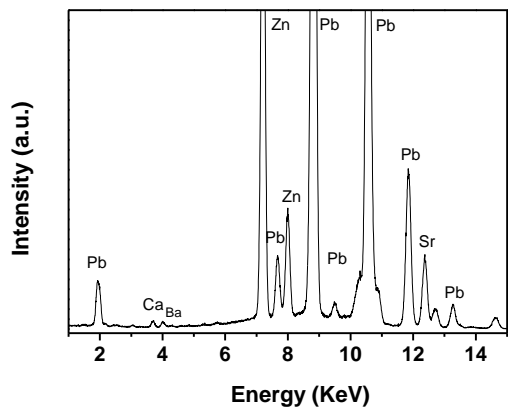
Red (R6b)



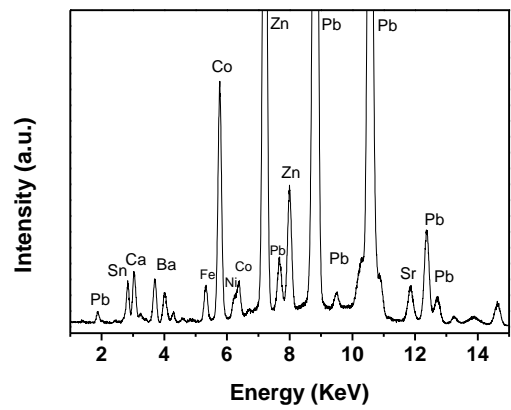
Signature (Sg1b)



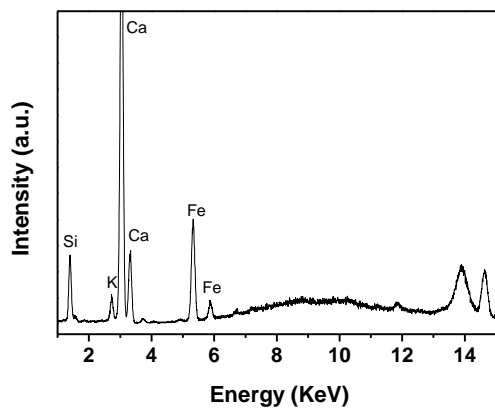
Pink (Pk1a)



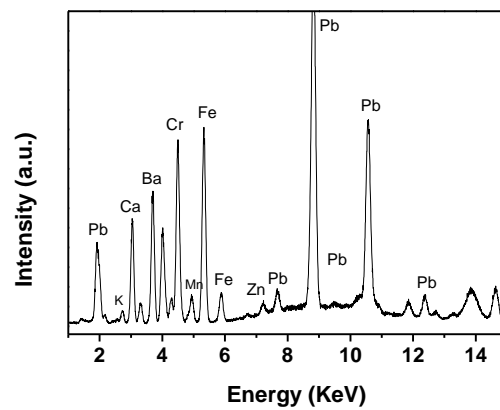
White paint number "2" (Ltw1a)



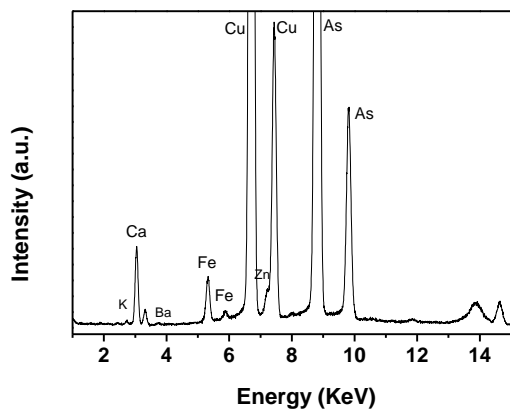
Blue paint number "2" (Ltl1a)



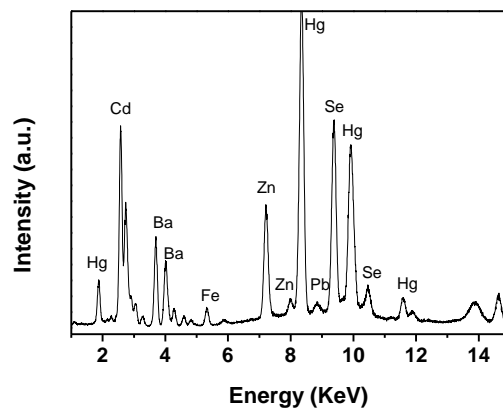
Glass (G11a)



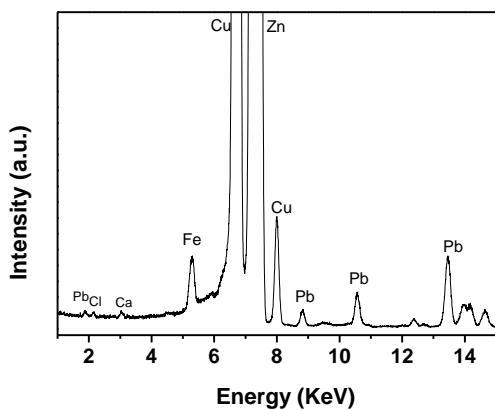
Mirror #1 (G1G1a)



Green paint on glass #3 (GIG3a)



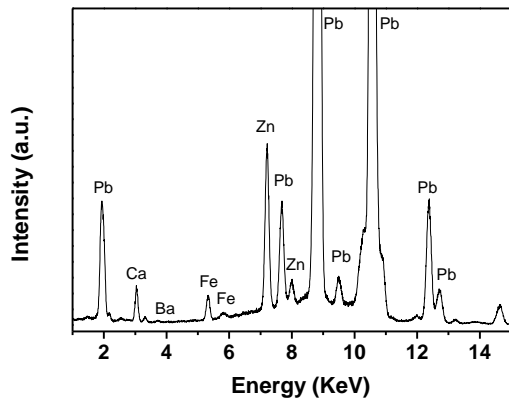
Red paint on glass #1 (GIR1a)



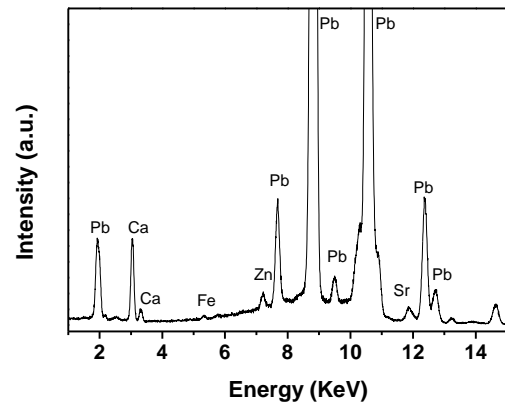
Golden (Gd1a)

**Figure V.2** Representative  $\mu$ -EDXRF spectra of preparation layer and white, black, violet, blue, green, yellow, orange, brown, pink, red, glass, mirror, golden areas from *Entrada* painting.

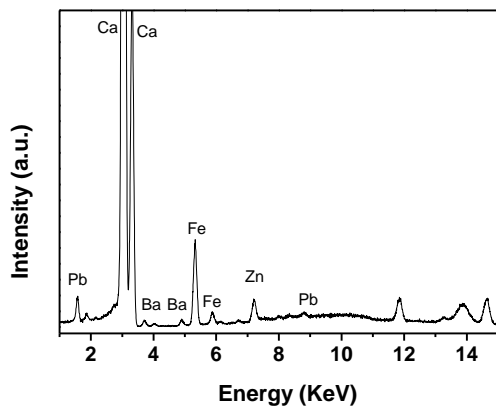
Representative  $\mu$ -EDXRF from Coty painting.



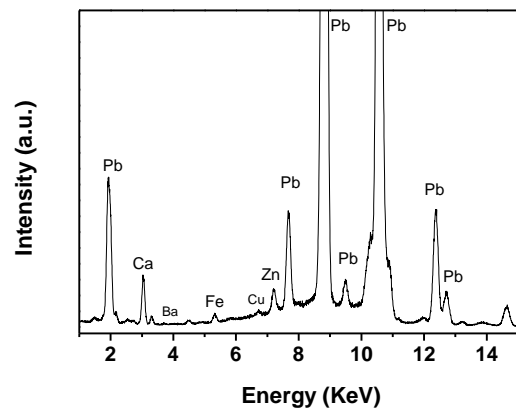
Preparation (P11a)



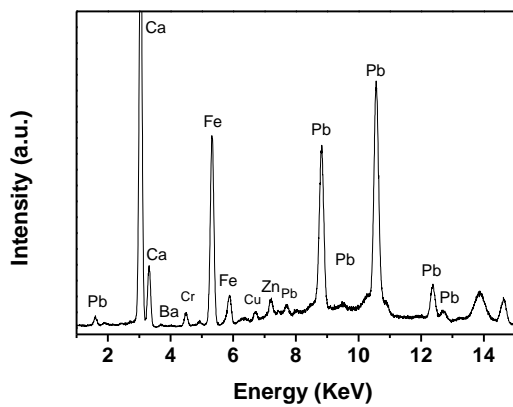
White (Wh2a)



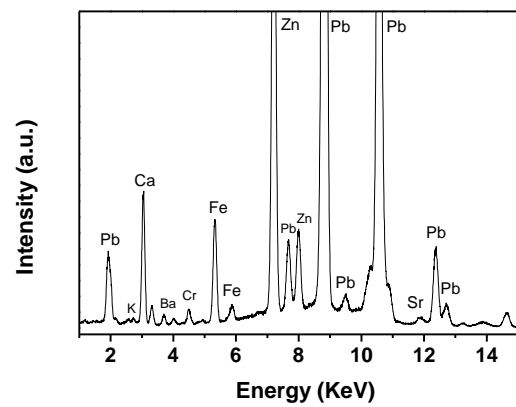
White (Wh8a)



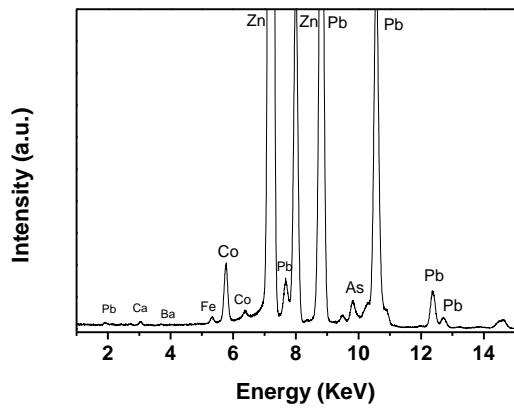
White "COTY" (Wh7a)



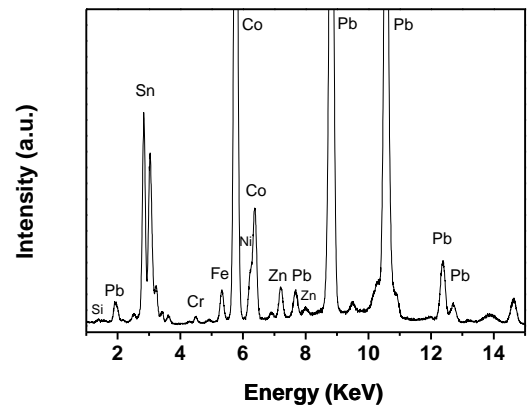
Black (Bk2a)



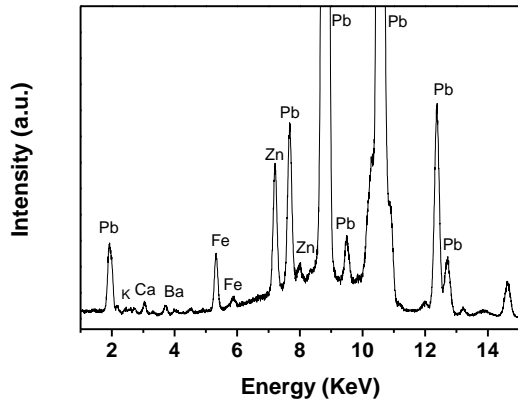
Grey (Grey1a)



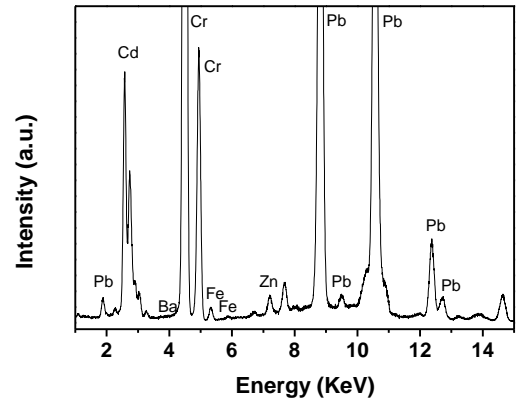
Violet (Vi3b)



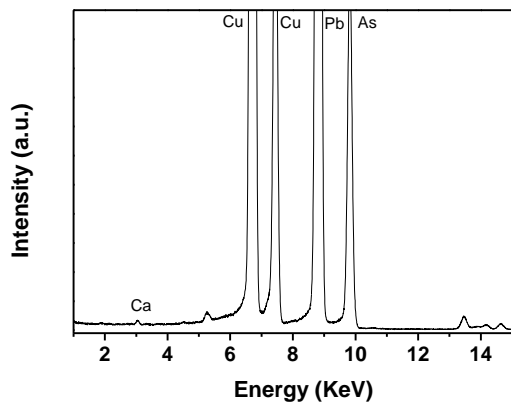
Blue (Bl1a)



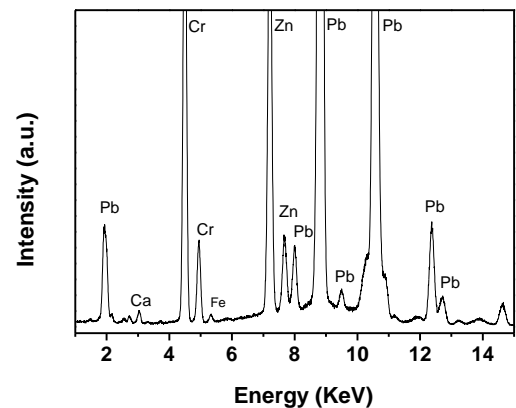
Blue (Bl8a)



Green (Gr2a)

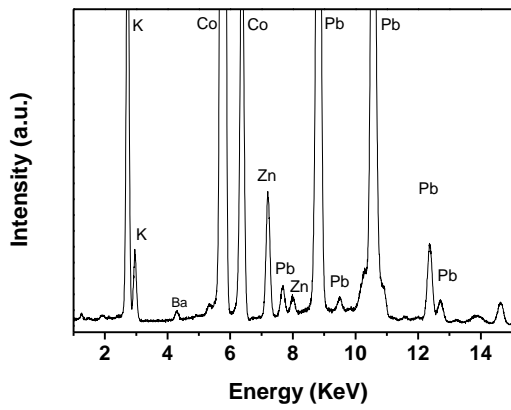


Green (Gr11a)

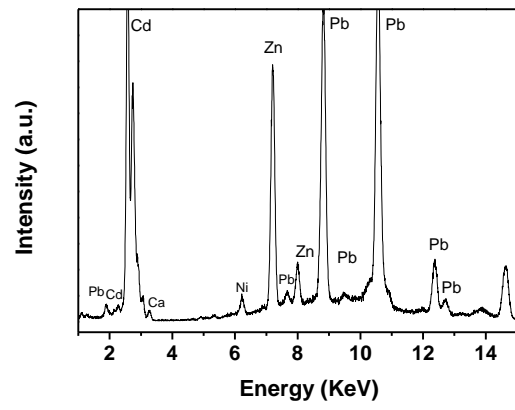


Yellow (Y4a)

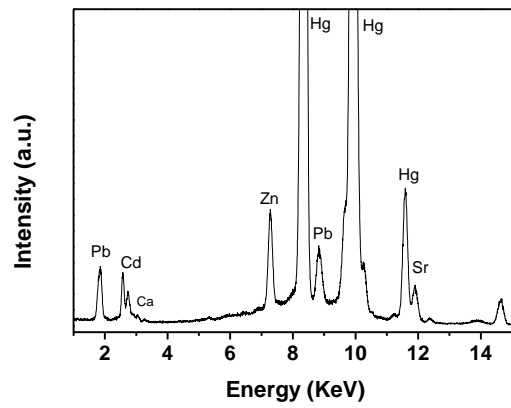




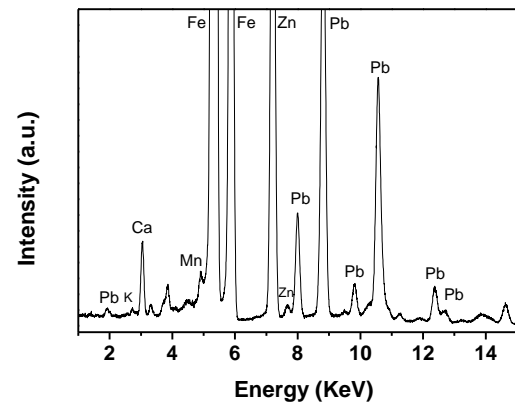
*Yellow (Y15a)*



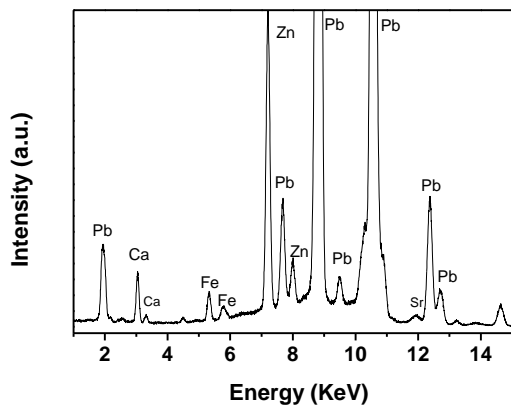
*Yellow (Y16a)*



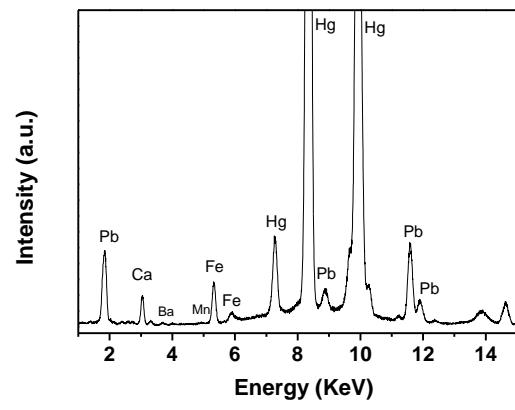
*Orange (O2a)*



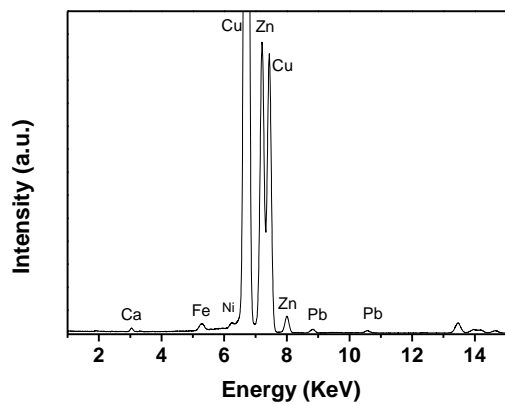
*Brown (Br9a)*



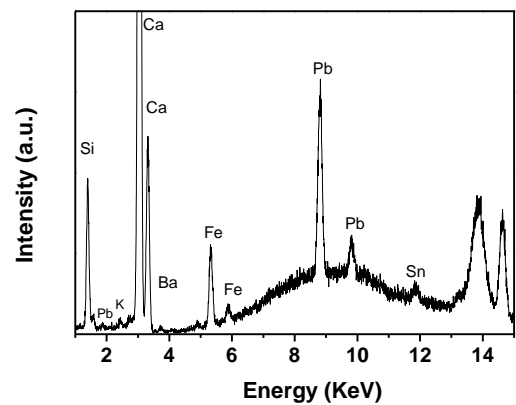
*Pink (Pk2b)*



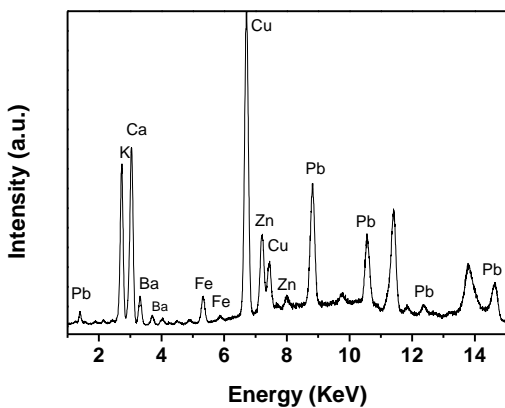
*Red (R4a)*



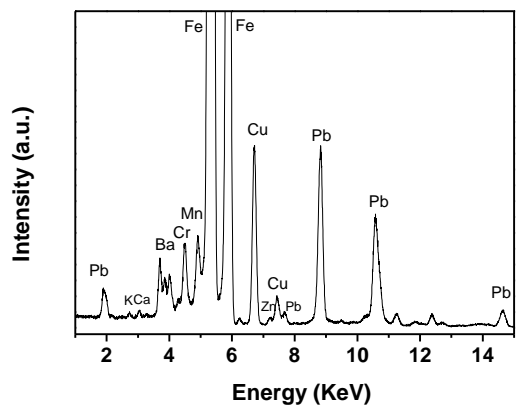
Golden (Gd1a)



Glass (Gl2a)



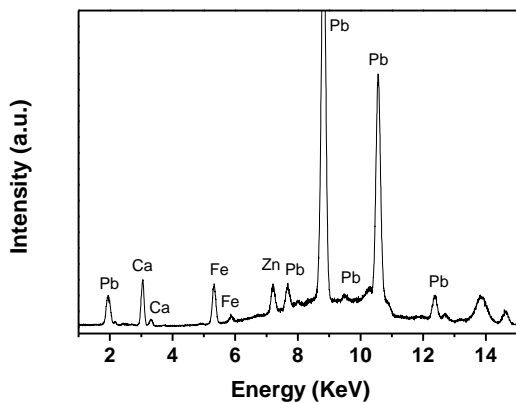
Pearl (Co2a)



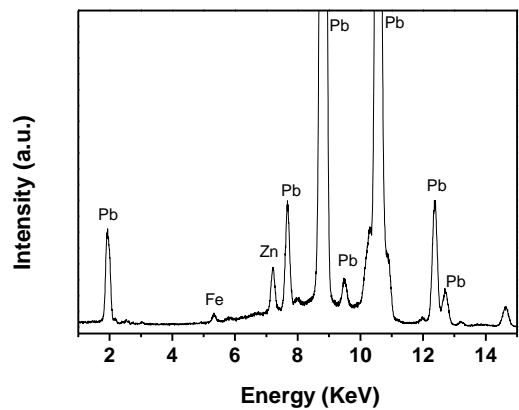
Metal hair clip

**Figure V.3** Representative  $\mu$ -EDXRF spectra of preparation layer and white, black, grey, violet, blue, green, yellow, orange, brown, pink, red, golden, areas and glass, pearl, metal hair clip from *Coty* painting.

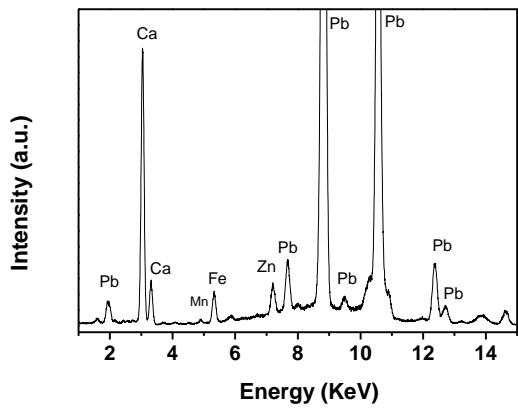
**Representative  $\mu$ -EDXRF from *Untitled* painting.**



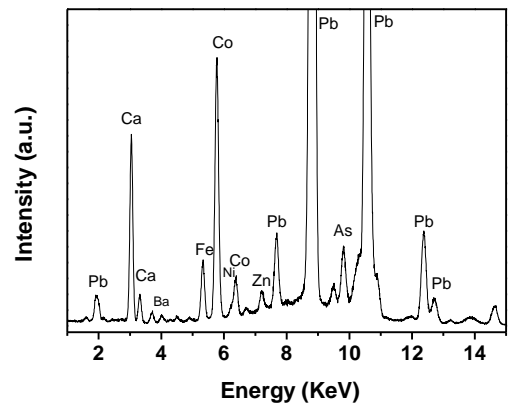
Preparation (Pl1a)



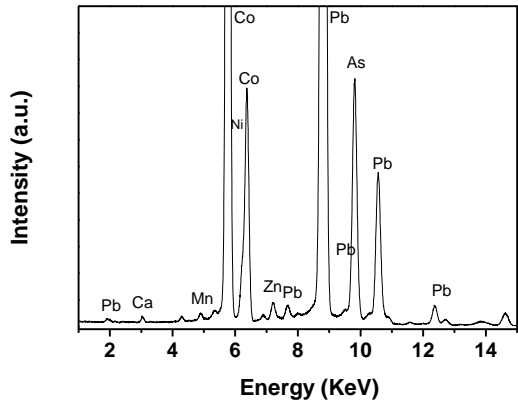
White (Wh1a)



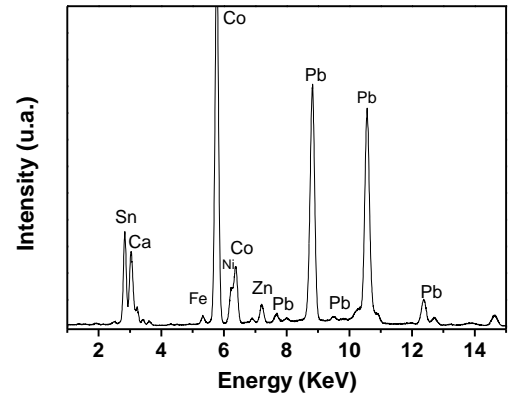
*Black (Bk1a)*



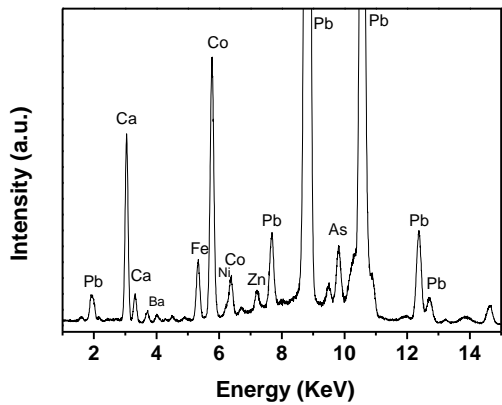
*Black (Bk3a)*



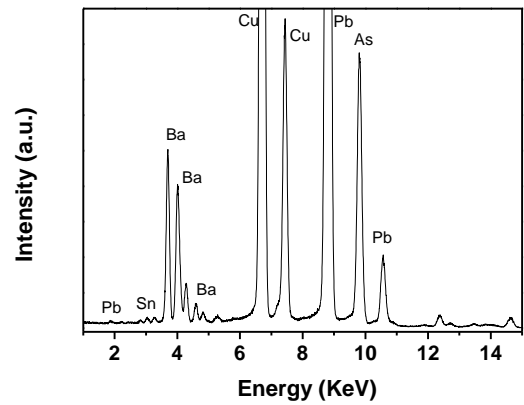
*Violet (Vi2a)*



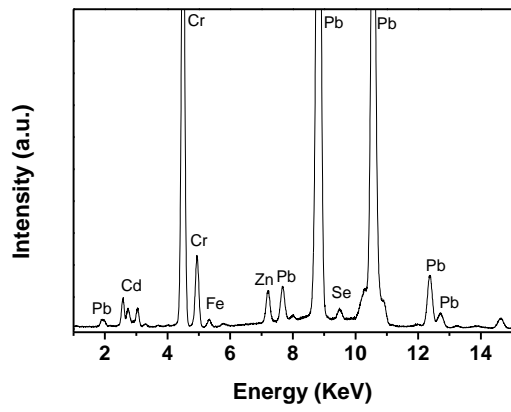
*Blue (Bl2a)*



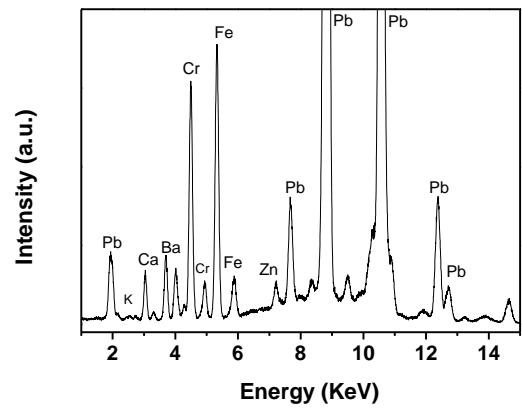
*Blue (Bl8a)*



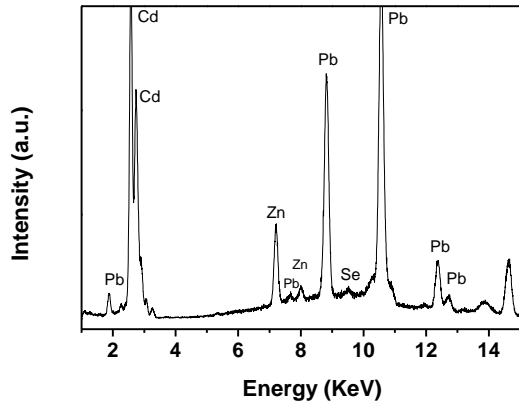
*Green (G1a)*



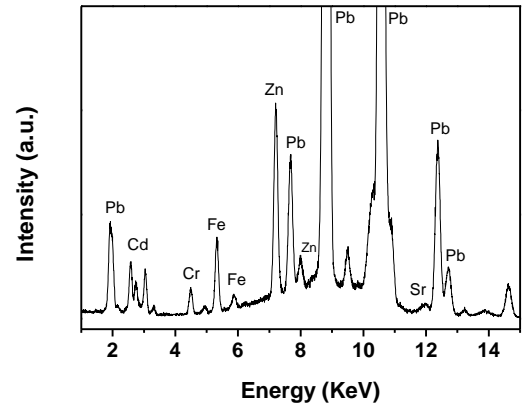
Green (G2a)



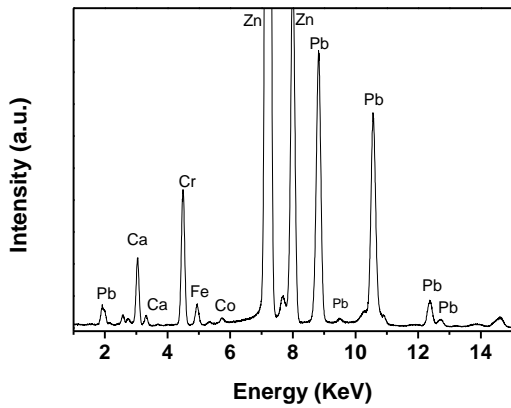
Green (G9a)



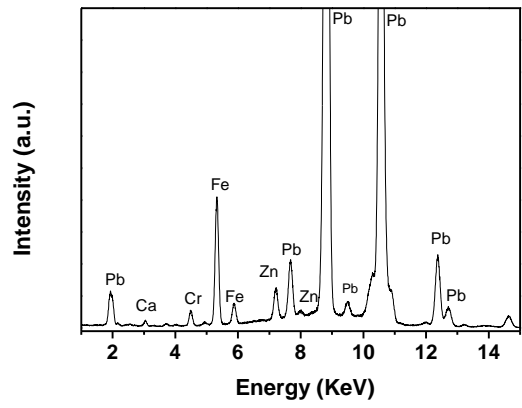
Yellow (Y1b)



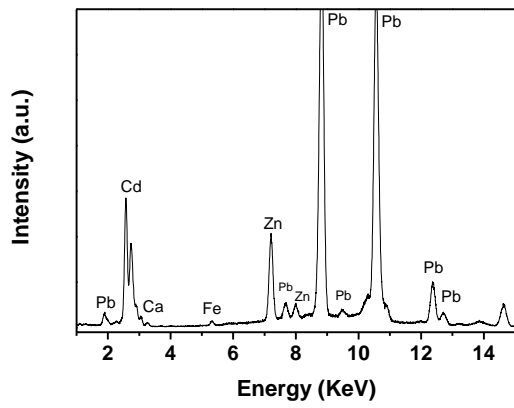
Yellow (Y3a)



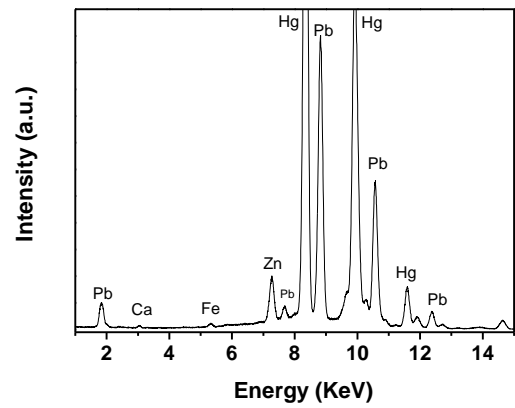
Yellow (Y7a)



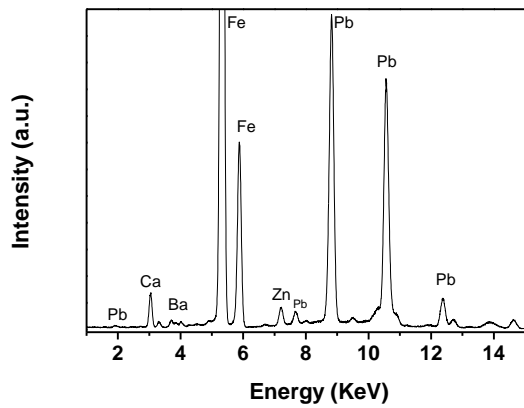
Yellow (Y15c)



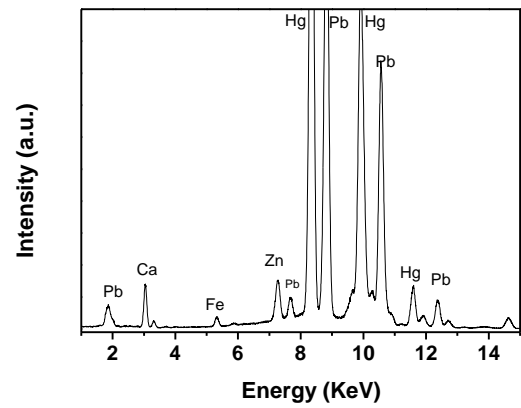
Orange (O2a)



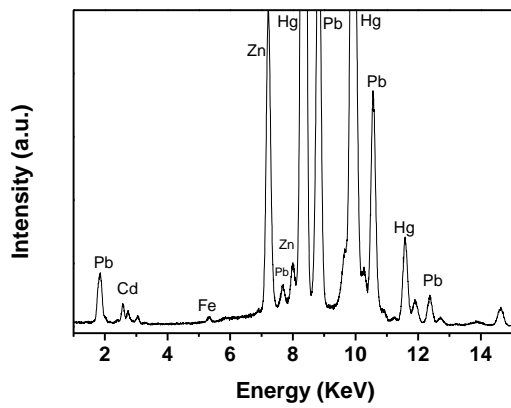
Orange (O3b)



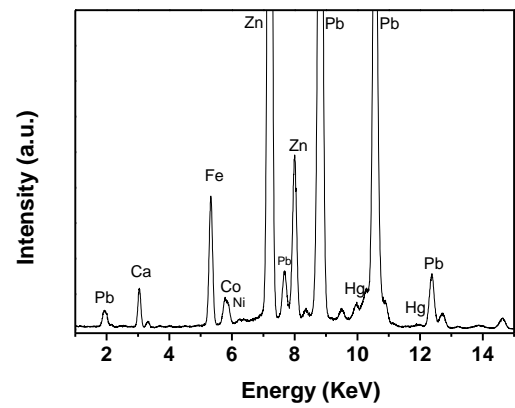
Brown (Br3a)



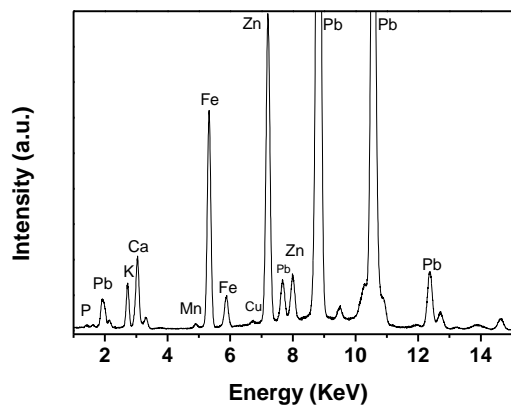
Red (R2a)



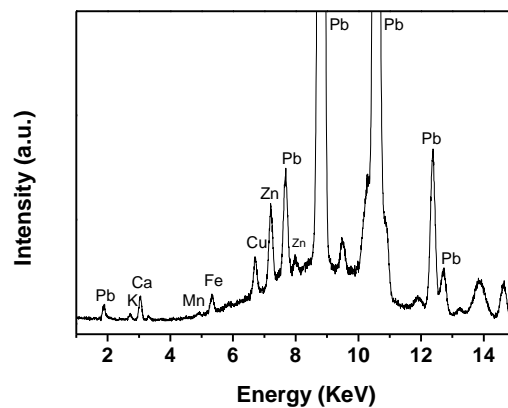
Red (R3a)



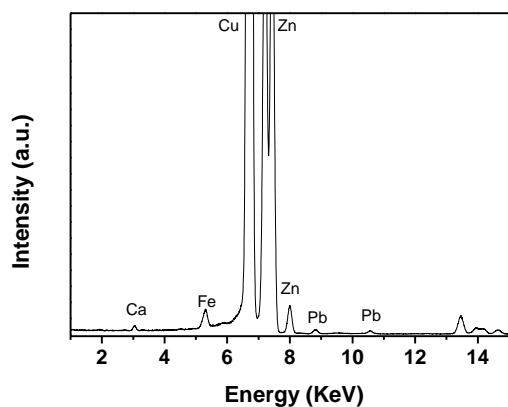
Pink (Ro1a)



Matches (Fosf1c)



Matches box (Fosf1d)



Golden over matches box (Fosf1e)

**Figure V.4** Representative  $\mu$ -EDXRF spectra of preparation layer and white, black, grey, violet, blue, green, yellow, orange, brown, red, pink, golden areas and matches from *Untitled* painting.

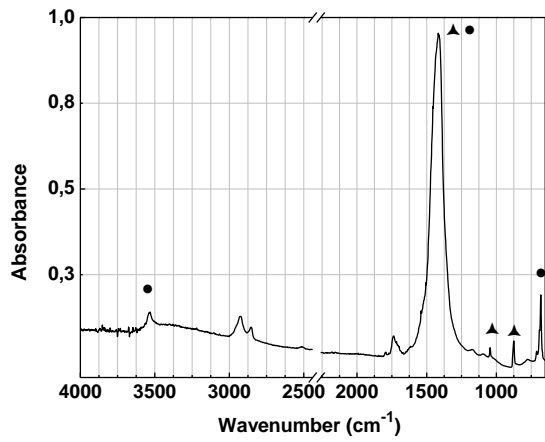
**Table V.5.** Characteristic energies of the X-rays (KeV) used to identify the elements in the EDXRF analysis.

Elements	K $\alpha$	K $\beta$	L $\alpha$	L $\beta_1$	L $\beta_2$	L $\gamma_1$	M $\alpha$
<sup>15</sup> P	2,014	2,139					
<sup>19</sup> K	3,314	3,590					
<sup>20</sup> Ca	3,690	4,012					
<sup>24</sup> Cr	5,414	5,946					
<sup>26</sup> Fe	6,396	7,057					
<sup>27</sup> Co	6,922	7,648					
<sup>28</sup> Ni	7,477	8,264					
<sup>29</sup> Cu	8,040	8,904					
<sup>30</sup> Zn	8,630	9,570					
<sup>33</sup> As	10,543	11,725					
<sup>56</sup> Ba			4,467	4,828	5,156	5,531	
<sup>80</sup> Hg			9,987	11,823	11,923	13,828	
<sup>82</sup> Pb			10,550	12,812	12,621	14,782	2,342

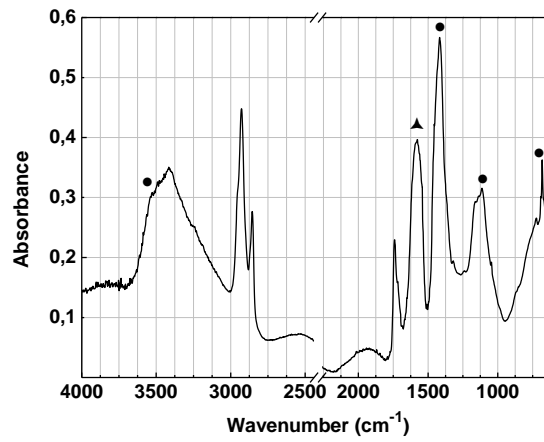


## V.2 $\mu$ -FTIR

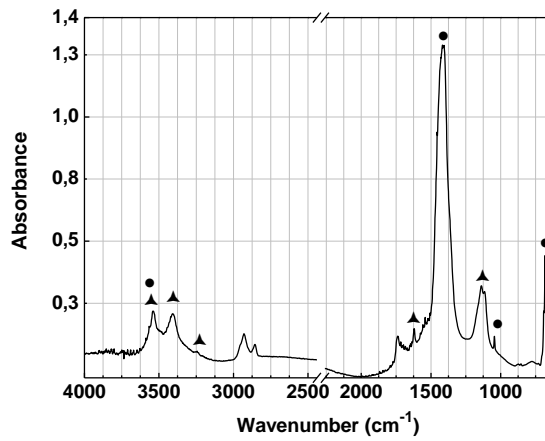
Representative from *BRUT* painting.



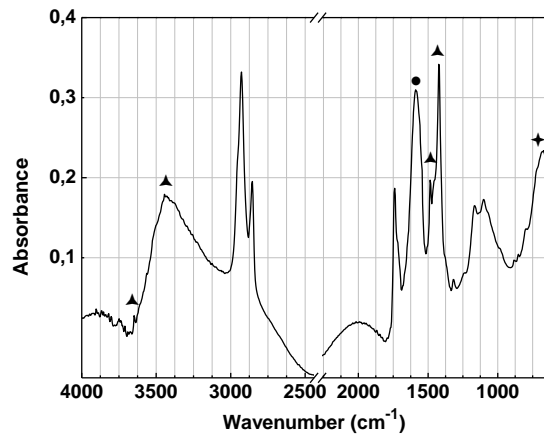
Preparation ( $\mu$ 1), ( $\blacktriangle$ ) calcium carbonate;  
( $\bullet$ ) lead white.



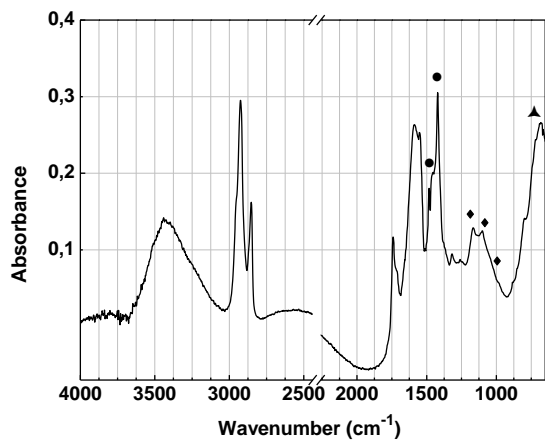
White ( $\mu$ 25), ( $\bullet$ ) lead white;  
( $\blacktriangle$ ) zinc carboxylate.



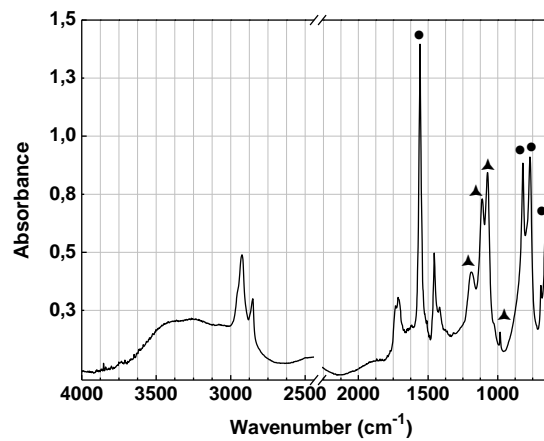
White ( $\mu$ 29), ( $\bullet$ ) lead white;  
( $\blacktriangle$ ) gypsum.



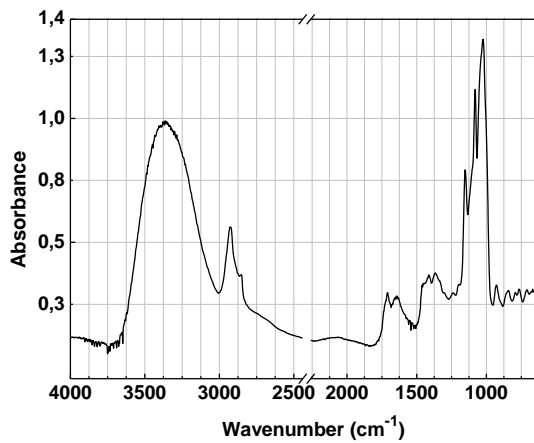
Violet ( $\mu$ 19), ( $\blacktriangle$ ) cerulean blue;  
( $\bullet$ ) zinc carboxylate; ( $\blacktriangle$ ) magnesium carbonate.



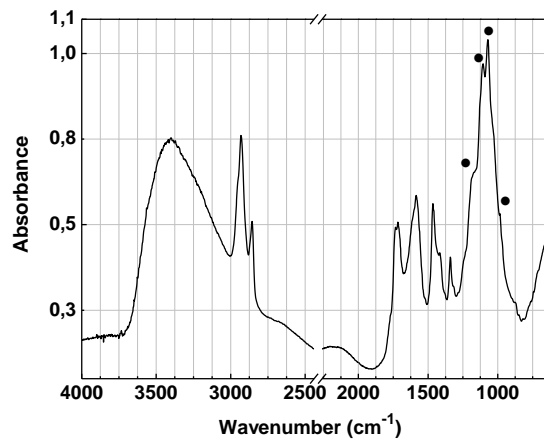
Blue ( $\mu$ 18), ( $\blacktriangle$ ) cobalt blue; ( $\blacklozenge$ ) barium sulphate.  
( $\bullet$ ) magnesium carbonate;



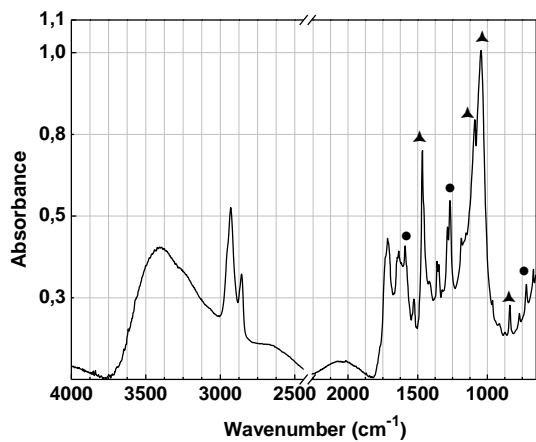
Green ( $\mu$ 7), ( $\bullet$ ) emerald green;  
( $\blacktriangle$ ) barium sulphate.



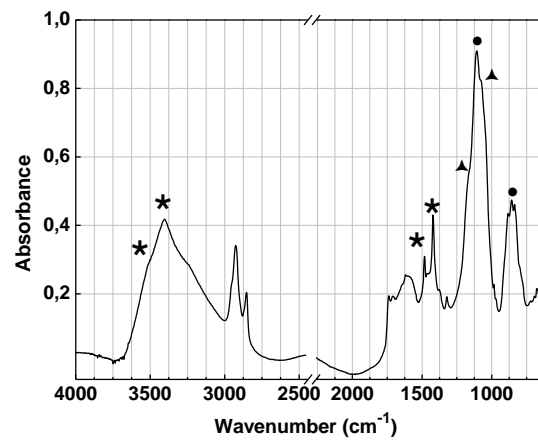
Green, starch ( $\mu 6$ ).



Red ( $\mu 11$ ), (●) sulfato de bário.



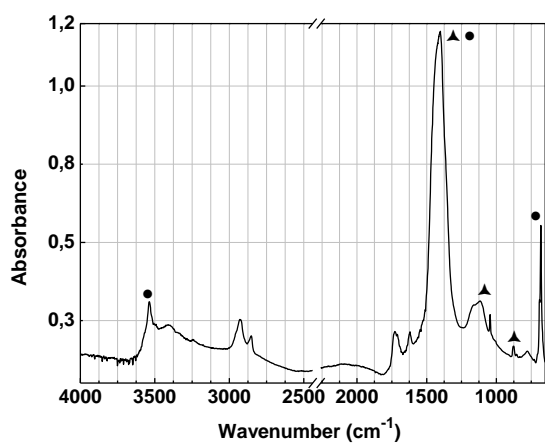
Red ( $\mu 14$ ), (●) alizarin;  
(▲) calcium phosphate.



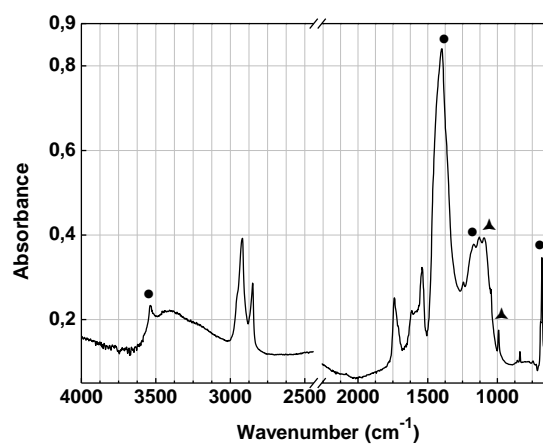
Yellow ( $\mu 3$ ), (●) chrome yellow; (▲) barium sulphate;  
(★) magnesium carbonate.

**Figure V.5** Representative infrared spectra of preparation layer and white, violet, blue, green, yellow, red areas from *BRUT* painting

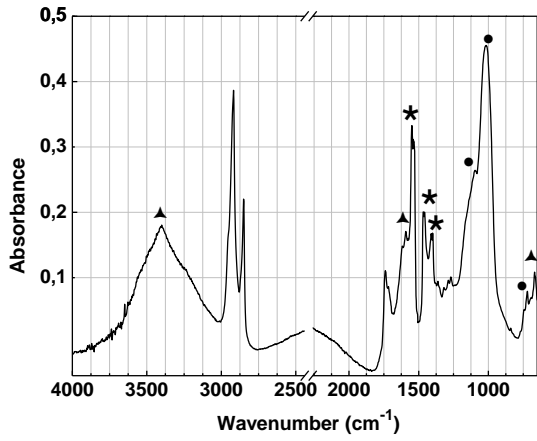
**Representative from *Entrada* painting.**



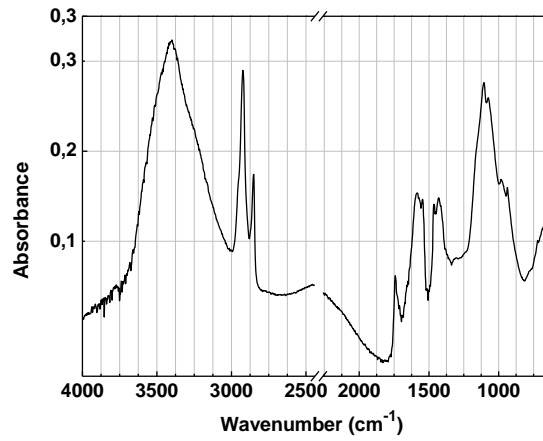
Preparation ( $\mu 33$ ),  
(▲) calcium carbonate; (●) lead white.



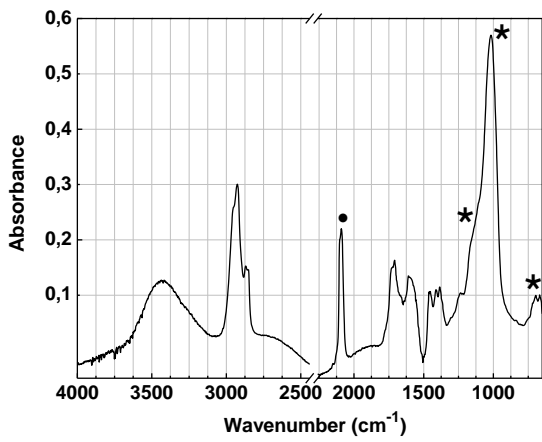
White ( $\mu 23$ ),  
(●) lead white; (▲) strontium sulphate.



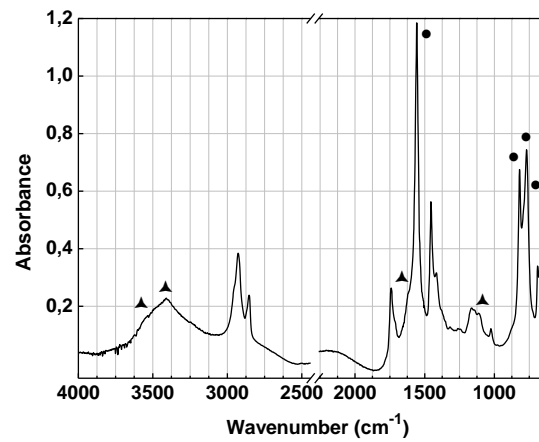
Violet ( $\mu 24$ ), (●) ultramarine blue;  
(▲) gypsum; (★) zinc carboxylate.



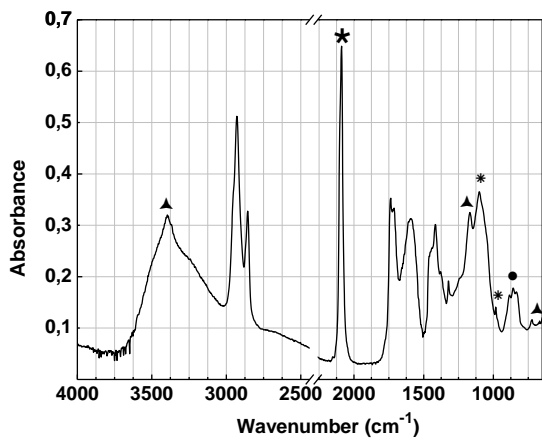
Violet ( $\mu 20$ ),  
Madder lake.



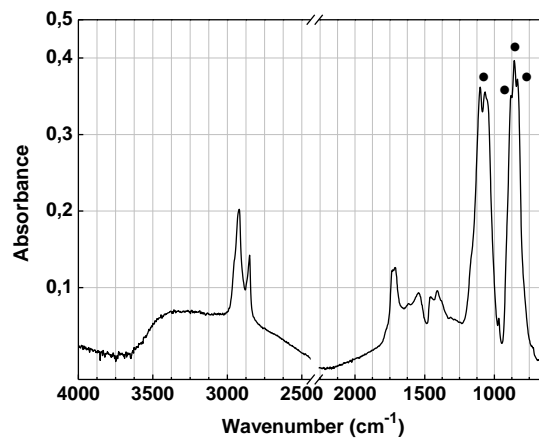
Blue ( $\mu 3$ ), (●) Prussian blue;  
(★) ultramarine blue.



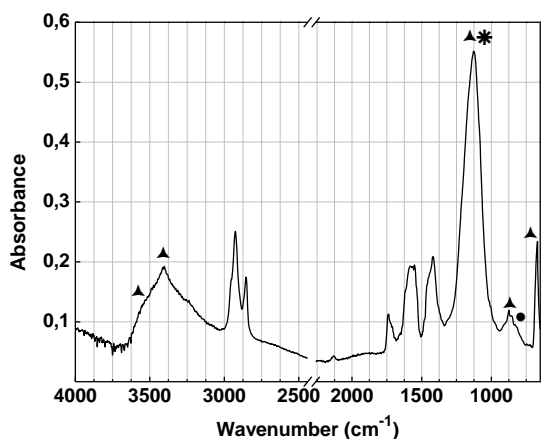
Light green ( $\mu 5$ ),  
(●) emerald green; (▲) gypsum.



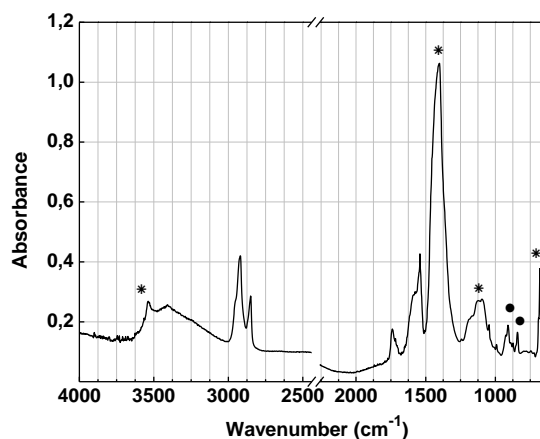
Green ( $\mu 14$ ), (●) chrome yellow; (▲) gypsum; (★)  
Prussian blue; (★) barium sulphate.



Yellow ( $\mu 17$ ),  
(●) chrome yellow.



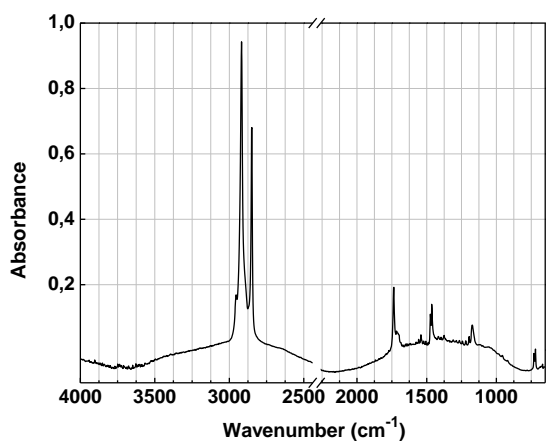
Yellow ( $\mu 19$ ), (●) chrome yellow;  
( $\blacktriangle$ ) gypsum; (\* ) strontium sulphate.



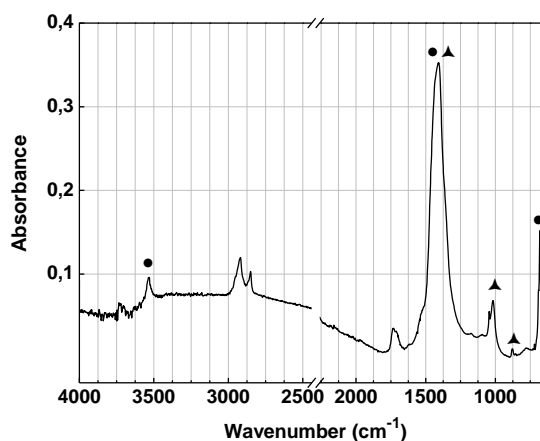
Yellow ( $\mu 26$ ),  
(●) strontium yellow; (\* ) lead white.

**Figure V.6** Representative infrared spectra of preparation layer and white, violet, blue, green, yellow areas from *Entrada* painting.

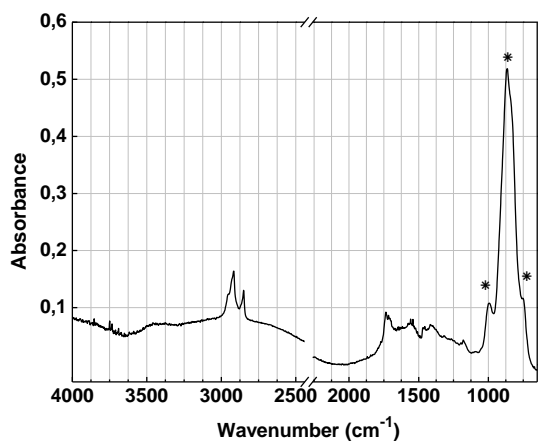
**Representative infrared spectra from *Coty* painting.**



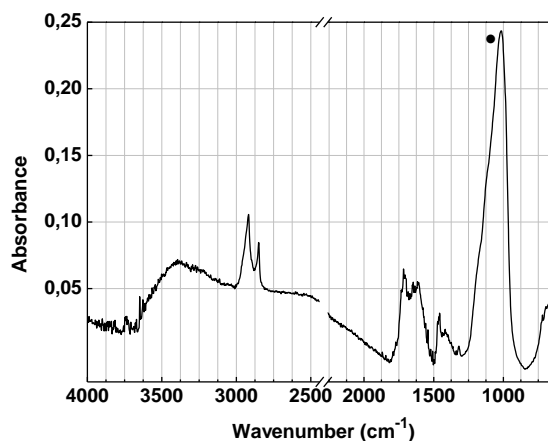
Varnish ( $\mu 2$ ),  
ketone resin varnish.



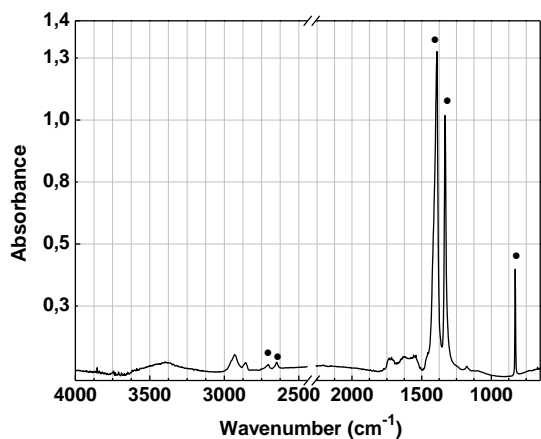
Preparation ( $\mu 6$ ),  
( $\blacktriangle$ ) calcium carbonate; (●) lead white.



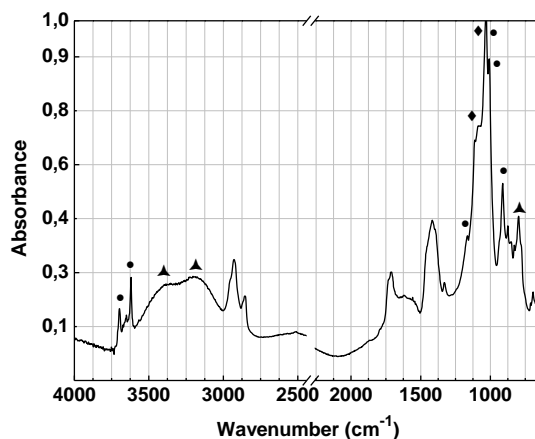
Violet ( $\mu 13$ ), (\* ) cobalt violet.



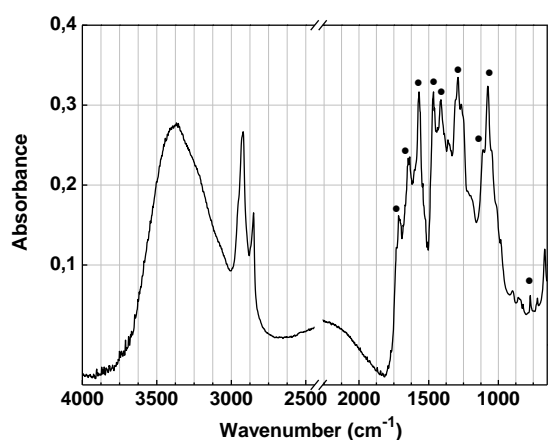
Blue ( $\mu 12$ ), (●) ultramarine blue.



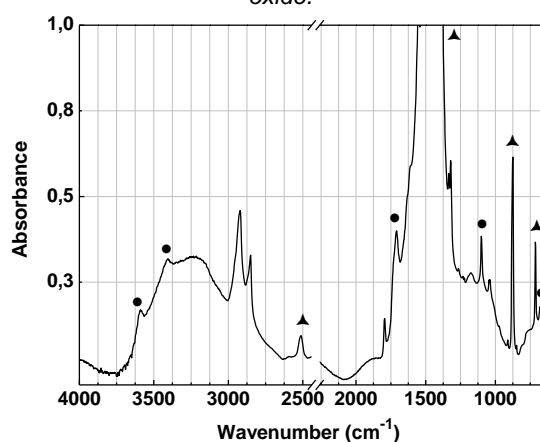
Yellow ( $\mu 3$ ), (●) cobalt yellow.



Yellow ( $\mu 4$ ), (◆) chrome yellow; (●) kaolin; (▲) iron oxide.



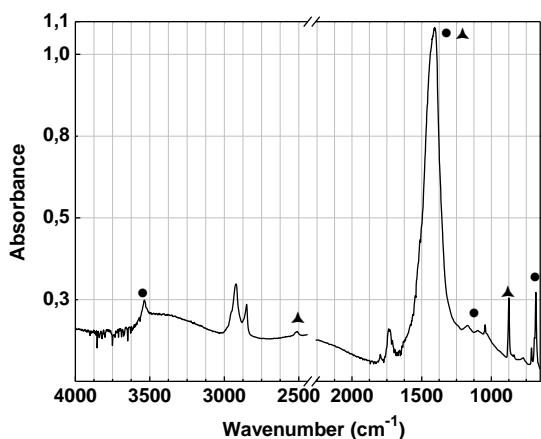
Red ( $\mu 6$ ), (●) carminic acid.



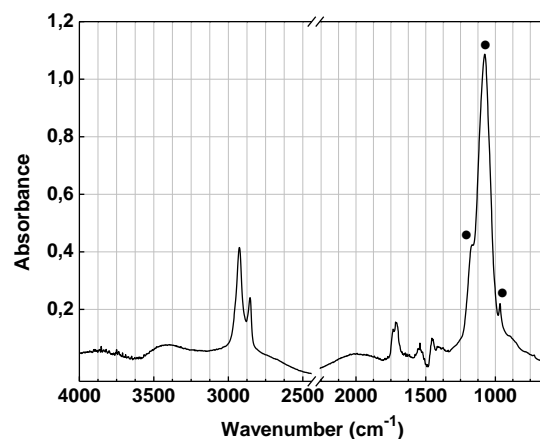
White mass round the glass ( $\mu 10$ ), (●) gypsum; (▲) calcium carbonate.

**Figure V.7** Representative infrared spectra of varnish, preparation layer and white, violet, blue, yellow, red areas from *Coty* painting.

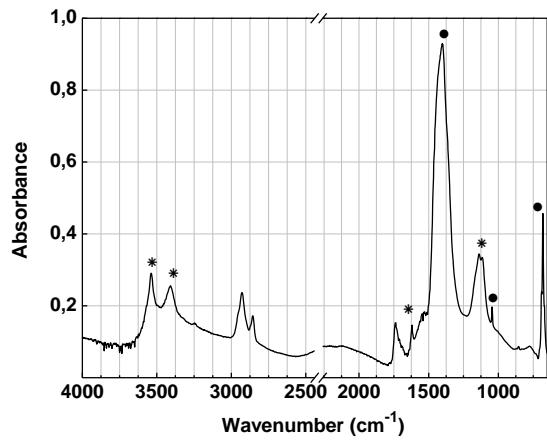
**Representative infrared spectra from *Untitled* painting.**



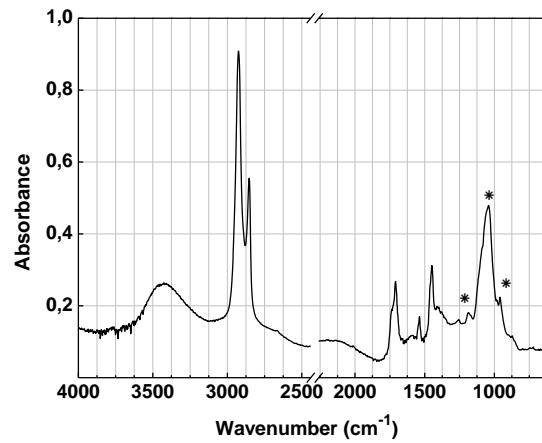
Preparation ( $\mu 2$ ), (▲) calcium carbonate; (●) lead white.



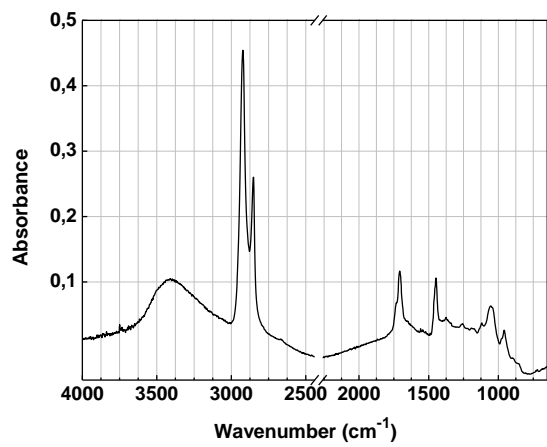
White ( $\mu 7$ ), (●) lead sulphate



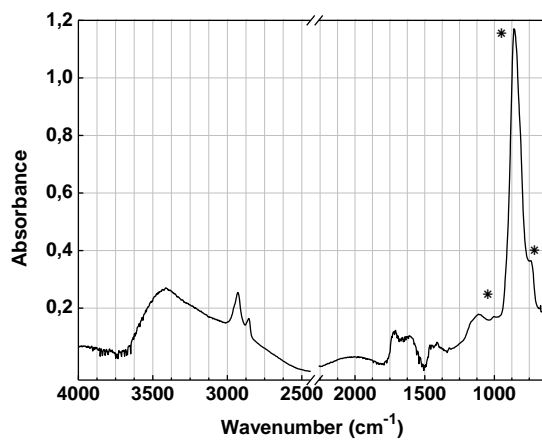
*White (μ43),*  
 (●) lead white; (\*) gypsum.



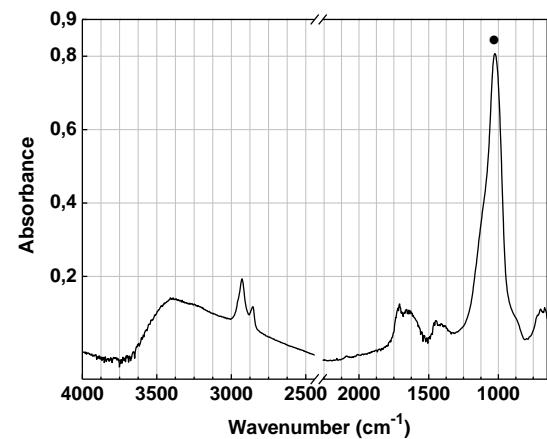
*Black (μ3),*  
 (\*) carbon black



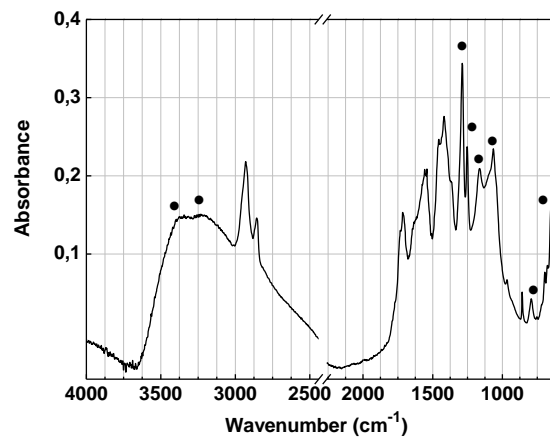
*Varnish over black area (μ3),*  
 beeswax.



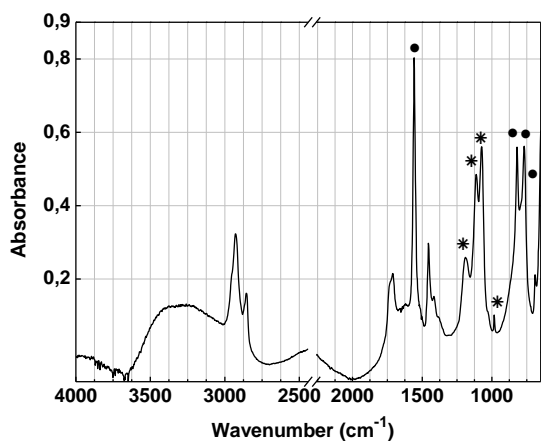
*Violet (μ9),*  
 (\*) cobalt violet.



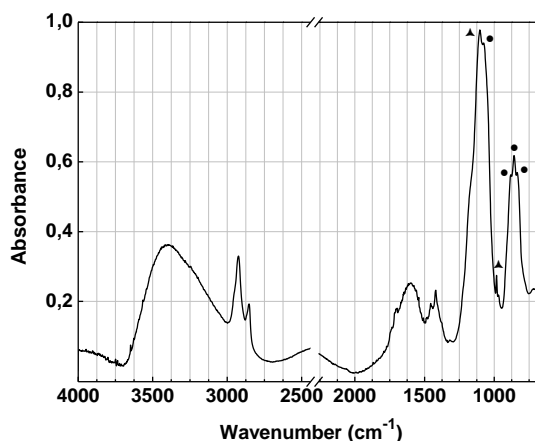
*Dark blue (μ32),*  
 (●) ultramarine blue.



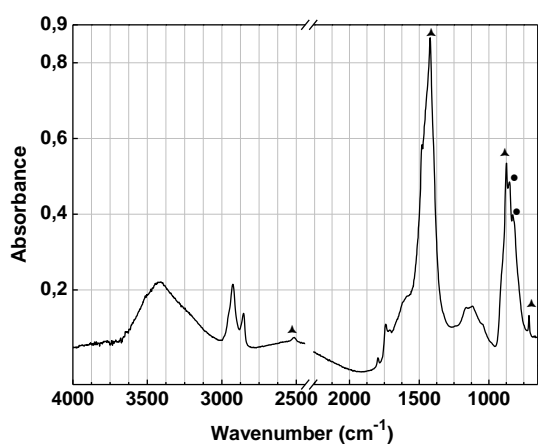
*Green (μ19),*  
 (●) viridian.



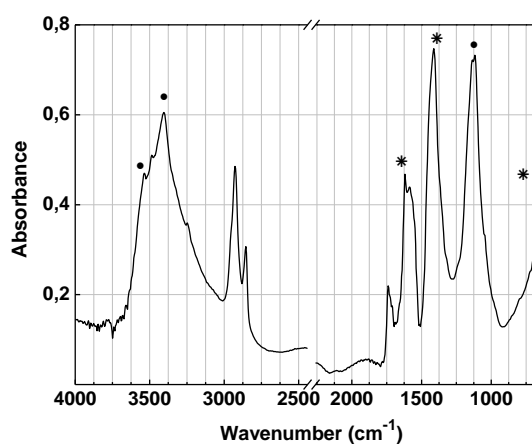
Light green ( $\mu 31$ ),  
 (●) emerald green; (\*) barium sulphate.



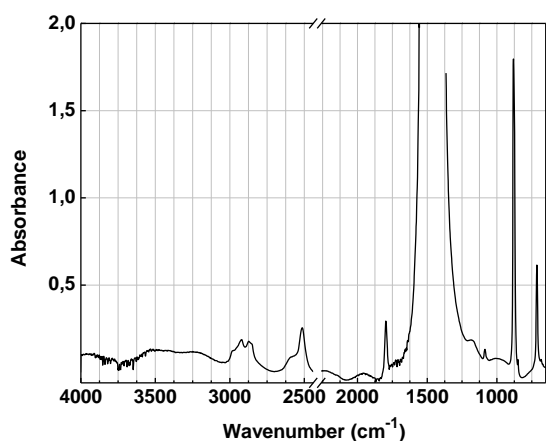
Yellow ( $\mu 1$ ),  
 (●) chrome yellow; (▲) barium sulphate.



Yellow ( $\mu 29$ ),  
 (●) chrome yellow; (▲) calcium carbonate.



Pink ( $\mu 23$ ),  
 (●) gypsum; (\*) lead white.



Transparent sphere of calcium carbonate ( $\mu 16$ ).

**Figure V.8** Representative infrared spectra of varnish, preparation layer and white, black, violet, dark blue, green, light green, yellow, red areas and transparent sphere from *Untitled* painting.



**Table V.6.** Characteristic bands of FTIR spectra of the pigments identified.

Pigment	Bands (cm <sup>-1</sup> ) and intensity	Assignment*
<b>Lead white</b> 2PbCO <sub>3</sub> .Pb(OH) <sub>2</sub>	3536, medium 1400, strong and broad 1047, weak 686, medium	v (OH) v <sub>as</sub> (CO <sub>3</sub> <sup>2-</sup> ) δ (OH) δ <sub>as</sub> (CO <sub>3</sub> <sup>2-</sup> )
<b>Barium sulphate</b> BaSO <sub>4</sub>	1200-1050, strong and broad 983, weak	v <sub>as</sub> (SO <sub>4</sub> ) v <sub>as</sub> (SO <sub>4</sub> )
<b>Quartz</b> SiO <sub>2</sub>	1164, 1063, forte e weak 799, 781, weak	v <sub>as</sub> (Si-O-Si) δ (-O-Si-)
<b>Gypsum</b> CaSO <sub>4</sub> .2H <sub>2</sub> O	3404, medium 1618, weak 1140, 1116, strong 669, weak	v (HO) δ (H <sub>2</sub> O) v <sub>as</sub> (SO <sub>4</sub> <sup>2-</sup> ) δ <sub>as</sub> (SO <sub>4</sub> <sup>2-</sup> )
<b>Carbon black</b> C+Ca <sub>3</sub> (PO <sub>4</sub> ) <sub>2</sub> +MgSO <sub>4</sub> +CaCO <sub>3</sub>	1457, medium and broad 1031, strong 873, weak 700, weak	δ <sub>as</sub> (CO <sub>3</sub> <sup>2-</sup> ) v <sub>as</sub> (PO <sub>4</sub> <sup>2-</sup> ) e v <sub>as</sub> (SO <sub>4</sub> <sup>2-</sup> ) δ <sub>as</sub> (CO <sub>3</sub> <sup>2-</sup> ) δ <sub>as</sub> (CO <sub>3</sub> <sup>2-</sup> )
<b>Cobalt violet</b> Co <sub>3</sub> (AsO <sub>4</sub> ) <sub>2</sub>	878, strong	v <sub>as</sub> (As-O)
<b>Ultramarine blue</b> Na <sub>8</sub> [Al <sub>6</sub> Si <sub>6</sub> O <sub>24</sub> ]S <sub>n</sub>	1150-950, strong and broad 696, weak	v (Si-O-Si e Si-O-Al) δ (-O-Si-)
<b>Prussian Blue</b> Fe <sub>4</sub> [Fe(CN) <sub>6</sub> ] <sub>3</sub>	2082, strong	v (CN)
<b>Emerald green</b> Cu(C <sub>2</sub> H <sub>3</sub> O <sub>2</sub> ) <sub>2</sub> .3Cu(AsO <sub>2</sub> ) <sub>2</sub>	1557, strong 1454, weak 820, medium 768, media 647, strong	carboxylate " (As-O) (As-O) (As-O)
<b>Viridian</b> Cr <sub>2</sub> O <sub>3</sub> .2H <sub>2</sub> O	3630-2630, very broad 1288, medium 1064, strong 794, medium/ strong 650, strong	v (OH) - - - γ (OH)
<b>Cobalt yellow</b> K <sub>3</sub> [NaCo(NO <sub>2</sub> ) <sub>6</sub> ]	2704, weak 2649, weak 1390, very strong 1334, very strong 827, medium	- - v <sub>as</sub> (NO <sub>2</sub> ) v <sub>as</sub> (NO <sub>2</sub> ) v <sub>as</sub> (NO <sub>2</sub> )
<b>Chrome yellow</b> PbCrO <sub>4</sub>	857/830, strong and broad	v <sub>as</sub> (CrO <sub>4</sub> <sup>2-</sup> )
<b>Strontium yellow</b> SrCrO <sub>4</sub>	911/888/874/843, strong and broad	v <sub>as</sub> (SrO <sub>4</sub> <sup>2-</sup> )
<b>Ochre</b> Fe <sub>2</sub> O <sub>3</sub> .H <sub>2</sub> O	3689, 3670, 3650, 3622 medium 1036 strong 917 medium 800 medium	v (OH) v <sub>as</sub> (Si-O-Si) v (Al-O-H) δ (Fe-O-H) goethite and δ (-O-Si-) kaolin

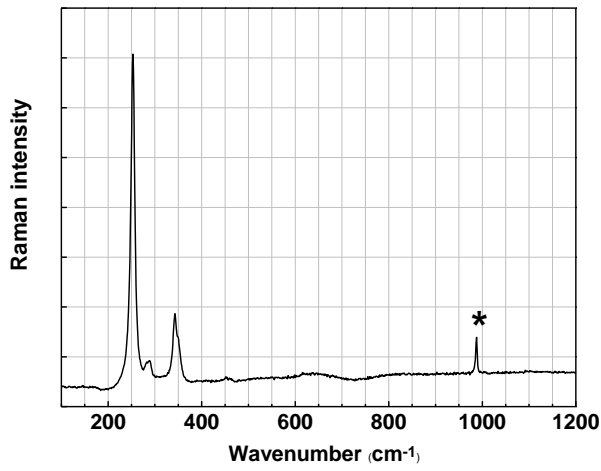
**Table V.6. (continued)**

<b>Pigment</b>	<b>Bands (cm<sup>-1</sup>) and intensity</b>	<b>Assignment*</b>
<b>Purpurine</b>	1627, 1614, strong 1581, medium 1066, medium 719, 709, weak	v (CO <sub>3</sub> <sup>-2</sup> ) v (aromatic ring) δ H- aromatic ring v H- aromatic ring
<b>Alizarin</b>	1662, 1633, strong 1587, 1286, medium 1047, medium 713, weak	v (CO <sub>3</sub> <sup>-2</sup> ) v (aromatic ring) δ H- aromatic ring v H- aromatic ring
<b>Carminic acid</b>	3424, strong 1717, medium 1572, strong 1448, strong 1285 should, 1255 strong, 1229 shoulder 1083, 1045 forte 983, 888, weak 820, 768 weak	v (OH) v <sub>acid</sub> (C=O) v(CC)/ δ (C <sub>8</sub> OH)/ δ (OH) v(CC)/ δ (CH <sub>3</sub> )/ δ (OH) v(CC)/ δ (COH) v(CC)/ δ (COH) ρ(CH <sub>3</sub> )/ δ(CCC) γ (COH)

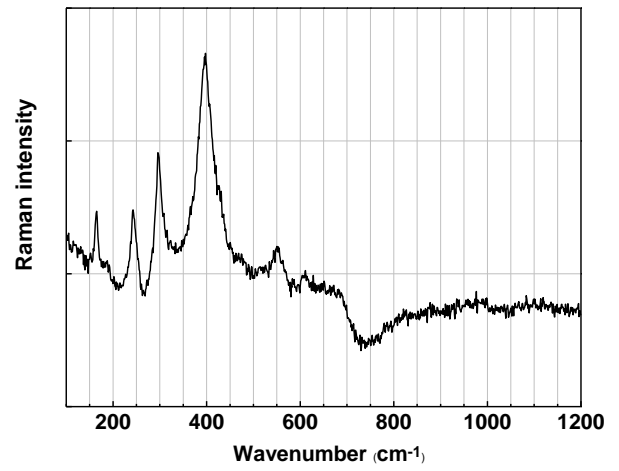
\* Assignment based on [Derrick *et al.* 1999; Genestar and Pons 2005; Humel 2002; Hitchman 1982; Vendilo 2011; Weerd *et al.* 2005; Prasad *et al.* 2005; Stuart and Ando 1996]

### V.3 $\mu$ -Raman

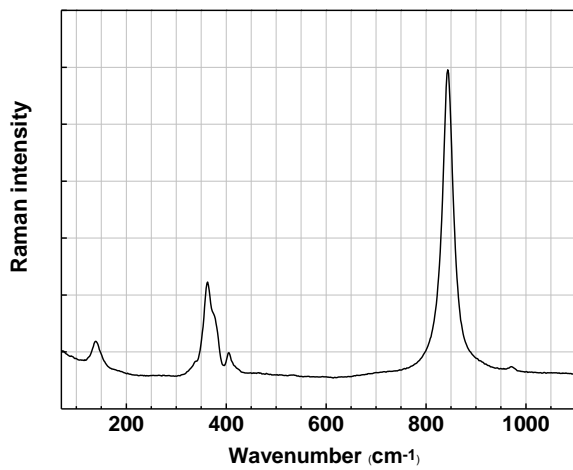
Representative Raman spectra from *BRUT* painting.



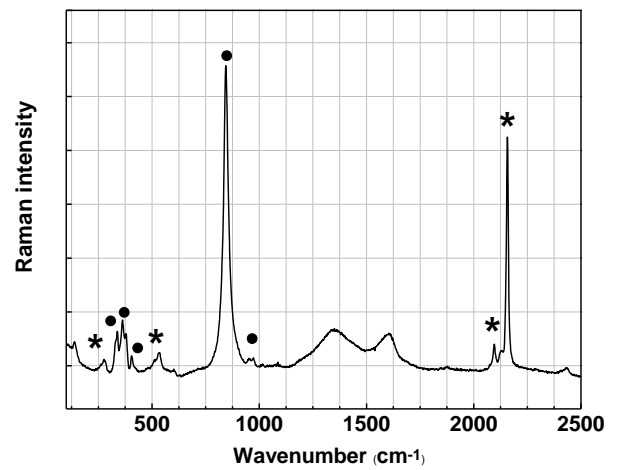
Red ( $\mu 1$ ); vermilion; (\*) barium sulphate.



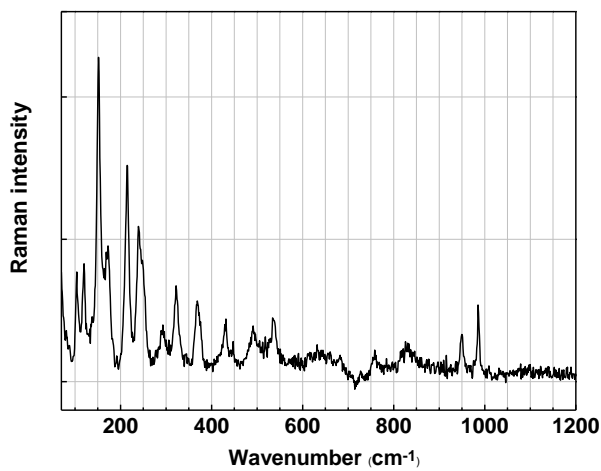
Red, goethite ( $\mu 1$ ).



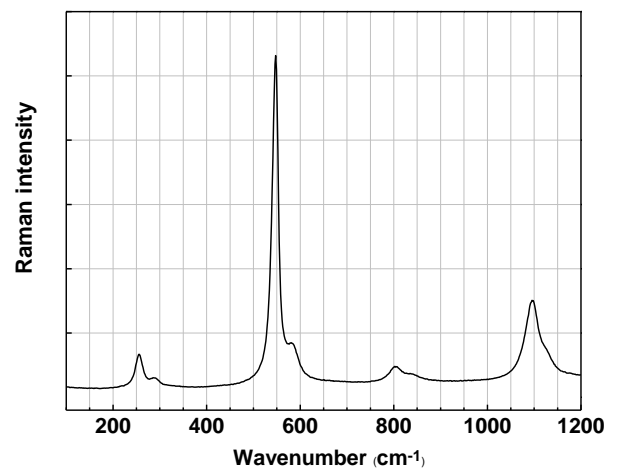
Chrome yellow ( $\mu 5$ ).



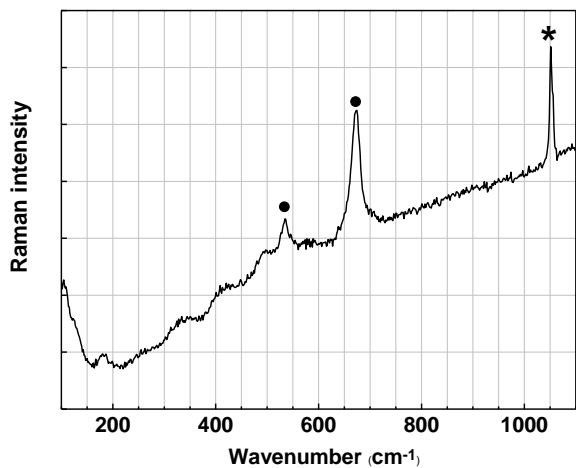
Chrome yellow (●); (\*) Prussian blue ( $\mu 5$ ).



Emerald green ( $\mu 33$ ).



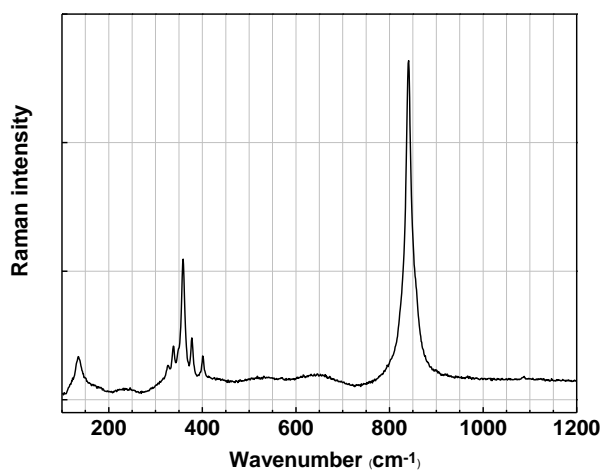
Ultramarine blue ( $\mu 10$ ).



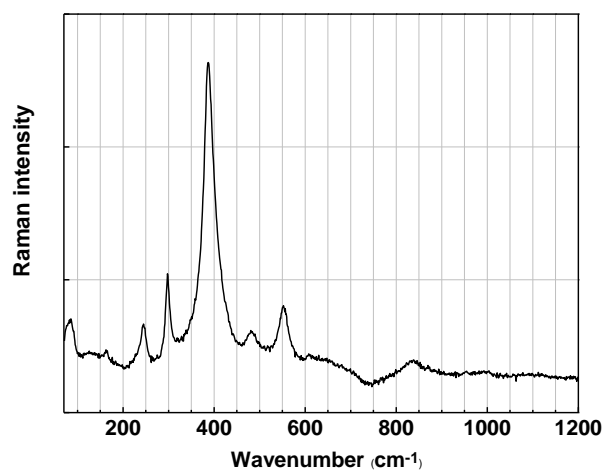
Cerulean blue (●); lead carbonate (\*); ( $\mu 27$ ).

**Figure V.9** Representative Raman spectra of red, yellow, green blue areas from *BRUT* painting.

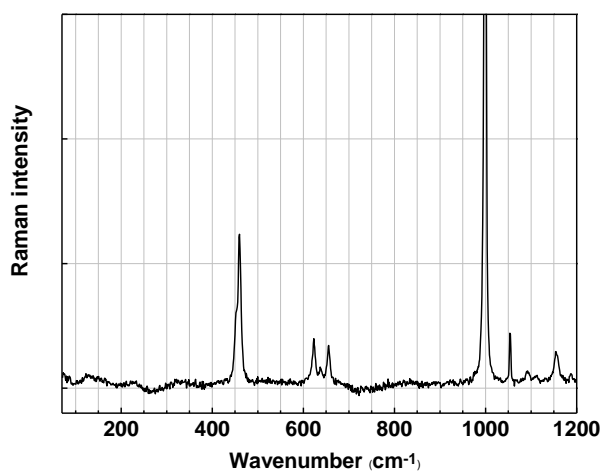
**Representative Raman spectra from *Entrada* painting.**



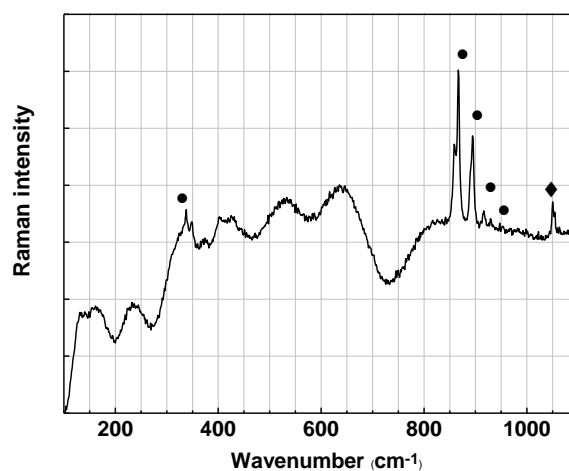
Chrome yellow ( $\mu 8$ ).



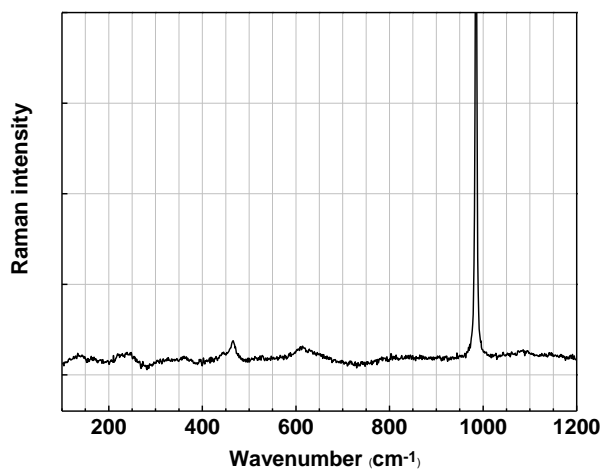
Brown, goethite ( $\mu 11$ ).



Green, strontium sulphate ( $\mu 14$ ).



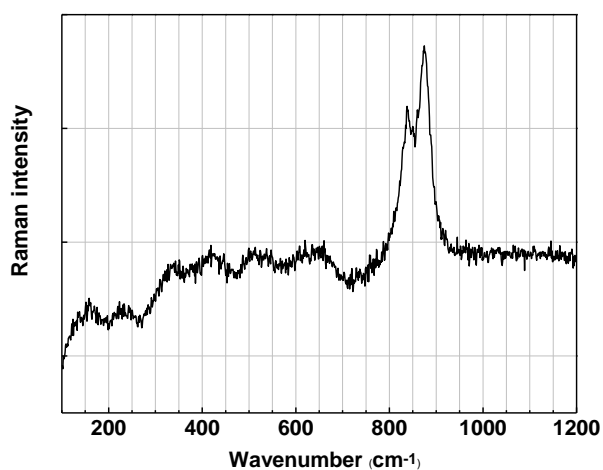
Yellow ( $\mu 26$ ), strontium yellow (●); lead white (◆).



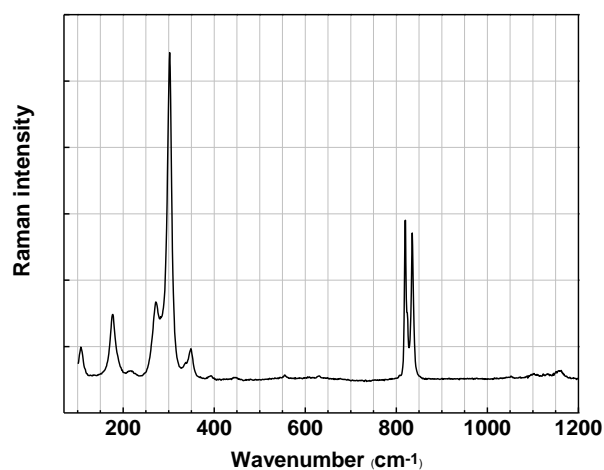
*Magnesium sulphate (μ37).*

**Figure V.10** Representative Raman spectra of yellow, brown, green areas from *Entrada* painting.

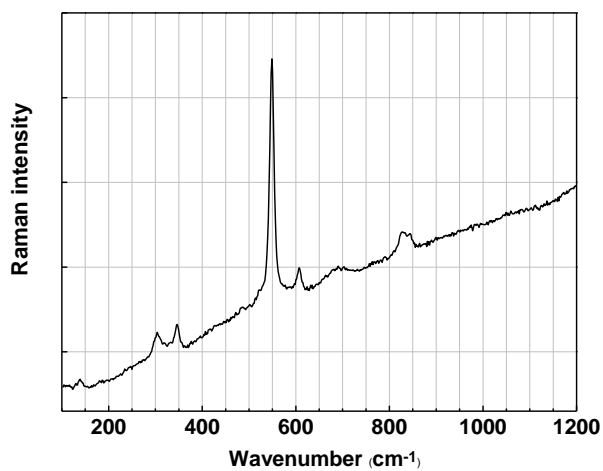
**Representative Raman spectra from *Coty* painting.**



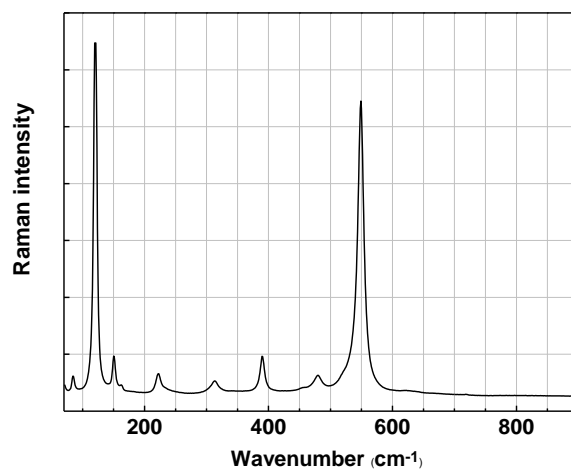
*Cobalt violet (μ13).*



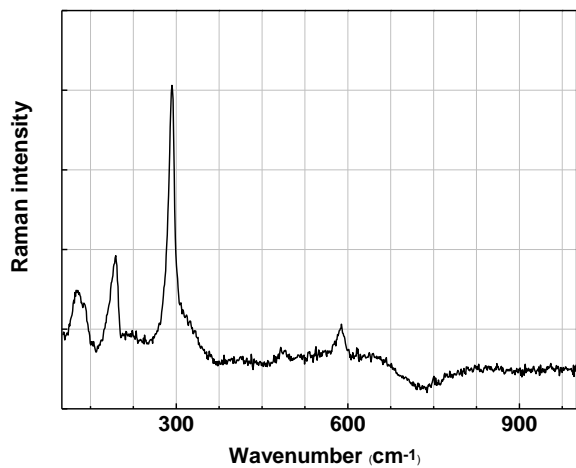
*Cobalt yellow (μ3).*



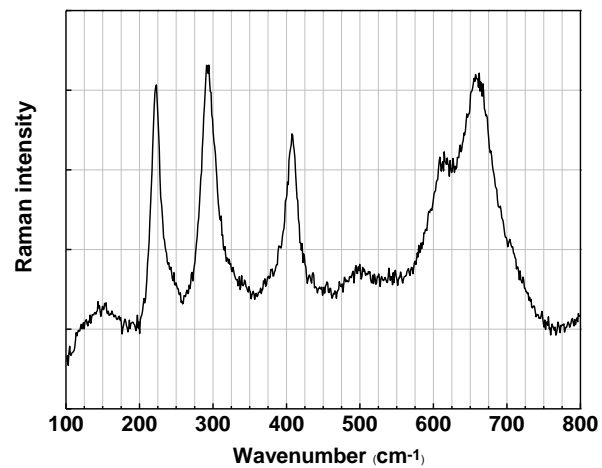
*Viridian (μ14).*



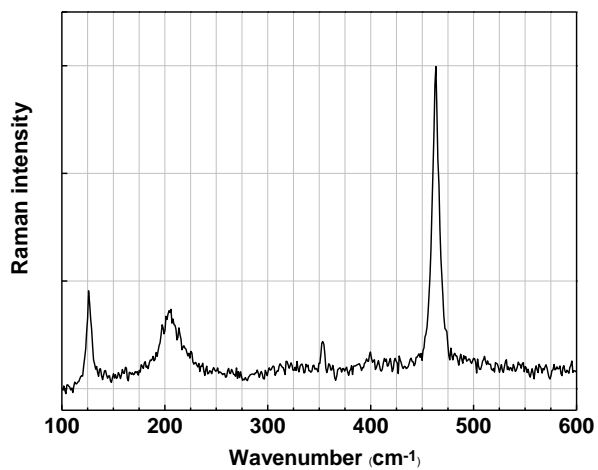
*Minium (μ2)*



*Cadmium orange ( $\mu 1$ ).*



*Brown, hematite ( $\mu 1$ ).*



*Transparent sphere, quartz ( $\mu 8$ ).*

**Figure V.11** Representative Raman spectra of violet, blue, green, red, orange, brown areas and a transparent sphere from *Coty* painting.

Representative Raman spectra from *Untitled* painting.

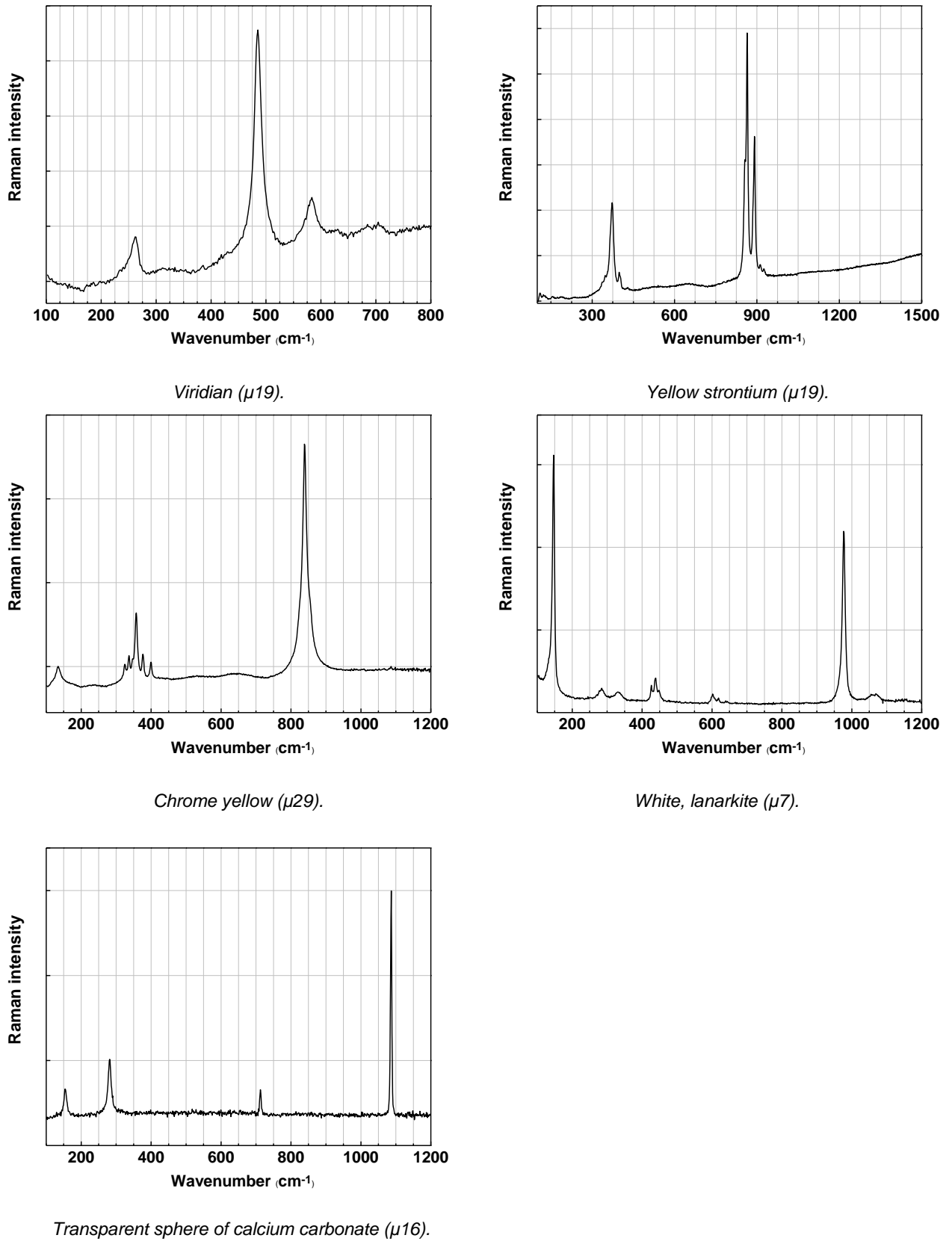


**Figure V.12** Representative Raman spectra of green, yellow, white, areas and calcium carbonate sphere from *Untitled* painting.



**Table V.7** Raman band and assignments of the pigments identified on the paintings.

Pigment	Band wavenumber (cm <sup>-1</sup> )	Assignment*
<b>Ultramarine blue</b> 3Na <sub>2</sub> O.3Al <sub>2</sub> O <sub>3</sub> .6SiO <sub>2</sub> .2Na <sub>2</sub> S	258 weak	δ (S <sub>3</sub> <sup>-</sup> )
	548 (vs)	ν <sub>s</sub> (S <sub>3</sub> <sup>-</sup> )
	822 (w)	
	1096 (m)	overtone
<b>Prussian blue</b> Fe <sub>4</sub> [Fe(CN) <sub>6</sub> ] <sub>3</sub>	277, very weak	δ (C-Fe-C)
	531, strong	δ (Fe-C≡N)
	2092, weak	ν (C≡N)
	2127, weak, shoulder	ν (C≡N)
	2154, very strong	ν (C≡N)
<b>Cerulean blue</b> CoO.nSnO <sub>2</sub>	482 (m,sh)	ν <sub>s</sub> (Sn-O)
	532 (s)	ν (Co-O)
	670 (vs)	ν <sub>as</sub> (Sn-O)
<b>Cobalt blue</b> CoO.Al <sub>2</sub> O <sub>3</sub>	202, very strong	
	520, very strong	ν (Co-O)
<b>Viridian</b> Cr <sub>2</sub> O <sub>3</sub> .2H <sub>2</sub> O	266, weak	δ (O-Cr <sup>III</sup> -O)
	490, very weak	δ <sub>s</sub> (O-Cr <sup>III</sup> -O)
	552, very weak	ν <sub>as</sub> (O-Cr <sup>III</sup> -O)
	585, very weak	ν <sub>as</sub> (O-Cr <sup>III</sup> -O)
<b>Emerald Green</b> Cu[C <sub>2</sub> H <sub>3</sub> O <sub>2</sub> ].3Cu[AsO <sub>2</sub> ] <sub>2</sub>	117, very weak	
	151, medium	δ (O-Cu-O)
	171, medium	δ (O-Cu-O)
	214, very strong	δ (O-Cu-O)
	241, strong	δ (O-Cu-O)
	292, weak	δ (Cu-O)
	321, weak	δ (As-O) or ν (Cu-O)
	365, weak	δ <sub>s</sub> (As-O)
	427, very weak	ν (Cu-O)
	489, medium	ν (Cu-O)
	536, medium	ν (Cu-O) or <i>bridge</i> (As-O)
	633, very weak	δ <sub>s</sub> (COO)
	683, very weak	δ <sub>s</sub> (COO)
	760, weak	ν <sub>s</sub> (As-O)
	835, weak, broad	ν <sub>as</sub> (As-O)
	948, strong	ν (C-C)
1440, weak, broad	ν <sub>s</sub> (COO <sup>-</sup> )	
1556, weak	ν <sub>as</sub> (COO <sup>-</sup> )	
2926, strong	ν <sub>s</sub> (CH <sub>3</sub> )	
<b>Chrome yellow</b> PbCrO <sub>4</sub>	134, weak	lattice mode
	325, very weak	δ (CrO <sub>4</sub> <sup>2-</sup> )
	337, weak-medium	δ (CrO <sub>4</sub> <sup>2-</sup> )
	347, weak	δ (CrO <sub>4</sub> <sup>2-</sup> )
	357, medium	δ (CrO <sub>4</sub> <sup>2-</sup> )
	375, medium	δ (CrO <sub>4</sub> <sup>2-</sup> )
	39, very weak	δ (CrO <sub>4</sub> <sup>2-</sup> )
	839, very strong	ν <sub>s</sub> (CrO <sub>4</sub> <sup>2-</sup> )

Table V.7. (continued)

Pigment	Band wavenumber (cm <sup>-1</sup> )	Assignment*
<b>Cobalt yellow</b> K <sub>3</sub> [Co(NO <sub>2</sub> ) <sub>6</sub> ].nH <sub>2</sub> O	178, weak	
	302, very strong	v (Co-N)
	821, strong	δ (N-O)
	836, medium	δ (N-O)
	1326, strong	v <sub>as</sub> (N-O)
<b>Strontium chromate</b> SrCrO <sub>4</sub>	338, weak	
	347, weak	δ (CrO <sub>4</sub> <sup>2-</sup> )
	373, medium	δ (CrO <sub>4</sub> <sup>2-</sup> )
	399, weak	δ (CrO <sub>4</sub> <sup>2-</sup> )
	403, weak	
	861, strong	
	865, very strong	v <sub>as</sub> (CrO <sub>4</sub> <sup>2-</sup> )
	894, strong	v <sub>as</sub> (CrO <sub>4</sub> <sup>2-</sup> )
	915, weak	
	931, very weak	
<b>Cadmium yellow</b> CdS	304, very strong	v (Cd-S)
	609, strong	v (Cd-S)
<b>Goethite</b> α-FeOOH	242, very weak	
	297, weak	δ <sub>s</sub> (Fe-O)
	394, very strong	δ <sub>s</sub> (Fe-O)
	477, very weak	δ <sub>as</sub> (Fe-O)
	554, weak	v <sub>as</sub> (Fe-O)
<b>Vermilion</b> HgS	253, very strong	δ (S-Hg-S)
	282, weak-shoulder	δ (S-Hg-S)
	343, medium	v (Hg-S)
<b>β-naphthol</b>	165, medium	
	204, weak	
	310, media	
	356, weak	
	405-418, weak	
	592, weak	
	628, media	
	69, weak	
	711, weak	
	735, weak	
	773, weak	
	895, weak	
	986, weak	
	1039, weak	
	1092, shoulder	v azobenzene
	1121, media	v azobenzene
	1186, media	v azobenzene
1226-1236, weak	v azobenzene	
1315, shoulder	v azobenzene	
1334, strong	v azobenzene	

Table V.7. (continued)

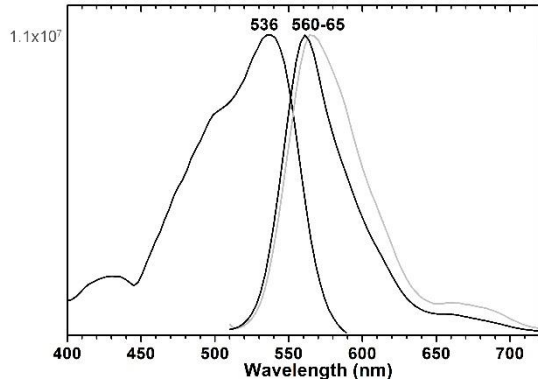
Pigment	Band wavenumber (cm <sup>-1</sup> )	Assignment*
<b>β-naphthol (continued)</b>	1394, medium	v azobenzene
	1453, weak	v azobenzene
	1488, medium	v azobenzene
	1558, shoulder	v (NO <sub>2</sub> )
<b>Haematite</b> α-Fe <sub>2</sub> O <sub>3</sub>	224, very strong	δ <sub>s</sub> (Fe-O)
	291, strong	
	407, medium	δ <sub>s</sub> (Fe-O)
	610, weak	ν <sub>s</sub> (Fe-O)
	1315, medium broad	
<b>Cobalt violet</b> Co <sub>3</sub> (AsO <sub>4</sub> ) <sub>2</sub>	204, very weak	(As-O) in the plane
	351, weak, broad	(As-O) out of plane
	375, weak, shoulder	(As-O) out of plane
	420, weak, broad	(As-O) out of plane
	508, weak	(As-O) out of plane
	738, very weak	ν <sub>s/s</sub> (As-O)
	765, very weak	ν <sub>s/s</sub> (As-O)
	837, medium, shoulder	ν <sub>s/s</sub> (As-O)
	865, very strong	ν <sub>s/s</sub> (As-O)
<b>Lead carbonate or Lead White</b> PbCO <sub>3</sub> or 2PbCO <sub>3</sub> .Pb(OH) <sub>2</sub>	665, very weak	δ <sub>s</sub> (CO <sub>3</sub> <sup>2-</sup> )
	687, very weak	δ <sub>s</sub> (CO <sub>3</sub> <sup>2-</sup> )
	829, very weak	ν <sub>as</sub> (CO <sub>3</sub> <sup>2-</sup> )
	1050, very strong	ν <sub>s</sub> (CO <sub>3</sub> <sup>2-</sup> )
<b>Barium sulphate</b> BaSO <sub>4</sub>	453, médium	δ (SO <sub>4</sub> <sup>2-</sup> )
	461, médium, should	δ (SO <sub>4</sub> <sup>2-</sup> )
	616, weak	δ <sub>out-of-plane</sub> (SO <sub>4</sub> <sup>2-</sup> )
	647, weak	δ <sub>out-of-plane</sub> (SO <sub>4</sub> <sup>2-</sup> )
	987, very strong	ν <sub>s</sub> (SO <sub>4</sub> <sup>2-</sup> )
<b>Calcium Carbonate</b> CaCO <sub>3</sub>	157, weak	lattice mode
	281, weak	lattice mode
	711, very weak	δ <sub>s</sub> (CO <sub>3</sub> <sup>2-</sup> )
	1085, very strong	ν <sub>s</sub> (CO <sub>3</sub> <sup>2-</sup> )
<b>Lanarkite**</b> Pb <sub>2</sub> (SO <sub>4</sub> )O	103, medium	
	146, very strong	
	285, medium, broad	
	426, medium	
	440, medium	
	602, weak	
	978, very strong	
	1055, very weak	
1072, very weak		

\* Assignment based on [Bersani *et al.* 1999; Bouchard *et al.* 2010; Casadio *et al.* 2011; Frausto-Reyes *et al.* 2009; Frost 2004; Frost *et al.* 2010; Quilès and Burneau 1998; Roncaglia *et al.* 1985; Shebanova and Lazor 2003; Vandenberghe *et al.* 2000; Yang *et al.* 2010; Zumbühl *et al.* 2009].

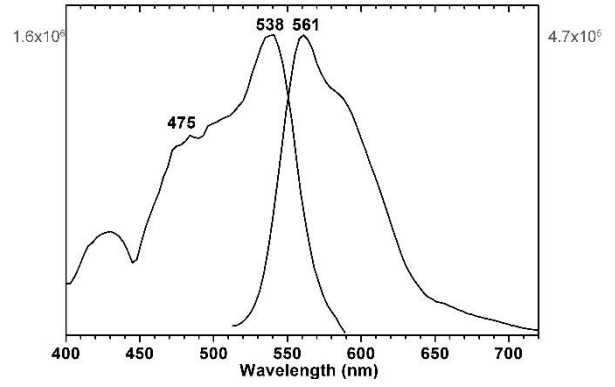
\*\* Attribution made by comparison with the mineral.

## V.4 $\mu$ -SPEX

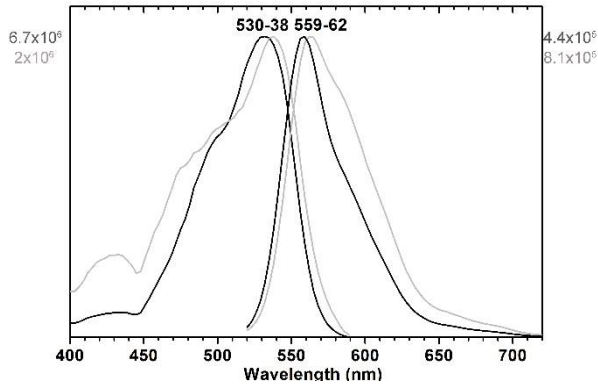
Representative spectra of Emission and excitation spectra *BRUT* painting.



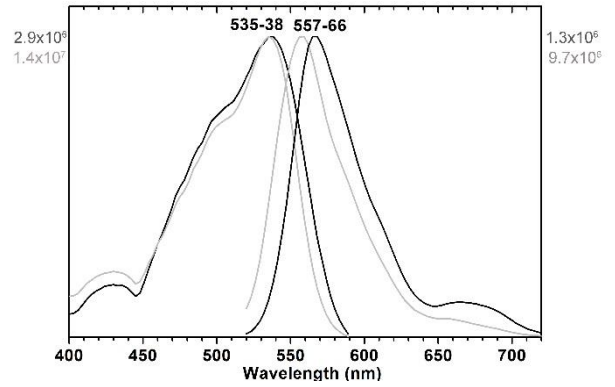
*Pink areas ( $\mu$ Red1).*



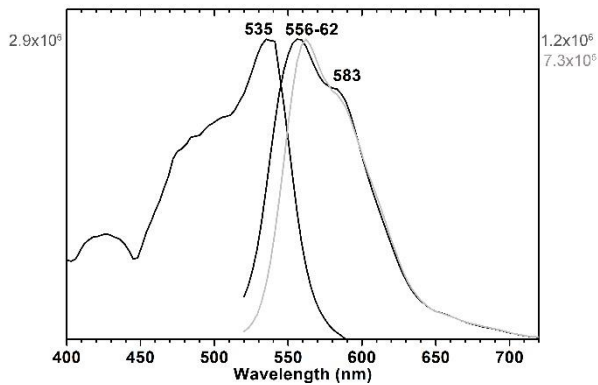
*Red areas ( $\mu$ Red1).*



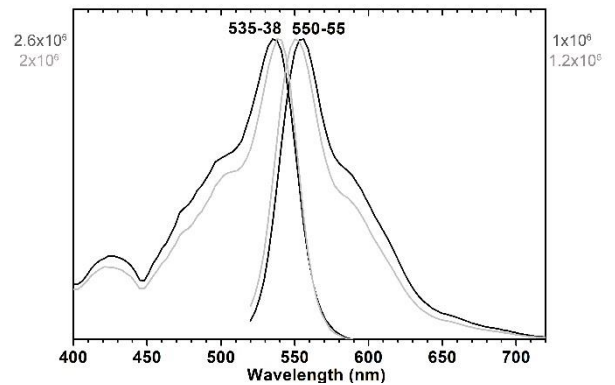
*Pink areas ( $\mu$ 11).*



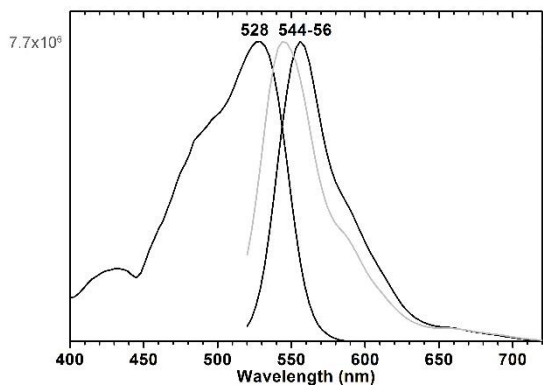
*Pink areas ( $\mu$ 11).*



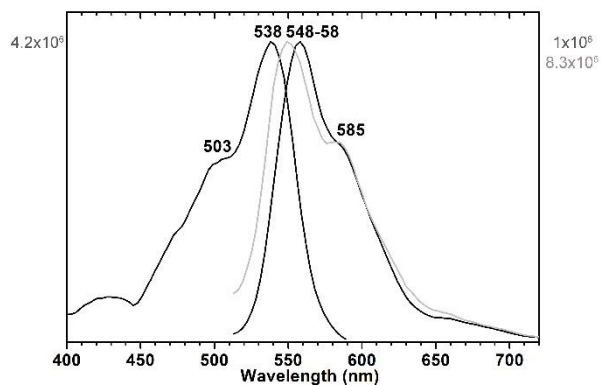
*Red areas ( $\mu$ 11).*



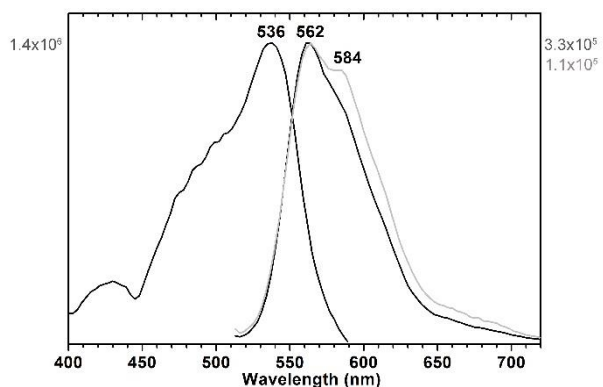
*Red areas ( $\mu$ 14).*



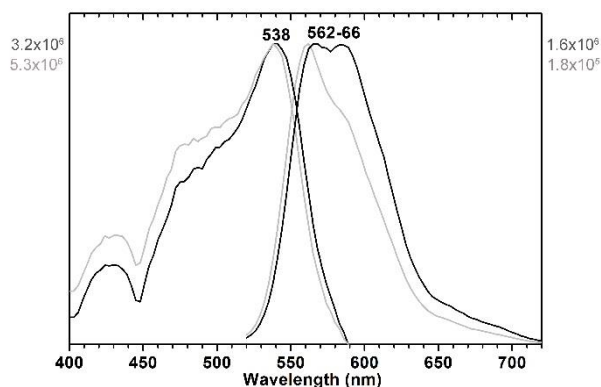
*Pink and violet areas ( $\mu 19$ ).*



*Pink areas ( $\mu 28$ ).*



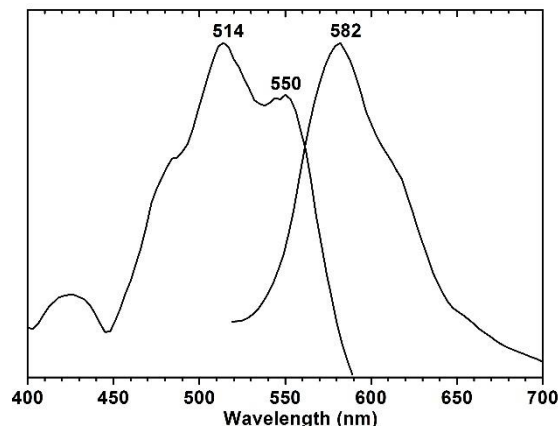
*Red areas ( $\mu 26$ ).*



*Red areas ( $\mu 30$ ).*

**Figure V.13** Representative spectra of Emission and excitation spectra ( $\lambda_{exc} = 490 \text{ nm}$ ; dichroic = 500 nm;  $\lambda_{em} = 610 \text{ nm}$ ; dichroic = 600 nm) acquired on pink, red and violet samples from *BRUT* painting.

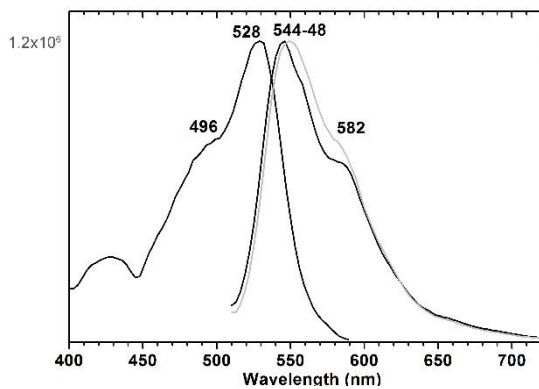
Representative spectrum of Emission and excitation spectra from *Entrada* painting.



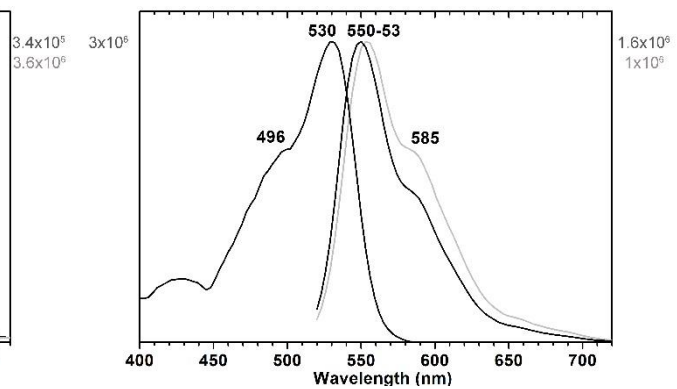
*Pink areas (μ20).*

**Figure V.14** Representative spectrum of Emission and excitation spectra ( $\lambda_{exc} = 490$  nm; dichroic = 500 nm;  $\lambda_{em} = 610$  nm; dichroic = 600 nm) acquired on pink sample from *Entrada* painting.

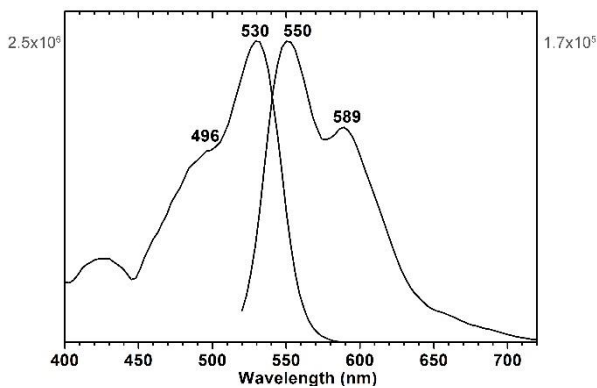
Representative spectrum of Emission and excitation spectra from *Untitled* painting.



*Pink areas (μ21).*



*Pink areas (μ28).*

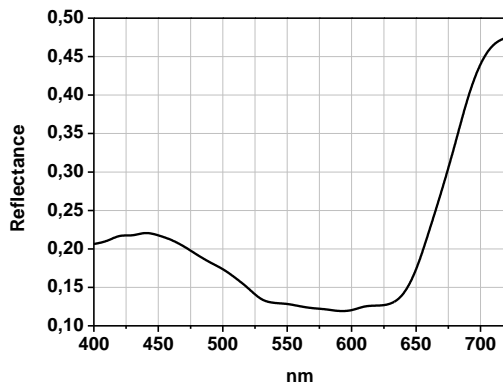


*Red areas (μ28).*

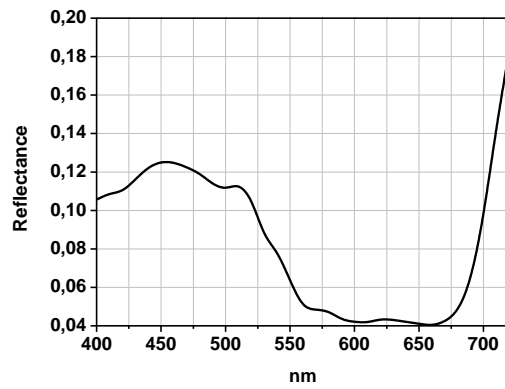
**Figure V.15** Representative spectra of Emission and excitation spectra ( $\lambda_{exc} = 490$  nm; dichroic = 500 nm;  $\lambda_{em} = 610$  nm; dichroic = 600 nm) acquired on pink and red samples from *Untitled* painting.

## V.5 Reflectance spectroscopy (hyperspectral imaging)

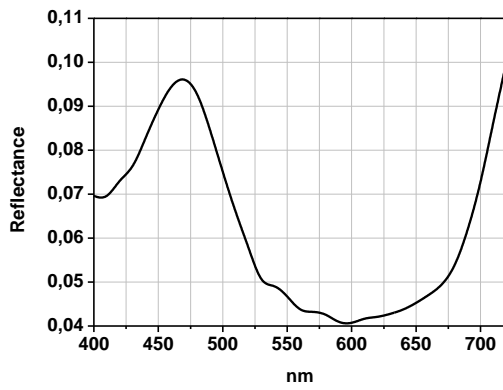
Representative Reflectance (hyperspectral imaging) spectra from the painting *BRUT*.



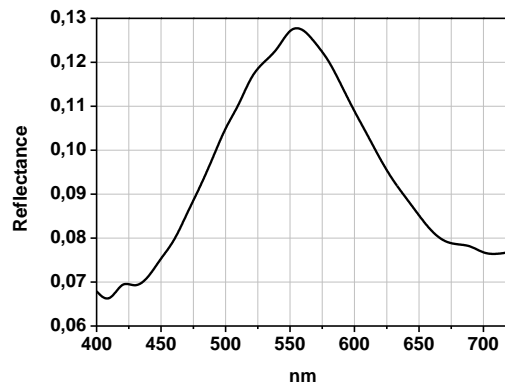
*Violet area*



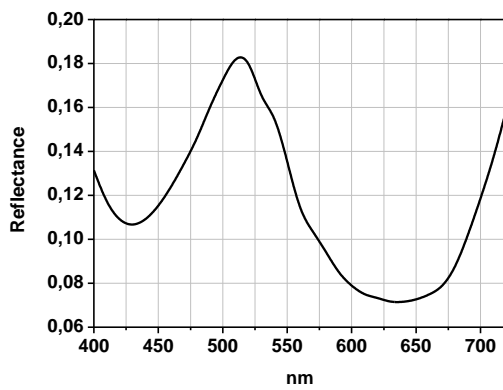
*Blue area*



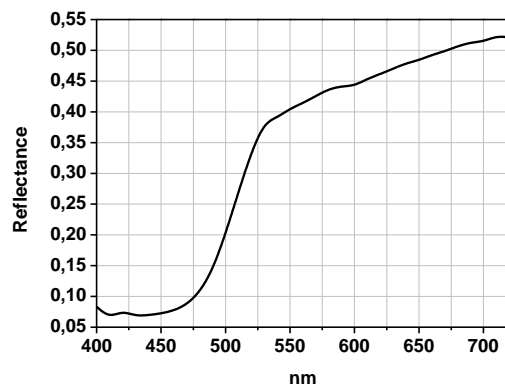
*Blue area*



*Green area*

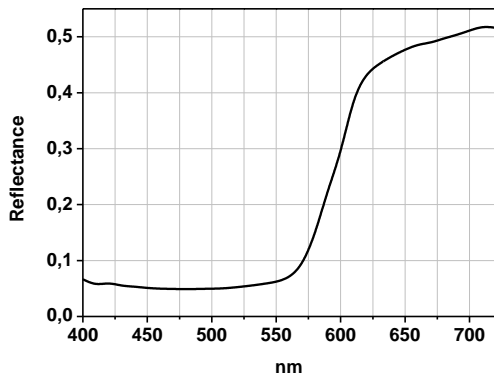


*Green area*

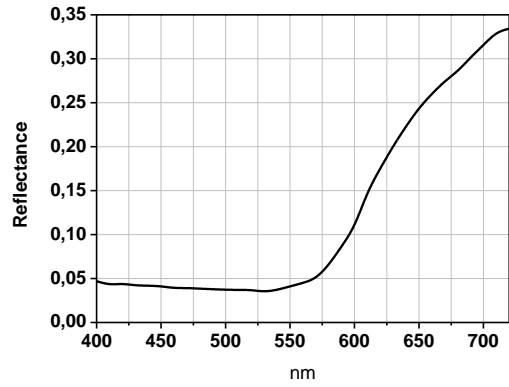


*Yellow area*





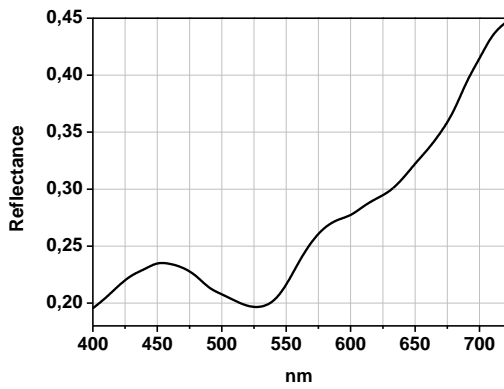
*Red area*



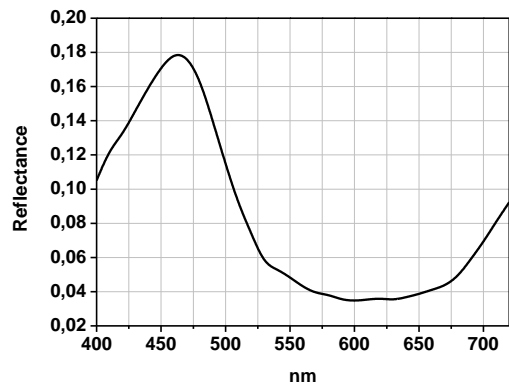
*Red area*

**Figure V.16** Representative Reflectance (hyperspectral imaging) spectra of violet, blue, green, yellow, red areas from *BRUT*.

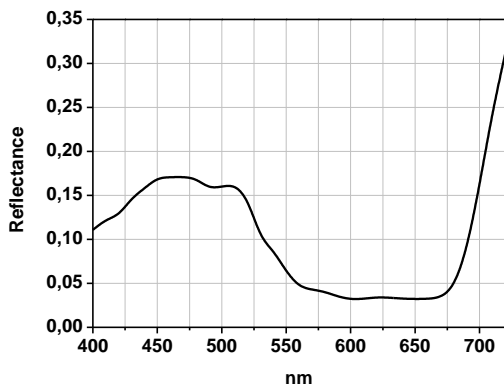
**Representative Reflectance (hyperspectral imaging) spectra from the painting *Entrada*.**



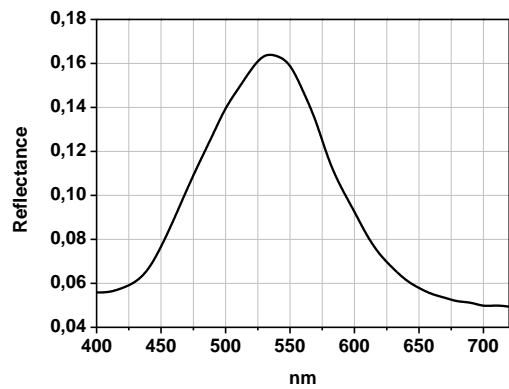
*Violet area*



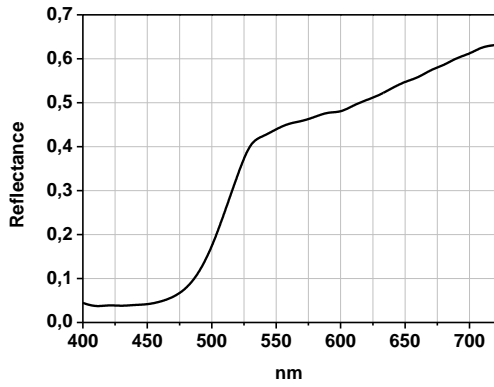
*Blue area*



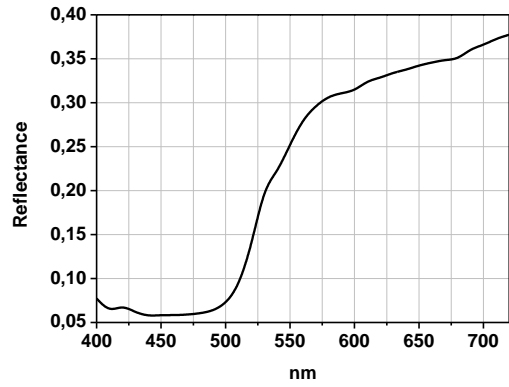
*Blue area*



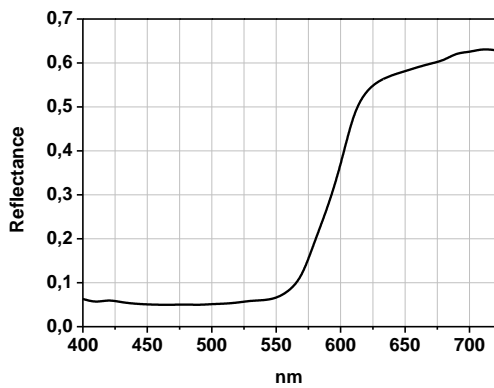
*Green area*



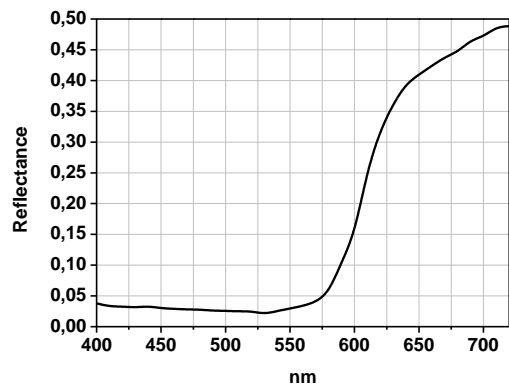
Yellow area



Orange area



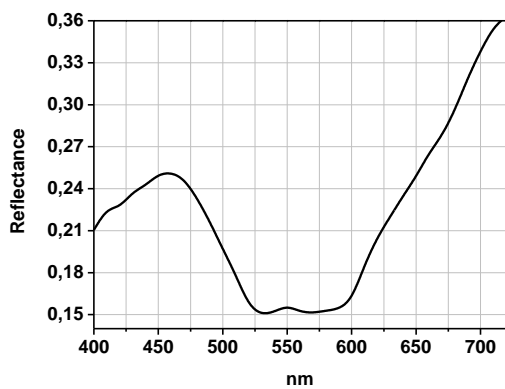
Red area



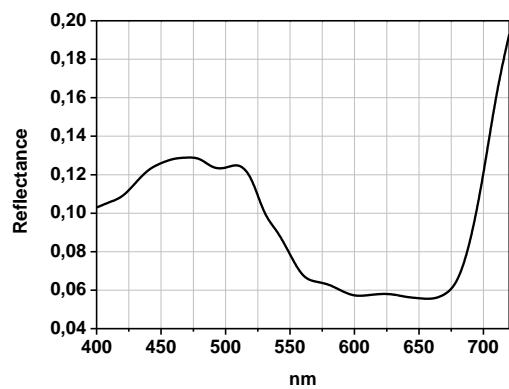
Red area

**Figure V.17** Representative Reflectance (hyperspectral imaging) spectra of violet, blue, green, yellow, orange, red areas from *Entrada*.

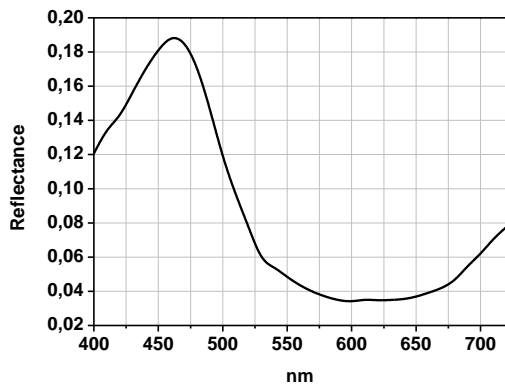
**Representative Reflectance (hyperspectral imaging) from the painting *Coty*.**



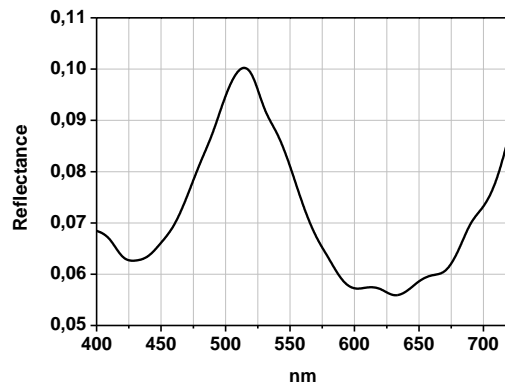
Violet area



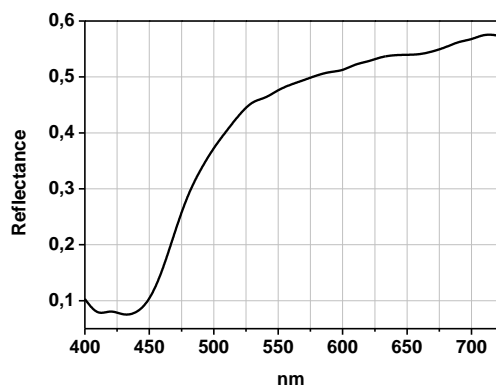
Blue area



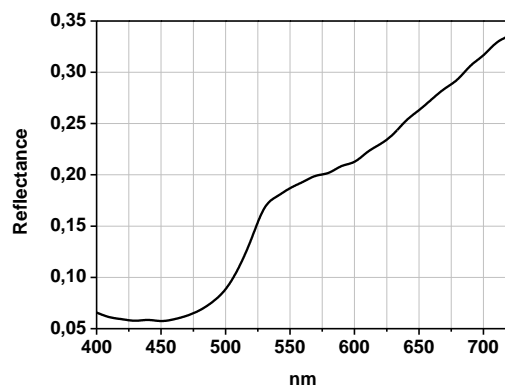
Blue area



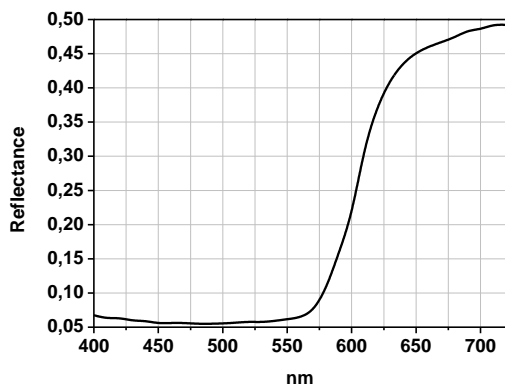
Green area



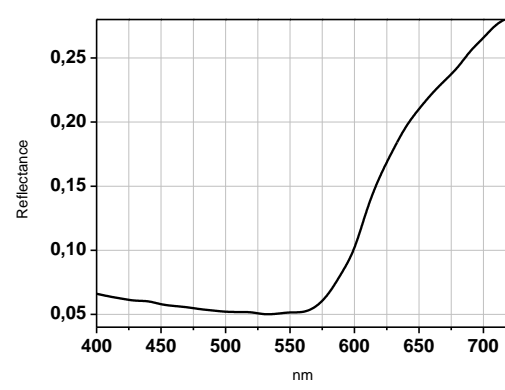
Yellow area



Yellow area



Red area



Red area

**Figure V.18** Representative Reflectance (hyperspectral imaging) spectra of violet, blue, green, yellow, red areas from *Coty*

Representative Reflectance (hyperspectral imaging) spectra from the painting *Untitled*.

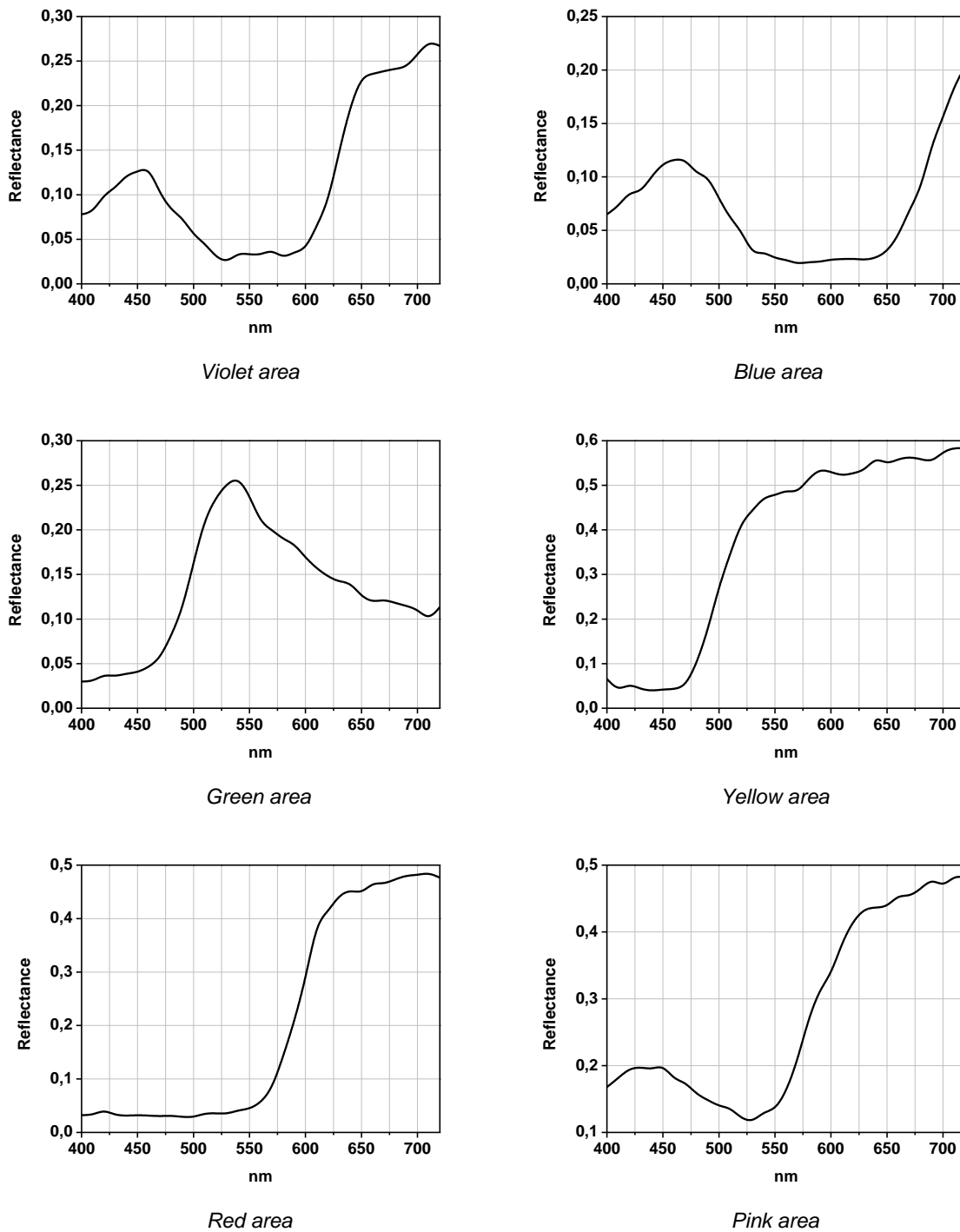


Figure V.19 Representative Reflectance (hyperspectral imaging) spectra of violet, blue, green, yellow, red, pink, areas from *Untitled*.

Appendix VI: SEM-EDS analysis on cross-sections and micro-samples

VI.1 Sampling areas



Figure VI.1 BRUT, areas of sampling of cross-section (•) and micro-samples (•)



Figure VI.2 Entrada, areas of sampling of cross-section (•) and micro-samples (•)



Figure VI.3 *Coty*, areas of sampling of cross-section (•) and micro-samples (•)

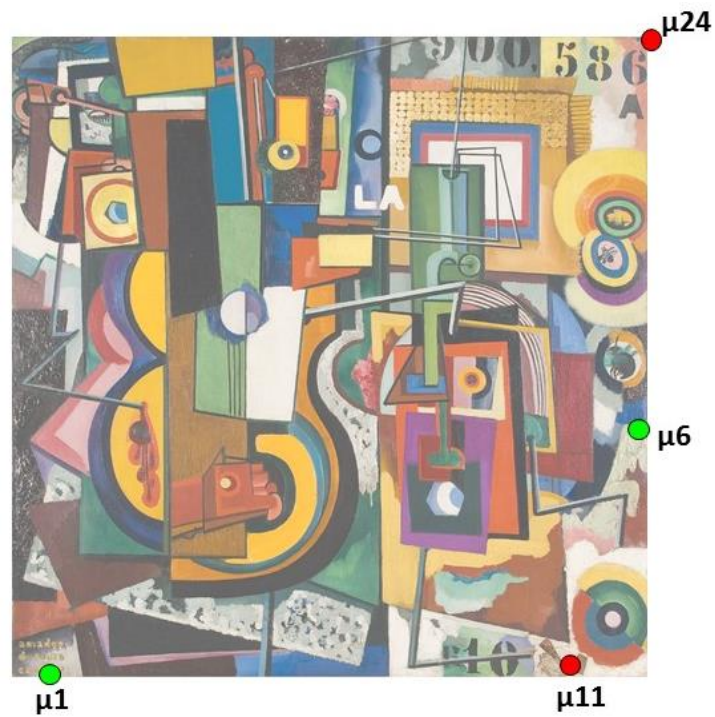


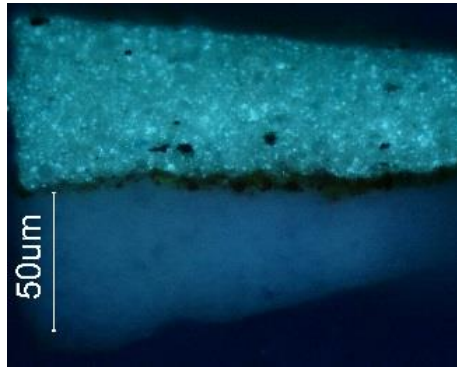
Figure VI.4 *Untitled*, areas of sampling of cross-section (•) and micro-samples (•)



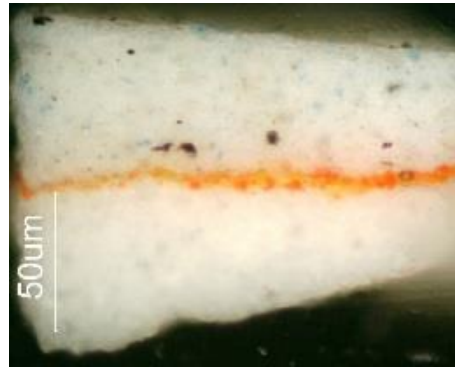
## VI.2 Cross-sections

### BRUT

μ12

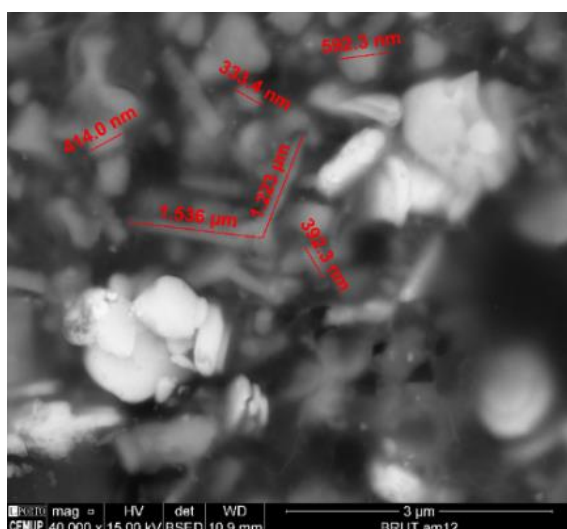
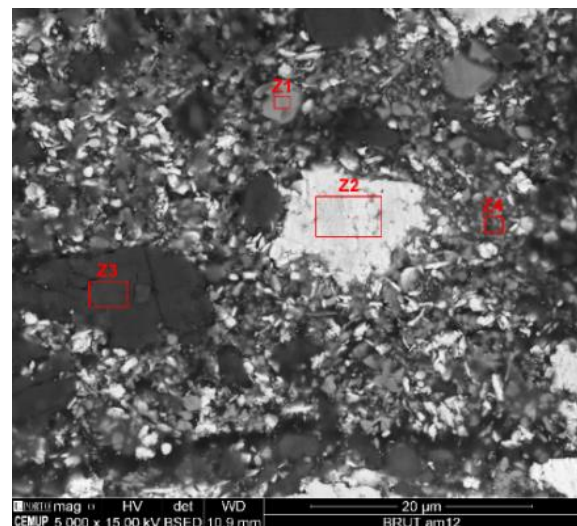
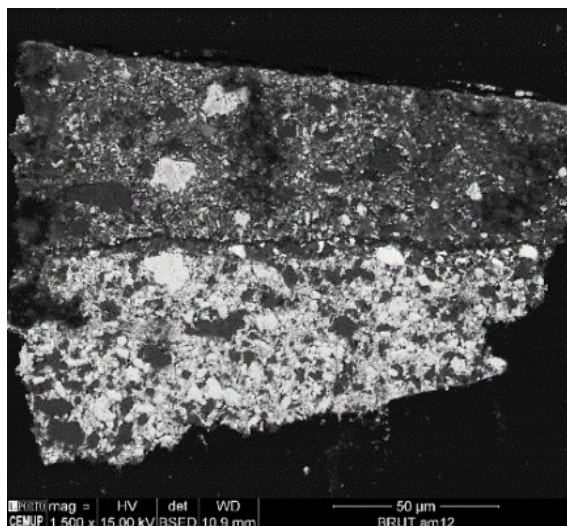


UV light



Visible light

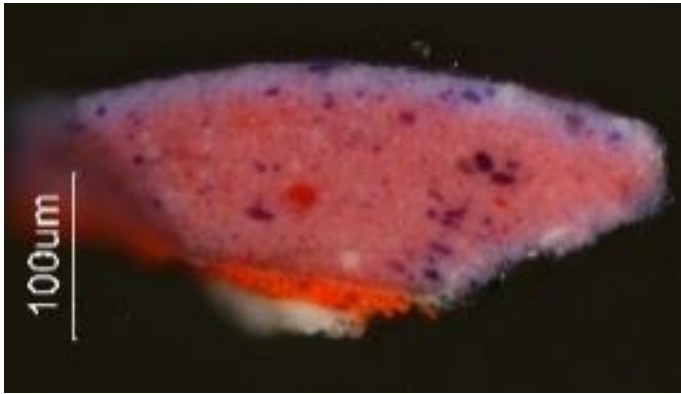
Gypsum; dark crystal pyrite (FeS<sub>2</sub>); zinc oxide; cerulean blue.  
 Vermilion; hematite; magnetite; baryte; lead white; SiO<sub>2</sub>.  
 Lead white; calcium carbonate; SiO<sub>2</sub> (SEM).



**Ground layer** lead white and calcium carbonate. **The red layer** is composed by vermilion, iron based pigment with the presence of Mg, Na, Al and BaSO<sub>4</sub>. The **top layer** (thickness ca. 50 μm) is characterized by the presence of large agglomerates of lead white (Z2) and large particles of gypsum (Z3). It also visible zinc white (c) with difference particle shape (tripod and rounded) and size (0.33-15 μm). On the blue particle it was detected Co and Sn (Z1) that suggest the presence of cerulean blue.

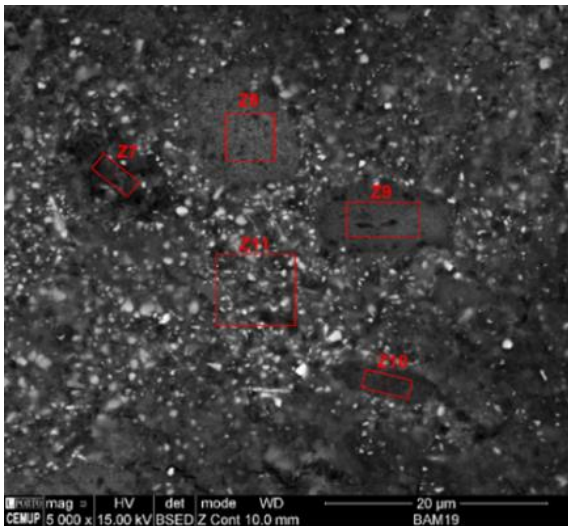
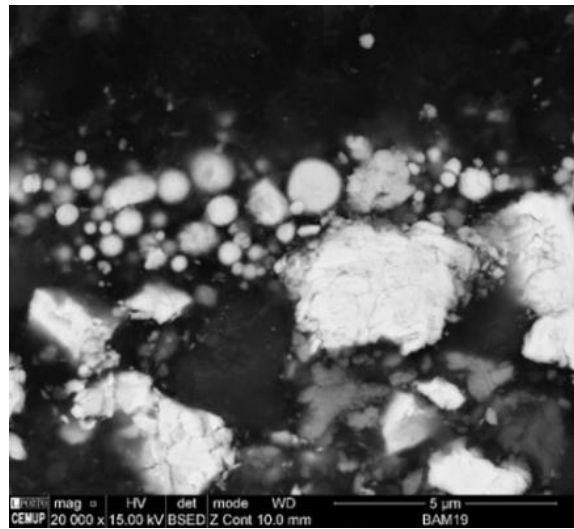
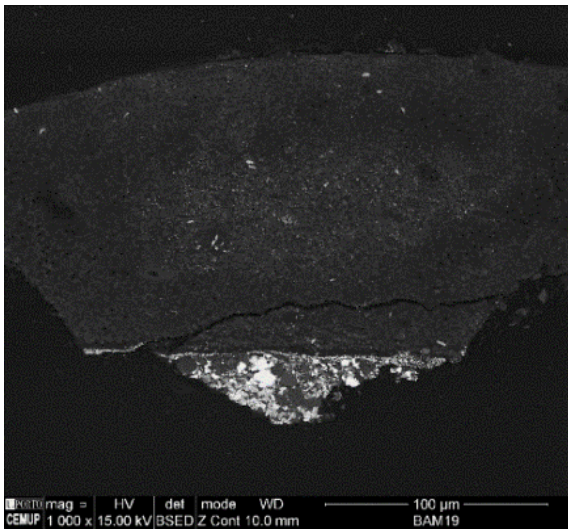


μ19



Visible light

- Cobalt blue, zinc white.
- Lead sulphate ; zinc white; Al in dark purple and red; Eosine based lake (SPEX); cobalt blue;
- Vermilion; hematite; magnetite; baryte; lead white; SiO<sub>2</sub>.
- Lead white; calcium carbonate.



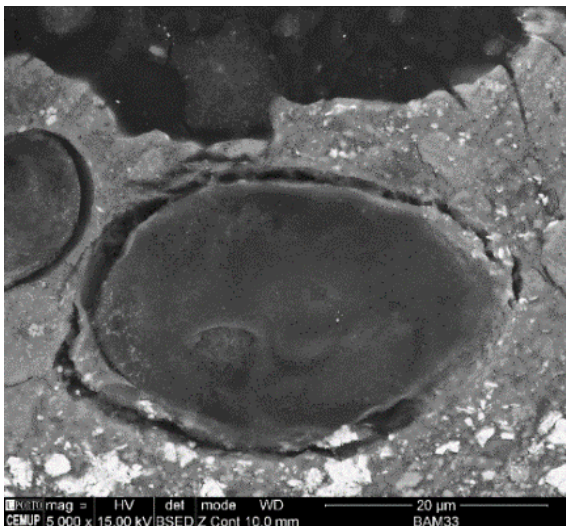
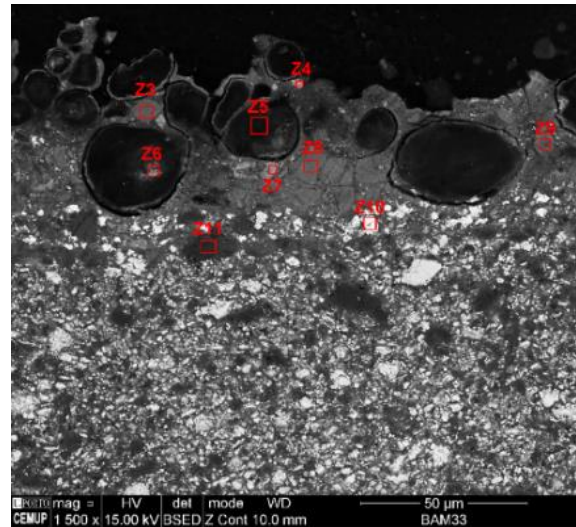
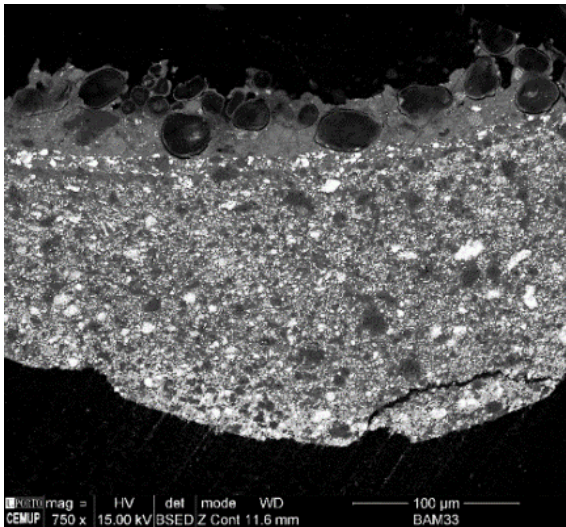
Over the red layer it is visible a thin layer of spherical particle of Pb (b). **Purple** (thickness ca. 130 μm). BSE image does not show a separation between the purple and blue layer. Al is clearly associated to the presence of dark purple, blue and red crystals. In the dark purple and blue crystal it was detected also the presence of cobalt, as for example in Z8, Z9, Z12 (dark purples) and Z14 (blue). This distribution could suggest the use of cobalt blue pigments and red lake. Finally magnesium was detected in correspondence with dark red crystals as for example Z7. **Zn** is homogenous distributed.

μ33



Visible light

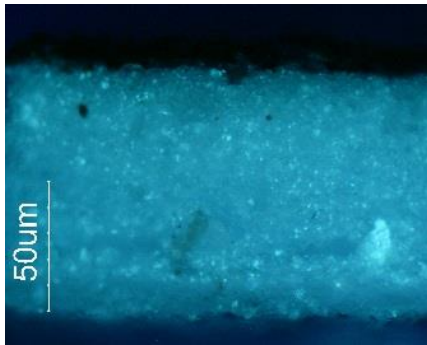
- Emerald green; barite. Starch (FITR)
- Vermilion; hematite; magnetite; barite; lead white; SiO<sub>2</sub>.
- Lead white; calcium carbonate



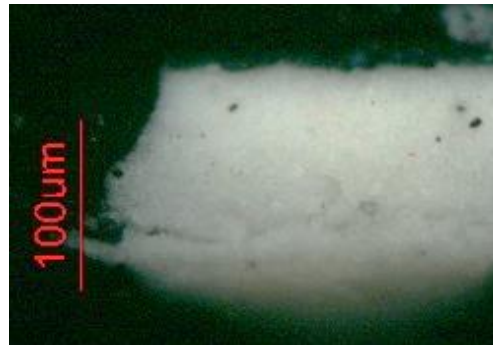
Green layer was detected Cu and As (Z3 and Z8), BaSO<sub>4</sub> (Z4 and Z7). On the green to layer are visible dark circular areas, similar to *bubbles*. These areas show different sizes from less than 10 μm to ca. 40 μm. In these areas SEM-EDS analysis detected high content of carbon and lower amount of Pb, As and Cu (Z5). The fractures, around the *bubbles*, suggest that the organic material that has filled the cavities reduced in the volume causing breakage of the adjacent area. FTIR analysis in this area and in the area am6 detected high amount of starch. The presence of the same kind of *bubbles* in the am6 excluded the possibility that the cavity were filled by the resin used to prepare the cross-section.



μ5

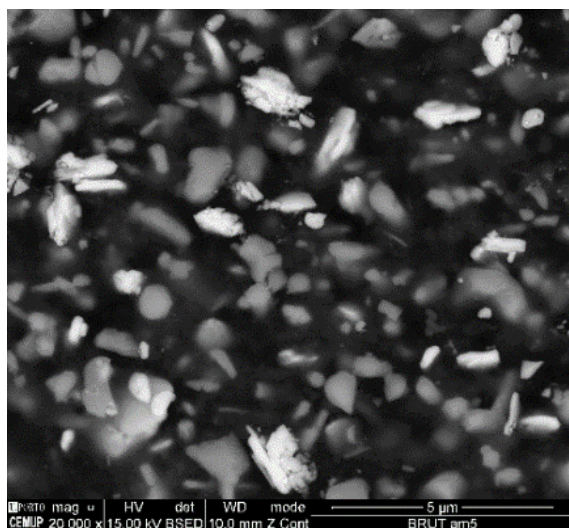
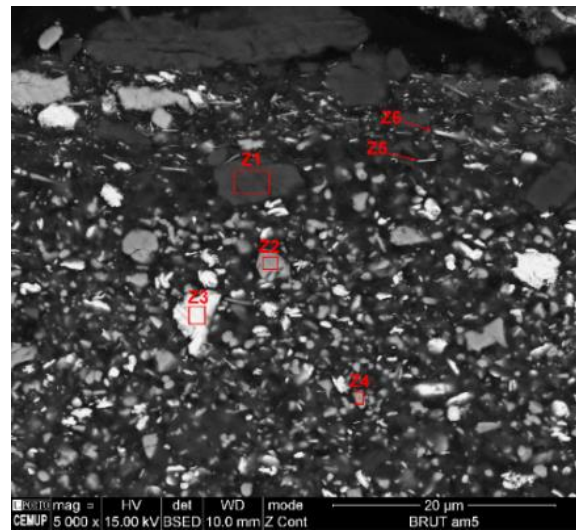
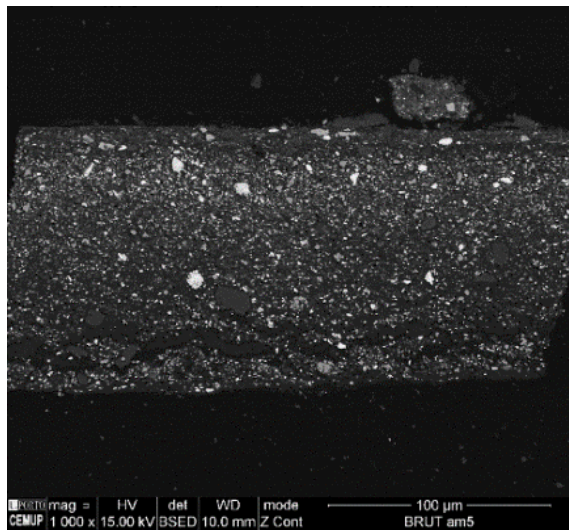


UV light



Visible light

Prussian blue; chrome yellow; lead white; calcium carbonate  
Zinc oxide; lead white; zinc soap;



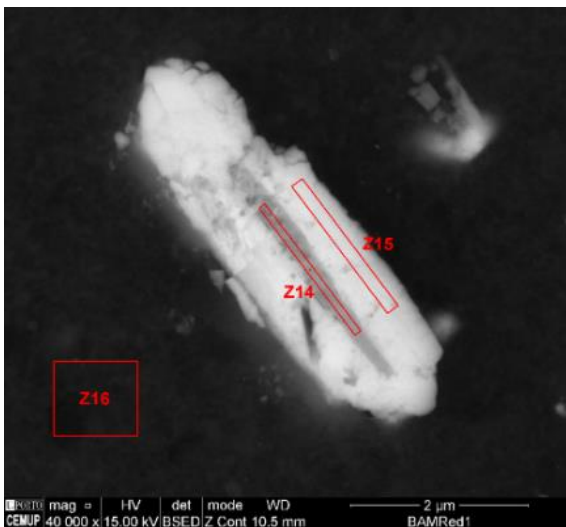
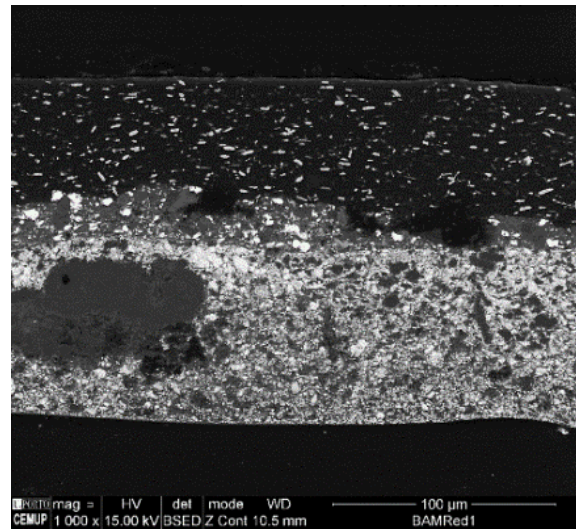
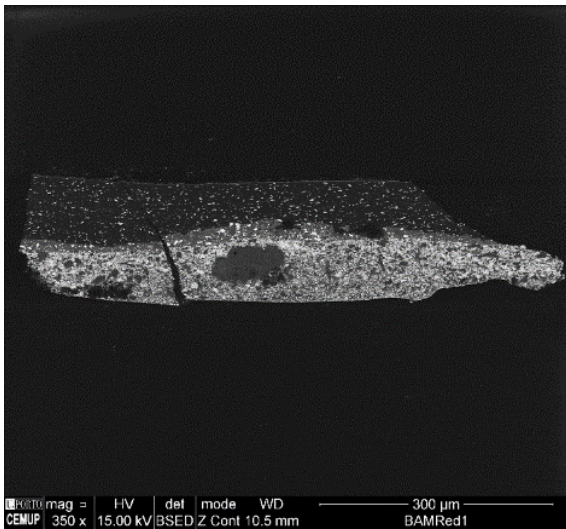
In the **white** layer (thickness ca.100 μm) was detected particle aggregates of lead white. SEM-EDS analysis detected the presence of zinc with the particles size from 0,24 and 1.3 μm (c) . In the **green** layer it was detected Cr, Fe, K (Z6 and Z7) that results support those obtained by Raman in the identification of Prussian blue and chrome yellow. The chrome yellow particles have rod-like shape. Calcium and phosphate were detected in the same particle that suggest the presence of carbon black. In all the cross-section it was detected aluminium.

# µRed1



Visible light

- Alizarine; purpurine (SPEX, FTIR). Al in the matrix (SEM) and elongates white particles of barium sulphate covered with lead.
- Vermilion; hematite; magnetite; baryte; lead white; SiO<sub>2</sub> (SEM).
- Lead white; calcium carbonate.



The **ground** layer (thickness ca.75 µm) is composed by lead white and calcium carbonate. The **red** layer show a uniform thickness (min. 5 µm and max. 20 µm). The layer is composed by vermilion, iron oxide, manganese and silica. In the **top** layer it is visible elongated white particles on a “dark matrix”. In the matrix was detected Al and a small amount of Pb ( Z16). The Al could be associated to the presence of a red lake. The lead is probably related with the surrounding particles. The white particles show a core of BaSO<sub>4</sub> (Z14) covered by Pb (Z15), possibly PbSO<sub>4</sub>. The particles measure 7.5 µm in length and 2 µm of thinness. The core measures a thinness of 0.3 µm



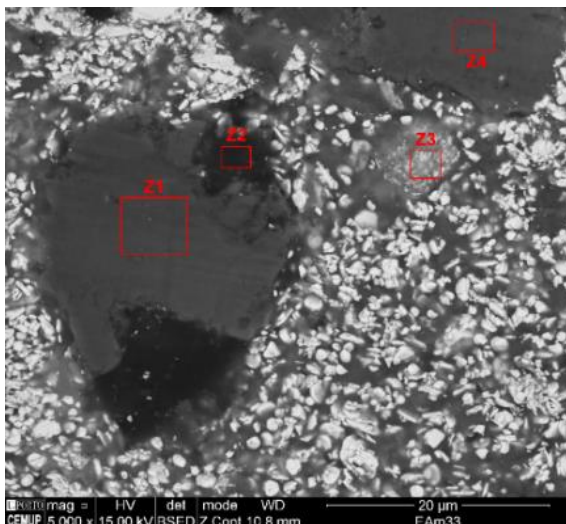
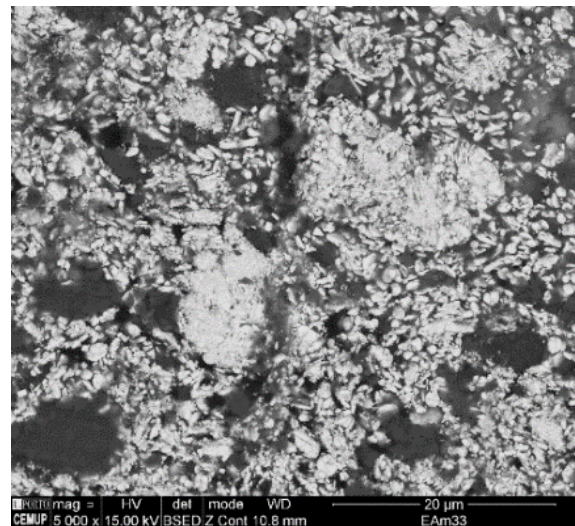
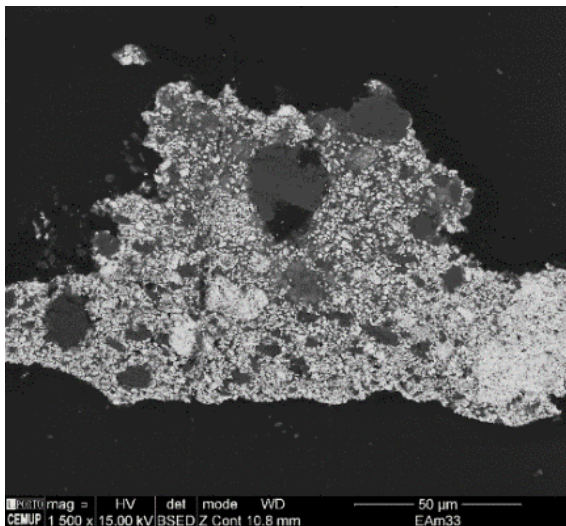
## Entrada

μ33



Visible light

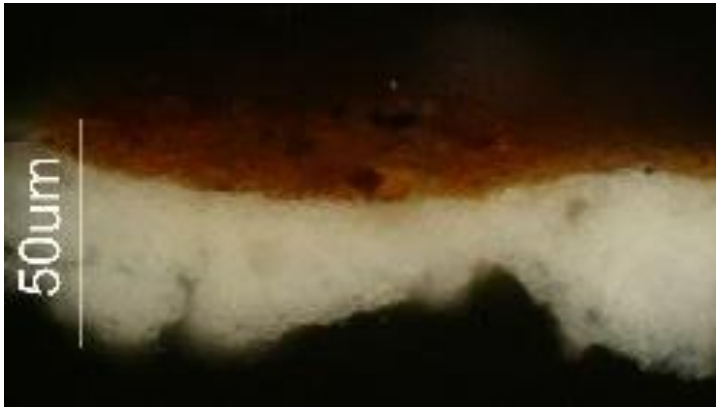
Lead white, calcium carbonate. Black crystal: carbon black; yellow crystal: silica (SiO<sub>2</sub>); hematite.



This cross-section include only the ground and it is partial covered by the resin. The maximum thickness is ca. 100 μm. Similar to the other ground layer it is visible an agglomerate of lead white particle Dutch method, (b). It is present particles of CaCO<sub>3</sub> with different sizes, the biggest one measures ca. 30 μm. Al was detected in Z1, Z2 and Z4 associated to Ca. In Z4 was detected also a small amount of Mg.

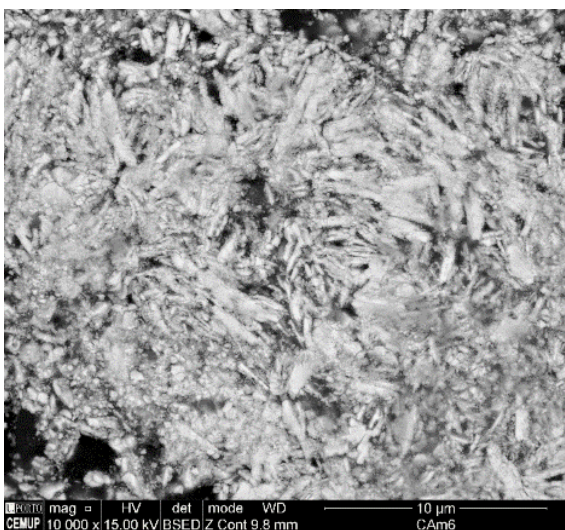
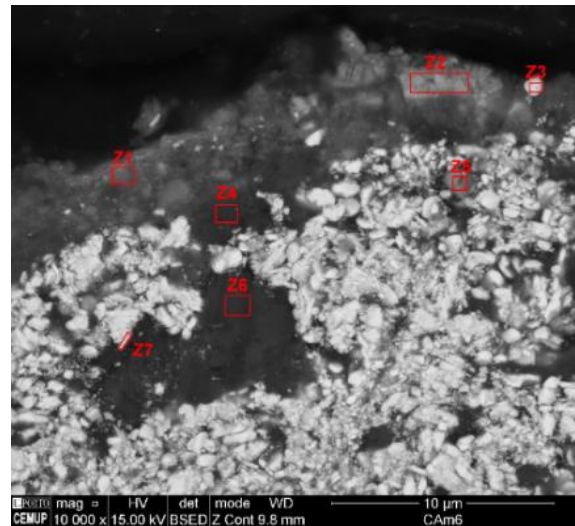
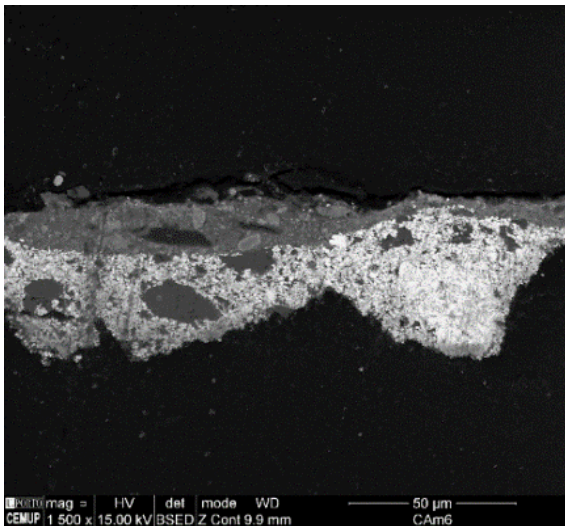
# Coty

μ6



Visible light

■ Hematite; magnetite; goethite; lead white.  
■ Lead white, calcium carbonate

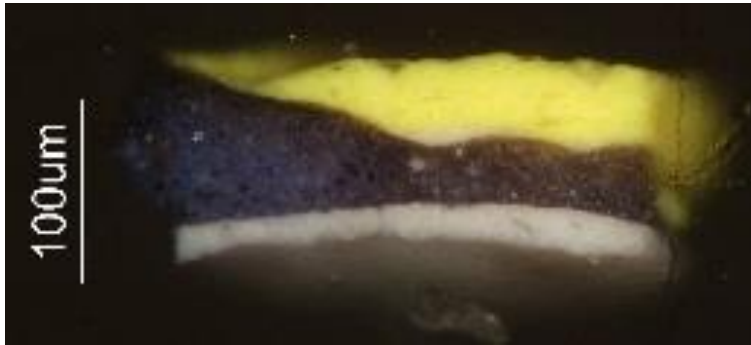


In the **ground** layer detected lead white and calcium carbonate. In © an agglomerate of lead white particle (Dutch method). The maximum thickness of the ground is 45 μm. The **brown-red** layer is composed by iron based pigment and lead white (Z3). Iron was detected associated with manganese (Z5), silicon and magnesium (Z11).



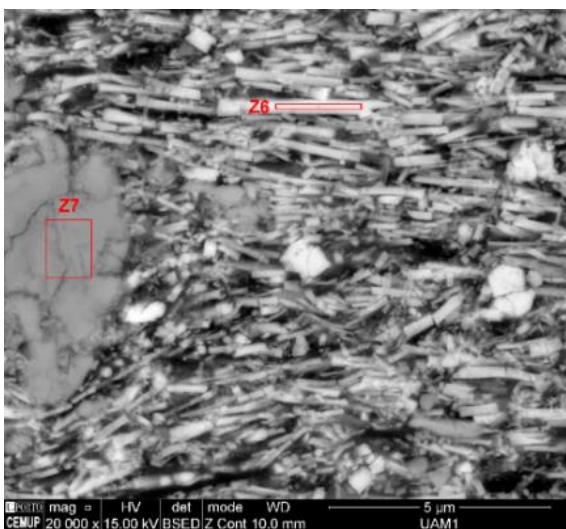
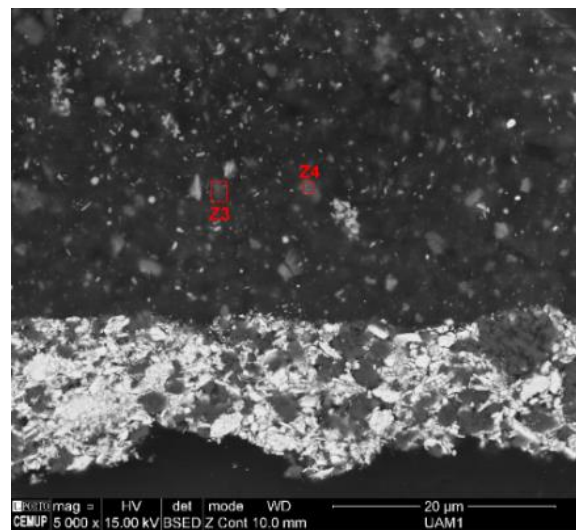
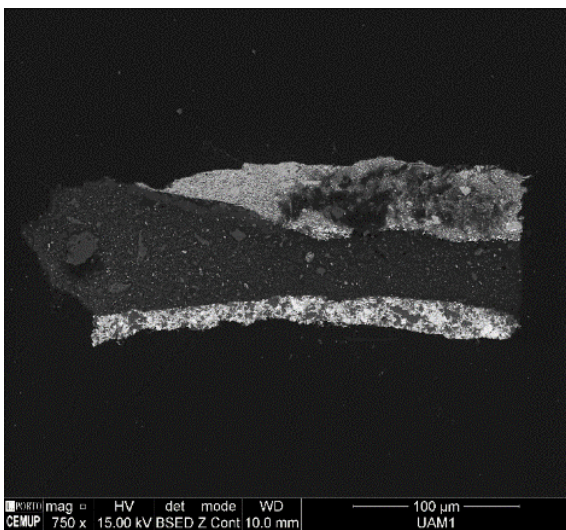
# Untitled

μ1



Visible light

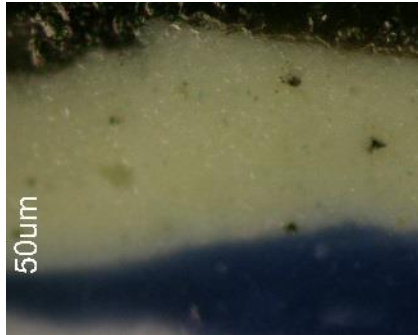
- Mixed chrome yellow; barite; zinc soap.
- Lead white; gypsum.
- Ultramarine blue; ivory black; zinc white (SEM)
- Lead white; calcium carbonate



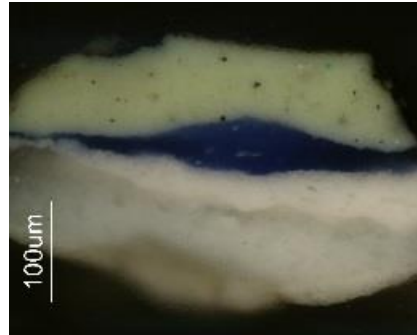
In the **ground** layer (max. thickness 22 μm) was detected lead white and calcium carbonate. In the **blue** particles (Z3) was detected Na, Al, S and Si that confirm the presence of Ultramarine blue detected by Raman. In the same particles were detected small amount of Fe and K. In the Z4 it was detected calcium and phosphorus that suggest the presence of ivory black. Zinc was detected in all the point of analysis performed in the blue layer. The maximum thickness of the layer is ca. 75 μm. Between the blue and the yellow layer it is visible a **white** layer composed by lead white and gypsum. In the **yellow** layer was detected lead chromate (Z6) rod-like particles with different dimensions, 0.4 - 4 μm in length and 0.07-0.4 μm in width. Large aggregates of BaSO<sub>4</sub> (Z7) sub-rounded particles are also observed.



μ6

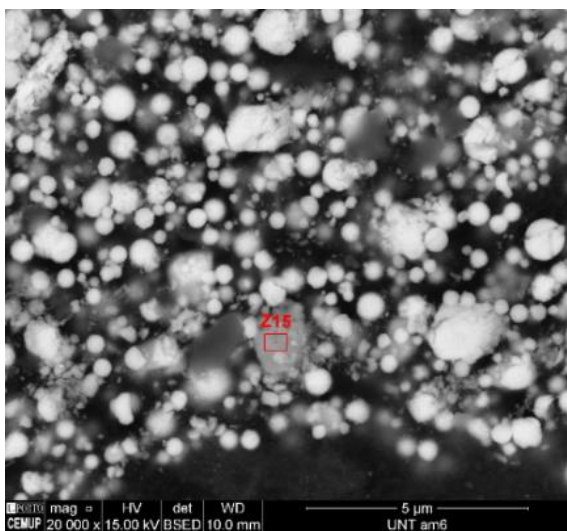
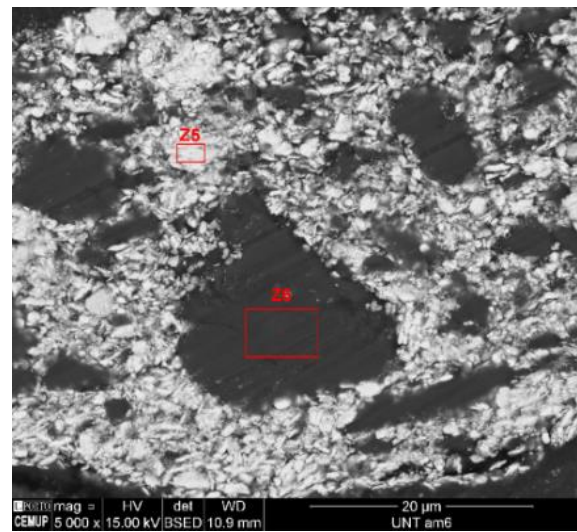
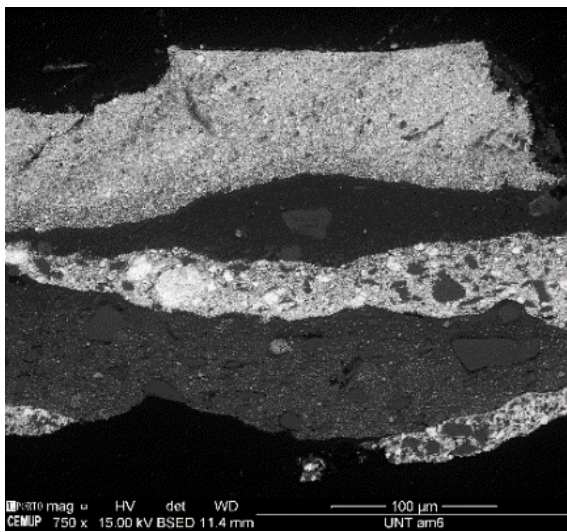


Visible light



Visible light

- Lanarkite ( $Pb_2(SO_4)O$ ), black crystal: carbon black; red crystal: hematite; blue crystal: cerulean blue (SEM), barite; Cobalt blue; zinc white; Fluorescence (RAMAN).
- Gypsum; lead white.
- Gypsum; zinc white
- Calcium carbonate; lead white.



By SEM-EDS analysis it is possible to observe 5 layers. In the **ground** layer was detected calcium carbonate and lead.

Over the ground layer are visible two white layers: the 1<sup>st</sup> with gypsum and zinc white and in the 2<sup>nd</sup> gypsum (Z6) and lead white (Z5).

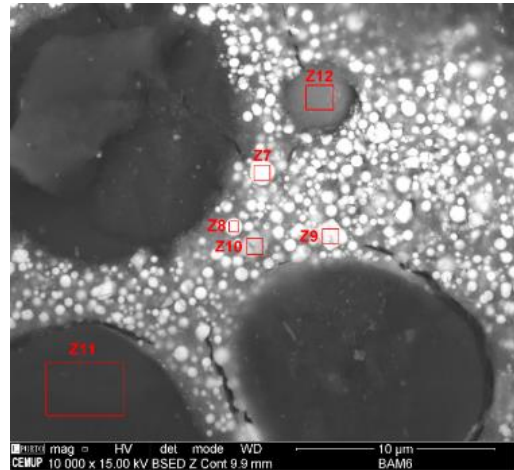
In the **blue** layer it was detected Zn and Co associate with Al that suggest the presence of cobalt blue.

In the **yellow-greenish** layer are visible few particles of Aluminium oxide, cerulean blue; barite (Z15) but the mainly are round particle of lead or lead oxide (c).

## VI.3 Micro-samples

### BRUT

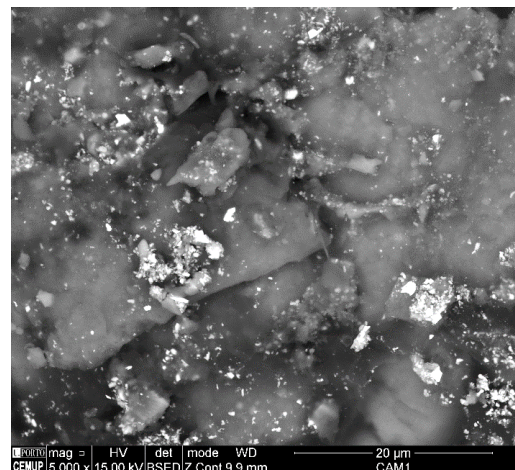
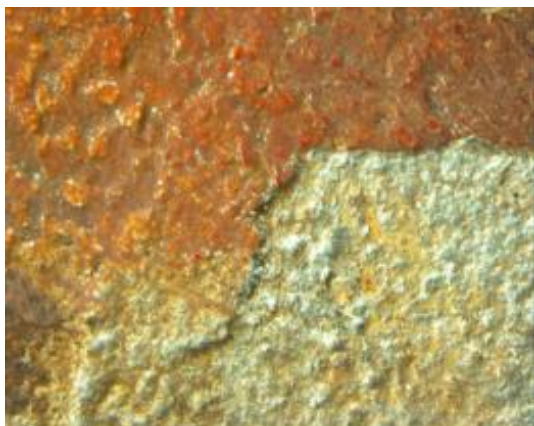
**μ6** Starch (FTIR); emerald green; aluminium-silicate and iron based pigments; barite; lead *spheres*.



SEM-EDS analysis detected the presence of Cu associated with As, that suggest the use of emerald green. In this sample are visible dark circular *bubbles*, similar those present in the cross-section BRUT am33. SEM-EDS analysis detected high amount of C and low amount of Cu, As and Pb. In few particles it was detected Si, Al associated with Fe iron (Z12) and with titanium (Z1 and Z13). These elements suggest the presence of aluminium-silicate and iron based pigments. On all the sample spherical particles of lead (Z7, Z8 and Z9) were present. Few particles of BaSO<sub>4</sub> were also detected.

### Coty

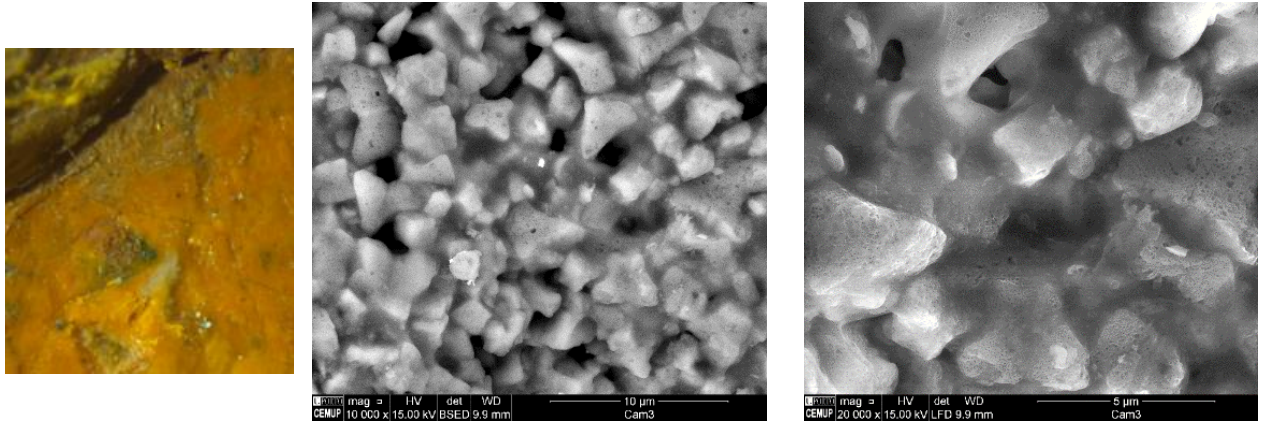
**μ1** Brown: hematite, barite. Silver: Al, Zn.



The BSE image doesn't allow to understand the morphology of the silver coloured materials. SEM-EDS analysis detected Al, Zn, Ca and Pb. Ca and Pb are related to the preparation layer where the silver coloured material was applied (Z1).

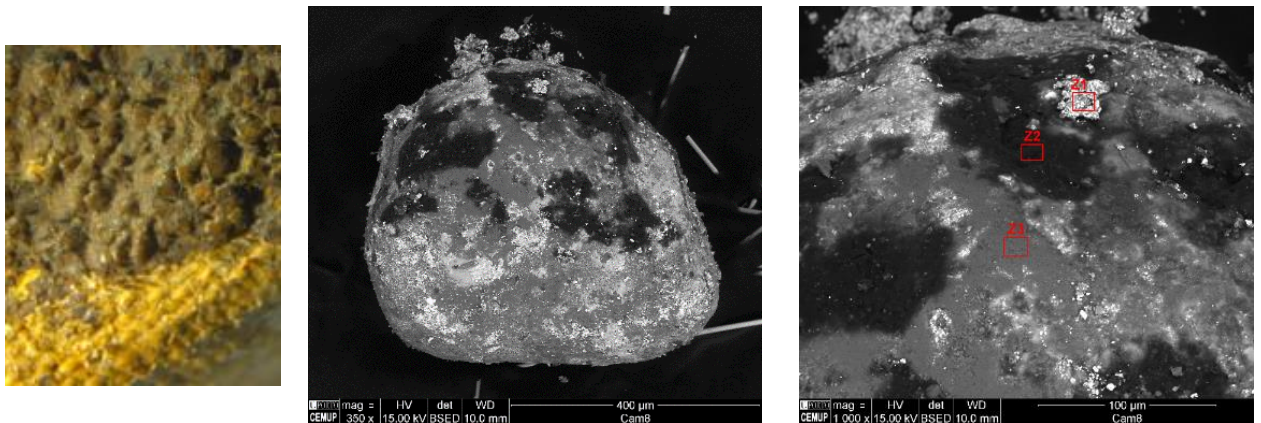


**μ3** Cobalt yellow



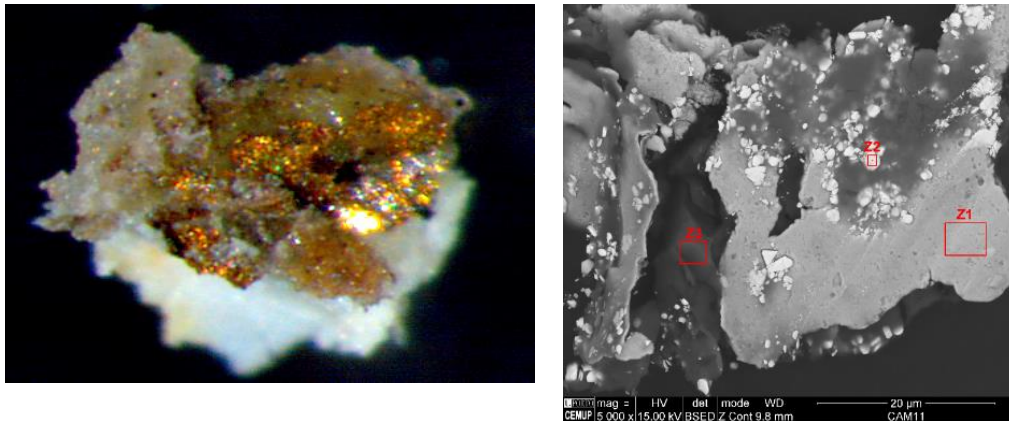
The BSE image shows a tetrahedron –like particles. The elemental maps show a uniform distribution of Co, Na and K. The distribution of the Al is not uniform but localised, it was not possible to make a correlation between the map of the distribution of Al and the presence of particles shape different from those of the yellow cobalt. In the surface of the particles are visible small hole.

**μ8** Brown: hematite, manganese oxide, gypsum, lead white. Sphere: silica (SiO<sub>2</sub>)



SEM-EDS analysis confirm the presence of silica. The silica shows a round shape with a diameter around 530 μm. The elements Fe, Mn and Pb are related with the presence of iron and manganese based pigments used in the brown paint that covered the silica particles

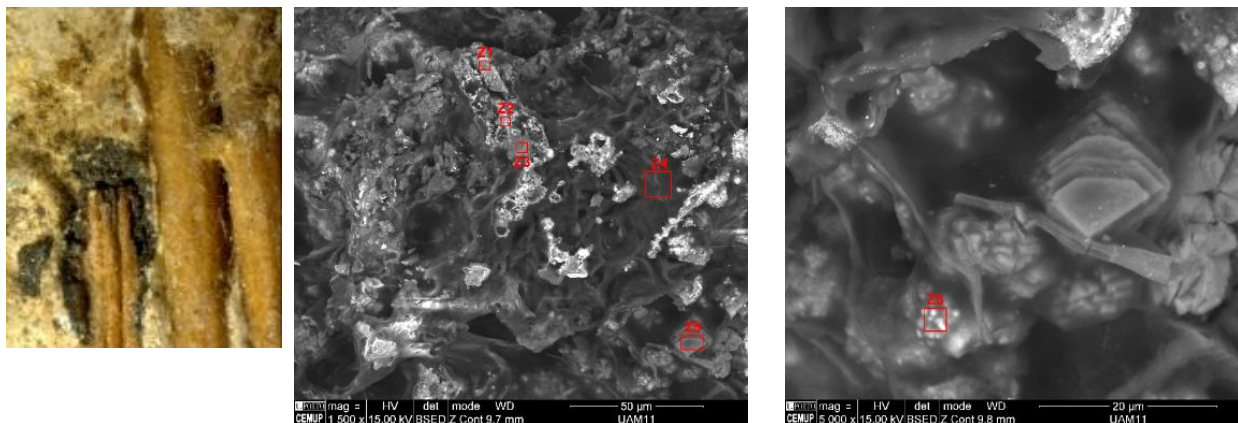
**μ11** White: calcium carbonate, gypsum. Gold: copper and zinc.



From the BSE image seems that the gold coloured material was applied as foil. The thickness of the foil is around 350 nm. SEM-EDS analysis detected copper and Zn (Z1). Also in this case the Ca and Pb (Z2) could be related to the preparation layer.

### Untitled

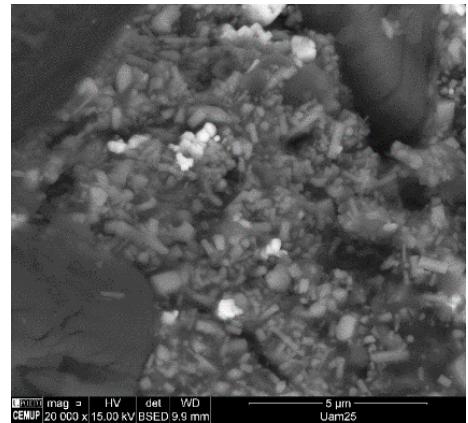
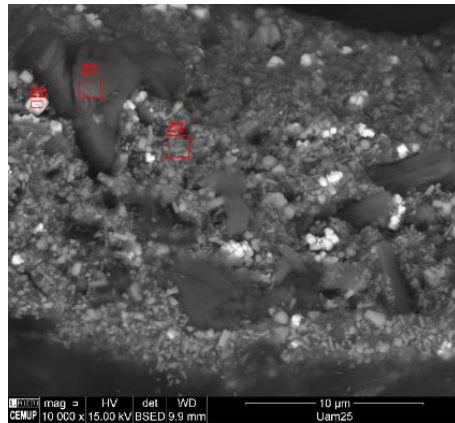
**μ11**



This sample comes from the *heat* of the matches applied in the painting. The samples is extremely porous. The SEM-EDS analysis revealed  $\text{CaCO}_3$  and  $\text{Al}_2\text{O}_3$  that are usually used as inert materials in matches.

Pb, P, Sb, Cl and K were also detected. It is possible suggest presence of antimony trisulfide ( $\text{SbS}_3$ ) and potassium chlorate as ignite materials. The presence of phosphorus can be attributed to the presence of white phosphorous or to phosphorus sesquisulfide ( $\text{P}_4\text{S}_3$ ). The phosphorus sesquisulfide was introduced in France in the 1897 to replace the toxic white phosphorus ( $\text{P}_4$ ). Berne Convention (1906) with which the European countries banned the 'use matches made with white phosphorus.

## $\mu$ 24 Pink



SEM-EDS analysis detected the presence of gypsum (Z1) and a mixture of vermilion (HgS) and zinc white (Z3).

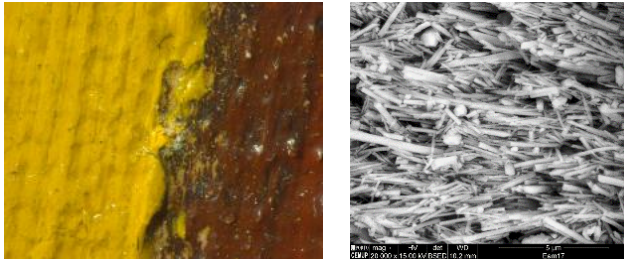


## Appendix VII: Chrome yellow samples analysis

This appendix presents the characterization of the chrome yellows samples collected on the paintings *BRUT*, *Entrada* and *Untitled*.

### VII.1 SEM-EDS analysis of *Entrada*, *BRUT* and *Untitled* samples

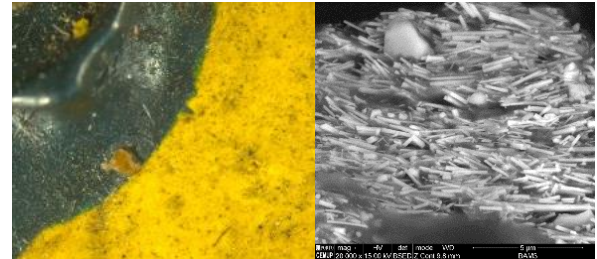
#### *Entrada*



$\mu 17$

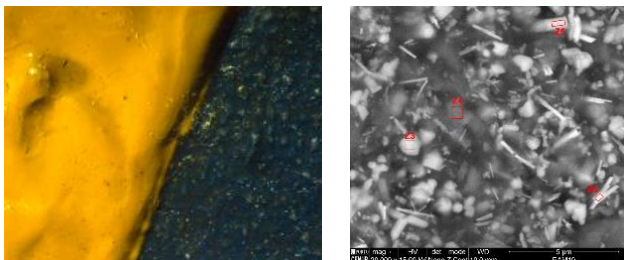
**Mixed-crystals of lead chromate and lead sulphate** rod-like particles (0.3 - 3  $\mu\text{m}$  in length and 0.07 - 0.4  $\mu\text{m}$  in width). Sub-rounded particles probably corresponds to a **phoenicochroite**. **No fillers** were detected.

#### *BRUT*



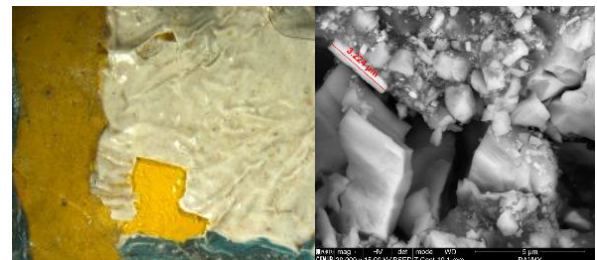
$\mu 3$

**Lead chromate** rod-like particles (0.3 - 3  $\mu\text{m}$  in length and 0.07 - 0.3  $\mu\text{m}$  in width). Possibly a particle of **phoenicochroite**. **BaSO<sub>4</sub>** rough and irregular shape. **Al** and **Mg** were detected in all analysed areas



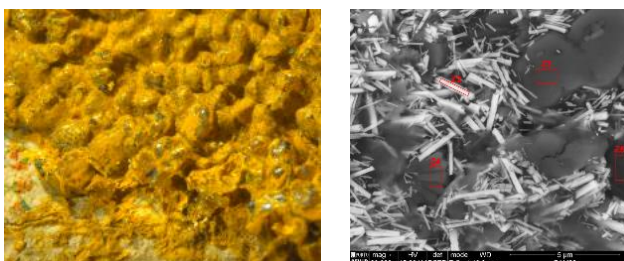
$\mu 19$

A small content of **lead chromate** rod-like particles (0.4 - 2  $\mu\text{m}$  in length and 0.07-0.3  $\mu\text{m}$  in width). High content of **CaSO<sub>4</sub>** and several rounded, rod-like and tetrapod-like, particles of **ZnO**. Rough and irregular shape of **SrSO<sub>4</sub>** and an aggregate of **CaCO<sub>3</sub>**.



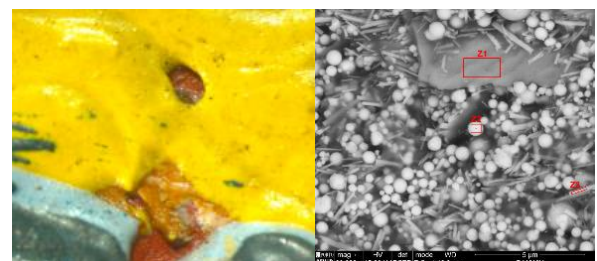
$\mu 4$

Small particles **lead chromate** rod-like particles (0.4 - 3  $\mu\text{m}$  in length and 0.1 - 0.6  $\mu\text{m}$  in width). High content of **BaSO<sub>4</sub>**, **CaSO<sub>4</sub>** and **Si**-based particle.



$\mu 32$

SEM-EDS analysis shows a high content of **lead chromate** rod-like particles (Z2) with dimensions between 0.3 and 2  $\mu\text{m}$  in length and 0.07 and 0.3  $\mu\text{m}$  in width.



$\mu 16$  orange and yellow

SEM-EDS analysis revealed the presence of a high content of spherical **lead particles** (Z2) together with **lead chromate** rod-like particles (Z3) with dimensions





## VII.2 $\mu$ FTIR

### Entrada

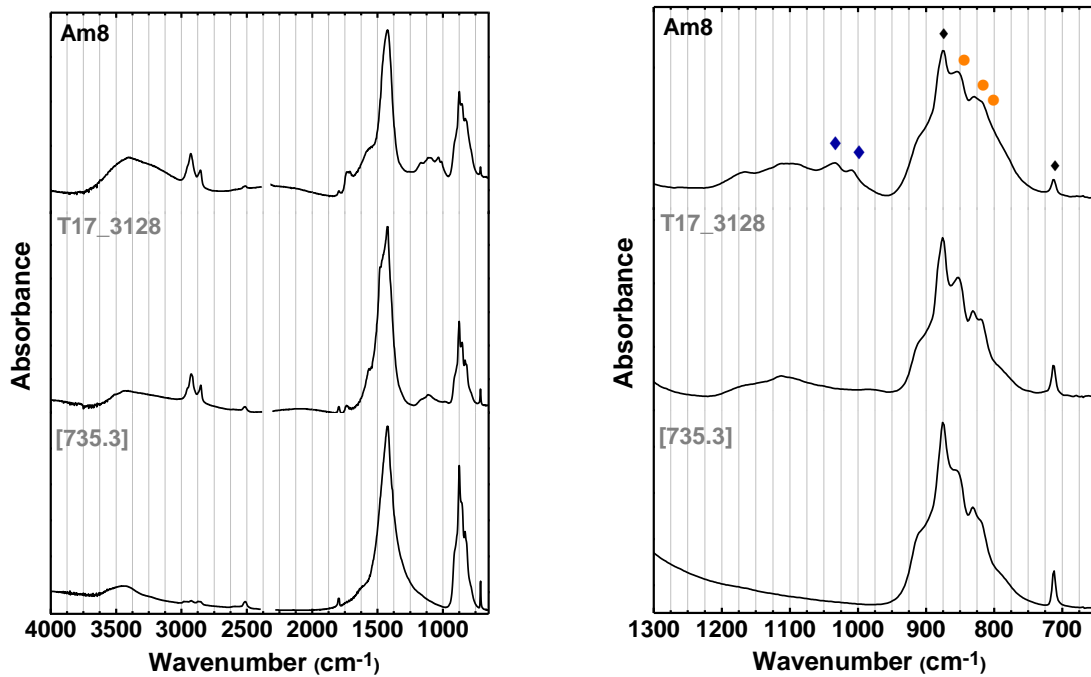


**Figure VII.1.** Infrared spectra sample  $\mu 8$  *Entrada*; Columbano Tube T17\_3128 and 735.5 reconstruction  
 ●  $\text{PbCrO}_4$ ; ◆  $\text{CaCO}_3$ ; ◆ kaolinite.

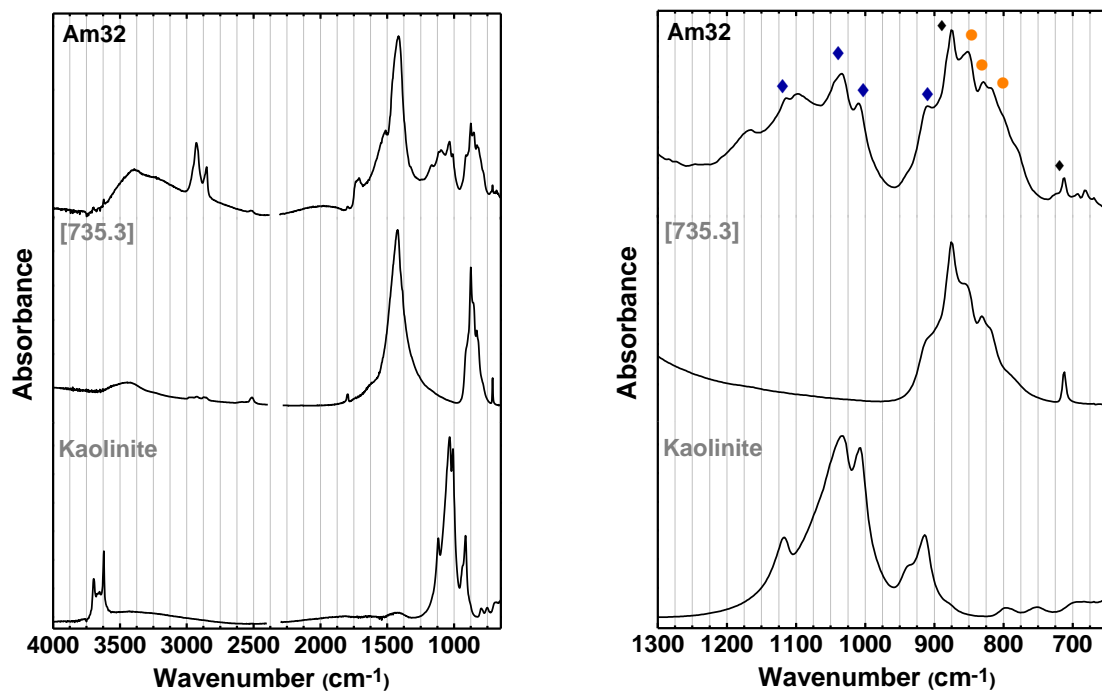


**Figure VII.2** Infrared spectra sample  $\mu 32$  *Entrada*; Columbano Tube T17\_3128 and 735.5 reconstruction.  
 ●  $\text{PbCrO}_4$ ; ◆  $\text{CaCO}_3$ ; ◆ kaolinite

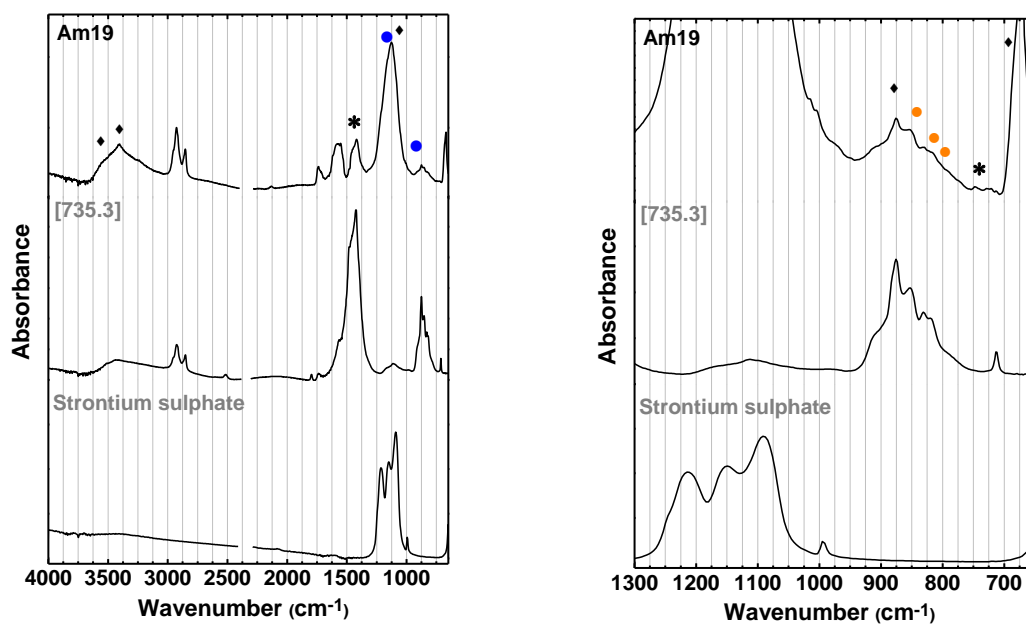


**Figure VII.3.** Infrared spectra sample  $\mu 19$  Entrada; Columbano Tube T17\_3128 and 735.5 reconstruction.  
 ● PbCrO<sub>4</sub>; ◆ Gypsum; \* CaCO<sub>3</sub>; ● SrSO<sub>4</sub>.

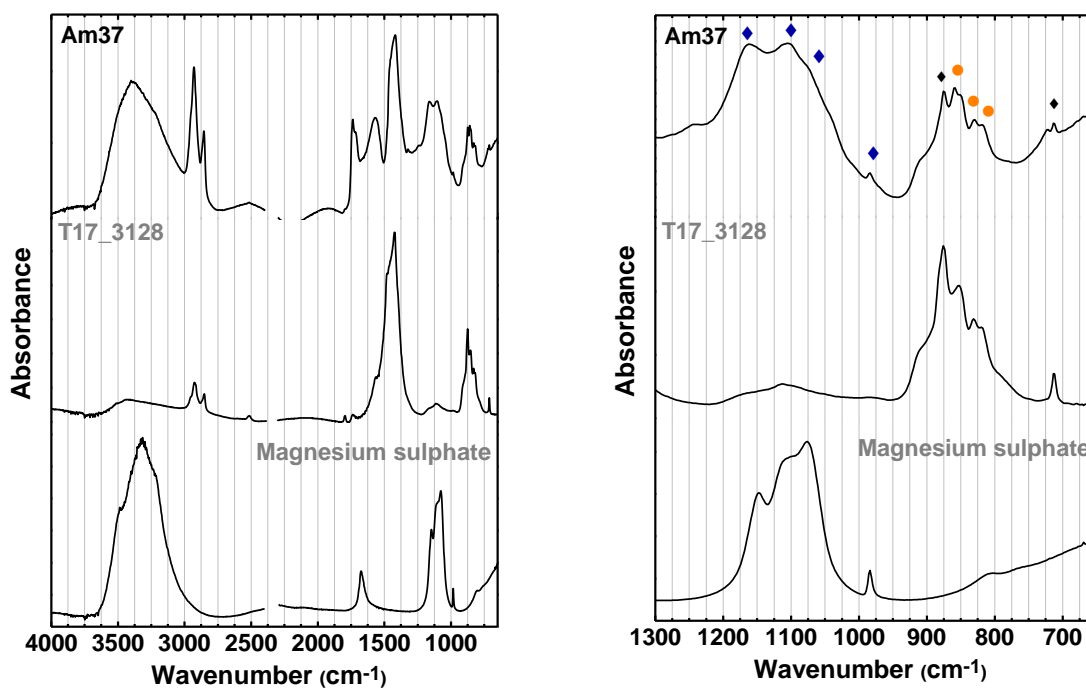


**Figure VII.4.** Infrared spectra sample  $\mu 37$  Entrada; Columbano Tube T17\_3128 and magnesium sulphate heptahydrate.  
 ● PbCrO<sub>4</sub>; ◆ CaCO<sub>3</sub>; ◆ MgSO<sub>4</sub> 7H<sub>2</sub>O

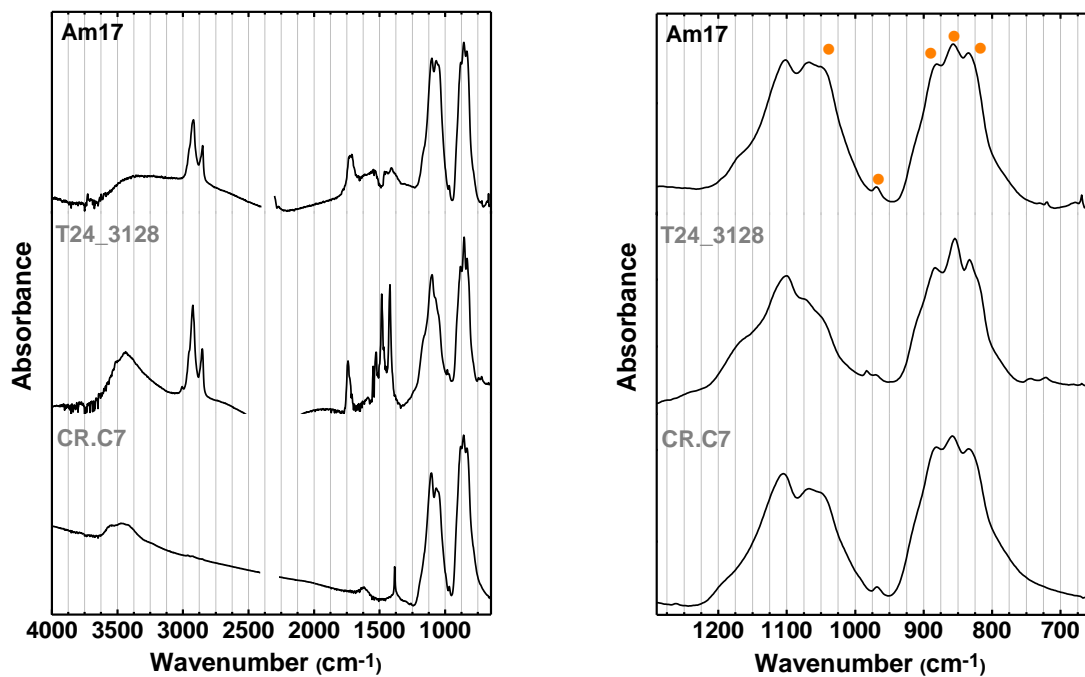


Figure VII.5. Infrared spectra sample  $\mu 17$  *Entrada*; Columbano tube T24\_3128 and CR.C7 0.4 Molar fraction chromate and 0.6 sulphate. ●  $\text{Pb}(\text{Cr,S})\text{O}_4$ .

### BRUT

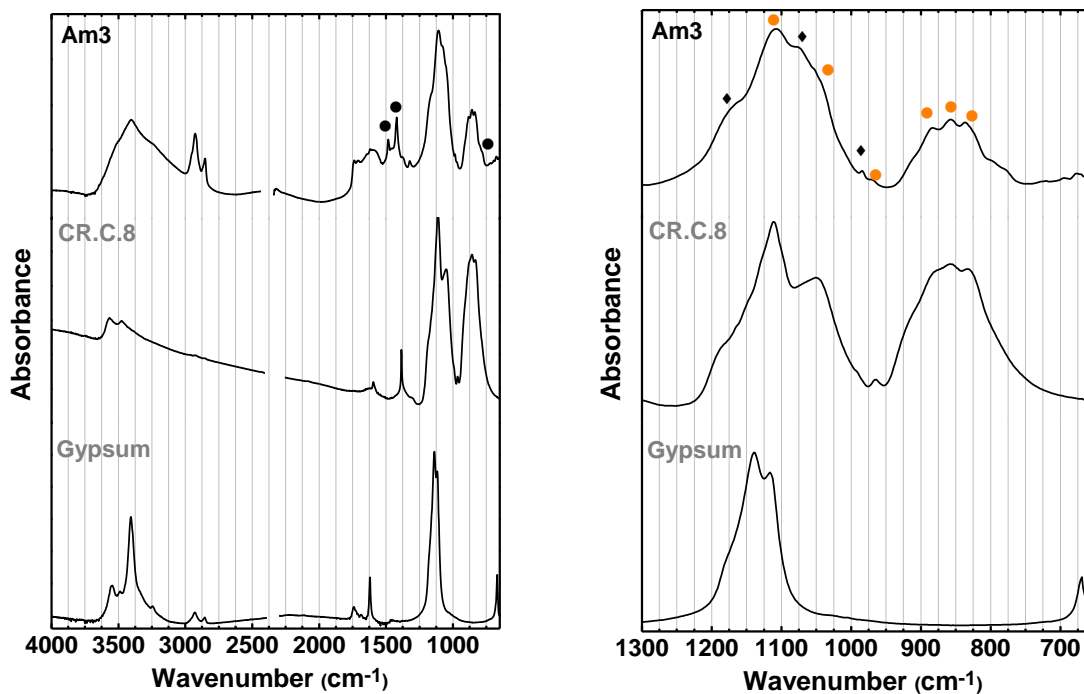


Figure VII.6. Infrared spectra sample  $\mu 3$  *BRUT*; CR.C.8 with 0.3 Molar fraction chromate and 0.7 sulphate  
●  $\text{Pb}(\text{Cr,S})\text{O}_4$ ; ◆  $\text{BaSO}_4$ ; ●  $\text{MgCO}_3$ .

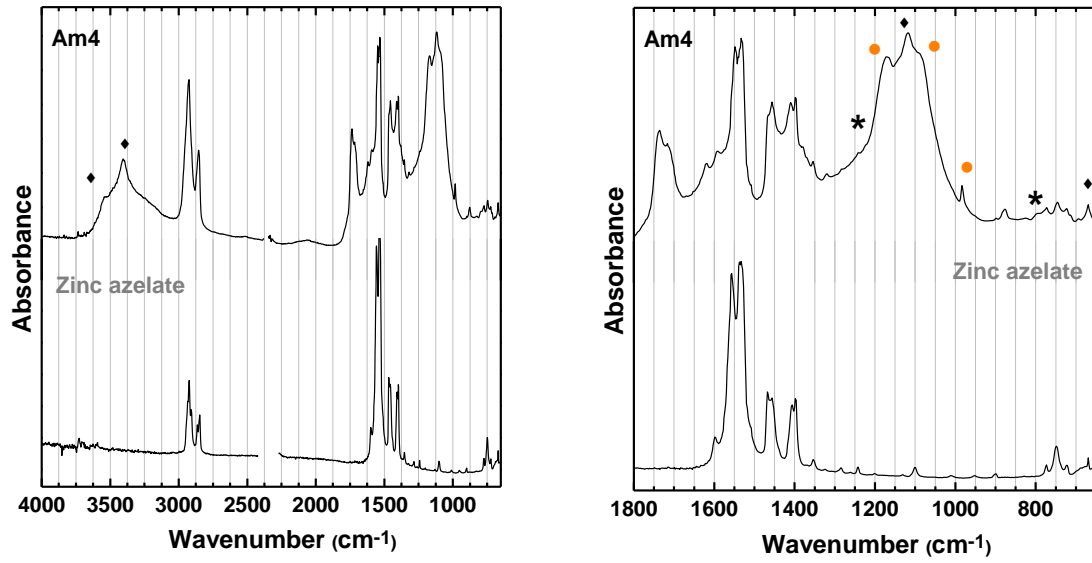


Figure VII.7. Infrared spectra sample  $\mu 4$  BRUT; ● BaSO<sub>4</sub>; ◆ gypsum; \* quartz.

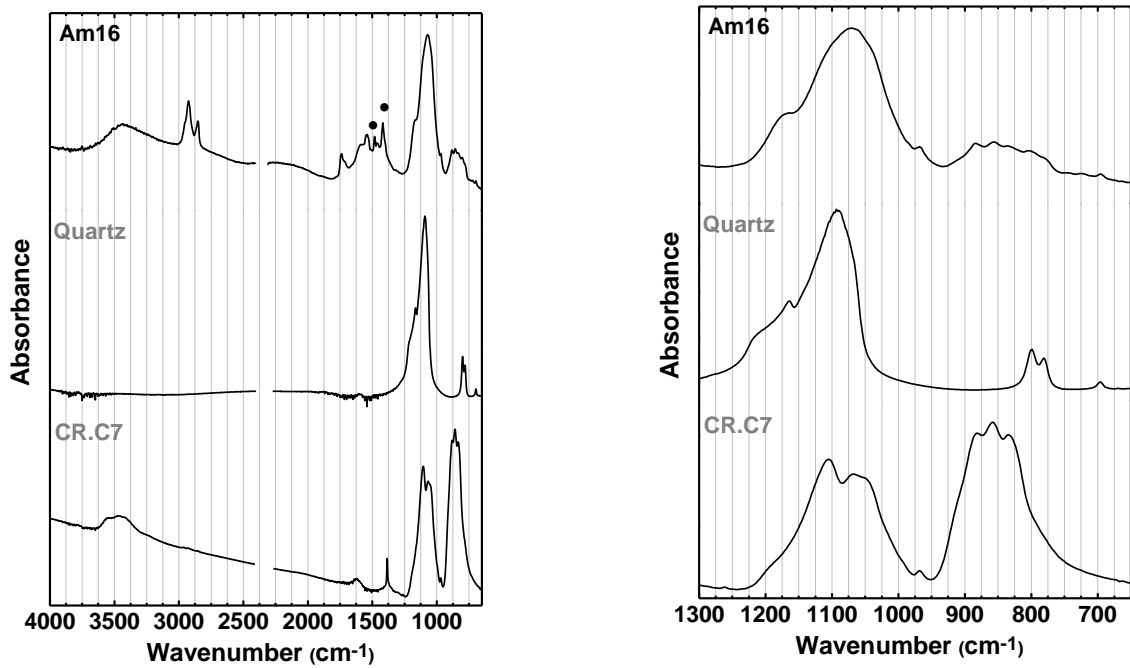


Figure VII.8. Infrared spectra sample  $\mu 16$  BRUT, CR.C7 0.4 Molar fraction chromate and 0.6 sulphate. ● MgCO<sub>3</sub>

## VII.3 Synchrotron analysis

Two sample from the paintings BRUT and Entrada were analyzed by SR  $\mu$ -IR spectroscopy, SR  $\mu$ -XRF and  $\mu$ -XANES. Both of the samples are a solid mixed phase crystal of lead chromate and lead sulfate,  $\text{Pb}(\text{Cr},\text{S})\text{O}_4$ . In the BRUT sample it was detected the presence of magnesium carbonate, barytes and quartz. Metal carboxylates were also found, comparing the IR spectra with reference carboxylate suggests the presence of zinc azelate. The absorption of the carboxylate is homogenous in all the sample, no aggregates are visible. The intensity profile of Cr K line calculated from the XRF maps at 6.12 and 6.02 keV beam energies in the Entrada sample suggests that no degradation has occurred. XANES analysis performed in both the samples identified Cr(VI) compound(s), supporting that no degradation is visible.

### Post-processing data

PyMca program was used to fit the different absorption region for the IR spectra and the different elemental contribution in the fluorescence spectra. The same program was used as a batch fitting procedure for IR and XRF maps.

All XANES spectra were normalized using ATHENA software program. Edge-step normalization of the data was carry out by means of linear pre-edge subtraction and by regression of a quadratic polynominal beyond the edge. *ATHENA was also used to perform a linear combination fitting of the unknown XANES spectra with a library of Cr-species compounds. The best fitting was selected from a large number of different combination of the reference spectra.*

## Results

### **BRUTam17**

$\mu$ -IR spectroscopy and  $\mu$ -XRF analysis of BRUT a17 samples confirmed the presence a solid mixed phase crystal,  $\text{Pb}(\text{Cr},\text{S})\text{O}_4$ . Barium was detected in few points of the sample otherwise,  $\text{MgCO}_3$  was found almost homogeneously distributed in the entire sample (Figure VII.9).

In the region between 1250 and 950  $\text{cm}^{-1}$  it is visible the contribution of the  $\nu\text{SO}_4^{2-}$  of barite as well as the sulphate of the chrome mixed crystal. The widening of the band suggest also the presence of quartz. Elemental analysis detected the presence of Si that is mapped on Figure VII.10. The IR spectra of quartz is characterized for the absorption bands at 1094  $\text{cm}^{-1}$ , 790, 780 and 696  $\text{cm}^{-1}$ . Unfortunately the low ration S/N of the SR-IR spectra difficult the identification of these absorptions.

Figure VII.11 compares two spectra acquired from the same paint area, one obtained by SR- $\mu$ IR in  $\text{BaF}_2$  cell and one by  $\mu$ -FTIR in diamond cell with the range 4000-650  $\text{cm}^{-1}$  ( $\mu$ 15 BRUT) where it is visible the absorption bands of the quartz at lower wavenumbers. The characteristic bands of metal carboxylates are visible in the region 1550-1537  $\text{cm}^{-1}$  and in the broad band centred at 1581  $\text{cm}^{-1}$  these two regions are mapped in the Figure VII.9 E and F, respectively and are attributed to the presence of zinc azelate. Similar spectroscopic features were detected in the zinc white sample tube (ASC8).

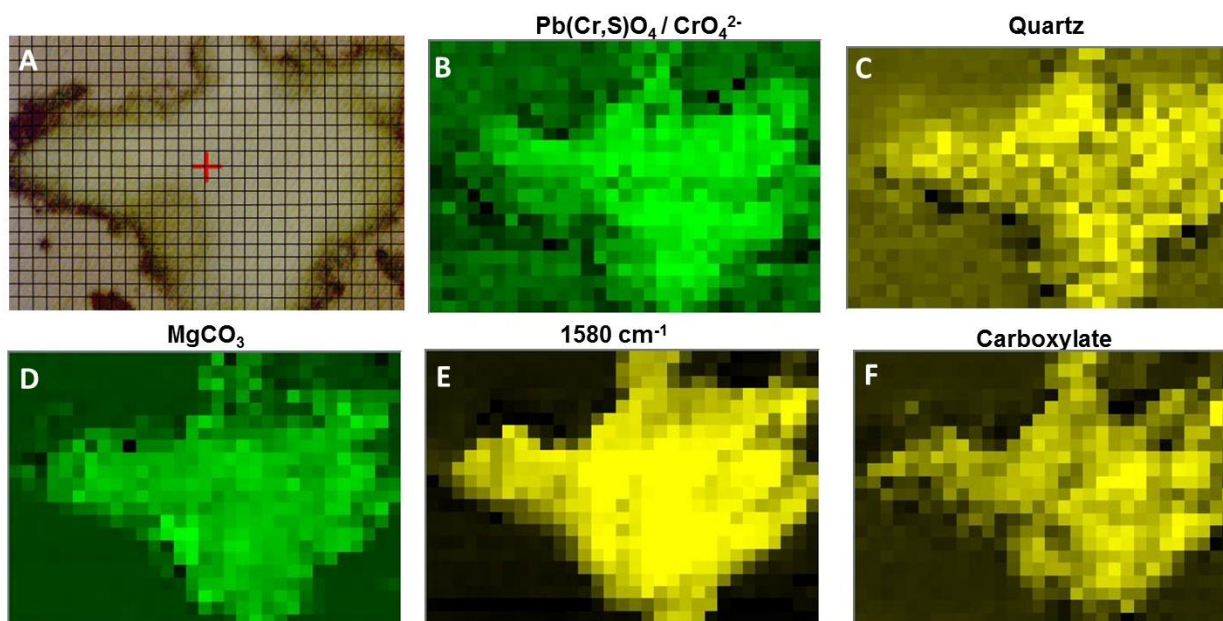


**Figure VII.9.** Visible light microscope with the mapping area marked in red; RGB composite images obtained by  $\mu$ -IR: **B** mixed lead chromate (975-966  $\text{cm}^{-1}$ ); **C** Quartz (1170-1157  $\text{cm}^{-1}$ ); **D**  $\text{MgCO}_3$  (1500-1398  $\text{cm}^{-1}$ ); **E** broad band centred at 1580  $\text{cm}^{-1}$ ; **F** Carboxylate (1525-1560  $\text{cm}^{-1}$ ).

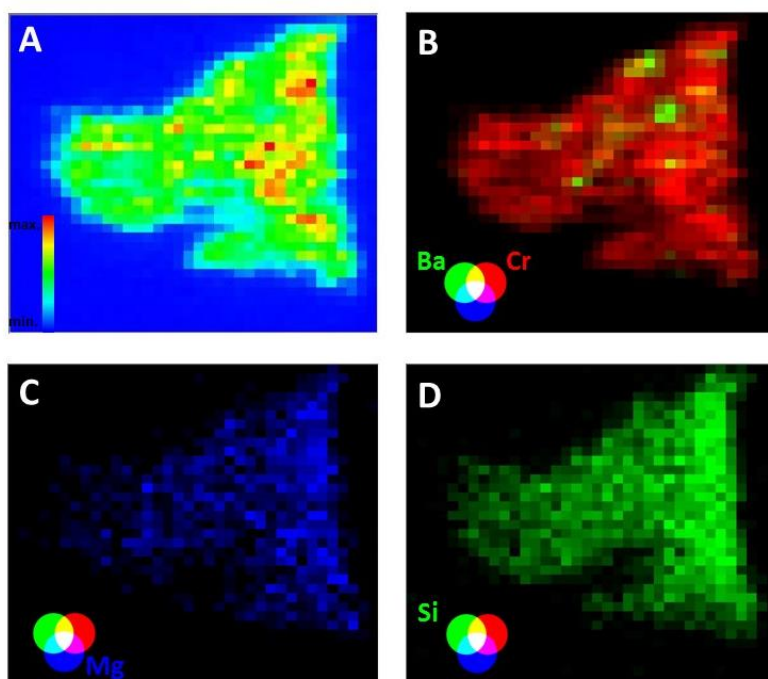


**Figure VII.10.** XRF Chromium map intensity; RGB composite images obtained by  $\mu$ -XRF at a primary beam energy of 6.12 keV **B** Ba in green, Cr in red; **C** Mg in blue; **D** Si in green.

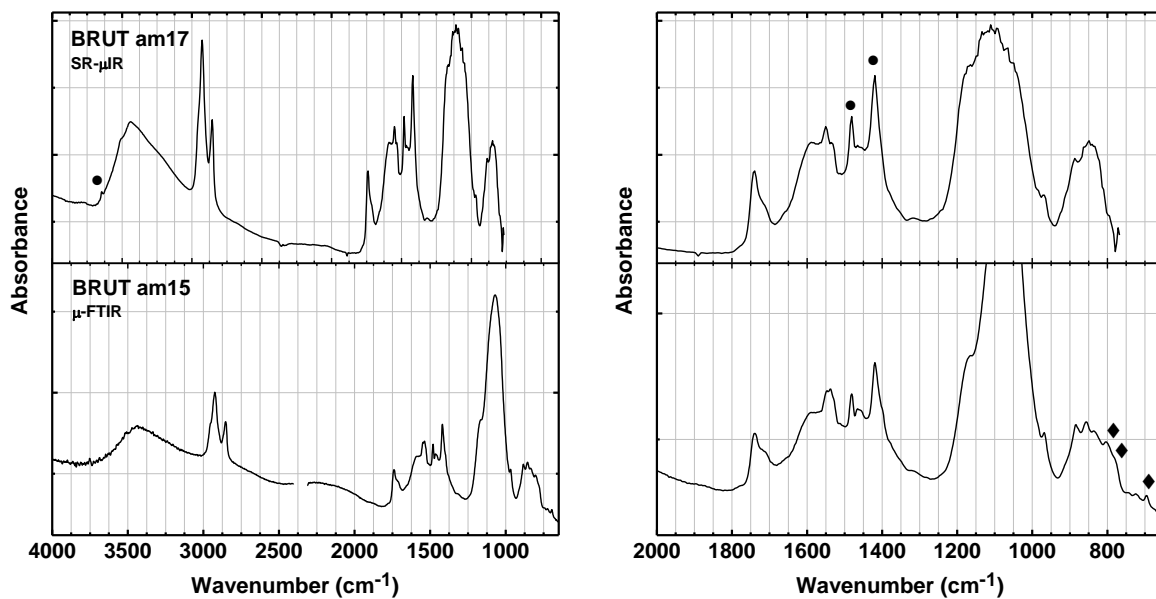


**Figure VII.11.** Infrared spectra sample am17 BRUT acquired with SR- $\mu$ IR in BaF<sub>2</sub> cell (top) and sample am15 BRUT acquired with  $\mu$ -FTIR in diamond cell (down); ● MgCO<sub>3</sub>; ♦ Quartz.

XANES analysis was performed on 9 points over the sample indicated in Figure VII.12, the comparison of the spectra with the Cr-species compounds allow to see that the main spectra feature belong to Cr(VI) compound, therefore no degradation signal are visible.

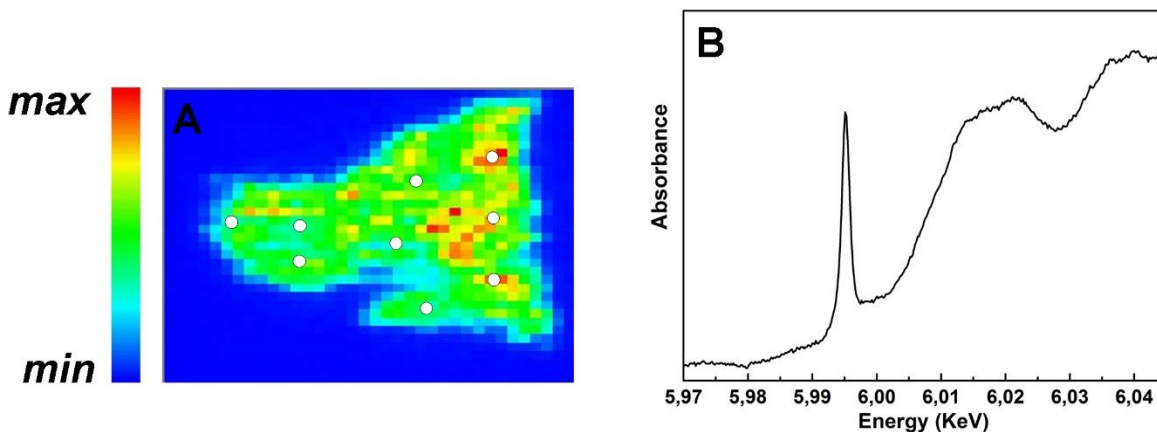


**Figure VII.12.** XRF chromium map intensity with the XANES points of analysis; **B** average XANES spectrum.

### **Entrada am17**

Two IR maps, in diamond cell and BaF<sub>2</sub>, were carry out on the am 17  $\mu$ -sample of Entrada painting. The IR analysis confirm the presence a solid mixed phase crystal, Pb(Cr,S)O<sub>4</sub>.

The XRF analysis detected the presence of Ba and K in few points, marked in the Figure VII.13A, barium sulphate were no identify in the IR spectrum. Figure VII.13C shows the profile obtained comparing the intensity of the Cr peak in the XRF maps acquired at 6.12 (black) and 6.02 (red) keV. The profile correspond to and area of the average value calculated in the area marked with the black grid in the



Figure VII.13B This profile indicates that no species of Cr(III) are present in the sample, in other words there is no degradation signal. XANES analysis was performed on 12 points on the samples, marked in Figure VII.13D, also that analysis confirmed the presence of Cr(VI).

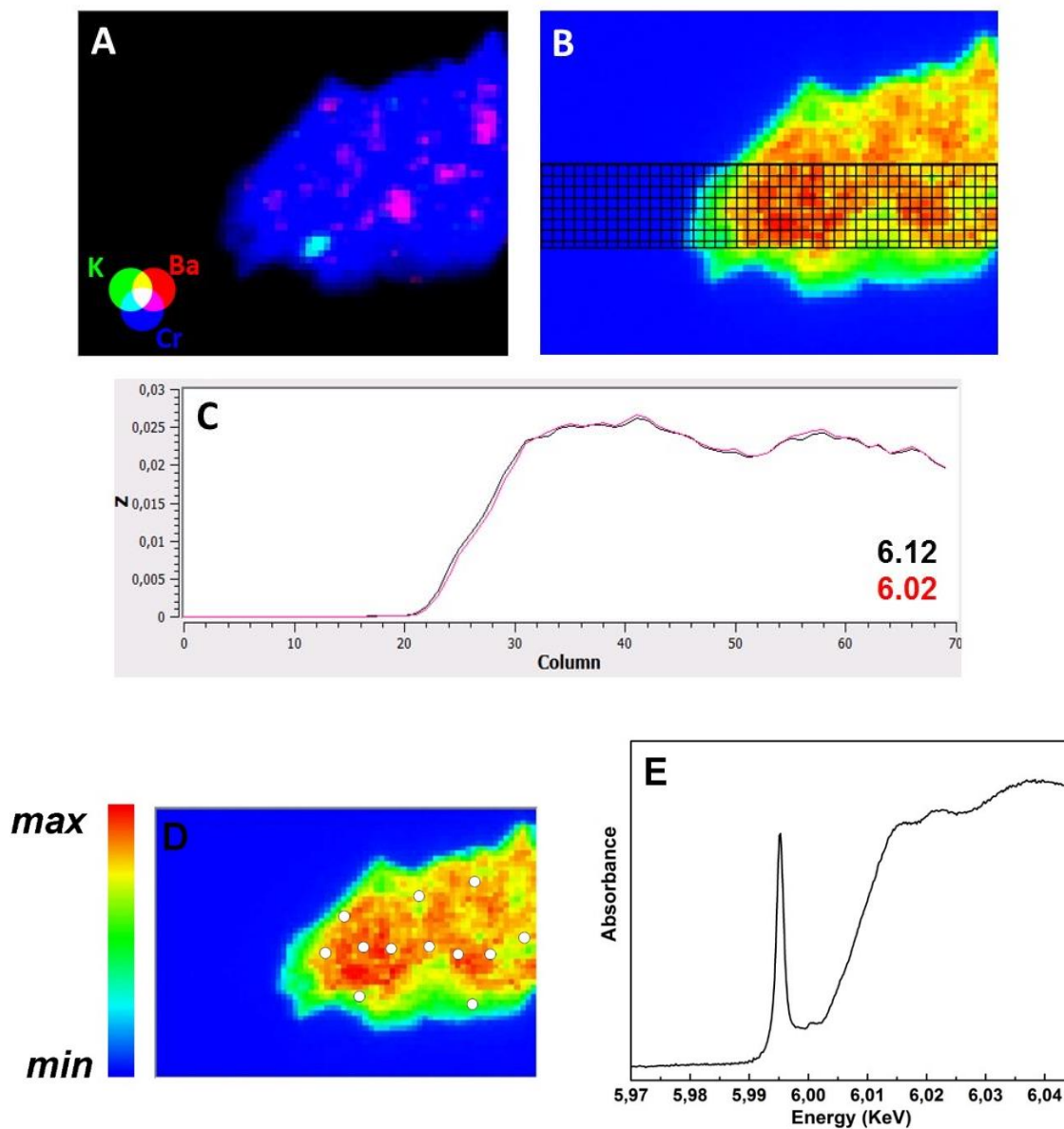


**Figure VII.13.** RGB composite images obtained by  $\mu$ -XRF at a primary beam energy of 6.12 keV with K in green, Ba in red and Cr in blue; **B** XRF Chromium map intensity in black the area used to create the calculate the intensity profile reported in C; **C** intensity profile of Cr K line on the XRF maps at beam energy of 6.12 keV (black) and 6.02 keV (red); **D** XANES points of analysis; **E** average XANES spectrum.

**Table VII.1** Roi region in  $\text{cm}^{-1}$  used for IR mapping.

ROI		From	To
Quartz	1	807	790
	2	1170	1157
CaCO <sub>3</sub>	1	890	860
	2	1805	1785
Chromate		940	800
PbSO <sub>4</sub> / CrO <sub>4</sub>		975	960
BaSO <sub>4</sub>	1	990	975
	2	1050	1090
SrSO <sub>4</sub>		1005	980
PbSO <sub>4</sub>		1200	1140
Viridian	1	1270	1240
	2	1300	1270
Oxalates	1	1350	1300
	2	1600	1650
Cobalt Yellow	1	1360	1300
	2	1440	1360

ROI		From	To
MgCO <sub>3</sub>	1	1450	1380
	2	1540	1450
	3	3480	3410
Zinc Soap	1	1525	1560
	2	1563	1650
COO- Soaps		1600	1475
Gypsum	1	1600	1635
	2	3460	3360
C=O Acid		1725	1685
C=O Ester		1760	1725
Prussian Blue		2130	2050
CH stretching		2980	2830
Lead White		3580	3500
Kaolin		3720	3610

**Table VII.2** X-ray adsorption edges and X-ray line energies (keV) used for XRF mapping.

Element	Line	Energy (keV)
S	K KL <sub>III</sub>	2.308
K	K KL <sub>III</sub>	0.293
Ca	K KL <sub>III</sub>	3.692
Cr	K KL <sub>III</sub>	5.415
Ba	L L <sub>III</sub> N <sub>V</sub>	5.158
Pb	M M <sub>III</sub> N <sub>I</sub> ; M M <sub>III</sub> N <sub>V</sub>	2.658

## Appendix VIII: Oil paint tubes

In the following Table the transcription of the labels from the 31 oil tubes sampled during the analysis made by DCR at the time of the edition of the Catalogue Raisonné of Paintings of Amadeo de Souza-Cardoso. For more details on the analysis of the paint tube samples please see Melo *et al.* 2009.

**Table VIII.1** Oil pain tubes analysed in Melo *et al.* 2009, relative code and label's transcription.

CODE	LABEL	CODE	LABEL
<b>ASC2</b>	TEMPERA FARGE Chromgelb dunkel Jaune de chrome foncé Chrome yellow deep (...) Neisli & Co, Dresden (?)	<b>ASC3</b>	ROUGE DE CADMIUM FONCÉ (...) Cadmium red deep Cadmiumrot dunkel --- LEFRANC PARIS On the back: SÉRIE P
<b>ASC7</b>	WINSOR & NEWTON (LIMITED) ---- CERULEAN BLUE Bleu Cerulean Coelin Blau --- Rathbone Place, London, England	<b>ASC8</b>	BLANC DE ZINC OXIDE DE ZINC Zinc White Zinkweiss --- LEFRANC – PARIS
<b>ASC10</b>	Bourgeois GOMME-GUTTE 1re Série GAMBOGE	<b>ASC13</b>	VIOLET DE COBALT (...) COBALT --- LEFRANC – PARIS
<b>ASC14</b>	CARMI(...) (...) LEFRANC – PARIS	<b>ASC15</b>	Bourgeois VERT DE COBALT (...)me Série COBALT GREEN
<b>ASC16</b>	Bourgeois JAUNE DE (...) Naples (?) (...)	<b>ASC17</b>	J. DE CHROME FONCÉ CHROMATE DE PLOMBE Chrome yellow deep Chromgelb dunkel --- LEFRANC – PARIS
<b>ASC18</b>	VERT DE CADMIUM (...)CADMI(...) --- LEFRANC - PARIS	<b>ASC19</b>	WINSOR & NEWTON (LIMITED) --- ANTWERP BLUE Blue Mineral Antwerpen Blau --- Rathbone Place, London, England.

Table VIII.1 (continued)

CODE	LABEL	CODE	LABEL
<b>ASC20</b>	VERT EMERALD OXIDE DE CHROME Emerald oxide of chrome Smaragd(...) --- LEFRANC – PARIS	<b>MG1</b>	WINSOR & NEWTON (LIMITED) --- BROWN MADDER --- Rathbone Place London, England
<b>MG2</b>	WINSOR & NEWTON (LIMITED) --- CADMIUM ORANGE Jaune de cadmium orange Cadmium Orange --- Rathbone Place London, England	<b>MG3</b>	WINSOR & NEWTON (LIMITED) ---- FRENCH VERMILION Vermillion Française Französischen Zinber ---- Rathbone Place, London, England
<b>MG4</b>	WINSOR & NEWTON Rathbone Place, London, England ---- OIL COLOUR COBALT BLUE Bleu de cobalt Kobalt Blaut Bleu di Cobalto Azul Cobalto	<b>MG5</b>	ROUGE DE CADMIUM CLAIRE SELENIO SUL(...) DE CADMIUM Cadmium red pale Cadmium ret bell (?) LEFRANC – PARIS
<b>MG6</b>	WINSOR & NEWTON (LIMITED) --- CHINESE VERMILION Vermillion de Chine (...) (tradução em alemão) --- Rathbone Place London, England	<b>MG7</b>	WINSOR & NEWTON (LIMITED) --- RAW SIENNA --- Rathbone Place London, England
<b>MG8</b>	WINSOR & NEWTON (LIMITED) MOIST COLOUR 38, Rathbone Place LONDON W. OLIVE GREEN	<b>MG10</b>	CARMINE FINE (...) Andrinople (...) alumina chau(...) (...) lake permanent Andrinople Lack LEFRANC – PARIS
<b>MG11</b> <b>MG12</b>	WINSOR & NEWTON Rathbone Place, London, England ---- OIL COLOUR YELLOW OCHRE Ocre jaune Lichter Ochre Ocria Giallo Ocre Amarillo	<b>MG13</b>	WINSOR & NEWTON (LIMITED) ---- CASSEL EARTH. --- Rathbone Place, London, England.

Table VIII.1 (continued)

CODE	LABEL	CODE	LABEL
<b>MG14</b>	WINSOR & NEWTON (LIMITED) ---- INDIGO --- Rathbone Place, London, England.	<b>MG15</b>	WINSOR & NEWTON (LIMITED) ---- (...) vert --- Rathbone Place, London, England.
<b>MG16</b>	(...)	<b>MG17</b>	WINSOR & NEWTON (LIMITED) ---- IVORY BLACK --- Rathbone Place, London, England.
<b>MG18</b>	REMBRANDT Oil Color Talens & Son I(...) Ington Apeldor N.J. Holland U.S.A. TERRA ROSA		

With ASC the samples take from the oil pant tubes from the box with the 'Amadeo'.

With MG the samples take from the oil pant tubes from the box with the 'Maria da Graça' [Melo *et al.* 2009].

## Appendix IX: Ripolin chart



Figure IX.1 Front of the Ripolin's colour chart: *Glacis Ripolin a Finir Spécial Pour Voitures*, dated 1925.

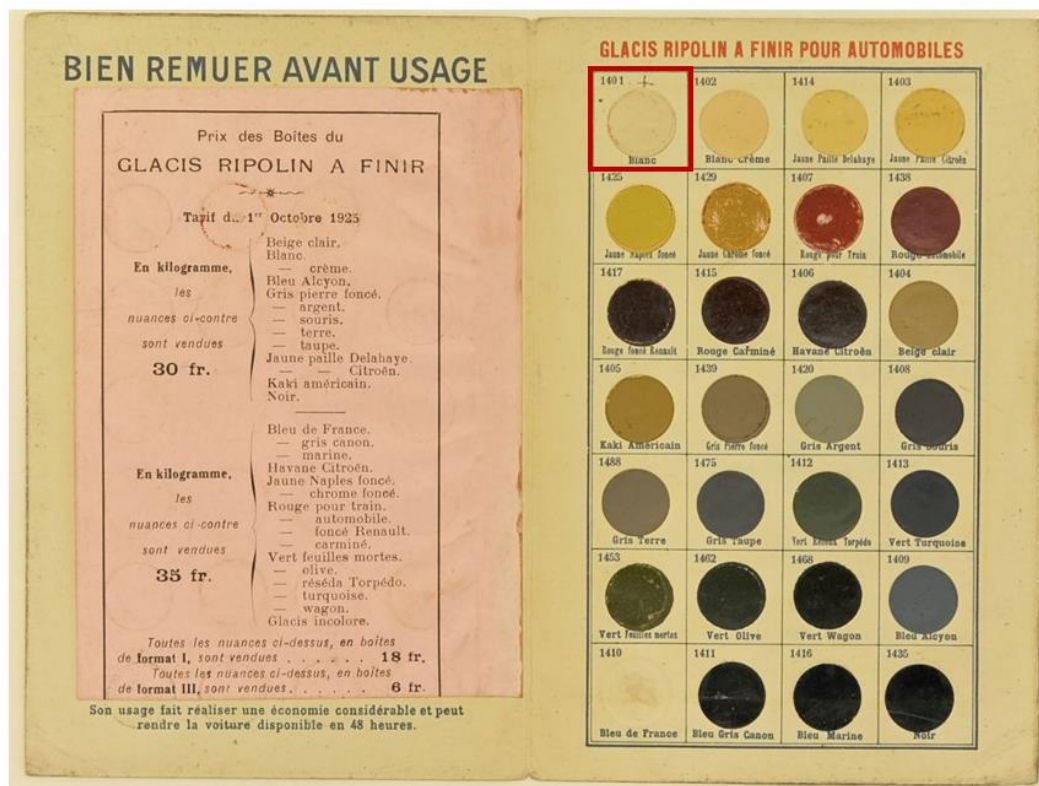


Figure IX.2 Inside of the Ripolin's colour chart: *Glacis Ripolin a Finir Spécial Pour Voitures*, dated 1925. In the red squared is identified the swatch Blanc 1401.

## **APPENDICES PART III**





## Appendix I: Images painting (A) *Collage*

*Image not available*

**Figure I.1.** Painting A, “The collage”, assigned Amadeo de Souza-Cardoso.

*Image not available*

**Figure I.2** **A** Image of the collage with normal light; **B** mapping of the areas painted with pigments not included in the Amadeo’s palette: (●) copper phthalocyanine and dioxazine violet; (●)  $\beta$ -naphthol; (●) dioxazine violet and  $\beta$ -naphthol; (●) Hansa yellow and red  $\beta$ -naphthol; (●) dioxazine violet and copper phthalocyanine; (●) red  $\beta$ -naphthol and yellow ochre. The green line indicates the papers glued.

## Appendix II: Area of analysis case studies paintings.

### II.1 Painting (A) *Collage*

*Image not available*

**Figure II.1** Painting (A) *Collage*, points where it was performed EDXRF analysis (○).

*Image not available*

**Figure II.2** Painting (A) *Collage*, samples for FTIR (●) and Raman analysis (○).

## II.2 Painting (B) *Geometric*

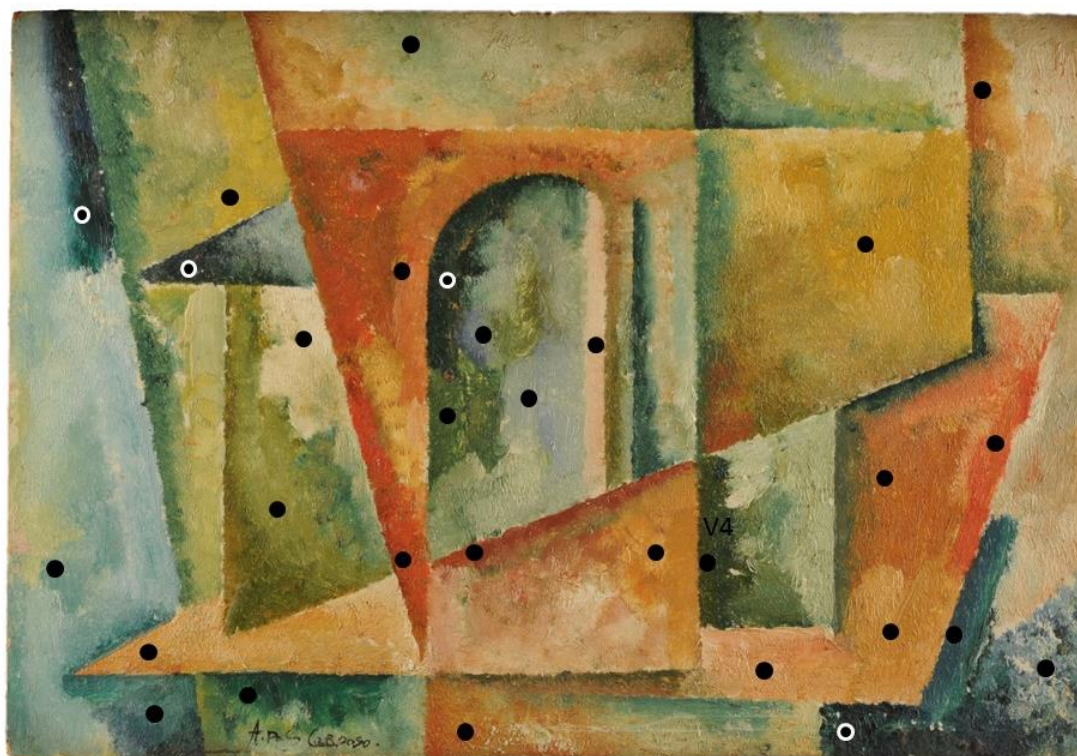


Figure II.3 Painting (B), points where it was performed EDXRF analysis (●).

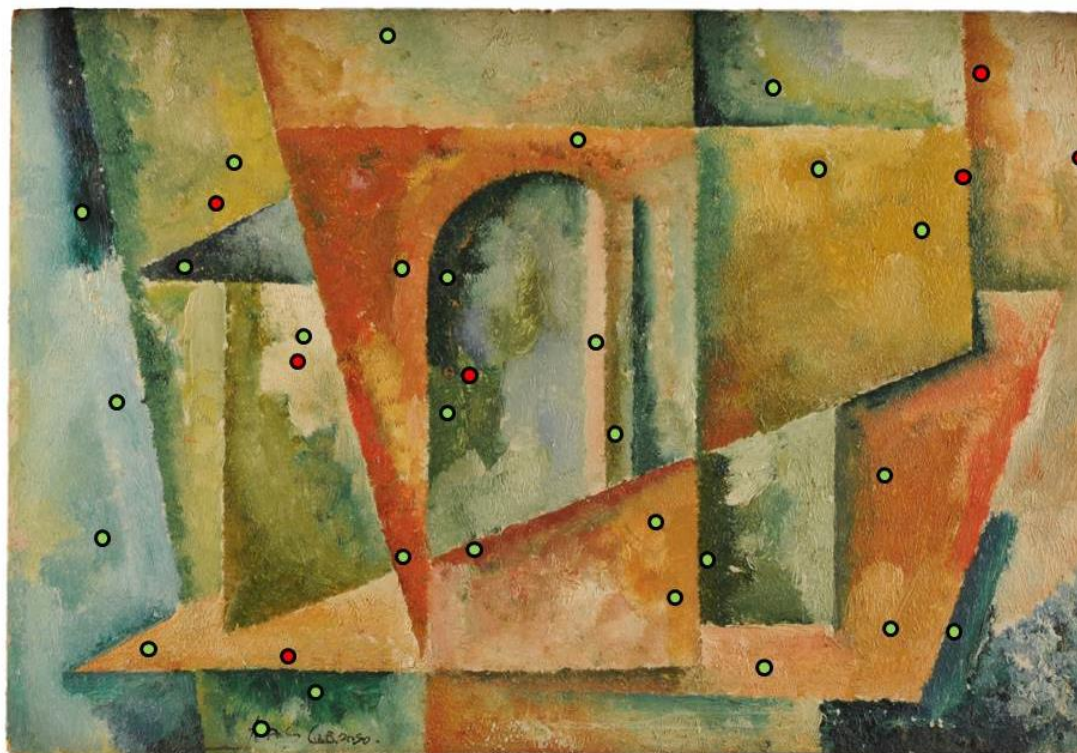
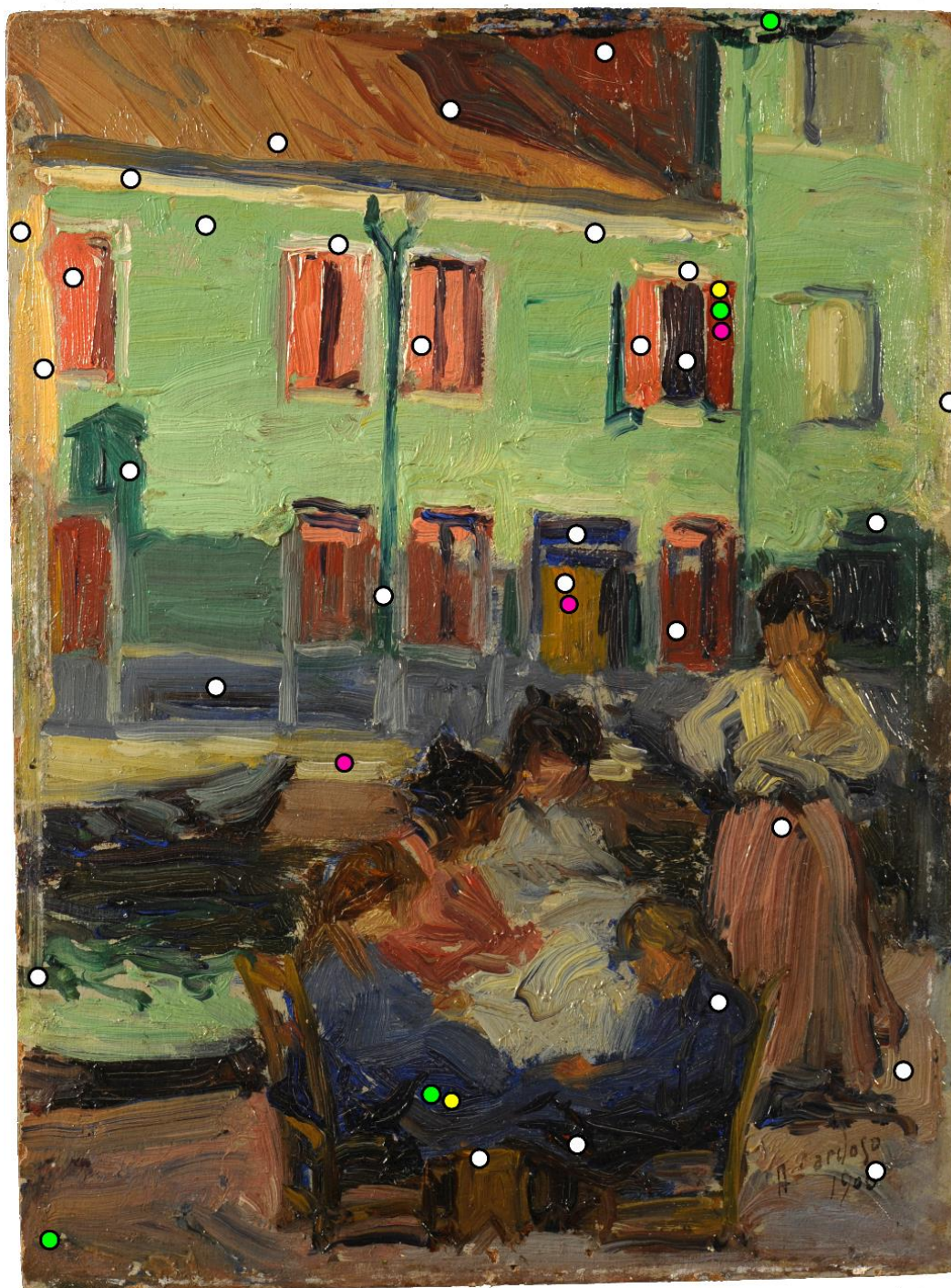


Figure II.4 Painting (B), samples for FTIR (●) and Raman analysis (●)



### II.3 Painting (C) *Embroiderers*



**Figure II.5** Painting (C) points where it was performed EDXRF and FORS analysis (O); Raman *in-situ* (●); points of sampling for FTIR and Raman (●); samples for cross-sections (●).

## II.4 Painting (D) *Café*



**Figure II.6** Painting C, points where it was performed EDXRF analysis (O); points of sampling for FTIR and Raman (●); samples for cross-sections (●).

### Appendix III: Analysis and representative spectra of the case studies paintings

In this appendix are presented the representative spectra of  $\mu$ -EDXRF,  $\mu$ -FTIR,  $\mu$ -Raman, FORS acquired in the paintings studied in the chapter Case Studies. In this appendix are also presented the cross-sections prepared. To help the reader in the following tables (Tables II.1-4) are presented the samples analysed, divided for colour and the result obtained by each analytical techniques used.

#### III.1 Results

**Table III.1** Colour areas analysed on Painting (A) *Collage* by  $\mu$ -EDXRF;  $\mu$ -Raman and  $\mu$ -FTIR.

Colour	$\mu$ -EDXRF	$\mu$ -Raman	$\mu$ -FTIR
<b>BLUE</b>	(Al), Si, S, (Cl), K, Ca, Fe, Cu, (Zn), (Sr), Ba	ultramarine blue, copper phthalocyanine, dioxazine violet	ultramarine blue, Prussian blue
<b>RED</b>	(Si), (S), Cl, K, Ca, Fe, (Cu), (Zn), (Sr), Ba	red $\beta$ -naphthol	red $\beta$ -naphthol
<b>VIOLET</b>	(Al), Si, (P), S, (Cl), K, Ca, Fe, Cu, (Zn), Sr, Ba	ultramarine blue, copper phthalocyanine, dioxazine violet, red $\beta$ -naphthol, carbon black	n.a.
<b>ORANGE</b>	Si, S, (Cl), K, Ca, Fe, (Cu), (Zn), Se <sup>‡</sup> , (Sr), Cd, Ba	red $\beta$ -naphthol, yellow Hansa	yellow Hansa
	(Si), (S), K, Ca, Ti, Fe, (Cu), (Zn), (Sr), Ba	goethite, titanium dioxide	n.a.
<b>BROWN</b>	(Al), (Si), (P), (S), (Cl), K, Ca, Ti, Fe, (Cu), (Zn), (Sr), Ba	Goethite, dioxazine violet, copper phthalocyanine	n.a.
	(Al), (Si), (P), (S), (Cl), K, Ca, Ti, Cr, Fe, (Cu), (Zn), (Sr), Ba	goethite, red $\beta$ -naphthol, carbon black	n.a.
<b>BLACK</b>	(Si), (P), (S), (Cl), (K), Ca, Ti <sup>#</sup> , Cr <sup>#</sup> , Fe, (Ni), (Cu), (Zn), (Sr), Ba	carbon black	n.a.
<b>SIGNATURE</b>	(Si), P, (S), (Cl), K, Ca, Fe, (Cu), Zn, (Sr), Ba	carbon black	n.a.

<sup>‡</sup> Selenium (Se) was detected in large amount in the dark orange areas; <sup>#</sup> Titanium (Ti) and chromium (Cr) was detected in the mixtures of black and brown; n.a. No analysed by FTIR

**Table III.2** Colour areas of the paper analysed on Painting (A) *Collage* by  $\mu$ -EDXRF and  $\mu$ -Raman.

Paper	Colour	$\mu$ -EDXRF	$\mu$ -Raman
<b>Paper A</b>	Green	(Si), S, K, Ca, Cr, Fe, Cu, (Zn), (Hg?), (Pb?), (As?), (Sr), Ba	n.s.
	White	(Si), (S), (Cl), K, Ca, Fe, (Cu), (Zn), (Sr), Ba	n.s.
<b>Paper B</b>	Blue	(Si), (P), (S), (Cl), K, Ca, Mn, Fe, (Cu), (Zn), (Sr), Ba	Indigo
	Yellow	(Si), (P), (S), (Cl), K, Ca, Mn, Fe, (Cu), (Zn), (Sr), Ba	n.s.
<b>Support</b>	---	(Si), (P), (S), (Cl), K, Ca, Mn, Fe, (Cu), (Zn), (Sr), Ba	n.s.

n.s. No Raman signal



### III.2 Painting (B) *Geometric*

**Table III.3** Colour areas analysed on Painting (B) *Geometric* by  $\mu$ -EDXRF;  $\mu$ -Raman and  $\mu$ -FTIR.

Colour	$\mu$ -EDXRF	$\mu$ -Raman	$\mu$ -FTIR
WHITE	Ca, Pb, (Ba), (Cr), (Fe)	lead white	lead white
YELLOW	Ca, Pb, Ba, Fe, Cr, (Hg)	ochre, vermilion	yellow ochre
RED	Ca, Pb, Ba, Hg, Cr, Fe	vermilion	n.a
PINK	Ca, Pb, Ba, Cr, Fe, (Hg)	vermilion, lead white	n.a
BROWN	Ca, Pb, Ba, Hg, Cr, Fe	vermilion	yellow ochre
LIGHT GREEN	Ca, Pb, (Ba), Fe, Cr	Viridian	n.a
DARK GREEN	Ca, Pb, Ba, Cr, Co, Ni, Fe	Viridian	n.a
BLUE	Ca, Pb, Fe, Cr, Co,(Ni)	viridian + cobalt blue	cobalt blue
GREEN ON THE BACK	Ca, Pb, Ba, Fe, Cu, As	emerald green	n.a

n.a. No analysed by FTIR

### III.3 Painting (C) *Embroiderers*

**Table III.4** Colour areas analysed on Painting (C) *Embroiderers* by  $\mu$ -EDXRF; FORS;  $\mu$ -Raman and  $\mu$ -FTIR.

Colour	$\mu$ -EDXRF	FORS	$\mu$ -Raman	$\mu$ -FTIR
BLUE	Co, Ni, (Cr, Hg), Pb (Ba, Fe, Ca, Sr, Zn)	cobalt or cerulean blue	cobalt and cerulean blue, goethite, hematite	cobalt based blue. Silicate matrix <sup>‡</sup>
GREEN	Cr, Co, Ni, Fe, Pb (Ba, Ca, Sr, Zn)	viridian	n.a	viridian
RED	Ba, Co, Ni, Pb Ba, (Fe, Ca, Sr, Zn)	organic pigments n.i.	red $\beta$ -naphthol, barium sulphate	organic pigment, barium sulphate
YELLOW	Fe, Cr, Cd, Pb, Co, Ni, (Ba, Ca, Sr, Zn)	n.i.	chrome yellow, barium sulphate, quartz	n.a.
WHITE	Pb, (Cr, Co) (Ba, Ca, Sr, Zn)	n.a.	lead white	lead white
PINK	Pb, (Cr, Co) (Ba, Ca, Sr, Zn)	organic pigments n.i.	n.a	n.a
BROWN	Fe, Co, Ni, Cr, Pb (Ba, Fe, Ca, Sr, Zn)	n.i.	n.a.	n.a.
PREPARATION	Pb, Co, Fe, Zn, Cr, Ca, (Sr, Ba)	n.a.	lead white, barium sulphate	n.a.
SUPPORT <sup>§</sup>	Ba, Fe, Ca, Sr, (Pb, Cu, Zn)	n.a.	n.a.	n.a

# in *italic* the elements associated to the millboard support; <sup>‡</sup> Usually associate to earth pigments; <sup>§</sup> Elements from the preparation layer could be detected; n.a. No analysed; n.i No identified

### III.4 Painting (D) *Café*

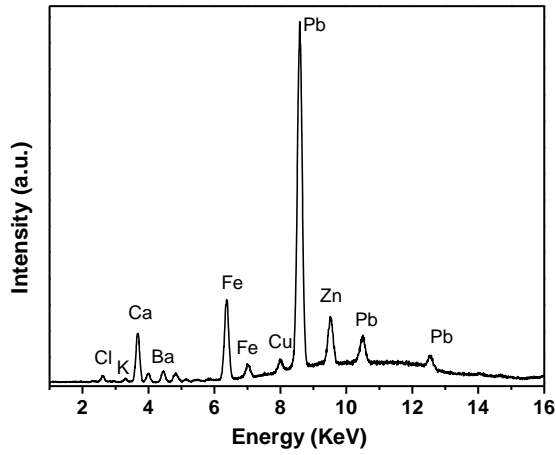
**Table III.5** Colour areas analysed on Painting (D) *Café* by  $\mu$ -EDXRF;  $\mu$ -Raman and  $\mu$ -FTIR.

<b>Colour</b>	<b><math>\mu</math>-EDXRF</b>	<b><math>\mu</math>-Raman</b>	<b><math>\mu</math>-FTIR</b>
<b>BLUE</b>	Co, Pb, Ba, (Sr), (Ni) <i>Zn Cu, Fe, (Ca)</i>	ultramarine blue, barium sulphate, lead white	
<b>GREEN</b>	Cr, Pb, Co, Ba Hg, Ni, Sr <i>Zn, Fe, Cu, Ca, (K)</i>	viridian ultramarine blue, lead white, vermilion	viridian ultramarine blue barium sulphate, lead white
<b>RED</b>	Hg, Pb, Zn, Ba, Cr, Sr, <i>Fe, Cu, (Ca)</i>	vermilion	n.a.
<b>YELLOW</b>	Pb, Cr, Ba, Hg, (Sr) <i>Fe, Zn, (Cu), (Ca)</i>	chrome yellow, barium sulphate, lead white, vermilion	chrome yellow, barium sulphate,
<b>WHITE</b>	Pb, Ba, Hg, Sr, Cr <i>Cu, Fe, Zn, (Ca)</i>	lead white, barium sulphate, vermilion	lead white, barium sulphate
<b>VIOLET</b>	Pb, Fe, Hg, Ba, Cr, Co, Sr <i>Zn, Cu, (Ca), (K)</i>	Lead white, barium sulphate, ultramarine blue, vermilion	Lead white, barium sulphate, ultramarine blue,
<b>BROWN</b>	Pb, Fe, Ba, Hg, Co, Cr, (Sr), <i>Zn, Cu (Ca)</i>	n.a.	n.a.
<b>BLACK</b>	Fe, Pb, Hg, Cr, Ba, Sr <i>Zn Ca, Cu K</i>	n.a.	n.a.
<b>SIGNATURE</b>	Pb, Cr, Ba, Co, Hg, Sr, <i>Zn, Fe, Cu, Ca, (K)</i>	n.a.	n.a.
<b>SUPPORT</b>	Zn, Fe, Ca, Pb, Ba, Cu, Cl, (K)	n.a.	n.a.

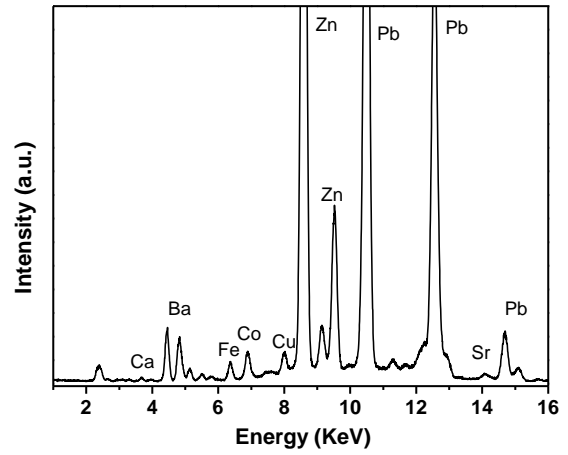
# in *italic* the elements associated to the millboard support;  
n.a. No analysed

### III.2 $\mu$ -EDXRF

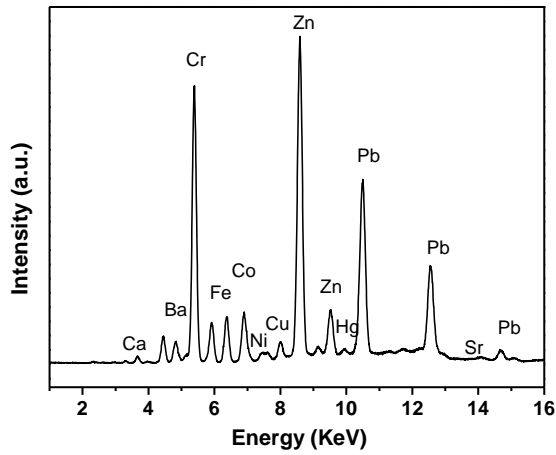
Representative  $\mu$ -EDXRF spectra from Painting (A) *Collage*.



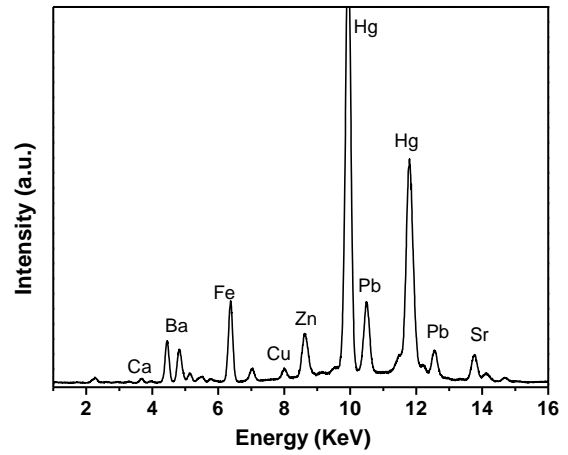
*Paper support*



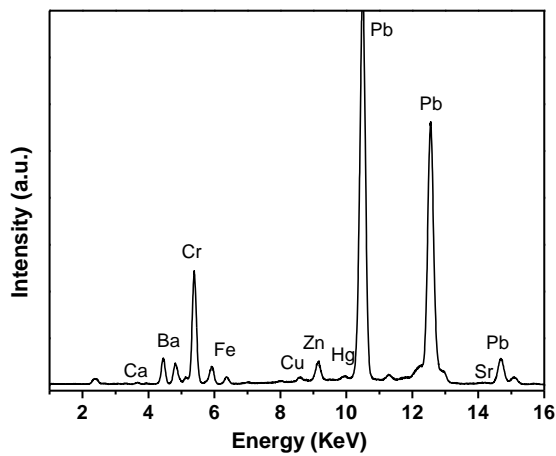
*Blue*



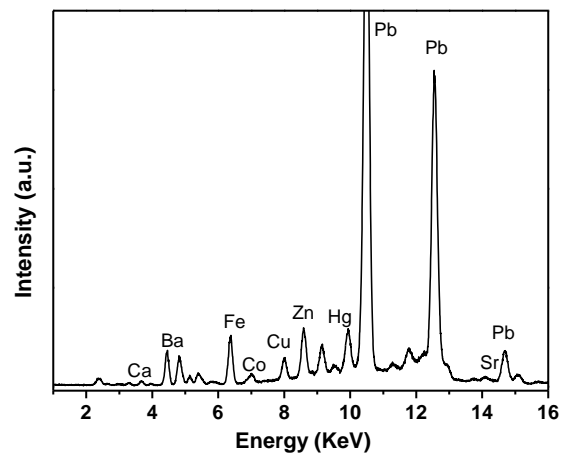
*Green*



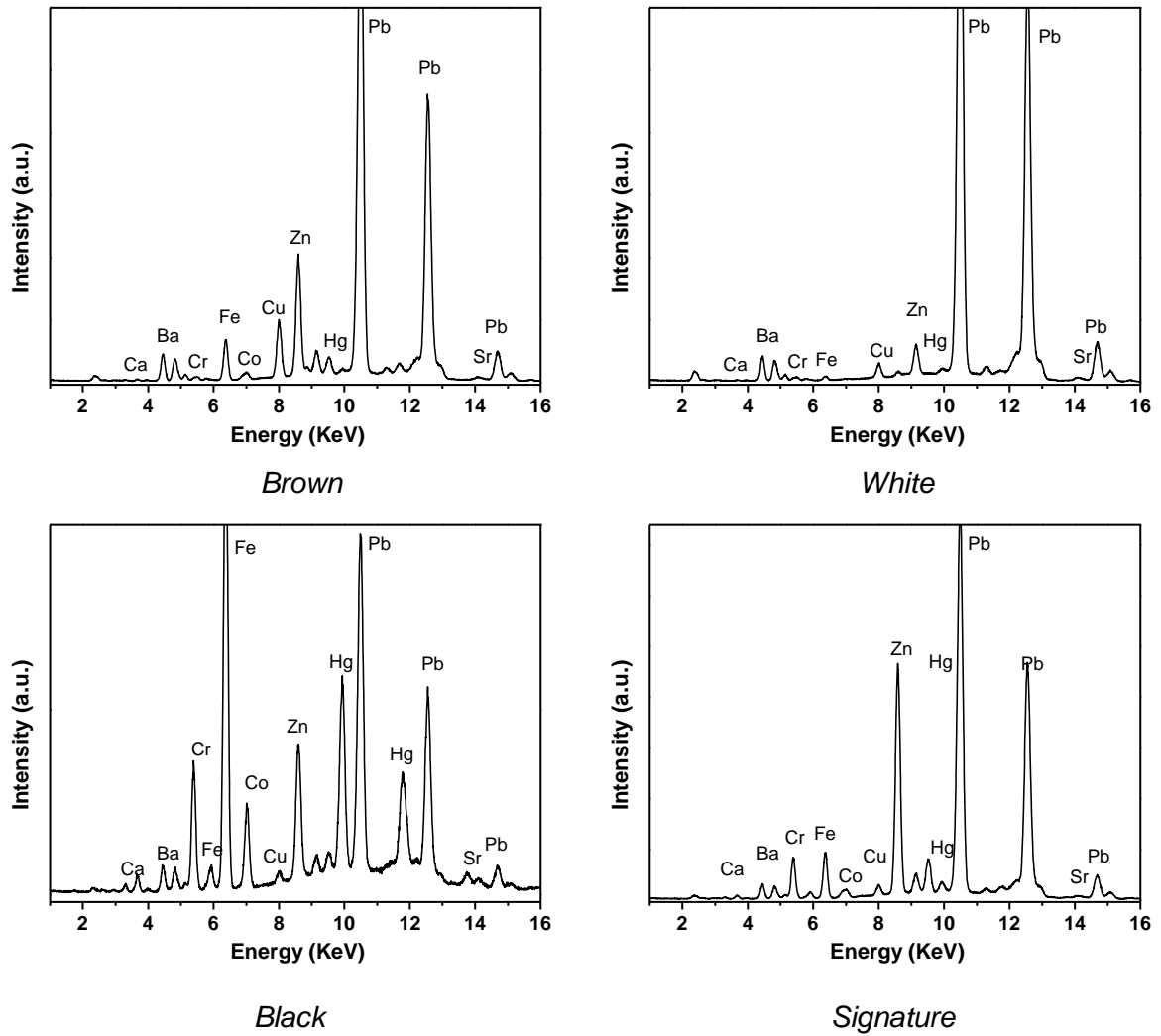
*Red*



*Yellow*

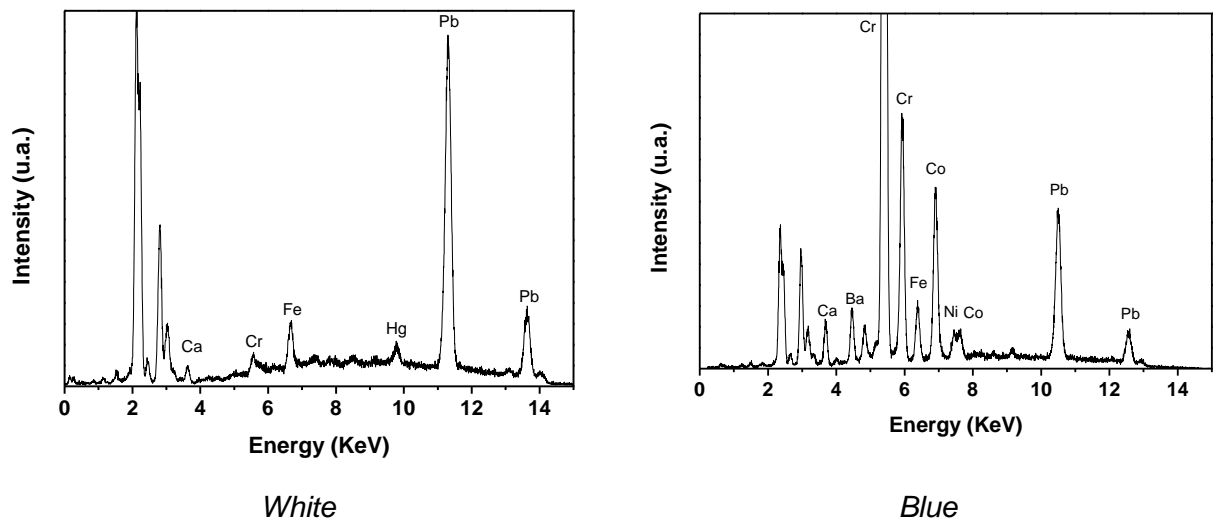


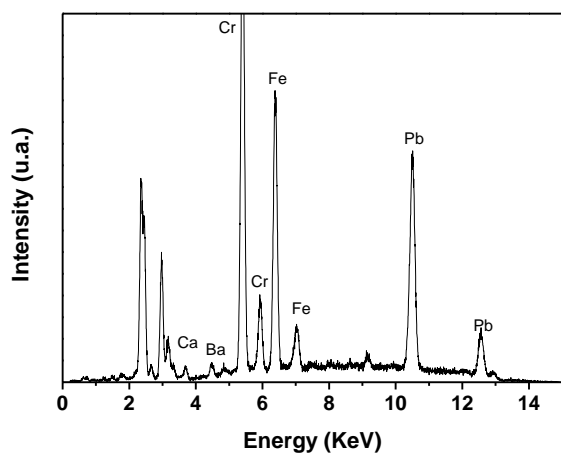
*Violet*



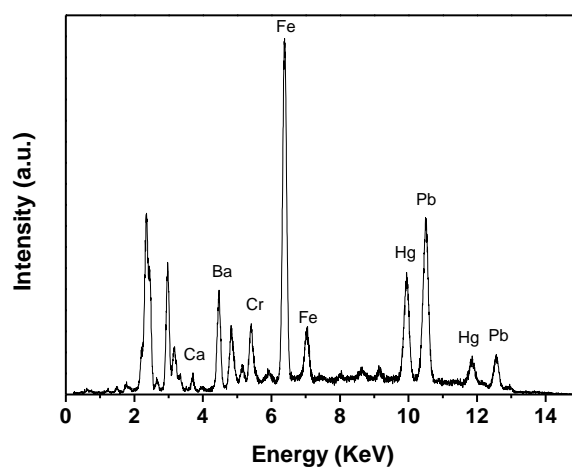
**Figure III.1** Representative  $\mu$ -EDXRF spectra of the paper support; blue; green; red; yellow; violet; brown; white; black areas and the signature from *Painting A (the collage)*.

**Representative  $\mu$ -EDXRF spectra from *Painting (B) Geometric*.**

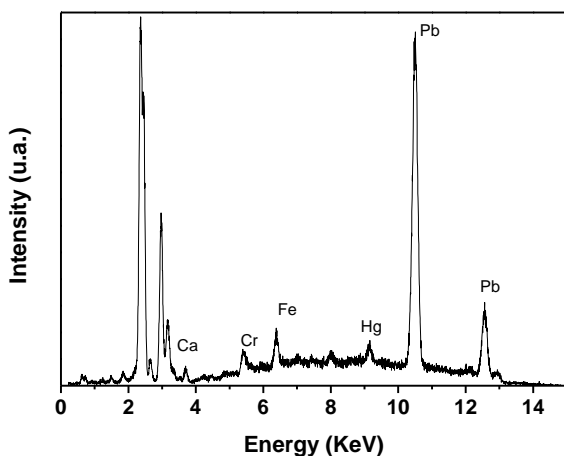




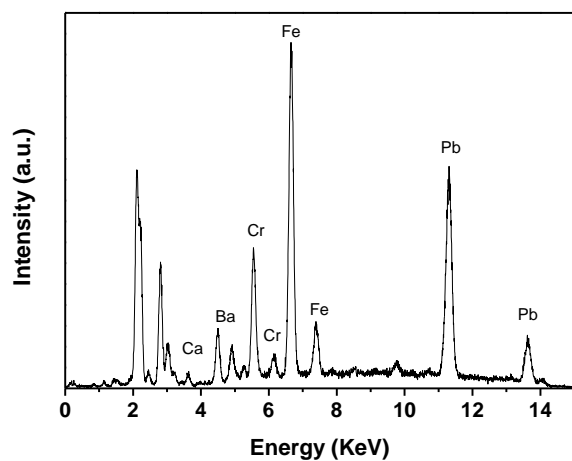
*Green*



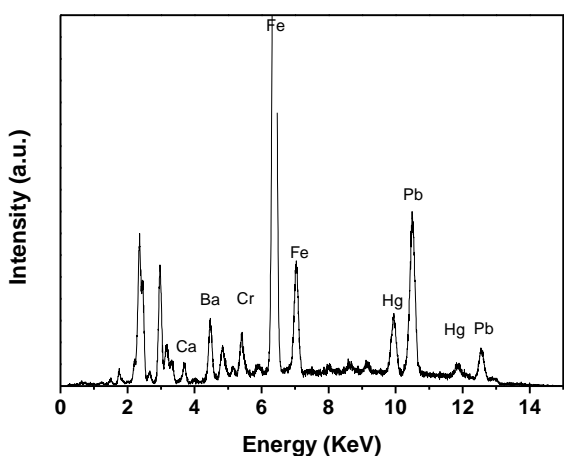
*Red*



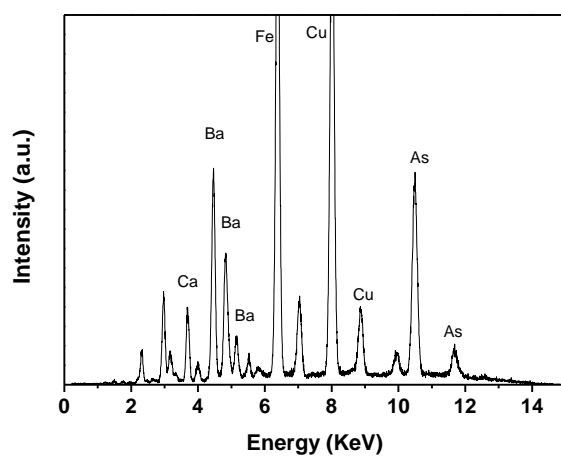
*Pink*



*Yellow*



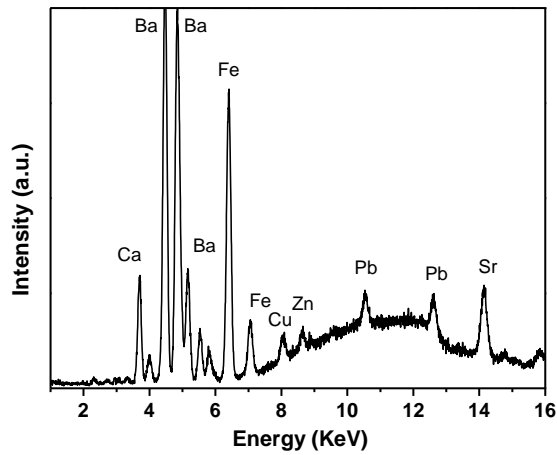
*Brown*



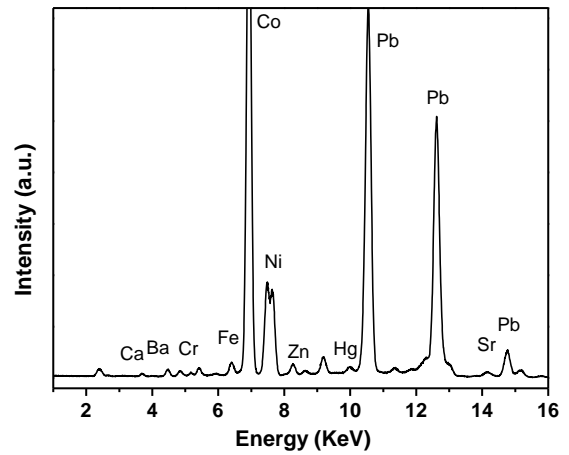
*Green on the back*

**Figure III.2** Representative  $\mu$ -EDXRF spectra of white; blue; green; red; pink; yellow; brown areas from Painting (B) *Geometric*.

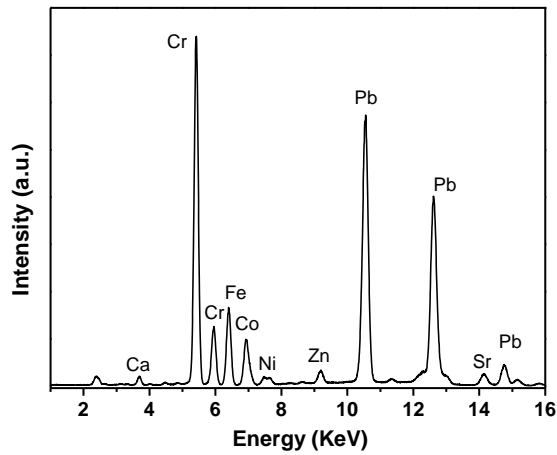
Representative  $\mu$ -EDXRF spectra from Painting (C) *Embroiderers*.



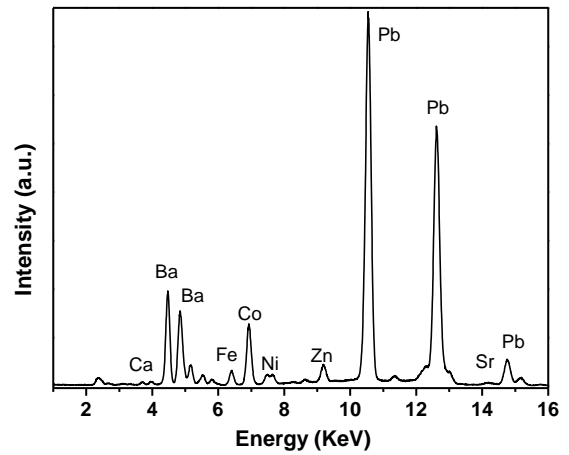
*Paper support*



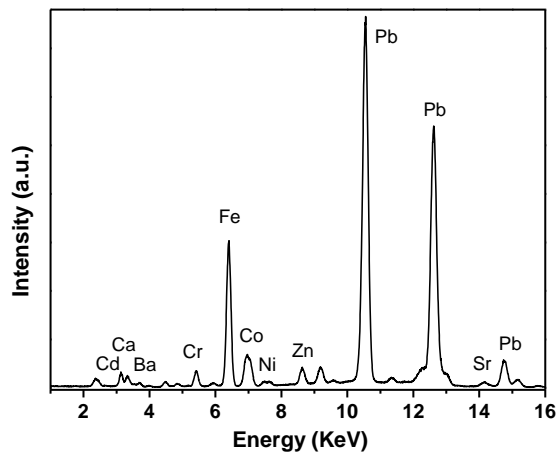
*Blue*



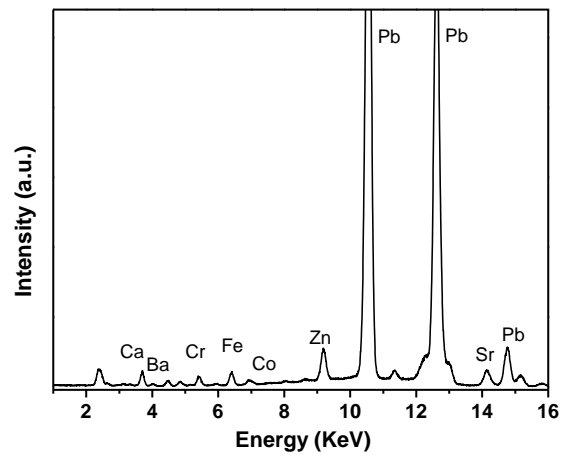
*Green*



*Red*

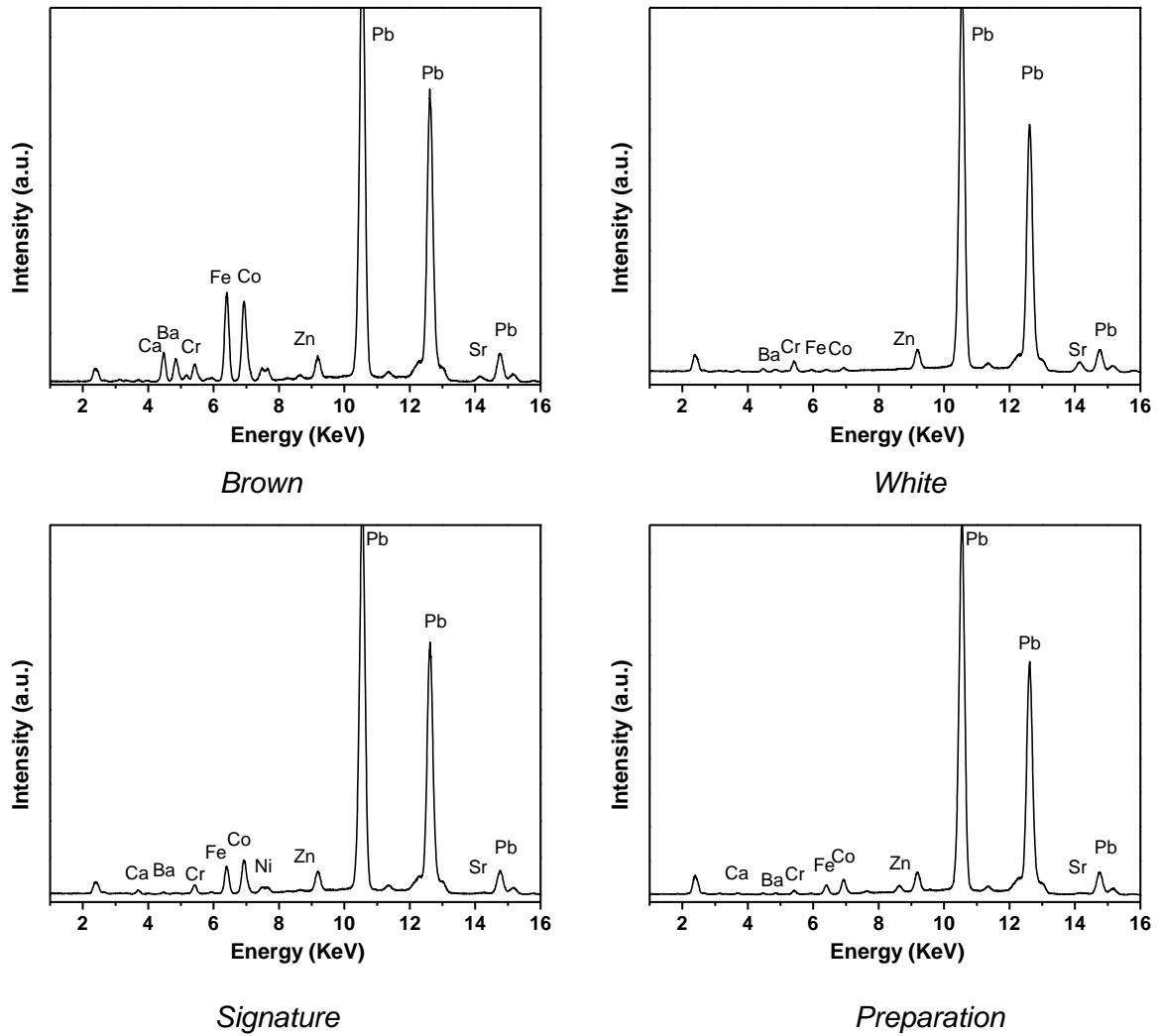


*Yellow*



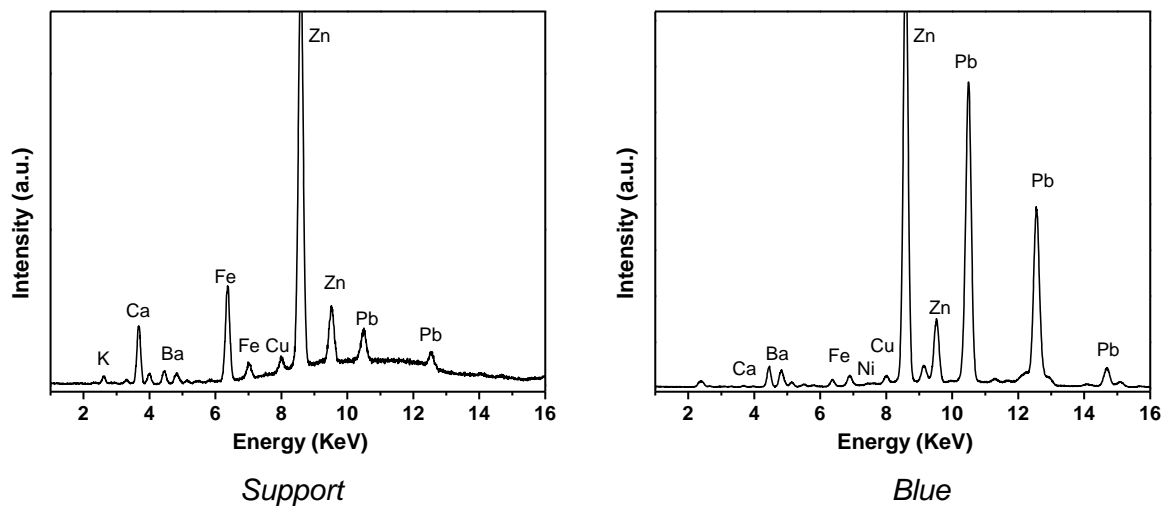
*Pink*

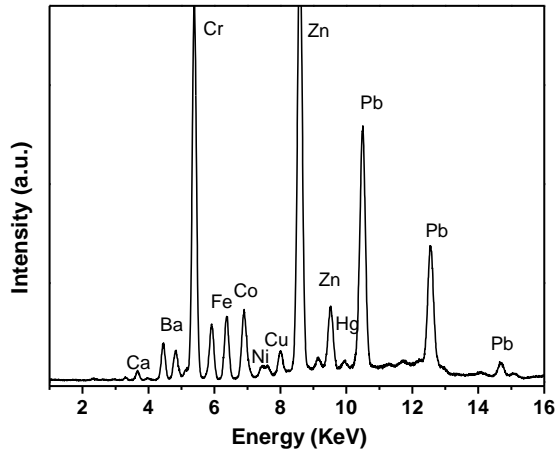




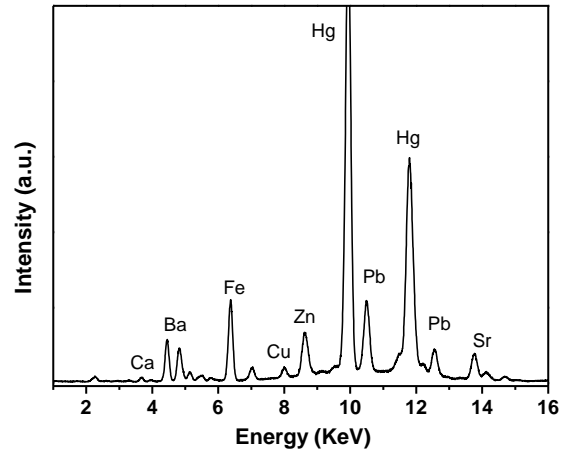
**Figure III.3** Representative  $\mu$ -EDXRF spectra of the support; blue; green; red; yellow; pink; brown; white areas; signature and preparation layer from Painting (C) *Embroiderers*.

Representative  $\mu$ -EDXRF spectra from Painting (D) *Café*.

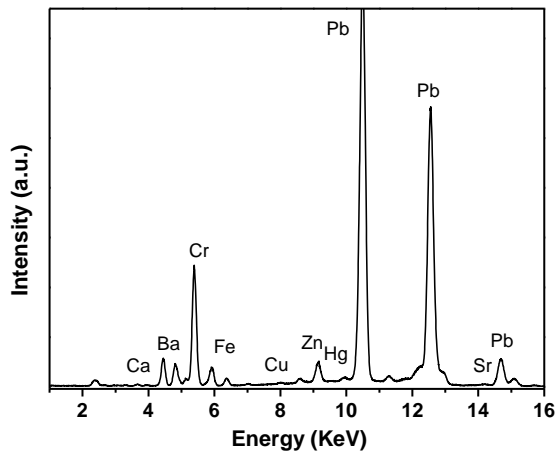




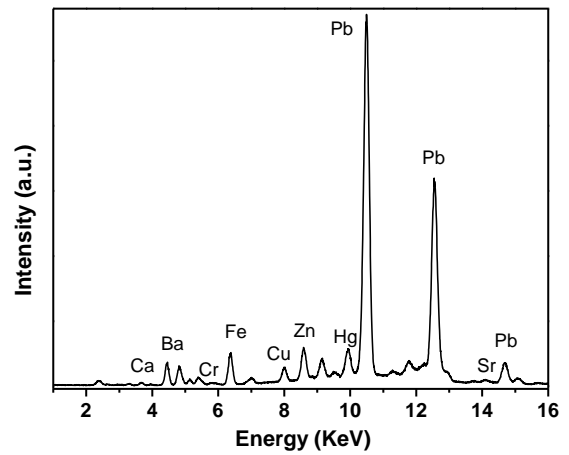
*Green*



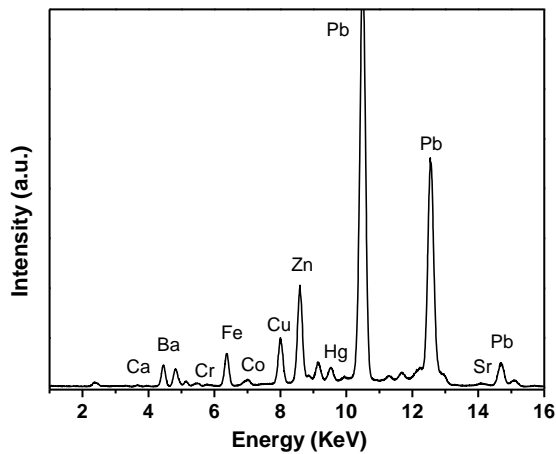
*Red*



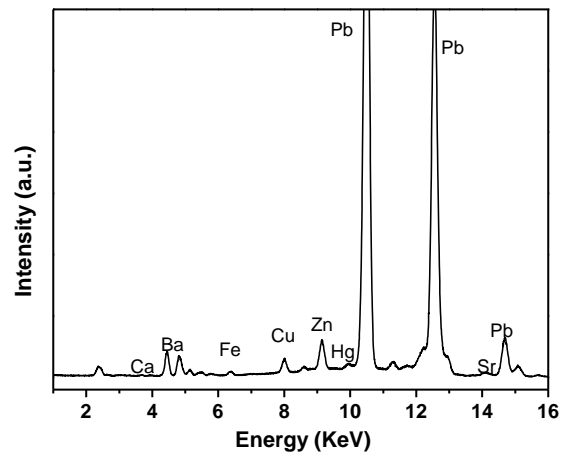
*Yellow*



*Violet*



*Brown*



*White*

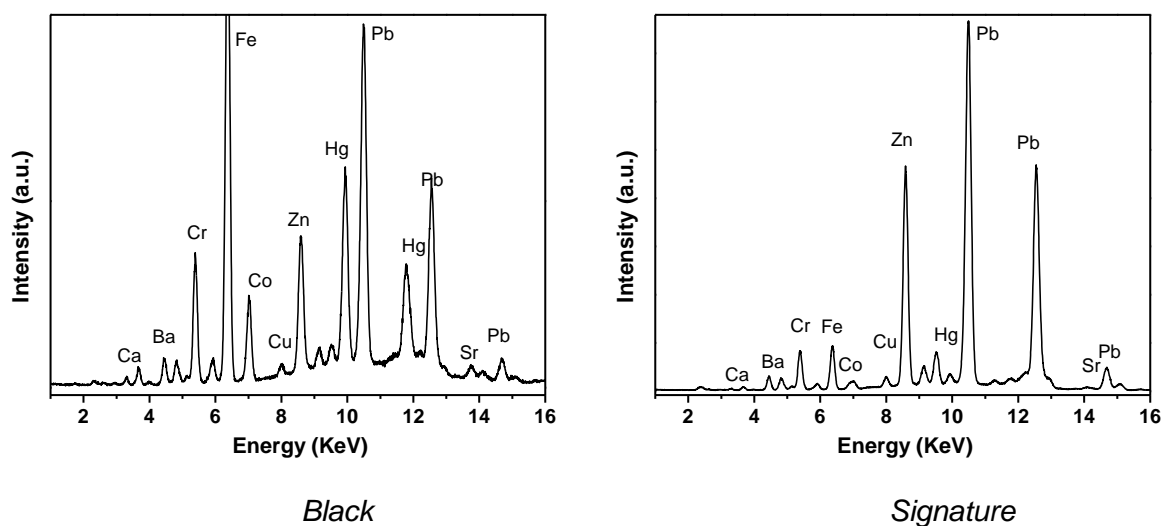


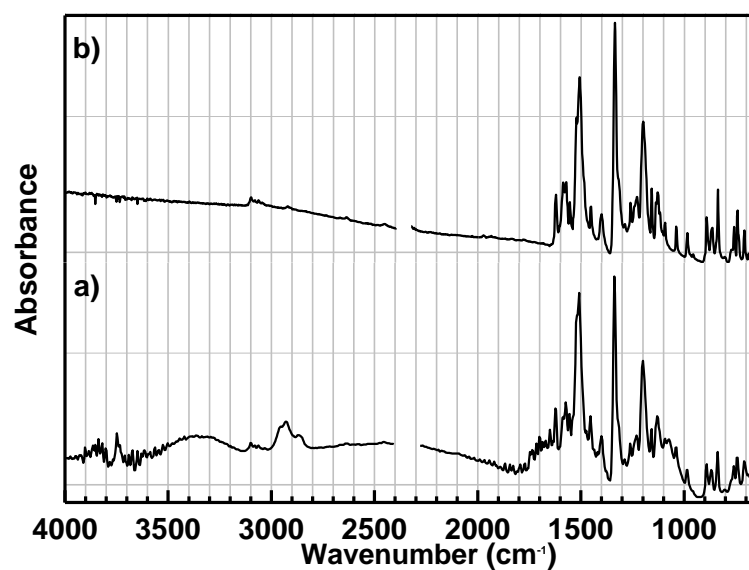
**Figure III.4** Representative  $\mu$ -EDXRF spectra of the support; blue; green; red; yellow; violet; brown; white; black areas and preparation layer from Painting (D) *Café*

**Table III.6.** Characteristic energies of the X-rays (KeV) used to identify the elements in the EDXRF analysis.

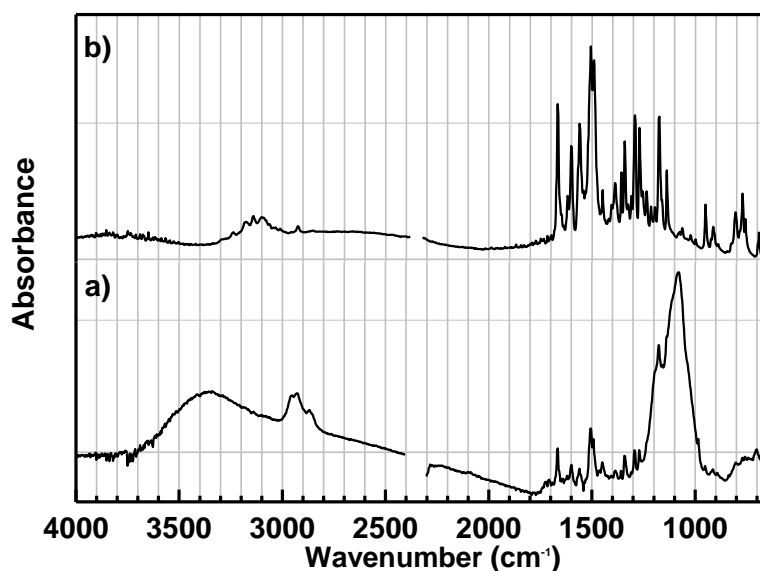
Elements	K $\alpha$	K $\beta$	L $\alpha$	L $\beta_1$	L $\beta_2$	L $\gamma_1$	M $\alpha$
<sup>15</sup> P	2,014	2,139					
<sup>19</sup> K	3,314	3,590					
<sup>20</sup> Ca	3,690	4,012					
<sup>24</sup> Cr	5,414	5,946					
<sup>26</sup> Fe	6,396	7,057					
<sup>27</sup> Co	6,922	7,648					
<sup>28</sup> Ni	7,477	8,264					
<sup>29</sup> Cu	8,040	8,904					
<sup>30</sup> Zn	8,630	9,570					
<sup>33</sup> As	10,543	11,725					
<sup>56</sup> Ba			4,467	4,828	5,156	5,531	
<sup>80</sup> Hg			9,987	11,823	11,923	13,828	
<sup>82</sup> Pb			10,550	12,812	12,621	14,782	2,342

### III.3 $\mu$ -FTIR

Representative  $\mu$ -FTIR spectra from Painting (A) *Collage* and the reference pigments.



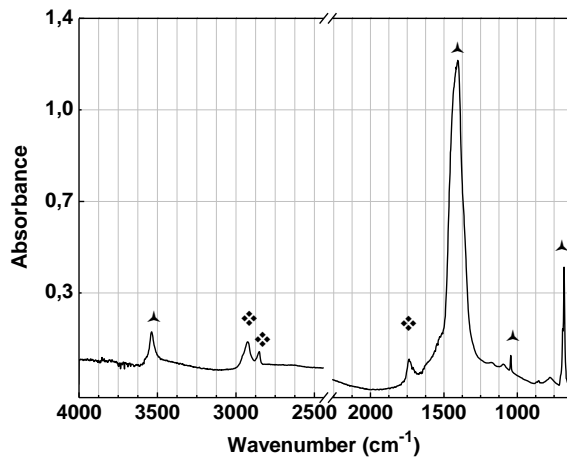
Red sample (a) and  $\beta$ -naphthol PR4 (Clariant) (b).



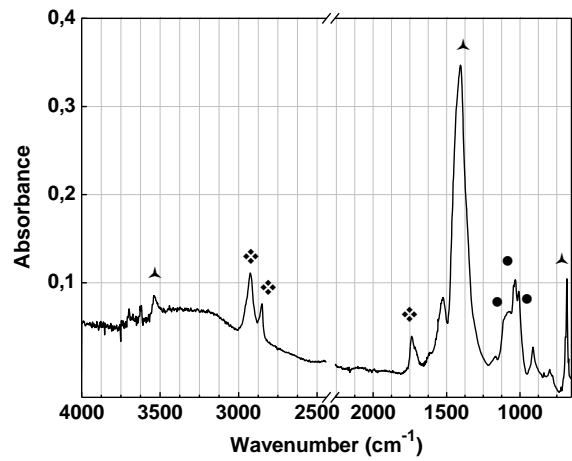
Yellow sample (a) and Hansa PY1 (Clariant).

**Figure III.5** Representative  $\mu$ -FTIR spectra of the red and yellow areas from Painting (A) *Collage* and the reference pigments  $\beta$ -naphthol PR4 (Clariant) and Hansa yellow PY1 (Clariant).

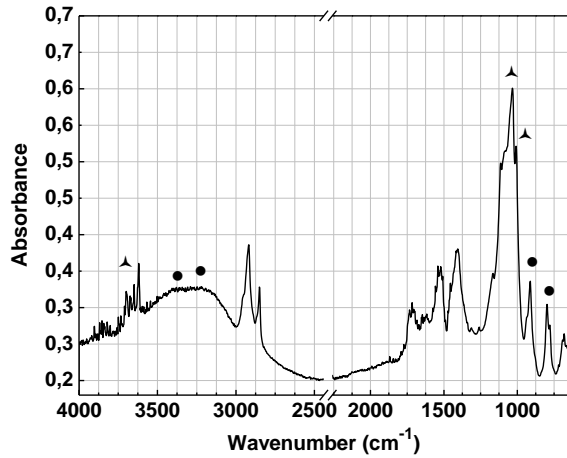
Representative  $\mu$ -FTIR spectra from Painting (B) *Geometric*.



White sample,  
oil (◆) and lead white (▲).



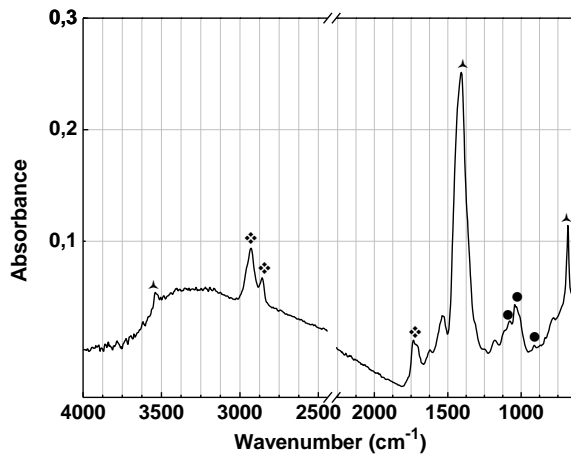
White sample, oil (◆);  
lead white (▲) and barium sulphate (●).



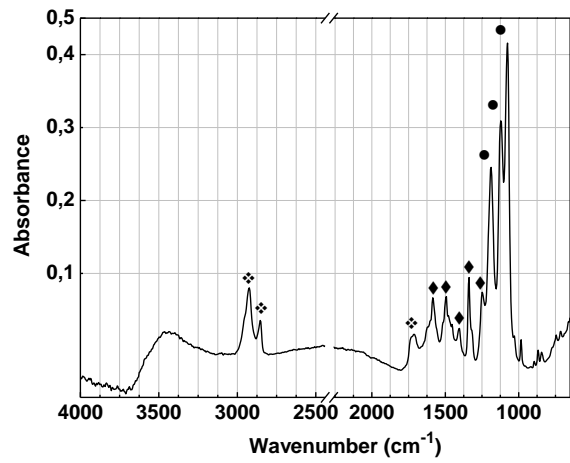
Brown sample,  
kaolin (▲) and iron oxide (●).

Figure III.6 Representative  $\mu$ -FTIR spectra of the white and brown areas from Painting (B) *Geometric*.

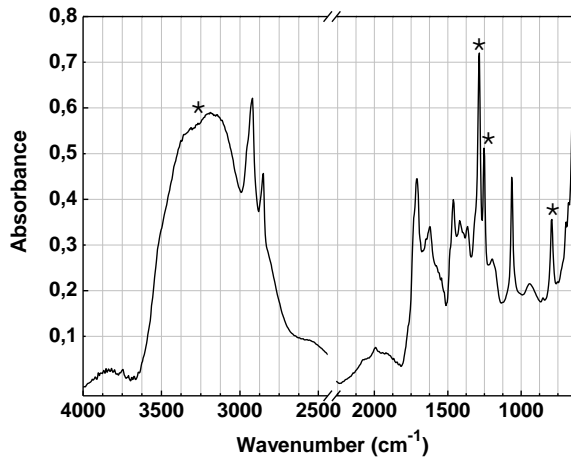
Representative  $\mu$ -FTIR spectra from Painting (C) *Embroiderers*.



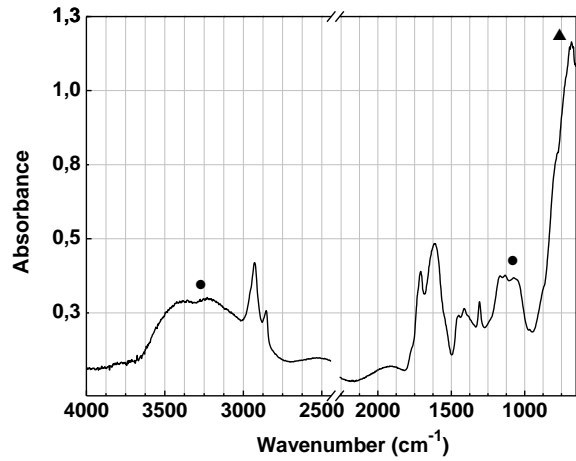
Grey sample, oil (⚡); lead white (▲) and barium sulphate (●).



Red sample, oil (⚡), barium sulphate (●) synthetic red of  $\beta$ -naphthol class (◆).



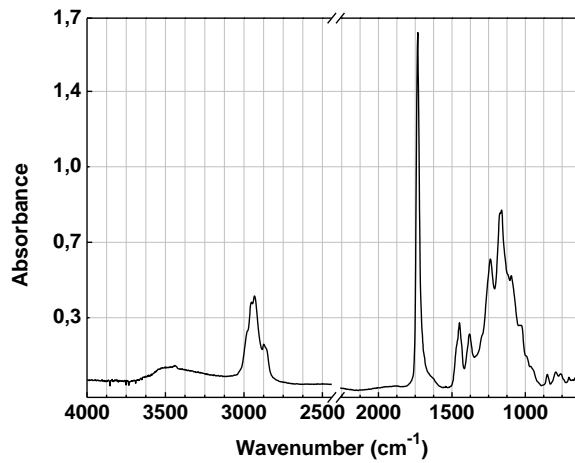
Green sample, viridian (★).



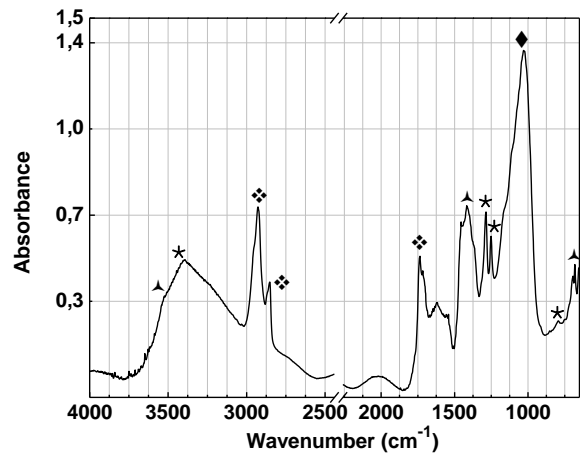
Blue sample, blue cobalt based pigment (▲); silicate matrix (●).

Figure III.7 Representative  $\mu$ -FTIR spectra of the grey, red, green and blue areas from Painting (C) *Embroiderers*.

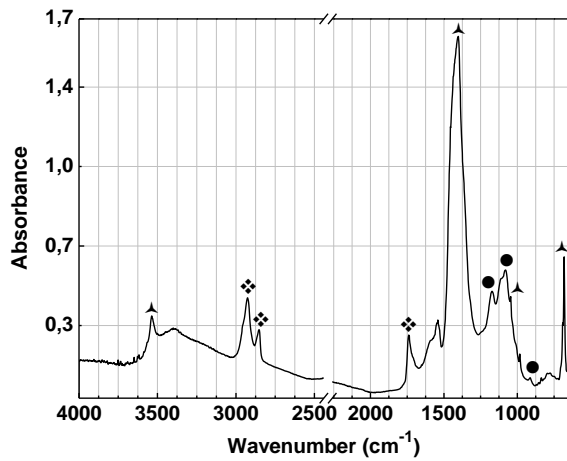
Representative  $\mu$ -FTIR spectra from Painting (D) *Café*.



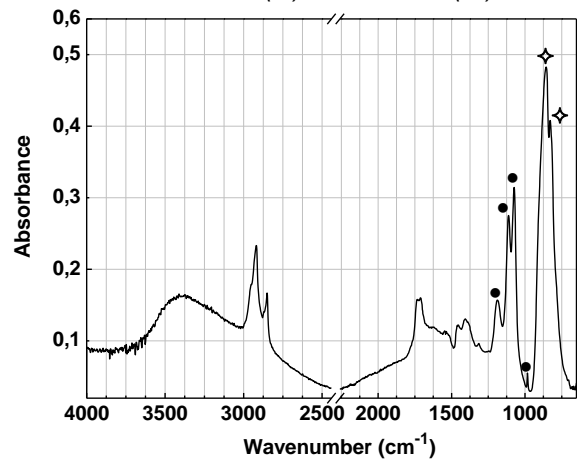
Varnish sample.



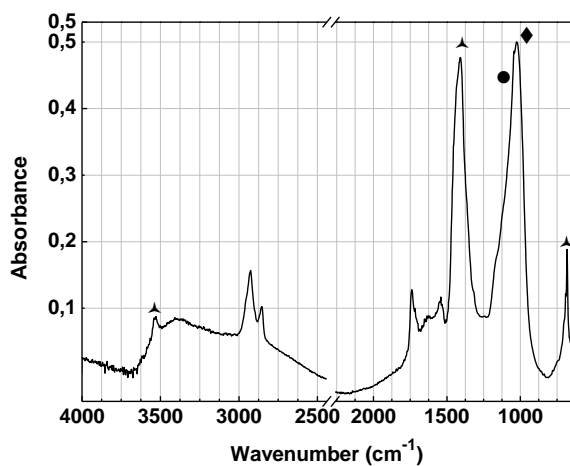
Green sample, oil ( $\blacklozenge$ ); lead white ( $\blacktriangle$ ); ultramarine blue ( $\blacklozenge$ ) and viridian ( $\blackstar$ ).



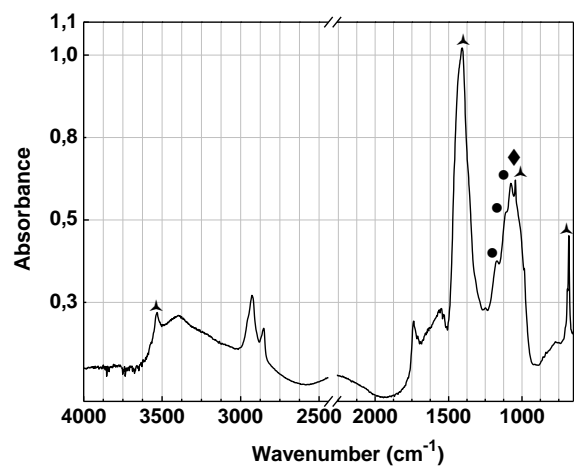
White sample, oil ( $\blacklozenge$ ); lead white ( $\blacktriangle$ ) and barium sulphate ( $\bullet$ ).



Yellow sample, barium sulphate ( $\bullet$ ) and chrome yellow ( $\blacklozenge$ ).



Blue sample, lead white ( $\blacktriangle$ ); barium sulphate ( $\bullet$ ) and ultramarine ( $\blacklozenge$ ).



Violet sample, lead white ( $\blacktriangle$ ); barium sulphate ( $\bullet$ ) and ultramarine ( $\blacklozenge$ ).

**Figure III.8** Representative  $\mu$ -FTIR spectra of the varnish and the green; white; yellow; blue and violet areas from Painting (D) *Café*.



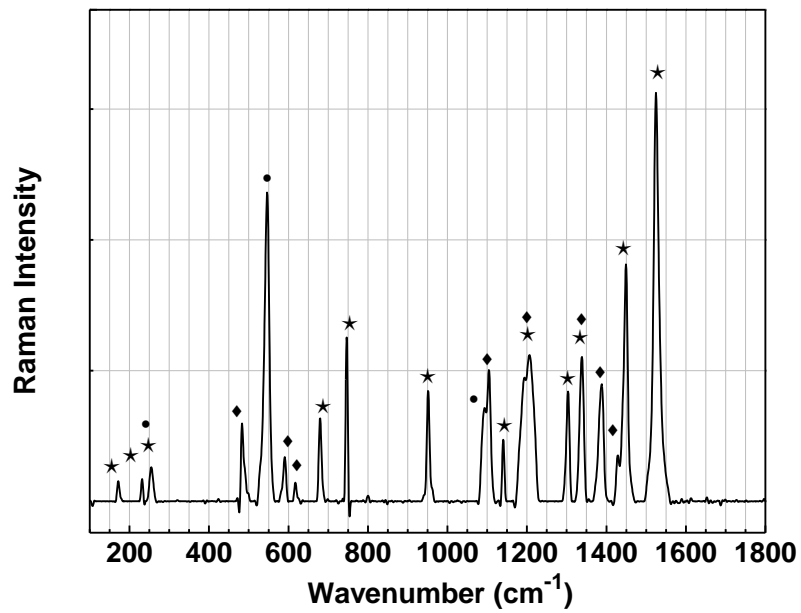
**Table III.7.** Characteristic bands of FTIR spectra of the pigments identified.

Pigment	Bands (cm <sup>-1</sup> ) and intensity	Assignment*
<b>Lead white</b> 2PbCO <sub>3</sub> .Pb(OH) <sub>2</sub>	3536, medium 1400, strong and broad 1047, weak 686, medium	v (OH) v <sub>as</sub> (CO <sub>3</sub> <sup>2-</sup> ) δ (OH) δ <sub>as</sub> (CO <sub>3</sub> <sup>2-</sup> )
<b>Barium sulphate</b> BaSO <sub>4</sub>	1200-1050, strong and broad 983, weak	v <sub>as</sub> (SO <sub>4</sub> ) v <sub>as</sub> (SO <sub>4</sub> )
<b>Ultramarine blue</b> Na <sub>8</sub> [Al <sub>6</sub> Si <sub>6</sub> O <sub>24</sub> ]S <sub>n</sub>	1150-950, strong and broad 696, weak	v (Si-O-Si e Si-O-Al) δ (-O-Si-)
<b>Viridian</b> Cr <sub>2</sub> O <sub>3</sub> .2H <sub>2</sub> O	3630-2630, very broad 1288, medium 1064, strong 794, medium/ strong 650, strong	v (OH) - - - γ (OH)
<b>Chrome yellow</b> PbCrO <sub>4</sub>	857/830, strong and broad	v <sub>as</sub> (CrO <sub>4</sub> <sup>2-</sup> )
<b>Hansa Yellow</b>	1666, medium 1599, weak 1560, weak 1506, media 1493, media 1449, weak 1386, weak 1358, weak 1292, weak 1270, weak 1175, strong 951, weak 914, weak 702, weak	v (C=O) - - v <sub>as</sub> (NO <sub>2</sub> ) - v (N=N) - v <sub>as</sub> (NO <sub>2</sub> ) - - - - - -
<b>Goethite</b> Fe <sub>2</sub> O <sub>3</sub> .H <sub>2</sub> O	3689, 3670, 3650, 3622 medium 1036, strong 917, medium 800, medium	v (OH) v <sub>as</sub> (Si-O-Si) v (Al-O-H) δ (Fe-O-H) goethite and δ (-O-Si-)
<b>β-naphthol red</b>	2929, medium broad 1572, medium 1509, strong 1453, weak 1400, weak 1337, forte 1199, medium 1129, weak 984, weak 891, weak 867, weak 837, weak 742, weak 708, weak	- - v <sub>as</sub> (NO <sub>2</sub> ) - - v <sub>s</sub> (NO <sub>2</sub> ) - - - - - - - -

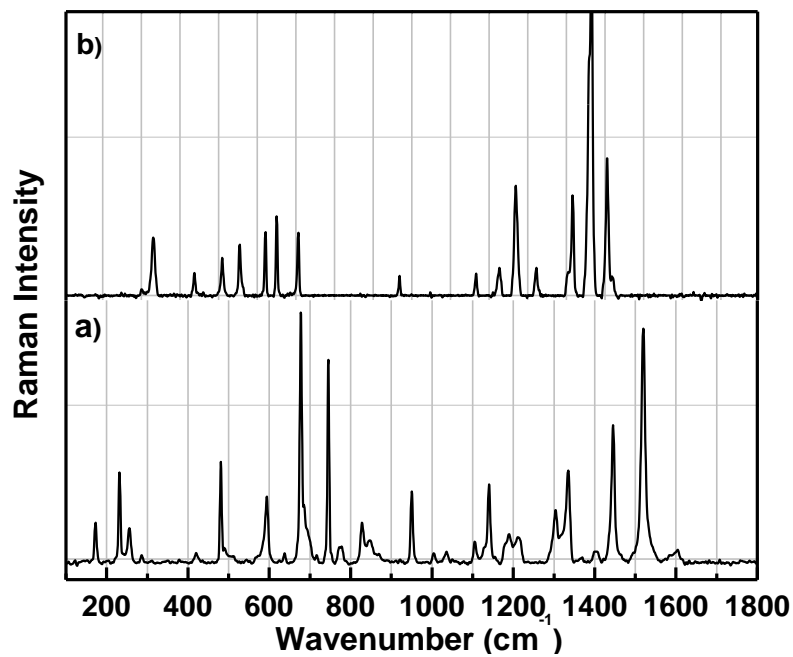
\* Assignment based on [Bouchard *et al.* 2009; Derrick *et al.* 1999; Genestar and Pons 2005; Humel 2002; Weerd *et al.* 2005; Prasad *et al.* 2005; Stuart *et al.* 1996]

### III.4 $\mu$ -Raman

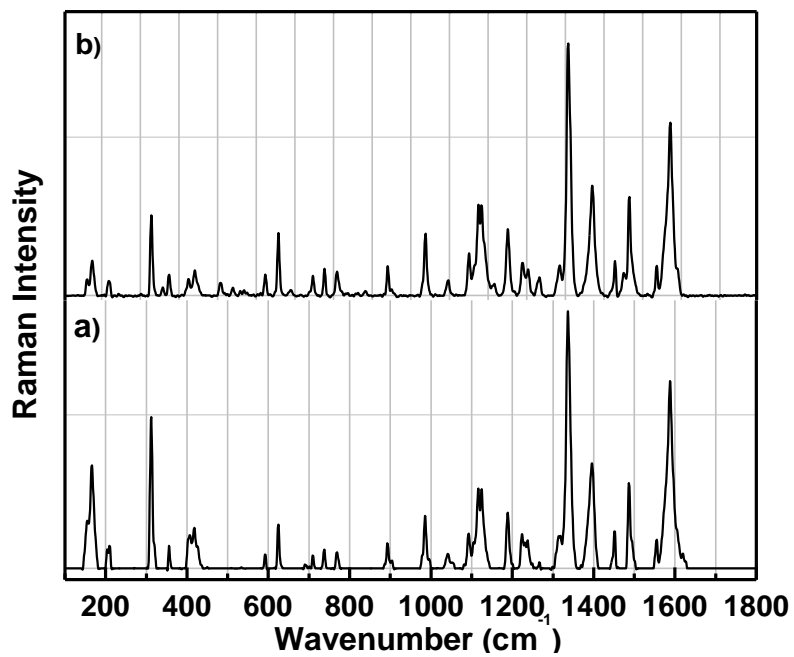
Representative  $\mu$ -Raman spectra from Painting (A) *Collage* and the reference pigments.



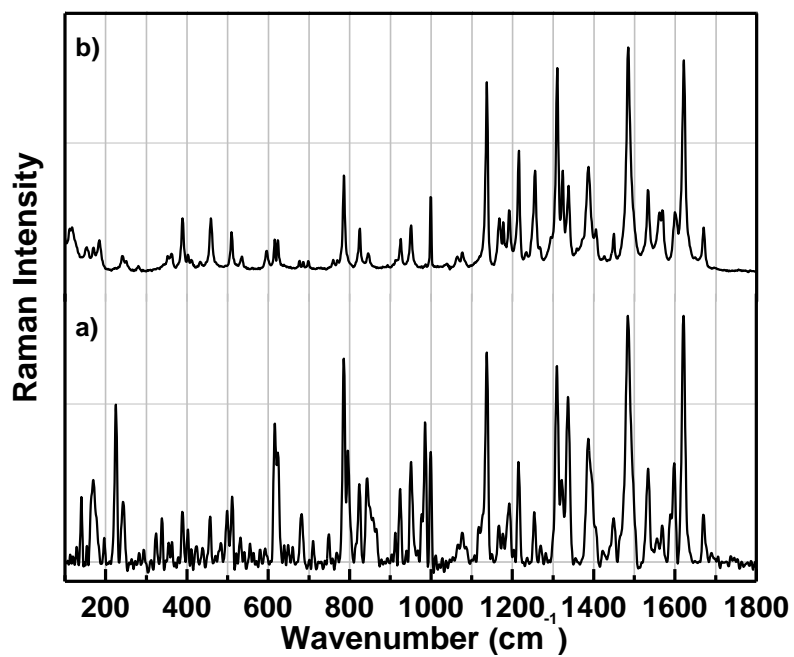
Blue; copper phthalocyanine blue (☆); dioxazine violet (◆); ultramarine blue (●)



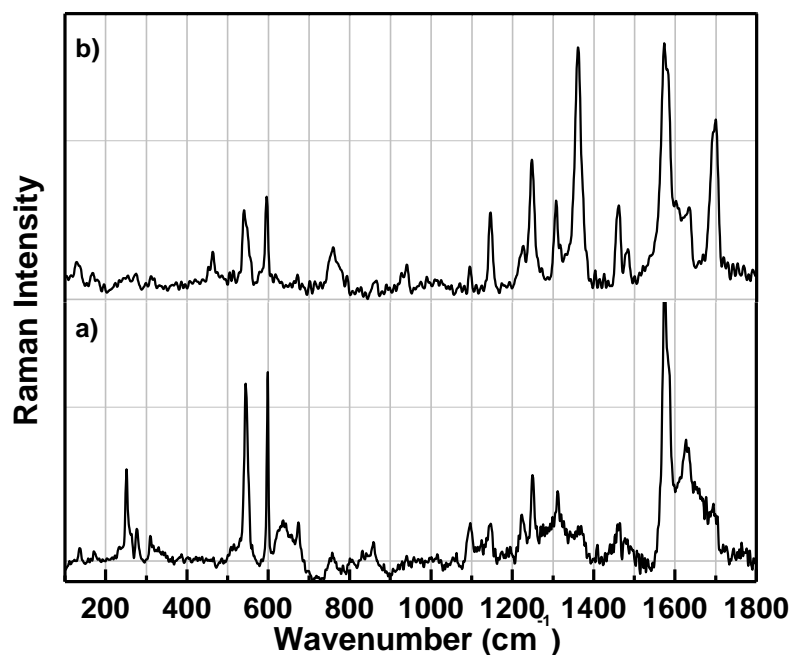
Copper phthalocyanine blue PB15 (Aldrich) (a) and dioxazine violet PV23 (Clariant)(b);



Red area (a) and red  $\beta$ -naphthol PR4 (Clariant) (b).



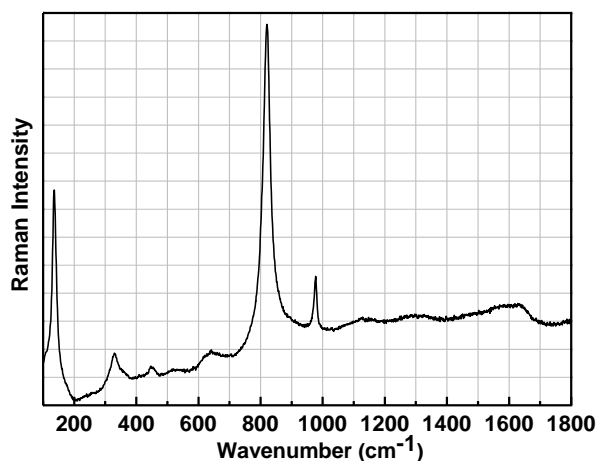
Yellow area (a) and Hansa yellow PY1 (Clariant) (b).



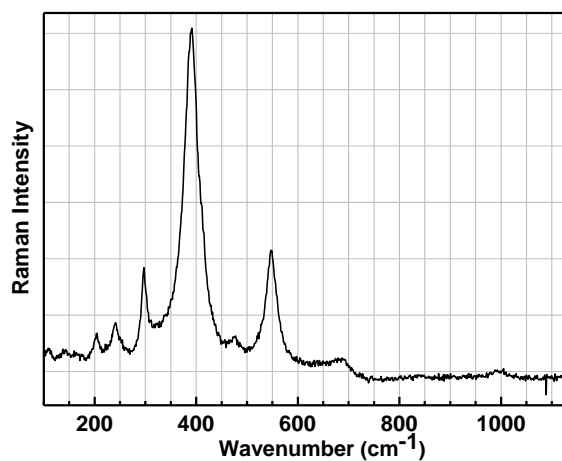
*Blue area on paper B (a) and indigo (Thermo Database) (b).*

**Figure III.9** Representative  $\mu$ -Raman spectra of the blue; red; yellow painted areas and blue area on paper B from Painting (A) *Collage* and the reference pigments Copper phthalocyanine blue PB15 (Aldrich); dioxazine violet PV23 (Clariant);  $\beta$ -naphthol PR4 (Clariant), Hansa yellow PY1 (Clariant) and indigo (Thermo Database).

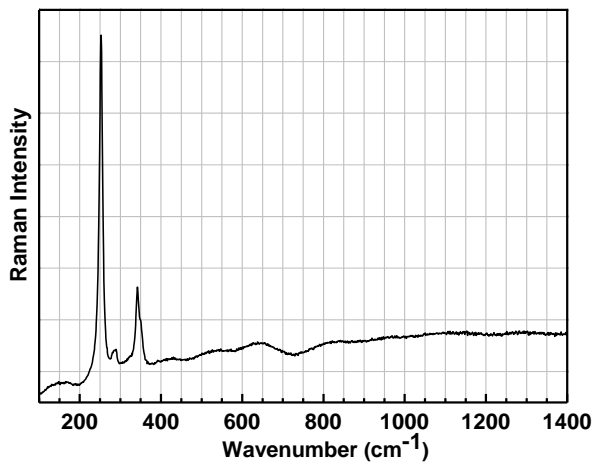
**Representative  $\mu$ -Raman spectra from Painting (B) *Geometric*.**



*Yellow; chrome yellow*



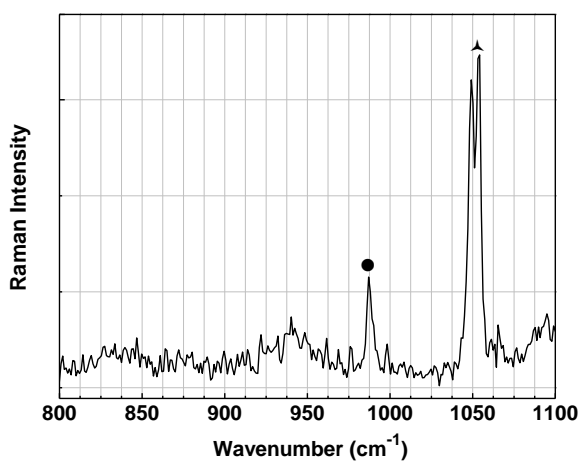
*Brown; goethite.*



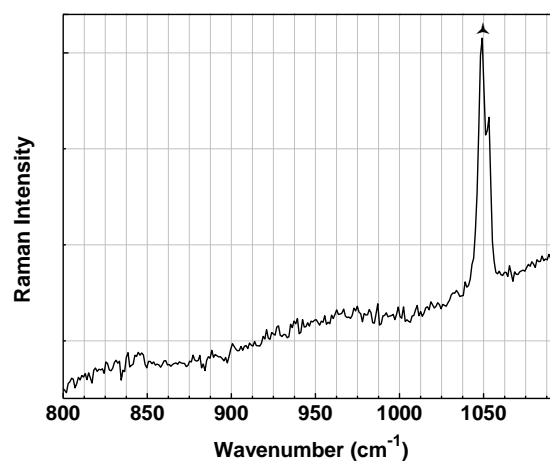
*Red; vermilion.*

**Figure III.10** Representative  $\mu$ -Raman spectra of the yellow; brow and red from Painting (B) *Geometric*.

Representative  $\mu$ -Raman spectra from Painting (C) *Embroiderers*.



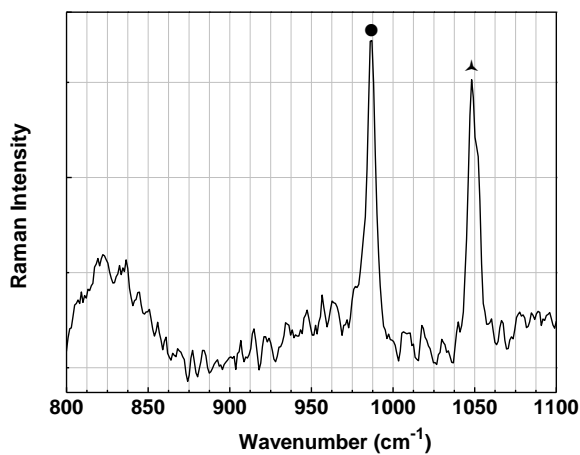
*Preparation layer;*  
 (▲) lead white; (●) barium sulphate



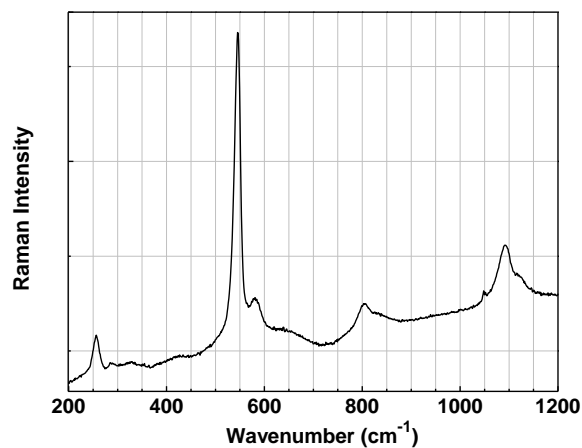
*White;*  
 (▲) lead white.

**Figure III.11** Representative  $\mu$ -Raman spectra of the preparation and white area from Painting (C) *Embroiderers*.

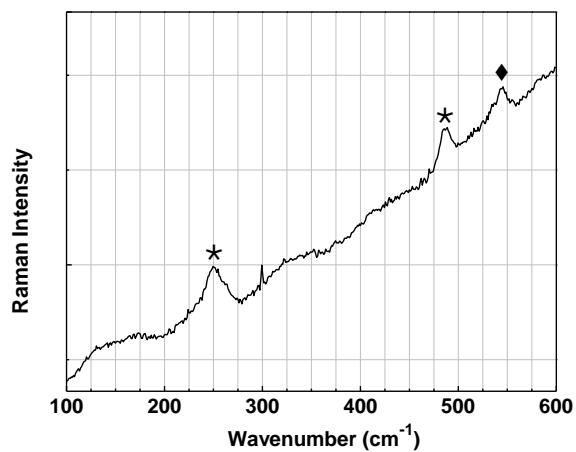
Representative  $\mu$ -Raman spectra from Painting (D) *Café*.



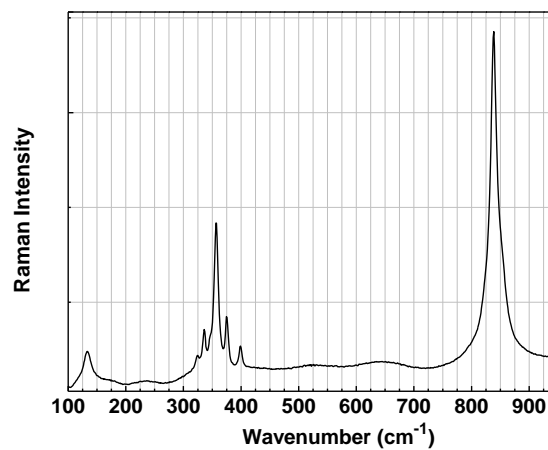
White sample,  
barium sulphate (●) and lead white (▲).



Blue sample  
of ultramarine blue.



Green sample,  
viridian (★) and ultramarine blue (◆).



Yellow sample  
of chrome yellow.

**Figure III.12** Representative  $\mu$ -Raman spectra of the white; blue; green and yellow areas from Painting (D) *Café*.

**Table III.8.** Characteristic bands of Raman spectra of the pigments identified.

Pigment	Band wavenumber (cm <sup>-1</sup> )	Assignment*
<b>Ultramarine blue</b> 3Na <sub>2</sub> O.3Al <sub>2</sub> O <sub>3</sub> .6SiO <sub>2</sub> .2Na <sub>2</sub> S	258 weak	δ (S <sub>3</sub> <sup>-</sup> )
	548 (vs)	ν <sub>s</sub> (S <sub>3</sub> <sup>-</sup> )
	822 (w)	
	1096 (m)	overtone
	520, very strong	ν (Co-O)
<b>Copper Phthalocyanine Blue</b>	173, weak	Aromatic ring deformation
	226, weak	
	256, weak	
	678, medium	
	747, strong	
	952, medium	
	1142, weak	
	1206, medium	
1301, medium	ν (C-C) isoindol group ν (C-C) isoindol group	
<b>Indigo</b>	250, weak	δ (C=C-CO-H) δ (C=O), δ (C-H), δ (C-NH-C) δ (C-H), δ (C=O) ν (C-C), ν (C=C), ν (C=O) ν (C-C), δ (C-H)
	277, very weak	
	545, medium	
	600, medium	
	1250, weak	
	1574, strong	
	1630, weak	
<b>Viridian</b> Cr <sub>2</sub> O <sub>3</sub> .2H <sub>2</sub> O	266, weak	δ (O-Cr <sup>III</sup> -O)
	490, very weak	δ <sub>s</sub> (O-Cr <sup>III</sup> -O)
	552, very weak	ν <sub>as</sub> (O-Cr <sup>III</sup> -O)
	585, very weak	ν <sub>as</sub> (O-Cr <sup>III</sup> -O)
<b>Chrome yellow</b> PbCrO <sub>4</sub>	134, weak	lattice mode
	325, very weak	δ (CrO <sub>4</sub> <sup>2-</sup> )
	337, weak-medium	δ (CrO <sub>4</sub> <sup>2-</sup> )
	347, weak	δ (CrO <sub>4</sub> <sup>2-</sup> )
	357, medium	δ (CrO <sub>4</sub> <sup>2-</sup> )
	375, medium	δ (CrO <sub>4</sub> <sup>2-</sup> )
	39, very weak	δ (CrO <sub>4</sub> <sup>2-</sup> )
	839, very strong	ν <sub>s</sub> (CrO <sub>4</sub> <sup>2-</sup> )
<b>Goethite</b> α-FeOOH	242, very weak	δ <sub>s</sub> (Fe-O) δ <sub>s</sub> (Fe-O) δ <sub>as</sub> (Fe-O) ν <sub>as</sub> (Fe-O)
	297, weak	
	394, very strong	
	477, very weak	
	554, weak	



Table III.8 (continued).

Pigment	Band wavenumber (cm <sup>-1</sup> )	Assignment*		
<b>Hansa Yellow</b>	168, medium	ρ(OCC)		
	240, medium			
	354, weak			
	361, weak			
	387, weak			
	400, weak			
	454, medium		δ (C=O)	
	509, medium			
	538, weak			
	593, weak			
	616, strong			Aromatic ring deformation
	679, medium			
	789, strong			
	823, medium			
	842, medium			
	922, medium			
	950, medium			
	996, medium			
	1077, weak	ν (CONH), Amide III		
	1135, strong			
	1166, weak			
	1190, medium			
	1214, medium			
	1253, medium			
	1308, strong			
	1322, medium			
	1335, medium			
1385, strong				
1422, weak				
1448, medium				
1483, strong				
1533, medium				
1567, weak	ν (NO <sub>2</sub> )			
1597, medium				
1622, strong	Aromatic ring			
1670, medium				
<b>Goethite</b> α-FeOOH	242, very weak	δ <sub>s</sub> (Fe-O)		
	297, weak			
	394, very strong			
	477, very weak			
	554, weak			
<b>Vermilion</b> HgS	253, very strong	δ (S-Hg-S)		
	282, weak-shoulder	δ (S-Hg-S)		
	343, medium	ν (Hg-S)		

Table III.8 (continued).

Pigment	Band wavenumber (cm <sup>-1</sup> )	Assignment*	
<b>β-naphthol</b>	165, medium	Aromatic ring deformation	
	204, weak		
	310, media		
	356, weak		
	405-418, weak		
	592, weak		
	628, media		
	69, weak		
	711, weak		
	735, weak		
	773, weak		
	895, weak		δ (NO <sub>2</sub> )
	986, weak		
	1039, weak		
	1092, shoulder		
	1121, media		
	1186, media		
	1226-1236, weak		
1315, shoulder	v azobenzene		
1334, strong			
1394, medium			
1453, weak			
1488, medium			
1558, shoulder	v (NO <sub>2</sub> )		
<b>Cobalt violet</b> Co <sub>3</sub> (AsO <sub>4</sub> ) <sub>2</sub>	204 very weak	(As-O) in the plane	
	351 weak, broad	As-O) out of plane	
	375 weak shoulder	As-O) out of plane	
	420 weak, broad	As-O) out of plane	
	508 weak	(As-O) out of plane	
	738 very weak	v <sub>s/s</sub> (As-O)	
	837 medium	v <sub>s/s</sub> (As-O)	
	865 very strong	v <sub>s/s</sub> (As-O)	
<b>Dioxazine violet</b>	482, weak	v <sub>s</sub> (naphthalene) v (C=N); v (C=C) v aromatic ring	
	592, weak		
	617, weak		
	1106, medium		
	1207, medium		
	1337, medium		
	1387, medium		
1431, shoulder			
<b>Lead carbonate or Lead White</b> PbCO <sub>3</sub> or 2PbCO <sub>3</sub> .Pb(OH) <sub>2</sub>	665, very weak	δ <sub>s</sub> (CO <sub>3</sub> <sup>2-</sup> )	
	687, very weak	δ <sub>s</sub> (CO <sub>3</sub> <sup>2-</sup> )	
	829, very weak	v <sub>as</sub> (CO <sub>3</sub> <sup>2-</sup> )	
	1050, very strong	v <sub>s</sub> (CO <sub>3</sub> <sup>2-</sup> )	

<b>Barium sulphate</b> <b>Barite</b> BaSO <sub>4</sub>	453, medium	$\delta$ (SO <sub>4</sub> <sup>2-</sup> )
	461, medium, should	$\delta$ (SO <sub>4</sub> <sup>2-</sup> )
	616, weak	$\delta_{\text{out-of-plane}}$ (SO <sub>4</sub> <sup>2-</sup> )
	647, weak	$\delta_{\text{out-of-plane}}$ (SO <sub>4</sub> <sup>2-</sup> )
	987, very strong	$\nu_s$ (SO <sub>4</sub> <sup>2-</sup> )

\* Assignment based on [Bersani *et al.* 1999; Bouchard *et al.* 2010; Casadio *et al.* 2011; Frausto-Reyes *et al.* 2009; Frost 2004; Frost *et al.* 2010; Quilès and Burneau 1998; Roncaglia *et al.* 1985; Ropret *et al.* 2008; Scherren *et al.* 2009; Shebanova and Lazor 2003; Schulte *et al.* 2008; Vandenabeele *et al.* 2000; Yang *et al.* 2010; Zumbuehl *et al.* 2009].

### III.5 FORS

Representative FORS spectra from Painting (C) *Embroiderers*.

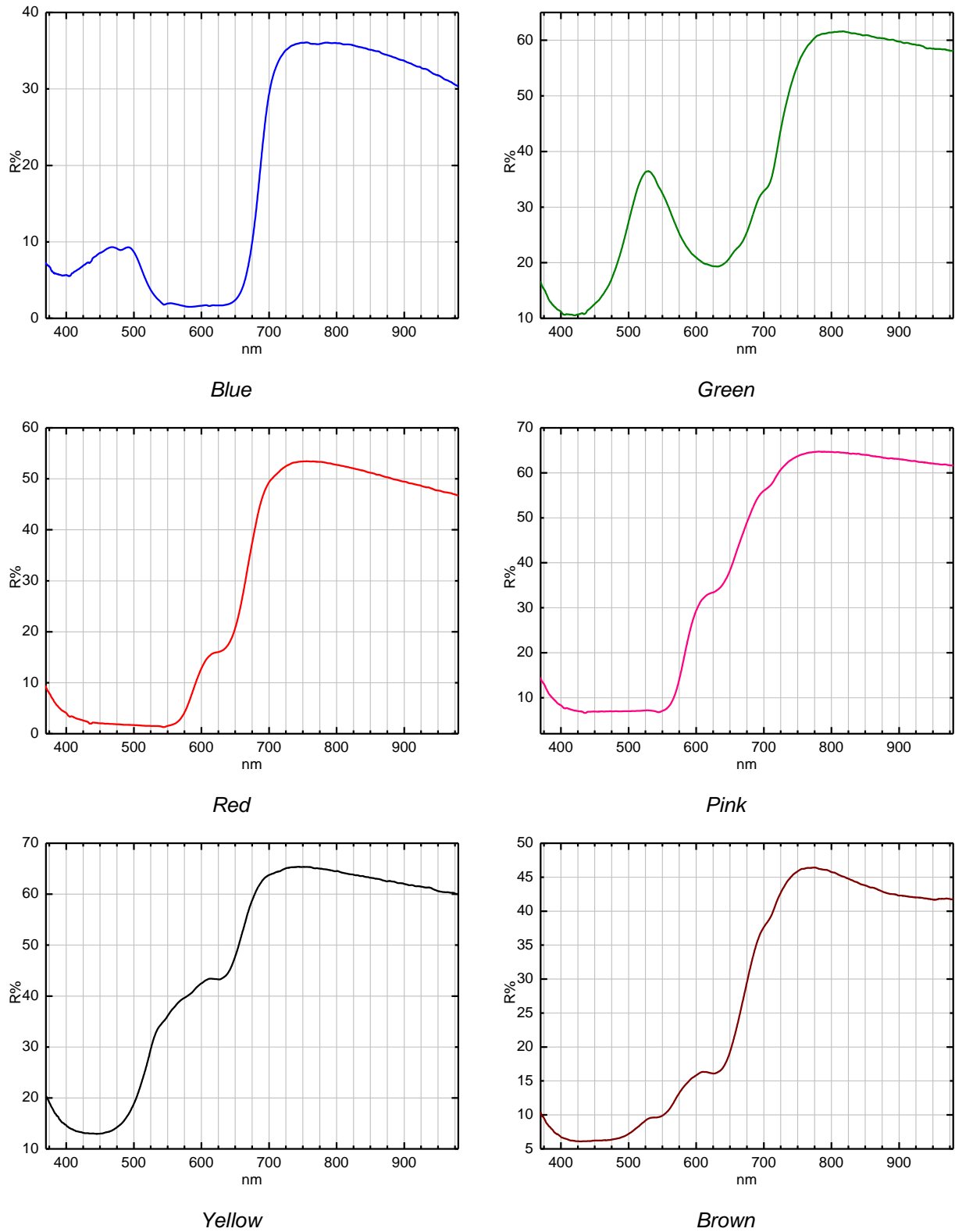


**Figure III.13** Representative FORS spectra of the support; blue; green; red; pink; yellow; brown areas from Painting (C) *Embroiderers*.

Appendix IV: Image documentation



Figure IV.1. Infrared photography Painting (A), *Collage*, attributed Amadeo de Souza-Cardoso.



**Figure V.2.** Infrared photography Painting (C), *Embroiderers*, attributed Amadeo de Souza-Cardoso.



**Figure V.3.** Ultraviolet photograph (covered in black and white) of the Painting (D), *Café*, attributed Amadeo de Souza-Cardoso.



**Figure V.4.** X-ray image of the Painting (D), *Café*, attributed Amadeo de Souza-Cardoso.



**Appendix V: Paintings cited in the main text**

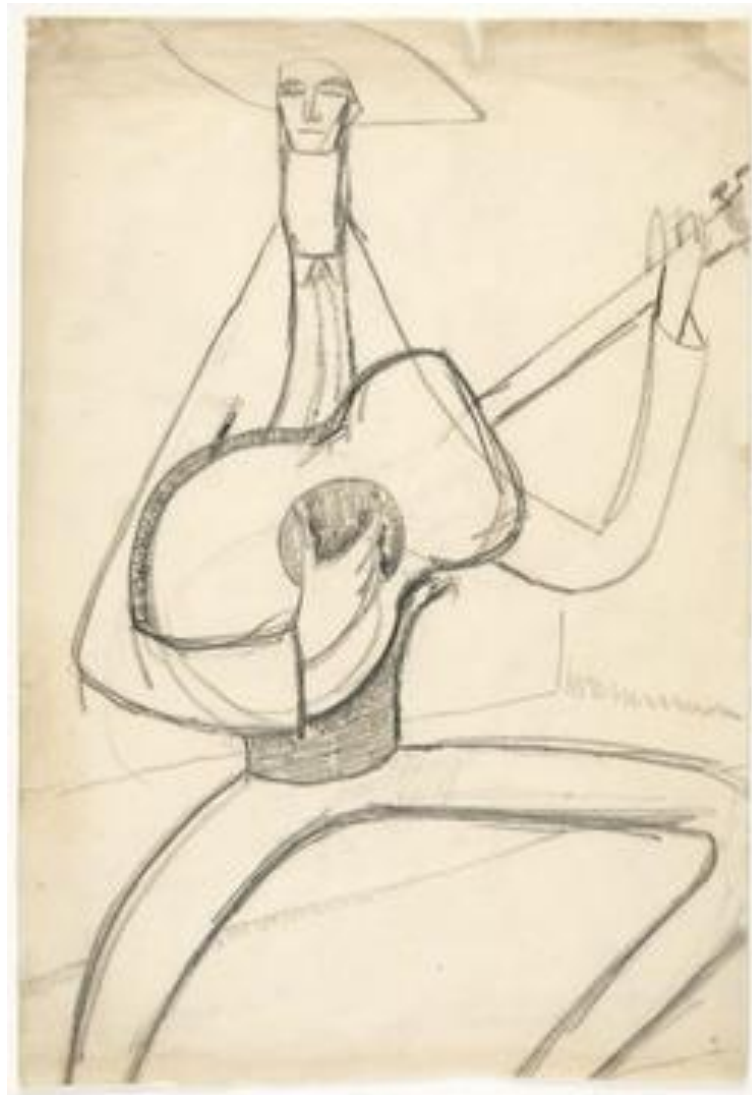


**Figure VI.1** Amadeo de Souza-Cardoso, *Untitled*, 1910, graphite on paper. 36 x 24.7 cm. Collection of Centro de Arte Moderna, Fundação Calouste Gulbenkian (Inv. 92DP1586).



**Figure VI.2** Amadeo de Souza-Cardoso, Untitled, 1910, graphite on paper. 25 x 35 cm. Collection of Centro de Arte Moderna, Fundação Calouste Gulbenkian (Inv. 86DP372).

